

## INFORMATION TO USERS

This manuscript has been reproduced from the microfilm master. UMI films the text directly from the original or copy submitted. Thus, some thesis and dissertation copies are in typewriter face, while others may be from any type of computer printer.

**The quality of this reproduction is dependent upon the quality of the copy submitted.** Broken or indistinct print, colored or poor quality illustrations and photographs, print bleedthrough, substandard margins, and improper alignment can adversely affect reproduction.

In the unlikely event that the author did not send UMI a complete manuscript and there are missing pages, these will be noted. Also, if unauthorized copyright material had to be removed, a note will indicate the deletion.

Oversize materials (e.g., maps, drawings, charts) are reproduced by sectioning the original, beginning at the upper left-hand corner and continuing from left to right in equal sections with small overlaps.

Photographs included in the original manuscript have been reproduced xerographically in this copy. Higher quality 6" x 9" black and white photographic prints are available for any photographs or illustrations appearing in this copy for an additional charge. Contact UMI directly to order.

ProQuest Information and Learning  
300 North Zeeb Road, Ann Arbor, MI 48106-1346 USA  
800-521-0600

**UMI<sup>®</sup>**



**University of Alberta**

**Instrumentation, capillary coating, and labeling chemistry for capillary  
electrophoresis with laser-induced fluorescence detection**

by

**Hossein Ahmadzadeh**



A thesis submitted to the Faculty of Graduate Studies and Research in partial fulfillment of  
the requirements for the degree of **Doctor of Philosophy**

Department of Chemistry

Edmonton, Alberta

Spring 2000



**National Library  
of Canada**

**Acquisitions and  
Bibliographic Services**

**395 Wellington Street  
Ottawa ON K1A 0N4  
Canada**

**Bibliothèque nationale  
du Canada**

**Acquisitions et  
services bibliographiques**

**395, rue Wellington  
Ottawa ON K1A 0N4  
Canada**

*Your file Votre référence*

*Our file Notre référence*

**The author has granted a non-exclusive licence allowing the National Library of Canada to reproduce, loan, distribute or sell copies of this thesis in microform, paper or electronic formats.**

**L'auteur a accordé une licence non exclusive permettant à la Bibliothèque nationale du Canada de reproduire, prêter, distribuer ou vendre des copies de cette thèse sous la forme de microfiche/film, de reproduction sur papier ou sur format électronique.**

**The author retains ownership of the copyright in this thesis. Neither the thesis nor substantial extracts from it may be printed or otherwise reproduced without the author's permission.**

**L'auteur conserve la propriété du droit d'auteur qui protège cette thèse. Ni la thèse ni des extraits substantiels de celle-ci ne doivent être imprimés ou autrement reproduits sans son autorisation.**

**0-612-59923-X**

**Canada**



**University of Alberta**

**Library release form**

**Name of Author:** Hossein Ahmadzadeh

**Title of Thesis:** Instrumentation, capillary coating, and labeling chemistry for  
capillary electrophoresis with laser-induced fluorescence detection

**Year this Degree Granted:** 2000

Permission is hereby granted to the University of Alberta Library to reproduce single copies of this thesis and to lend or sell such copies for private, scholarly, or scientific research purposes only.

The author reserves all other publication and other rights in association with the copyright in the thesis, and except as herein before provided, neither the thesis nor any substantial portion thereof may be printed or otherwise reproduced in any material form whatever without the author's prior written permission.

Ahmadzadeh

Hossein Ahmadzadeh

Chemistry Department

University of Alberta

Edmonton, AB, T6G2G2

Dec. 6/ 1999

**University of Alberta**

**Faculty of Graduate Studies and Research**

The undersigned certify that they have read, and recommend to the Faculty of Graduate Studies and Research for acceptance, a thesis entitled **Instrumentation, capillary coating, and labeling chemistry for capillary electrophoresis with laser-induced fluorescence detection** submitted by **Hossein Ahmadzadeh** in partial fulfillment of the requirements for the degree of **Doctor of Philosophy**.



Dr. N. J. Dovichi



Dr. F. F. Cantwell



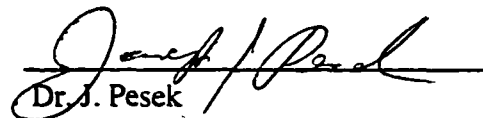
Dr. M. McDermott



Dr. M. Palcic



Dr. X. C. Le



Dr. J. Pesek

12 November 1999

**Instrumentation, capillary coating,  
and labeling chemistry for  
capillary electrophoresis with  
laser-induced fluorescence detection**

## **Dedication**

To the memory of my mother who all the time wanted me to finish my education and there were no sacrifices that she did not do for me, to my father whose financial support was critical for me, to my wife who took care of the family and made a quiet home for me to study and made the ends meet with a student salary, to Arezoo who pretended to read science along with me, to Arman whose letters from a remote distance encouraged me. to all of my family members and closest friends who gave moral support all the time. I would also like to dedicate my thesis to all of my past and present teachers who taught me the logic of scientific approach to problems.

## **Abstract**

A miniaturized Capillary Electrophoresis (CE) instrument with Laser-Induced Fluorescence (LIF) detection (CE-LIF) and its performance optimization is shown. Different injection techniques in CE are discussed and experimental results show the high sensitivity of the CE-LIF method. Limit of detection of 150 fluorescein molecules is presented. A light shield was designed for the instrument and it was shown that the major contribution to the background noise comes from the laser and not from the room light.

A method is presented for electroosmotic flow (EOF) measurement in the case that the instrument does not have a UV detector, as is the case for CE-LIF. The method validation is shown and statistical data analysis shows that this new method is as precise as the neutral marker injection method for EOF measurement. Basic principles of CE were investigated including the effect of pH, ionic strength, temperature and electric field on EOF.

Coating the capillary inner surface with a polymer to eliminate EOF is also presented. A series of polymers from the most hydrophobic to the most hydrophilic one are compared to find which polymer shows the lowest EOF and minimum adsorption of proteins and antibody (Ab) to the capillary wall. It was shown that a Si-C sub-layer is much more stable than Si-O sub-layer and acryloylaminopropanol (AAP) monomer, when polymerized on the capillary surface, has the least EOF and also the minimum adsorption of proteins.

A high-sensitive method to measure natural toxins in water (microcystins) using CE is also studied. The immunoassay technique was chosen because it was already used for this class of toxins that are liver carcinogens, but the classical immunoassay technique lacked sensitivity. The first step was to fluorescently label the analyte, called antigen in immunoassay, and this process involved studying amine labeling chemistry, developing carboxylic acid labeling, and finally synthesizing an arginine-specific labeling reagent.

Labeling chemistry for CE-LIF Immunoassay of carboxylic acids is presented. Despite being optimized by the author, amine-labeling chemistry with FQ fluorogenic dye is not discussed because it is widely used in CE and the analytes of interest lack an amine group. Microcystin lacks an amine group, but it has two carboxylic acid groups and one arginine group.

Microgram-scale organic synthesis of an arginine-specific reagent is also studied. Microcystin contains an arginine group. In this study an optimized procedure to label the arginine group is presented. Because the sample quantity is very limited, the synthesis approach was developed in a way to cut down the weight of starting material to the microgram level to reduce reagent consumption.

## ACKNOWLEDGEMENT

If we perceive learning to be a many-sided collaborative effort, then writing a thesis is the embodiment of that principle. In that respect, I am indebted to my supervisor, Professor N. J. Dovichi, who encouraged me, and produced the anthology of learning. I am particularly grateful to the insights, intelligence, guidance, support, patience, and constructive criticism of my supervisor and all of the committee members of my PhD. I am grateful and perhaps fortunate to have had in my life a variety of inspired teachers who taught me how to have a scientific logic.

I would like to thank Dr. J. Stryker and Dr. Ole Hindsgaul for their useful discussions in organic synthesis.

There are many other people I must thank for their contribution: Kym Schreiner very helpfully edited the entire thesis chapter by chapter and commented on the fluency of writing, Monica Palcic let me use her laboratory to do organic chemistry, Keiko Sujino discussed the organic synthesis, and Ole Hindsgaul let me use his MALDI-MS instrument and also discussed the results of organic synthesis with me.

I would also like to thank Dr. Xc. Le for his collaboration on the arginine project and Dr. Jed Harrison for his collaboration on the TNT immunoassay project. The generous donation from National Research Laboratory (NRL) of all the chemicals used in TNT immunoassay is also greatly appreciated.

Finally financial support from Natural Science and Engineering Research Council (NSERC) and Canadian Genetic Diseases Network (CGDN) and Department of Chemistry of the University of Alberta are very much appreciated.

In particular, I would like to thank my Professors at Shiraz (A. Safavi and A. Masoumi) and Mashhad (F. Milani-nejad, F. Tayari, and M. Rahimzadeh) universities who taught me the true value of research and especially I would like to thank Professor Issa Yavari who encouraged me to continue my education abroad.

## Table of contents

<b>Volume 1</b>	1
<b>Part I: Capillary electrophoresis, laser induced fluorescence detection, sample introduction, and sample depletion</b>	2
<b>Chapter 1: Introduction and theory</b>	3
<b>1.1 Historical background and development of electrophoresis</b>	4
<b>1.2 Basic principles of CE</b>	8
<b>1.2.1 Some definitions and fundamental equations of CE</b>	11
<b>1.2.2 Electroosmotic Flow (EOF)</b>	13
<b>1.2.3 Resolution and efficiency</b>	17
<b>1.2.4 Variance caused by injection</b>	19
<b>1.2.5 Variance caused by diffusion</b>	19
<b>1.2.6 Variance due to hydrodynamic flow</b>	21
<b>1.2.7 Variance caused by Joule heating</b>	21
<b>1.2.8 Variance due to adsorption</b>	22
<b>1.2.9 Variance caused by conductivity difference</b>	24
<b>1.3 Detection methods in CE</b>	25
<b>1.3.1 UV-Visible Absorbance</b>	25
<b>1.3.2 Laser Induced Fluorescence (LIF) detection with a sheath flow cuvette as a very sensitive post column detector</b>	27
<b>1.3.2a) LASER: Light Amplification by Stimulated Emission of Radiation</b>	27
<b>1.3.2b) Fluorescence spectroscopy</b>	30



<b>1.3.3 Laser Induced Fluorescence (LIF)</b>	34
<b>1.3.4 The sheath flow cuvette</b>	35
<b>1.3.5 Derivatization for fluorescence detection</b>	38
<b>1.4 Mass spectrometry</b>	41
<b>1.5 Applications of capillary electrophoresis</b>	42
<b>1.6 Thesis overview</b>	48
<b>1.7 References</b>	51
<b>Chapter 2: Performance optimization of a miniaturized CE-LIF system</b>	55
<b>2.1 Introduction</b>	56
<b>2.1.1 A sheath flow cuvette with Laser Induced Fluorescence</b>	
(LIF) detection for capillary electrophoresis	56
<b>2.1.1a) The sheath flow cuvette</b>	57
<b>2.1.1b) LIF detection</b>	58
<b>2.1.1c) Application of a sheath flow cuvette</b>	
with LIF detection	60
<b>2.1.2 Sample introduction in capillary electrophoresis</b>	60
<b>2.1.3 Contribution of injection volume on bandbroadening in CE</b>	64
<b>2.1.4 Electrokinetic injection</b>	65
<b>2.1.5 Hydrodynamic injection</b>	66
<b>2.1.6 Limit of Detection (LOD)</b>	68
<b>2.2 Experimental</b>	70
<b>2.2.1 Instrument design and improvement</b>	70
<b>2.2.2 Methods and materials</b>	74
<b>2.2.2.1 Reagents</b>	74
<b>2.2.2.2 Methods</b>	74
<b>2.2.2.3 Vacuum Injector modification</b>	74

<b>2.3 Results and discussion</b>	78
<b>2.3.1 Vacuum Injection</b>	78
<b>2.3.2 Modification of the commercial vacuum injector</b>	82
<b>2.3.3 Electrokinetic Injection</b>	82
<b>2.3.4 Siphoning effect</b>	82
<b>2.3.5 Limit of Detection (LOD)</b>	85
<b>2.3.6 Further modification of DRES instrument</b>	
(Room light blocking)	91
<b>2.4 Conclusions</b>	94
<b>Appendix I</b>	95
<b>A1.1 Procedure for operation of DRES Capillary</b>	
Electrophoresis Instrument	95
<b>A1.2 Alignment</b>	95
<b>A1.3 CE separation</b>	97
<b>2.5 References</b>	98
<b>CHAPTER 3: Pseudo-Coulometric Sample Introduction In Capillary Gel</b>	
Electrophoresis DNA Sequencing	100
<b>3.1 Theoretical background in DNA sequencing and</b>	
electrokinetic sample introduction onto a gel-filled capillary	101
<b>3.1.1 DNA structure</b>	101
<b>3.1.2 Cycle sequencing</b>	105
<b>3.1.3 Change of transference (or transport) number at</b>	
solution-gel interface in electrokinetic injection	105
<b>3.1.4 An efficient method of sample introduction for</b>	
capillary gel electrophoresis DNA sequencing	113
<b>3.2 Experimental</b>	116

<b>3.2.1</b> Reagents and material	116
<b>3.2.2</b> Instrument	116
<b>3.2.3</b> Methods and procedures	117
<b>3.3</b> Results and discussion	120
<b>3.3.1</b> Injection	121
<b>3.3.2</b> Depletion of the sample	123
<b>3.3.3</b> Sequencing	129
<b>3.4</b> Conclusions	131
<b>3.5</b> References	134
<b>Part II: Electroosmotic flow: measurement and elimination</b>	136
<b>Chapter 4: Fast, accurate and universal method for electroosmotic flow rate measurement and evaluation of fundamental parameters affecting separation in capillary electrophoresis</b>	137
<b>4.1</b> Introduction	138
<b>4.1.2</b> History of EOF	138
<b>4.1.3</b> Theory of EOF	139
<b>4.1.3.1</b> Double-layer theory	141
<b>4.1.3.2</b> Stern-Gouy-Chapman model	144
<b>4.1.4</b> Mismatch of electroosmotic flows	149
<b>4.1.5</b> The methods of EOF measurement	151
<b>4.2</b> Experimental	155
<b>4.2.1</b> EOF calculation	155
<b>4.2.2</b> Instrument	156
<b>4.2.3</b> Reagents	157
<b>4.3</b> Results and discussions	159

<b>4.3.1</b> Method validation	159
<b>4.3.2</b> Study of fundamental properties in CE using current monitoring method	177
<b>4.3.2.1</b> Effect of concentration on EOF	177
<b>4.3.2.2</b> Electric field effect on EOF velocity	177
<b>4.3.2.3</b> pH effect on EOF	180
<b>4.3.2.4</b> The effect of temperature on EOF	184
<b>4.4</b> Conclusions	185
<b>4.5</b> References	187
<b>Volume 2</b>	<b>189</b>
<b>Chapter 5: Surface modification based on Si-O and Si-C sub-layers and a series of N-substituted acrylamide top-layers for capillary electrophoresis</b>	188
<b>5.1</b> Introduction	191
<b>5.2</b> Experimental	197
<b>5.2.1</b> Instrument	197
<b>5.2.2</b> Reagents	199
<b>5.2.3</b> Capillary coating protocol	200
<b>5.2.3.1</b> Capillary pre-treatment	202
<b>5.2.3.2</b> Chlorinating of silanol groups	202
<b>5.2.3.3</b> Grignard reaction	203
<b>5.2.3.4</b> Polymerization step	204
<b>5.2.3.5</b> FQ labeling	204
<b>5.2.3.6</b> Electro-osmotic flow (EOF) mobility	

measurement	205
5.2.3.7 Safety precautions	205
5.3 Results and discussion	205
5.3.1 EOF comparison	205
5.3.2 Temperature stability	208
5.3.3 pH stability	211
5.3.4 Peak shape comparison and adsorption study	213
5.3.5 Five-capillary instrument	224
5.3.6 Migration time reproducibility	234
5.3.7 Long-term stability	236
5.3.8 Si-C-polyDMA coated capillary	239
5.3.9 Separation of alkaline protein markers	239
5.4 Conclusions	242
5.5 References	244

<b>PART III: Development of labeling chemistry and its characterization for ultrasensitive assay of natural toxins and environmental samples using capillary electrophoresis and flow injection analysis with laser-induced fluorescence detection</b>	246
--	-----

<b>Chapter 6: Carboxylic acid labeling and method development for microcystin analysis</b>	247
6.1 Introduction	248
6.1.1 Microcystins and shellfish toxins	248
6.1.2 Objectives	251
6.1.3 Carboxylic acid labeling	252

6.1.4	The use of penicillins as model analytes	254
6.1.5	Organic synthesis	255
6.2	Experimental	255
6.2.1	Reagents	255
6.2.2	Instruments	257
6.2.3	Reaction conditions optimization	258
6.2.3.1	Procedure 1	258
6.2.3.2	Procedure 2	258
6.2.3.3	Procedure 3	259
6.2.3.4	Procedure 4	260
6.2.3.5	Procedure 5	260
6.2.3.6	Procedure 6	260
6.2.3.7	Procedure 7	261
6.2.3.8	Preparative TLC and purification method	261
6.2.3.9	Quantitation and Calibration curve	262
6.3	Results and Discussion	262
6.4	Conclusion	293
6.5	References	294
<b>Chapter 7:</b>	<b>Arginine labeling chemistry and microgram-scale organic synthesis of an arginine-specific reagent for microcystin chemical analysis</b>	<b>296</b>
7.1	Introduction	297
7.1.1	Model compounds for microcystin labeling	298
7.1.2	Microgram-scale organic synthesis and labeling	299
7.1.3	Introduction to arginine-labeling chemistry	299
7.1.4	The chemical properties of the guanidinium group of arginine	300

7.1.5 Microgram-scale organic synthesis of an arginine-specific fluorescent labeling reagent	300
<b>7.2 Experimental</b>	301
7.2.1 Reagents	301
7.2.2 Instruments	302
7.2.3 Visualizing spots on TLC	302
7.2.3.1 ninhydrine solution	303
7.2.3.2 Iodine vapor	303
7.2.3.3 sulfuric acid solution	303
7.2.3.4 Molibdo-Cerric solution	303
7.2.4 Developing solvent for TLC	304
7.2.5 Free amine generation from N <sub>α</sub> -acetyl-L-arginine model compound	304
7.2.6 Direct labeling of arginine with amine-labeling reagent FQ	304
7.2.7 Direct labeling of N-acetyl-L-arginine with tetramethylrhodamine N-hydroxysuccinimidyl ester at pH 12	306
7.2.8 Hydrazine reaction	307
7.2.9 Hydrazinolysis reaction time optimization	307
7.2.10 Ornithine TMR labeling reaction	307
7.2.11 Hydroxylamine reaction	308
7.2.12 Sodium hydride reaction	308
7.2.13 TMR labeling reaction on the NaH reaction mixture before separation	309
7.2.14 Ion-exchange separation of the hydrazinolysis and NaH reaction products	309

<b>7.2.15</b>	Preparative TLC for NaH and hydrazinolysis reaction product	309
<b>7.2.16</b>	C <sub>18</sub> Sep-Pak separation of the NaH and hydrazinolysis reaction products	310
<b>7.2.17</b>	TMR labeling of the NaH reaction after ion exchange separation of the product	310
<b>7.2.18</b>	Two-layer sample deposition for MALDI	311
<b>7.2.19</b>	Hydrazine reaction on cyclic peptide	312
<b>7.2.20</b>	TMR labeling on the product of hydrazinolysis reaction of cyclic peptide	312
<b>7.2.21</b>	NaH reaction on cyclic peptide	313
<b>7.2.22</b>	TMR labeling on the product of NaH reaction of cyclic peptide	313
<b>7.2.23</b>	Furfurylamine reaction with 5-BrMF	314
<b>7.2.24</b>	Ozonolysis of 5-BrMF and furfurylamine reaction	315
<b>7.2.25</b>	4-aminoacetophenone reaction with 5-BrMF	315
<b>7.2.26</b>	SeO <sub>2</sub> oxidation of 5-BrMF and aminoacetophenone reaction	316
<b>7.2.27</b>	2, 3-butanedione reaction with benzylbromide	316
<b>7.2.28</b>	2, 3-butanedione reaction with 5-BrMF	317
<b>7.2.29</b>	Arginine labeling using 5 (pentane 2,3 dione) methyl fluorescein	317
<b>7.2.30</b>	Microcystin labeling with TMR using NaH deprotonation	317
<b>7.2.31</b>	Separation of the labeled microcystin-LR	318
<b>7.2.32</b>	Microcystin labeling using 5-BrMF	318
<b>7.2.33</b>	Microcystin immunoassay	319
<b>7.3</b>	Results and discussion	319



<b>7.3.1</b>	Direct labeling of arginine with amine labeling reagent FQ	319
<b>7.3.2</b>	Direct labeling of arginine with TMR at pH 12	323
<b>7.3.3</b>	Hydrazine reaction with arginine and reaction time optimization	323
<b>7.3.4</b>	Hydrazine reaction time optimization	325
<b>7.3.5</b>	Ornithine TMR labeling reaction	325
<b>7.3.6</b>	Hydroxylamine reaction with arginine	329
<b>7.3.7</b>	Sodium hydride reaction with arginine and TMR labeling of the product before separation	329
<b>7.3.8</b>	Hydrazine and NaH reactions with arginine and TMR labeling of the product after separation with ion-exchange resin	333
<b>7.3.9</b>	Hydrazine and NaH reactions with arginine and TMR labeling of the product after separation with Sep-Pak	336
<b>7.3.10</b>	Hydrazine and NaH reactions with cyclic peptide	339
<b>7.3.11</b>	Furfurylamine and 4-aminoacetophenon reactions with 5-BrMF followed by the oxidation of the resulting products	349
<b>7.3.12</b>	Butanedione reaction with benzylbromide	354
<b>7.3.13</b>	Butanedione reaction with 5-BrMF	354
<b>7.3.14</b>	Arginine labeling reaction with synthesized 5 (pentane 2, 3 dione) methylfluorescein	359
<b>7.3.15</b>	Microcystin labeling with TMR using NaH deprotonation	362
<b>7.3.16</b>	Separation of the labeled microcystin	366
<b>7.3.17</b>	Microcystin labeling with 5-BrMF	369
<b>7.3.18</b>	Microcystin immunoassay	372
<b>7.4</b>	Conclusions	376

7.5 References	378
<b>Chapter 8: Capillary-based and microchip flow injection analysis of TNT using displacement immunoassay with laser-induced fluorescence detection</b>	381
<b>8.1 Introduction</b>	382
<b>8.1.1 Immunoassay techniques for environmental/clinical sample analysis</b>	382
<b>8.1.2 Microfabrication devices for performing capillary electrophoresis and flow injection analysis of explosives</b>	385
<b>8.1.3 Capillary electrophoresis for performing immunoassay analysis of explosives</b>	385
<b>8.1.4 The analysis of explosive compounds</b>	386
<b>8.1.5 Antibody immobilization on silica surfaces</b>	387
<b>8.2 Experimental</b>	389
<b>8.2.1 Reagents and materials</b>	389
<b>8.2.2 Equipment</b>	389
<b>8.2.3 Flow buffer</b>	394
<b>8.2.4 Antibody immobilization on a capillary</b>	394
<b>8.2.5 Antibody immobilization on a microchip</b>	395
<b>8.2.6 Displacement immunoassay</b>	395
<b>8.3 Results and discussion</b>	396
<b>8.3.1 Injection time and flow rate optimization for flow injection analysis of Cy5-TNB with a sheath-flow cuvette and LIF detection</b>	396
<b>8.3.2 Comparison of calibration curves for Cy5-TNB using flow injection analysis with a sheath-flow cuvette and a comercial Beckman instrument</b>	

and a microchip system	396
<b>8.3.3</b> Displacement immunoassay of TNT using flow injection analysis with a sheath-flow cuvette, microchip, and a Beckman instrument	399
<b>8.3.4</b> Cross-reactivity studies of explosive compounds	403
<b>8.3.5</b> Comparison of electroosmotic and hydrodynamic analysis	411
<b>8.3.6</b> LOD comparison among a sheath-flow cuvette, a microchip, and a commercial Beckman instrument	411
<b>8.4</b> Conclusions	415
<b>8.5</b> References	416
<b>Chapter 9: Conclusions and future work</b>	418
<b>9.1</b> Introduction	419
<b>9.2</b> CE-LIF instrument and performance optimization	419
<b>9.3</b> Electroosmotic flow measurement and manipulation	421
<b>9.4</b> Labeling chemistry and environmental sample analysis	423

## List of tables

<b>Table 1.1:</b> Advantages and disadvantages of detection techniques in CE	45
<b>Table 2.1:</b> A comparison of surface-to-volume ratio for a 50 cm long capillary having varied ID	61
<b>Table 2.2:</b> Multiplier constants for LOD of Knoll's method	71
<b>Table 2.3:</b> The reproducibility results of a 1 s vacuum injection of $10^{-11}$ M fluorescein solution.	80
<b>Table 2.4:</b> The reproducibility results of a 5 s vacuum injection of $10^{-11}$ M fluorescein solution	81
<b>Table 2.5:</b> The results of 5 s at 1000 v electrokinetic injection of 1 pM fluorescein solution for LOD calculation	89
<b>Table 2.6:</b> LOD calculation using the data in Table 2.5	90
<b>Table 2.7:</b> Background fluctuation due to laser and room light	93
<b>Table 4.1:</b> Neutral marker and current monitoring method comparison for a series of concentration difference between run buffers	164
<b>Table 4.2:</b> t-test calculation for the highest difference between the means of neutral marker and current monitoring methods	166
<b>Table 4.3:</b> t-test calculation for the lowest difference (in %) between the means of neutral marker and current monitoring methods	168
<b>Table 5.1:</b> Migration time reproducibility of coated capillaries using single-capillary instrument with the capillaries being washed with run buffer in between runs. Sample FQ-labeled ovalbumin injected for 5 s at 1 kV. Capillary length 35 cm, voltage run	

400 V/cm, and 22 identical injections	237
<b>Table 6.1:</b> $R_f$ values for separation of the reaction components of procedure 5 (labeling reaction in acetone in the absence of tetramethylammonium hydroxide)	272
<b>Table 6.2:</b> $\lambda_{\max}$ for starting material and different collected fractions of reaction mixture of procedure 4	273
<b>Table 8.1:</b> Theoretical calculations of surface-to-volume ratio versus capillary ID	410
<b>Table 8.2:</b> LOD comparison among FIA and LIF detection with a) on-column detection using a commercial Beckman instrument, b) on-column detection on a microchip, and c) post-column detection with a sheath flow cuvette	414

## Table of Figures

<b>Figure 1.1:</b> Some of the important historical events in the development of capillary electrophoresis	9
<b>Figure 1.2:</b> Number of papers related to capillary AND electrophoresis in MEDLINE since 1985	10
<b>Figure 1.3:</b> Schematic diagram of the counter ions accumulating at silica-solution interface and change in the potential generated versus distance	14
<b>Figure 1.4:</b> Schematic diagram of a) diffusion, b) hydrodynamic, and c) electrokinetic flow profile	20
<b>Figure 1.5:</b> Schematic diagram of temperature gradients from capillary center to the surrounding	23
<b>Figure 1.6:</b> Schematic diagram of peak shapes if a) sample conductivity is more than run buffer conductivity, b) sample conductivity is less than run buffer conductivity, and c) sample conductivity is the same as run buffer conductivity	26
<b>Figure 1.7:</b> Generalized energy level diagrams showing the three basic processes of a laser involving the a) absorption, b) spontaneous emission and c) stimulated emission of radiation.	29
<b>Figure 1.8:</b> Deactivation processes for an excited molecule for a) absorption; b) vibrational relaxation; c) internal conversion; d) fluorescence; e) external conversion; f) intersystem crossing; and g) phosphorescence	31
<b>Figure 1.9:</b> Schematic diagram of a laser induced fluorescence detector	32
<b>Figure 1.10:</b> Schematic diagram of a) CE instrument with b) sheath flow cuvette	37
<b>Figure 1.11:</b> Schematic diagram of ESI mechanism	43
<b>Figure 1.12:</b> Schematic diagram of a MALDI-MS with a commercial sample probe	44

<b>Figure 1.13:</b> Range of separation techniques for particles with different sizes	47
<b>Figure 2.1:</b> Schematic diagram of a) CE instrument with b) a sheath flow cuvette and c) LIF detection	59
<b>Figure 2.2:</b> Schematic diagram of a) pressure, b) Vacuum, c) gravity, and d) electrokinetic injection techniques in CE	63
<b>Figure 2.3:</b> Plug-like injection by applying voltage or a pressure difference	69
<b>Figure 2.4:</b> Top view of a second generation CE-LIF instrument built for DRES	72
<b>Figure 2.5:</b> Schematic diagram of commercial vacuum injector before modification	76
<b>Figure 2.6:</b> Commercial vacuum injector after modification. a) A general block diagram of the sheath flow tubings with arrows showing the direction of the flow, b) The valve position before and after injection, c) The valve position during the injection time	77
<b>Figure 2.7:</b> Three seconds vacuum injection of $10^{-10}$ M fluorescein solution using commercial vacuum injector before modification	79
<b>Figure 2.8:</b> Three seconds vacuum injection of $10^{-10}$ M fluorescein solution after modification of commercial vacuum injector	83
<b>Figure 2.9:</b> Electropherograms of 5 s electrokinetic injection of $10^{-10}$ M fluorescein solution	84
<b>Figure 2.10:</b> Electropherograms showing the siphoning effect of 5 s injection at 0 kV for a) 1 pM, b) 100 pM, c) 500 pM fluorescein solution	86
<b>Figure 2.11:</b> Electropherograms of 5 s injection of 1 pM fluorescein solution at 1000 v for LOD calculation	87
<b>Figure 2.12:</b> A CE-LIF instrument with a Light Shield that operates at room light	92

<b>Figure 3.1:</b> General chemical structure of a) a nucleotide and b) sugar in DNA and RNA	102
<b>Figure 3.2:</b> Chemical structure of a) four bases found in DNA and their hydrogen bonds and b) phosphate group bond to a base	103
<b>Figure 3.3:</b> The chemical structure of a short polynucleotide	104
<b>Figure 3.4:</b> Cycle sequencing process includes a) annealing (47 °C), b) extension and termination (70 °C) and c) Denaturation (95 °C)	106
<b>Figure 3.5:</b> Effect of medium viscosity on transference number of an imaginary system of a) free solution and b) gel phase (polyacrylamide media)	108
<b>Figure 3.6:</b> A change in ionic concentration at the capillary:sample solution interface induced by change in transference numbers at a) time $t_0$ when the concentration of ions is uniform, and b) at time $t_1$ when five electrons have passed the outside circuit and the ionic composition is lower in the interface. but it has changed in the bulk of the capillary and sample solution interface	110
<b>Figure 3.7:</b> Chemical equations showing the silanized coating procedure	118
<b>Figure 3.8:</b> Chemical reactions showing free radical polymerization of acrylamide	119
<b>Figure 3.9:</b> Comparison of formamide and deionized formamide solution on signal intensity when a $4 \times 10^{-12}$ M Rox-primer solution was prepared first in a conventional formamide-EDTA solution and then in a deionized formamide resuspension solvent	122
<b>Figure 3.10:</b> Linearity of injection time and signal intensity in constant current mode	124
<b>Figure 3.11:</b> Peak width versus injection time	125
<b>Figure 3.12:</b> Peak height versus the injection number for 75 s and 150 s injections	127
<b>Figure 3.13:</b> Signal intensity versus injection number for 3, 9,	



and 20 $\mu$ L of sample	130
<b>Figure 3.14:</b> Sequencing M13mp18 ddTTP using commercial formamide:EDTA	132
<b>Figure 3.15:</b> Sequencing M13mp18 ddTTP using deionized formamide	133
<b>Figure 4.1:</b> Differential solute migration in a column under a potential gradient	140
<b>Figure 4.2:</b> Schematic representation of the double layer structure according to Stern's model	142
<b>Figure 4.3:</b> Flow profile and resulting peak shape with a) electrokinetic, and (b) pressure driven flow	143
<b>Figure 4.4:</b> Schematic diagram showing the adsorption effect on surface potential versus distance from the surface if a) polyvalent counter ions, and b) co-ions are adsorbed	148
<b>Figure 4.5:</b> Schematic apparatus used to measure EOF by Zare's group	154
<b>Figure 4.6:</b> Chemical structure of Atto-Fluor and its ionization equilibria	158
<b>Figure 4.7:</b> Current monitoring method to measure EOF of (a) an uncoated and (b) a coated capillary	160
<b>Figure 4.8:</b> EOF measurement using a) neutral marker for 5 consecutive injections of Atto-Fluor for 10 s injections and 12 kV run voltage, and b) current monitoring method for 10% concentration difference	162
<b>Figure 4.9:</b> Current Monitoring method for a) 15%, b) 40% , and c) 80% change in concentration between run buffer and replacing buffer	170
<b>Figure 4.10:</b> Comparison of RSD of a) current monitoring method for coated and uncoated capillaries, b) neutral marker method at different run buffer concentrations for an uncoated capillary	171

<b>Figure 4.11:</b> Electroosmotic Flow Mobility of coated (bottom) and uncoated (top) capillary versus % of concentration difference measured using current monitoring method	173
<b>Figure 4.12:</b> Expansion of Figure 4.11 showing the current monitoring method for EOF measurement of a) an uncoated and b) a coated capillary at different % of concentration difference	174
<b>Figure 4.13:</b> Concentration effect on EOF for a) EOF versus concentration, and b) EOF versus inverse square root of concentration	178
<b>Figure 4.14:</b> Electric field effect on a) EOF mobility b) EOF velocity	179
<b>Figure 4.15:</b> The effect of pH on EOF for an uncoated capillary (upper trace) and a coated capillary (lower trace)	181
<b>Figure 4.16:</b> Chemical formulas showing a) siloxane, b) free silanol group, c) geminal silanol group, d) vicinal or bound silanol group, and e) bound water that are present as different types of active silanol groups on fused-silica capillary wall	182
<b>Figure 4.17:</b> Temperature effect on EOF for an uncoated capillary (upper part) and a coated capillary (lower part)	183
<b>Figure 4.18:</b> Decrease in viscosity by increasing temperature and corresponding increase in EOF by increasing temperature for an uncoated capillary	186
<b>Figure 5.1:</b> Schematic diagram showing the strategy for permanent coating	192
<b>Figure 5.2:</b> Chemical formulas for Hjerten coating method	194
<b>Figure 5.3:</b> Chemical formulas and reaction steps in making a Si-C bond using Grignard method and polymerization of acrylamide as a top-layer	195
<b>Figure 5.4:</b> Chemical formulas of the monomers introduced by Righetti	196
<b>Figure 5.5:</b> Apparatus for filling capillaries. Nitrogen gas pressure was	

used to force different reagents through the capillary. The reagents were held in a disposable vial held by Reacti-vial. The fittings were used to connect the capillary to the reagents.	201
<b>Figure 5.6:</b> Ohm's plot for si-O and Si-C coated capillaries with polyAA, polyAAEE, poly AAP and polyDMA top-layers	206
<b>Figure 5.7:</b> EOF values and relative standard deviations for 1) an uncoated capillary , 2) Si-O-polyAA, 3) Si-CH <sub>2</sub> -CH=CH <sub>2</sub> 4) Si-C-polyAA, 5) Si-C-polyAAEE, 6) Si-C-polyDMA and 7) Si-C-polyAAP coated capillaries	209
<b>Figure 5.8:</b> Temperature effect on EOF of A) uncoated capillary compared with a Si-C-polyAA coated one, and B) Si-C-polyAA, Si-C-polyAAEE, Si-C-polyDMA and Si-C-polyAAP coated capillaries	210
<b>Figure 5.9:</b> pH effect on EOF for A) uncoated capillary compared with Si-C-polyAA, and B) Si-C-polyAAP, Si-C-polyDMA, Si-C-polyAAEE and Sic-polyAA comparison	212
<b>Figure 5.10:</b> Peak shape comparison of 22 successive injections onto a Si-C-polyAA coated capillary	214
<b>Figure 5.11:</b> Peak shape comparison for a Si-C-polyDMA coated capillary selected from 22 successive injection of FQ-labeled protein	215
<b>Figure 5.12:</b> Peak shape comparison of a Si-C-polyAAEE coated capillary	217
<b>Figure 5.13:</b> Peak shape comparison for a Si-C-polyAAP coated capillary	218
<b>Figure 5.14:</b> Protein adsorption onto a Si-C-polyAA coated capillary	219
<b>Figure 5.15:</b> Adsorption of proteins onto a Si-C-polyAAEE coated capillary	221
<b>Figure 5.16:</b> Protein adsorption onto a Si-C-polyAAP coated capillary	222
<b>Figure 5.17:</b> Peak width comparison among Si-C-polyAA, Si-C-polyAAEE and Si-C-polyAAP coated capillaries	223
<b>Figure 5.18:</b> The 10th run of simultaneous evaluation of coated	

capillaries using 5-capillary instrument (1 nM fluorescein injection for 5 sec at 100 V/cm, voltage run 400 V/cm and capillary length 42 cm)	225
<b>Figure 5.19:</b> Simultaneous evaluation of coated capillaries using 5-capillary instrument (conditions the same as Fig. 5.18, run number 20)	227
<b>Figure 5.20:</b> Simultaneous evaluation of five coated capillaries using 5-capillary instrument (FQ-labelled ovalbumin injection for 5 s at 100 V/cm, voltage run 400 V/cm, capillary length 42 cm, run number 1)	228
<b>Figure 5.21:</b> Comparison of Si-C-polyAAP and Si-C-polyAAEE coated capillaries using 5-capillary instrument (run number 1)	230
<b>Figure 5.22:</b> Comparison of Si-C-polyAAP and Si-C-polyAAEE coated capillaries using 5-capillary instrument (run number 20)	231
<b>Figure 5.23:</b> Peak area comparison for 22 injection onto Si-C-polyAAP and Si-C-polyAAEE coated capillaries using 5-capillary instrument	232
<b>Figure 5.24:</b> Theoretical plate comparison for a) Si-C-polyAAEE and b) Si-C-polyAAP coated capillaries using 5-capillary instrument	233
<b>Figure 5.25:</b> Migration time reproducibility comparison of Si-C-polyAAP and Si-C-polyAAEE coated capillaries using 5-capillary instrument	235
<b>Figure 5.26:</b> Long term stability of a) Si-C-polyAAP, and b) Si-C-polyAA coated capillaries	238
<b>Figure 5.27:</b> EOF regeneration of a Si-C-polyAA and a Si-C-polyAAP coated capillary	240
<b>Figure 5.28:</b> Separation of alkaline protein markers using a) Si-C-polyAAP and b) Si-C-polyAA coated capillaries	241
<b>Figure 6.1:</b> Chemical structure of microcystin-LR	250
<b>Figure 6.2:</b> Excitation/emission spectra of 5-BrMF as a fluorescent labeling reagent for carboxylic acid derivatization	253

<b>Figure 6.3:</b> The chemical equation showing the labeling of penicillin-G with a fluorescent tag 5-BrMF	256
<b>Figure 6.4:</b> Penicillin-G labeling reaction with 5-BrMF in aqueous potassium carbonate solution (procedure 1)	263
<b>Figure 6.5:</b> Labeling reaction in MeOH solution (procedure 2)	264
<b>Figure 6.6:</b> Possible side reactions for penicillin-G labeling with 5-BrMF in aqueous KOH solution	266
<b>Figure 6.7:</b> ESI/MS for the product of procedure 3	267
<b>Figure 6.8:</b> Dianion, monoanion, neutral, cationic and lactone form of fluorescein	268
<b>Figure 6.9:</b> ESI/MS spectrum of the labeling reaction in acetone solvent in the presence of an organic base	269
<b>Figure 6.10:</b> Labeling reaction in acetone (procedure 5)	274
<b>Figure 6.11:</b> ESI/MS spectra of reaction in acetone in the absence of tetraethyl ammonium hydroxide organic base after passing the reaction mixture from a silica gel column	275
<b>Figure 6.12:</b> ESI/MS spectra of reaction in acetone in the absence of an organic base. From top to bottom a) blank 5-BrMF, b) blank penicillin-G, c) 5-BrMF without heating, d) penicillin-G without heating, e) mixture of 5-BrMF and penicillin-G without heating	277
<b>Figure 6.13:</b> Negative ion mode ESI/MS of labeling reaction in acetone in the absence of an organic base. The reaction mixture is passed through a column and a) fraction 20, b) fraction 15, c) fraction 10, and e) fraction 5 are collected from the silica gel column	278
<b>Figure 6.14:</b> Negative ion mode ESI/MS of reaction in acetone in the absence of an organic base. a) blank reaction of 5-BrMF, b) 5-BrMF without heating, c) blank reaction of penicillin-G	

and d) mixture of 5-BrMF and penicillin-G without heating	279
<b>Figure 6.15:</b> Electropherograms of labeling reaction products in DMF solvent	281
<b>Figure 6.16:</b> HPLC separation of the labeling reaction component	282
<b>Figure 6.17:</b> Positive ion ESI/MS spectra of the labeling reaction in DMF (procedure 6) before HPLC separation (preparation TLC purification)	283
<b>Figure 6.18:</b> Hydrogen and potassium adducts of the labeling reaction in DMF. The top spectra are the expansion of the experimental positive ESI/MS spectra and the bottom ones are theoretical molecular weight calculations and corresponding isotope patterns of the molecular weights with relative abundances for the isotopes	284
<b>Figure 6.19:</b> Positive ion ESI/MS spectrum of the HPLC-purified product of labeling reaction in DMF (procedure 6). The potassium adduct of the 18-crown-6 is separated and the potassium adduct of the labeled penicillin-G is the major ion	286
<b>Figure 6.20:</b> Positive ion mode ESI/MS of the labeling reaction in DMF with no 18-crown6 present (procedure 7)	287
<b>Figure 6.21:</b> Positive ion mode (top) and negative ion mode ESI/MS of the labeling reaction in DMF with no 18-crown-6 present (Procedure 7)	288
<b>Figure 6.22:</b> 600 MHz NMR <sup>1</sup> H NMR spectrum of labeled penicillin-G	289
<b>Figure 6.23:</b> Calibration curve of labeled penicillin-G	290
<b>Figure 6.24:</b> Immunoassay reaction of labeled penicillin-G with anti penicillin-G	292
<b>Figure 7.1:</b> Four different feasible strategies to deprotonate Na-acetyl-L-arginine	305
<b>Figure 7.2:</b> Arginine deprotonation and labeling reaction electropherogram	320
<b>Figure 7.3:</b> Direct arginine labeling reaction at high pH with TMR	321

<b>Figure 7.4:</b> ESI-MS spectra of a) reaction mixture of TMR with arginine at high pH and b) blank MeOH / HOAc 9 / 1	322
<b>Figure 7.5:</b> Schematic representation of arginine-to-ornithine conversion reaction and purification processes of a) before running the TLC, b) after running the TLC, c) removal of the desired spot for further purification, d) extraction of the product from silica gel, and e) Sep-Pak separation and purification of the product	324
<b>Figure 7.6:</b> ESI-MS spectra of the arginine-to-ornithine conversion reaction of a) blank reaction of arginine in the absence of hydrazine for 1 h heating, b) 1h, c) 5 h, and d) 64 h heating of arginine in the presence of hydrazine	326
<b>Figure 7.7:</b> TMR labeling reaction formula of ornithine by hydrazinolysis of N-acetyl-L-arginine	327
<b>Figure 7.8:</b> ESI-MS spectra of the hydrazinolysis reaction of N-acetyl-L-arginine, a) before labeling reaction with TMR, and b) after labeling reaction with TMR	328
<b>Figure 7.9:</b> ESI-MS spectra of hydroxylamine reaction with N-acetyl-L-arginine a) before and b) after TMR labeling reaction	330
<b>Figure 7.10:</b> Chemical equations of NaH deprotonation of N-acetyl-L-arginine and TMR labeling of the product	331
<b>Figure 7.11:</b> ESI-MS spectra of NaH reaction with N-acetyl-L-arginine a) before and b) after labeling reaction with TMR	332
<b>Figure 7.12:</b> MALDI-MS spectra of a) dihydroxy benzoic acid (DHB) used as a matrix, b) N-acetylarginine used as a sample and c) 5-TMR used as a labeling reagent	334
<b>Figure 7.13:</b> MALDI analysis of hydrazine reaction mixture passed through AG50W and AGMP-50 cation-exchange resin and washed	

with a) MeOH, b) 2M NaCl, c) TMR labeling reaction on a and	
d) TMR labeling reaction on b	335
<b>Figure 7.14:</b> MALDI analysis of hydrazine reaction mixture labeled with TMR and separated by C18 Sep-Pak cartridge. a) first fraction washed with 5 mL of water, b) fourth fraction washed with 5 mL of water and c) first fraction washed with 5 mL of MeOH	337
<b>Figure 7.15:</b> MALDI analysis of sodium hydride reaction mixture labeled with TMR and separated by C <sub>18</sub> Sep-Pak cartridge, a) first fraction washed with 5ml of water and b) first fraction washed with 5 mL of MeOH	338
<b>Figure 7.16:</b> Chemical reaction of cyclo (Arg-Gly-Asp-Phe-Val) by hydrazine and TMR labeling of the product	340
<b>Figure 7.17:</b> NaH reaction with arginine containing cyclic peptide and TMR labeling of the resulting product	341
<b>Figure 7.18:</b> TLC of a) TMR, b) hydrazinolysis reaction product of cyclo (Arg-Gly-Asp-Phe-Val), and c) NaH reaction product of cyclic peptide	342
<b>Figure 7.19:</b> MALDI-MS spectra of a) DHB matrix, b) cyclic peptide, c) expansion of b, and d) TMR in DMF	343
<b>Figure 7.20:</b> MALDI-MS spectra of the hydrazine reaction products of cyclic peptide a) before labeling reaction and before separation, b) after labeling reaction but before separation, c) after labeling reaction and the first water washed out of the Sep-Pak cartridge, d) after labeling reaction and first MeOH washed out of Sep-Pak cartridge, e) after labeling reaction and 5th MeOH wash, f) 10th MeOH wash and g) 15th MeOH wash out of the Sep-Pak cartridge	344
<b>Figure 7.21:</b> MALDI-MS spectra for NaH reaction with cyclic peptide followed by TMR labeling of the product, a) cyclic peptide reaction with NaH before labeling, b) after labeling but before separation,	



c) Sep-Pak separation of first MeOH washed fraction, d) second MeOH washed, e) third MeOH washed and f) expansion of e	346
<b>Figure 7.22:</b> MALDI-MS spectra of blank reaction of TMR dissolved in DMF and separated by preparative TLC, a) DHB matrix, b) band 1 recovered from TLC, and c) band 2 recovered from TLC	347
<b>Figure 7.23:</b> MALDI-MS spectra of the hydrazinolysis reaction of cyclic peptide followed by TMR labeling of the products. The labeled product is separated by preparative TLC and spectra a - g show fractions 1 to 7, respectively	348
<b>Figure 7.24:</b> Chemical equations for the synthesis of an arginine-specific reagent using furfurylamine followed by ozonolysis of the product	350
<b>Figure 7.25:</b> Chemical equations for the synthesis of an arginine-specific reagent using aminoacetophenone followed by ozonolysis of the product	351
<b>Figure 7.26:</b> MALDI-MS spectra of a) furfurylamine condensation reaction with 5 BrMF and b) ozonolysis of the furfurylamine condensation product	352
<b>Figure 7.27:</b> MALDI-MS spectra of a) 4-aminoacetophenone condensation reaction with 5-BrMF and b) SeO <sub>2</sub> oxidation of the resulting product from condensation	353
<b>Figure 7.28:</b> Chemical equations showing 2, 3 butanedione coupling to benzylbromide and dimerization of diketone	355
<b>Figure 7.29:</b> MALDI-MS spectra of a) 2, 3, butane dione, b) benzylbromide and c) 2, 3, butane dione condensation reaction with benzylbromide	356
<b>Figure 7.30:</b> Chemical equations showing 2, 3 butanedione trimerization and its reaction with 5-BrMF to synthesize an arginine-specific labeling reagent	357
<b>Figure 7.31:</b> MALDI-MS spectra of 2, 3, butane dione reaction with	

5-BrMF for the synthesis of an arginine-specific fluorescent reagent	358
<b>Figure 7.32:</b> Chemical equations of arginine labeling with the diketone derivative of fluorescein	360
<b>Figure 7.33:</b> MALDI-MS spectra of a) N-acetyl-L-arginine, b) arginine-labeling reaction with 5(2, 3 butanedione) methyl fluorescein in the absence of borate and c) arginine-labeling reaction with 5(2, 3 butane-dione) methyl fluorescein in the presence of borate	361
<b>Figure 7.34:</b> Chemical equations of microcystin-LR labeling reaction with TMR using NaH to deprotonate arginine group	363
<b>Figure 7.35:</b> Schematic diagram of the apparatus for performing labeling reaction of microcystin	364
<b>Figure 7.36:</b> MALDI-MS spectra of microcystine-LR labeled with TMR, a) positive-ion mode spectrum of microcystine, b) negative-ion mode of TMR, and c) negative-ion mode MALDI-MS spectrum of the labeled microcystin with TMR	365
<b>Figure 7.37:</b> MALDI-MS spectra of gel chromatography separation of labeled microcystin with TMR for a) first fraction (positive polarity), b) expansion of a, c) 2nd fraction (negative polarity), and d) 50th fraction (negative polarity)	367
<b>Figure 7.38:</b> MALDI-MS spectra of Sep-Pak separation of labeled microcystin with TMR for collected fractions of a) first, b) 5th, c) 10th, d) 15th, e) 20th MeOH washed fraction, and f) no Sep-Pak separation	368
<b>Figure 7.39:</b> Microcystin-LR labeling reaction with 5-BrMF using NaH to deprotonate arginine group	370
<b>Figure 7.40:</b> Negative-ion mode ESIMS spectrum of microcystine-LR labeled with TMR	371
<b>Figure 7.41:</b> Reproducibility of CE experiment for labeled antigen	

(labeled microcystin)	373
<b>Figure 7.42:</b> Titration of labeled microcystin by adding 0, 2, 4, 6, 8, and 10 $\mu\text{L}$ of anti-microcystin antibody	374
<b>Figure 7.43:</b> Calibration curve for the addition of anti-microcystin antibody to labeled microcystine	375
<b>Figure 8.1:</b> Schematic diagram of displacement immunoassay	384
<b>Figure 8.2:</b> Chemical equations of the antibody immobilization on the capillary wall	388
<b>Figure 8.3:</b> Schematic diagram of the displacement immunoassay flow injection analysis with a sheath-flow cuvette and LIF detection	391
<b>Figure 8.4:</b> a) Schematic of the optical detection system for flow injection analysis of TNT with LIF detection using a microfabricated chip, and b) The top view of the channels integrated on a planar glass substrate used as a microchip	392
<b>Figure 8.5:</b> The effect of injection time on peak area for displacement immunoassay flow injection analysis of TNT with a sheath-flow cuvette and LIF detection	397
<b>Figure 8.6:</b> The effect of the flow rate on retention time in displacement flow injection analysis of TNT using a sheath-flow cuvette with LIF detection	398
<b>Figure 8.7:</b> Calibration curve for Cy5-TNB using flow injection analysis with a sheath-flow cuvette and LIF detection	400
<b>Figure 8.8:</b> Calibration curve for Cy5-TNB using flow injection analysis with on-column LIF detection. The Beckman instrument has been used for this experiment with 20 s injection at 0.5 psi and 20 psi for separation	401

<b>Figure 8.9:</b> a) Peak shape for flow injection analysis of Cy5-TNB on a microchip with on-column LIF detection, and b) Calibration curve for Cy5-TNB using the peak areas of part a	402
<b>Figure 8.10:</b> TNT analysis using Cy5-TNB displacement immunoassay and a sheath-flow cuvette with LIF detection	404
<b>Figure 8.11:</b> a) Peak shape for TNT analysis using microchip with flow injection analysis and on-channel LIF detection, and b) Calibration curve for TNT using the peak areas from Fig. 11a	405
<b>Figure 8.12:</b> a) Peak shape for TNT flow injection analysis with on-column LIF detection, and b) Calibration curve for TNT with 20 s injection at 0.5 psi	406
<b>Figure 8.13:</b> Chemical formulas for different explosives used for cross-reactivity studies	407
<b>Figure 8.14:</b> Cross-reactivity of explosive compounds as compared to TNT using Flow Injection Analysis with a sheath-flow cuvette and LIF detection	408
<b>Figure 8.15:</b> Cross-reactivity of explosive compounds compared to TNT using flow injection analysis with LIF detection on a microchip channel with 1 mL injection of the explosives each at 500 ng/mL concentration	412
<b>Figure 8.16:</b> Displacement immunoassay of TNT using a sheath-flow cuvette and LIF detection with a) Hydrodynamic injection, and b) Electrokinetic injection of TNT. Capillary length is 20 cm and 400 V/cm voltage was applied to transfer the TNT to the detection end using EOF	413

### List of Abbreviations and Symbols Used:

1, 3, 5-trinitrobenzene	TNB
2, 4, 6-trinitrotoluene	TNT
2, 4-dinitrotoluene	DNT
2-nitrotoluene	NT
3-amino-9-methoxy-2, 6, 8-trimethyl-10-phenyldeca-4,6-dienoic acid	Adda
3-mercaptopropyltrimethoxysilane	MTS
3-methacryloxypropyltrimethoxysilane	silane
4-amino-2, 6-dinitrotoluene	ADNT
5-bromomethyl fluorescein	5-BrMF
5-furoyl quinoline-3-carboxaldehyde	FQ
A calculated result	Z
A constant that is determined for the time period that is a multiple analyte's peak width at half maximum	$K_{LOD}$
Absolute errors for measured quantities of A, B, C,...	$\Delta Z, \Delta A, \Delta B, \Delta C, \dots$
Acetic acid	HOAc
Acetonitrile	AcN
Acrylamide	AA
Acryloylaminopropanol	AAP
Altered ionic concentration	$C_a$
Amonium fluoride	$NH_4F$
Amount of analyte injected onto the capillary	$C_s$
An antigen-antibody complex that antibody is fluorescently labeled	Ab*.Ag
An antigen-antibody complex that antigen is fluorescently labeled	Ab.Ag*
Analysis time	t

Analyte peak height	$h_s$
Antibody	Ab
Antigen	Ag
Apparent mobility	$\mu_{app}$
Argon	Ar
Atomic mass unit	amu
Attomole ( $10^{-18}$ moles)	amole
Average linear velocity of the liquid through the capillary	$U^*$
Average linear velocity	$v_{eof}$
Average mobilities	$\mu_{ave}$
Avogadro's constant	$N_A$
Capillary electrophoresis with Laser Induced Fluorescence detection	CE-LIF
Capillary electrophoresis	CE
Capillary gel electrophoresis	CGE
Capillary length	L
Change of concentration in time	$(\partial C/\partial t)_x$
Change of transference number with concentration	$(dT/dC)$
Charge on ion i	$N_{i \text{ ion}}$
Collision-induced dissociation	CID
Column cross-section	A
Concentration limit of detection	$C_{LOD}$
Concentration of each ionic species in bulk electrolyte	$n_0$
Concentration of the analyte in Columb / mL	$C_{ep}$
Concentration of the analyte	C
Conductivity of the migrating analyte	$\kappa_{ep}$

Conductivity of the run buffer	$\kappa$
Conductivity of the surrounding run buffer	$\kappa_{AB}$
Corrected injection volume	$V_{inj}$
Coulomb	C
Current	i
Current monitoring method for EOF measurement	CM
Current	I
Cy5-trinitrobenzene	Cy5-TNB
Cyclo (Arg-Gly-Asp-D-Phe-Val)	Cyclic peptide
Defense Research and Establishment at Suffield	DRES
Degrees of centgrade	$^{\circ}\text{C}$
Degrees of freedom	n
Density of the liquid inside the capillary	$\rho$
Deoxy nucleic acid	DNA
Diazomethyl derivative is 9-anthryldiazomethane	ADAM
Dielectric constant	$\epsilon$
Difference in conductivity	$\Delta\kappa$
Diffusion coefficient of the components	D
Dihydroxybenzoic acid	DHB
Dimethylacrylamide	DMA
Dimethylformamide	DMF
Displacement efficiency	$D_e$
Distance from the injection end of the capillary	x
Efficiency of the detector as a function of the fluorescence wavelength	

incident on it	$g(\lambda)$
Electric field strength	$E$
Electrokinetic injection time	$t_{inj}$
Electrokinetic injection voltage	$E_{inj}$
Electronic charge	$e$
Electroosmotic flow	EOF
Electroosmotic mobility due to EOF	$\mu_{eof}$
Electrophoretic mobility	$\mu_e$
Electrospray ionization mass spectrometer	ESI-MS
Electrospray Ionization	ESI
Enzyme Linked ImmunoSorbant Assay	ELISA
Equivalent ion conductivities for cations and anions	$\lambda_+$ and $\lambda_-$
Ethanol	EtOH
Flow Injection Analysis	FIA
Fluorescently labeled antibody	Ab*
Fluorescently labeled antigen	Ag*
Free-solution mobility of ion i	$\mu_{i \text{ ion}}$
Frictional coefficient	$f$
Geometrical factor that is determined by the solid angle of the radiation subtended by the detector (fluorescence is emitted in all directions but is viewed only through a limited aperture)	$f(\theta)$
Gravity constant	$g$
Height difference between the two ends of the capillary	$\Delta h$
Helium-Cadmium	He-Cd



Helium-Neon	He-Ne
Hexahydro 1, 3, 5 trinitrotriazine	RDX
High performance capillary electrophoresis	HPCE
High performance liquid chromatographic	HPLC
High voltage applied for capillary electrophoresis	$E_{CE}$
Hour	h
Hydrogen fluoride	HF
Hydroxyl group	OH
Initial ionic concentration	C
Initial light intensity	$I_0$
Initial plate height	B
Injection number	n
Internal diameter	ID
Ion spray voltage	IS
Isoelectric focusing	IEF
Kilogram	Kg
Krypton fluoride	KrF
Laser excitation wavelength	$\lambda$
Laser Induced Fluorescence	LIF
Laser-induced fluorescence polarization	LIFP
Length of the cell containing the analyte	b
Length of the sample plug injected onto the capillary	$l_{inj}$
Light Amplification by Stimulated Emission of Radiation	Laser
Light frequency	$\nu$
Light intensity after passing through the solution	I
Limit of Detection	LOD

Mass spectrometry	MS
Mass-to-charge ratio	m / z
Matrix Assisted Laser Desorption Ionization Mass Spectrometry	MALDI-MS
Matrix Assisted Laser Desorption Ionization	MALDI
Maximum noise fluctuation in the background signal	$h_n$
Measured quantities	A, B, C, ...
Meter	m
Micellar electrokinetic chromatography	MEKC
Micro molar concentration ( $10^{-6}$ M)	$\mu\text{M}$
Microliter ( $10^{-6}$ L)	$\mu\text{L}$
Micrometer ( $10^{-6}$ m)	$\mu\text{m}$
Migration time of the component	$t_{\text{mig}}$
Migration time	t
Milli Watt ( $10^{-3}$ Watt)	mW
Millimeter	mm
Mobility of an anion	$\mu_-$
Mobility of the analyte	$\mu_{\text{ep}}$
Mobility of the buffer	$\mu_A$
Mobility of the counter ion	$\mu_B$
Mobility of a cation	$\mu_+$
Molar absorptivity of the analyte	a
N,N,N',N'-tetramethylethylenediamine	TEMED
N-acryloylaminoethoxyethanol	AAEE

Nanoliter ( $10^{-9}$ L)	nL
Nanometer ( $10^{-9}$ m)	nm
Net volume charge density at points where the potential is $\psi$	$\rho$
Neutral marker method for EOF measurement	NM
Nitrobenzene	NB
N-methyl-dehydroalanine	Mdha
N-succinimidyl-4-maleimidobutyrates	GMBS
Nuclear magnetic resonance	NMR
Number of charges on the particle	Z
Number of injections to decrease the peak height to 1/e of its initial value	$n_c$
Number of moles injected onto the capillary	$n_{inj}$
Octahydro 1, 3, 5, 7 tetranitro 1, 3, 5, 7-tetrazocine	HMX
Orifice voltage	OR
Outer diameter	OD
Outer Helmholtz Plane	OHP
Ozone gas	$O_3$
Particle radius	r
Peak width at half the peak height of the analyte	$w_{1/2}$
Photomultiplier tube	PMT
Plank's constant	h
Plate number	N
Polyacrylamide gel electrophoresis	PAGE
Potassium cyanide	KCN
Pressure drop because of the height difference between sample vial and sheath flow levels	$\Delta P$

Radius of the capillary	$r_{\text{cap}}$
Radius of the capillary	R
Relative standard deviation	RSD
Residual offset	A
Resistance x Capacitance	RC
Resistance	R
Resistivities of buffer 1 and buffer 2	$\rho_1$ and $\rho_2$
Resolution	$R_s$
Retarded transference number	$T_r$
Retarding factor of an anion	$R_-$
Retarding factor of a cation	$R_+$
Ring voltage	RNG
Second order nucleophilic substitution reaction	$SN^2$
Second	s
Selenium dioxide	$SeO_2$
Silanol group	SiOH
Silicon-Carbon bond	Si-C
Silicon-Oxygen bond	Si-O
Sodium azide	$NaN_3$
Sodium chloride	NaCl
Sodium dodecyl sulfate	SDS
Sodium dodecyl sulfate- Polyacrylamide gel electrophoresis	SDS-PAGE
Sodium hydride	NaH
Sodium hydroxide	NaOH
Spin quantum number of the electron	s
Square centimeters	$cm^2$

Square millimeter	$\text{mm}^2$
Standard deviation in the background signal when the laser is off	$\sigma_{\text{laser off}}$
Standard deviation in the background signal when the laser is on	$\sigma_{\text{laser on}}$
Standard deviation of the blank signal	$\sigma$
Standard deviation of the pooled data	$\text{Std.Dev.}_{\text{pooled}}$
Tetrahydrofurane	THF
Tetramethylrhodamine succinimidyl ester	TMR
The electric potential at the capillary surface at a distance x from the surface in the electrolyte solution	$\psi$
The electric potential at the capillary surface	$\psi_0$
The electric potential energy for anions	$-Z e \psi$
The electric potential energy for cations	$+Z e \psi$
The Faraday constant	F
The numbers of negative ions per unit volume at points where the potentials are $\psi$	$n_-$
The numbers of positive ions per unit volume at points where the potentials are $\psi$	$n_+$
Thickness of the diffuse layer	$l / \kappa$
Thin layer chromatography	TLC
Total ion chromatogram	TIC
Total standard deviation in the background signal when the laser is on	$\sigma_{\text{total}}$
Total variance in the background signal	$\sigma_{\text{total}}^2$

Total variance	$\sigma_{\text{tot}}^2$
Transference number at infinite dilution	$T^0$
Transference number of a cation	$T_+$
Transference number of an anion	$T_-$
Transference number of an ion	$T_i$
TRIS, borate and EDTA buffer	TBE
Ultra violet light	UV
UV / Vis maximum absorption wavelength	$\lambda_{\text{max}}$
Variance in the background signal when the laser is off	$\sigma_{\text{laser off}}^2$
Variance in the background signal when the laser is on	$\sigma_{\text{laser on}}^2$
Variances due to adsorption	$\sigma_{\text{ads}}^2$
Variances due to all the other parameters	$\sigma_{\text{other}}^2$
Variances due to diffusion	$\sigma_{\text{diff}}^2$
Variances due to hydrodynamic flow	$\sigma_{\text{hf}}^2$
Variances due to injection	$\sigma_{\text{inj}}^2$
Variances due to conductivity difference between the solute zone and the sample zone	$\sigma_{\Delta K}^2$
Variances due to Joule heating	$\sigma_{\text{Jh}}^2$
Velocity	$v$
Viscosity of the medium	$\eta$
Voltage	$V$
Volume of the capillary	$V_{\text{Cap}}$

Widths of the peaks at base line	w
Zeptomole ( $10^{-21}$ moles)	Zmole
Zeta potential of the charged particle	$\xi$
Zone electrophoresis	ZE

# *Volume 1*



# **Part I**

## **Capillary electrophoresis, laser induced fluorescence detection, sample introduction, and sample depletion**

# **Chapter 1**

## **Introduction and theory**

## 1.1 Historical background and development of electrophoresis

Electrophoresis is the differential migration of electrically charged species by attraction or repulsion in an electric field. In 1809, Reuss observed that clay particles in an aqueous dispersion migrate when an electric field is applied.<sup>1</sup> In the 19<sup>th</sup> century, a number of scientists described practical methods of electrophoresis.<sup>2</sup> At the end of 19<sup>th</sup> century, Kohlrausch developed a theory of ionic migration that could be used to describe different electrophoretic phenomena.<sup>3</sup> Kohlrausch's work was a basic theoretical foundation for electrophoresis.

In the beginning of the 20<sup>th</sup> century, electrophoresis found its way to applications in analytical chemistry. Since the middle of 20<sup>th</sup> century slab gel electrophoresis has been used to separate a wide range of biological molecules including peptides, proteins and polynucleotides. Electrophoretic experiments can be performed in different formats and in different media, such as filter paper, cellulose acetate, starch, agarose and polyacrylamide.<sup>4</sup>

In 1909, Michaelis discovered that proteins separate based on their isoelectric points and he was the first one who used the term "electrophoresis". In the 1930s, Tiselius' pioneering experiments introduced moving boundary electrophoresis as a separation technique.<sup>5</sup> In moving boundary electrophoresis, the sample is continuously fed and the leading edges of the sample components are resolved. In this method all the sample components of the mixture overlap except the fastest component. In zone electrophoresis (ZE), however, the sample is applied as a plug; after applying high voltage the sample components are resolved into discrete zones by electrophoresis. As an analytical technique or as a preparative method, ZE is superior to moving boundary electrophoresis because ZE separates the sample components into spatially resolved zones. Sample components in ZE could be individually detected or even collected. Tiselius filled a tube with serum proteins and applied an electric field across the tube (moving boundary electrophoresis). By using this technique, he found that sample components migrated in a direction and at a rate

determined by their charge and their mobility. For his work in separation science, Tiselius was awarded a Nobel prize in 1948.

In the 1950s and 1960s, research continued on the development of moving boundary electrophoresis, zone electrophoresis, and isotachopheresis. Thermal diffusion and convection limited separation efficiency in free solution. Because of thermal diffusion and convection problems most of the efforts were directed toward the improvement of anti-convective media for ZE. Traditionally, anti-convective media, such as polyacrylamide, starch or agarose gels has been used in electrophoresis. Gel-filled tubes and slab gel electrophoresis have been primarily used for the size-dependent separation of biological macromolecules, such as nucleic acids and proteins. Despite being one of the most frequently used separation techniques, slab gel electrophoresis generally suffers from long analysis times, low efficiencies, and difficulties in detection and automation. Since the 1960s, polyacrylamide gels have been optimized for high resolution separations of native proteins and sodium dodecyl sulfate (SDS)-complexed proteins.<sup>6</sup> Polyacrylamide gel electrophoresis (PAGE) and SDS-PAGE have proven to be relatively rapid and inexpensive techniques for the characterization of protein mixtures, determination of protein molecular weights, and resolution of oligonucleotides. Today, PAGE and SDS-PAGE are found in almost every biochemistry laboratory.<sup>7</sup>

In the late 1960s, with combination of Isoelectric Focusing (IEF) and SDS-PAGE, two-dimensional gel electrophoresis was developed.<sup>8</sup> Two-dimensional PAGE is clearly superior in high resolution techniques. It is possible to separate over 1000 components from cellular homogenates using two-dimensional gel electrophoresis.

In parallel with developing electrophoresis techniques for larger molecules, chemists in the pharmaceutical industry were developing high performance liquid chromatographic (HPLC) techniques for the analysis of smaller molecules. HPLC proved to be ideal for industrial and clinical laboratories in terms of speed, resolution, quantitation,

and automation. The emergence of biotechnology and the need for quality control of the new products from gene cloning and protein expression led to the realization that neither electrophoresis nor HPLC were adequate for this need. Electrophoresis could not satisfy the demands of quantitative analysis, preparative isolation, due to poor resolution and recoveries with large molecules, particularly structural proteins.

In parallel with the development of gel electrophoresis, Hjerten in Uppsala University of Sweden continued working on moving boundary electrophoresis. He improved the technique by reducing the cross-sectional area of the U-tube, by eliminating electroosmosis, and by introducing a UV-scanning method to obtain high resolution and sensitivity.<sup>9</sup> But his approach was still limited by the inherent weaknesses of the moving boundary method, which are incomplete separation of the sample proteins and relatively large volume of the sample required. Therefore, Hjerten developed a new kind of electrophoresis apparatus where the components of a sample in a mixture could be resolved into distinct zones. This method was so-called free zone electrophoresis.<sup>9</sup> This technique allowed the zones to be withdrawn for preparative purposes. He used a quartz tube with an internal diameter (ID) of 1 to 3 mm and outer diameter (OD) of 7.8 mm. The tube was immersed in a cooling bath and was rotated around its horizontal axis in order to reduce convective mixing. To prevent solute adsorption and to reduce electroosmotic flow (EOF), the internal surface of the tube was coated with methylcellulose. A UV-scanning detector was employed for continuous monitoring of the separating components. By the use of these relatively smaller ID tubes in combination with efficient cooling, higher field strengths could be applied, and thus, resulted in an increase in separation efficiency. Hjerten's apparatus laid the foundation for high performance capillary electrophoresis (HPCE). He pointed out in his thesis that if a sufficiently small ID tube in combination with a thin wall, to dissipate the heat effectively, was employed even higher field strength could be used. In this case the rotation of the tube or the introduction of a stabilizing medium,

polyacrylamide gel, would not be needed.<sup>9</sup> However, it was not possible to test these ideas at that time because the technology required was not available, especially sensitive absorbance detectors.

In parallel with the growth of the biotechnology industry, there was increasing concern about the toxic compounds being introduced into the environment. Closer inspection and more restrictive regulations regarding environmental concerns resulted in increased cost for waste disposal. HPLC in the laboratories generated organic solvent waste that was a major problem to operating costs, and of concern for future disposal problems.

Because of this historical background there was increasing demands for high resolution, quantitative precision of biopharmaceuticals, and control of waste management costs. The necessity of having an analytical technique that produces less organic solvent waste and better resolution led to the arrival of capillary electrophoresis (CE) on the analytical chemistry scene. An alternative to the slab-gel format was to perform the electrophoretic separation in smaller ID tubes or capillaries as was pointed out by Hjerten.<sup>9</sup> Since small ID capillaries are themselves anticonvective, gel media were not essential to perform the analysis. This allowed the performance of free-solution electrophoresis, as well as the use of traditional gel media in the capillary.

The pioneering work of Hjerten was the foundation for the CE analysis of many kinds of analytes, ranging from small molecules (inorganic ions, nucleotides) to macromolecular structures, such as proteins and even viruses. Virtanen performed electrophoresis in approximately 200- $\mu\text{m}$  internal diameter (ID) Teflon capillaries and Mikkers repeated electrophoresis in glass-made capillaries.<sup>7, 10</sup> Jorgenson and Lukacs improved the technique by using 75- $\mu\text{m}$  ID fused-silica capillaries in the early 1980s.<sup>11</sup> Jorgenson also described the theory of CE by clarification of the relationships between

operational parameters and separation quality. He also demonstrated the potential of HPCE (high performance capillary electrophoresis) as an analytical technique. Since the 1980s, numerous reviews and a few books have been written describing various aspects of CE.<sup>12</sup> CE demonstrated the potential for high resolution separation of biopolymers, as well as smaller pharmaceutical molecules. This technique used very small amounts of both sample and reagents as compared to HPLC. The reappearance of CE after a twelve-year dormancy since Hjerten's work resulted from a combination of improvements in the sensitivity of detectors, advances in automation technology, and, most particularly, the wide-spread availability of high-quality smaller ID fused-silica capillaries.<sup>7</sup>

Within a few years after emergence of CE in the scientific world, research groups throughout the world had expanded the horizons of the applications of CE. Terabe pioneered micellar electrokinetic chromatography (MEKC).<sup>13-15</sup> Using micellar solutions, he demonstrated the possibility to separate neutral and charged species.

In summary, the following diagram (Figure 1.1) shows some key steps in the development of capillary electrophoresis techniques.

Interest in CE has increased exponentially over the past decade, and its incorporation into the modern analytical laboratory has begun. One indicator of this growth is the exponential growth of the number of research articles, with "capillary" AND (a logic operator) "electrophoresis" collected by Medline each year since 1985. Figure 1.2 shows the number of papers related to capillary electrophoresis published and collected in Medline in each year since 1985.

## **1.2 Basic principles of CE**

Electrophoresis is a technique frequently used in bioanalytical chemistry, molecular biology, biochemistry and medicine. It is applied to the separation and characterization of

**Figure 1.1: Some of the important historical events in the development of capillary electrophoresis. The time axis is not to scale**

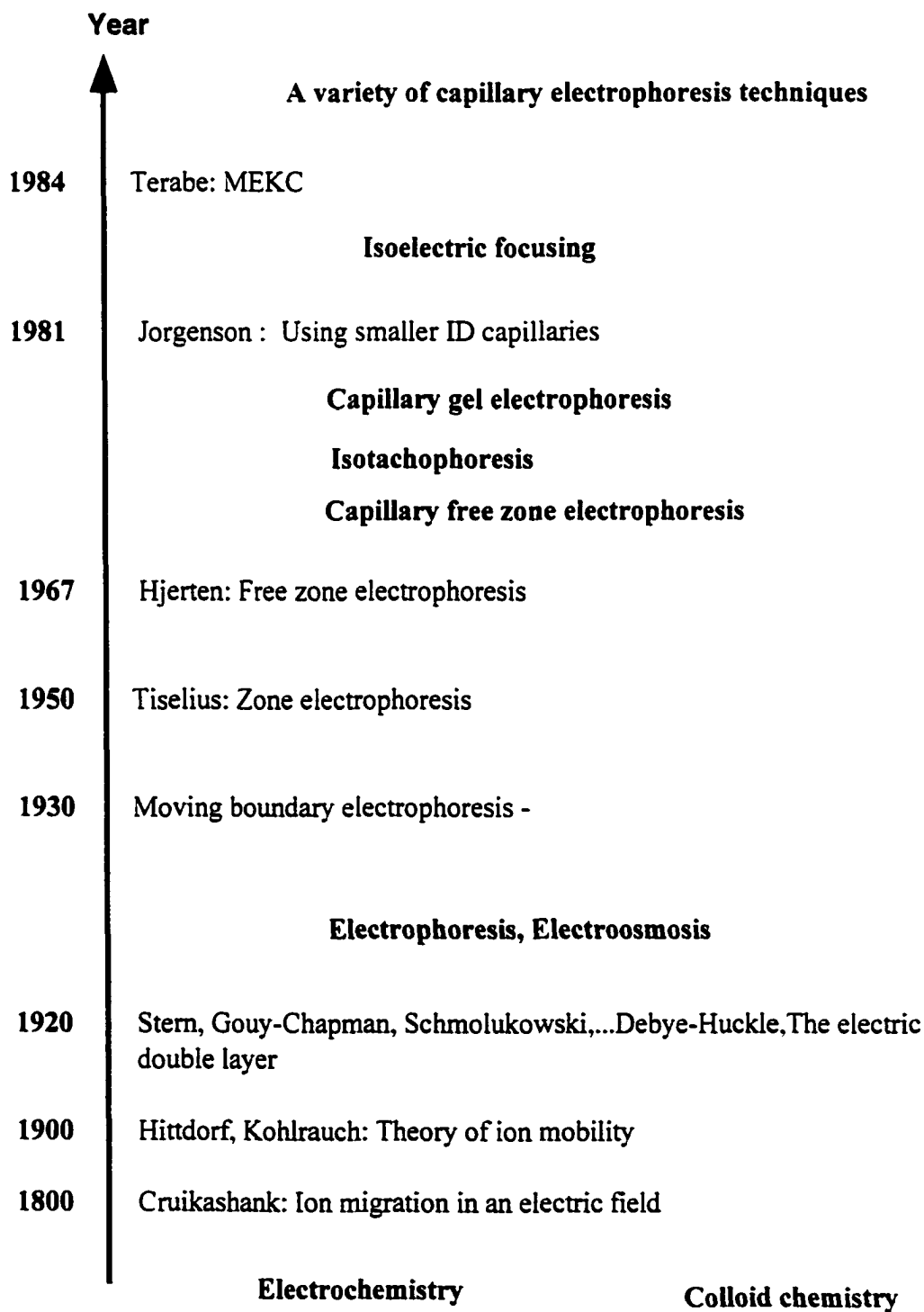
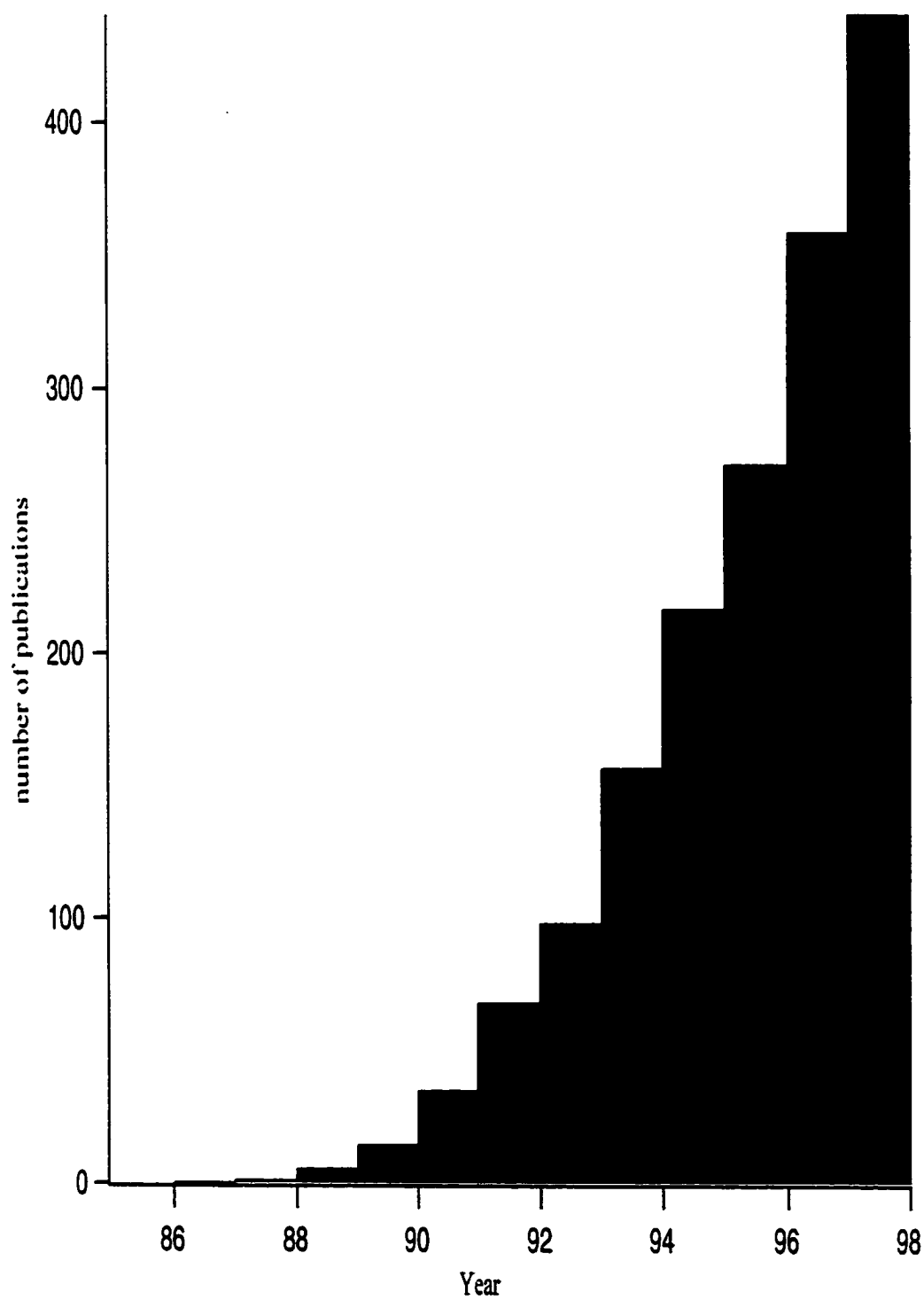




**Figure 1.2: Number of papers related to capillary AND electrophoresis in MEDLINE since 1985. AND is a logic term.**



many different kinds of molecules like anions, cations, and neutral molecules. It is also used for separation of biologically important molecules like proteins, nucleic acids and subcellular-sized particles like viruses and small organelles. Its principle is that the electric field is applied to a solution containing charged particles. This electric field will cause the migration of charged particles of the sample and separation according to the surface charge density of these charged particles. If the electric field is applied on a gel matrix, the separation is based on both charge and size of the particles.

### 1.2.1 Some definitions and fundamental equations of CE

The electrophoretic mobility  $\mu_e$  ( $C \text{ s Kg}^{-1}$  or  $\text{cm}^2 \text{ V}^{-1} \text{ s}^{-1}$ ) of a particle is defined as the average velocity  $v$  ( $\text{m} / \text{s}$ ) with which the particle moves divided by the applied electric field strength  $E$  ( $\text{m Kg s}^{-2}\text{C}^{-1}$  or  $\text{V} / \text{s}$ ).

$$\mu_e = v / E \quad (1.1)$$

$E$  (volts/cm) is a function of the applied voltage and capillary length. When the electric field is applied on a charged particle a steady-state will be achieved. In this case the product of the electric field strength,  $E$ , the number of charges on the particle,  $Z$ , and the electronic charge,  $e$  (coulomb, C), i.e.,  $Z e E$ , is the force that moves the particle in a forward direction. This force is balanced by another force of equal size but opposite to the migration direction. This opposing force is the product of a frictional coefficient,  $f$  ( $\text{kg s}^{-1}$ ), and the velocity,  $v$ , i.e.,  $f v$ .

$$Z e E = f v \quad (1.2)$$

Using Stokes law for frictional coefficient,  $f = 6 \pi r \eta$ , where  $r$  is the particle radius in m and  $\eta$  is the viscosity of the medium in  $\text{m}^{-1} \text{kg s}^{-1}$ , the mobility can be expressed by a combination of the equations 1.1 and 1.2 to give the equation 1.3:

$$\mu_e = z e / 6 \pi r \eta \quad (1.3)$$

From the equation 1.3, it is clear that electrophoretic mobility depends on the charge density of the particle ( $z / r$ ), as well as on the viscosity of the medium ( $\eta$ ). It should be remembered that equation 1.3 is a simplified equation for electrophoretic mobility. In fact, many more variables need to be taken into account. Smoluchowski has derived the following relationship for the electrophoretic mobility of a macromolecule:

$$\mu = \epsilon \xi / 4 \pi \eta \quad (1.4)$$

where  $\epsilon$  is the dielectric constant and  $\xi$  is the zeta potential of the charged particle. The zeta potential is defined as the potential at the slipping plane, called the plane of shear, in the electrochemical doublelayer (Stern layer). Zeta potential is due to an excess of ions in close proximity with a charged particle or a charged surface. This electrostatic interaction creates a thin region that is nonelectroneutral and called the electrical double layer. The electric double layer produces an ionic atmosphere surrounding the surface of the charged particle. When an external electric field is applied the electric double layer moves at the same speed as the charged particle. The plane of shear is located between a fixed adsorbed layer of ions at the surface of the charged particle and a diffuse region of ions in close proximity of the adsorbed layer. This plane of shear is a hypothetical one, since in practice there is a smooth

transition from freely moving water molecules to those firmly attached to the charged particle. The magnitude of the zeta potential, like mobility, is a function of the net charge density of the particle and the ionic strength and temperature of the medium. Therefore, the mobility of the analytes will be affected by the electrolyte buffer type (additives), total concentration of different ions, pH and temperature of the solution. Among the above mentioned parameters pH is the most important one because it strongly influences the net surface charge density of the particle.

In practice the mobility is often determined from electrophoresis experiments. The following equation can be obtained by replacing velocity with  $L/t$  and electric field with  $V/L$  in equation 1.1:

$$\mu = L^2 / t V \quad (1.5)$$

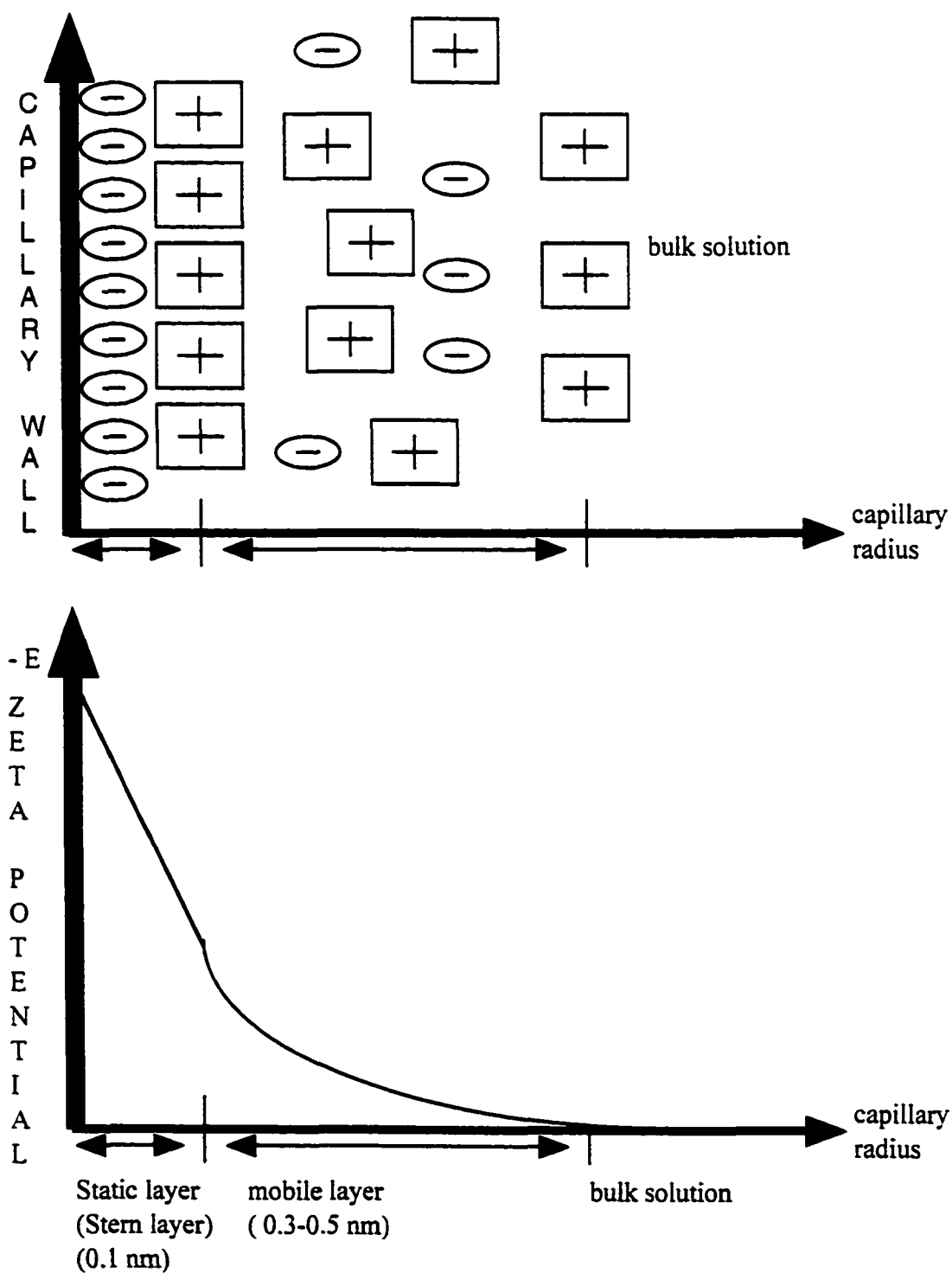
where  $L$  is the capillary length,  $t$  is the migration time and  $V$  is the applied voltage.

Equation 1.5 has been used to calculate the electrophoretic and/or electroosmotic mobility in most of the experiments presented in this thesis.

### **1.2.2 Electroosmotic Flow (EOF)**

EOF is defined as the movement of bulk liquid in an electrophoresis experiment. A fused-silica capillary is made of silanol groups ( $\text{SiOH}$ ) that are ionized ( $\text{SiO}^-$ ) above pH 2. When an electric field is applied over these negatively charged silanol groups on the inner surface of the capillary, the cationic species from the buffer solution are attracted toward the negatively charged surface to form a cationic layer along the surface. The adsorbed layer has a positive charge that decreases exponentially from the capillary wall (see Figure 1.3). This layer that is formed closest to the surface is essentially static and called the Stern layer. A second layer that is more diffuse is formed at a distance from the Stern layer. This

**Figure 1.3: Schematic diagram of the counter ions accumulating at silica-solution interface and change in the potential generated versus distance**



secondary layer is called the diffuse part of the double layer. When an electric field is applied across the capillary, cations in the OHP migrate toward the negative electrode carrying water of hydration with them. Figure 1.3 shows a schematic representation of ions at a silica-solution interface. Since these ions are solvated, when the electric field is applied, the bulk solution is dragged along with the counter ions. The extremely thin double layer starts moving and this leads to a flow that originates at the walls of the capillary. EOF results in flat flow (plug-like) profile which does not contribute to any significant broadening of a solute zone.

The thickness of the electric double layer is related to the ionic strength of the run buffer solution, according to Debye-Huckel theory

$$l / \kappa \approx 3 \times 10^{-8} (\text{Ionic strength})^{-1/2} \quad (1.6)$$

where  $l / \kappa$  is the thickness of the diffuse layer. For solutions with run buffer concentrations ranging from  $10^{-2}$  M to  $10^{-6}$  M, the thickness of the double layer will be from 3 to 300 nm. Since usually the double layer is very thin, EOF usually originates in the vicinity of the capillary wall. Because there is no stationary phase in the capillary, the flow profile will be flat, as long as the capillary radius is more than 7 times the thickness of the double layer.<sup>16</sup>

The average linear velocity of the EOF is given by:

$$v_{\text{eof}} = \epsilon \xi E / 4 \pi \eta \quad (1.7)$$

where  $\epsilon$  is the dielectric constant of the solution. In the presence of EOF, therefore, the

migration velocity for a charged particle is given by the following equation

$$v = \mu_{app} E = (\mu_e + \mu_{eof}) E \quad (1.8)$$

where  $\mu_{app}$  is the apparent mobility,  $\mu_e$  is the electrophoretic mobility due to the applied electric potential and  $\mu_{eof}$  is the electroosmotic mobility due to EOF.

In practice, however, the rate and direction of the EOF is mainly a function of the magnitude of the IR drop across the double layer and the viscosity of the buffer solution. In other words, an increase in  $\zeta$  potential increases the EOF and an increase in  $\eta$  decreases the EOF. Since pH strongly affects the ionization of silanol groups, the charge on the surface is primarily a function of pH. The charge on the surface determines the zeta potential, and therefore, EOF changes with pH. An increase in pH increases the zeta potential, and an increase in zeta potential increases the EOF. Other parameters that have been shown to influence the zeta potential are the run buffer type and its concentration, the presence of organic solvents in the run buffer and aging of the capillary. An increase in ionic strength decreases the EOF. The effect of these parameters on EOF and a more thorough discussion of the origin of EOF is presented in Chapter 4 of this thesis.

The EOF can be used advantageously in some analyses and is a prerequisite. At neutral pH the velocity of EOF is higher than the absolute migration velocity of most anions. As a result, cations, neutrals and anions all move toward the detector in a single CE experiment. Any separation ultimately is determined by the differences in the electrophoretic mobility of the individual analytes, and therefore, it is possible to separate and identify anions, cations, and neutral species in a single CE experiment. One of the problems with taking advantage of EOF in CE is the difficulty to obtain reproducible flow

rates and, therefore, migration time of the analytes. The EOF can be eliminated in different ways, which will be discussed in Chapter 5 of this thesis.

### 1.2.3 Resolution and efficiency

Resolution ( $R_s$ ) is a criterion that characterizes the separation of two components. It is defined as the difference in migration time of the two components divided by the average peak width of those components.

$$R_s = 2 (t_2 - t_1) / (w_2 + w_1) \quad (1.9)$$

where  $t_2$  and  $t_1$  are the migration times of components 2 and 1, and  $w_2$  and  $w_1$  are the widths of the peaks at base line, respectively. According to equation 1.9, a high resolution requires a large difference in migration times and/or minimum peak width.

Normally, it is more practical to use the peak width at half the peak height of the analyte,  $w_{1/2}$ , instead of  $w$ . In this case the resolution is given by the following expression:

$$R_s = (t_2 - t_1) / (w_{(1/2)2} + w_{(1/2)1}) \quad (1.10)$$

However, in order to be able to predict the actual resolution between any two components, the following formula can be derived:

$$R_s = N^{1/2} (\mu_2 - \mu_1) / 4 \mu_{ave} \quad (1.11)$$



where  $\mu_2$  and  $\mu_1$  are the mobilities of components 2 and 1, respectively, and  $\mu_{ave}$  is their average mobilities.

Equation 1.11 permits the assessment of the two factors that affect resolution independently, selectivity and efficiency. The selectivity is defined as the relative differences of mobilities of the analytes ( $\Delta\mu/\mu$ ). The efficiency of the separation process is defined by N, the plate number, which is derived from the definition using the width at half-height of a Gaussian peak,

$$N = 5.54 (t / W_{1/2})^2 \quad (1.12)$$

where t is the migration time of the analyte and  $W_{1/2}$  is the peak width at half maximum.

The number of theoretical plates can be defined in terms of the total variance of the separation:

$$N = \sigma_{tot}^2 / L^2 \quad (1.13)$$

where  $\sigma_{tot}^2$  is the total variance. To consider all the factors that influences  $\sigma_{tot}^2$ , we should include variances due to injection ( $\sigma_{inj}^2$ ), diffusion ( $\sigma_{diff}^2$ ), hydrodynamic flow ( $\sigma_{hf}^2$ ), Joule heating ( $\sigma_{jh}^2$ ), adsorption ( $\sigma_{ads}^2$ ), and conductivity difference ( $\sigma_{\Delta K}^2$ ) between the solute zone and the background run buffer. The total variance  $\sigma_{tot}^2$  of the system may be expressed as:

$$\sigma_{tot}^2 = \sigma_{inj}^2 + \sigma_{diff}^2 + \sigma_{hf}^2 + \sigma_{jh}^2 + \sigma_{ads}^2 + \sigma_{\Delta K}^2 + \sigma_{other}^2 \quad (1.14)$$

Equation 1.14 is valid if the variances are independent of each other.

#### 1.2.4 Variance caused by injection

Sternberg derived an equation that describes the variance due to sample injection. This equation is the most commonly used for sample injection if the sample is introduced onto the capillary as a plug.

$$\sigma_{inj}^2 = l_{inj}^2 / 12 \quad (1.15)$$

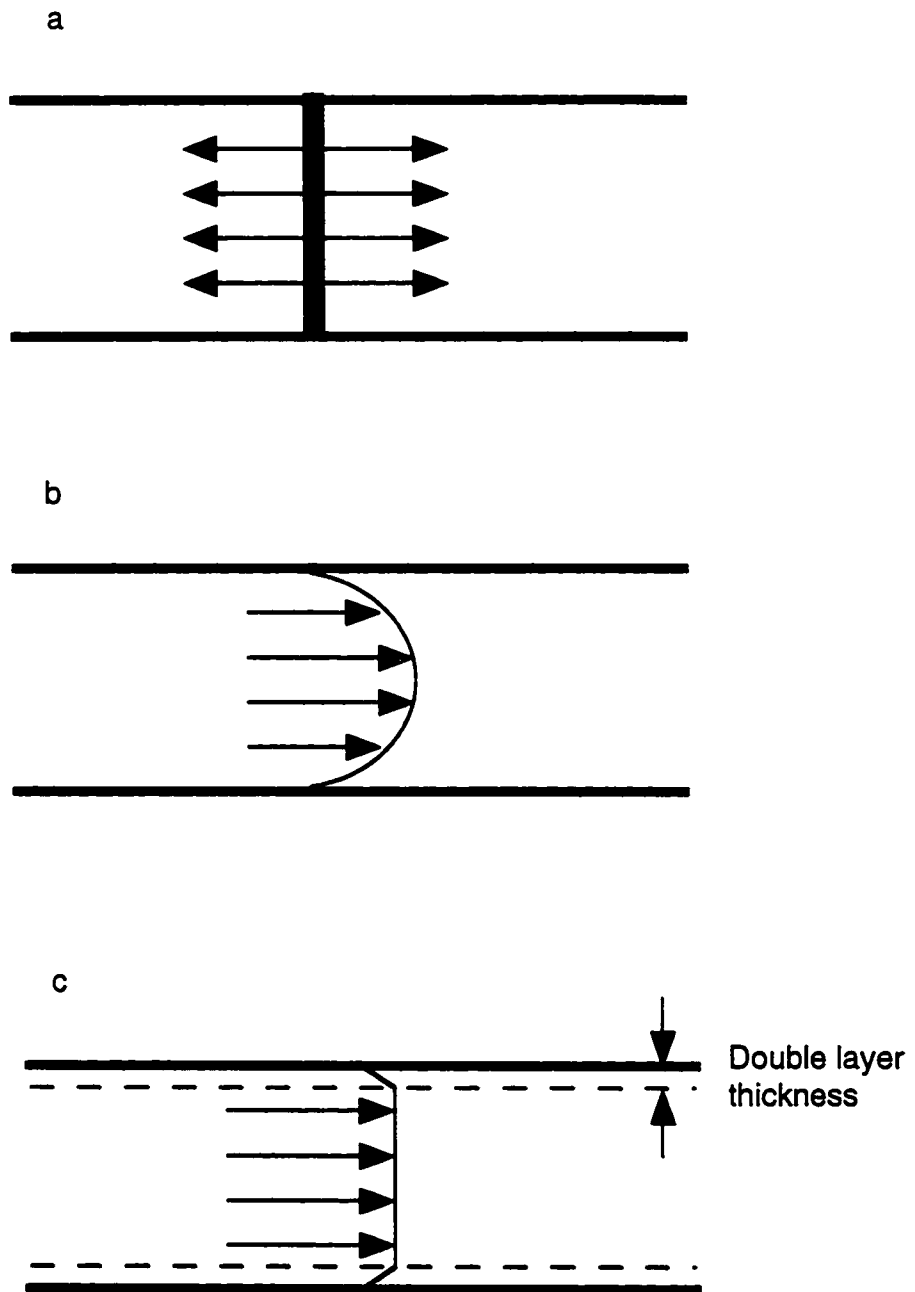
In this equation  $l_{inj}$  is the length of the sample plug injected onto the capillary, assuming a rectangular plug.<sup>17</sup> If the ratio of plug length to capillary length is less than 1% there will not be excessive band broadening due to injection.<sup>18</sup> Therefore, in an ideal injection, this band broadening effect could be negligible. However, for lower concentration samples a longer injection plug is required to facilitate detection of the analytes but at the expense of band broadening.

#### 1.2.5 Variance caused by diffusion

If there is a concentration difference between two points inside the capillary, diffusion will be observed and migration of the molecules from the higher concentration region to the lower concentration region. As soon as the sample is introduced onto the capillary, a boundary between the sample zone and the background run buffer is created and diffusion occurs (see Figure 1.4a). The variance can be expressed as:

$$\sigma_{diff}^2 = 2 D t \quad (1.15)$$

**Figure 1.4: Schematic diagram of a) diffusion, b) hydrodynamic, and c) electrokinetic flow profile**



where  $D$  is the diffusion coefficient of the components and  $t$  is the analysis time. Molecules with a smaller diffusion coefficient, such as proteins and DNA, will show less band broadening.<sup>17, 18</sup>

### 1.2.6 Variance due to hydrodynamic flow

Hydrodynamic flow in a capillary is created by a height difference between the run buffer level and sheath flow level. Practically, it is very difficult to maintain both run buffer level and sheath flow level exactly at the same height and having a slight hydrodynamic flow is unavoidable. While EOF has a plug-like flow profile, hydrodynamic flow has a parabolic one (see figure 1.4). This parabolic flow profile contributes to band broadening. The variance due to hydrodynamic flow can be expressed as:

$$\sigma_{\text{hf}}^2 = (R^6 \Delta P^2 t) / (1536 L^2 \eta^2 D) \quad (1.17)$$

where  $R$  is the radius of the capillary and  $\Delta P$  is the pressure drop because of the height difference between sample vial and sheath flow levels.<sup>19</sup> Capillary radius plays the most significant contribution to band broadening.

Because of hydrodynamic flow contribution to band broadening, it should be eliminated in most cases. However, hydrodynamic flow can be utilized for some particular purposes. For example it is possible to increase the resolution by using a hydrodynamic counter flow.<sup>20</sup>

### 1.2.7 Variance caused by Joule heating

When high voltage is applied across the capillary, a current will pass through the conducting run buffer solution. This current-generated heat is called Joule heating. It

depends on the conductivity of the run buffer inside the capillary and the voltage applied. The Joule heating increases the temperature at the center of the capillary relative to that of the walls. The temperature difference leads to a viscosity difference that affects the migration rate of the solutes. Therefore, the migration velocity will be highest at the center and lowest at the wall and the sample zone will acquire a parabolic shape (see Figure 1.5). According to Hjerten, this variance can be expressed as:<sup>21</sup>

$$\sigma_{jh}^2 = 1/12 (B \kappa L / \lambda)^2 (R E / 2 T_0)^4 \quad (1.18)$$

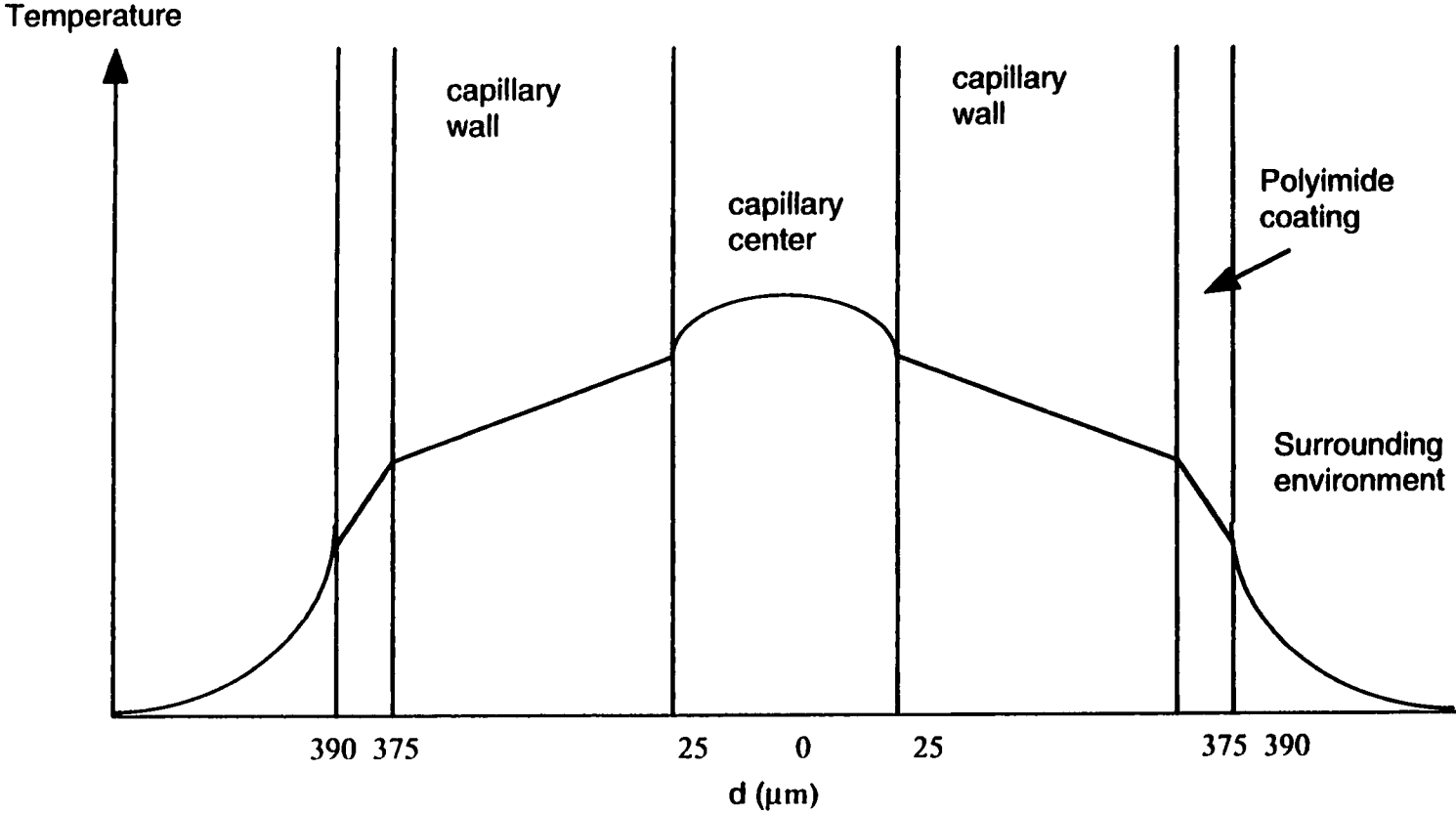
where B is a constant (2400 °K) and T<sub>0</sub> is the temperature of the coolant liquid.

The strong dependence of  $\sigma_{jh}^2$  on the radius of the capillary (R), conductivity of the run buffer ( $\kappa$ ) and the field strength (E) shows the importance of performing electrophoresis at high voltage using small ID capillaries and low conductivity buffers with good buffering capacity.<sup>22</sup> The thermal gradient between the center of the capillary and the surroundings is illustrated in Figure 1.5.<sup>23</sup>

### 1.2.8 Variance due to adsorption

As discussed above, a small ID capillary is important to obtain high separation efficiency in CE. The ratio of the internal surface of the capillary to its volume is  $2 \pi R L / \pi R^2 L = 2 / R$  that means capillaries with smaller ID show increasingly larger wall effects. A silica surface is well known to adsorb different substances. The interaction between analyte and the capillary wall can be both electrostatic and hydrophobic. Basic and / or hydrophobic proteins show the most interactions with the silica surface. This wall adsorption causes not only band broadening but also irreproducible migration times. Very

**Figure 1.5: Schematic diagram of temperature gradients from capillary center to the surrounding**



strong adsorption may prevent the analytes from reaching the detector (see Figure 5.11).

The variance of band broadening due to adsorption can be expressed:

$$\sigma_{\text{ads}}^2 = A L E \quad (1.19)$$

where A is a constant for a given solute.

There are several methods available to decrease adsorption. Since both wall adsorption and EOF originate from the charge on the capillary wall, methods developed to suppress EOF also suppress adsorption. The different methods are based on:

- Low pH<sup>24</sup>
- High ionic strength<sup>24</sup>
- Dynamic coating, which can be achieved by adding surfactants and hydrophilic polymers to the run buffer.<sup>25</sup>
- Covalent coating by some hydrophilic polymers, such as methylcellulose and polyacrylamide or a silanizing reagent.<sup>21,25-28</sup>

In Chapter 5 of this thesis a new approach to coat the capillaries is discussed and the experimental results show that the protein adsorption was minimized to nearly zero.

### 1.2.9 Variance caused by conductivity difference

The electric current in a conducting solution is equivalent to the transport of ions. Analyte ions and buffer ions with different mobilities transport the current differently. The conductivity of the migrating analyte ( $\kappa_{\text{ep}}$ ) will, therefore, differ from the conductivity of the surrounding run buffer ( $\kappa_{\text{AB}}$ ).<sup>21, 29</sup>

$$\Delta\kappa = (C_{ep} / \mu_{ep})(\mu_A - \mu_{ep})(\mu_B - \mu_{ep}) \quad (1.20)$$

where  $C_{ep}$  is the concentration of the analyte in Columbs/mL,  $\mu_{ep}$  is the mobility of the analyte,  $\mu_A$  is the mobility of the buffer and  $\mu_B$  is the mobility of the counter ion.

The conductivity difference causes peak asymmetry with either a fronting ( $\kappa_{ep} > \kappa_{AB}$ ) or a tailing ( $\kappa_{ep} < \kappa_{AB}$ ) peak shape (see Figure 1.6). The variance under specified conditions is:<sup>21, 31</sup>

$$\sigma_{\Delta\kappa}^2 = (\mu_{app} E t)^2 (\Delta\kappa / \kappa_{AB}) / 16 \quad (1.21)$$

From equation 1.21, it is evident that minimization of  $\Delta\kappa$  can be achieved by decreasing the sample concentration and choosing a buffer ion with the same mobility as the analyte ion.

### 1.3 Detection methods in CE

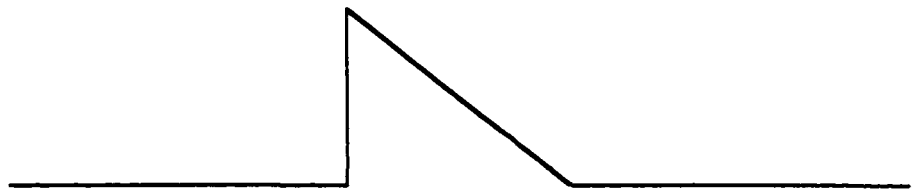
#### 1.3.1 UV-Visible Absorbance

UV-Visible absorbance detection is the most common, straightforward, method of on-column detection for CE. Its sensitivity, however, is limited. Most of the commercial CE instruments use on-column UV absorbance detection. This detection method suffers from two main problems. First, the path length is very short, less than 100  $\mu\text{m}$ , and this will impose the need for higher concentration of the analyte. The second problem of UV detection, unlike the plane-parallel arrangements in conventional detection cells, is that the

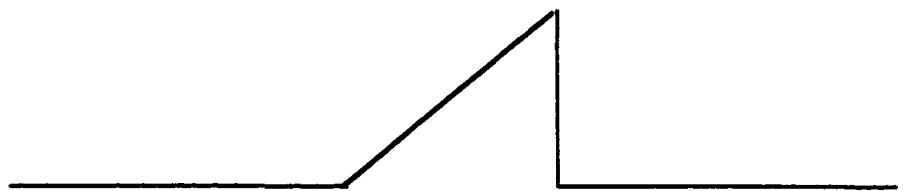


**Figure 1.6: Schematic diagram of peak shapes if a) sample conductivity is more than run buffer conductivity (a tailing peak), b) sample conductivity is less than run buffer conductivity (a fronting peak), and c) sample conductivity is the same as run buffer conductivity (no zone distortion)**

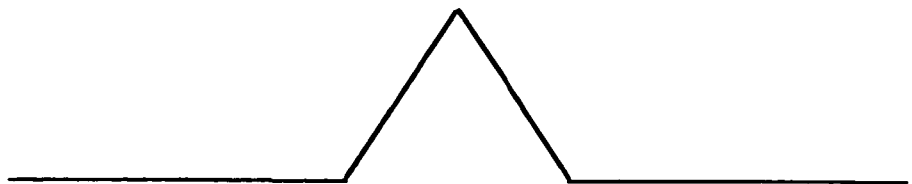
**a**



**b**



**c**



UV light has to enter onto and exit from the capillary through the curved borders. This will cause refractive index effects, and the illuminated column will act as a lens.<sup>30</sup>

### **1.3.2 Laser Induced Fluorescence (LIF) detection with a sheath flow cuvette as a very sensitive post-column detector**

Fluorescence detection is more sensitive than UV absorbance detection.

Fluorescently labeled amino acids have been reported to be 15 times more sensitive when using fluorescence detection as compared to UV-Visible absorbance detection.<sup>31</sup> However, with conventional light sources for UV (deuterium or tungsten lamps) the gain is limited, and therefore, the sensitivity is low. With lasers, however, more light can be focused into small capillaries. This will result in impressive mass detection limits. Wu and Dovichi have reported the detection of 1100 molecules of tagged arginine.<sup>32</sup> For this thesis we have used laser induced fluorescence (LIF) detection with a sheath flow cuvette. Before discussing LIF, it is convenient to discuss the basic principles of lasers and fluorescence spectroscopy and then the sheath flow cuvette.

#### **1.3.2a) LASER: Light Amplification by Stimulated Emission of Radiation**

Laser is an acronym standing for Light Amplification by Stimulated Emission of Radiation. It is a device that emits high-intensity radiation that is coherent (in-phase) and has a narrow (typically 0.001 to 0.01 nm) bandwidth. The high intensity and narrow bandwidth of radiation that is emitted from a laser are two important parameters that makes the laser an almost ideal light source for fluorescence spectroscopy at those wavelengths for which lasers are available.

A laser consists of three sub-units. The first sub-unit is an optical amplifier. It is a collection of atoms, ions, or molecules with a non-Boltzman distribution of energy among some set of quantum states. This non-Boltzman distribution is called a population

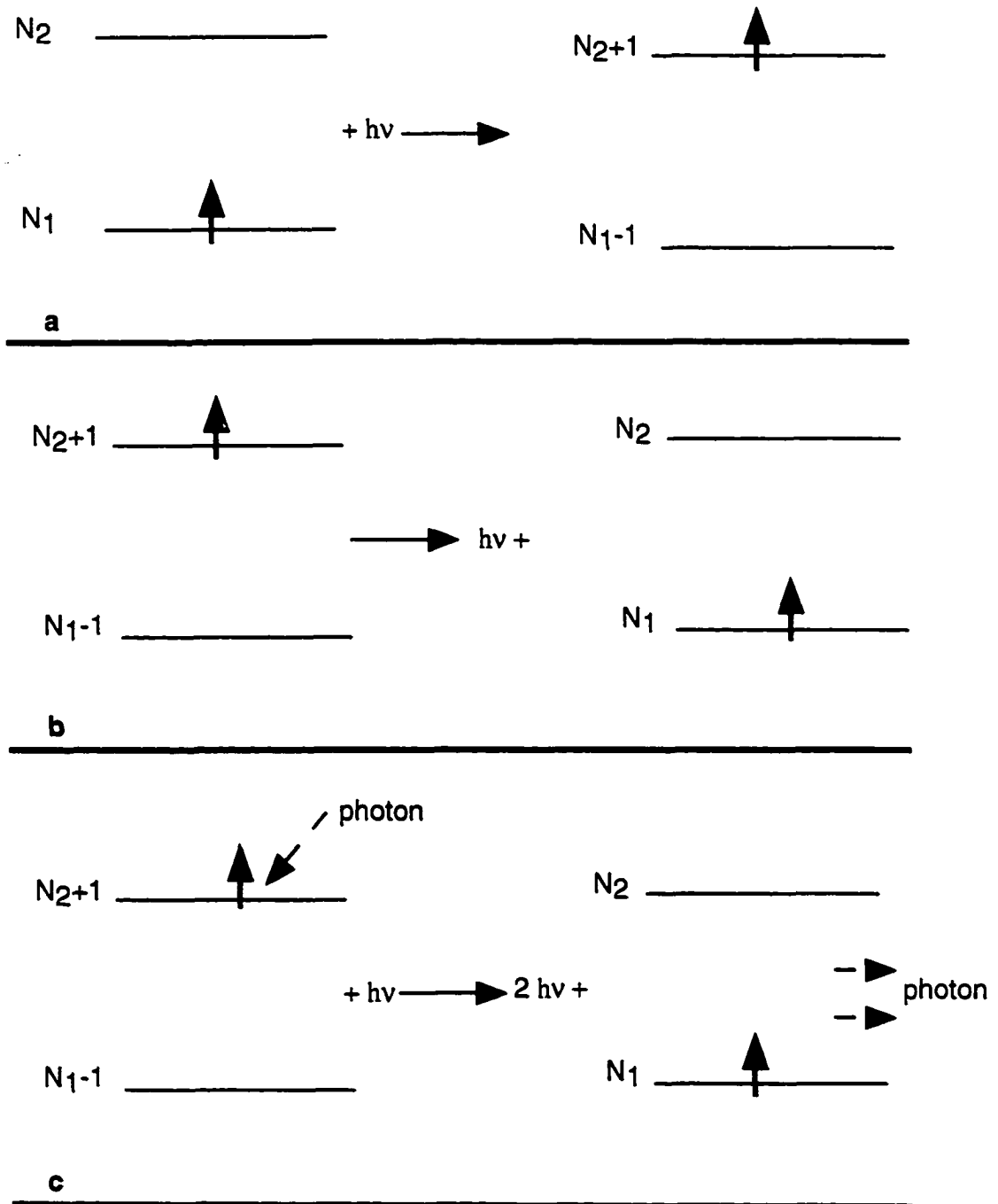
inversion. It has the unique property of amplifying certain frequencies of light via the stimulated emission of radiation. The second subunit is an excited state pump. It is the device or mechanism used to generate and maintain the population inversion. The exact mechanism to reach the population inversion depends upon the details of the energy levels and the matrix that the atom, ion, or molecule is found. The third subunit is an optical resonator. It is used to convert the amplifier into an optical oscillator. Although this final step may seem to involve only passive components, the resultant laser radiation has many properties that is primarily due to the resonator design. Figure 1.7 shows the energy level diagrams and the three basic processes of adsorption, emission and stimulated emission of radiation.

Because of their light amplifying properties, lasers produce spatially narrow and extremely intense beams of radiation. The process of stimulated emission is the key step. It produces a beam of highly monochromatic (bandwidth of 0.01 nm or less) and remarkably coherent radiation.

Lasers can provide higher peak powers to be focused on a small spot as compared to conventional light sources. The effect is that lasers can be used to illuminate very small volumes on a capillary or beneath the capillary tip. Therefore, laser power can be more effectively utilized.

Lasers have many applications in areas such as Raman spectroscopy, absorbance, fluorescence, refractive index, photothermal defraction, and capillary electrophoresis with on-column or post-column LIF detection. LIF detection has produced excellent detection limits for chemical analysis. The importance of the laser can be seen in the tremendous increase of laser being used in research since the first paper for laser analysis was published in 1966.<sup>33</sup>

**Figure 1.7: Generalized energy level diagrams showing the three basic processes of a laser involving the a) absorption, b) spontaneous emission and c) stimulated emission of radiation. The term  $h\nu$  represents a photon with a frequency satisfying Plank's law.**



### 1.3.2b Fluorescence spectroscopy

The various activation and deactivation processes are shown in the self-explanatory Jablonski diagram (Figure 1.8)

A radiational transition between electronic states of the same multiplicity is called fluorescence. The electrons in the ground state of most molecules are paired and their multiplicity ( $2s + 1$ ) is one. It means that fluorescence involves a singlet-singlet transition. Because internal conversion to  $S_1$  (see Fig. 1.8) and vibrational relaxation are more rapid processes than fluorescence, fluorescence usually occurs from the lowest ground vibrational state of  $S_1$  to various vibrational levels in  $S_0$  ( $S_1 \rightarrow S_0 + h\nu$ ). That is why only one fluorescence band is normally observed even if absorption to different excited singlet states may happen. Fluorescence lifetime is typically  $10^{-10}$  to  $10^{-6}$ s. Fluorescence usually occurs at longer wavelengths than absorption because absorption transitions are to higher excited electronic states or to higher vibrational levels of the  $S_1$  but fluorescence is always from the lowest energy level of the excited state.

The first application of fluorescence detection in CE was reported by Jorgenson and Lukacs in 1981.<sup>11</sup> They showed high sensitivity and high selectivity of a fluorescence detector for CE.

Figure 1.9 shows a typical fluorescence detector. It consists of an excitation source and a monochromator or a filter to select the proper excitation wavelength. If the excitation source is a laser, because it is a monochromatic light source, there is no need for a filter. A fluorescence detector also has optics to focus the excitation beam onto the capillary for on-column detection or on a sheath flow cuvette for post-column LIF detection. Fluorescence is collected at right angles. After being filtered, it is detected with a photomultiplier tube.

Fluorescence intensity is a function of analyte concentration and excitation source intensity. In order to be able to measure low analyte concentration, it is convenient to

**Figure 1.8: Deactivation processes for an excited molecule for a) absorption ( $10^{-15}$  s); b) vibrational relaxation ( $10^{-11}$  -  $10^{-10}$  s); c) internal conversion; d) fluorescence ( $10^{-10}$  -  $10^{-6}$ ); e) external conversion; f) intersystem crossing; and g) phosphorescence ( $10^{-4}$  -  $10^{+4}$  s). (S is a singlet state and T is a triplet state)**

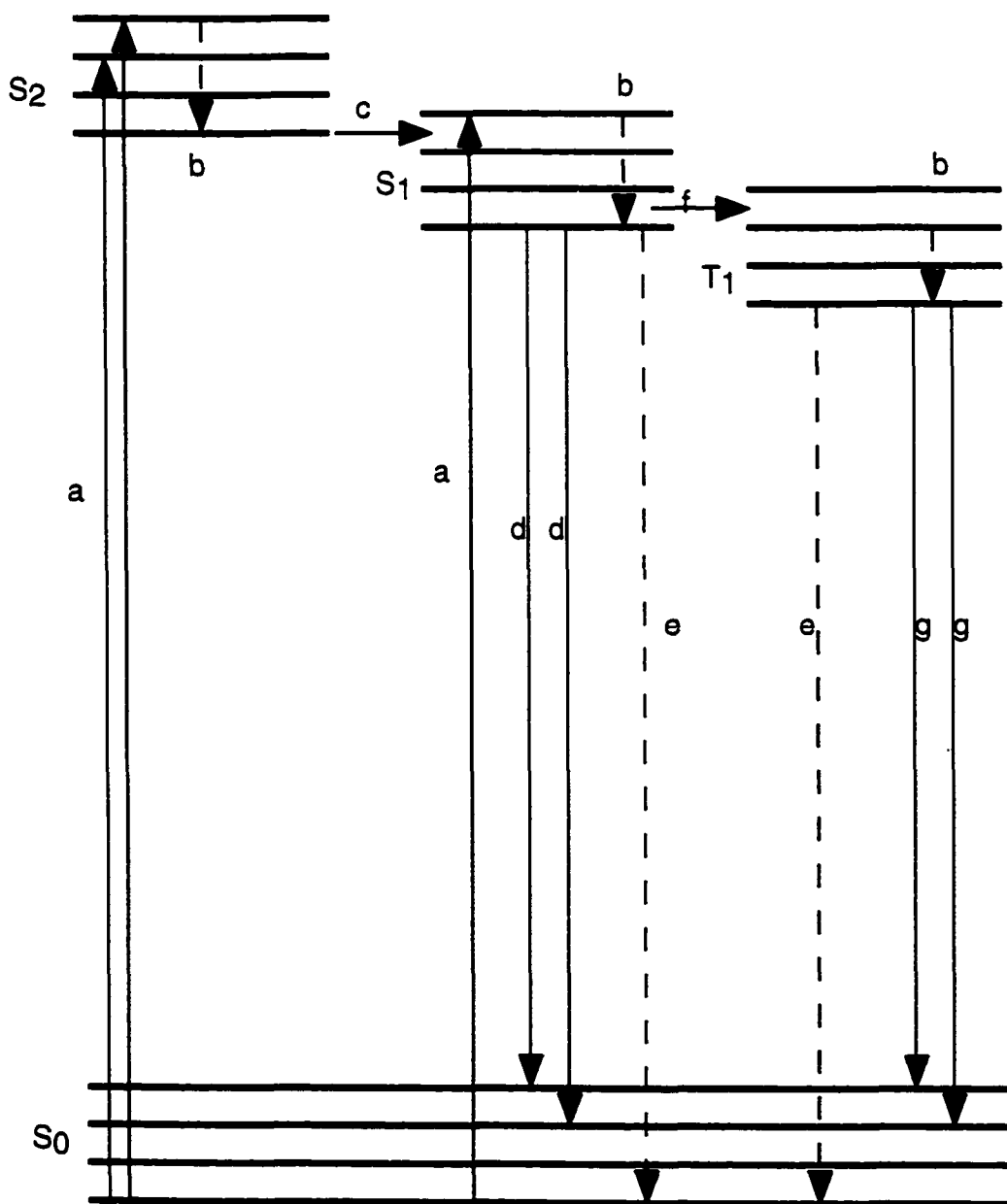
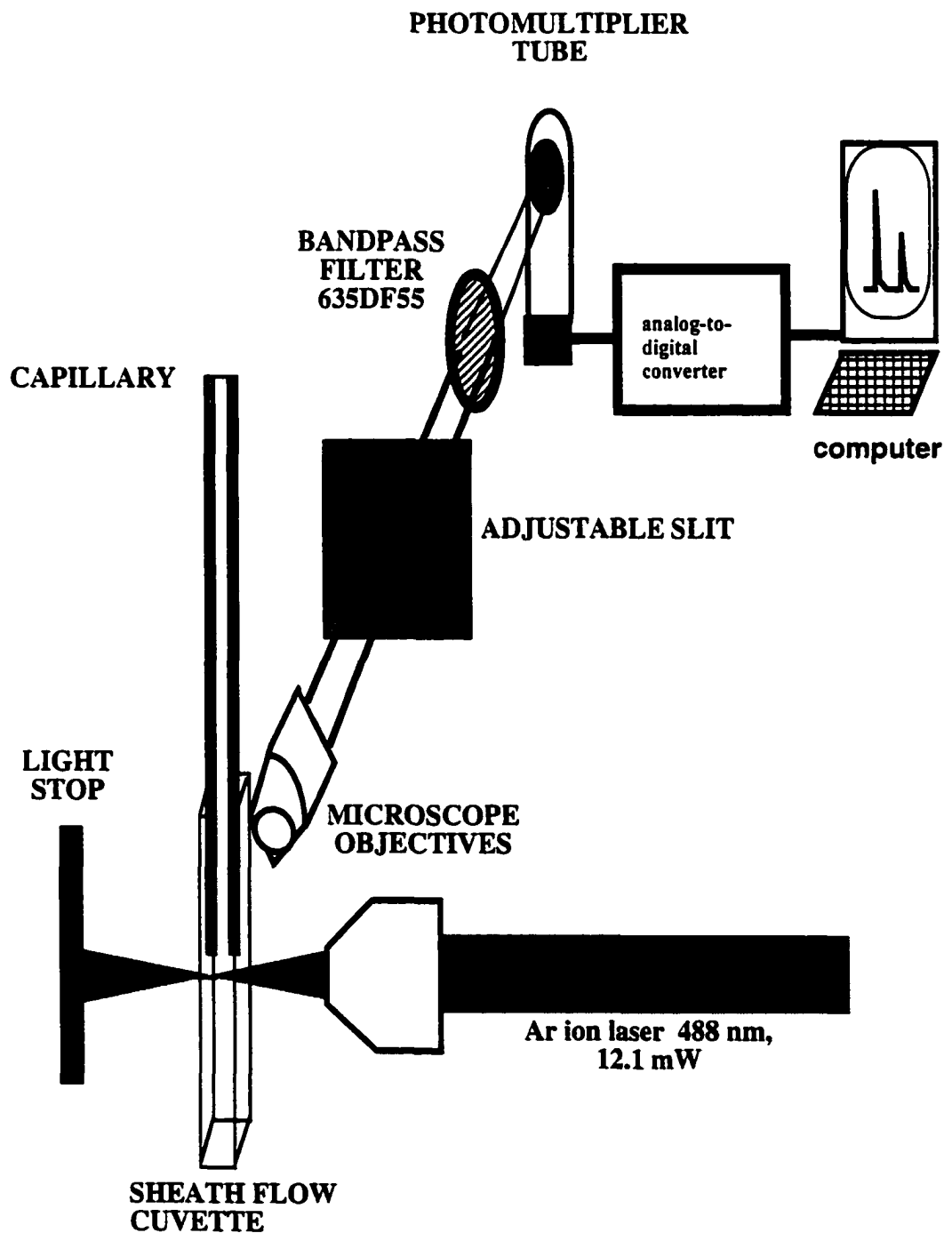


**Figure 1.9: Schematic diagram of a laser induced fluorescence detector**



increase the source intensity and hence lasers are ideal sources for fluorescence spectroscopy. The quantitative relationship between fluorescence (or phosphorescence) intensity and concentration may be derived from Beer's law. The fraction of light transmitted through the solution is:

$$I / I_0 = 10^{-abC} \quad (1.22)$$

Where I is the light intensity after passing through the solution,  $I_0$  is the initial light intensity, a is molar absorptivity of the analyte, b is length of the cell containing the analyte, and C is the concentration of the analyte. The corresponding fraction of light absorbed is

$$1 - I / I_0 = 1 - 10^{-abC} \quad (1.23)$$

Rearranging, the fraction of light absorbed by the sample is

$$I_0 - I = I_0 (1 - 10^{-abC}) \quad (1.24)$$

The total fluorescence intensity is proportional to the quanta of light absorbed and to the fluorescence quantum efficiency,  $\phi$ , which is the ratio of quanta absorbed to the quanta emitted; that is, the fraction of excited species that fluoresces rather than undergoes intersystem crossing. Thus, for fluorescence

$$F = (I_0 - I) \phi f(\theta) g(\lambda) = I_0 \phi (1 - 10^{-abC}) f(\theta) g(\lambda) \quad (1.25)$$



where  $f(\theta)$  represents the geometrical factor and is determined by the solid angle of the fluorescence radiation collected by the detector (fluorescence is emitted in all directions but is viewed only through a limited aperture), and  $g(\lambda)$  defines the efficiency of the detector as a function of the fluorescence wavelength incident on it. The above equation can be written in the following exponential power series as:

$$F = I_0 \phi f(\theta) g(\lambda) \{ 2.3 a b C - (2.3 a b C)^2 / 2! + (2.3 a b C)^3 / 3! - \dots + (2.3 a b C)^n / n! \} \quad (1.26)$$

For very dilute solutions in which not over 2% of the total excitation energy is absorbed, and the term  $abC$  is not greater than 0.05 in fluorescence (and 0.01 in phosphorescence), Equation 1.26 simplifies to:

$$F = 2.3 I_0 \phi f(\theta) g(\lambda) a b C \quad (1.27)$$

Of particular interest in Equation 1.27 is the linear dependence of fluorescence on the source excitation intensity. This means sensitivity can be increased by working at high source excitation intensities (i.e. laser) to give large signal to noise ratios.<sup>34</sup>

### 1.3.3 Laser Induced Fluorescence (LIF)

LIF detection with a sheath flow cuvette for neat sample solutions was in the range of single molecule limits in 1984. This work was conducted by Dovichi, Keller, and others.<sup>35</sup> Their detection limit was reported to be  $8.9 \times 10^{-14}$  M at two times background noise for aqueous rhodamine-6G.

Figure 1.10 shows the schematic diagram of a CE instrument with a sheath flow cuvette and LIF detection. The instrument components are a high-voltage power supply (0 to 30 kV), a capillary which is usually made of fused silica with an ID < 50  $\mu\text{m}$  and a length of 20-50 cm, one buffer reservoir that can accommodate the electrode connected to the power supply, and a PMT detector. The sheath flow that is connected to a waste reservoir acts as the ground electrode. The sheath flow cuvette system will be described later in this chapter.

LIF produces remarkable improvement in detection limit compared with the use of conventional incoherent sources. In 1985, Zare's group reported the first application of lasers for fluorescence detection in CE.<sup>37</sup> They used a 5-mW helium-cadmium laser that produced an excitation beam with 325 nm wavelength. The fluorescence from the sample was collected with optical fibers. After being spectrally filtered, the fluorescence was detected with a photomultiplier tube. They reported the detection of femtomole amounts of dansyl-amino acids with their LIF detection system.

The major problem for on-column fluorescence detection is a relatively large amount of light scattering. This will generate a large amount of reflection and refraction at the capillary walls. The result is a high background signal, and therefore, a relatively low sensitivity.<sup>44</sup> Fluorescence should be, ideally, measured in a flow chamber with good optical quality. Flat windows are required to eliminate or reduce the light scattering. While it is possible to use a square capillary for electrophoresis, it is not possible to manufacture long pieces of small dimension capillaries with flat windows. Instead, it is a better option to use a post-column fluorescence chamber to achieve extremely high-sensitivity fluorescence detection.

#### **1.3.4 The sheath flow cuvette**

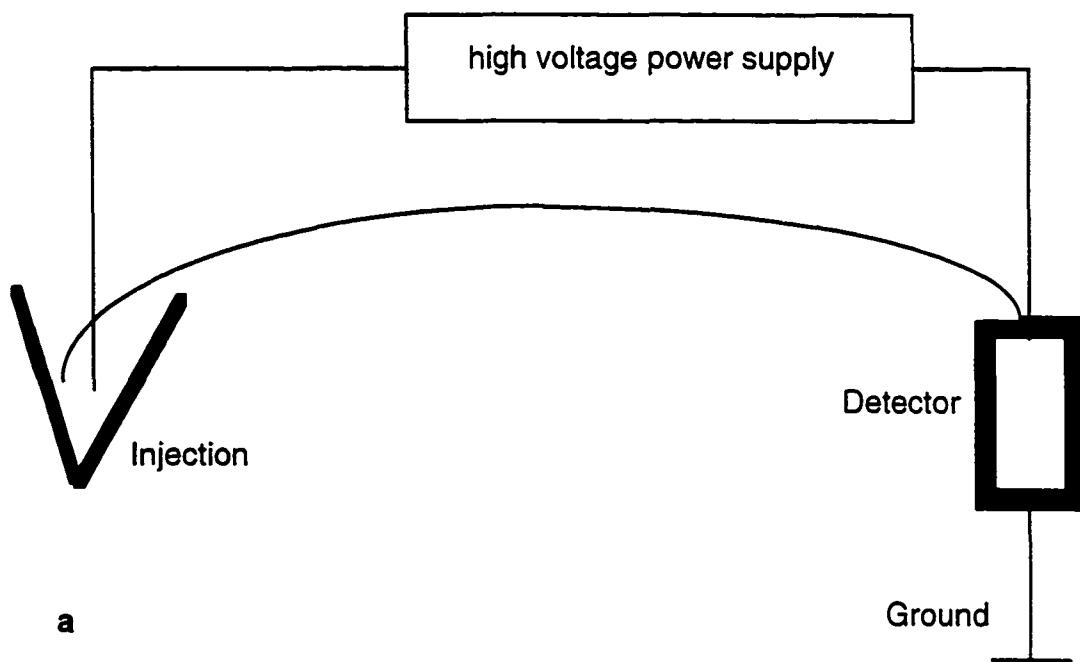
Figure 1.10b shows a schematic diagram of a sheath flow cuvette. This kind of

cuvette is very important when manipulating small sample volumes. When the sample migrates out of the capillary, it enters into the center of a sheath flow cuvette and produces a stream under laminar conditions. The internal diameter of cuvette narrows to smaller ID flow chamber and this creates the process of hydrodynamic focusing. The small sample stream out of the capillary is surrounded by the flowing sheath stream. This flowing sheath stream does not change the sample concentration by dilution. The cuvette is a 250- $\mu\text{m}$  square chamber that holds the capillary in its center. The sheath flow enters from the top of the cuvette and exits from the bottom part of the cuvette to the waste reservoir. Sheath flow cuvettes use a square flow chamber with flat windows of good optical quality. The square flow chamber and flat windows minimize the scattering of excitation light into the emission optics in a fluorescence experiment.<sup>38</sup>

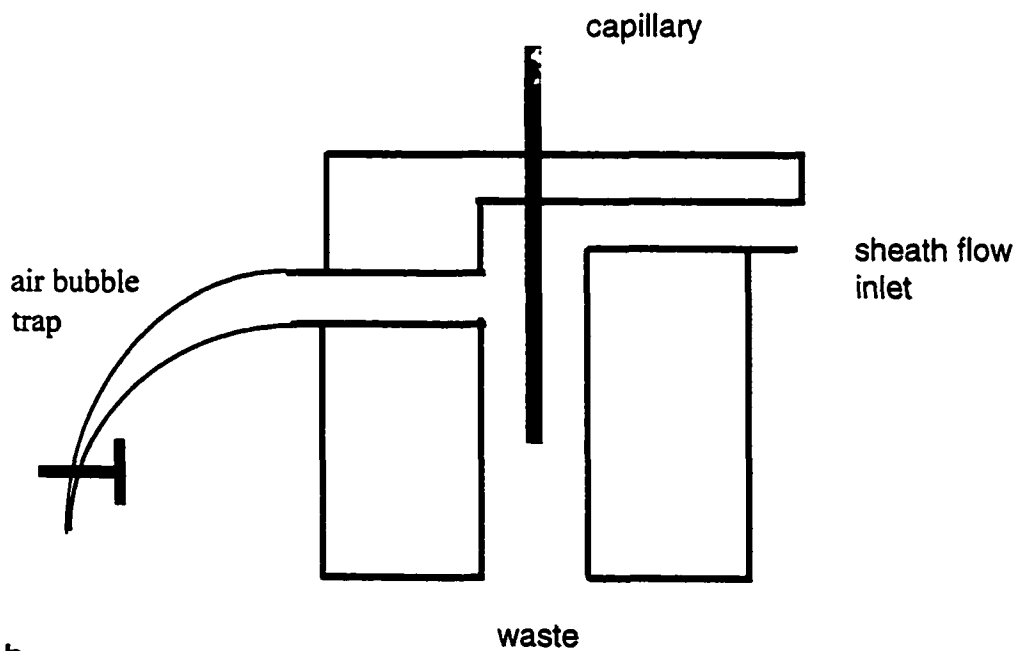
The other advantage of sheath flow cuvette is that it focuses the sample stream far away from the cuvette windows within a sheath stream of CE run buffer. Therefore, no contamination occurs inside the cuvette window when the sheath stream is flowing. Most importantly, since the sheath flow buffer and CE run buffer are exactly the same buffer with similar concentration, they have the same refractive index. Therefore, the excitation beam is not scattered at the interface of the sample and sheath flow streams. A spatial filter is located in the emission optical path of the fluorescence detector. This filter reduces the small amount of scatter light generated by the cuvette windows.

The cuvette used for a sheath flow system has three main advantages as a detector cell. The first advantage is that very small detection volume can be easily obtained. This small detection volume eliminates the detector dead volume and, therefore, extra column band broadening is reduced. The second advantage is that the sample stream never contacts the cuvette windows. This prevents contamination of the windows. The third advantage of a sheath flow cuvette is that the light scattered due to the cell window can be easily eliminated because the sample stream is located far away from the windows.

**Figure 1.10: Schematic diagram of a) CE instrument with b) sheath flow cuvette**



**a**



**b**

Dovichi and Zarrin applied this cuvette for particle size analysis in 1985<sup>39-41</sup>. In this application, the cuvette was used as a light scattering detector to count individual particles that were eluted out of a capillary column hydrodynamic chromatograph. The elution order was based on the particle size. Concentration detection limits were about 1000 particles / mL. Particles as small as 45 nm radius were detected with a right angle collection geometry. Since 1985, this detector has been used routinely in Dr. Dovichi's laboratory for high sensitivity detection.<sup>42-47</sup>

High sensitivity LIF detection system has many applications in biological analysis. For example, in DNA sequencing, the total amount of sequencing sample introduced onto the capillary is about 1 amol. The amount of each fragment averages perhaps 1 zeptomole.<sup>48</sup>

If the laser beam intensity is too strong, the analyte may decompose photochemically. This process is called photobleaching that is the fundamental limitation of LIF detection system.<sup>45</sup>

### **1.3.5 Derivatization for fluorescence detection**

Despite being the most sensitive detection technique, LIF suffers from the limitation that most biologically important molecules are not naturally fluorescent. There are a vast number of publications on the subject of changing non-fluorescent molecules to fluorescent molecules by chemical labeling reactions. The Molecular Probes catalog (Eugene, OR) is one of the best resources that contains over 5000 references on labeling and detection of a large number of analytes. The analytes of interest are amino acids, peptides, proteins, DNA, enzymes and antibodies. The fluorescence labeling chemistry is not restricted to CE, but the small size of the capillary and nL sample consumption make the labeling reaction chemistry a serious challenge.

Those proteins and peptides that contain tryptophan residues naturally fluoresce. The excitation wavelength is about 280 nm. There are no inexpensive lasers available to provide 280 nm excitation wavelength and, therefore, high-sensitivity detection of native fluorescence molecules is difficult. That is why the labeling chemistry plays an important role to derivatize the biologically important molecule for high-sensitivity LIF detection.

Novotny pointed out that it is much more appropriate to choose a labeling reagent with spectral properties that match those of commercially available lasers<sup>49</sup>. There are many commercial inexpensive lasers that provide different excitation wavelengths. For example KrF laser provides excitation wavelength in the UV region (248 nm), the He-Cd laser at 325 and 442 nm, the He-Ne laser at 543.5, 594, and 633 nm, and the Ar-ion laser at 488 and 514.5 nm. The labeling reagent chosen to derivatize a molecule should have an excitation wavelength that matches with the wavelength provided by one of these commercial lasers. Diode lasers have a long life and relatively inexpensive cost and provide excitation wavelengths in the range of 650 to 700 nm. That is the reason that there is great effort in the development of new dyes that absorb strongly in the red and emit in the near infrared.

Labeling reagents with strong absorbance in the range of 440 to 600 nm are most useful and common. Molecular Probes offers a complete list of these kind of fluorescent labeling reagents.<sup>50</sup> There are labeling reagents for almost all of the functional groups, but most of the labeling reagents that are commercially available are amine labeling reagents. There are few labeling reagents for other functional groups like carboxylic acid. In Chapter 6 of this thesis 5-bromomethyl fluorescein (5-BrMF) has been used to label the carboxylic acid functional groups.

There is no labeling reagent commercially available for the arginine amino acid.<sup>50</sup> In Chapter 7 of this thesis a new fluorescent labeling reagent for arginine functional group is introduced.

Protein labeling chemistry suffers from one intrinsic problem. There are quite a few primary amines, lysine side chains, present in a protein molecule. This problem imposes the possibility of multiple labeling of the protein. For example, if a protein contains  $N$  primary amino groups including lysine side chains and N-terminal amino group, then a total of  $2^{N-1}$  possible multiple labeling products can be formed.<sup>51, 52</sup> Larger proteins have many lysine groups and this will cause a massive number of multiple labeling products. In this case either separation by CE is a formidable task or band broadening is unavoidable. One solution to prevent the multiple labeling problem is the old method that is used in organic synthesis. All primary amino groups have to be protected by reaction with an amine protecting agent, like phenyl isothiocyanate, to produce the phenyl thiocarbamyl derivative.<sup>53</sup> Then, the protein has to be reacted with an acid. Acid cleavage produces a free N-terminal amino group that could be labeled with an amine labeling reagent. This chemistry replaces a positively charged  $\epsilon$  amino group of the lysine side chain with a positively charged phenyl carbamyl group. The overall charge of the protein remains constant, and solubility is not affected significantly.

The labeling technique can be categorized into pre-column, post-column, and on-column labeling methods. Pre-column labeling is the most common method used for CE. Almost all off-line pre-column labeling uses a large volume of analytes and reagents. In practice, however, a small fraction of the labeled molecule is injected onto the capillary and the rest of the labeled analyte is wasted. A post-column labeling reaction is compatible with sheath flow designs. An on-column "T" has been constructed to introduce labeling reagent for a post-column detector during the separation.<sup>54-56</sup> The major drawback of a post-column labeling reaction is the slow reaction rate. This will cause extra column band broadening. On-column labeling drastically reduces the volume of analyte and reagents.

## 1.4 Mass spectrometry

Despite being the most sensitive detector, LIF does not provide structural information regarding the analytes of interest. MS detection could provide both structural information and molecular weight determination of the analyte. CE works based on the differential migration of charged particles in a solution, while MS works based on mass-to-charge ratio ( $m/z$ ) of the ions in the gas phase. This is an intrinsic problem that makes the interfacing of these two techniques a challenge because separations are based on the ion motion in two completely different environments: conductive liquid buffer for CE and high vacuum gas phase for MS. CE also separates large biological molecules that have traditionally presented problems to the mass spectroscopists using conventional ionization techniques such as electron impact. The electron impact ionization technique is, usually, applicable to a wide range of organic compounds and the method is limited by two factors. First, the sample has to be vaporized before ionization. This may cause thermal decomposition of involatile or thermally labile compounds before ionization. The second limitation of electron impact ionization is that the electron energy usually used for ionization of the molecules is about 70 eV. This high energy frequently causes extensive fragmentation and/or lack of molecular weight information. Using softer ionization technique reduces the fragmentation, but obtaining molecular weight information of intact biological molecules has proved to be challenging to the mass spectrometry community.

In Electrospray Ionization (ESI) the liquid flow out of the CE capillary at atmospheric pressure has to be nebulized to the gas phase before entering into the MS at very low pressures. The nebulization takes place by the exposure of the liquid surface to a high electric field. In an ESI source, the analyte solution is introduced into dry air or nitrogen at atmospheric pressure through a metal capillary tube that is held at a potential of several kilovolts relative to the walls of the ion source. The charges will be built-up at the liquid surface. This creates such an instability in the liquid where coulombic repulsion



forces are sufficient to overcome the surface tension so that small ( $<1\ \mu\text{m}$ ) charged droplets separate from the liquid emerging from the capillary tube.<sup>59</sup> Figure 11 shows the ESI process.

Matrix Assisted Laser Desorption Ionization (MALDI) is another soft ionization technique. In this method, sample is mixed with a matrix such as dihydroxybenzoic acid (DHB) or cinnamic acid with a ratio of 1 to 100 or even 1 to 500. The analyte molecules will coprecipitate with matrix molecules. A nitrogen laser is focused on the sample. When the matrix is vaporized with the laser energy, analyte molecules will also transfer to the gas phase along with the matrix molecule. The gas phase molecules will, then, enter into the MS system. Figure 12 shows the schematic diagram of a MALDI process.

In Chapter 7 of this thesis ESI was used as a tool for molecular weight determination of synthesized dyes, but not as a detector for CE. MALDI was also used for the same purpose.

For a thorough discussion of other detection techniques in CE, including thermo-optical detection, see reference 48. Table 1, however, compares different methods of detection in CE with respect to mass detection limit and concentration detection limit. It also lists the advantages and disadvantages of each technique.

### **1.5 Applications of capillary electrophoresis**

Capillary electrophoresis has many advantages that make it a technique with a wide range of applications. Some of the advantages of CE are summarized as the following:

- High resolution (up to 1,000,000 theoretical plates).
- High speed (separation time under 10 minutes).
- Allows rapid method development.

**Figure 1.11: Schematic diagram of ESI mechanism. Ions from solution are transferred directly to the gas phase by applying high voltage to the tip of the syringe.**

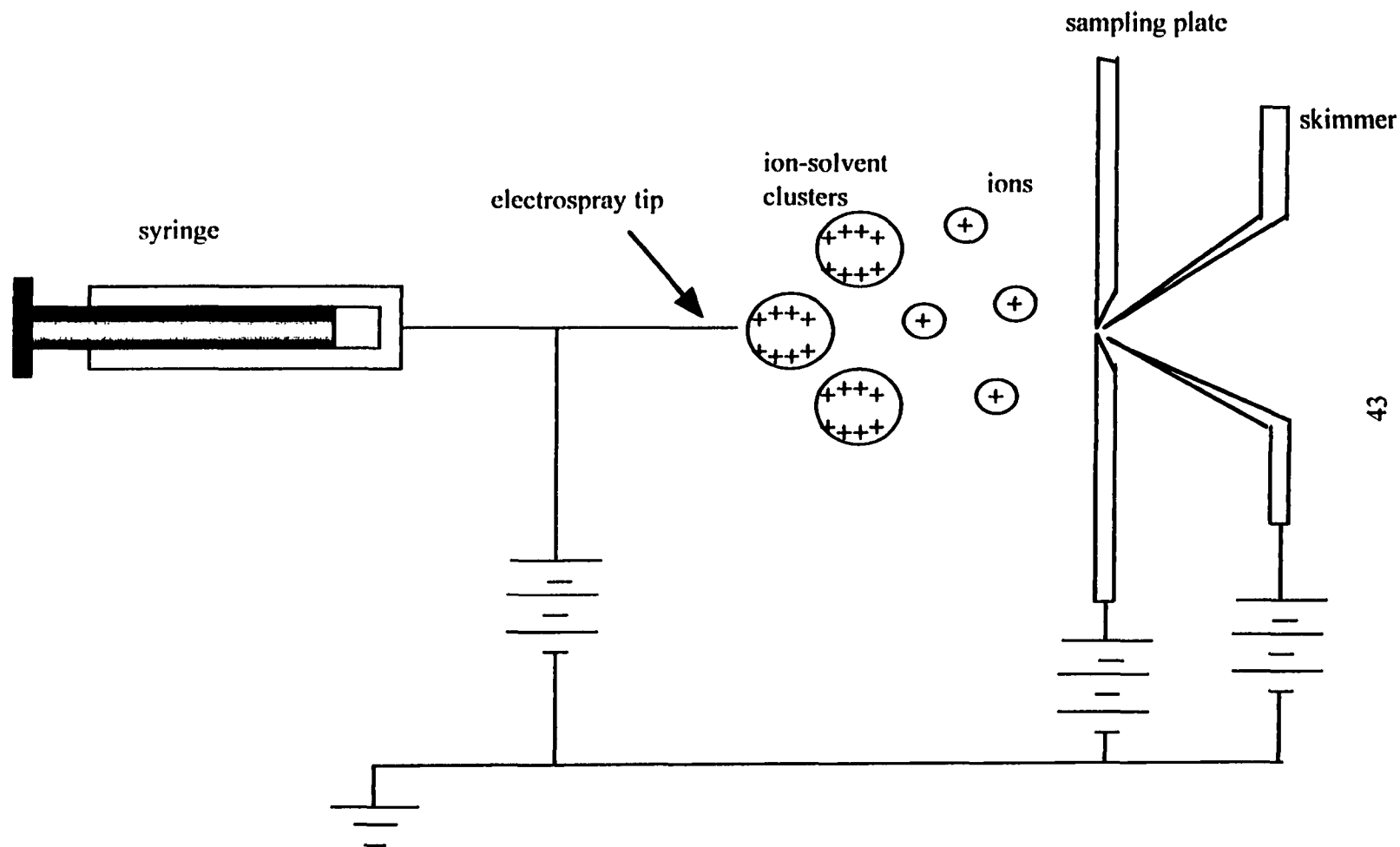


**Figure 1.12: Schematic diagram of a MALDI mechanism with a commercial sample probe**

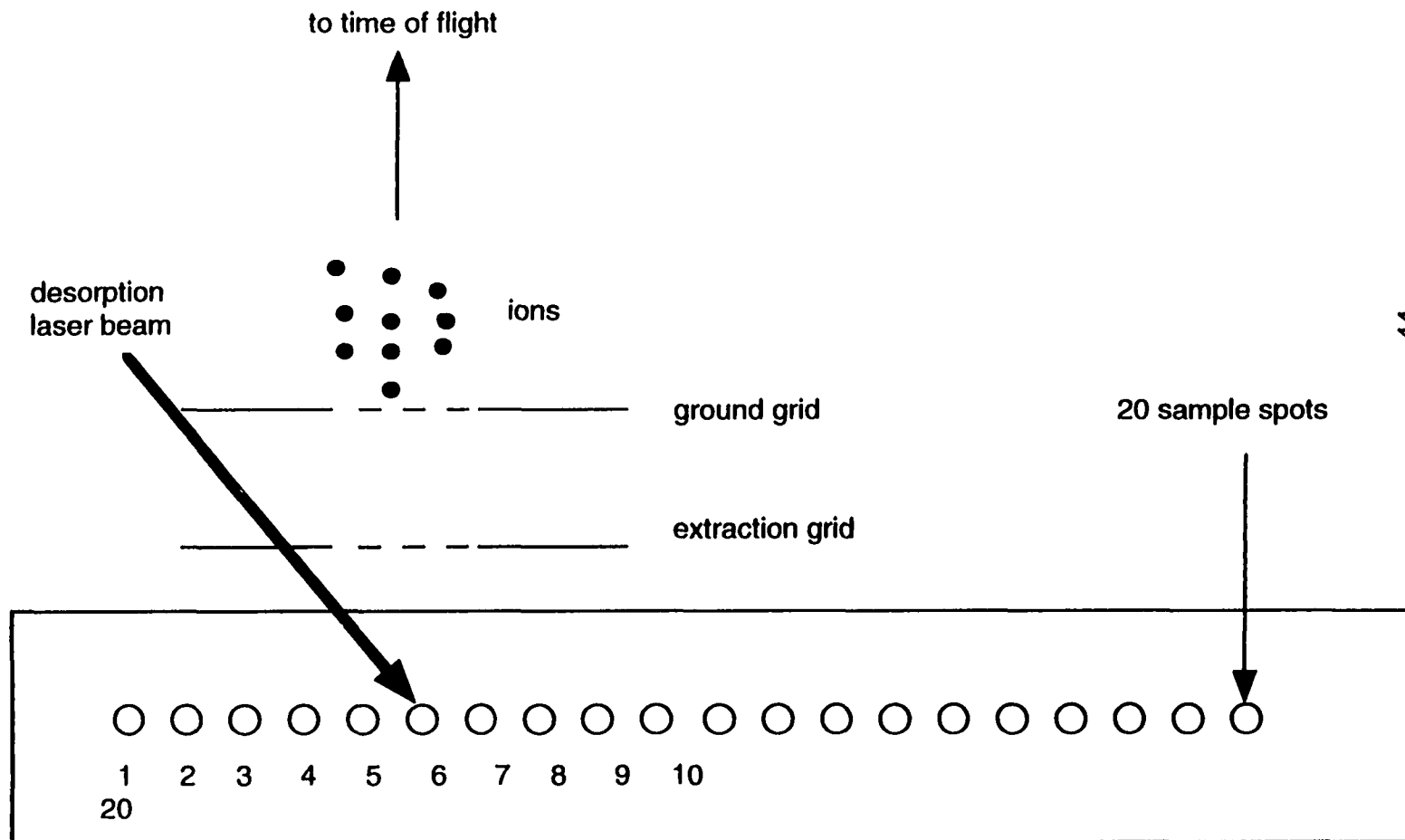


**Table 1.1: Advantages (+) and disadvantages (-) of detection techniques in CE**

<b>Method</b>	<b>Mass detection limit (moles)</b>	<b>Concentration detection limit (moles) (10 nL injection)</b>	<b>Advantages/ disadvantages</b>
UV-Vis absorption	$10^{-13}$ - $10^{-16}$	$10^{-5}$ - $10^{-8}$	+ Universal + Diode Array offers spectra
Fluorescence	$10^{-15}$ - $10^{-17}$	$10^{-7}$ - $10^{-9}$	+ Sensitive, Selective - Usually requires sample derivatization
Laser-induced fluorescence ( <b>LIF</b> )	$10^{-18}$ - $10^{-20}$	$10^{-14}$ - $10^{-16}$	+ Extremely sensitive - Usually requires sample derivatization - Expensive
Amperometry	$10^{-18}$ - $10^{-19}$	$10^{-10}$ - $10^{-11}$	+ Sensitive - Selective but useful for electroactive analytes - Requires special electronics and capillary modification
Conductivity	$10^{-15}$ - $10^{-16}$	$10^{-7}$ - $10^{-8}$	+ Universal - Requires electronics and capillary modification
Mass Spectrometry	$10^{-16}$ - $10^{-17}$	$10^{-8}$ - $10^{-9}$	+ Sensitive and offers structural information - CE-MS interface is complicated
Indirect UV, fluorescence, amperometry	10-100 times less than direct method	-	

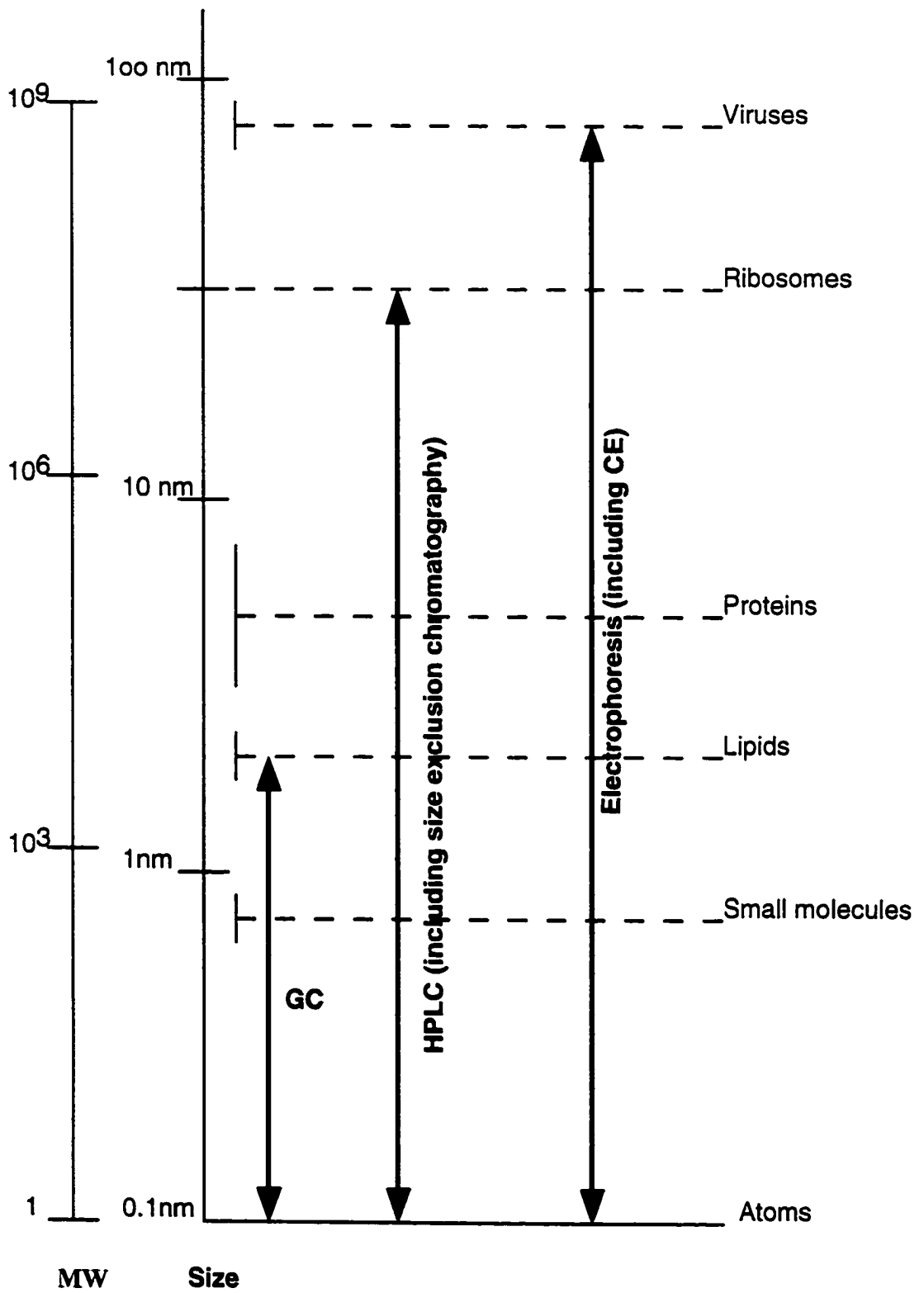
- Migration times often predicted by structure.
- Large selection of CE modes and buffer modifiers.
- Ease of switching among the different modes of CE.
- Very low sample consumption (nL).
- Very low cost of columns, reagents and operation.
- Very low sample waste.
- Versatility

Because of the above mentioned advantages, CE is used for the separation of many different classes of compounds; including proteins, nucleic acids, carbohydrates, lipids and cell organelles. Figure 1.13 compares chromatographic techniques with CE in terms of molecular weight and size of the species that can be separated by that technique. CE is a rapidly growing separation technique. One of its greatest advantages is its diverse application range. Originally considered primarily for the analysis of biological macromolecules, it has proven useful for separations of compounds such as amino acids, chiral drugs, vitamins, pesticides, inorganic ions, organic acids, dyes, surfactants, peptides and proteins, carbohydrates, oligonucleotides and DNA restriction fragments, and even whole cells and virus particles.

The mechanisms responsible for separation in CE are different from those in chromatography, and thus can offer orthogonal, complementary analysis. In addition, CE may offer simpler method development, minimal sample volume requirements, and lack of organic waste.

While numerous advances are being made in CE, the technique is still in a development and growth stage. Incumbent with new technology is a lag time between

**Figure 1.13: Range of separation techniques for particles with different sizes**



published results generated by researchers developing the technique and the formation of a workable knowledge base for the user. Scientists should be aware that CE is not totally mature, relative to HPLC for example. This implies, for example, that methods may need to be developed and optimized for each application by the user.

In different chapters of this thesis, we will see some practical applications of capillary electrophoresis showing the diversity of CE applications.

## **1.6 Thesis overview**

It was the object of the author's research to develop a high-sensitive method to measure natural toxins in water (microcystins) using CE. The immunoassay technique was chosen because it was already used for this class of toxins that are liver carcinogens, but the classical immunoassay technique lacked sensitivity. The first step was to fluorescently label the analyte, called antigen in immunoassay, and this labeling process involved studying amine labeling chemistry, developing carboxylic acid labeling, and finally synthesizing an arginine-specific labeling reagent. The labeling chemistry and synthesis are presented in Chapters 6 and 7.

This thesis is divided onto two volumes or three parts. In volume one and part one, building the instrument and evaluating the injection techniques are presented. Because of very low concentration of analyte and because of bias in electrokinetic injection, different injection methods were studied. Finally, sample depletion in electrokinetic injection was studied to evaluate the effect of multiple injections on the original concentration of the analyte. Part one includes three chapters: Chapters 1, 2, and 3.

In Chapter 2 of the volume 1, the CE-LIF instrument and performance optimization of this miniaturized CE is shown. Different injection techniques in CE are discussed and experimental results show the high sensitivity of the CE-LIF method. The limit of detection of 150 fluorescein molecules is presented. It is shown that the major contribution to the

background noise comes from the laser and not from the room light when a light shield is designed for the instrument.

In Chapter 3 sample depletion in electrokinetic injection is presented. There are several techniques to introduce the sample onto the capillary. The most common one is electrokinetic injection that is biased and components with higher mobility are differentially injected onto the capillary. The analyte concentration changes with subsequent injections.

The microcystin antibody is a huge protein which adsorbs significantly to the capillary wall and, hence, obscures the separation. This problem is addressed in part two of the thesis. To combat the adsorption, a capillary was coated with a hydrophilic polymer to minimize the adsorption. To evaluate the efficiency of the surface coverage, a reliable method for EOF measurement was developed and used as a criterion to evaluate the effectiveness of surface coverage. Part two includes Chapters 4 and 5.

In Chapter 4, a method is presented for EOF measurement in the case that the instrument does not have a UV detector as is the case for CE-LIF. The method validation is shown and statistical data analysis shows that this new method is as precise as the neutral marker injection method for EOF measurement. Basic principles of CE were investigated including the effect of pH, ionic strength, temperature and electric field on EOF.

Coating the capillary inner surface with a polymer to eliminate EOF is presented in Chapter 5. A series of polymers from the most hydrophobic to the most hydrophilic one are compared to find which polymer shows the lowest EOF and minimum adsorption of proteins and Ab to the capillary wall.

Having gained experience in introducing the sample effectively onto the capillary and preventing the sample loss by adsorption, the third part of the thesis in volume 2 involved fluorescently labeling the analyte in order to be able to detect it. This part includes Chapters 6, 7, and 8.



Labeling chemistry for CE-LIF Immunoassay of carboxylic acid labeling is presented in Chapter 6. Despite being optimized by the author, amine labeling chemistry with FQ fluorogenic dye is not discussed because it is widely used in CE and the analytes of interest lack an amine group. Microcystin lacks an amine group, but it has two carboxylic acid groups and one arginine group. Carboxylic acid labeling chemistry is discussed in Chapter 6.

Microgram-scale organic synthesis of an arginine-specific reagent is shown in Chapter 7. Microcystin contains an arginine group. In this chapter an optimized procedure to label the arginine group is presented. Because the sample quantity is very limited, the synthesis approach was developed in a way to reduce the weight of the starting material to a microgram to reduce the reagent consumption.

In Chapter 8 different immunoassay techniques are discussed and displacement immunoassay of explosive compounds are presented in order to have another example for environmental samples.

Finally, the conclusions and future work are presented in Chapter 9.

## 1.7: References

1. Overbeek, J. T. G., and Bijsterbosch, B. H., *Electrokinetic Separation Methods*: Righetti, P. G., Oss, C. J. V., Vanderhoff, J. W., Eds.; Elsevier/North Holland Biomedical Press, pp 1-32, 1979.
2. Vesterberg, O., *J. Chromatogr.*, 480, 1, 1989.
3. Kohlrauch, F., *Wiedemanns Ann. (Ann. Phys. Leipzig)*, 62, 1887.
4. Michaelis, L., *Biochem. Z* 16, 81, 1909.
5. Tiselius, A., *Transactions of the Faraday Society* 33, 524, 1937.
6. Raymond, S. and Weintraub, L., *Science*, 130, 711, 1959.
7. Landers J. P., *Handbook of Capillary Electrophoresis*, 2<sup>nd</sup> Ed., CRC Press Inc., 1997.
8. Dale, G., and Latner, A. L., *Clin. Chem. Acta*, 24, 61, 1969.
9. Hjerten, S., *Chromatogr Rev.*, 9, 122-219, 1967.
10. Virtanen, R., *Acta Polytechnica Scand.*, 123, 1, 1974.
11. Jorgenson, J. W. and Lukacs, K.D., *Anal. Chem.*, 53, 1298, 1981.
12. Heiger, D. N., *High Performance Capillary Electrophoresis - An Introduction*, 2<sup>nd</sup> edition, Hewlett-Packard Company, 1992.
13. Terabe, S., Otsuka, K., Ichikawa, K., Tsuchiya, A., and Ando, T., *Anal. Chem.* 56, 111, 1984.
14. Terabe, S., Otsuka, K., and Ando, T., *Anal. Chem.*, 57, 834, 1984.
15. Vindevogel, J., and Sandra, P., *Introduction to Micellar Electrokinetic Chromatography*, Huthig 1992.
16. Stevens, T. S. and Corets, H. J., *Anal. Chem.*, 55, 1365, 1983.
17. Stenberg, J. C., *Adv. Chromatogr.*, 2, 206, 1966.
18. Huang, X., Coleman, W. F., and Zare, R. N., *J. Chromatogr.*, 480, 95, 1989.
19. Grossman, P. D., and Colburn, J. C., *Capillary Electrophoresis, theory and practice*, Academic Press Inc. New York 1992.

20. Hjerten, S., and Palm, A., *Acta Universitatis Upsaliensis* 1996.
21. Hjerten, S., *Electrophoresis*, 11, 665-690, 1990.
22. Hjerten, S., Valtcheva, L., Elenbring, K., and Liao, J. L., *Electrophoresis*, 16, 584. 1995.
23. Heiger, D. N., *High Performance Capillary Electrophoresis- An Introduction*, 2<sup>nd</sup> Ed., Hewlett-Packard p29, 1992.
24. McCormik, R. M., *Anal. Chem.*, 60, 2322-2328, 1988.
25. Schomburg, G., Belder, D., Gilges, M., and Motsch, S. J., *Cap. Elec.* 1, 219-230. 1994.
26. Hjerten, S., *J. Chromatogr.*, 347, 191-198, 1985.
27. Zhao, Z., Malik, A., and Lee, M. L., *Anal. Chem.*, 65, 2742-2752, 1985.
28. Hjerten, S., and Kubo, K., *Electrophoresis*, 14, 390-395, 1993.
29. Grossman, P. D., and Colburn, J. C., *Capillary Electrophoresis, theory and practice*. Academic Press Inc., New York 1992.
30. Vindevogel, J., Schuddink, G., Dewaele, C., and Verzele, M., *J. High Resolut. Chromatogr. Chromatogr. Commun.*, 11, 317, 1988.
31. Albin, M., Weinberger, R., Sapp, E., Moring, S., *Anal. Chem.*, 63, 417, 1991.
32. Wu, S., Dovichi, N. J., *J. Chromatogr.*, 480, 141, 1989.
33. Horrocks, D. L., Studier, M. H. *Anal. Chem.*, 1782, 1966.
34. Willard, Merritt, Dean, Settle, and Litton, *Instrumental Methods of Analysis*, 6<sup>th</sup> Ed., Educational Publishing, Inc., 1981.
35. Dovichi, N. J., Martin, J. C., Jett, J. H., Trkula, M., Keller, R. A., *Anal. Chem.* 56. 348, 1984.
36. Gassman, E., Kuo, J. E., and Zare, R. N., *Science*, 230, 813, 1985.
37. Lycons, J. W., and Faulkner, L. R., *Anal. Chem.*, 54, 1060, 1982.
38. Lynos, J. W., Faulkner, L.R., *Anal. Chem.*, 54, 1960, 1982.

39. Zarrin, F., Dovichi, N. J., *Anal. Chem.*, 57, 1826, 1985.
40. Zarrin, F., Risfelt, J. A., Dovichi, N. J., *Anal. Chem.*, 59, 850, 1987.
41. Zarrin, F., Bornhop, D.J., Dovichi, N. J., *Anal. Chem.*, 59, 854, 1987.
42. Cheng, Y. F. and Dovichi, N. J., *Science*, 242, 562, 1988.
43. Cheng Y. F., Wu S., Chen D. Y., and Dovichi N. J., *Anal. Chem.*, 62, 496, 1990.
44. Swerdlow, H., Zhang, J. Z., Chen, D. Y., Harke, H. R., Wu, S., Fuller, C., and Dovichi, N. J., *Anal. Chem.*, 63, 2835, 1991.
45. Wu, S., and Dovichi, N. J., *Talanta*, 39, 173, 1992.
46. Chen, D. Y., Swerdlow, H. P., Harke, H. R., Zhang, J. Z., and Dovichi, N. J., *J. Chromatogr.*, 559, 237, 1991.
47. Zhang, J. Z., Chen, D. Y., Wu, S., Harke, H. R., and Dovichi, N. J., *Clin. Chem.*, 37, 1492, 1991.
48. Camilleri, P., *Capillary Electrophoresis, Theory and Practice*, Chapter 2, 25-64, CRC Press Inc., 1993.
49. Novotny, M., *Anal. Chem.*, 60, 500A, 1988.
50. Haugland, R. P., *Handbook of Fluorescent Probes and Research Chemicals, Molecular Probes*, Eugene, OR, 1989.
51. Liu, J., Hsieh, Y. Z., Wiesler, D., and Novotny, M., *Anal. Chem.*, 63, 408, 1991.
52. Camilleri, P., *Capillary Electrophoresis, Theory and Practice*, Chapter 8, 311-370, CRC Press Inc., 1993.
53. Zhao, J. Y., Waldron, K. C., Miller, J. Z., Harke, H. R., and Dovichi, N. J., *J. Chromatogr.*, 1993.
54. Tsuda, T., Kobayashi, Y., Hori, A., Matsumoto, T., and Suzuki, O., *J. Chromatogr.*, 456, 375, 1988.
55. Roze, D. J. and Jorgenson, J. W., *J. Chromatogr.*, 447, 117, 1988.

56. Pentoney, S. L., Huang, X., Burgi, D. S., and Zare, R. N., *Anal. Chem.*, 60, 2625. 1988.

# Chapter 2

## Performance optimization of a miniaturized CE-LIF system<sup>1</sup>

---

<sup>1</sup> Part of the results of this chapter is under preparation for a publication in collaboration with D. Lewis and E. Arriaga who have designed the electronics of the DRES instrument.

## **2.1 Introduction**

### **2.1.1 A sheath flow cuvette with Laser Induced Fluorescence (LIF) detection for capillary electrophoresis**

Since 1984, Dr Dovichi's research group has been using LIF detection for charged molecules using the sheath flow cuvette. The reported detection limit was approaching single molecule levels. Their limit of detection at two times signal-to-background noise ratio was  $8.9 \times 10^{-14}$  M solution of rhodamine-6G.<sup>1</sup>

Figure 2.1 shows the schematic diagram of a CE instrument with a sheath flow cuvette and LIF detection. The instrument components are a high-voltage power supply (0 to 30 kV), a capillary which is usually made of fused-silica with an ID < 50  $\mu$ m and a length of 20-50 cm, one buffer reservoir that can accommodate the electrode connected to the power supply and a PMT detector. The sheath flow cuvette that is connected to a waste reservoir acts as the ground electrode.

LIF produces remarkable improvement in detection limit compared with the use of conventional incoherent sources. In 1985, Zare's group reported the first application of lasers for fluorescence detection in CE.<sup>2</sup> They used a 5-mW helium-cadmium laser that produced an excitation beam with 325 nm wavelength. The fluorescence from the sample was collected with optical fibers. After being spectrally filtered, the fluorescence was detected with a photomultiplier tube. They reported the detection of femtomole amounts of dansyl-amino acids with their LIF detection system.

The major problem for on-column fluorescence detection is a relatively large amount of light scattering that is generated by reflection and refraction at the capillary walls. The result is a high background signal, and therefore, a relatively poor detection.<sup>3</sup> Fluorescence should be, ideally, measured in a flow chamber with good optical quality. Flat windows are required to eliminate or reduce the light scattering. It is possible to use a

square capillary for electrophoresis, but it is not possible to manufacture long pieces of small dimension capillaries with flat windows. Instead, it is a better option to use a post-column fluorescence chamber to achieve extremely high-sensitivity fluorescence detection.

### **2.1.1a) The sheath flow cuvette**

Figure 2.1b shows a schematic diagram of a sheath flow cuvette. The cuvette is a 200- $\mu\text{m}$  square chamber that holds the capillary in its center. The sheath flow buffer enters from the top of the cuvette and exits from the bottom part of the cuvette to the waste reservoir. When the sample exits out of the capillary, it enters into the center of this sheath flow cuvette, and produces a stream under laminar conditions. This sample stream that migrates out of the capillary is surrounded by the flowing sheath stream.

Sheath flow cuvettes use a square flow chamber with flat windows of good optical quality. The flow chamber is made of optically flat quartz, with 2-mm thick windows, and has a 200- $\mu\text{m}$  square hole in the center. The square flow chamber and flat windows minimize the scattering of excitation light into the emission optics in a fluorescence experiment.<sup>4</sup> Most importantly, since the sheath flow buffer and CE run buffer are exactly the same buffer with similar concentration, they have the same refractive index. Therefore, the excitation beam is not scattered at the interface of the sample and sheath flow streams. A spatial filter is located in the emission optical path of the fluorescence detector. This filter reduces the small amount of scatter light generated by the cuvette windows.

The cuvette used for a sheath flow system has three main advantages as a detector cell. The first advantage is that very small detection volume can be easily obtained. This small detection volume minimizes the detector dead volume and, therefore, extra column band broadening is reduced in capillary electrophoresis with a sheath flow cuvette detector. The second advantage is that the sample stream never contacts the cuvette windows which



prevents contamination of the windows. The third advantage of a sheath flow cuvette is that the light scattered due to the cell window can be easily eliminated because the sample stream is located far away from the windows. Using the sheath flow design, not only the separation efficiency is not lost and very high separation sensitivity is gained.

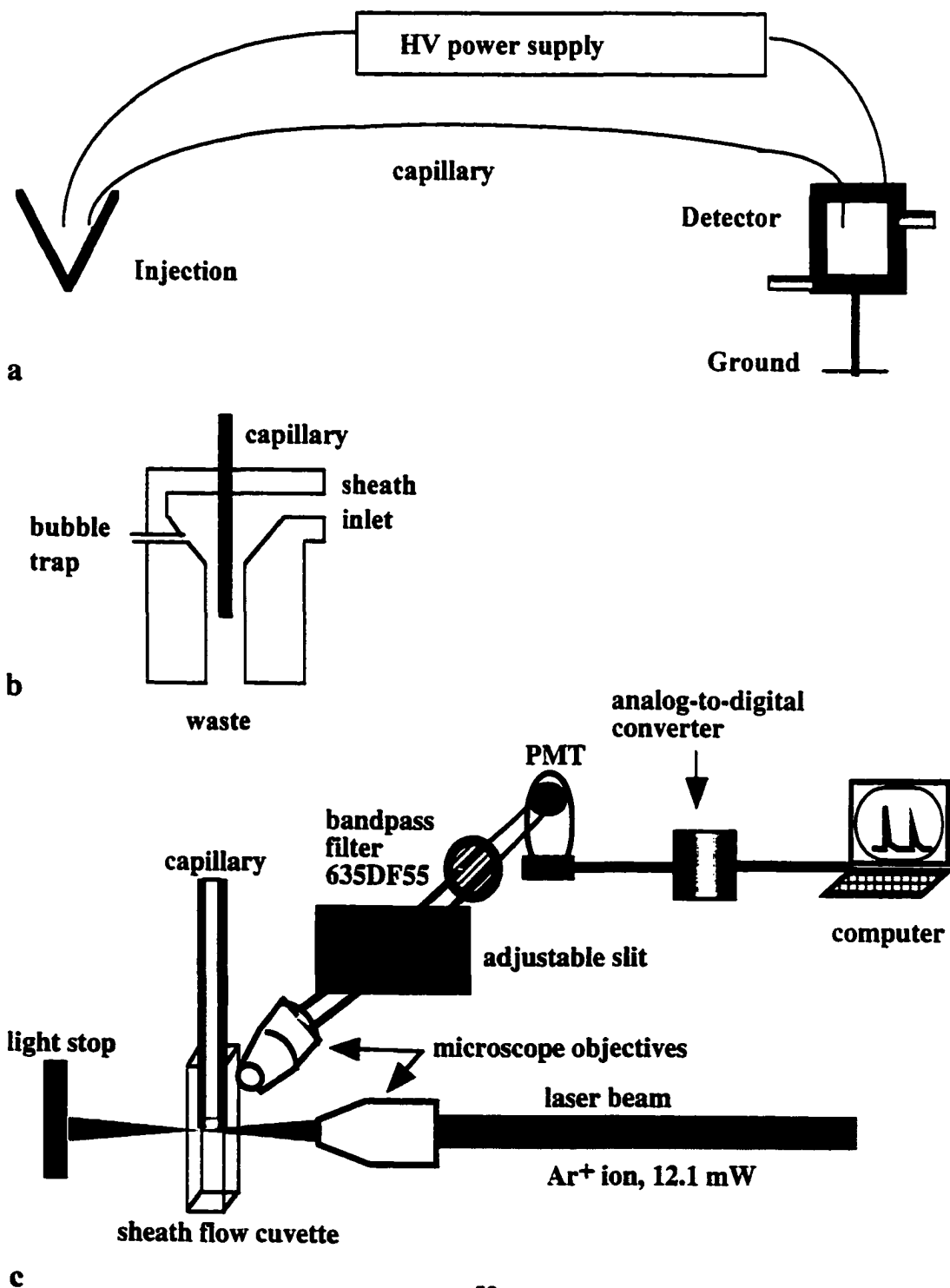
Dead volume in the tubing, used to transfer the sample from the capillary to the detection end, is the major source of band broadening for a post-column detector. Much care is needed to design such a post-column detector with no extra-column band broadening. Our group has developed such a post-column fluorescence detector based on the sheath flow cuvette with minimized band broadening (Figure 2.1c).<sup>5-11</sup>

Sheath fluid, having the same composition as the separation buffer, is introduced onto the cuvette at a flow rate of a few microliters per hour. The flow can be provided by a high-precision syringe pump; instead, we are using a very simple alternative by generating a siphon while holding the sheath fluid in a vial that is raised a few centimeters above the waste collection vial. Under the very low flow rate produced by electroosmosis, the sample stream travels as an approximately 10- $\mu\text{m}$  diameter stream through the center of the cuvette.

### **2.1.1b) LIF detection**

The fluorescence excitation source is a low-power laser beam focused to a 10- $\mu\text{m}$  spot about 200  $\mu\text{m}$  downstream from the capillary exit. Fluorescence is collected at right angles to both the sample stream and laser beam with a microscope objective. Spectral filters are used to eliminate the scattered laser light. A 200- $\mu\text{m}$  radius pinhole is located in the reticle position of the microscope objective to restrict the scattered light from the illuminated sample stream to reach the photomultiplier tube (PMT) as a detector. If single

**Figure 2.1: Schematic diagram of a) CE instrument with b) a sheath flow cuvette and c) LIF detection**



molecule detection is the goal, the PMT is cooled to  $-15\text{ }^{\circ}\text{C}$  to minimize detector dark current. The choice of a laser depends on the spectral properties of the analyte. In general, lower background signals are observed for long-wavelength excitation because the Raman scattering decreases at longer wavelengths. The decreased background signal is roughly proportional to  $\lambda^{-4}$ , where  $\lambda$  is the laser excitation wavelength. Also, there are relatively few impurity molecules that absorb long-wavelength light to generate background fluorescence signals. Longer wavelength excitation sources have another advantage. The longer excitation wavelength provides smaller excitation energy and this can reduce photobleaching of the analyte under the intense laser beam. Photobleaching is the fundamental limit of fluorescence detection.<sup>9</sup>

### **2.1.1c) Application of a sheath flow cuvette with LIF detection**

Dovich and Zarrin applied this cuvette for particle size analysis in 1985.<sup>12-14</sup> In this application, the cuvette was used as a light scattering detector to count individual particles that were eluted out of a capillary column hydrodynamic chromatograph. The elution order was based on the particle size. Concentration detection limits were about 1000 particles / mL. Particles as small as 45 nm radius were detected with a right angle collection geometry. Since 1986, this detector has been used routinely in Dr. Dovich's laboratory for high sensitivity fluorescence detection. A high sensitivity LIF detection system with a sheath flow cuvette has many applications in biological analysis. For example, in DNA sequencing, the total amount of sequencing sample introduced onto the capillary is about 1 amol. The amount of each fragment averages perhaps 1 zeptomole.<sup>15</sup>

### **2.1.2 Sample introduction in capillary electrophoresis**

In capillary electrophoresis the dimensions of the capillaries are so small that the total capillary volume is typically in the microliter range. See Table 2.1 for a list of capillary

**Table 2.1: A comparison of surface-to-volume ratio for a 50 cm long capillary having varied ID**

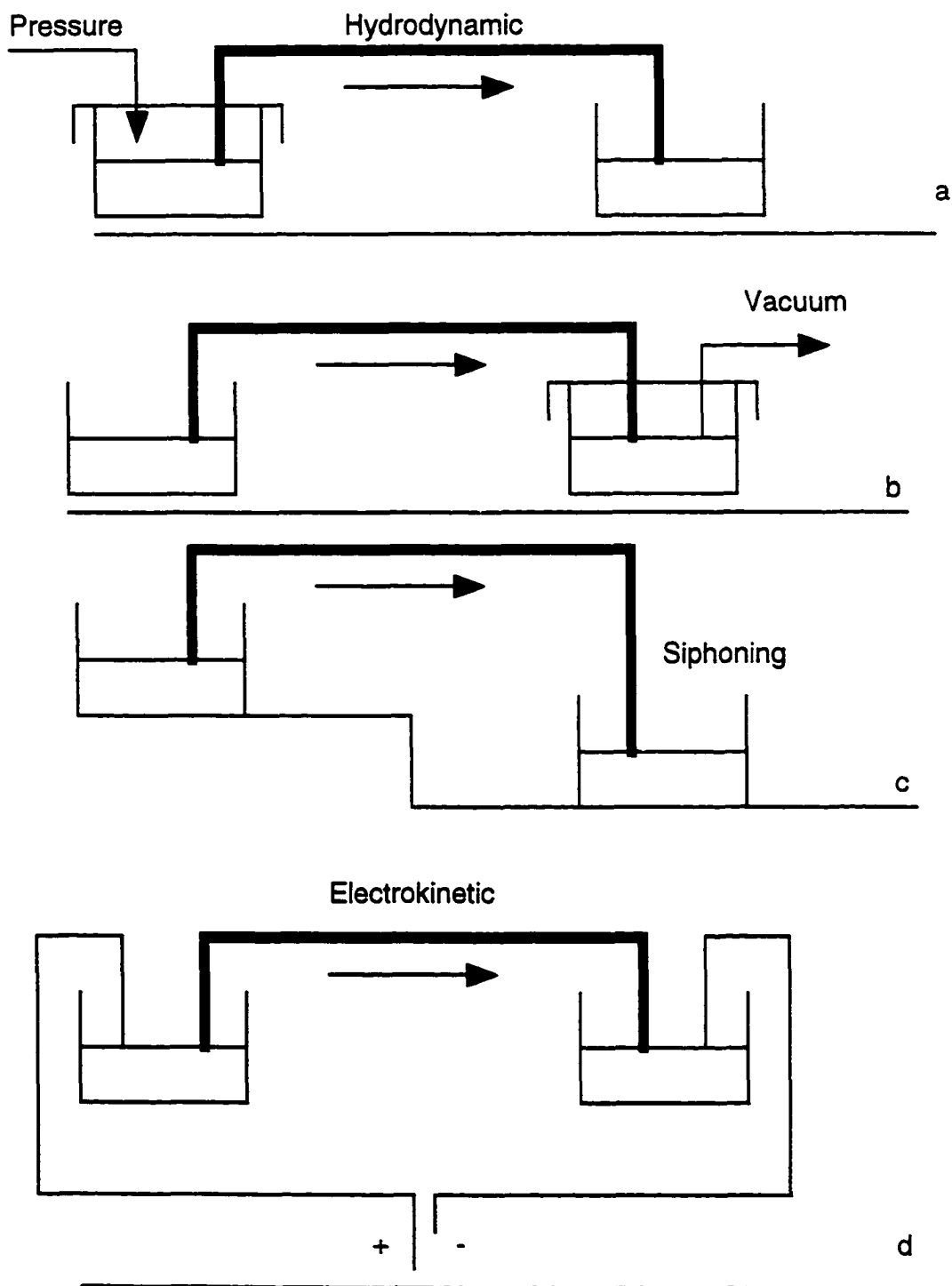
<b>Capillary ID (<math>\mu\text{m}</math>)</b>	<b>Surface area (<math>\text{mm}^2</math>)</b>	<b>Volume (<math>\mu\text{L}</math>)</b>	<b>Surface-to-volume Ratio (<math>\text{mm}^{-1}</math>)</b>
200	314	15.71	20
100	157	3.92	40
75	117.75	2.21	53
50	78.5	0.99	80
20	31.4	0.16	200
10	15.7	0.04	400

volumes and surface-to-volume ratios.

If overloading is to be avoided, the sample volume should be 1-5% of the total capillary volume, i.e. sample volumes must be in the nanoliter range.<sup>16</sup> There are four accepted methods for small sample volume introduction onto a capillary. Injection of the sample onto the capillary can be accomplished by vacuum, gravity or by applying high voltage (electrokinetic injection). For the first two cases, the sample is introduced by immersing the capillary inlet into a vial containing the sample and either pressurizing the inlet vial containing the sample (pressure injection) or applying a vacuum to the outlet vial (vacuum injection). Gravity injection is more commonly used with non-commercial systems.<sup>17-18</sup> This method relies on the siphoning of sample onto the capillary by elevating the injection end of the capillary relative to the outlet end. For electrokinetic injection, the injection end of the capillary is immersed into the sample vial and the outlet in the separation buffer (sheath flow buffer for in-house instrument). A low voltage (1-10 kV) is applied for a duration of 1 to 99 seconds depending on the capillary length and ID.<sup>19</sup> Figure 2.2 depicts different techniques of sample introduction onto a capillary.

In electrokinetic injection, the quantity of sample introduced onto the capillary depends on a number of parameters. The most important of these parameters are electrophoretic mobilities of the sample components and the electroosmotic flow rate (EOF). EOF is defined as bulk flow of a liquid inside the capillary. For a discussion of EOF, you may refer to chapter 1 and/or chapter 4 of this thesis. Other parameters that can affect this mode of injection include the buffer type, ionic strength, pH and the composition of the sample matrix. The electrokinetic mode is a biased sample introduction; sample components with the highest electrophoretic mobility will be preferentially injected. In contrast, electrokinetic injection may be advantageous if the concentration of the analyte is a small percentage of the sample, but the analyte of interest has a much higher electrophoretic

**Figure 2.2: Schematic diagram of a) pressure, b) vacuum, c) gravity, and d) electrokinetic injection techniques in CE**



mobility than those of other constituents. Under these conditions, electrokinetic injection provides a positive sample loading bias and may enhance the sensitivity of the analysis. The other situation where electrokinetic injection is advantageous is the case of capillary gel electrophoresis (CGE). In CGE, the capillary contains a polymerized or cross-linked matrix and pressure injection may damage the gel or extrude the gel out of the capillary. For example, DNA or SDS-protein complexes are introduced electrokinetically onto the capillary to do CGE. Sample matrices containing significant concentrations of electrolyte are not efficiently introduced by electrokinetic injection. Shihabi has discussed in detail the problems associated with high-salt sample matrices and approaches to manipulating the matrix for satisfactorily CE analysis.<sup>20</sup>

The objectives of this chapter are performance optimization and characterization of a miniaturized CELIF system constructed in our laboratory for the Defense Research and Establishment at Suffield (DRES). There is a trend in analytical instrumentation design towards mobile instruments.<sup>21</sup> The ultimate goal is to design a portable instrument to do the analysis on site to avoid sample degradation.

In this chapter, I compare different injection modes. In the next chapter, bias in electrokinetic injection will be presented. Despite being biased, electrokinetic injection was used to introduce the analyte onto the capillary in most chapters of this thesis because of its simplicity and its high precision.

### **2.1.3 Contribution of injection volume on band broadening in CE**

If the injection is the major source of band broadening, the total peak variance ( $\sigma_{\text{total}}^2$ ) can be written as:

$$\sigma_{\text{total}}^2 = \sigma_{\text{other}}^2 + \sigma_{\text{inj}}^2 = \sigma_{\text{other}}^2 + l_{\text{inj}}^2/12 \quad (2.1)$$

where  $\sigma_{\text{other}}^2$  is due to all the possible sources of band broadening,  $\sigma_{\text{inj}}^2$  is the variance due to injection and  $l$  is the injection length.

Accepting 10% loss in plate count from injection, for a 50 cm capillary with a modest theoretical plate number  $N = 100,000$ , the length of the injection plug is limited to less than 1.8 mm. For a 50  $\mu\text{m}$  ID capillary, this plug volume is only 3.6 nL. With shorter and smaller columns the allowed injection volume drops rapidly into the picoliter range with plug lengths of less than 1 mm. Microsyringes have been used to deliver small volumes of a sample solution onto a capillary.<sup>22</sup> Using a split-flow technique, nanoliter injections onto 75  $\mu\text{m}$  ID capillaries have been demonstrated with a microsyringe and a piece of split vent capillary tubing.<sup>23</sup> In the majority of cases, two injection techniques that are typical for CE are electrokinetic injection and hydrodynamic injection<sup>22</sup>. A plug-like injection profile is obtained by inserting the capillary in the sample solution and applying a high voltage for a controlled length of time, but pressure injection gives a parabolic flow profile.

In the experimental section of this chapter, electrokinetic injection, vacuum injection, and pressure injection for a miniaturized CELIF system will be studied.

#### **2.1.4 Electrokinetic injection**

Despite being biased for the analytes with higher mobility, electrokinetic injection is the most widely used injection mode of CE. The sample is dissolved in a buffer solution and then introduced onto the capillary by applying a low potential across the capillary for a short period of time. The injection voltage and time are controlled easily by a computer program.

When a voltage is applied, components with different charges (e.g. cations, neutrals, anions) or with different sizes will migrate according to their velocities onto the



capillary. Analytes with higher electrophoretic mobilities move faster and thus are injected to a greater extent than slower moving analytes. The injection volume of individual component can be calculated if the ionic strength of the sample and separation buffer are equal. The following equation is used to calculate the injection volume:

$$V_{inj} = V_{cap} (t_{mig} / t_{inj}) (E_{inj} / E_{CE}) \quad (2.2)$$

where  $V_{inj}$  is the corrected injection volume of a specific component in the sample solution.  $V_{cap}$  is the volume of the capillary ( $\pi r^2 L$ ),  $t_{mig}$  is the migration time of the component,  $t_{inj}$  is the electrokinetic injection time,  $E_{inj}$  is the electrokinetic injection voltage, and  $E_{CE}$  is the high voltage applied for capillary electrophoresis.<sup>24</sup>

### 2.1.5 Hydrodynamic injection

Hydrodynamic injection is done by lifting the sample vial with the injection end of the capillary for a period of time to a certain height above the waste reservoir level at the detection end of the capillary. This method is also known as hydrostatic or siphoning injection. A narrow zone of the sample solution flows onto the injection end of the capillary due to gravity. The siphoning injection can be performed manually or automatically. Manual siphoning injection gives very poor reproducibility unless the injection time is long enough. Precision of a few percent or less can be achieved by automated hydrodynamic injection.<sup>25, 26</sup>

The volume of the sample solution injected hydrodynamically can be calculated by the following equation:

$$V_{inj} = (\pi r_{cap}^4 \rho g \Delta h t_{inj}) / (8 \eta L) \quad (2.3)$$

where  $r_{\text{cap}}$  is the radius of the capillary,  $\rho$  is the density of the liquid inside the capillary,  $g$  is the gravity constant ( $9.8 \text{ m/s}^2$ ),  $\Delta h$  is the height difference between the two ends of the capillary,  $t_{\text{inj}}$  is the injection time,  $\eta$  is the viscosity of the sample solution and  $L$  is the total length of the capillary.<sup>27</sup> In hydrodynamic injection there is no discrimination against components with different electrophoretic mobilities and the injected volume is the same for all components in the bulk sample solution. However, hydrodynamic injection cannot be used for gel-filled columns as the required pressure would disrupt the gel in the column.

D. Y. Chen introduced a hydrodynamic injector with a three-way electronically actuated valve.<sup>27</sup> Using this injector, he obtained an injection volume precision of about 2.5%.

For low flow rates and a pressure-induced flow of a liquid in an open tube, the flow profile is laminar and the average flow velocity is described by the Poiseuille's equation<sup>27</sup>:

$$U^* = (\Delta P r_{\text{cap}}^2) / (8 \eta L) \quad (2.4)$$

where  $U^*$  is the average linear velocity of the liquid through the capillary.  $U^*$  is obtained by integrating the linear velocity in the cross section of the tube dividing by the capillary cross sectional area. The injection volume can be calculated by equation 2.3.

When electrokinetic injection is used, it is necessary to balance the liquid levels in injection vial and waste reservoir to avoid supplementary siphoning effects during the injection. Hydrodynamic flow introduces laminar flow that causes extra-column band broadening.

The length of the injection plug is determined by the product of the driving force (voltage or pressure) and the injection time (Figure 2.3). Electronic control of the injection time and automation are decisive in obtaining good reproducibility.<sup>25, 29-30</sup> Siphoning is more reproducible than electrokinetic injection.<sup>25, 28</sup> Almost any application of the voltage or pressure will show some inertia (Figure 2.3): lifting time of the injection vial, initial ramp when applying voltage for electrokinetic injection and building up of pressure for pressure injection.<sup>29</sup> Therefore, for a constant product of force and time, injected quantities may differ from one injection to the other. Variations in injection volume can also be minimized by selecting a relatively low voltage or low pressure with a corresponding longer injection time and computer controlled correction for the lifting time of the sample vial and initial ramp when applying a high voltage or pressure.<sup>30, 31</sup>

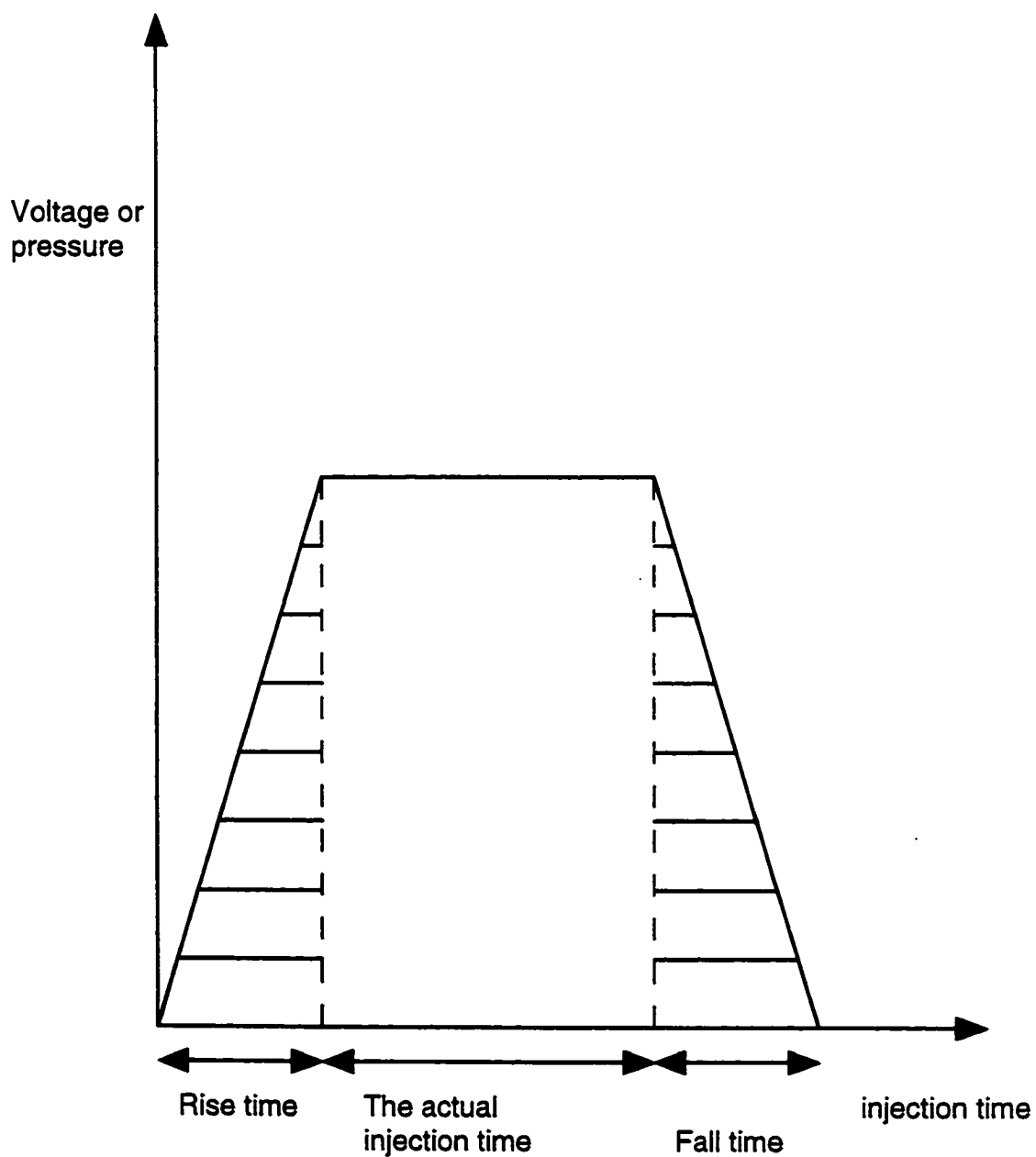
### 2.1.6 Limit of Detection (LOD)

LOD is defined as the minimum amount of an analyte that gives a signal three times higher than the standard deviation of the blank signal. The background noise can be measured by recording the blank electropherogram and determining the standard deviation. LOD in CE may be more conveniently calculated by Knoll's method which is used in chromatography.<sup>32, 33</sup> The electropherogram for the baseline is recorded over a time period that is 10-100 times the full peak-width in terms of time at one-half peak height ( $W_{1/2}$ ). The maximum deviation ( $h_n$ ) from the average baseline is used to estimate the  $3\sigma$  detection limit:

$$C_{\text{LOD}} = K_{\text{LOD}} h_n C_s / h_s \quad (2.5)$$

where  $C_{\text{LOD}}$  is the concentration limit of detection,  $C_s$  is the amount of analyte injected and  $h_s$  is the analyte peak height and  $h_n$  is the maximum noise fluctuation in the background signal.  $K_{\text{LOD}}$  is a constant that is determined for the time period that is a multiple of the

**Figure 2.3: Plug-like injection by applying voltage or a pressure difference. The dashed area cause error in calculating the amount of sample injected**



analyte's peak width at half-maximum ( $W_{1/2}$ ). The largest noise fluctuation is also measured in an interval that is the same multiple of  $W_{1/2}$  as the  $K_{LOD}$  multiplier. Values of  $K_{LOD}$  for different multiplier of  $W_{1/2}$  are listed in table 2.2.<sup>32</sup>

The assumptions on the underlying noise distribution in the data are very weak. Most importantly, correlation between adjacent data points due to filtering underestimate the standard deviation of the baseline.

The peak height and the maximum deviation are obtained from the electropherogram of a very dilute sample ( $C_S$ ) and then the LOD is calculated. The number of moles of analyte corresponding to the LOD can be calculated.

The injected volume is calculated using the equation 2.2 and then the number of moles injected,  $n_{inj}$ , is estimated by:

$$n_{inj} = C_S V_{inj} \quad (2.6)$$

The limit of detection in terms of mass of analyte injected,  $n_{LOD}$ , is given by:

$$n_{LOD} = K_{LOD} n_{inj} (h_n / h_S) \quad (2.7)$$

## 2.2 Experimental

### 2.2.1 Instrument design and improvement

Figure 2.4 shows the top-view of a miniaturized CE-LIF instrument that was assembled for the Defense Research and Establishment at Suffield (DRES). The instrument used a 0-30 kV dc power supply (CZE1000, Spellman, Plainview, NY). For the sheath flow cuvette detector, excitation was provided by the 488-nm line of an argon ion laser

**Table 2.2: Multiplier constants for LOD of Knoll's method<sup>12</sup>**

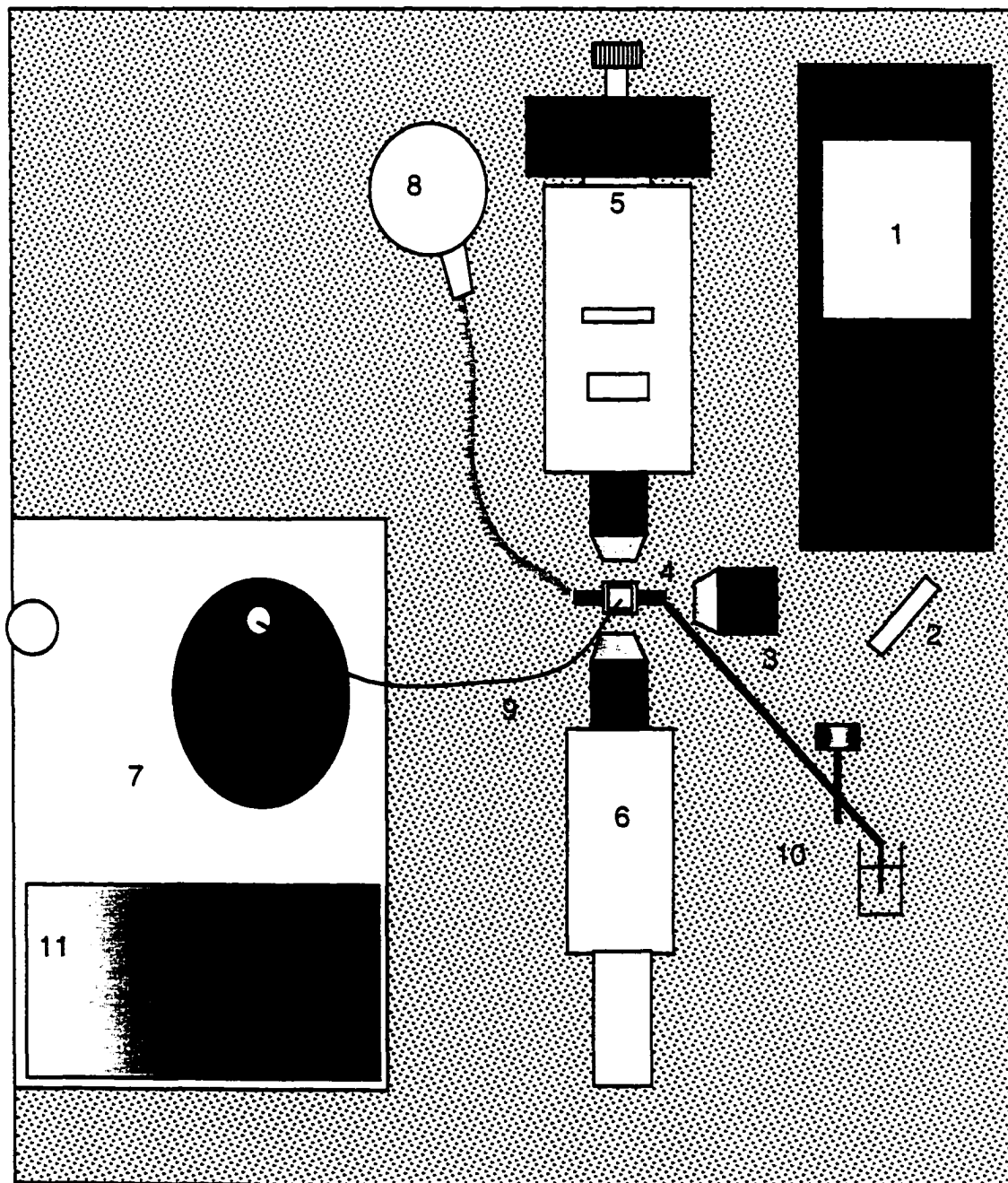
---

<b>Peak width multiplier</b>	<b>10</b>	<b>20</b>	<b>50</b>	<b>100</b>
<b><math>K_{1,000}</math></b>	<b>1.9718</b>	<b>1.4309</b>	<b>0.9194</b>	<b>0.6536</b>

---

**Figure 2.4: Top view of a second generation CE-LIF instrument built for DRES.**

1. Laser, 2. Mirror, 3. Focusing mechanism, 4. Sheath flow cuvette,
5. Detector box, 6. Microscope, 7. Spectraphoresis, 8. Buffer reservoir,
9. Capillary, 10. Bubble trap, 11. Power supply



operated at 12.1 mW (Model 2211-15SL, Uniphase, San Jose, CA or Model Innova 90-4, Coherent, Mountain View, CA), which was focused  $\approx 30 \mu\text{m}$  from the tip of the capillary with a 6.3x objective (Melles Griot, Nepean, ON, Canada). Fluorescence was collected by a 60x, 0.7 NA microscope objective (MO-0060LWD, Universe Kokagu, Oyster Bay, NY) and filtered with a spatial filter to remove stray light. Either a 615DF45 or a 630DF30 bandpass spectral filter (Omega Optical, Brattleboro, VT) was used to remove scattered light and fluorescence was imaged onto a photomultiplier tube (R1477, Hamamatsu, Middlesex, NJ) biased at 1.0 kV. The photocurrent was passed through a low-pass filter (RC = 47 ms) and then digitized with a 16-bit data acquisition board (NB-MIO16XH-18, National Instrument, Austin, TX) connected to a Macintosh computer.

A first generation system was constructed by Edgar Arriaga of this group. To improve the instrument's performance, especially in summer when room temperature fluctuation is more significant, I replaced the detector box that was made of Delrin (a polymeric material) with one made of aluminum, which results in less temperature drift of the delicate optical alignment. Alignment drift using the aluminum detector box is expected to be ten times less than when using the Delrin detector box because temperature fluctuation will cause less expansion of the aluminum. After this modification, the instrument withstood larger temperature changes, which are likely to be found during field operation. The migration time RSD of the day to day reproducibility when  $10^{-10}$  M fluorescein solution was injected onto the capillary with the Delrin box was 10% while after replacing the detector box it was reduced to 1%.

Appendix 1 of this chapter lists step by step procedure to operate the DRES electrophoresis instrument. This appendix also explains how to align the optical parts of the instrument and how to perform a CE separation.



## **2.2.2 Methods and materials**

### **2.2.2.1 Reagents**

Sodium tetraborate (borax) and sodium dodecyl sulfate (SDS) were purchased from BDH (Toronto, ON, Canada). For most experiments the running buffer and sheath flow buffers were 2.5 mM borax (10 mM borate) and 5 mM SDS with pH of 9.2. A  $10^{-3}$ M Fluorescein stock solution in MeOH was prepared and all the standard solution was made by diluting the stock solution with 10 mM borate.

### **2.2.2.2 Methods**

For the vacuum injection, by applying vacuum at the detection end of a 40-cm long capillary, the sample was introduced onto the capillary. The sample was  $10^{-10}$  M fluorescein dissolved in 2.5 mM borax and 5 mM SDS. A 3 s vacuum injection was done onto a 40 cm long capillary. The applied voltage was 16 kV (400 V / cm). For electrokinetic injection the same capillary length and the same voltage as vacuum injection were used.

To evaluate the reproducibility of the electrokinetic injection, a  $10^{-10}$  M fluorescein solution in 2.5 mM borax and 5 mM SDS was prepared. After each injection, the fluorescein solution was changed to a fresh one to prevent sample depletion (see chapter 3 of this thesis for a discussion of sample depletion in electrokinetic injection). The injection conditions for electrokinetic injection was 5 s at 1000 V. The PMT voltage was biased to 1000 V and the laser power was adjusted to 12.1 mW. The capillary length and CE voltage were similar to vacuum injection, i.e. 40-cm long capillary and 400 V / cm electric field.

### **2.2.2.3 Vacuum Injector modification**

The injector, designed by D. Y. Chen, was constructed by connecting the inlet and

one outlet of a three-way electrically actuated valve (LFAA1200118H, The Lee Co.) between the end of the sheath flow cuvette and the waste reservoir of the CE-LIF.<sup>27</sup>

Figure 2.5 shows the schematic diagram of the commercial vacuum injector before modification. Before injection, the capillary was filled with run buffer solution and all tubing in the system was filled with sheath flow buffer solution. In all the experiments, run buffer solution and sheath flow buffer solution both were 10 mM borate and 5 mM SDS.

Initially there was no vacuum applied and the flow was from the sheath-flow buffer to the waste-reservoir buffer. During the injection, vacuum was applied on a closed-system waste reservoir. The flow, in this case, was both from sheath-flow buffer and sample vial to the waste buffer. Applying vacuum in this situation introduced the sample onto the capillary, but generated air bubbles because the vacuum was applied on the sheath-flow buffer. The air bubbles were visible inside the tubing after each injection and it was clear that the source of these bubbles were the vacuum applied on the sheath-flow buffer. The injection was not reproducible, mostly due to the siphoning effect.

The height of the liquid surfaces of the sample and waste reservoirs were carefully measured with a ruler and then set to the same level. The liquid level in the injector reservoir was set lower than the sheath flow buffer and waste reservoirs to form a height difference,  $\Delta h$ .

The commercial vacuum injector was modified using the same principle that D. Y. Chen introduced.<sup>27</sup>

I modified the system in a way that is shown in Figure 2.6. The cuvette had two side arms. One side arm delivered the sheath flow buffer into the cuvette and the second arm trapped bubbles (not shown in the figure). A three-way valve was placed in the input flow arm. During the injection (Figure 2.6c) the electric valve was closed in a way that there was no sheath-flow to the cuvette. Applying vacuum in this situation introduced the

**Figure 2.5: Schematic diagram of a commercial vacuum injector before modification. Flow direction is shown in bold.**

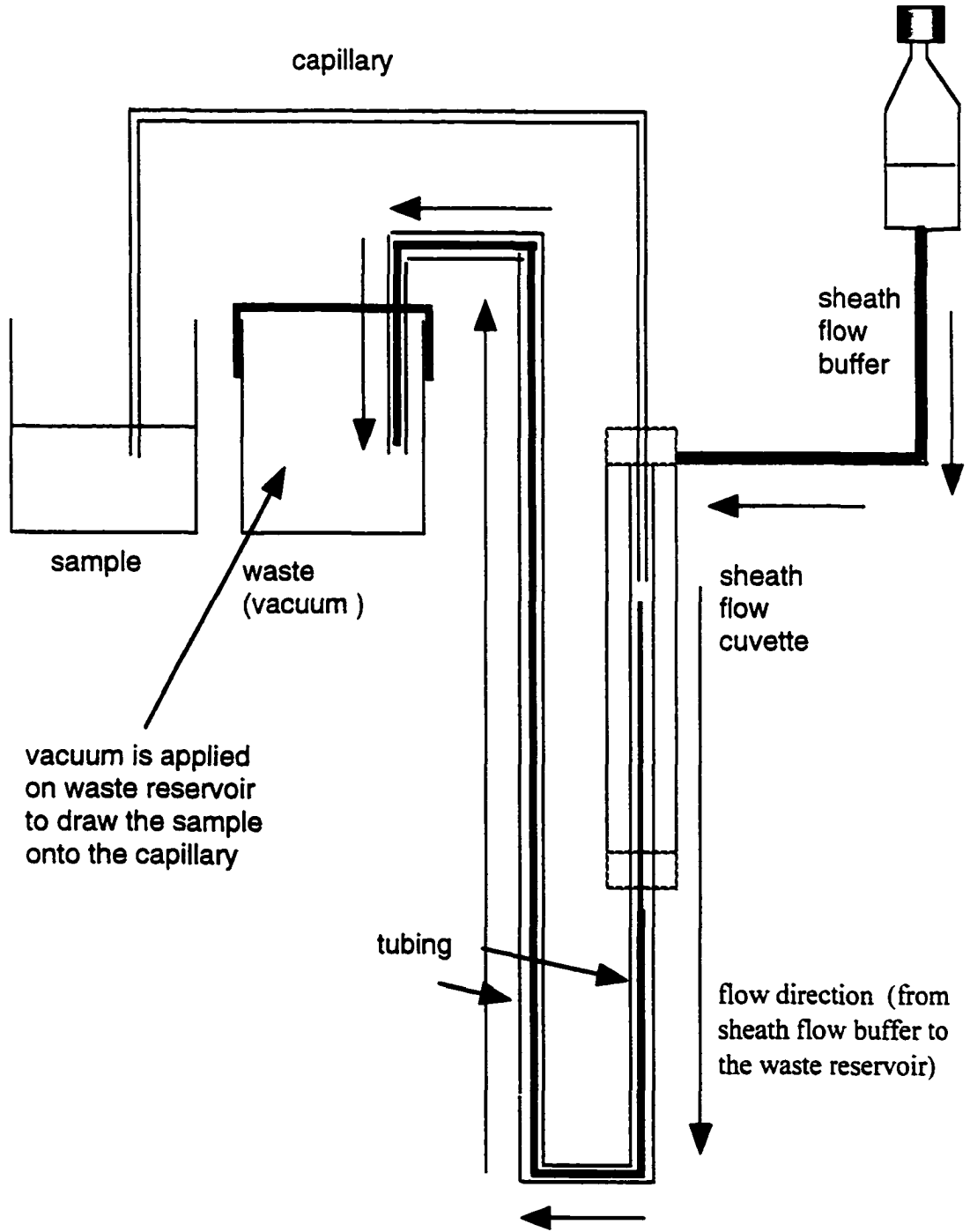
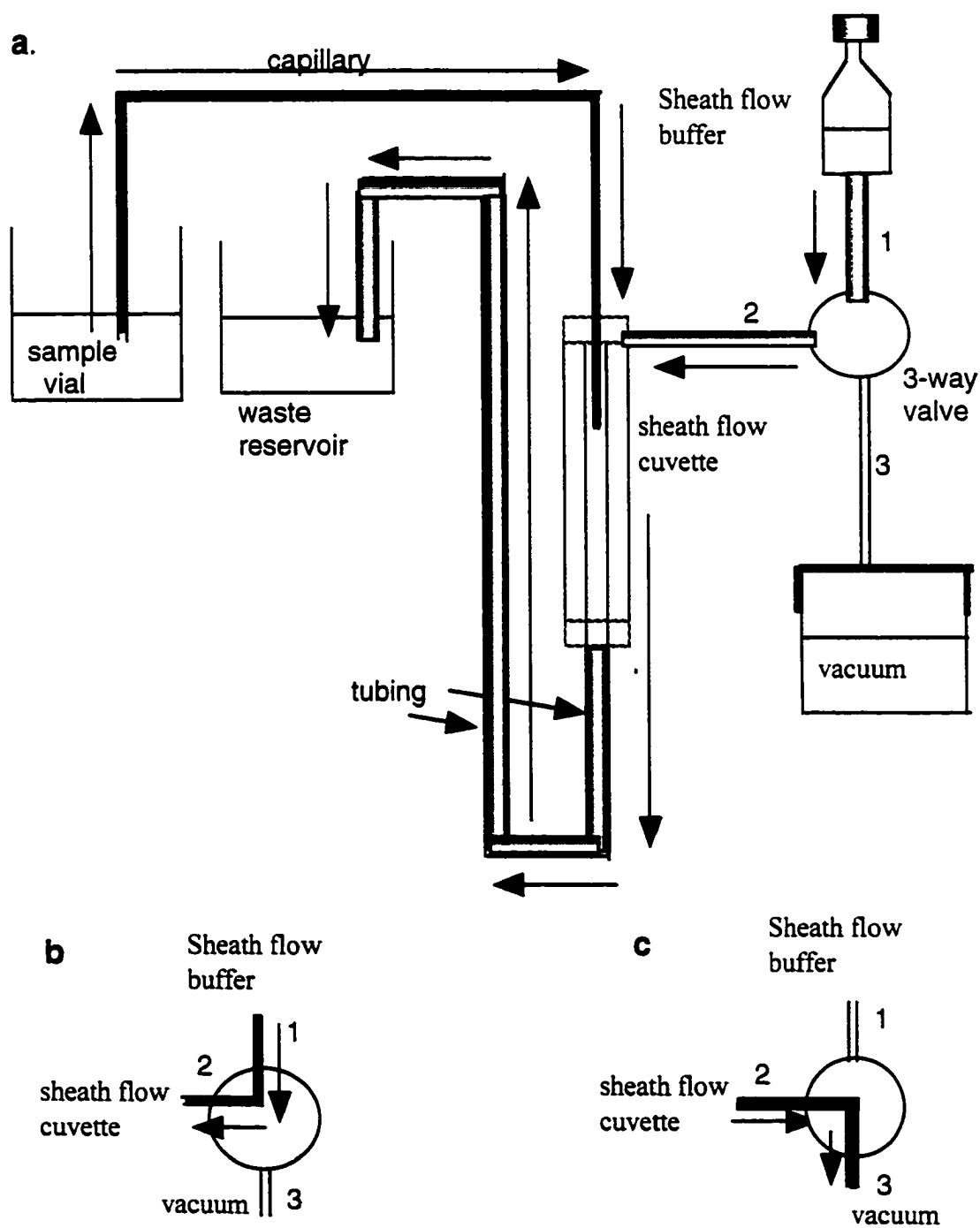


**Figure 2.6: Commercial vacuum injector after modification. a) A general block diagram of the sheath flow tubings with arrows showing the direction of the flow, b) The valve position before and after injection, c) The valve position during the injection time**



sample onto the capillary and generated fewer air bubbles than those of the commercial vacuum injector. After injection, the electronics readjusted the three-way valve to allow sheath flow through the cuvette (Figure 2.6a). Figure 2.6b schematically depicts the direction of the flow before and after the injection.

## **2.3 Results and discussion**

### **2.3.1 Vacuum Injection**

Figure 2.7 shows 5 consecutive injections of  $10^{-10}$  M fluorescein solution with 3 s injection time using the commercial vacuum injector for the DRES instrument. RSD of the migration time is 0.5%, but for the signal intensity RSD is 46%. Using this injection mode, the peak width fluctuates so much that the number of theoretical plates,  $N$ , changes from 0.2 to  $1.5 \times 10^6$ .

Using this injection mode, the RSD in signal intensity is not very impressive (62% for 1 s injection and 13% for 5 s injection). Furthermore, applying vacuum on the sheath flow end of the capillary caused air-bubble generation and current fluctuations. The data for Figure 2 have been filtered using Igor Pro software to remove the air bubbles.

One way to improve RSD in signal intensity is to increase the injection time, which compensates for the initial ramp when applying vacuum to build up the pressure difference. Tables 2.3 and 2.4 show the results of 2 different experiments with 1 s and 5 s injection times. RSD in signal intensity, peak width and peak area all improved by increasing the injection time. But as we discussed earlier, the larger injection volume will cause extra column band broadening.

Increasing the injection time improved the fluctuation in signal intensity. The RSD in signal intensity declined from 62% to 13%, RSD in peak width improved from 12.5% to 2% and peak area RSD from 60% to 14%. In practice it was very difficult to use the

Figure 2.7: Three-second vacuum injection of  $10^{-10}$  M fluorescein solution using commercial vacuum injector before modification

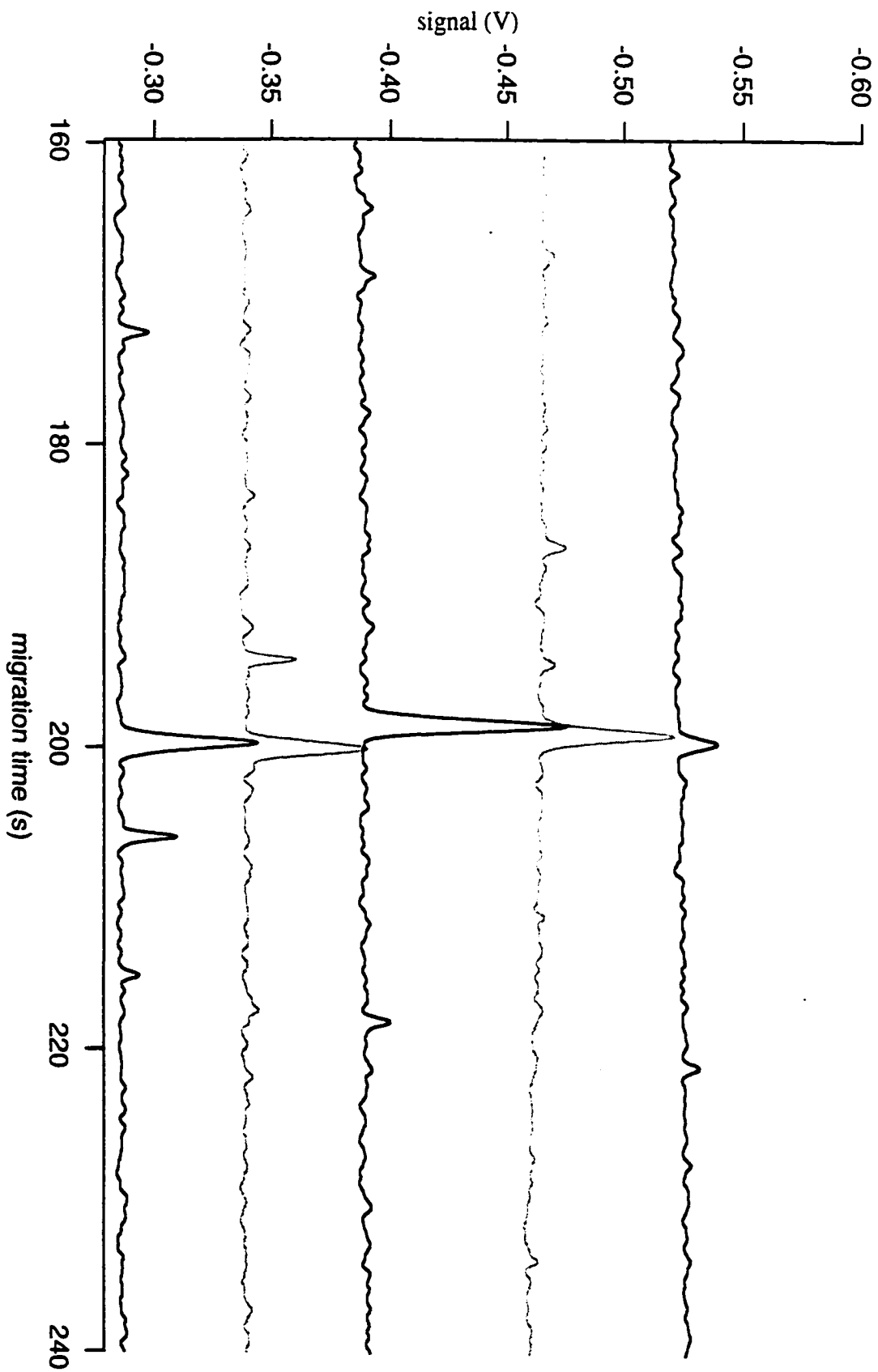


**Table 2.3: The reproducibility results of a 1 s vacuum injection of  $10^{-11}$  M fluorescein solution. The capillary length was 40 cm and 400 V / cm was the applied CE voltage**

<b>Injection Number</b>	<b>Signal Intensity</b>	<b>Migration Time (s)</b>	<b>Peak width (s)</b>	<b>Area</b>	<b>N (x 10<sup>6</sup>)</b>
1	0.049	199.7	1.05	0.055	0.57
2	0.044	200.0	1.09	0.051	0.53
3	0.075	199.2	1.02	0.082	0.61
4	0.048	199.1	1.07	0.055	0.56
5	0.013	200.0	0.92	0.013	0.76
6	0.009	200.0	1.33	0.013	0.36
<b>Mean</b>	<b>0.040 ± 0.02</b>	<b>199.7 ± 0.4</b>	<b>1.08 ± 0.13</b>	<b>0.045 ± 0.027</b>	<b>0.57 ± 0.129</b>
<b>RSD</b>	<b>62%</b>	<b>0.2%</b>	<b>12.5%</b>	<b>60%</b>	<b>23%</b>

**Table 2.4: The reproducibility results of a 5 s vacuum injection of  $10^{-11}$ M fluorescein solution**

<b>Injection Number</b>	<b>Signal Intensity</b>	<b>Migration Time (sec)</b>	<b>Peak width (s)</b>	<b>Area</b>	<b>N (x <math>10^6</math>)</b>
1	0.075	200.2	1.13	0.090	0.50
2	0.096	200.0	1.13	0.116	0.50
3	0.068	199.4	1.09	0.079	0.54
4	0.084	200.0	1.12	0.101	0.51
5	0.085	200.5	1.14	0.103	0.50
Mean	$0.082 \pm 0.010$	$200.0 \pm 0.4$	$1.12 \pm 0.02$	$0.098 \pm 0.014$	$0.51 \pm 0.017$
RSD	13%	0.2%	2.0%	14.3%	3%



commercial vacuum injector mode because of air bubbles generated during long injection times.

### **2.3.2 Modification of the commercial vacuum injector**

Figure 2.8 shows an electropherogram of a 3 s vacuum injection of  $10^{-10}$  M fluorescein. This injection was done when the three-way electrical valve was installed to apply the suction before the sheath flow buffer tubing to reduce the bubble formation. Comparing Figure 2.7 with Figure 2.8 shows that for the same injection time, 3 s, and the same fluorescein concentration,  $10^{-10}$  M, the RSD of the signal intensity improved from 46% to 12%. After modification, air bubbles were still generated after each vacuum injection but were significantly fewer (see Figure 2.5 and Figure 2.6).

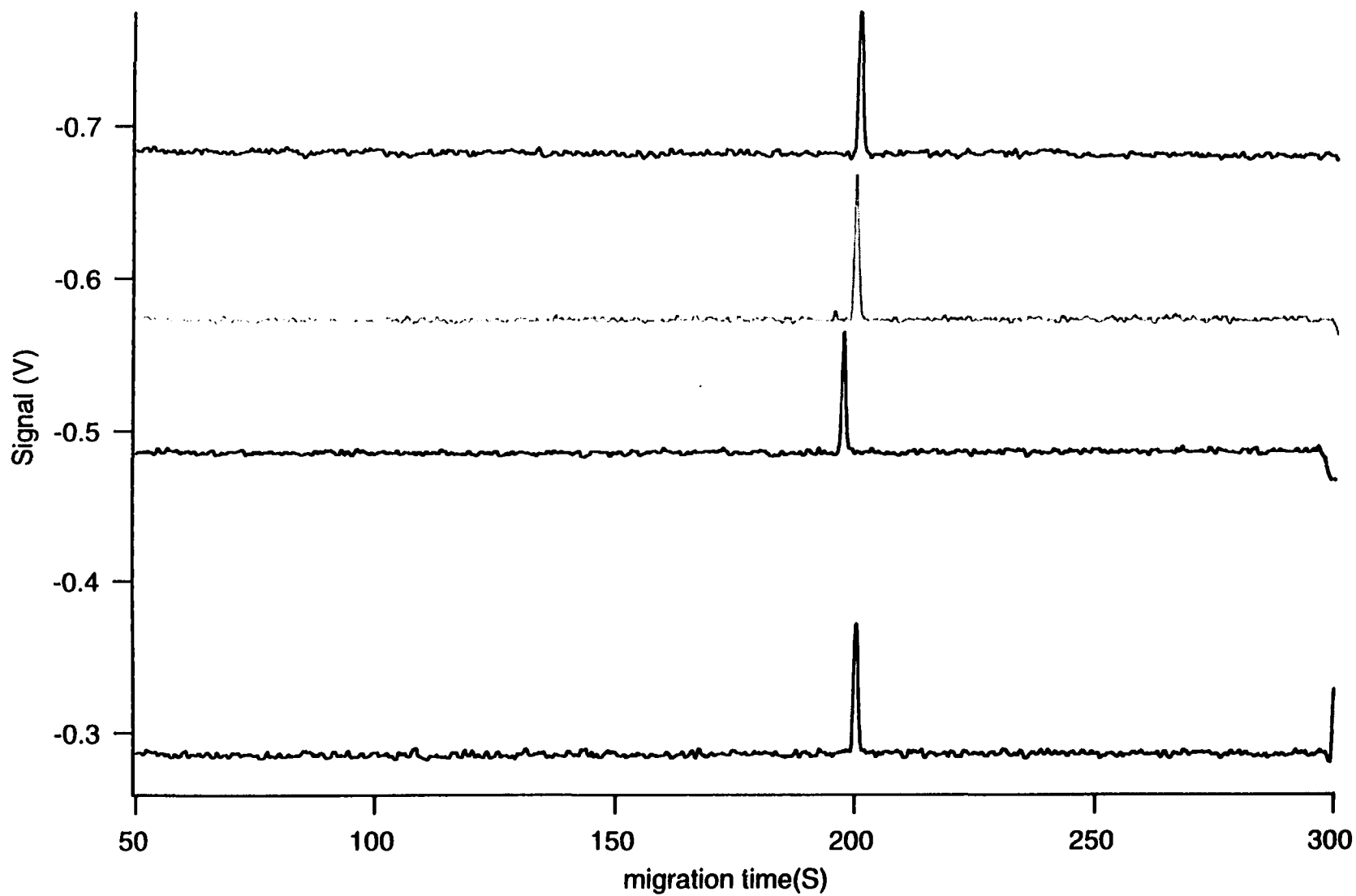
### **2.3.3 Electrokinetic Injection**

Figure 2.9 shows 5 electropherograms of consecutive electrokinetic injections, each with a fresh solution. Signal intensity and peak width improved as compared to vacuum injection before modification. RSD for migration time is 0.4%. The RSD for signal intensity is 2.6% that is also better than vacuum injection (13%). This mode of injection, despite being biased against low mobility ions, was chosen for the other projects in this thesis except for immunoassay, which was done in the flow injection format.

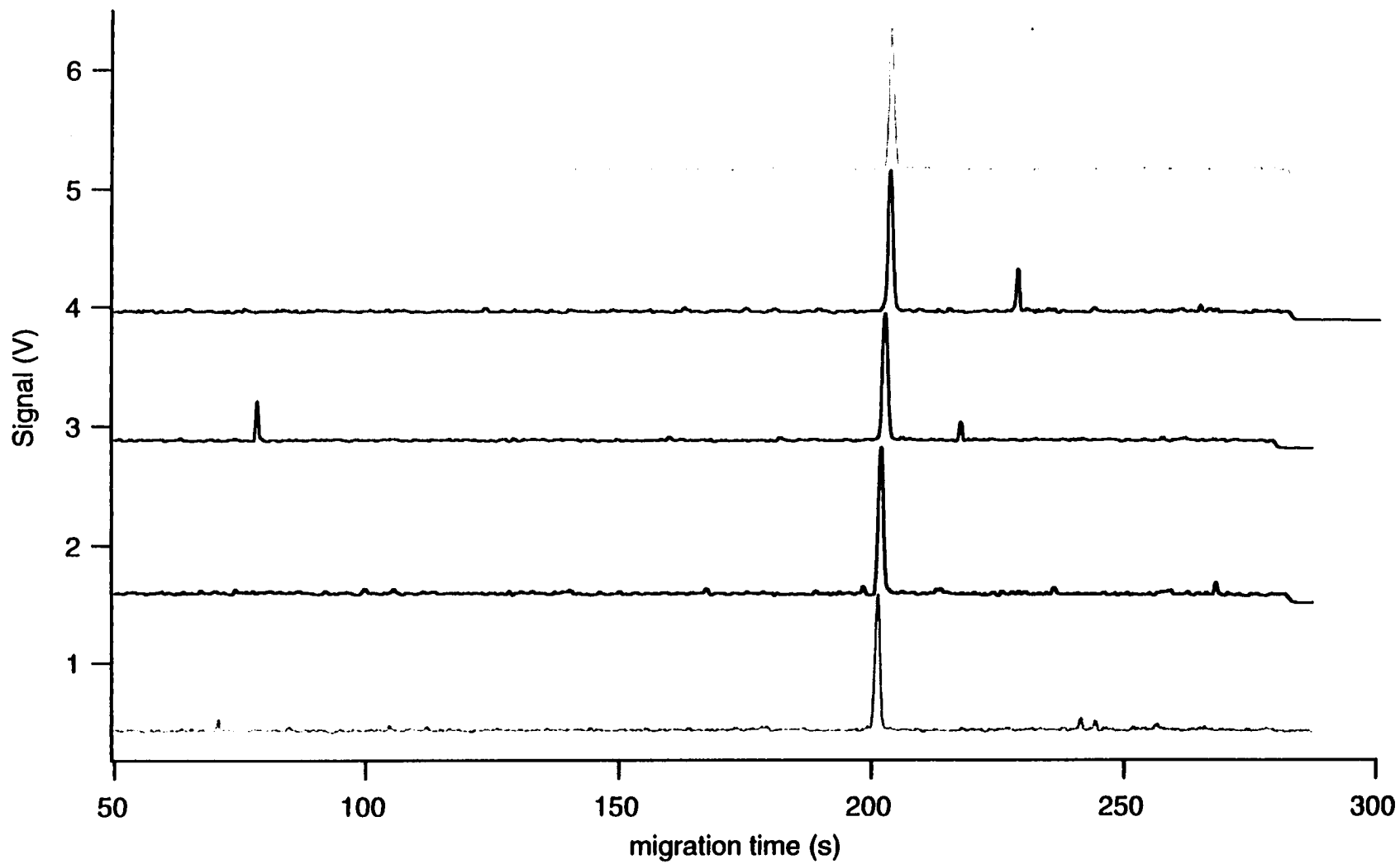
### **2.3.4 Siphoning effect**

Practically, it is very difficult to adjust the levels of sample reservoir and waste to the same height. Failure to do so will cause a contribution of gravity (hydrodynamic) injection while doing electrokinetic injection. One reason for fluctuations in signal intensity in Figures 2.7, 2.8, and 2.9 is this siphoning effect, because sheath flow is continuously flowing and its level is gradually changing. It is advantageous to measure the

**Figure 2.8: Three-second vacuum injection of  $10^{-10}$  M fluorescein solution after modification of commercial vacuum injector**



**Figure 2.9: Electropherograms of 5 s electrokinetic injection of  $10^{-10}$  M fluorescein solution at 1000 v injection voltage, 40 cm capillary length and 400 V / cm CE run voltage**



siphoning flow rate in order to correct for this effect especially when the analyte concentration is very low or when the LOD determination is the goal. The contribution of siphoning on signal intensity is a function of both analyte concentration and injection time. To correct for siphoning, we have to inject the analyte of the same concentration while applying a 0 kV electric field for the same injection time as electrokinetic injection.

Figure 2.10 shows electropherograms after 5 s injection at 0 kV and then running CE with the same voltage, i.e. 16 kV. Fluorescein concentration was varied from 500 pM to 100 pM and then to 1 pM which is the same concentration that was used to measure the LOD. The mean of signal intensity for 5 injections at each concentration, which is due to siphoning effect, was 0.025 for a 500 pM solution, 0.0020 for a 100 pM and 0.00005 for a 1 pM fluorescein solution. The last number (0.00005 for the 1 pM fluorescein solution) was used to correct for siphoning effect when measuring the LOD.

### 2.3.5 Limit of Detection (LOD)

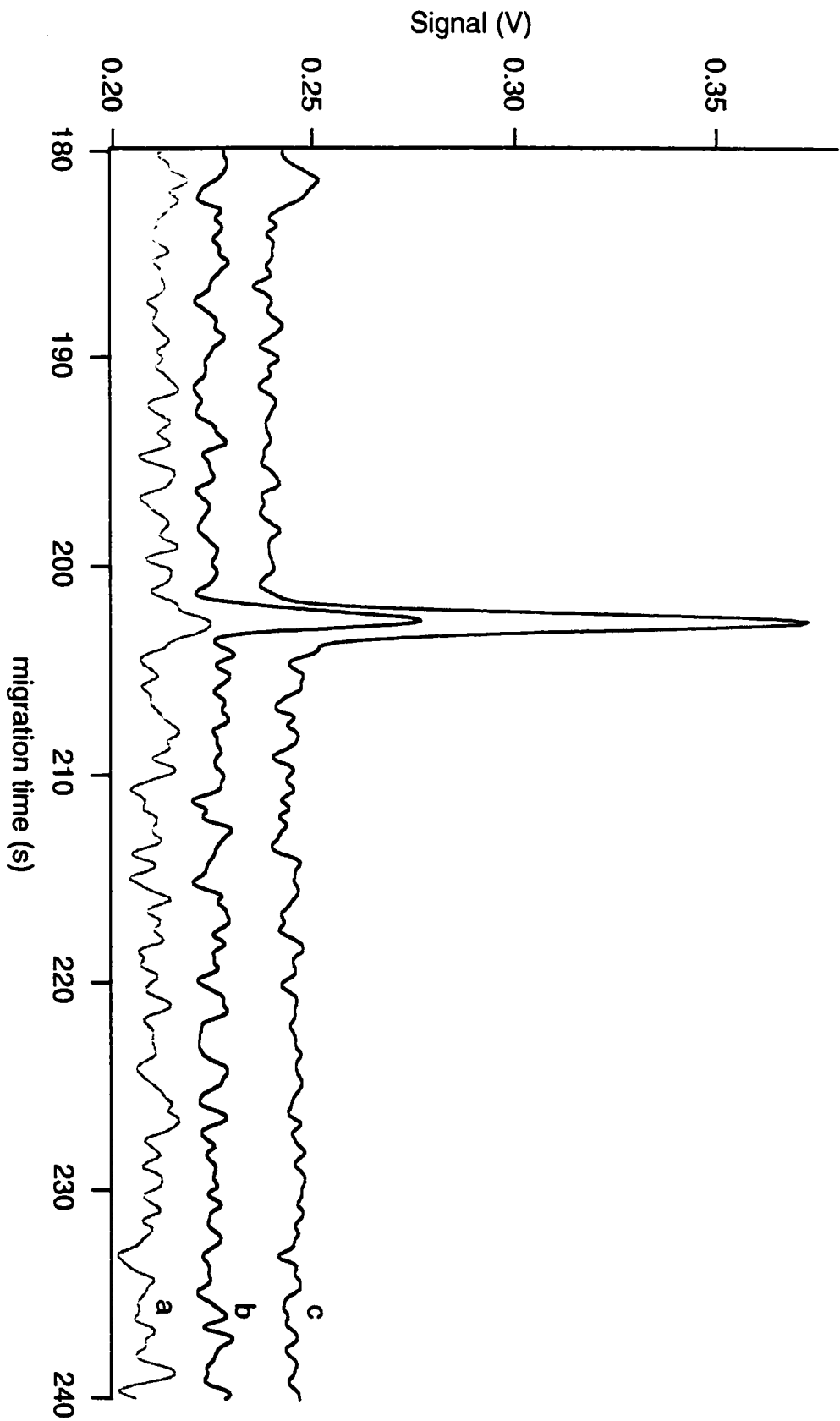
1 pM fluorescein solution ( $10^{-12}$  M) was electrokinetically injected at 1 kV for 5 second. The same capillary length, 40 cm, and the same voltage, 16 kV, as the previous experiments was used. Figure 2.11 depicts the electropherograms.

Table 2.5 shows background, migration time, signal intensity, peak width, peak area and plate number for each electropherogram. These data have been extracted from the electropherograms in Figure 2.11 and are used to calculate the LOD which is shown below.

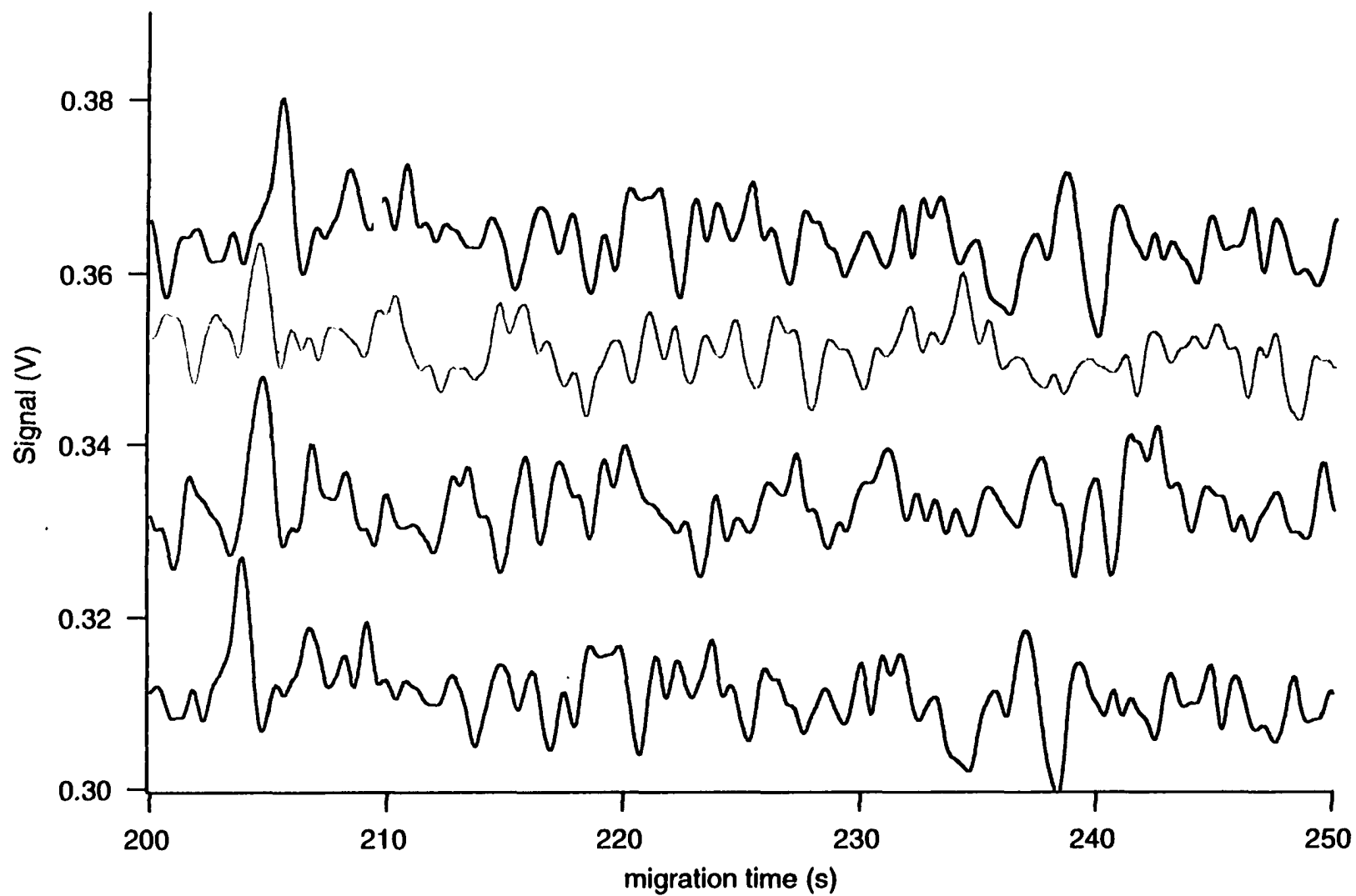
To calculate LOD, the first step is to calculate the capillary volume. The volume of the 40-cm long and 50- $\mu$ m capillary is:

$$V_{\text{cap}} = \pi r^2 L = \pi (25 \times 10^{-6})^2 (0.40) = 7.85 \times 10^{-10} \text{ m}^3 (1000 \text{ L/m}^3) = 7.85 \times 10^{-7} \text{ L} = 0.78 \text{ } \mu\text{L}$$

**Figure 2.10: Electropherograms showing the siphoning effect of 5 s injection at 0 kV for a) 1, b) 100, c) 500 pM Fluorescein solution**



**Figure 2.11: Electropherograms of 5 s injection of 1 pM fluorescein solution at 1000 v for LOD calculation. Capillary length is 40 cm and CE applied voltage is 400 V/cm**



The second step is to calculate the injected volume of the fluorescein solution from equation 2.2, where  $E_{inj}$  is 1 kV,  $E_{CE}$  is 16 kV,  $t_{inj}$  is 5 sec and  $t_{mig}$  is migration time of the analyte out of the capillary. Using migration times listed in Table 2.5, the injected volume could be calculated:

$$V_{inj} = 7.85 \times 10^{-7} (1 / 16)(5 / t_{mig}) \quad (2.8)$$

If we use the average migration time, the injected volume is 1.19 nL. The ratio of injected volume to capillary volume is:  $V_{inj} / V_{cap} = (1.19 \times 10^{-9} \text{ L}) / (7.85 \times 10^{-7} \text{ L}) = 0.15 \%$  which is much less than 1% and there is minimal contribution to band broadening from the injection.

Finally, the LOD is calculated using the following equation:

$$\text{LOD} = (V_{inj})(\text{concentration})(N_{avo})(3)(\text{background SD} / \text{signal intensity}) \quad (2.9)$$

To correct for siphoning effect, the signal intensity in siphoning experiment (Fig. 2.9a) should be subtracted from the signal intensity of the run that we wish to calculate LOD.

$$\text{LOD} = (1.2 \times 10^{-9} \text{ L})(1 \times 10^{-12} \text{ mole} / \text{L})(3 N_{avo} \text{ molecule} / \text{mole})(\text{Bk}_{sd}) / (\text{signal} - 0.00005)$$

$$\text{LOD} = 2152 (\sigma_{Bk}) / (\text{signal} - 0.00005) \quad (2.10)$$

Using background standard deviations,  $\sigma_{Bk}$ , and signal intensities from Table 2.5, LOD is calculated and shown in Table. 2.6. The average LOD is 158 fluorescein molecules with the standard deviation of 23, i.e. RSD = 14%.

**Table 2.5: The results of 5 s at 1000 v electrokinetic injection of 1 pM fluorescein solution for LOD calculation**

<b>Injection number</b>	<b>Background signal (v)</b>	<b>Migration time (s)</b>	<b>Signal intensity (v)</b>	<b>Peak width (s)</b>	<b>Peak area (Vs)</b>	<b>N (x 10<sup>6</sup>)</b>
1	0.467 ± 0.0009	206.0	0.011	0.74	0.009	1.25
2	0.460 ± 0.0010	206.8	0.017	1.09	0.019	0.57
3	0.445 ± 0.0009	206.3	0.013	1.22	0.017	0.46
4	0.445 ± 0.0011	206.3	0.013	1.20	0.016	0.47
<b>Mean</b>	0.457 ± 0.0092	206.4 ± 0.3	0.013 ± 0.002	1.06 ± 0.22	0.015 ± 0.004	0.68 ± 0.38
<b>RSD</b>	2%	0.2%	16%	21%	29%	56%



**Table 2.6: LOD calculation using the data in Table 2.5**

<b>Injection</b>	<b>1</b>	<b>2</b>	<b>3</b>	<b>4</b>
<b>LOD (number of molecules)</b>	168	131	148	185

**Mean = 158 and RSD = 14%**

### 2.3.6 Further modification of DRES instrument (Room light blocking)

The DRES instrument was designed to be a portable CE to be used in a battle-field situation. One major draw-back of the CE-LIF instrument is the need to work in the dark. Room light leaks into the PMT and the background is so high that the PMT will be saturated. Covering the microscope eye piece did not help because room light leaked from the sides of the cuvette into the PMT and the background was still high. A light shield was designed that surrounds the cuvette (Figure 2.12). It connects the two microscope objectives so that little room light can leak in. There is a tiny hole approximately equal or slightly bigger than the laser beam size that focuses the laser onto the cuvette. Another tiny hole is made in the opposite direction for the exiting laser beam. This simple design prevented room light from reaching the detector and, therefore, the DRES instrument could be operational in a day-light environment.

Table 2.7 shows the results of the experiment which proves that the background noise is due to the laser itself and not due to the stray light from the environment. For this experiment while both laser and room lights were on, the background was recorded. Then the room lights were turned off and the background signal was collected. Finally all room lights and laser were off, and again the background was recorded.

Total variance is the sum of variances if we assume the contribution of room light and laser on background are independent processes, hence:

For the case that the light room is on:

$$\sigma_{\text{total}}^2 = \sigma_{\text{laser on}}^2 + \sigma_{\text{laser off}}^2 \quad (2.11)$$

$$\sigma_{\text{total}}^2 = (0.001)^2 + (0.0003)^2$$

**Figure 2.12: A CE-LIF instrument with a Light Shield that covers both eye-piece of the microscope and the detector box focusing lens**

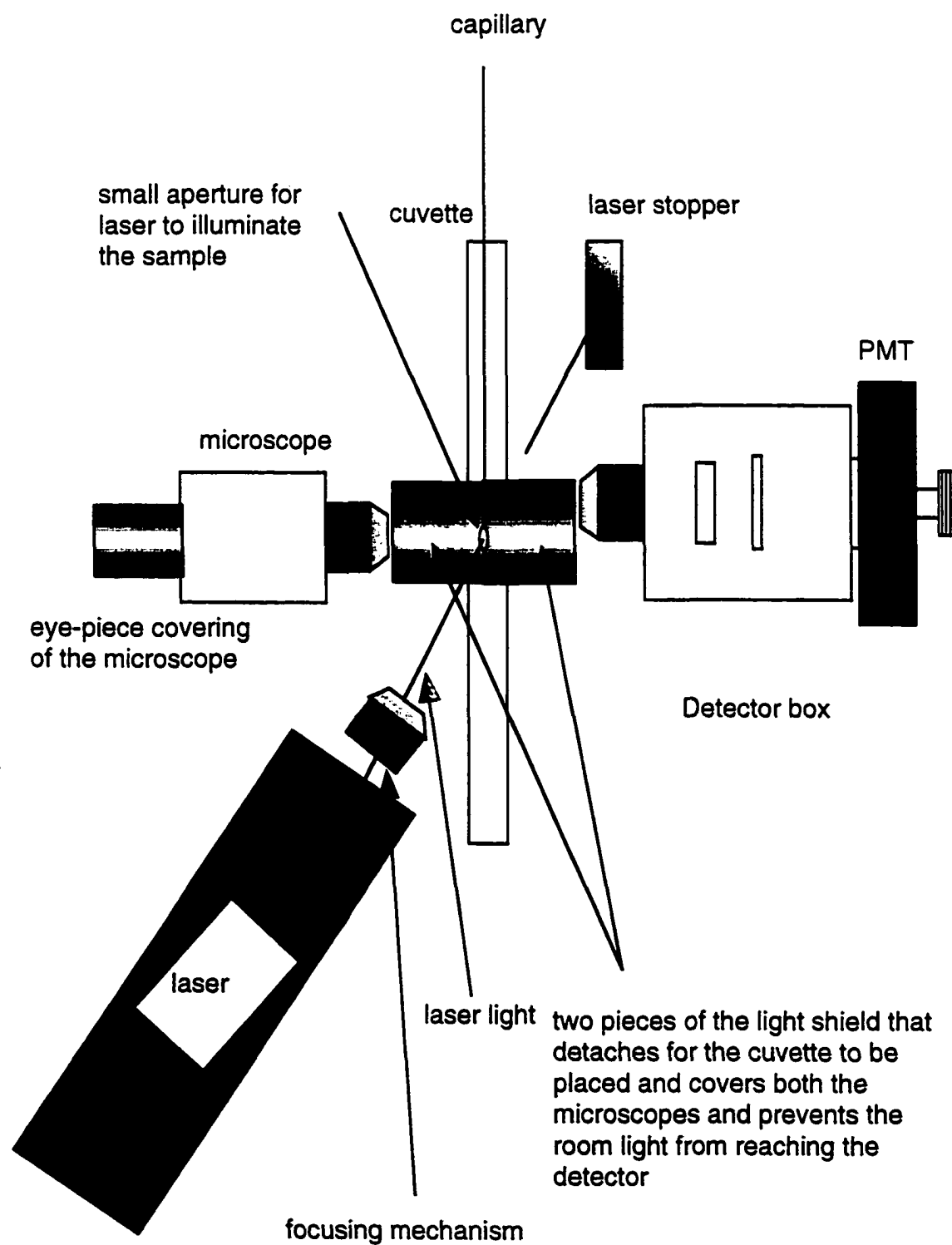


**Table 2.7: Background fluctuation due to laser and room light**

	<b>Room lights on</b>	<b>Room lights off</b>
<b>Laser on</b>	$0.444 \pm 0.001$	$0.443 \pm 0.002$
<b>Laser off</b>	$0.007 \pm 0.0003$	$0.004 \pm 0.0002$

$\sigma_{\text{total}} = 0.001$  which is the same standard deviation as when the laser is on and room lights are also on.

For the case when the lights are off:

$$\sigma_{\text{total}}^2 = (0.002)^2 + (0.0002)^2$$

and  $\sigma_{\text{total}} = 0.002$  which is the same standard deviation as when the laser is on.

This simple experiment shows that the major source of noise is due to the laser itself and not the room light. It is a good indication that the light shield is functioning effectively.

## 2.4 Conclusions

A compact CE-LIF instrument was assembled. This CE-LIF instrument is the first generation of mobile instruments. The injector box had to be modified for reproducible vacuum injection. The electrokinetic injection is very precise. The limit of detection of the instrument is 150 fluorescein molecules.

The first generation of the instrument had to be operated in the dark because of light leakage into the PMT. To avoid this difficulty, a light shield was designed. It was proved that this simple design prevents stray light from reaching the detector. The light shield allows the CE-LIF instrument to be operated in day light and takes us one step forward in having a mobile CE-LIF instrument.

## **Appendix 1**

### **A1.1 Procedure for operation of DRES Capillary Electrophoresis**

#### **Instrument**

1. Turn on the laser (12.1 mW), Spectrophoresis control module, power supply, photomultiplier tube power supply (600 V), and computer. See Figure 2.4 for identification of different instrument parts.

2. Check for the sheath flow buffer tubings not to have any bubbles. In particular, check with the microscope that there are no bubbles in the detector region of the cuvette. If there are, apply pressure to the buffer reservoir until bubbles are forced out. Bubbles that are trapped between the buffer reservoir and the sheath flow cuvette tubing can be eliminated through the bubble trap line in the sheath flow cuvette. If the bubble trap valve is opened, there will be a flow of buffer from the sheath-flow buffer reservoir to a second waste vial. This second vial bypasses the flow from the cuvette and this will help to get rid of the bubbles very quickly.

3. Calculate the voltage required to apply 400 V/cm for the capillary being used. Apply the selected voltage.

4. Open the Labview file Cobra (data acquisition program) and start data acquisition.

5. Monitor the current (upper channel). If the current is erratic, there might be bubbles inside the capillary. Stop the high voltage. Using a syringe with a capillary adapter, flush the capillary with the running buffer for 30 seconds. Restart the high voltage and check if the current is stable.

#### **A1.2 Alignment**

1. Rough alignment: Prepare a fresh  $10^{-9}$  M fluorescein solution in the run buffer by diluting a stock solution of  $10^{-3}$  M fluorescein in MeOH. Run CE at 400 V / cm to inject the fluorescence solution continuously. When the fluorescein solution starts to migrate, the

signal (channel 2) will increase sharply. The maximum waiting time is 7 minutes for a 40 cm uncoated capillary. Check under the microscope region (detection volume) to observe an intense fluorescence signal. Its shape has to match the shape of light emitting diode (LED) used as an alignment guide. If the shape is different, the iris (lever on top of the detector) can be adjusted or the beam width and height can be changed by adjusting the position of the focusing objective.

2. Fine alignment. Cover the eyepiece of the microscope with a piece of cylindrical dark plastic. Do a fine alignment by monitoring the signal on the computer monitor while tuning the different translation stages. Corroborate that the signal is due to migration of the dye and not to capillary scattering by checking the background frequently. To check the background, the high voltage is set to zero. Signal in this zero CE voltage situation corresponds to background. The signal when CE voltage is applied has to be maximum, while the signal when the CE voltage is set to zero has to be minimum.

3. Washing. When the fine alignment is done, change the fluorescein containing vial with a fresh running buffer vial. Apply high voltage and run the instrument for another 5 minutes to replace the dye solution inside the capillary with running buffer. The background drops sharply when all the fluorescein solution is replaced with the running buffer.

4. Adjusting the PMT voltage. Change the PMT voltage to 1000 V. Make sure that the background signal is constant and that there is only a small background change (maximum 10 mV) when the CE power supply is turned on and off. If there is a larger change in background signal despite the power supply being on and off, it means that probably there are some micro-particles suspended in sheath flow buffer. In this case you have to re-filter the sheath flow buffer.

### **A1.3 CE separation**

- 1.** Select injection time in the front panel of the Spectrophoresis unit. Dial the selected voltage for the injection. (Suggested conditions: 5 s at 1000 V).
- 2.** Place the sample in the injection position. Immerse the electrode and capillary into the sample and press the injection button.
- 3.** After the injection is finished, change the sample vial to a running buffer vial, immerse the electrode and capillary into two washing vials. Rotate the carousel to select the running buffer vial.
- 4.** Readjust voltage to the selected running voltage (400 V/cm is the commonly used electric field).
- 5.** Start data acquisition. Name the file and start the Spectrophoresis unit. Each run takes approximately 5-8 minutes. The total time depends on sample, CE voltage, capillary length and it also depends on whether the capillary is coated or not.



## 2.5: References

1. Dovichi, N. J., Martin, J. C., Jett, J. H., Trkula, M., Keller, R. A., *Anal. Chem.*, 56, 348, 1984.
2. Gassman, E., Kuo, J. E., and Zare, R. N., *Science*, 230, 813, 1985.
3. Lycons, J. W., and Faulkner, L. R., *Anal. Chem.*, 54, 1060, 1982.
4. Lynos, J. W., and Faulkner, L.R., *Anal. Chem.*, 54, 1960, 1982.
5. Cheng, Y. F. and Dovichi, N. J., *Science*, 242, 562, 1988.
6. Wu, S., and Dovich, N. J., *J. Chromatogr.*, 480, 141, 1989.
7. Cheng, Y. F., Wu, S., Chen, D. Y., and Dovichi, N. J., *Anal. Chem.*, 62, 496, 1990.
8. Swerdlow, H., Zhang, J. Z., Chen, D. Y., Harke, H. R., Wu, S., Fuller, C., and Dovichi, N. J., *Anal. Chem.*, 63, 2835, 1991.
9. Wu, S. and Dovichi, N. J., *Talanta*, 39, 173, 1992.
10. Chen, D. Y., Swerdlow, H. P., Harke, H. R., Zhang, J. Z., and Dovichi, N. J., *J. Chromatogr.*, 559, 237, 1991.
11. Zhang, J. Z., Chen, D. Y., Wu, S., Harke, H. R., and Dovichi, N. J., *Clin. Chem.*, 37, 1492, 1991.
12. Zarrin, F., Dovichi, N. J., *Anal. Chem.*, 57, 1826, 1985.
13. Zarrin, F., Risfelt, J. A., Dovichi, N. J., *Anal. Chem.*, 59, 850, 1987.
14. Zarrin, F., Bornhop, D.J., Dovichi, N. J., *Anal. Chem.*, 59, 854, 1987.
15. Dovichi, N. J., *Capillary Electrophoresis, Theory and Practice*, Edited by Patrick Camilleri, Chapter 2, 25-65, CRC Press Inc., 1993.
16. Abersold, R., and Morrison, H. D., *J. Chromatogr.*, 516, 79, 1990.
17. Foret, F., Deml M., Kahle, V., and Bocek, P., *Electrophoresis*, 7, 430, 1986.
18. Fujiwara, S., and Honda, S., *Anal. Chem.*, 59, 487, 1987.
19. Jorgenson, J. W., and Lukacs, K. D., *Anal. Chem.*, 53, 1298, 1981.

20. Landers, J. P., Handbook of Capillary Electrophoresis, Second Edition. 1996. Chapter 15, 457-478, CRC Press Inc., 1997.
21. Kappes, T., and Hauser, P. C., Anal. Commun., 35, 325-329, 1998.
22. Sudor, J., Stransky, Z., Pospichal, J., Deml, M., Bocek, P., Electrophoresis (Weinheim), 10, 802, 1989.
23. Tehrani, J., Macomber, R., and Day, L., J. High Resolut. Chromatogr., 14, 10, 1991.
24. Huang, X., Gordon, M. J., Zare, R. N., Anal. Chem., 60, 375-377, 1988.
25. Honda, S., Iwase, S., Fujiwara, S., J. Chromatogr., 404, 313-320, 1987.
26. McCabe, J., Canadian Chemical News, 16-18, , February 1991.
27. Chen, D. Y., Ph.D. Thesis in chemistry, University of Alberta, 1993.
28. Rose, D. J., Jorgenson, J. W., Anal. Chem., 60, 642, 1988.
29. Fanali, S., Ossicini, L., Foret, F., and Bocek, P., J. Micocol. Sep., 1, 190, 1989.
30. Schwartz, H. E., Merela, M., and Brownlee, R. G., J. Chromatogr., 480, 129, 1989.
31. Vindevogel, J., and Sandra, P., Introduction to Micellar Electrokinetic Chromatography, Huthig Buch Verlag, Gmbh, Heidelberg, 1992.
32. Knoll, J. E., J. Chrom. Sci., 23, 422-425, 1985.
33. Zhao, J. Y., Ph.D. thesis in chemistry, University of Alberta, 1994.

**CHAPTER 3**

**PSEUDO-COULOMETRIC SAMPLE**

**INTRODUCTION IN**

**CAPILLARY GEL ELECTROPHORESIS**

**DNA SEQUENCING<sup>1</sup>**

---

<sup>1</sup> Some parts of this chapter have been published as "Pseudo-coulometric loading in capillary electrophoresis DNA sequencing" by Daniel Figeys, Hossein Ahmadzadeh, Edgar Arriaga, Norman J. Dovichi, *J. Chromatogr. A*, 744, 325-331, 1996.

### **3.1 Theoretical background in DNA sequencing and electrokinetic sample introduction onto a gel-filled capillary**

#### **3.1.1 DNA structure**

DNA is a long-chain natural polymer made of four different monomers linked together in a linear configuration.<sup>1-2</sup> The major unit of DNA is the nucleotide monomer (Figure 3.1a). Nucleotides have three parts: a sugar, a base, and a phosphate. The sugar is a pentose called 2'-deoxyribose (Figure 3.1b). Ribose has a hydroxyl group (-OH) in the 2' position, but in DNA, this -OH group is replaced by a hydrogen.

The chemical structures of the four bases that are encountered in DNA are shown in Figure 3.2a. These bases are linked to the sugar at the 1' position via a C-N bond replacing the -OH group of the 2'-deoxyribose sugar.

The phosphate component of the nucleotide usually consists of three individual phosphate groups attached together linearly (Figure 3.2b).

Different nucleotide monomers are linked together to make the DNA molecule. DNA is a polynucleotide in which the monomers are linked together by the formation of a phosphodiester bond between the 5'-phosphate group and the 3'-end of the 2'-deoxyribose. Only one phosphate group is involved in the phosphodiester bond; the other phosphate groups are removed during the polymerization. DNA has two ends: (Figure 3.3), a 5'-end (a triphosphate) and a 3'-end (a -OH group). These terminal groups cause different reactivity for each end of the polynucleotide.

Hundred of millions of nucleotides can link together to form a polynucleotide. There is no limitation to the order in which the nucleotides may link together. Thus, the different sequence possibilities are  $4^n$ , where  $n$  is the number of bases. For a short polynucleotide of 20 nucleotides the number of different sequences is  $4^{20} = 1 \times 10^{12}$ .

**Figure 3.1: General chemical structure of a) a nucleotide and  
b) sugar in DNA and RNA**

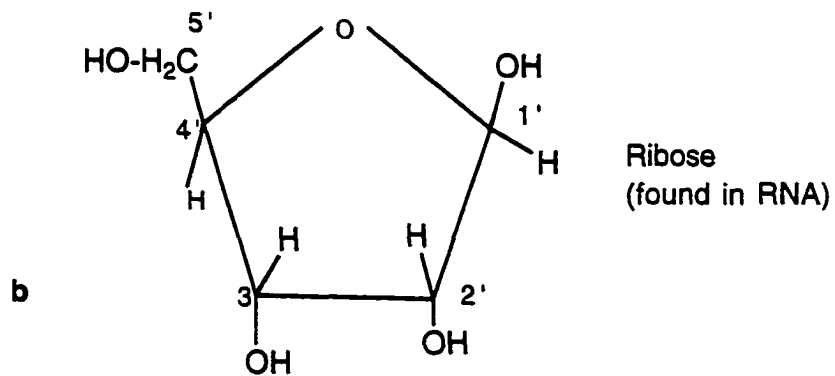
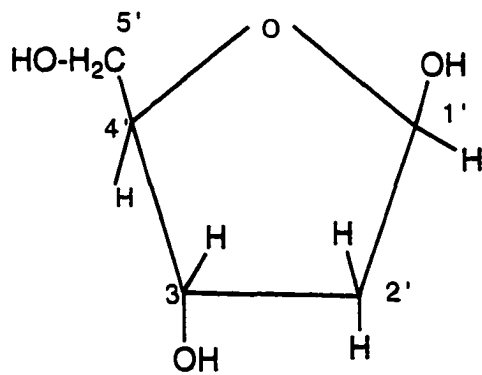
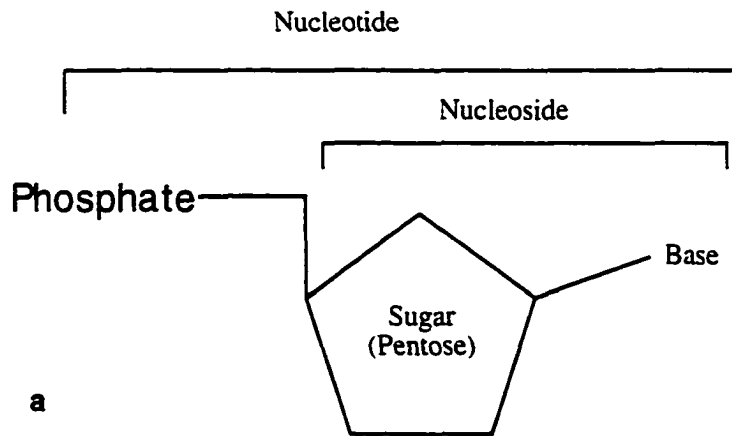


**Figure 3.2: Chemical structure of a) four bases found in DNA and their hydrogen bonds and b) phosphate group bond to a base**

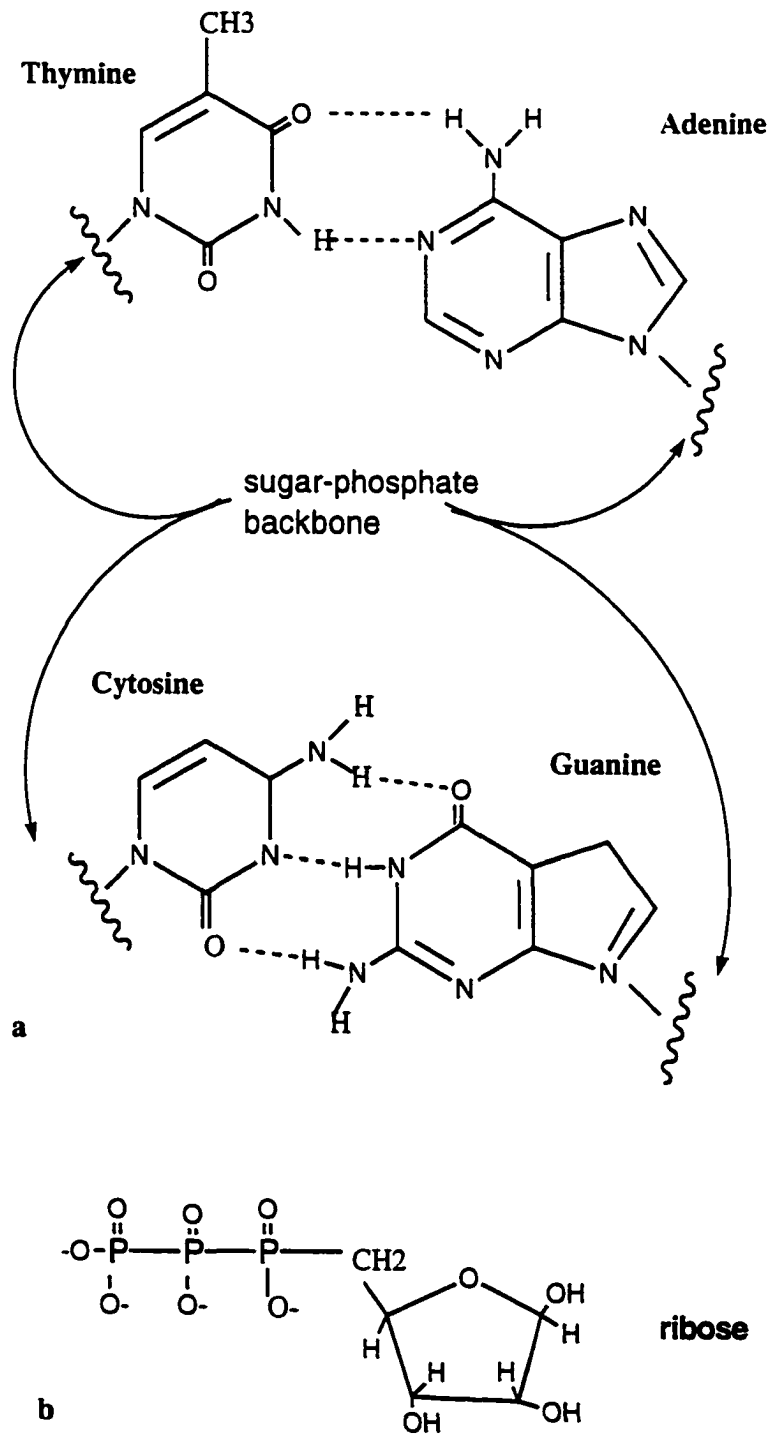
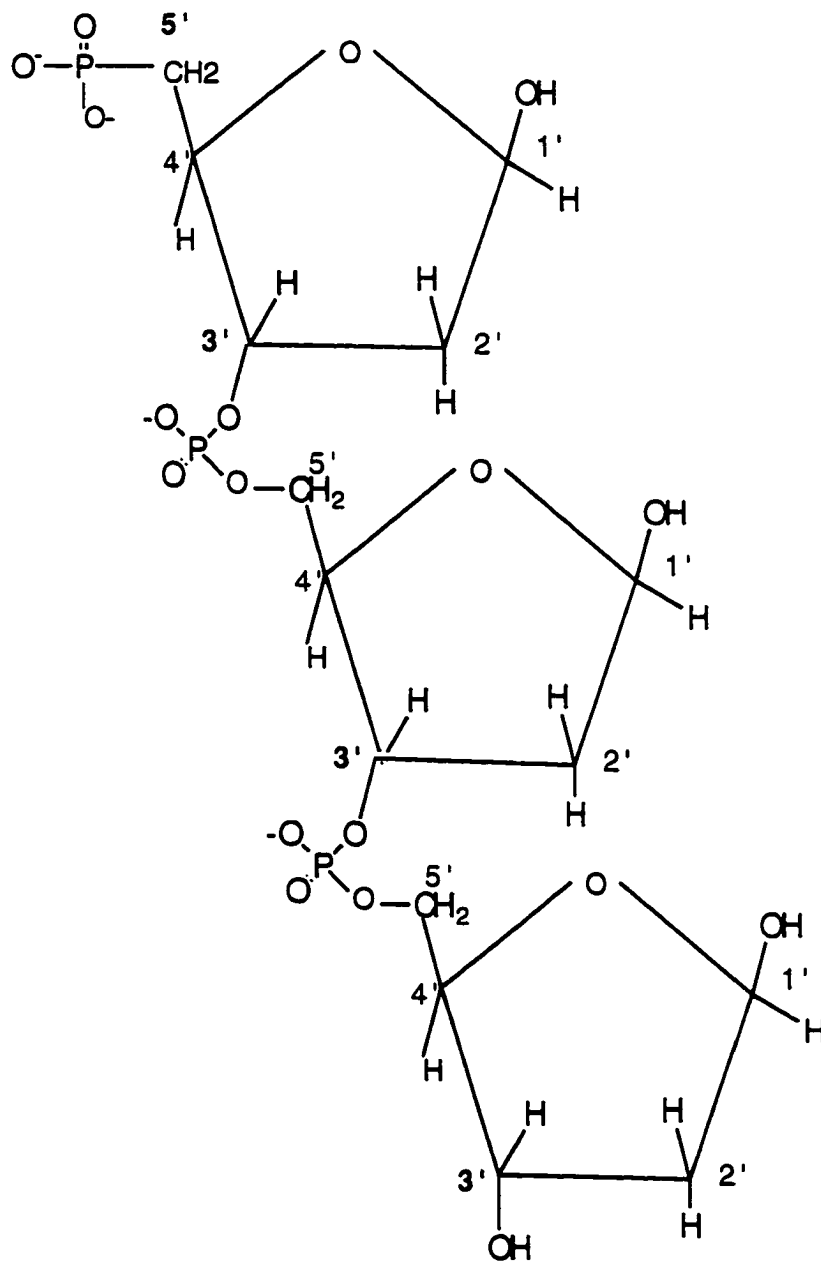


**Figure 3.3: The chemical structure of a short polynucleotide**



Two DNA molecules bind together by hydrogen bonds between the bases to form a double-stranded DNA. The DNA used in this chapter is single-stranded DNA (M13mp18).

### **3.1.2 Cycle sequencing**

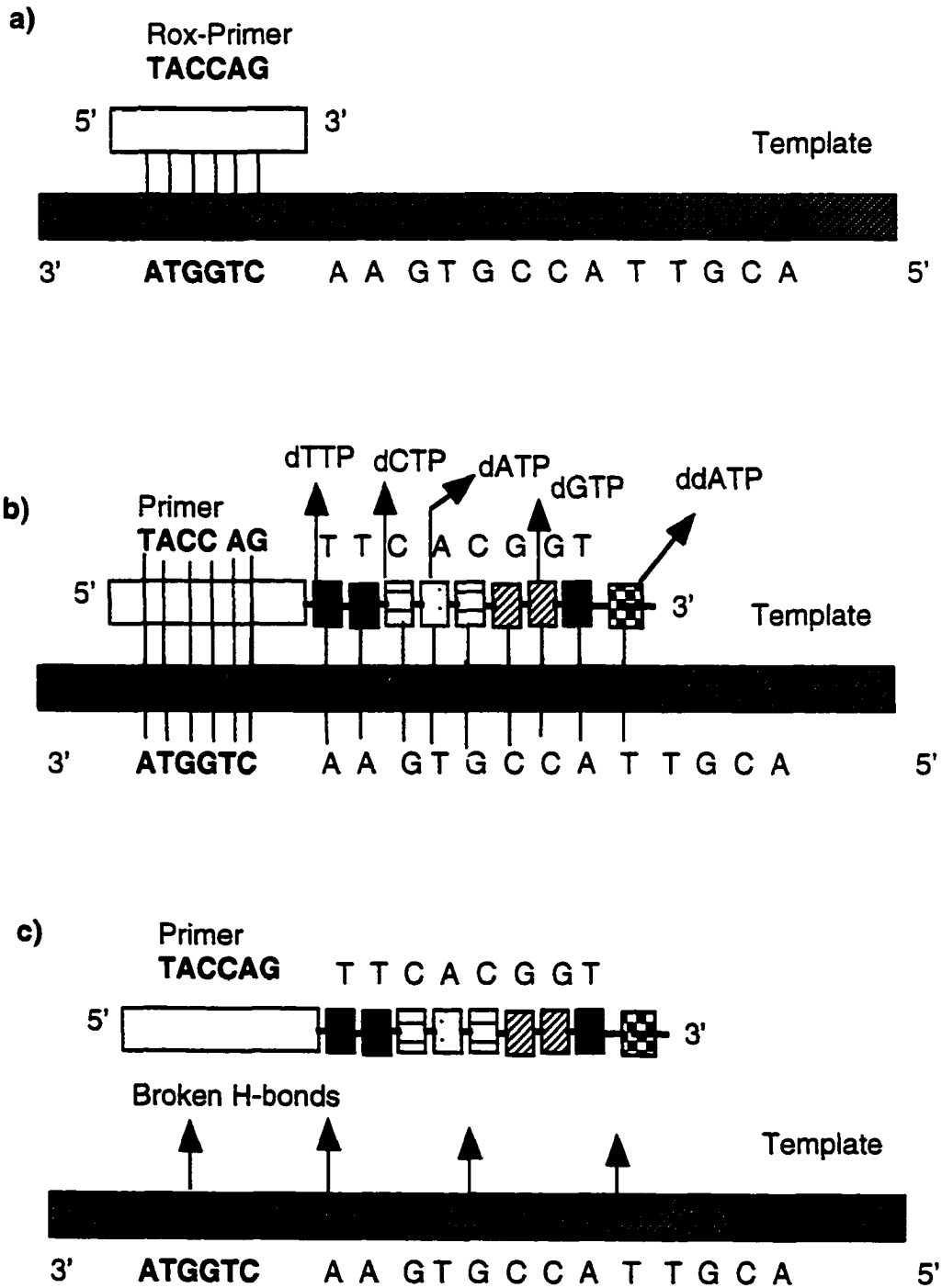
We used M13mp18 as a template in cycle sequencing. A template is a piece of DNA that has to be sequenced. A primer, a short piece of DNA with known sequence and complementary to one part of the template, is added to the template solution. A ROX-labeled universal primer was used. Figure 3.4 depicts different steps used in cycle sequencing reaction. In step a, Fig. 3.4a, the primer anneals to the template. By annealing, the templates and the primers form hydrogen bonds between the complementary bases. In step b, Fig. 3.4b, the annealed primer is extended at its 3'-end by a DNA polymerase thermostable enzyme (sequenase) in the presence of the four dNTPs and terminated using ddTTP. The enzyme adds bases at the 3'-end of the primers according to the complementary rule. Because the solution also contains one ddTTP sometimes the enzyme will incorporate a ddTTP. The extension will then stop because ddTTPs do not have a 3'-hydroxyl end. Then in step c, Fig. 3.4c, the temperature of the solution is raised to 95 °C. This high temperature causes the hydrogen bonds between the DNA fragment, template and its extended primer to break apart and the DNA fragment separates from the template. Because the templates are now free of any other DNA, it is possible to reanneal some primers and do the cycle again. The steps a, b, and c were cycled 30 times in our experiment.

### **3.1.3 Change of transference (or transport) number at solution-gel interface in electrokinetic injection**

Transference number ( $T_i$ ) of an ion is defined as the fraction of the total current



**Figure 3.4: Cycle sequencing process includes a) annealing (47 °C),  
b) extension and termination (70 °C) and c) Denaturation (95 °C)**



carried by that ion.  $T_+$  and  $T_-$  could be defined in terms of mobilities of the cation and anion ( $\mu_+$ , and  $\mu_-$ ).

$$T_+ = \mu_+ / (\mu_+ + \mu_-) \quad (3.1)$$

$$T_- = \mu_- / (\mu_+ + \mu_-) \quad (3.2)$$

For a single 1:1 electrolyte in a solution

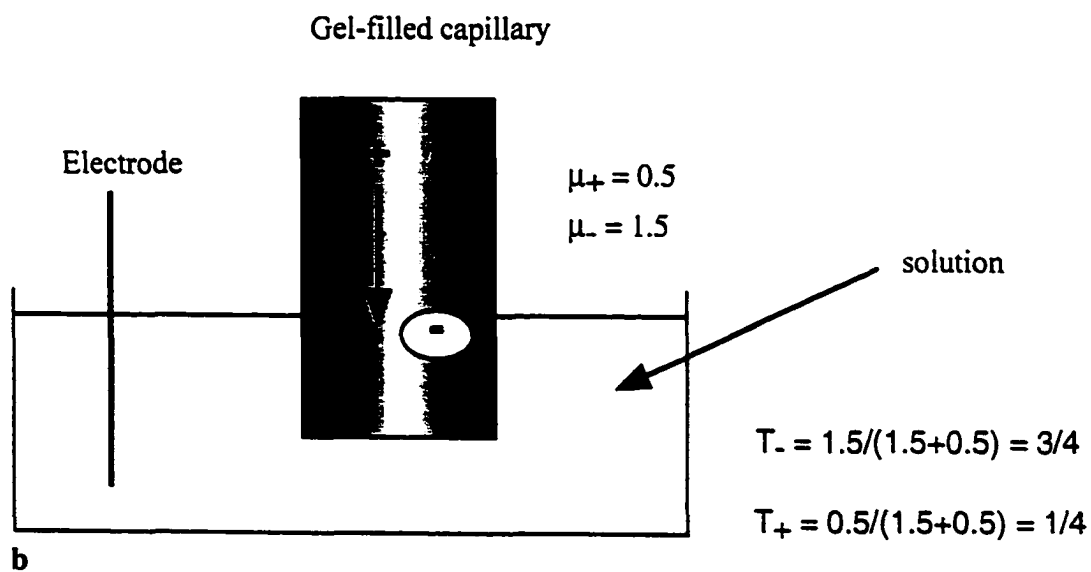
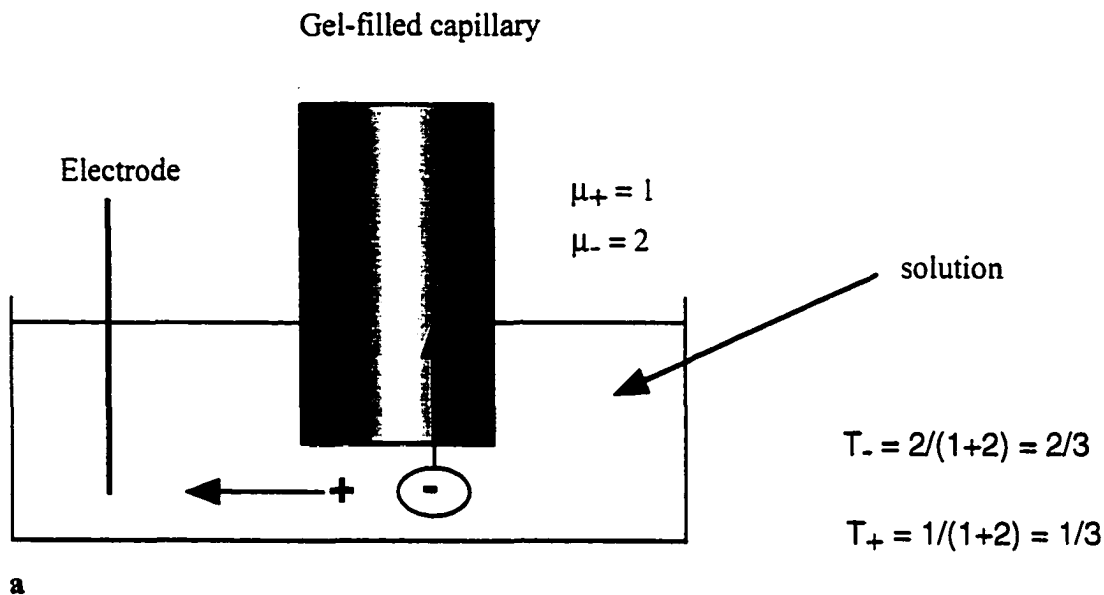
$$T_+ + T_- = 1 \quad (3.3)$$

where  $T_+$  and  $T_-$  are the cation and anion transference numbers. In most of our experiments, 1xTBE was used as a buffer to maintain conductivity. 1xTBE is a buffer made of TRIS, borate and EDTA. During electrophoresis, the borate migrates towards the anode and the TRIS migrates towards the cathode.

We assume that the mobilities change by retarding factors  $R_+$  and  $R_-$  when analytes pass from the solution phase to the more retarding gel medium, so that  $R_+$  and  $R_-$  are both less than unity.  $R_+$  and  $R_-$  are comparable to the "relative ion mobilities" determined by Stokes in sucrose and other nonelectrolytes.<sup>3</sup> Literature supports the assumption that  $R_+$  and  $R_-$  are substantially independent of concentration.<sup>5-7</sup>

Figure 3.5 shows the effect of medium viscosity on transference number. If we assume that in free solution, Fig. 3.5 a, the cation has a mobility of one and the anion, which is less solvated and hence smaller, has a mobility of 2, then the cation transports 1/3 of the total current and the anion transports 2/3.<sup>4</sup> The gel is more structured than free solution and, therefore, imposes more frictional forces on the ions. The cations are larger in

**Figure 3.5: Effect of medium viscosity on transference number of an imaginary system of a) free solution and b) gel phase (polyacrylamide media)**



size because they are more solvated than the anions. This causes the cations to encounter more frictional forces and their mobility decreases to 0.5. The anions also encounter more frictional forces than that in free solution, but not as much as the cations because the anions are smaller and less solvated. Thus, the anion mobility decreases to 1.5. Inside the gel, the cations transport 1/4 of the current and the anions transport the rest, i.e. 3/4 of the current (Fig. 3.5 b). Thus the amount of current transported by the ions in buffer reservoir is different from that of inside the capillary which is filled with higher viscosity gel.<sup>4</sup>

When the current starts to flow across the buffer reservoir/gel interface, the cation transference number in the less retarding medium (buffer solution) is

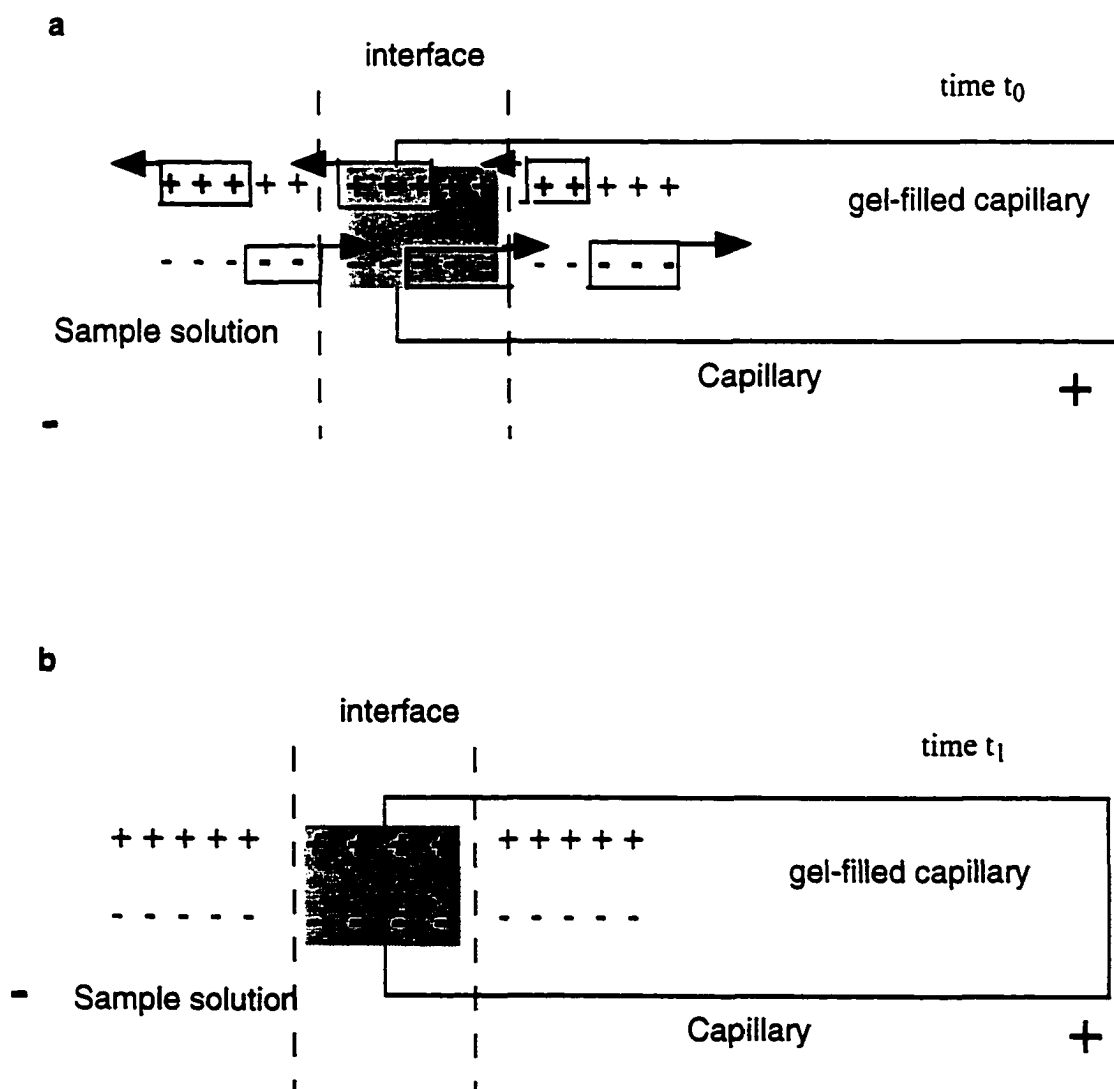
$$T_+ = \lambda_+ / (\lambda_+ + \lambda_-) \quad (3.4)$$

where  $\lambda_+$  and  $\lambda_-$  are equivalent ion conductivities (proportional to mobilities), measured in this medium at the given concentration of electrolyte. Similarly for the gel medium, the retarded transference number is called  $T_r$ ,

$$T_r = R_+ \lambda_+ / (R_+ \lambda_+ + R_- \lambda_-) = T R_+ / (T R_+ + (1-T) R_-) \quad (3.5)$$

If a steady state exists,  $T_r = T$ , which for a medium of unchanging composition demands that  $R_+ = R_-$ . When this is not true, there will be unequal rates of transport of each ion on the two sides of the interface, and changes in ionic composition must develop. A steady-state may, however, be achieved by the establishment of a change in electrolyte concentration on crossing the interface, because the conductivities  $\lambda_+$  and  $\lambda_-$  will then take different values on the two sides. Figure 3.6 shows the change in ionic concentration at the

**Figure 3.6: A change in ionic concentration at the capillary:sample solution interface induced by change in transference numbers at a) time  $t_0$  when the concentration of ions is uniform, and b) at time  $t_1$  when five electrons have passed the outside circuit and the ionic composition is lower in the interface, but it has changed in the bulk of the capillary and sample solution interface**



capillary/sample-solution interface when the transference number changes from one medium to another medium of a different viscosity.

The rate of depletion depends on the difference between the transference numbers in the two media. If we consider the transport of charge across planes of unit area parallel to the interface, but situated at some distance from either side of it so as to include the whole range of variable concentration, the net difference in transport during time  $dt$  will be  $(T - T_r) i dt$  coulombs per unit area, where  $i$  is the current density. At the end of a given time, the change in concentration (measured in equivalents per unit volume), integrated across the interface region, is given in equivalents per unit area by

$$\int (C_a - C) dx = (T - T_r) / F \int i dt \quad (3.6)$$

where  $C$  and  $C_a$  are the initial and altered ionic concentrations,  $x$  is distance, and  $F$  is the Faraday constant;  $i$  is taken as positive when cations move in the positive  $x$  direction, i.e. from the less retarding medium into the gel.<sup>5-7</sup>

Von Lau derived an equation, called extended Kohlrausch equation, for a general case which, when restricted to a linear system of uniform cross-section containing only two species of ion, leads to the following equation<sup>5-7</sup>.

$$\left(\frac{\partial C}{\partial t}\right)_x = (-i / F) (dT / dC) \left(\frac{\partial C}{\partial x}\right)_t \quad (3.7)$$

This equation relates the change of concentration in time,  $(\partial C / \partial t)_x$ , with the change of transference number with concentration  $(dT / dC)$ . In this equation,  $C$  is the concentration of ion,  $t$  is the time,  $T$  is the transference number of an ion,  $x$  is distance from the injection end of the capillary,  $i$  is the current and  $F$  is the Faraday constant.

When the ionic mobilities are independent of concentration, T also does not vary with concentration so that  $dT / dC$  is zero: thus, whatever the variation of C with x (including the case of discontinuous system), the concentration profile will not change with time. If, however, T is a function of C, there must be a movement of the profile. Using the general mathematical relationship, equation 3.8, the velocity of each point could be derived (equation 3.9)<sup>5-7</sup>.

$$(\partial C / \partial t)_x (\partial t / \partial x)_C (\partial x / \partial C)_t = -1 \quad (3.8)$$

$$v = (\partial x / \partial t)_C = (i / F) (dT / dC) \quad (3.9)$$

It is clear that a concentration profile will start to move as soon as it develops, whenever  $dT/dC$  is not equal to zero.

In a technique such as capillary gel electrophoresis, a zone of increased concentration will appear at the detection end, which is washed away by the sheath flow, and a zone of depleted concentration will form at the injection end. The rate of depletion within a zone must remain constant, even after a steady state is attained at the interface. This can in principle be satisfied by a constant rate of enlargement of a zone of uniform concentration, so that equation 3.10 gives a boundary velocity.

$$v = dx/dt = (i/F) ((T - T_r) / (C_a - C)) \quad (3.10)$$

Equation 3.7 is fully consistent with equation 3.6 when T is linearly related to C, however, this will hold only approximately over a limited range of concentration. A better

approximation is given by an equation of the form  $T = T^0 + AC^{1/2}$ , where  $T^0$  is the transference number at infinite dilution.<sup>5-7</sup>

This gradient in transference number induces a movement of the two ionic areas with a velocity  $v$  related to change in transference number with the ionic concentration. In the case of 1xTBE, the high ionic concentration situated on the injection side of the system (cathodic side) moves out of the capillary and is washed away with sheath flow buffer at the anodic side of the CE instrument. The low ionic concentration area located on the detection side of the system (anodic side) progresses into the capillary. Thus, an ion-depleted area forms in time at the cathodic (injection) end of the capillary. This depleted area experiences a higher electric field, whereas there is a lower electric field in the rest of the capillary.

### **3.1.4 An efficient method of sample introduction for capillary gel electrophoresis DNA sequencing**

In capillary electrophoresis the amount of sample injected is usually in the nanoliter range. However, it is often difficult to inject one nanoliter of sample simply because it is difficult to manipulate such a small volume sample. While micromachining technology offers the possibility for automated manipulation of nanoliter samples, current technology is not able to use the nanoliter injection volume capabilities of capillary electrophoresis.<sup>8-9</sup>

Burgi and Chien have presented a series of publications that explains how the stacking conditions have been used in capillary zone electrophoresis.<sup>10-11</sup> A large plug of sample is injected onto the capillary. If the ionic strength of the sample is low enough, most of the electric field will drop across the high resistance sample buffer. At the front of the sample plug, the sample ions are stacked and ready for separation by capillary zone electrophoresis in the higher ionic strength running buffer.



Capillary gel electrophoresis is a powerful technique for DNA sequencing and most of the modern separation techniques are based on noncrosslinked polyacrylamide. Capillary gel electrophoresis with noncrosslinked polyacrylamide have generated sequencing read lengths of over 600 base pairs in two hours.<sup>12-15</sup> Efficient sample introduction onto the capillary would be useful in DNA sequencing applications because it reduces significantly the cost of enzymes, fluorescently labeled primers, and dideoxynucleotides used in the sequencing reaction. Because the viscous separation medium obstructs the physical loading of large sample volumes onto the capillary, on-column stacking is usually difficult in DNA sequencing applications. The low viscosity, short-chain polymers, such as those described by Righetti, could be useful for successful on-column stacking.<sup>16</sup>

In this chapter, we present a different method of sample introduction onto capillaries for DNA sequencing. To understand this sample introduction method, it is necessary to know about the sequencing sample itself. The fragments of DNA sequencing are relatively short, single-stranded oligonucleotides, ranging up to a few thousand base pairs in length, that incorporate a fluorescent tag. Associated with the fragments is a much larger template molecule; usually single stranded. The DNA sequencing fragments are complementary to the template that hybridizes to it. The hybrid of fragment and template has low mobility and, therefore, does not generate useful sequencing information. Hybrid formation has to be minimized to get useful sequencing information. Formamide is a denaturing agent. It disturbs intra-strand hydrogen bonds and as a result of that the sequencing template is free. A small amount of EDTA is often added to the formamide to complex divalent impurity metal ions that might be associated with the DNA. A large amount of salt is also present in the sequencing sample, particularly if a thermostable DNA polymerase and cycle sequencing are used to generate the DNA fragments. Finally, formamide slowly hydrolyses to ammonia and formic acid. Ammonia and formic acid produce ammonium ion and formate ion which further increase the concentration of ions in

the sample. Because of the presence of these ions, DNA sequencing fragments represent a low fraction of the total ionic content of the sample solution and biased electrokinetic injection introduces a low amount of DNA onto the capillary.

The transference number for DNA is given by

$$T_{\text{DNA}} = [\text{DNA}] N_{\text{DNA}} \mu_{\text{DNA}} / \sum [\text{ion}] N_{i \text{ ion}} \mu_{i \text{ ion}} \quad (3.11)$$

where  $N_{i \text{ ion}}$  is the charge on ion  $i$  and  $\mu_{i \text{ ion}}$  is the free-solution mobility of ion  $i$ . We measured the free-solution mobility of DNA in 1xTBE buffer,  $\mu_{\text{DNA}} = 5.0 \times 10^{-4} \text{ cm}^2 \text{ V}^{-1} \text{ s}^{-1}$ , which was essentially independent of the fragment size. This value was close to the free-solution mobility of most small ions. If we assume equal mobility for all ions in the solution, then the transference number for DNA is equal to its concentration times its charge divided by the total ionic strength.

DNA has to be a significant fraction of the total ionic strength of the solution in order to be injected efficiently onto the capillary. The amount of DNA injected during an injection is maximized by maximizing the transference number. Elimination of EDTA from the formamide loading solution, along with the use of deionized formamide, minimizes the total ionic strength. Further reduction in ionic strength is produced by desalting of the DNA sequencing sample through, for example, the use of a size exclusion membrane.

Conventional buffers for sample introduction contain 10 mM EDTA plus some impurity ions present in formamide and some miscellaneous ions present in the sequencing reaction. Therefore, only a small fraction of the DNA is injected onto the capillary. However, if contaminating ions are excluded from the sample, then a very large fraction of the DNA can be introduced from the sample onto the capillary. In this chapter, we document this coulometric loading procedure.

## **3.2 Experimental**

### **3.2.1 Reagents and material**

Formamide was purchased from Fluka, Switzerland. It was deionized by passing on a mixed bed ion exchange resin from Bio-Rad, AG501-x8.

The Sequitherm Cycle Sequencing Kit was purchased from Cedarline Laboratories, Hornby, UK. This kit was used to prepare sequencing samples of fluorescently labeled DNA. The manufacturer's protocol for cycle sequencing was used with the following changes: ROX-labeled M13 universal (-21) primer (ABI, Foster City, CA) was used with M13mp 18 RF1. Single-stranded DNA was bought from USB, Cleveland, OH.

$\gamma$ -methacryloxypropyl trimethoxy silane was purchased from Sigma Chemical, St. Louis, MO, USA. N,N,N',N'-tetramethylethylenediamine (TEMED) and urea were purchased from Gibco BRL, Gaithersburg, MD, USA and ammonium persulfate from Boehringer Mannheim, Indianapolis, IN, USA. TRIS was purchased from ICN Biomedicals Inc., Cleveland, OH, USA, boric acid from BDH Inc., Toronto, ON, Canada. Acrylamide was purchased from Bio-Rad, CA and boric acid from BDH Inc., Toronto, ON, Canada.

### **3.2.2 Instrument**

The conductivity of formamide was measured with a General Radio Corporation model 1650-A impedance bridge.

The fused-silica capillaries, with typical dimensions of 33 cm in length and 50  $\mu\text{m}$  ID and 143  $\mu\text{m}$  OD, were purchased from Polymicro, Phoenix, AZ, USA.

The capillary electrophoresis system and LIF detection system used for these experiments were in-house designed.<sup>17-18</sup> In this system, one end of the capillary was kept at high voltage using a Spellman CZE 1000R (Plainview, CA, USA) high voltage power

supply, while the other end was held in a grounded sheath flow cuvette. Excitation of sequencing samples was achieved using a 5-mW yellow,  $\lambda = 594$  nm, He-Ne laser (PMS, Electro-Optics, Boulder, CO, USA) focused on the sheath flow cuvette below the tip of the capillary. Fluorescence was collected at right angles to the laser beam with a 125X microscope objective (Leitz, Weizlar, Germany). The light collected was imaged onto an iris, passed through a 630DF30 band pass filter (Omega Optical, Brattleboro, VT, USA) and detected with an R1477 photomultiplier tube (Hamamatsu, Middlesex, NJ, USA). The signal from the photomultiplier tube was converted to voltage. Then signal was filtered and digitized by a Macintosh computer.

### 3.2.3 Methods and procedures

Samples were ddTTP terminated. The samples were covered with mineral oil and heated for five minutes at 95 °C. Cycle sequencing was performed using 30 cycles: each cycle consisting of 45 s at 95 °C, 45 s at 47 °C and 90 s at 70 °C.

To minimize hybrid formation between DNA sequencing fragments and template, samples were ethanol precipitated, washed and resuspended in 10  $\mu$ L deionized formamide. Then the sample was diluted again in deionized formamide or a (49:1) mixture of 0.5 M EDTA in formamide at pH 8.0.

The capillaries were treated for one hour with a silanizing solution. This solution was freshly prepared by mixing 0.5 mL of glacial acetic acid, 0.5 mL of water, and 5  $\mu$ L of  $\gamma$ -methacryloxypropyl trimethoxy silane. Then a 3% T solution of acrylamide, with the appropriate catalyst (TEMED), was introduced onto the capillary to coat the capillary wall with a layer of linear polyacrylamide. Once the capillary was filled with the silane solution, the reaction was allowed to proceed for 20 min (see Figures 3.7 and 3.8). Vacuum was

**Figure 3.7: Chemical equations showing the silanized coating procedure**

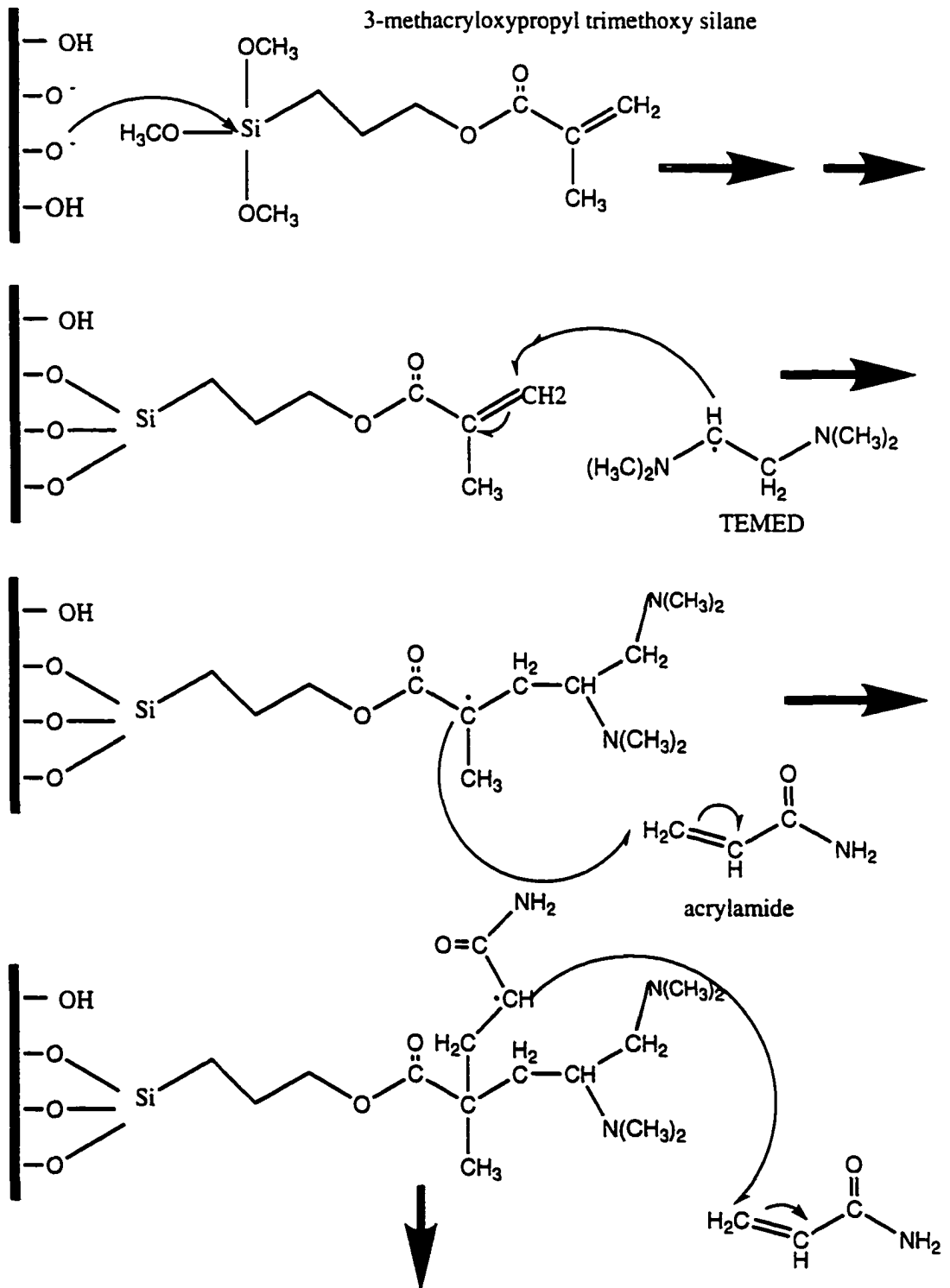
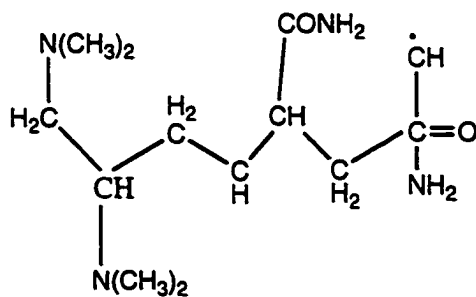
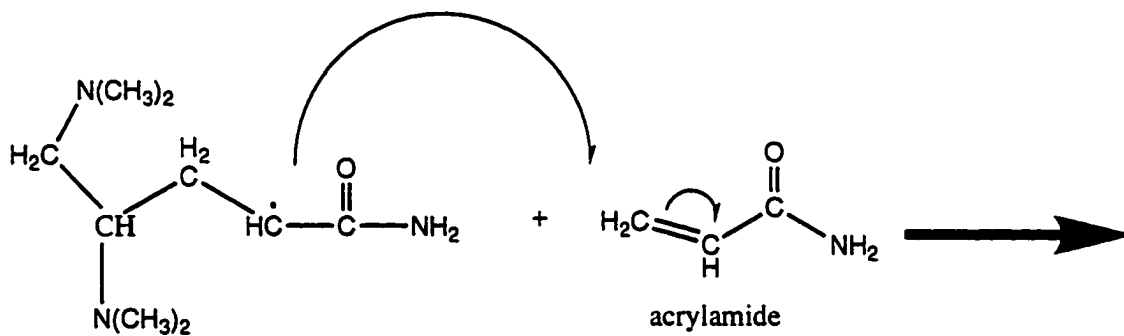
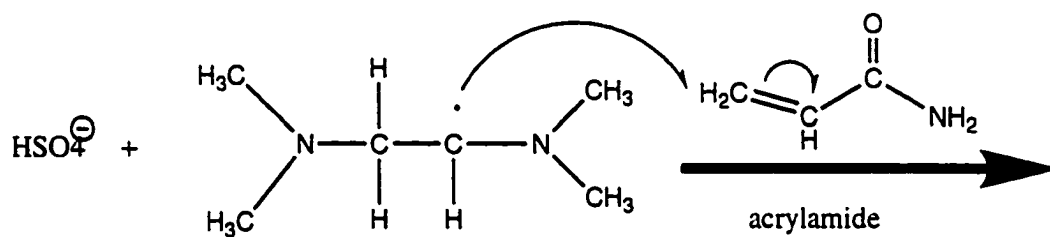
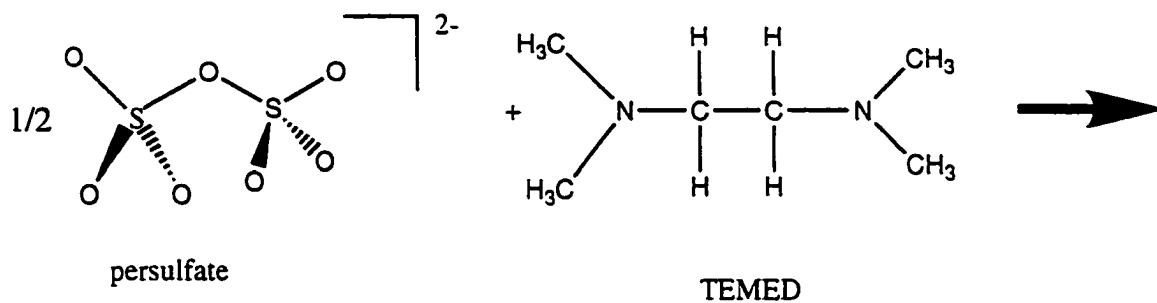


Figure 3.8: Chemical reactions showing free radical polymerization of acrylamide



then used to draw ethanol through the capillary to rinse residual unreacted silane solution. The vacuum was then used for air suction through the capillary.

Before using and whenever it was necessary, the capillary was refilled with 5%T 0%C 7M urea polyacrylamide. The capillary was filled by introducing the injection end of the capillary in a 200- $\mu$ L gas tight syringe (Hamilton, Reno, NV, USA) with a Valco fitting and then applying pressure using a low pressure syringe pump (Razel model A-99, Stanford, CA, USA) for 10 min. The noncrosslinked polyacrylamide sieving matrix (5%T 0%C) was prepared by mixing 1.25 mL of a 20% acrylamide stock solution, 1 mL of 5xTBE buffer (2.7 g TRIS, 1.37 g boric acid and 10 mL 0.5 M EDTA, diluted to 50 mL in deionized water) and 2.1 g of urea and making the solution up to 5.0 mL in deionized and filtered water. This solution was degassed for 20 minutes by bubbling argon gas through it. The polymerization reaction was initiated by adding 2  $\mu$ L N,N,N',N'-tetramethylethylenediamine (TEMED) and 20  $\mu$ L of 10% ammonium persulfate. The solution of 5%T-0%C-7M urea was used for 5 days or more after polymerization.

### 3.3 Results and discussion

The free-solution mobility of fluorescently labeled single-stranded DNA was measured with 1xTBE buffer at a potential of 29,000 V in a 73.8 cm long capillary. The electroosmotic mobility was determined by changing the ionic strength of the buffer by 10% and monitoring the change in current. In the next chapter, Chapter 4, this method of EOF measurement will be discussed thoroughly. The electroosmotic mobility was  $(9.9 \pm 0.1) \times 10^{-4} \text{ cm}^2 \text{ V}^{-1} \text{ s}^{-1}$ . Electrophoretic mobility was obtained by subtracting electroosmotic mobility from total mobility. The mobility of DNA sequencing samples was  $(-5.1 \pm 0.1) \times 10^{-4} \text{ cm}^2 \text{ V}^{-1} \text{ s}^{-1}$ . The free solution mobility of the primer was slightly

lower,  $\mu_{ep} = -5.0 \times 10^{-4} \text{ cm}^2 \text{ V}^{-1} \text{ s}^{-1}$ .

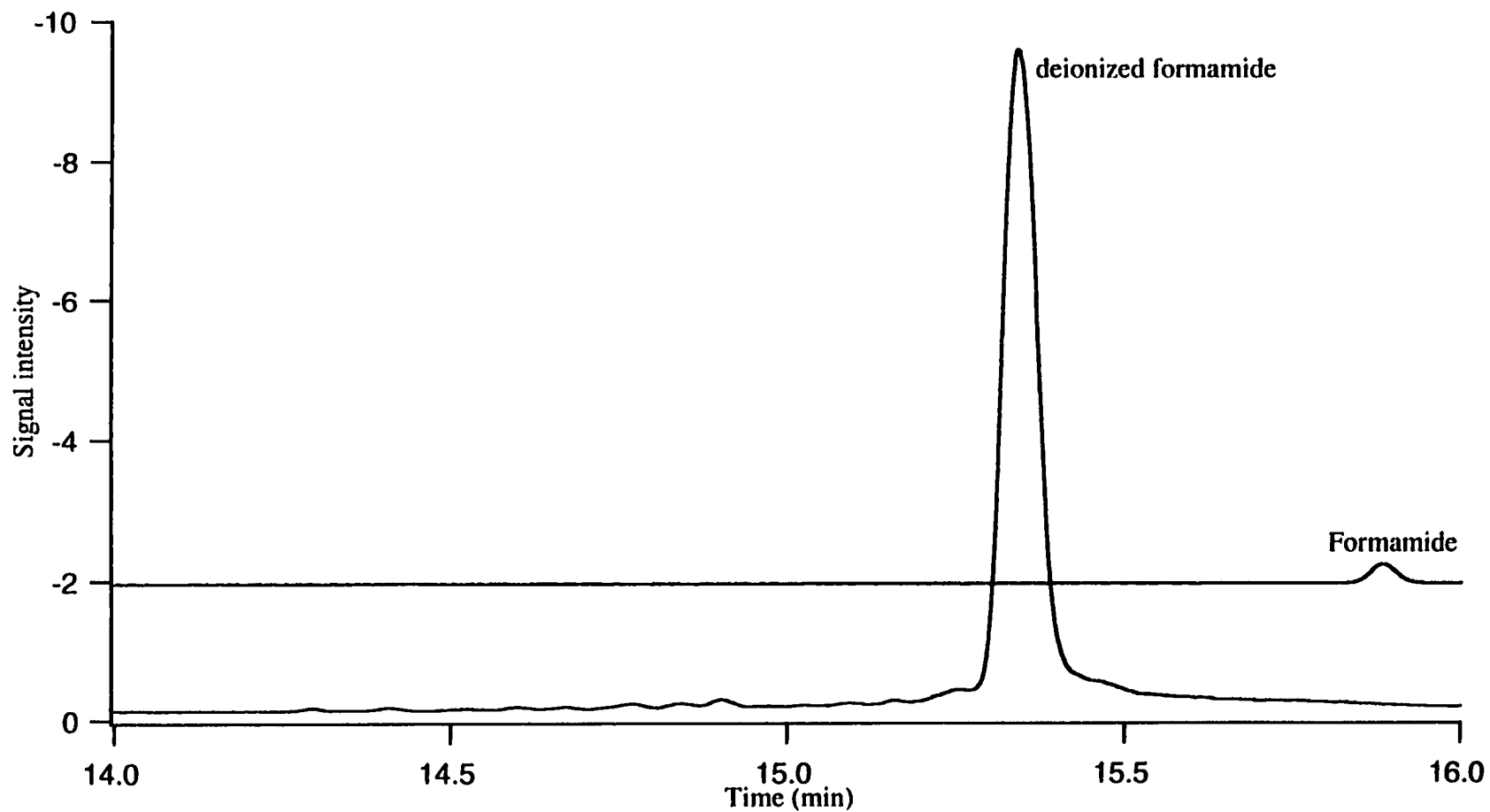
DNA sequencing samples were injected onto the capillary by applying a potential to the sample solution for a period  $t$ . The voltage induces a current,  $i$ , through the capillary. This current is carried by ions from the sample and buffer solution through the capillary; the total charge that passes through the capillary during the injection period is  $I \cdot t$  coulombs. Typical sample loading conditions were 7,800 V potential for 30 seconds. This voltage induces a current of  $2 \mu\text{A}$ , which transfers a total of  $I \cdot t = (2 \mu\text{A})(30 \text{ s}) = 6 \times 10^{-5}$  Coulombs or  $6 \times 10^{-5}$  Coulombs/ $6 \times 10^{-19}$  Coulombs per unit charge or  $4 \times 10^{14}$  unit charge (400 picomole of charge) onto the capillary.

### 3.3.1 Injection

A solution of  $4 \times 10^{-12} \text{ M}$  ROX-primer was injected onto the capillary for 30 seconds at a constant current of  $2 \mu\text{A}$ . The primer was prepared in a deionized formamide resuspension solvent. An 8 kV potential was then applied for 1.5 minutes. A second injection was made for 30 seconds, this time with the primer resuspended in the conventional formamide-EDTA solution. Peak heights were 20 to 40 times higher for the samples resuspended in deionized formamide as compared to samples resuspended in EDTA-formamide. Figure 3.9 shows the effect of deionizing formamide on the injection of ROX-labeled primer. This increase in peak height is inversely proportional to the conductivity of the formamide resuspension buffer. The deionized formamide had a resistivity of  $480 \text{ K}\Omega\text{-cm}$  while the conventional formamide-EDTA mixture had a resistivity of  $23 \text{ K}\Omega\text{-cm}$ . The same current was applied for both injections. In both cases the ions carrying  $4 \times 10^{14}$  units of charge were loaded onto the capillary. In the case of deionized



**Figure 3.9: Comparison of formamide and deionized formamide solution on signal intensity when a  $4 \times 10^{-12}$  M Rox-primer solution was prepared first in a conventional formamide-EDTA solution and then in a deionized formamide re-suspension solvent. Each solution injected for 30 s at a constant current of 2 micro-amp. CE run voltage was 8 kV and capillary length was 33 cm.**



formamide, DNA fragments have a higher transference number and, therefore, resulting in a larger sample loading.

Another way of increasing the amount of injected sample is to increase the injection time. Injection can be done in constant voltage or constant current mode. In the constant voltage mode, peak height is not linearly related to injection time. This non-linearity is due to a decrease in conductivity at the injection end of the capillary. This problem has been described by D. Figeys.<sup>19</sup> Nonlinearity between peak height and injection time is due to a difference in transference number of ions between the free solution and the polymer-filled capillary. The current drops during a constant-voltage injection because of the decreased conductivity at the capillary tip. This decreases the amount of sample injected per unit time. Figure 3.10 shows that in constant current injection mode, the intensity versus the injection time is linear with  $r > 0.999$ . During injection, the electric field increases to keep the voltage constant.

The peak width is inversely related to injection time. Figure 3.11 shows how the peak width decreases by changing the injection time from 20 to 400 s. Equation 3.12 shows the relationship between peak width,  $W$ , and injection time,  $t$ .

$$W = 0.6 + 37 / t \quad (3.12)$$

This result seems surprising because when DNA fragments are being injected onto the capillary, they are also being driven through the separation medium. In this case peak width should increase with increasing the injection time. Instead there is, presumably, an isotachophoretic focusing effect at the capillary tip.

### 3.3.2 Depletion of the sample

Using a low ionic strength DNA sample causes high loading efficiency. The

Figure 3.10: Linearity of injection time and signal intensity in constant current mode (injection conditions are similar to Figure 3.9)

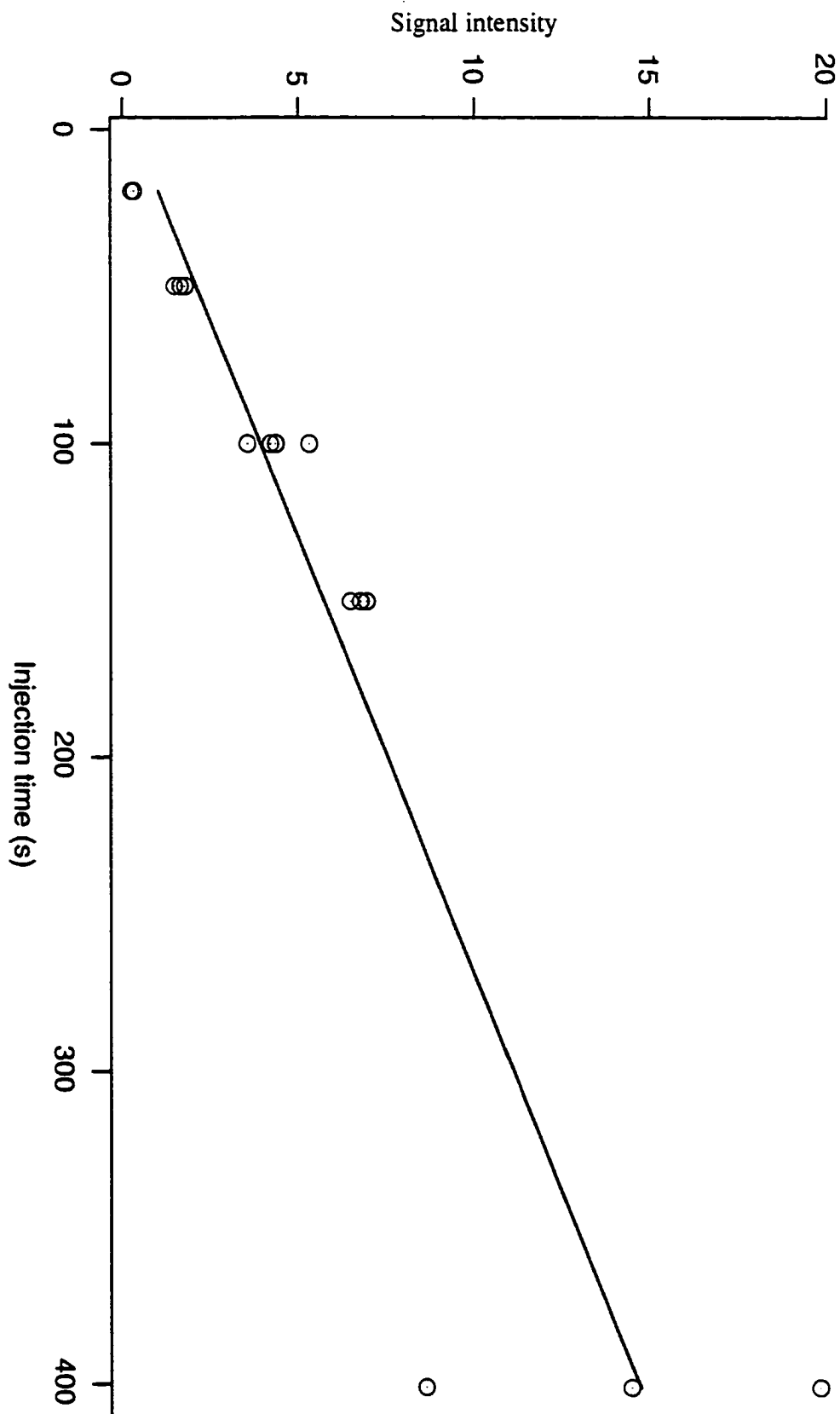
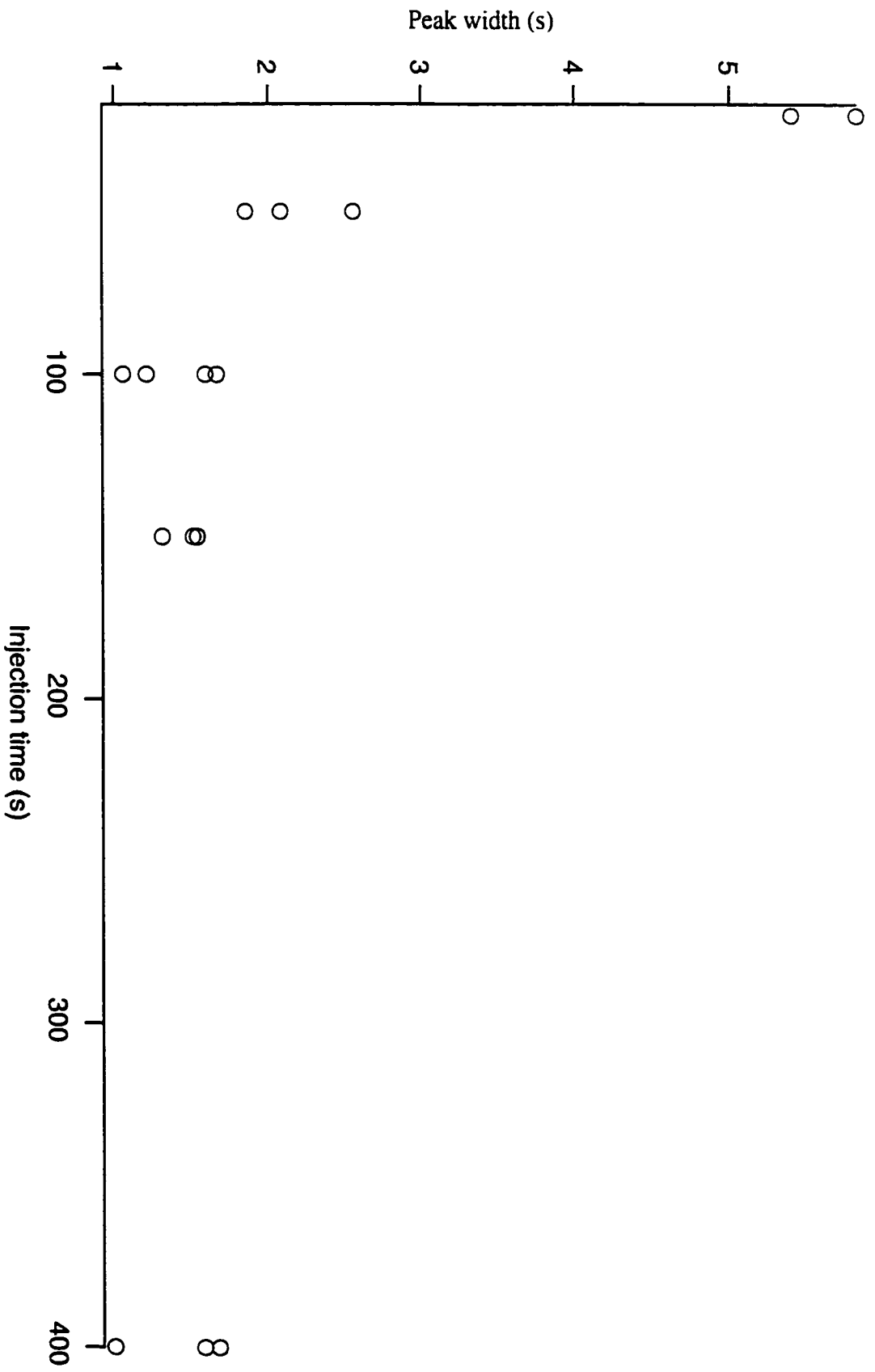


Figure 3.11: Peak width versus injection time (injection conditions and C/F parameters are similar to Figure 3.9)



efficiency of sample introduction was measured by replicate injections of the same sample. A dilute solution of ROX-primer (2 amol /  $\mu\text{L}$ ) and a 3  $\mu\text{L}$  sample volume of this solution in deionized formamide was used for subsequent injections.  $(2 \text{ amol} / \mu\text{L}) \times 3 \mu\text{L} \times 6 \times 10^{23} \text{ molecules} / \text{mole} \times 10^{-18} \text{ mole} / \text{amole} = 3.6 \times 10^4$  DNA molecules are contained within the sample. The first two injections generated peaks of roughly comparable height, while subsequent injections produced an exponential decrease in height with injection number.

Figure 3.12 shows the peak height versus the injection number. Two different constant injection times (75 and 150 s) are depicted in this Figure. A nonlinear least-squares regression analysis fit an exponential function to the peak height:

$$\text{Height} = A + B e^{-n/n_c} \quad (3.13)$$

In this equation A is a residual offset, B is the initial peak height, n is the injection number and  $n_c$  is the number of injections necessary to decrease the peak height to  $e^{-1}$  of the initial value. The results for the regression analysis are shown as the smooth curve in Figure 3.12 and the corresponding equations are shown below.

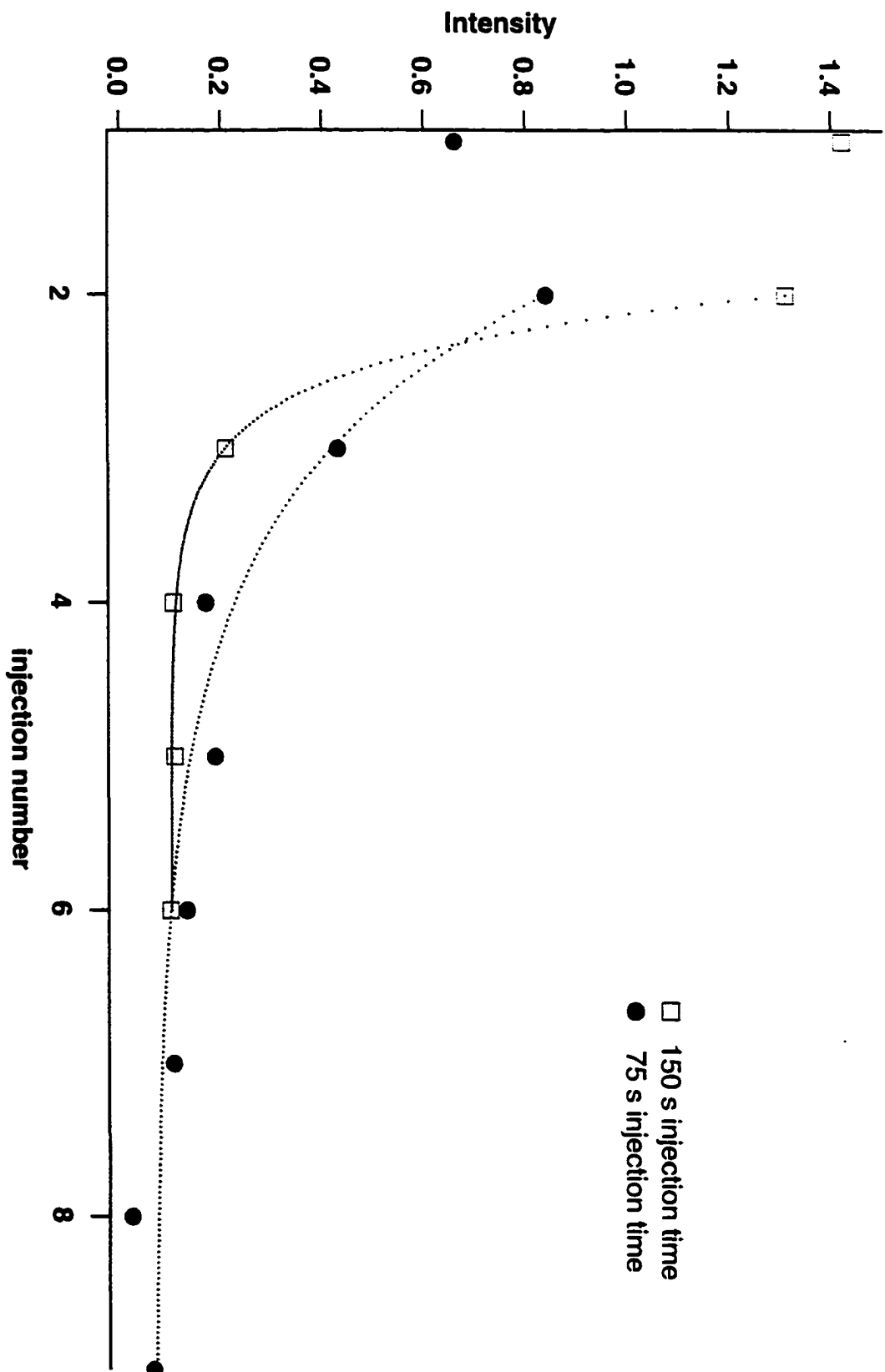
$$\text{Height} = (0.03 \pm 0.02) + (1.8 \pm 0.2) e^{-n/(2 \pm 0.2)} \quad (3.14)$$

$$N = 8 \quad \text{for 75 seconds injection}$$

$$\text{Height} = (0.06 \pm 0.04) + (7.8 \pm 2.2) e^{-n/(1 \pm 0.2)} \quad (3.15)$$

$$N = 5 \quad \text{for 150 seconds injection}$$

Figure 3.12: Peak height versus the injection number for 75 and 150 seconds of injection



In both experiments, the residual offset is zero within the experimental error. This means that the amount of DNA remaining in the sample goes to zero after many injections. For the first few injections, the peak height remains roughly constant. Then it drops exponentially with subsequent injections. Several injections are required to reduce the impurity ion concentration below the electrolysis level for a large-volume sample. Until the ionic strength drops to the electrolysis level, the transference number of DNA remains roughly constant and the number of moles of DNA loaded onto the capillary does not change with subsequent injections. Once the ionic strength drops to the electrolysis level, the transference number of DNA will drop exponentially with subsequent injections. The rate at which DNA is removed from the capillary is given by  $n_c$ . In the case of a 150 s injection, the peak height for a subsequent injection is  $e^{-1} = 37\%$  of the height of the preceding injection. This means that roughly 2/3 of the DNA is introduced onto the capillary in each injection. The exponential decrease in DNA concentration with subsequent injections is surprising. The amount of DNA removed from the sample is proportional to the fraction of charge carried by the DNA. This fraction of charge remains constant after each injection, because injection causes both DNA and impurity ions to be removed from the sample. The overall conductivity of the sample drops with subsequent injections but the fraction of charge carried by DNA remains constant. Solvent electrolysis generates additional ions to compensate for the number of solvent ions lost during injection. The transference number of DNA decreases exponentially with subsequent injections because DNA is depleted while the total ionic strength remains constant.

The rate of DNA removal from the sample is related to the sample volume. Larger sample volumes with the same concentration contain more DNA. Injection from larger sample volume removes a smaller fraction of DNA from larger samples. To investigate the depletion of DNA from large-volume samples, a series of experiments were performed with 150 s constant injection time and an increased sample volume. Figure 3.13 shows

peak height versus injection number for 3, 9 and 20  $\mu\text{L}$  sample volumes of the same concentration. The results of the regression analysis are included as the dotted curve in the figure. The equations describing these cases are shown below.

$$\text{Height} = (0.03 \pm 0.01) + (10.5 \pm 1.6) e^{-n/(0.7 \pm 0.1)} \quad (3.16)$$

$N = 5$             for 3  $\mu\text{L}$  sample

$$\text{Height} = (0.06 \pm 0.04) + (7.8 \pm 2.2) e^{-n/(1.3 \pm 0.3)} \quad (3.17)$$

$N = 6$             for 9  $\mu\text{L}$  sample

$$\text{Height} = (0.06 \pm 0.02) + (1.5 \pm 0.3) e^{-n/(5 \pm 2)} \quad (3.18)$$

$N = 12$            for 20  $\mu\text{L}$  sample

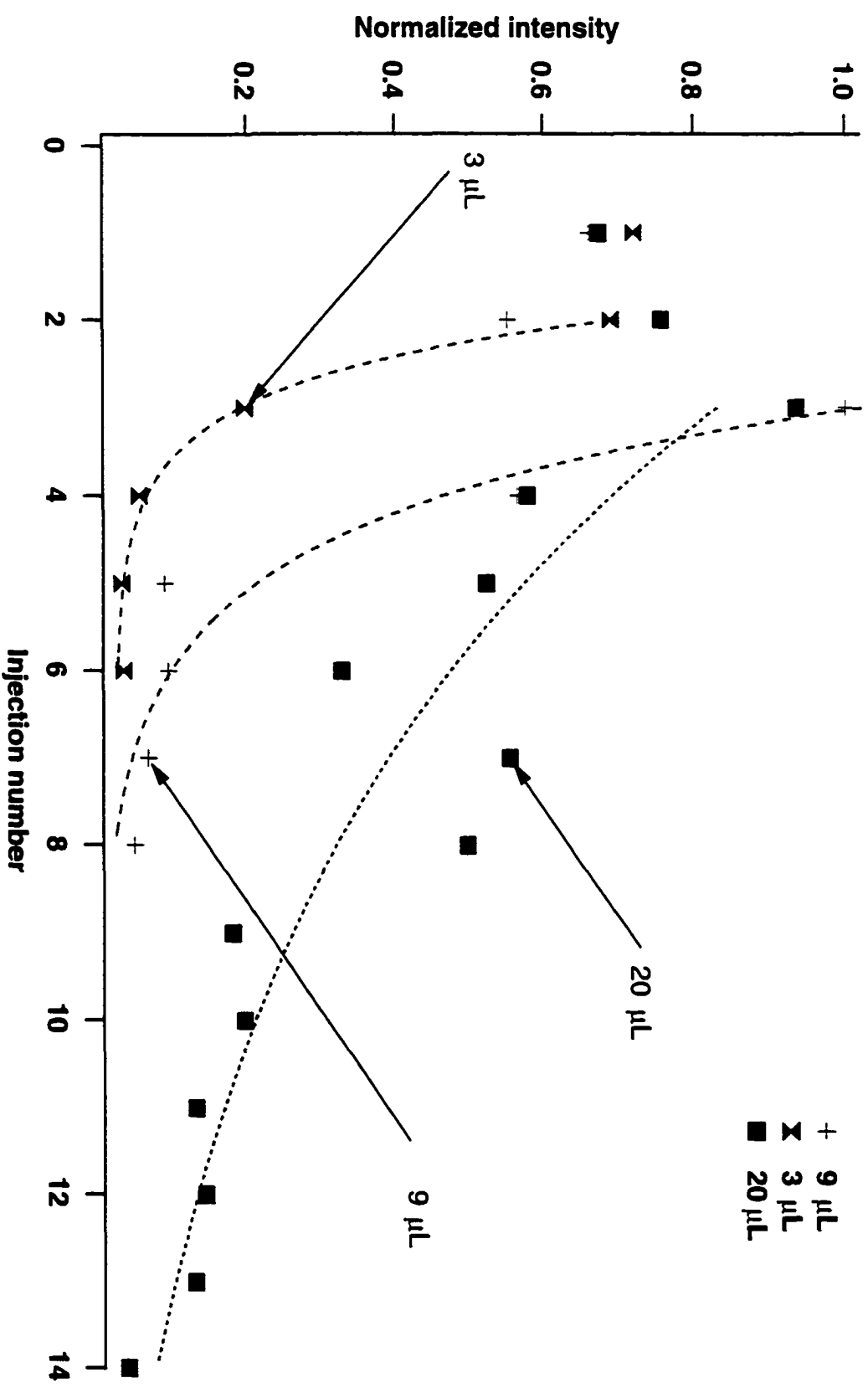
The residual offset for these equations is close to zero. This means that there is no long term retention of DNA in the sample vessel. The characteristic injection number increases roughly proportional to the sample volume. Five injections are required to decrease the DNA content of 20  $\mu\text{L}$  sample by 2/3 while less than one is required for 3  $\mu\text{L}$  sample.

### 3.3.3 Sequencing

Increasing the amount of sample injected is important for DNA sequencing because less of the expensive reagents or more dilute samples could be used for sequencing. Higher



Figure 3.13: Signal intensity versus injection number for 3, 9, and 20  $\mu\text{L}$  of sample



peak height was obtained by injecting a ddTTP sample of M13mp18 from deionized formamide (Figure 3.14) than for the same sample injected from a mixture of formamide:EDTA (Figure 3.15). The sequencing from deionized formamide was done on the same gel that was used for formamide:EDTA. Around 15 times higher peak height is obtained using deionized formamide as compare to than that of the formamide:EDTA. The resolution is slightly poorer in Figure 3.15 than in Figure 3.14 because the sequencing from deionized formamide was performed after the sequencing from formamide:EDTA and a decrease in resolution is often observed for subsequent sequencing. We believe that better results can be obtained if the salt from the sequencing reaction is removed.

### **3.4 Conclusions**

DNA samples that were resuspended in low ionic strength formamide were efficiently introduced onto a separation capillary. This efficient sample introduction technique suggests that dilute DNA sequencing samples were required for analysis. As a result, it should be possible to modify the DNA sequencing reaction to use lower concentration of template, enzyme, nucleotides, and primer. A significant cost savings could be achieved by decreased consumption of these reagents. This is particularly important in large-scale sequencing efforts, such as the human genome initiative and large-scale genomic disease screening efforts.

Figure 3.14: Sequencing M13mp18 ddtTTP using commercial formamide:EDTA

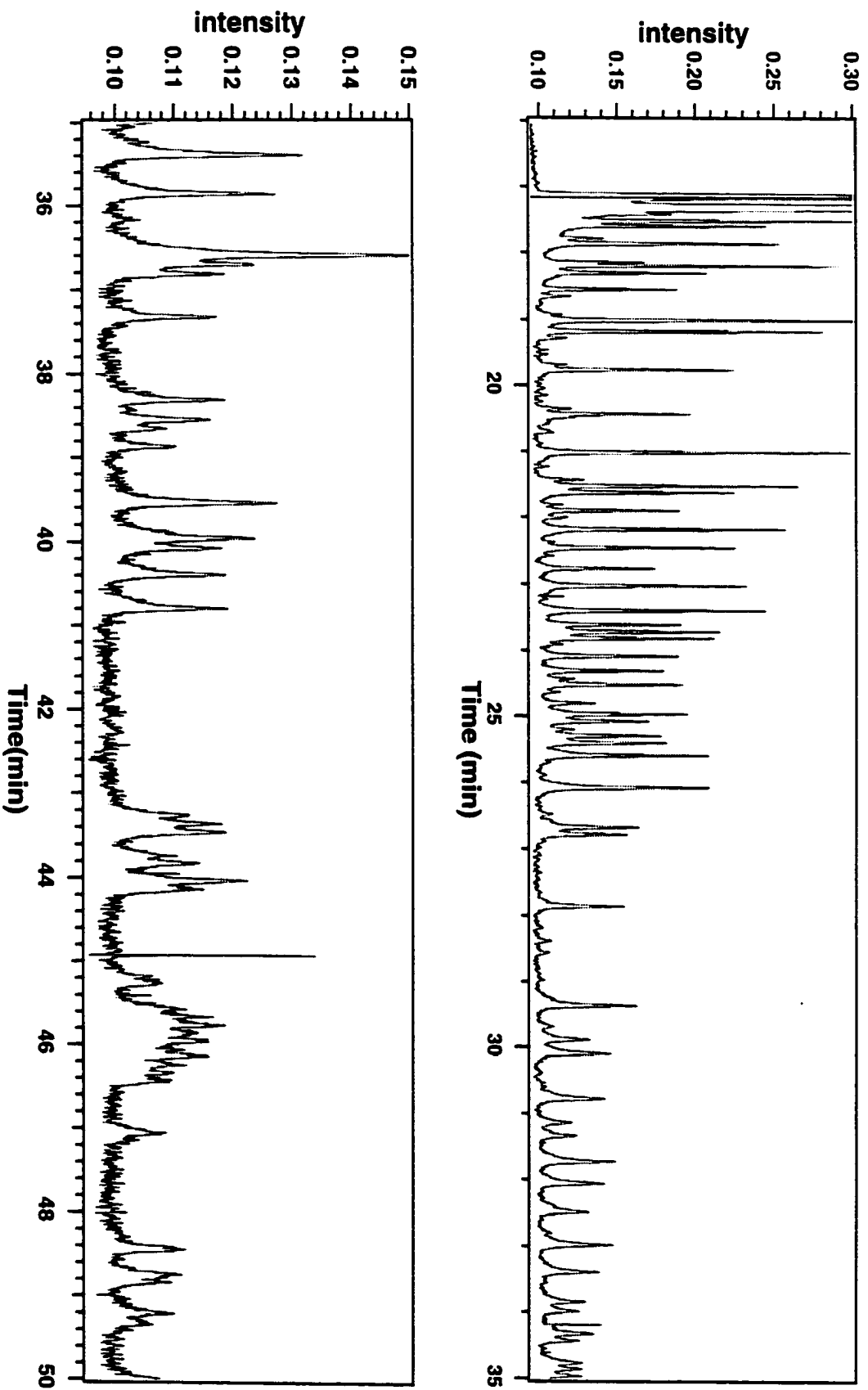
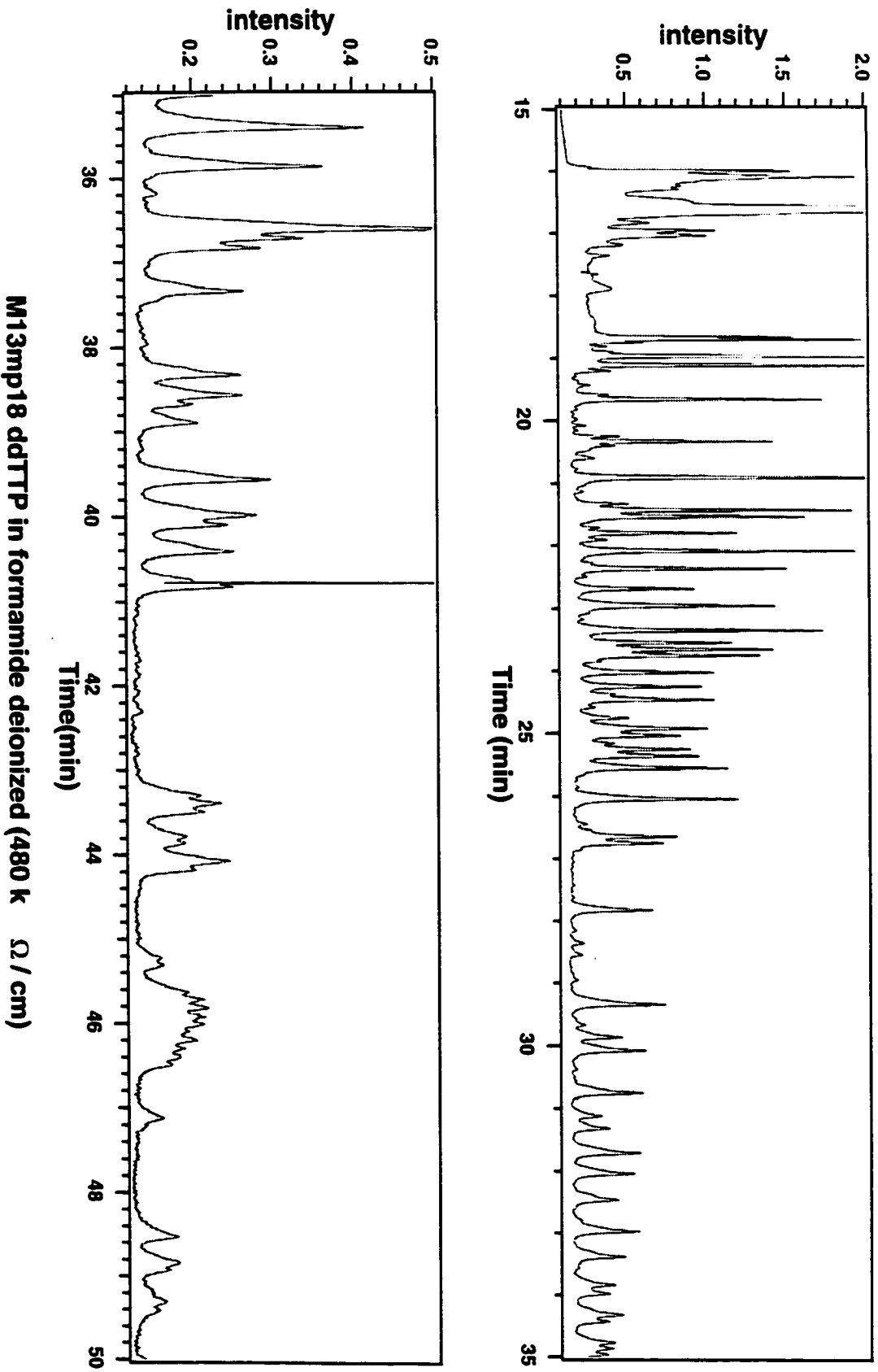


Figure 3.15: Sequencing M13mp18 ddTTP using deionized formamide



### 3.5: References

1. Brown, T. A. Genetics a Molecular Approach; Chapman & Hall: London, Vol. 2, pp 467, 1993.
2. Brown, T. A., Gene Cloning, an Introduction; 2<sup>nd</sup> ed.; Chapman & Hall, pp 286. 1990.
3. Robinson, R. A., and Stokes, R. H., Electrolyte Solutions. 2<sup>nd</sup> Edit. (Revised), Butterworths, London, p. 308, 1967.
4. Daniel Figeys, Ph.D. thesis, university of Alberta, 1995.
5. Spencer, M., Electrophoresis, 4, 36-41, 1983.
6. Spencer, M., Electrophoresis, 4, 41-45, 1983.
7. Spencer, M., Electrophoresis, 4, 46-52, 1983.
8. Harrison, D. J., Fluri, K., Seiler, K., Fan, Z., Effenhauser, C. S., and Manz, A., Science, 261, 895-897, 1993.
9. Manz, A., Effenhauser, C. S., Burggraf, N., Harrison, D. J., Seiler, K., and Fluri, K., J. Micromech. Microeng., 4, 257-65, 1994.
10. Chien, R. L. and Burgi, D. S., Anal. Chem., 64, A492-A496, 1992.
11. Burgi, D. S. and Chien, R. L., J. Microcolumn Sep., 3, 199-202, 1991.
12. Best, N., Arriaga, E., Chen, D. Y., and Dovichi, N. J., Anal. Chem., 66, 4063-7, 1994.
13. Chen, N., Manabe, T., Terabe, S., Yohda, M., and Endo, I., J. Microcolumn Sep., 6, 539-543, 1994.
14. Manabe, T., Chen, N., Terabe, S., Yohda, M., and Endo, I., Anal. Chem., 66, 4243-52, 1994.
15. Zhang, J. Z., Fang, Y., Hou, J. Y., Ren, H. J., Jiang, R., Roos, P., and Dovichi, N. J., Anal. Chem., 67, 4589-93, 1994.

16. Gelfi, C., Orsi, A., Leoncini, F., and Righetti, P. G., *J. Chromatogr. A.*, 689, 97-105, 1995.
17. Chen, D. Y., Swerdlow, H. P., Harke, H. R., Zhang, J. Z., and Dovichi, N. J., *J. Chromatogr.*, 559, 237-246, 1991.
18. Figeys, D., and Dovichi, N. J., *J. Chromatogr.*, 645, 311-317, 1993.
19. Figeys, D., Renborg, A., and Dovichi, N. J., *Electrophoresis*, 15, 1512-1517, 1994.

# **Part II**

## **Electroosmotic flow: measurement and elimination**

# Chapter 4

## **Fast, accurate and universal method for electroosmotic flow rate measurement and evaluation of fundamental parameters affecting separation in capillary electrophoresis<sup>1</sup>**

---

<sup>1</sup> Some parts of this chapter are being prepared for a publication entitled "Fast, accurate and universal method for electroosmotic flow rate measurement and evaluation of fundamental parameters affecting separation in capillary electrophoresis" by **Hossein Ahmadzadeh** and Norman J. Dovichi.



## 4.1 Introduction

Separation of analytes regardless of charge, i.e. anions, cations and neutrals, in a single experiment is possible in CE. This separation is possible because of electroosmotic flow (EOF) that drags the ion in a direction opposite of electrostatic attraction. EOF originates because capillary walls acquire a surface charge when in contact with a polar, aqueous medium. The capillary surface consists of silanol groups that will ionize in aqueous solutions above pH 2.0. Ions of opposite charge (counter-ions) are attracted towards the surface and ions of like charge (co-ions) are repelled from the surface. This attraction and repulsion leads to the formation of an electric double layer that is made up of the charged surface and a neutralizing excess of the counter-ions over co-ions distributed in a diffuse manner in the polar medium. The electric double-layer theory models this distribution of ions and, hence, the magnitudes of the electric potentials that are present near the charged surface. Understanding double-layer theory is the first necessary step towards understanding many of the experimental observations in capillary electrophoresis.<sup>1</sup> In this chapter we introduce a method to measure the EOF. The statistical data analysis has demonstrated that the method is a valid one to measure the EOF both for coated and uncoated capillaries. We have used the same method to evaluate fundamental properties of EOF that affect a separation.

### 4.1.2 History of EOF

EOF was first used in chromatography and reported in 1939 by Strain.<sup>2</sup> He recognized the difference between electrophoresis and electrochromatography and partitioning of the analytes between a mobile and a stationary phase. This early work on the separation of biological macromolecules used both electrophoretic and electroosmotic mobilities for the movement of the analytes through the separation medium. This was the first published report that showed the importance of EOF in separation science. Strain and

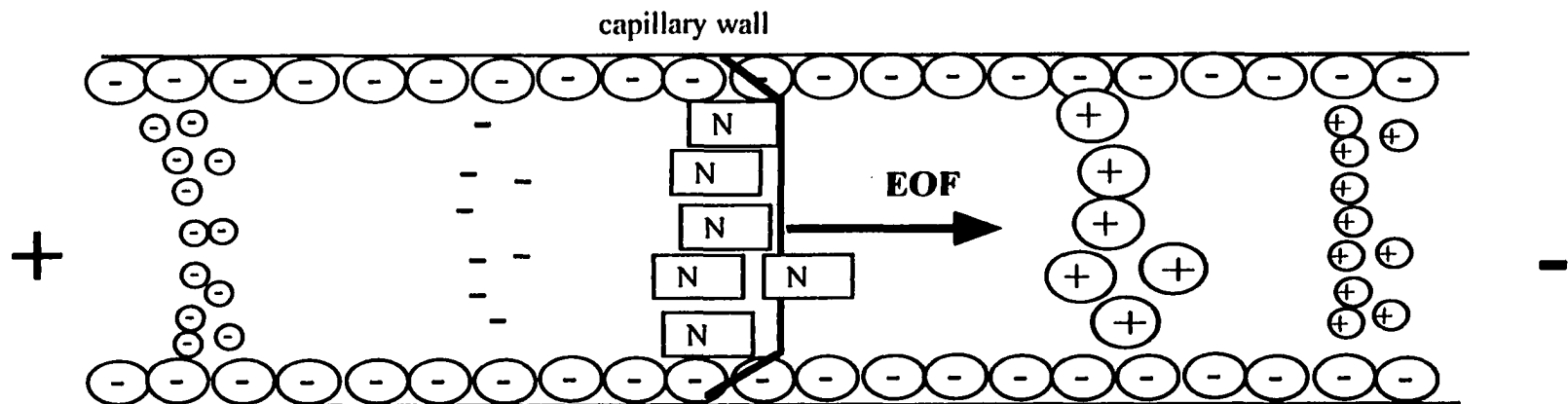
Sullivan reviewed early publications on electrically driven separation techniques that showed the possibility of analyzing basic, neutral, and acidic molecules using the EOF through a paper matrix.<sup>3</sup> Mould and Syngé reported the separation of polysaccharides using EOF through a colloidal membrane.<sup>4</sup> This report is perhaps the first unambiguous report where EOF is used to drive a mobile phase through a stationary phase. Kowalczyk measured the EOF velocity in a number of different thin-layer supports.<sup>5</sup> Jorgenson and Lukacs demonstrated the use of EOF in capillaries (0.17 mm ID) and showed the possibilities for reduced plate heights.<sup>6</sup>

#### 4.1.3 Theory of EOF

EOF was recognized as a distinct physical phenomenon by Wiedemann in 1852.<sup>7</sup> Figure 4.1 shows how EOF is used in CE to differentiate the movements of cations, anions and neutrals. An imaginary analyte containing anions, cations, and neutrals is injected onto the capillary. After high voltage is applied, the cations move toward the negative electrode and anions move toward the positive electrode. Smaller ions have higher mobility and, therefore, their movement towards the opposite sign electrode is faster than that of bigger ions with the same number of charges. The neutral molecules move with the velocity of EOF. Anions are moving against the direction of EOF, but the flow rate for EOF is higher than electrophoretic mobilities of the smallest anions and, therefore, anions also move toward the negative electrode. Because of this movement against the EOF directions, anions will reach the detector last. EOF allows for the separation and detection of anions, neutrals, and cations in a single CE run experiment. This situation is depicted in Figure 4.1

EOF, therefore, refers to the movement of bulk liquid relative to a stationary charged surface due to an applied electric field.<sup>8</sup> Most substances acquire a surface electric charge as a result of ionization of the surface and/or from adsorption of ionic species. For a

**Figure 4.1: Differential solute migration in a column under a potential gradient**



⊖ silanol groups on capillary wall

⊖ small anion

- bigger anion

N a neutral molecule

⊕ big cation

⊕ smaller cation

+ positive electrode

- negative electrode

fused-silica capillary, EOF arises mainly from ionization of the silanol groups on the internal wall of the capillary.

#### 4.1.3.1 Double-layer theory

The double layer (Figure 4.2) is generally explained using the Gouy-Chapman model in the revised version proposed by Stern, called SGC theory.<sup>1,9,10</sup> According to the SGC model, the double layer consists of a fixed layer of negative charges on the capillary wall and a positive part formed by a net excess of counter-ions, cations, in the background electrolyte. The counter-ions are arranged in a fixed layer (the Stern layer) and in a diffuse layer. At a position just outside of the compact-diffuse layer interface a plane of shear is established. The potential at this interface is known as the zeta potential,  $\zeta$ . While the potential in the diffuse part of the double layer falls exponentially to zero, the distance from the wall over which it drops by  $e^{-1}$  is referred to as the thickness of the double layer,  $1/\kappa$ . When a voltage is applied across the capillary to run a CE experiment, the cations in the diffuse layer migrate toward the cathode, negative electrode, dragging with them their hydration shells. Because of frictional forces among the solvent molecules, the bulk liquid also moves. Since the flow essentially originates at the silica surface, it is assumed to have a near plug-like flow profile, thus giving rise to less band broadening than HPLC where pressure driven flow results in a parabolic profile (Figure 4.3). Several groups have used microscope optics to provide images of the flow profiles within narrow capillaries. Taylor and Yeung observed the plug flow profile as predicted from theory.<sup>11</sup>

Practically, EOF profile depends on both the capillary diameter,  $d$ , and the thickness of the double layer,  $1/\kappa$ . Rice and Whitehead proposed that the flow profile

**Figure 4.2: Schematic representation of the double layer structure according to Stern's model**

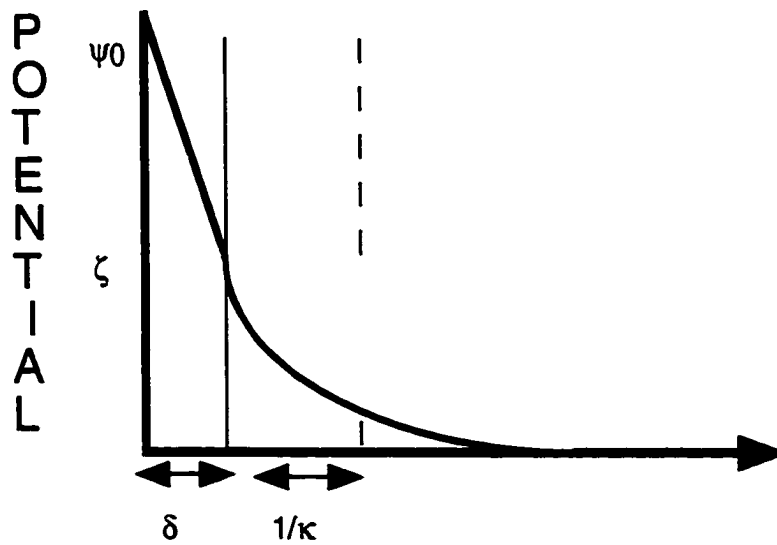
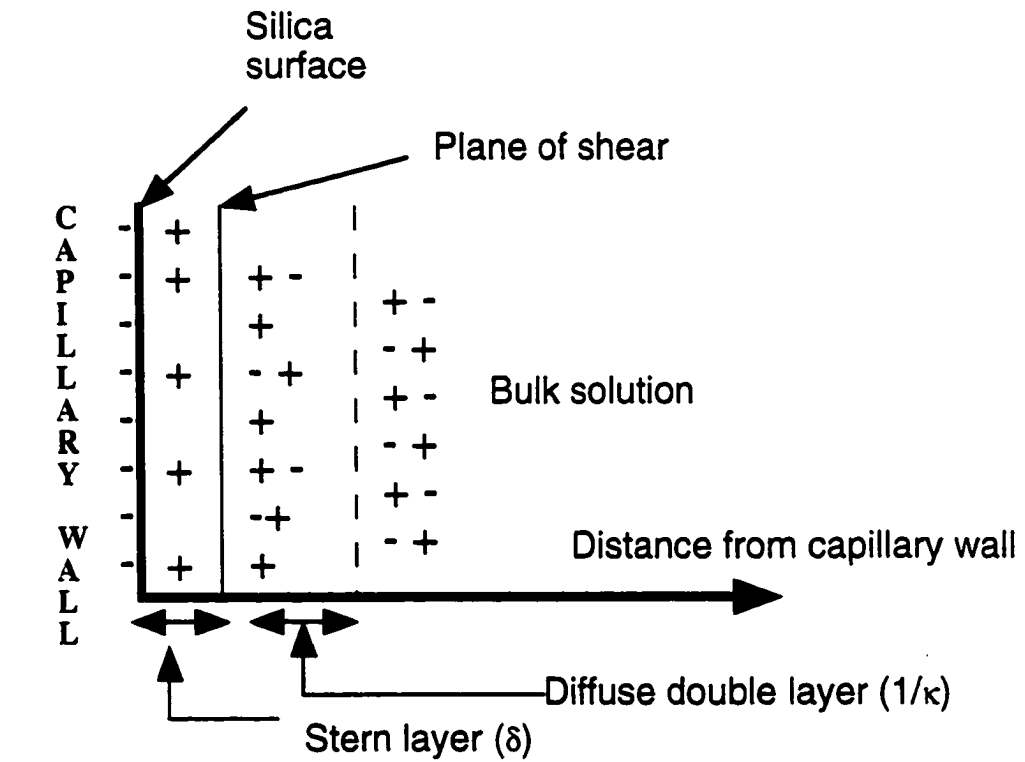
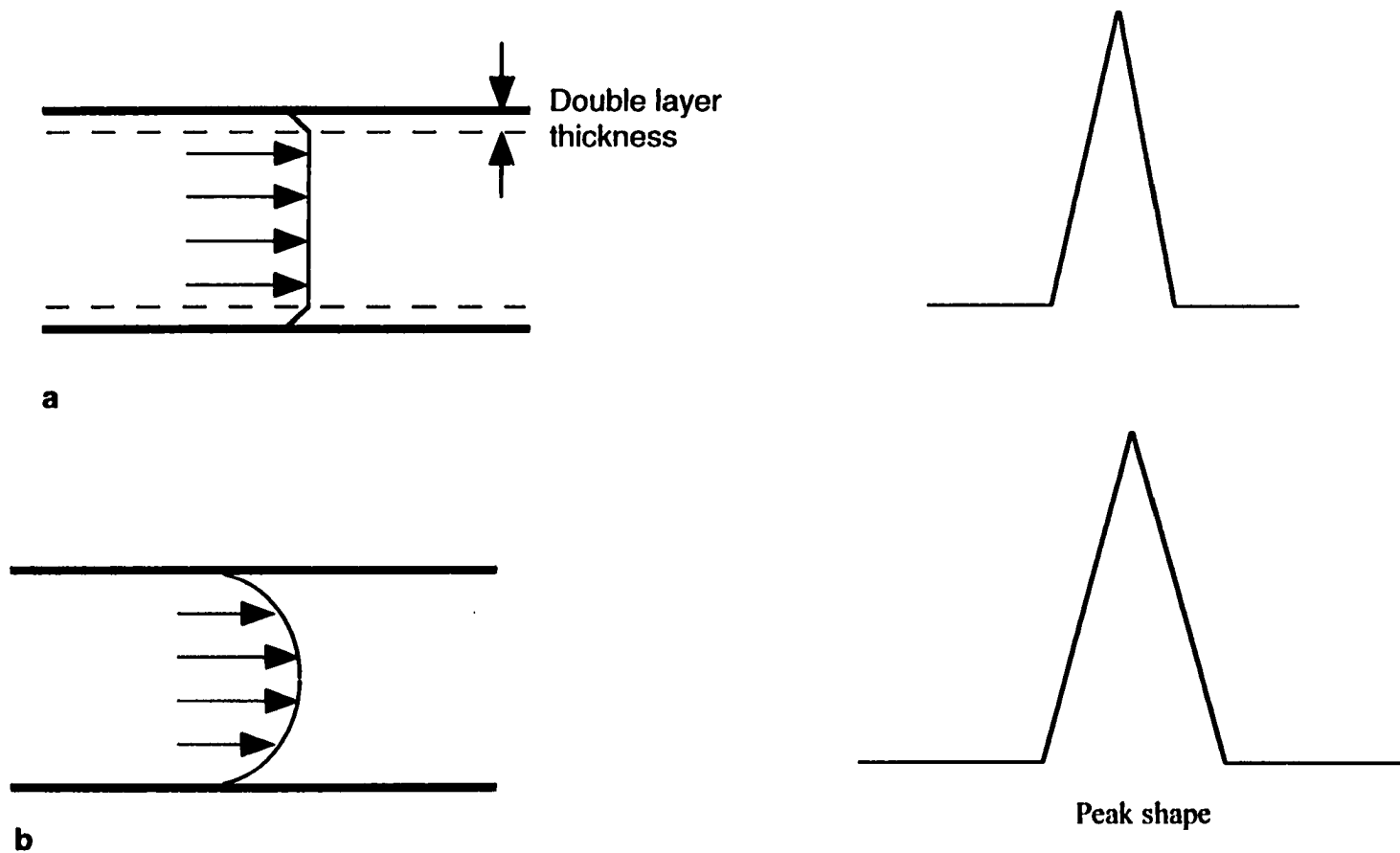


**Figure 4.3: Flow profile and resulting peak shape with a) electrokinetic, and (b) pressure driven flow. The arrows indicate vectors and corresponding solute profile**



would be plug-like if  $d$  is much greater than  $1/\kappa$ .<sup>12</sup> As  $d$  approaches  $1/\kappa$ , double-layer overlap occurs. Finally, when  $d$  and  $1/\kappa$  are of the same order, the parabolic form is expected. It was suggested that EOF velocity is acceptable when  $d \geq 10/\kappa$ .<sup>7</sup> Experimental observations are in good agreement with this theoretical approach, although at high interface potentials the theory is not strictly valid because of the failure of the Debye-Huckel approximations.<sup>13</sup>

#### 4.1.3.2 Stern-Gouy-Chapman model

It was already discussed that the electrical double layer consists of two layers. The inner layer includes adsorbed ions, and a diffuse layer that contains ions that are distributed according to the electro static forces and random thermal motion. To treat the double layer quantitatively, Gouy (1910) and Chapman (1931) made some assumptions for their model. <sup>1</sup> They assumed a flat surface with infinite dimensions and uniformly distributed charges on the surface. This assumption is acceptable for a capillary because the internal surface of the capillary could be considered flat at the molecular level. The adsorbed counter-ions in the diffuse part of the double layer were assumed to be point charges distributed according to the Boltzman distribution. This assumption can fail because ions have a finite size. To facilitate the mathematical treatment of the model, they also assumed a 1:1 symmetrical electrolyte with charge number of  $Z$ .

The electric potential at the capillary surface is  $\psi_0$  and at a distance  $x$  from the surface in the electrolyte solution is  $\psi$ . The fused-silica capillary inner surface is negatively charged (Figure 4.2) and if the Boltzman distribution is applied, the equations 4.1 and 4.2 are obtained:

$$n_+ = n_0 \exp (+ Z e \psi / \kappa T) \quad (4.1)$$

$$n_- = n_0 \exp (- Z e \psi / \kappa T) \quad (4.2)$$

where  $n_+$  and  $n_-$  are the numbers of positive and negative ions per unit volume at points where the potentials are  $\psi$ . The electric potential energy is  $- Z e \psi$  and  $+ Z e \psi$ , for anions and cations respectively.  $Z$  is the number of charges on each ion,  $e$  is the unit charge and  $n_0$  is the corresponding concentration of each ionic species in bulk electrolyte.

Therefore,  $\rho$ , the net volume charge density at points where the potential is  $\psi$  is given by the equation 4.3:<sup>1</sup>

$$\begin{aligned} \rho &= Z e (n_- - n_+) \\ &= Z e n_0 \{ \exp (- Z e \psi / \kappa T) - \exp (+ Z e \psi / \kappa T) \} \end{aligned} \quad (4.3)$$

$$\rho = 2 Z e n_0 \text{Sinh} (Z e \psi / \kappa T) \quad (4.4)$$

Poisson's equation relates  $\rho$  to  $\psi$  for a flat double layer as:

$$d^2 \psi / d x^2 = \rho / \epsilon \quad (4.5)$$

where  $\epsilon$  is the permittivity.

Combining equations 4.4 and 4.5 gives the equation 4.6:



$$d^2 \psi / dx^2 = (2 Z e n_0 / \epsilon) \text{Sinh} (Z e \psi / \kappa T) \quad (4.6)$$

The differential equation 4.6 can be solved with the Debye-Huckle approximation ( $e^x = 1 + x$  for small  $x$ , i.e  $\exp (+ Z e \psi / \kappa T) = 1 + Z e \psi / \kappa T$  for  $Z e \psi / \kappa T \ll 1$ ) and boundary conditions of  $\psi = \psi_0$  when  $x = 0$ ; and  $\psi = 0, d\psi / dx = 0$  when  $x = \infty$ . The results of solving the differential equation of 4.6 is shown by equation 4.7. The parameter  $\kappa$  is given by the equation 4.8.

$$\psi = \psi_0 \exp (-\kappa x) \quad (4.7)$$

$$\kappa = (2 e^2 n_0 Z^2 / \epsilon k T)^{1/2} = (2 e^2 N_A C Z^2 / \epsilon k T)^{1/2} \quad (4.8)$$

where  $N_A$  is Avogadro's constant and  $C$  is the electrolyte concentration. For a 1 mM 1:1 electrolyte, therefore, the thickness of the double layer is 10 nm.

Equation 4.7 shows that at low potentials, the surface potential decreases exponentially from the charged capillary surface. Close to the charged surface where the potential is relatively high, the Debye-Huckle approximation is not valid and it is predicted that the potential decreases at a rate greater than the exponential rate.

As mentioned before, the derivations for the diffuse double layer were based on the assumption of point charges in the electrolyte medium. But the ions do not have a zero radius and this will limit the inner boundary of the diffuse part of the double layer. The center of an ion cannot approach the surface closer than its hydrated radius without becoming specifically adsorbed. Stern modified the Gouy-Chapman model and proposed another model. According to the Stern model the double layer is divided into two parts

separated by a plane called the Stern plane. This plane is located at about a hydrated ion radius from the surface. Stern also considered the possibility of specific ion adsorption. In this kind of adsorption the ions are attached to the surface by electrostatic and/or Vander Waals forces strongly enough to overcome thermal motion. The centers of any specifically adsorbed ions are located in the Stern layer. Ions with centers located beyond the Stern plane form the diffuse part of the double layer.

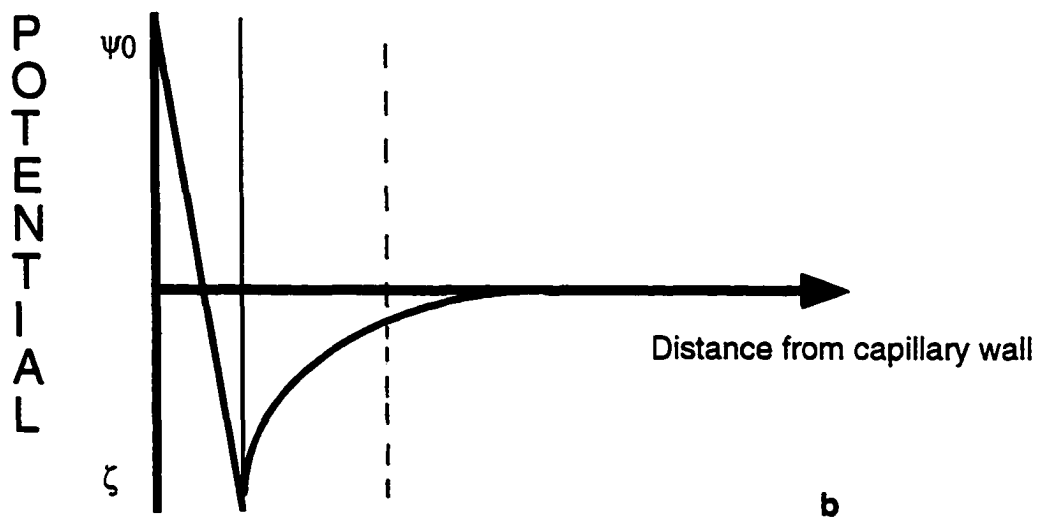
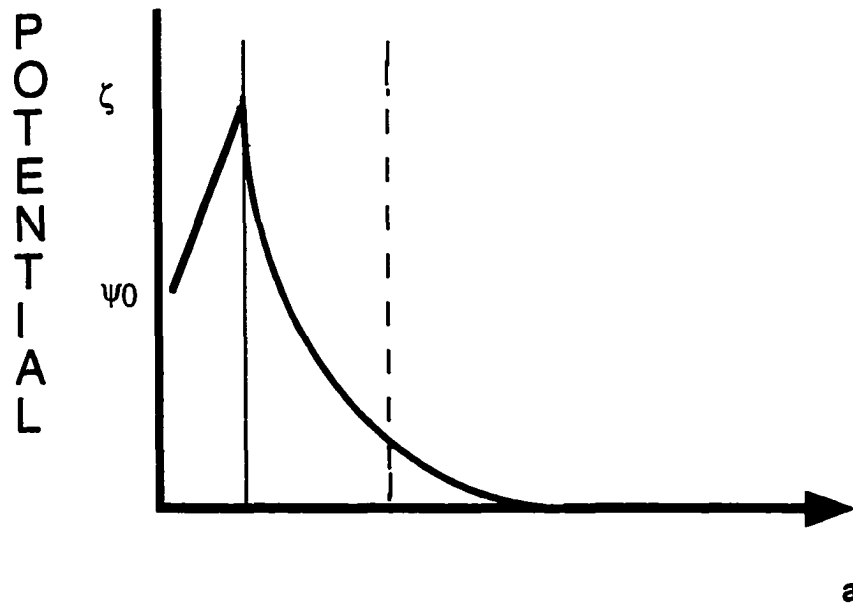
The potential changes from  $\psi_0$  (surface or wall potential) to  $\zeta$  (Stern potential) in the Stern layer, and decays from  $\zeta$  to zero in the diffuse part of the double layer. This is shown schematically in Figure 4.2.

If there is no specific ion adsorption, the charge densities at the surface and at the Stern plane are equal. When there is specific ion adsorption, counter-ion adsorption usually predominates over co-ion adsorption and a typical double layer situation is depicted in Figure 4.4 a. Polyvalent or surface active counter-ions may reverse the charge within the Stern layer. This will cause  $\psi_0$  and  $\zeta$  to have opposite signs and this situation in capillary electrophoresis causes a reversal in EOF direction. To get the analytes to the detector, the polarity of the power supply has to be reversed in this case. Adsorption of surface active co-ions could create a situation in which the sign of  $\psi_0$  is greater than  $\zeta$  potential (Figure 4.4 b)<sup>1</sup>.

The electrophoretic velocity of an ion is simply the product of its electrophoretic mobility and the electric field strength acting on it (equation 4.9), but the analysis of EOF velocity of the bulk solution is more complicated.

$$v_{ep} = \mu_{ep} E \quad (4.9)$$

**Figure 4.4: Schematic diagram showing the adsorption effect on surface potential versus distance from the surface if a) co-ions (increasing of surface charge) are adsorbed, and b) polyvalent counter ions (charge reversal)**



In columns where the electric field strength,  $E$ , and the zeta potential,  $\zeta$ , of the wall are homogeneous throughout the column, the bulk electroosmotic velocity,  $v_{\text{eof}}$ , can be expressed as:

$$v_{\text{eof}} = \mu_{\text{eof}} E \quad (4.10)$$

$$\mu_{\text{eof}} = \epsilon \zeta / 4 \pi \eta \quad (4.11)$$

where  $\mu_{\text{eof}}$  is called the electroosmotic flow (EOF) mobility and  $\epsilon$  is the dielectric constant and  $\eta$  is the viscosity of the double layer at the wall. However, in cases where there is a nonconstant distribution in either electric field strength or zeta potential throughout the column, the bulk velocity has to be averaged over the whole column. This latter case is useful for the way that we introduce in this chapter how to measure the EOF, therefore it is useful to elaborate on this concept.<sup>1</sup>

#### 4.1.4 Mismatch of electroosmotic flows

When a capillary column of length  $L$  is filled with two different concentration buffers of the same electrolyte, a length ( $x L$ ) of the column is filled with concentration 1 and a length  $(1 - x) L$  of the column is filled with concentration 2. If  $0 \leq x \leq L$ , then the total resistance  $R$  of the column, based on the equation  $R = \rho L/A$ , will be

$$R = (\rho_1 x + \rho_2 (1 - x)) L / A \quad (4.12)$$

where  $A$  is the column cross-section and  $\rho_1$  and  $\rho_2$  are the resistivities of buffer 1 and buffer 2, respectively.<sup>14</sup>

If now a voltage  $V$  is applied across the capillary, the electric current ( $I = V/R$ ) will then have a value according to the following equation:

$$I = V A / (L (\rho_1 x + \rho_2 (1 - x))) \quad (4.13)$$

This equation can be rearranged and solved for  $x$  as

$$x = ((I_2 / I) - 1) / ((I_2 / I_1) - 1) \quad (4.14)$$

The current when the column is completely filled with concentration 1 is

$$I_1 = V A / \rho_1 L \quad (4.15)$$

and when the column is filled with the same buffer but concentration 2 the current is:

$$I_2 = V A / \rho_2 L \quad (4.16)$$

The above equations (4.15 and 4.16) indicate that, if the currents  $I_1$  and  $I_2$  are known, it is possible to calculate the filled length,  $x$ , by monitoring the current  $I$  of the mixed system and using equation 4.14.

Because the electric field strength,  $E$ , is defined as the product of the current density and resistivity, the local field strengths,  $E_1$  and  $E_2$ , in two regions with different concentrations are given by:

$$E_{1,2} = E_0 \rho_{1,2} / (\rho_1 x + \rho_2 (1 - x)) \quad (4.17)$$

When only buffer 1 or buffer 2 is used, the system is uniform and the field strength is  $E_0 = V / L$ . The above equation shows that the field strength inside the lower resistance region is less than the original uniform field strength and the field strength inside the higher resistance region is higher.

While the absolute value of the electric field strength in regions 1 and 2 depends on  $x$ , the ratio between them remains a constant and only depends on the resistivities.

$$E_1 / E_2 = \rho_1 / \rho_2 \quad (4.18)$$

The resistivities  $\rho_1$  and  $\rho_2$  are inversely proportional to the concentration  $C_1$  and  $C_2$  for the same buffer composition. Hence, the ions inside the lower concentration region experience a higher electric field strength and move faster than the ions inside the higher concentration region. When they pass this concentration boundary, they experience lower electric field strength and slow down.<sup>14</sup>

#### 4.1.5 The methods of EOF measurement

The classical method to measure the EOF is to inject a neutral compound onto the capillary, called neutral marker, and then record its migration time when a high voltage is applied.<sup>15-17</sup> The accuracy of the neutral marker method depends on the neutral marker

itself, which has to have no partial charge at the applied pH. It may not be neutral at all pHs. Another restriction of the neutral marker method is that if there is a partial charge on the neutral marker, it may adsorb onto the capillary wall and this leads to false calculation of EOF. One last problem for the neutral marker method is the detectability of the neutral marker itself. Usually UV is used as a detector for CE and, therefore, the neutral marker has to be a good UV-absorber in order to be detected by the detector. In our case where laser-induced fluorescence is used as detection system, there are not many reagents that are both neutral and fluorescent at the same time. If there is a compound with these conditions it is very difficult to maintain its neutrality in a wide range of pH. The other problem is that fluorescence is also a function of pH and in acidic pHs the fluorescence sometimes quenches. It was because of the above mentioned difficulties that we used an alternative method to measure the EOF.

The other method of EOF measurement is to weigh the mass of electrolyte transferred from the capillary inlet to the capillary outlet over a constant period of time.<sup>18</sup> In this gravimetric method of EOF measurement, it is necessary to eliminate the losses caused by evaporation of the electrolyte eluted out of the capillary. The use of a digital balance in this method is recommended.

Williams and Vigh have proposed a method for EOF measurement that relies on pressure rinse available with most CE instrument.<sup>19</sup> The method has several steps. The first step is filling the capillary with background electrolyte and injection of a neutral marker dissolved in the same electrolyte. Then pressure is applied to move the injected band. The next step is injection of a second band of neutral marker followed by the background electrolyte and applying pressure to mobilize both bands. Finally, after applying high voltage, the third band of neutral marker is injected and by applying pressure all three bands will pass the detector. Both the injection times and CE run times have to be set precisely and the migration times for all three bands have to be measured carefully in order

to use the equations derived by William and Vigh for EOF measurement.<sup>19</sup>

Lee, Dadoo and Zare developed a method for measuring EOF rate continuously in capillary zone electrophoresis.<sup>20</sup> The method is based on introducing a reference flow of solution containing a fluorescent marker into the running buffer downstream from the detection zone. The EOF flow rate causes the dilution of the fluorescent dye. By monitoring the fluorescence intensity, it is possible to monitor the changes in EOF. Figure 4.5 depicts this post-column type of design for EOF measurement.

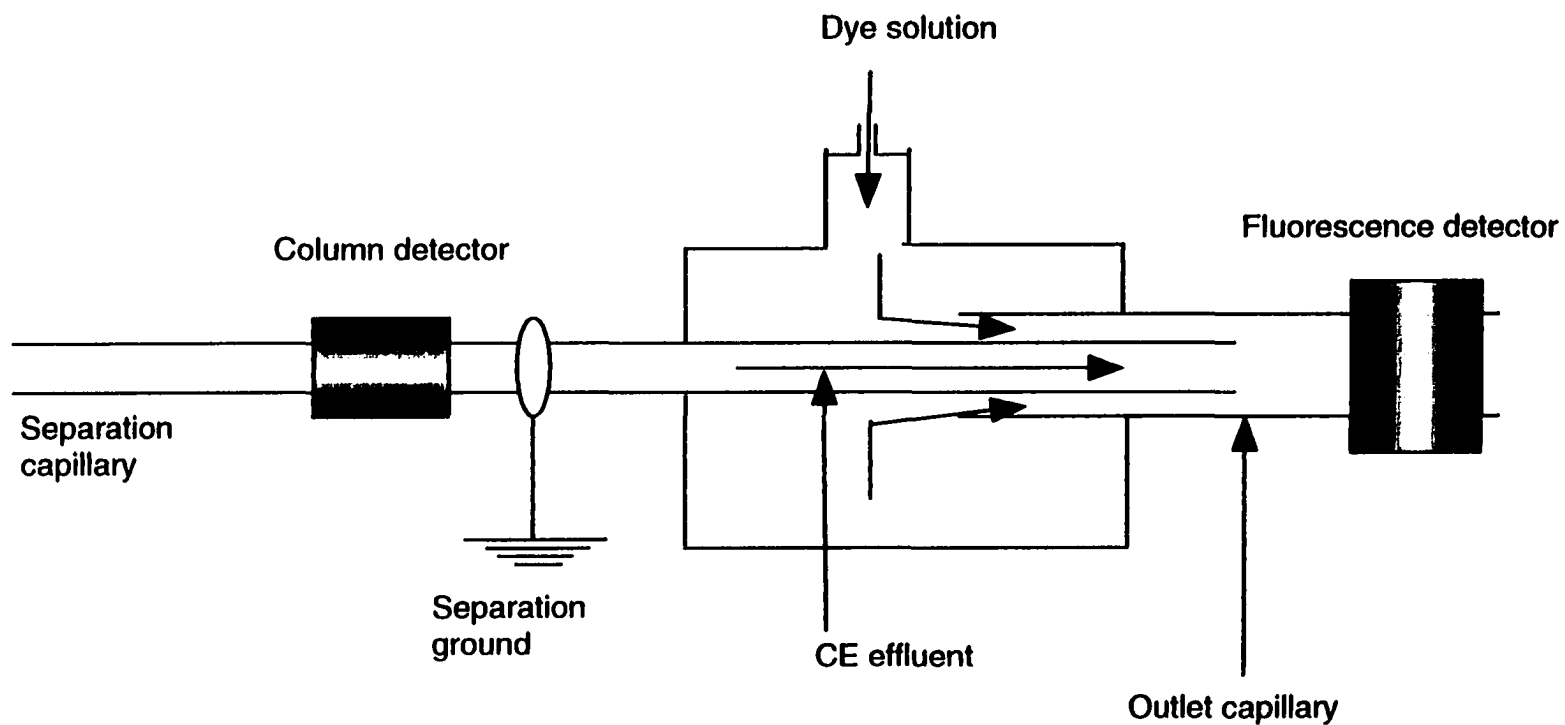
The clever design of Zare for post-column EOF monitoring eliminates the need for neutral marker, but still this method is not usable for CE-LIF instruments. In LIF detection the analyte itself is a fluorescent molecule and, therefore, it cannot be mixed with another fluorescent dye.

Zare's group introduced a second method to measure the EOF that was much faster and simpler than their first method.<sup>21</sup> The method that we used for EOF measurement in this chapter and in Chapter 5 is based on Zare's method.<sup>21</sup> This method was modified for better precision. EOF measurement is based on recording the time history of the current during a CE experiment. There is no need for a special type of injected solute, i.e. a neutral marker, and also there is no need for a special type of detector. Indeed there is no need for any kind of detector at all as long as the instrument can record the current during a capillary electrophoresis run. The operator does not worry about a neutral marker that fluoresces or if its fluorescence intensity quenches by change of pH.

The current monitoring method is based on the filling of the capillary with the background electrolyte and applying high voltage to run the CE. While the CE experiment is running, the current is monitored for a period of time until a constant background current is achieved. Then the background electrolyte is changed to a more dilute electrolyte and the current is monitored again. The current starts decreasing to a second constant level. By measuring the time for the current to drop to a stable value the EOF is calculated.



**Figure 4.5: Schematic apparatus used to measure EOF by Zare's group**



Zare used an electrolyte consisting of 20 mM sodium phosphate buffer with a pH of about 7.0. This solution was then diluted with water in a 19:20 ratio, so the diluted electrolyte has a concentration of 95% of the original background electrolyte or a 5% dilution. We have used different types of buffer with a different range of concentrations. The dilution was done from 1% all the way to 99% to show the applicability of the method in different conditions.

In all the experiments the measured EOF for both coated and uncoated capillaries were compared with the neutral marker method to check upon the accuracy of the method. The EOF was measured in a broad range of pH and compared by the neutral marker method to cross validate the method. Finally, the effect of concentration, pH, electric field and temperature on EOF was studied and the results were compared with literature data to show that this simple current monitoring method could be used for rapid method validation in capillary electrophoresis of coated and uncoated capillaries.

## 4.2 Experimental

### 4.2.1 EOF calculation

Electroosmotic flow rate velocity ( $V_{\text{eof}}$ ) and EOF mobility ( $\mu_{\text{eof}}$ ) were calculated using the following formulas:

$$V_{\text{eof}} = L / \Delta t \quad (4.19)$$

$$\mu_{\text{eof}} = V_{\text{eof}} / E = L^2 / V \Delta t \quad (4.20)$$

where  $\Delta t$  is time for the current drop,  $L$  is the capillary length, 30 cm, and  $V$  is the applied voltage (12 kV). It is worth mentioning that  $E$  is the electric field ( $E = V/L = 12,000 \text{ V}/30 \text{ cm} = 400 \text{ V/cm}$ ) and it was not used in EOF calculation.

The equations to calculate electroosmotic flow rate velocity ( $V_{\text{eof}}$ ) and electroosmotic flow mobility ( $\mu_{\text{eof}}$ ) for the neutral marker are quite similar to equations 4.19 and 4.20 except  $\Delta t$ , which is replaced by the migration time of a neutral marker ( $t_{\text{mig}}$ ). Equations 4.21 and 4.22 are equivalent to equations 4.19 and 4.20, but these are applied for the neutral marker method.

$$V_{\text{eof}} = L / t_{\text{mig}} \quad (4.21)$$

$$\mu_{\text{eof}} = V_{\text{eof}} / E = L^2 / V t_{\text{mig}} \quad (4.22)$$

#### 4.2.2 Instrument

Experiments were carried out using a single-capillary instrument with a sheath flow cuvette and LIF detection. The LIF detection was previously discussed in Chapters 1 and 2 of this thesis. The CE-LIF instrument was described in Chapter 2 as well.

Unless otherwise stated, fused-silica capillaries (Polymicro Technologies, Phoenix, AZ) were 30 cm long with 50  $\mu\text{m}$  ID and 141  $\mu\text{m}$  OD. The in-house constructed instrument used a 0-30 kV power supply (CZE 1000, Spellman, Plainview, NY).

For the neutral marker method, excitation was provided by the 488-nm line of an argon-ion laser operated at 12.1 mW (Model 2211-55 SL, Uniphase, San Jose, CA or Model Innova 90-4, Coherent, Mountainview, CA). The laser beam was focused approximately 30  $\mu\text{m}$  from the tip of the capillary with a 6.3x objective (Melles Griot,

Nepean, ON, Canada). Fluorescence was collected by a 60x and 0.7 NA microscope objective (Mo-0060LWD, Universe Kokagu, Oyster Bay, NY). It was then filtered with a spatial filter. Either a 615 DF 45 or a 630 DF 30 band pass filter (Omega Optical, Brattleboro, VT) was used to remove stray and scattered light. The filtered light was then imaged onto a photomultiplier tube (R1477, Hamamatsu, Middlesex, NJ) biased at 1,000 V. The photo current was passed through a current-to-voltage converter and a low pass filter (RC = 47 ms) and then digitized with a 16-bit data acquisition board (NB-MIO 16 XH-18, National Instruments, Austin, TX) connected to a Macintosh computer.

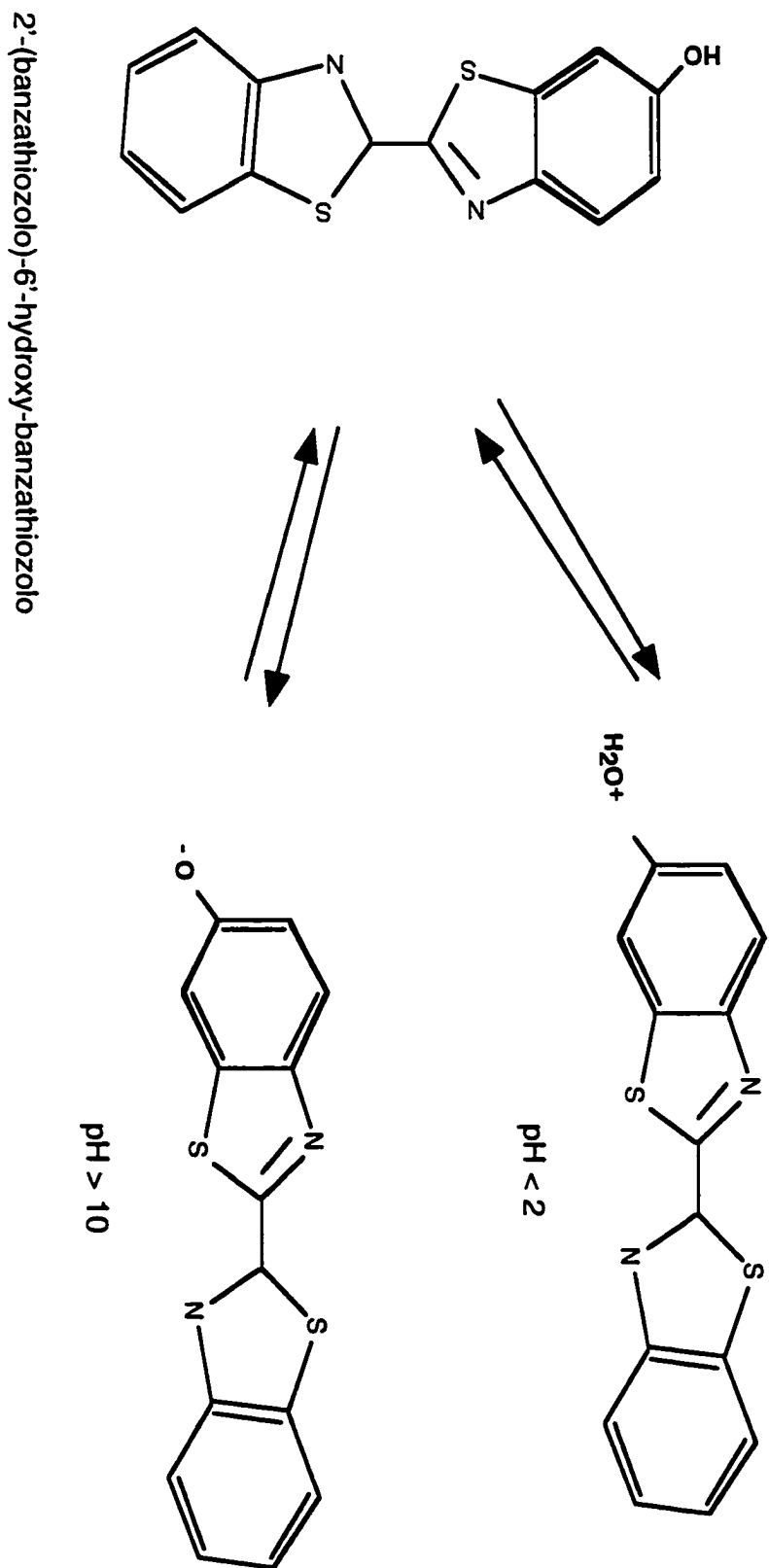
### 4.2.3 Reagents

Sodium tetraborate (borax), sodium dodecyl sulfate (SDS) and sodium citrate were purchased from BDH (Toronto, ON, Canada). For most of the experiments the running buffer and sheath flow buffer were 10 mM borate (2.5 mM borax) and 5 mM SDS or 10 mM borate with no SDS. All buffers were made with Milli-Q deionized water and were filtered using a 0.2- $\mu$ m filter. Atto Fluor was purchased from JBL (San Louis Obispo, CA, USA).

The neutral marker used for these experiments was Atto Fluor which is a commercial name for 2'-(banzathiozolo)-6'-hydroxy-banzathiozolo. Atto Fluor is a weakly fluorescent molecule and its structure is shown in figure 4.6. There is not a strong ionizable group in the structure of Atto Fluor and, therefore, it is a neutral molecule if the pH is not highly acidic or highly basic. At acidic pH two peaks for Atto Fluor were observed. One peak was the neutral form and the other peak was the protonated form of Atto Fluor. The phenolic group of the molecule has a pKa of 10 and, therefore, at pH more than 10 the molecule is partially charged.

While preparing a series of run buffers from pH 2.0 to 11.0, the ionic strength of each run buffer also changed due to different amounts of acid and/or its conjugated base.

Figure 4.6: Chemical structure of Atto-Fluor and its ionization equilibria



These solutions with varying pH were not suitable for pH studies because of the possibility of changes in ionic strength. To eliminate this problem, all the run buffers were swamped with 10 mM KCl solution to get a constant ionic strength for each pH.

10 mM solutions of KCl, phosphoric acid, sodium hydrogen phosphate, disodium hydrogen phosphate, and trisodium hydrogen phosphate were prepared in doubly distilled deionized water. 45 mL of the KCl solution and 5 mL of the phosphoric acid solution were mixed to get a 1 mM solution of phosphoric acid. Another solution was prepared by mixing 45 mL of the KCl solution and 5 mL of the monosodium hydrogen phosphate solution and the pH was adjusted to the desired pH by adding dilute solution of NaOH or HCl. Using the above mentioned procedure, a series of run buffers with varying pHs and constant ionic strength was prepared and used for pH studies.

### **4.3 Results and discussions**

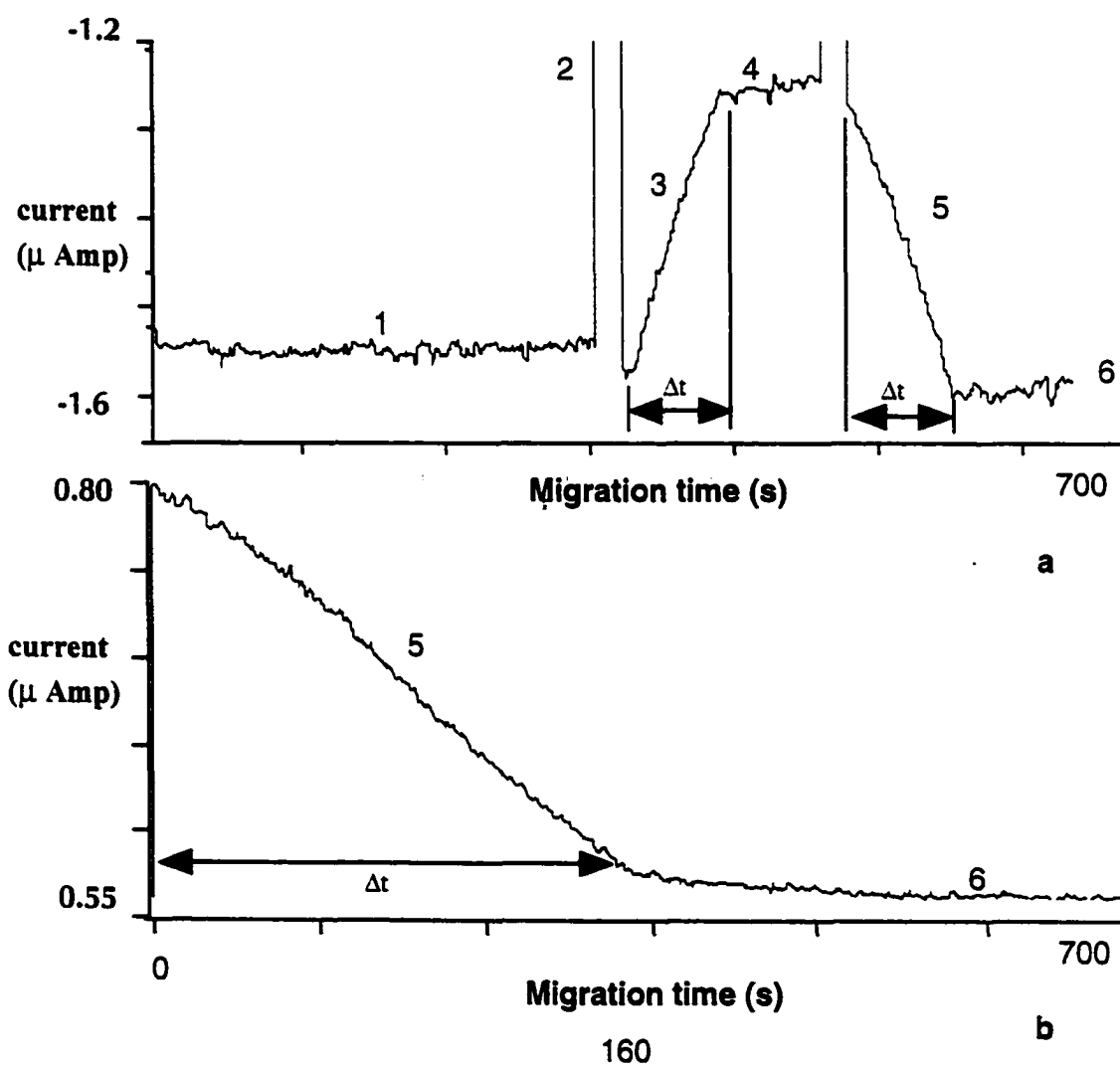
#### **4.3.1 Method validation**

A 30 cm piece of capillary was installed on the CE instrument and the current history of the capillary was monitored. In the case of neutral marker experiments a  $10^{-9}$ M solution of Atto Fluor in 10 mM borate was injected for 10 s and +5 kV. The running CE voltage for both neutral marker and current monitoring methods was +12 kV or +400 V/cm.

Figure 4.7a shows the way that current monitoring method was performed. First the capillary was filled with 9.5 mM borate and the high voltage was applied to get a constant current (1 in Figure 4.7a). Then the injector box door of the CE instrument was opened to replace the run buffer with 10 mM borate (2 in Figure 4.7a). While the 9.5 mM run buffer was replaced with 10 mM, the current rose (3) until it reached a new constant level (4 in Figure 4.7a). This current rise time from one constant level to another constant

**Figure 4.7: Current monitoring method to measure EOF of (a) an uncoated and**

**(b) a coated capillary. 1) constant current while running 9.5 mM borate, 2) the time that interlock is open to change the run buffer to 10 mM borate, 3) rise in current because of buffer replacement, 4) constant current when the capillary is filled with 10 mM borate, 5) Falling current because of change of run buffer to 9.5 mM borate, 6) constant current when all the capillary volume is filled with 9.5 mM borate**



level was measured and called  $\Delta t$ .

Parts 5 and 6 of Figure 4.7a show the reproducibility of the current monitoring method. In this experiment when the capillary was filled with 10 mM borate, the running buffer was changed to 9.5 mM. The rise time and the fall time of the current were equal within the experimental error, i.e.  $\Delta t_1 = \Delta t_2$

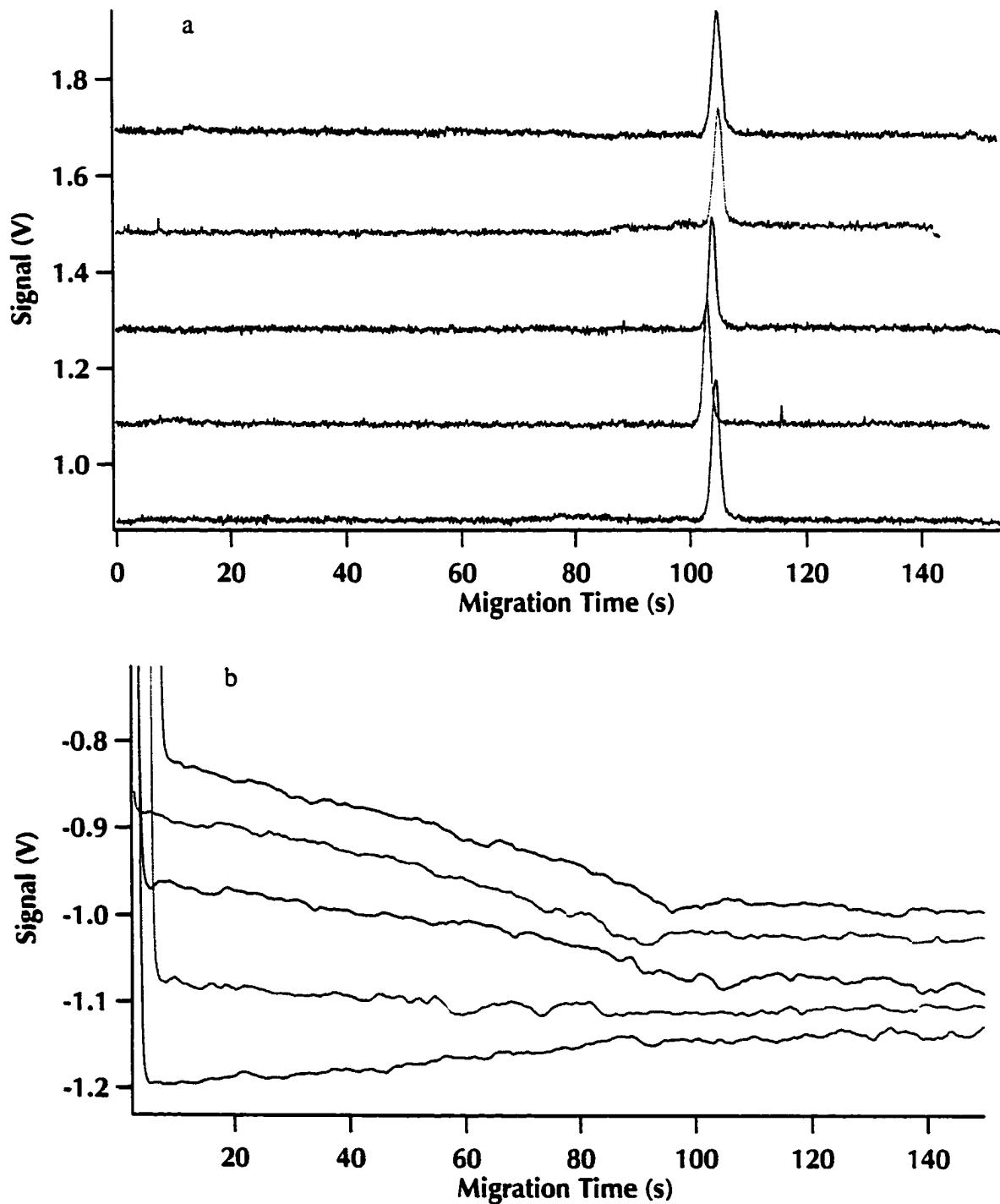
If we examine Figure 4.7a carefully, we see that when the capillary run buffer is changed from 10 mM (4) to 9.5 mM borate (6) the current does not level off exactly to the same level as the beginning of the experiment when the capillary was filled with 9.5 mM borate (1). The reason that the current levels in 1 and 6 are slightly different is due to depletion of ions during the replacement time. The 9.5 mM borate buffer in (1) is a fresh solution, but in (6) it has been depleted for the time  $\Delta t_2$ . When the ions in run buffer are depleted, the actual concentration is slightly less than 9.5 mM and, therefore, the current is slightly lower. The ion depletion phenomenon was already discussed in Chapter 3.

Figure 4.7b depicts the current monitoring for a coated capillary. In Chapter 5, we will discuss the coating methods to reduce EOF. The time that it takes for the 10 mM run buffer to be replaced by 9.5 mM is much longer than that of an uncoated capillary and the EOF, which is responsible for bulk flow and buffer replacement, is much lower than for coated capillaries. According to equations 4.9 and 4.10, which are applicable for coated capillaries as well, the longer  $\Delta t$  for the coated capillary accounts for the lower EOF. For a thorough discussion of coated capillaries and the reason that EOF is reduced, see Chapter 5.

Figure 4.8 compares current monitoring and neutral marker methods. For the current monitoring method the run buffer changed from 10 to 9.5 mM borate while for the neutral marker method the run buffer is 9.5 mM borate. The RSD in migration time for



**Figure 4.8: EOF measurement using a) neutral marker for 5 consecutive injections of Atto-Fluor for 10 s injections and 12 kV run voltage, and b) current monitoring method for 5% concentration difference**



neutral marker method is 2.4% and for the current monitoring method is 24%. From this experiment we may conclude that the neutral marker method is a more precise method, but the next experiment shows that the current monitoring method precision is a function of the concentration difference between the run buffer and the second buffer.

To address the problem of low precision for current monitoring method, a series of run buffers including 10, 9.5, 9.0, 8.5, 8.0, 7.5, 7.0, 6.0, 5.0, 4.0, 3.0, 2.0 and 1.0 mM borate was prepared. The sheath flow buffer was changed in each experiment to the same concentration as the replacing buffer. Each experiment was done by 5 injections of the neutral marker for each of the above mentioned run buffer concentrations. For the current monitoring method the capillary was filled with 10 mM borate with a manual syringe and high voltage was applied to replace the 10 mM borate with one of a 9.5, 9.0, 8.5, 8.0, 7.5, 7.0, 6.0, 5.0, 4.0, 3.0, 2.0 and 1.0 mM borate solutions. Each experiment was repeated 5 times. Table 4.1 shows the results of this experiment.

Table 4.1 shows the cross validation of neutral marker and current monitoring methods. As the table shows the RSD in migration time for current monitoring method is high when the difference in concentration between run buffer and replacing buffer is very low or very high. When this difference is 20%, the RSD is as good as the neutral marker method. When the difference in concentration is between 30% to 50%, the current monitoring method is about 2 times less precise. For 60% to 70% concentration difference, the current monitoring method is roughly 4 times less precise. For greater than 80% concentration difference, the current monitoring method precision becomes even poorer.

From Table 4.1 we may conclude that when the difference between run buffer and replacing buffer is low (5%) the RSD in migration time for the current monitoring method is very high, i.e. Figure 4.8 depicts the largest difference between the neutral marker and current monitoring methods. Zare recommended this concentration difference between run

**Table 4.1: Neutral marker and current monitoring method comparison for a series of concentration difference between run buffers**

<b>Neutral marker run buffer concentration (mM)</b>	<b>Neutral marker RSD</b>	<b>Current monitoring (change of concentration in %)</b>	<b>Current monitoring RSD</b>
10	2.5%		
9.5	2.4%	5%	24%
9	2.0%	10%	17%
8.5	1.4%	15%	5.5%
8.0	2.1%	20%	2.5%
7.0	3.2%	30%	6.0%
6.0	3.7%	40%	6.8%
5.0	3.0%	50%	7%
4.0	2.6%	60%	8.5%
3.0	1.8%	70%	8.9%
2.0	2.9%	80%	16%
1.0	3.8%	90%	22%

buffer and replacing buffer.<sup>21</sup> However, based on the results of this table, the best precision is obtained when the concentration difference is 20%.

To compare the means of the two EOF measurement methods (neutral marker and current monitoring), I repeated the experiment for the worst case scenario, i.e. the highest difference between RSDs of the means determined by two methods. The two means were compared using a t-test. The results show that there is no significant difference between the two methods. Table 4.2 shows the migration times of the 5 experiments for each method and the calculation for standard deviation of the pooled data for t-test to compare the two means.<sup>22</sup>

For a t-test we must have the standard deviation of the pooled data, i.e. the standard deviation of the CM and NM methods. The pooled standard deviation is calculated using the following equation.<sup>22</sup>

$$\text{Std.Dev.}_{\text{pooled}} = \{(\sum (X_i - X_1)^2 + \sum (X_j - X_2)^2) / (n_1 + n_2 - 2)\}^{1/2} \quad (4.23)$$

where  $X_1$  and  $X_2$  are the means for the current monitoring and neutral marker methods, respectively. The data for the current monitoring and neutral marker methods are  $X_1$  and  $X_2$ , respectively. Therefore, the standard deviation for the pooled data is calculated as:

$$\text{Std.Dev.}_{\text{pooled}} = \{(7.71 + 2557.2) / (5 + 5 - 2)\}^{1/2} = 17.9$$

Now t is calculated using the equation 4.24<sup>22</sup>

$$t = (X_1 - X_2) / (\text{Std.Dev.}_{\text{pooled}}) \{n_1 n_2 / (n_1 + n_2)\}^{1/2} \quad (4.24)$$

**Table 4.2: t-test calculation for the highest difference between the means of neutral marker and current monitoring methods**

Neutral marker ( $t_{mig}$ )	Deviation from mean	Square of deviation	Current monitoring ( $\Delta t$ )	Deviation from mean	Square of deviation
$X_i$	$X_i - X_1$	$(X_i - X_1)^2$	$X_j$	$X_j - X_2$	$(X_j - X_2)^2$
102.2	0.4	0.16	103	2.4	5.76
109	2.4	5.76	85	20.4	416.16
106.8	0.2	0.04	92	13.4	179.56
107.6	1	1	149	43.6	1900.96
107.5	0.9	0.81	98	7.4	54.76
$X_1 = 106.6$		$\sum(X_i - X_1)^2 = 7.71$	$X_2 = 105.4$		$\sum(X_j - X_2)^2 = 2557.2$
<b>Std. Dev.</b>			<b>Std. Dev.</b>		
<b>= 2.596</b>			<b>= 25.3</b>		

$$t = (106.6 - 105.4) / (17.9)\{25 / (5 + 5)\}^{1/2} = 0.106$$

At the 99% confidence level and  $n_1 + n_2 - 2 = 8$  degrees of freedom the t-value in the table is 3.355. Since the calculated t is less than the tabulated t, i.e.  $0.106 < 3.355$ , with 99% confidence level we can say that there is no significant difference between the two means. The F-test was done to compare the two variances ( $F = \max. S_1^2 / \min. S_2^2 = (25)^2 / (5)^2 = 25$  which is more than the tabulated F value for 4 and 4 degrees of freedom). The F-test indicates that there is a significant difference between the standard deviations of the two methods.<sup>29</sup>

Another experiment was performed for the case that the difference in RSD of the two methods is not as high as the previous experiment. The results of this experiment and t-test calculation are shown in Table 4.3.

From the equation 4.23 and the data in Table 4.3, the standard deviation of the pooled data is calculated,  $\text{Std.Dev.}_{\text{pooled}} = \{(42.58 + 172) / (5 + 5 - 2)\}^{1/2} = 5.18$ , and then from the equation 4.24 the t-value is calculated,  $t = (108.6 - 102.6) / (5.18)\{25/(5 + 5)\}^{1/2} = 1.83$ .

For the 99% confidence level and  $n_1 + n_2 - 2 = 8$  degrees of freedom the t-value in the table is 3.355. Since the calculated t is less than the tabulated t, i.e.  $1.83 < 3.355$ , with 99% confidence level we can say that there is no significant difference between the two means. The F-test indicated that there is a significant difference between the standard deviations of the two methods.

When the capillary is partially filled with a buffer of one concentration and contains a second buffer of the same composition but different concentration, the bulk EOF in this kind of mixed buffer system is a weighted average of the electroosmotic velocities of the pure buffers. That is the reason that when the difference in concentration is high, the standard deviation is also very high. When the difference in concentration is very low, still

**Table 4.3: t-test calculation for the lowest difference (in %) between the means of neutral marker and current monitoring methods**

<b>Neutral marker (<math>t_{mig}</math>)</b>	<b>Deviation from mean</b>	<b>Square of deviation</b>	<b>Current monitoring (<math>\Delta t</math>)</b>	<b>Deviation from mean</b>	<b>Square of deviation</b>
$X_i$	$X_i - X_1$	$(X_i - X_1)^2$	$X_j$	$X_j - X_2$	$(X_j - X_2)^2$
107.3	4.7	22.09	106	2.6	6.76
103.6	1	1	118	9.4	88.36
99.4	3.2	10.24	109	0.4	0.16
99.6	3	9	110	1.4	1.96
103.1	0.5	0.25	100	8.6	73.96
$X_1 =$ 102.6		$\Sigma(X_i - X_1)^2$ = 42.58	$X_2 = 108.6$		$\Sigma(X_j - X_2)^2 =$ 172
<b>Std. Dev. =</b> <b>2.596</b>			<b>Std. Dev. =</b> <b>25.3</b>		

the precision is low because of the instrument limitation to resolve the changes in current at a few percent of a micro ampere.

For 10%, 15%, and 20% concentration gradient (see Figure 4.10) between the run buffer and replacing buffer, both the F-test and the t-test indicate that there are no significant differences between the standard deviations and between the means of the two methods. This is the best range of concentration gradient that should be used for the current monitoring method in order to have a reliable results.

If there is no EOF, the flux of ions out of the concentration boundary will be exactly equal to the flux toward it. Consequently, this concentration boundary will be stationary, neglecting the effect of diffusion.<sup>23</sup> In other words, the apparent movement of the concentration boundary in mismatched EOF capillary electrophoresis comes solely from the EOF of the whole bulk solution. To check the idea that mismatch in EOF is the reason for low precision of the current monitoring method we coated a capillary to eliminate the EOF and the experiment was repeated using this polyacrylamide-coated capillary. The procedure to coat the capillaries is given in the Chapter 5.

Figure 4.9 compares the current monitoring method for different percentages of concentration between the run buffer and the replacement buffer. Each experiment was repeated 5 times. In three experiments a high concentration buffer replaced a lower one, and in two experiments a lower concentration buffer replaced a higher one. Figure 4.9 shows 15%, 40% and 80% dilutions respectively. As Figure 4.9 indicates, when we choose a higher concentration difference between run buffer and replacing buffer, the linearity of the variable current section changes. For example, in Figure 4.9c the dilution is 80% and we see a nonlinear fall/rise in the current. This will cause uncertainty in determining the exact time that all the buffer is replaced. This uncertainty in measuring the time will cause a high error in the EOF calculation. Similar experiments for different dilutions were performed on both coated and uncoated capillaries. For coated capillaries the



Figure 4.9: Current Monitoring method for a) 10 mM to 8.5 mM or 15%, b) 10 mM to 6 mM or 40% , and c) 10 mM to 2 mM or 80% change in concentration between run buffer and replacing buffer

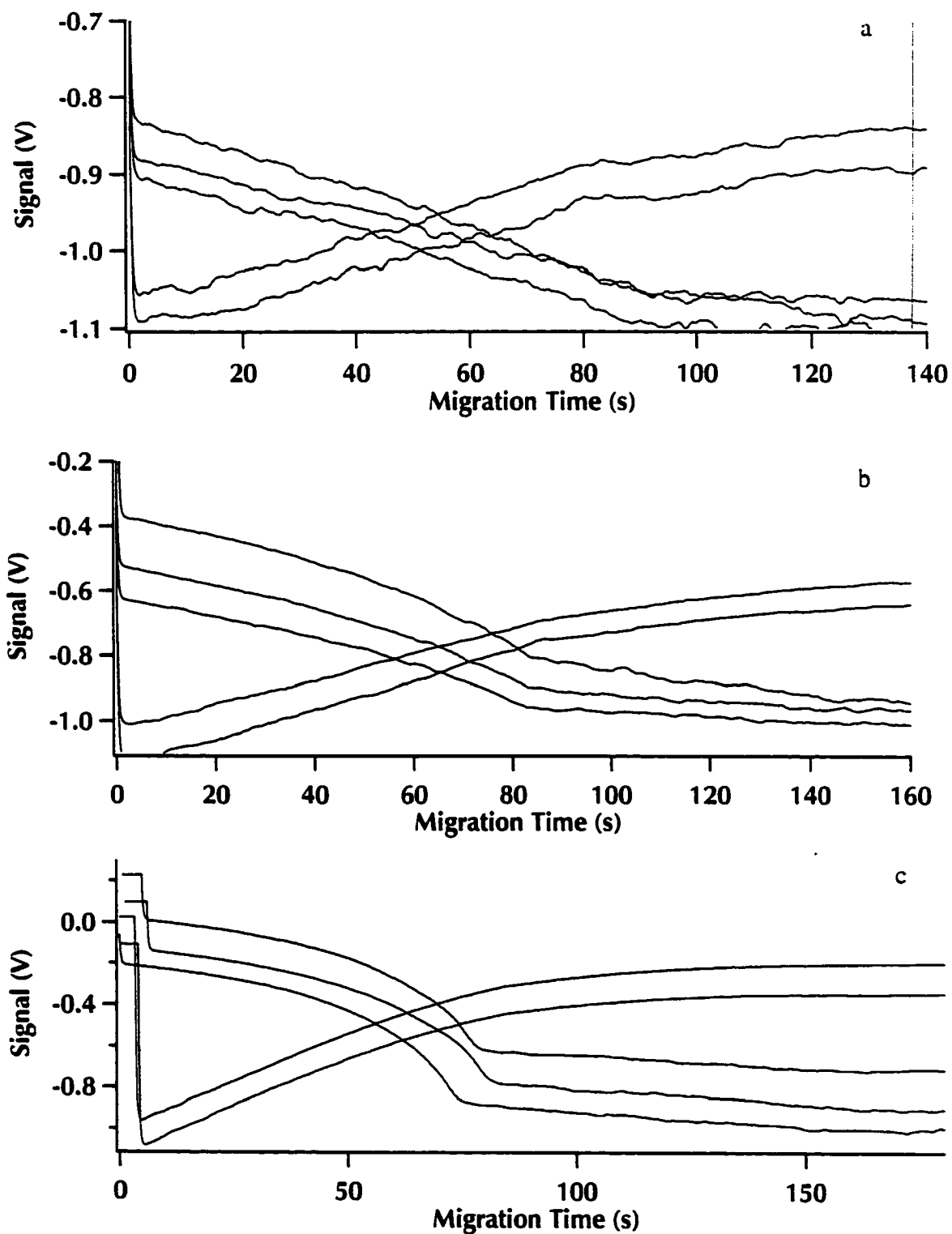
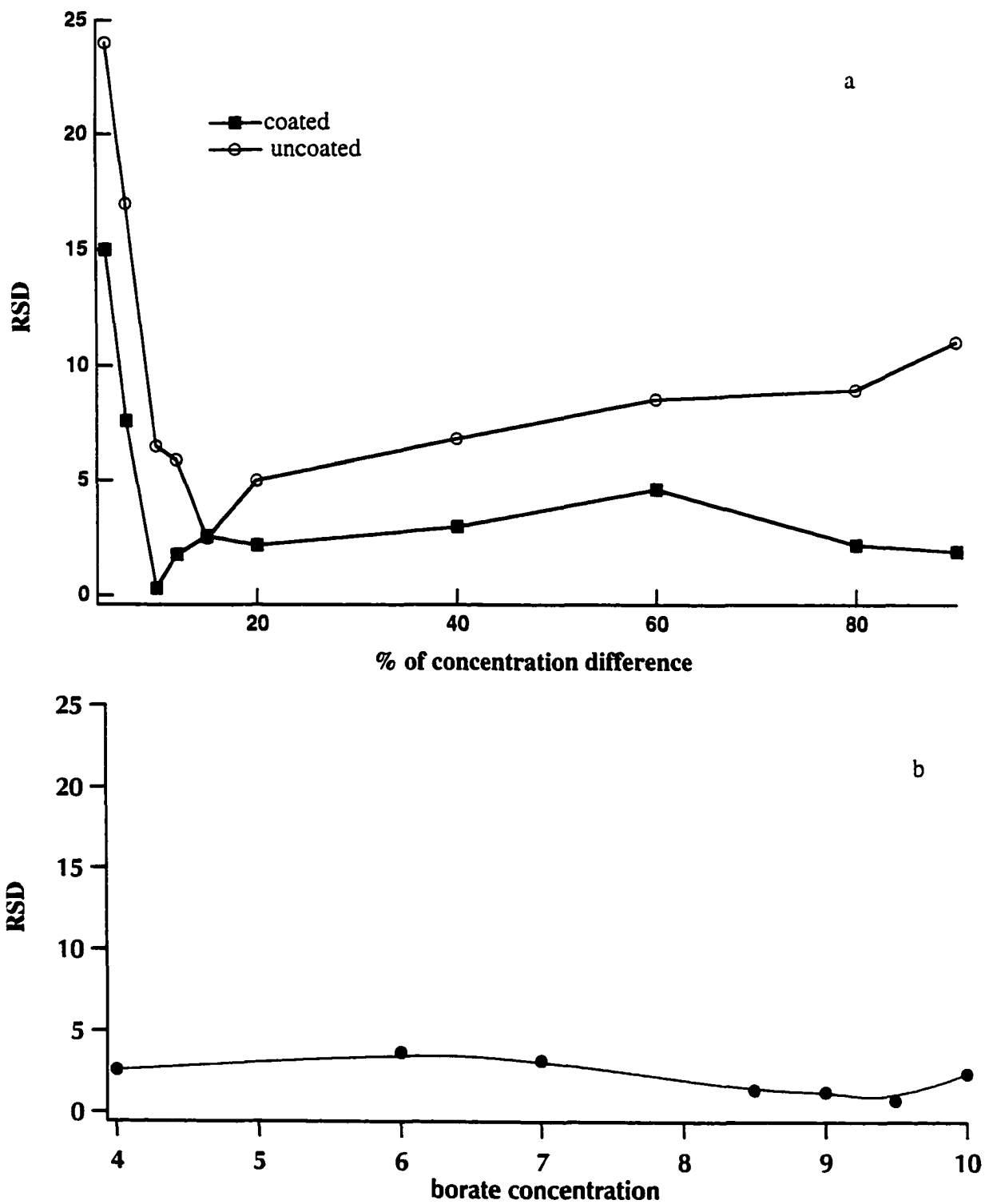


Figure 4.10: Comparison of RSD of a) current monitoring method for coated and uncoated capillaries, b) neutral marker method at different run buffer concentrations for an uncoated capillary



EOF is reduced by at least one order of magnitude and it can be seen that for each dilution the RSD is lower than that of an uncoated capillary.

Figure 4.10a compares the RSD in migration time for the EOF calculation of a coated and an uncoated capillary using the current monitoring method. The RSD in migration time, and hence the EOF, is constant over a wide range of concentration differences except for a very low concentration difference. If the dilution is below 5%, the change in current is so small that it is very difficult for the instrument to detect the difference and, therefore, the RSD is high at low concentration differences. The results of the neutral marker method for uncoated capillaries also are shown. For a coated capillary, the result of the neutral marker method is not shown because of the possibility of adsorption of the neutral marker molecule on the capillary wall and, therefore, invalidity of data. As Figure 4.10a shows for the neutral marker method only one buffer with a fixed concentration is run onto the capillary and there is no mismatch in EOF and, therefore, the RSD is a constant value with respect to the concentration of the run buffer used. It is worth mentioning that in each experiment by changing the run buffer concentration, the neutral marker was also diluted to  $10^{-9}$  M with the same run buffer.

In all experiments, including a concentration difference between the two run buffers, the RSD of the current monitoring method for a coated capillary is below that for an uncoated capillary. This is in agreement with the problem of mismatch of EOF when the capillary is filled with a buffer having two different concentrations. In coated capillaries the EOF is reduced and the difference in EOF in two regions is small and, therefore, the RSD is lower as compared to the RSD for uncoated capillaries.

Figure 4.11 compares the EOF for coated and uncoated capillaries in a wide range of concentration differences between run buffer and replacing buffer. As for the case of RSD in migration time, for coated capillaries EOF is relatively constant regardless of concentration difference. Similar to RSD in migration times, for uncoated capillaries

**Figure 4.11: Electroosmotic Flow Mobility (EOF) of coated (bottom) and uncoated (top) capillary versus % of concentration difference measured using current monitoring method. The error bars are RSD for EOF measurement (n = 5)**

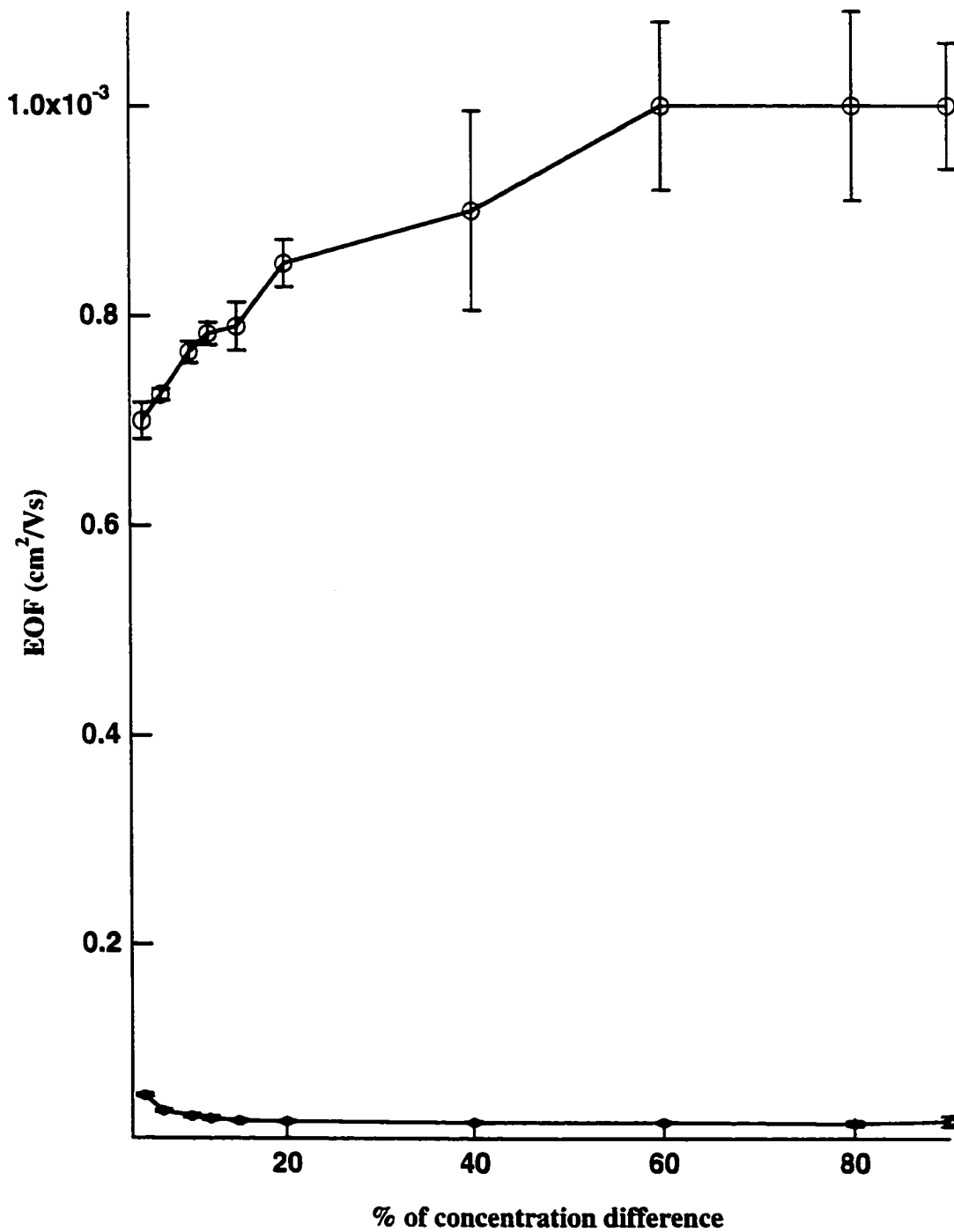
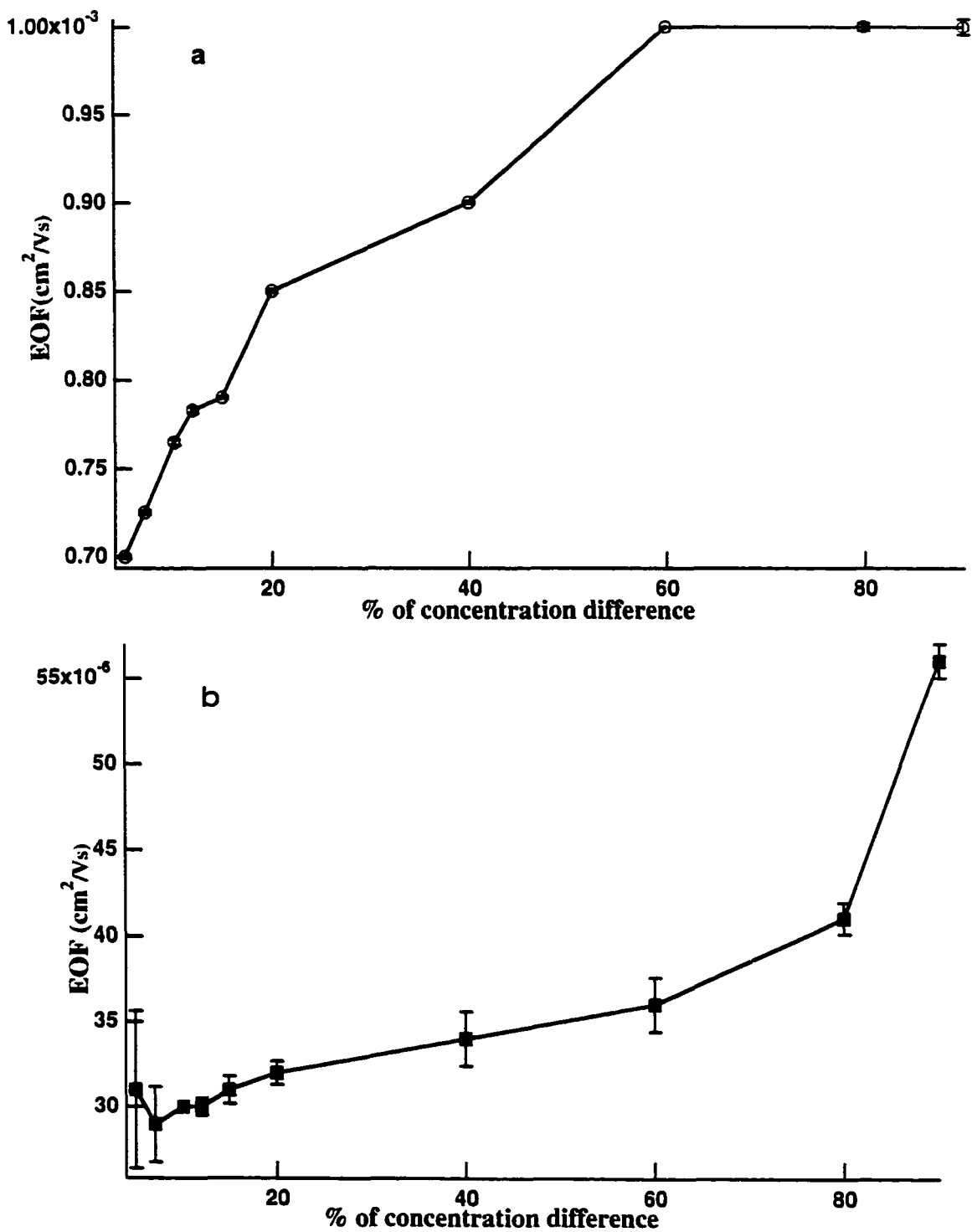


Figure 4.12: Expansion of Figure 4.11 showing the current monitoring method for EOF measurement of a) an uncoated and b) a coated capillary at different % of concentration difference. The error bars are RSD in EOF measurement (n = 5)



EOF increases by increasing the concentration difference between run buffer and replacing buffer. Figure 4.12a is the expansion of the EOF axis for uncoated capillaries to better visualize the change in EOF as a function of the concentration difference. Because we measure the time and EOF is calculated with respect to errors in this measurement, the error in calculated EOF has to be estimated. The error estimation in computed results could be done using the following approach.<sup>22</sup> In general if  $Z = f(A, B, C, \dots)$ , then for systematic errors we may use the following equation:

$$\Delta Z = (\partial Z / \partial A) \Delta A + (\partial Z / \partial B) \Delta B + (\partial Z / \partial C) \Delta C + \dots \quad (4.25)$$

and for random errors the equation is:

$$\Delta Z^2 = (\partial Z / \partial A)^2 \Delta A^2 + (\partial Z / \partial B)^2 \Delta B^2 + (\partial Z / \partial C)^2 \Delta C^2 + \dots \quad (4.26)$$

where  $Z$  is calculated result while  $A, B, C, \dots$  are measured quantities and  $\Delta Z, \Delta A, \Delta B, \Delta C, \dots$  are absolute errors.

The error bars in Figure 4.12 have been calculated using the following equations.

For electroosmotic flow velocity,  $v_{\text{eof}} = L/t_{\text{mig}}$ ,  $\Delta v_{\text{eof}} = (\Delta v_{\text{eof}} / \Delta t_{\text{mig}}) \Delta t_{\text{mig}}$  and therefore,

$$\begin{aligned} \Delta v_{\text{eof}} &= - (L / t_{\text{mig}}^2) \Delta t_{\text{mig}} \\ &= v_{\text{eof}} (\Delta t_{\text{mig}}) / t_{\text{mig}} \end{aligned} \quad (4.27)$$

Similarly, for electroosmotic mobility,  $\mu_{\text{eof}} = L^2 / V t_{\text{mig}}$ , we may use a similar approach

$$\begin{aligned}\Delta\mu_{\text{eof}} &= (-L^2/V t_{\text{mig}}^2) \Delta t_{\text{mig}} \\ &= \mu_{\text{eof}} (\Delta t_{\text{mig}} / t_{\text{mig}})\end{aligned}\tag{4.28}$$

Note that the negative sign resulting from differentiation is not considered in the final equation in order to obtain the maximum error.

The error bars in Figure 4.12 are calculated using the above equations. As discussed in the introductory section of this chapter, when a capillary is partially filled with two buffers of the same composition but different concentrations, the bulk EOF of the capillary is the weighted average of the two EOFs when the capillary is filled with one of the buffers at a time. This is the reason that by increasing the concentration difference, the EOF increases. The effect of concentration of run buffer on EOF will be studied next in this chapter. For the explanation of change in EOF by increasing the concentration difference, we have to know that at lower concentrations the EOF is higher. Hence, when the difference in concentration is high, the EOF is higher for the section of capillary that is filled with more dilute buffer and, therefore, the average EOF will increase. Figure 4.12b is also an expansion of the lower part of Figure 4.11 for a coated capillary. A similar trend is observed, but the change in EOF is smaller than that of an uncoated capillary.

By using the current monitoring method, not only can we measure the EOF, but we may also study the fundamental parameters that affect the EOF. To achieve this goal, we will show the effect of concentration, electric field, pH and temperature on zeta potential and, therefore, on EOF. In all of these experiments the dilution between the two buffers is 15% in order to have the maximum precision in measurements.

## **4.3.2 Study of fundamental properties in CE using current monitoring method**

### **4.3.2.1 Effect of concentration on EOF**

Figure 4.13a represents the concentration effect on EOF. As this figure shows, by increasing the concentration the EOF decreases but not linearly. Similar to what was discussed earlier, at low concentrations the error in EOF measurement is high. According to equations 4.7 and 4.8 by increasing concentration,  $\kappa$  will increase, and this decreases the  $\psi$  exponentially, i.e. EOF will decrease by increasing concentration.

The thickness of the double layer,  $1/\kappa$ , is inversely proportional to the square root of concentration. Figure 4.13b shows the EOF versus the inverse of square root of concentration. At higher concentration, EOF changes linearly with reciprocal of the square root of concentration. The non-linearity of the plot at low buffer concentration is still not understood.<sup>24</sup>

### **4.3.2.2 Electric field effect on EOF velocity**

Figure 4.14 shows the effect of increasing electric field on EOF. According to equation 4.10 ( $v_{eof} = \epsilon \zeta E / 4 \pi \eta$ ) and equation 4.11 ( $\mu_{eof} = \epsilon \zeta / 4 \pi \eta$ ) by increasing the applied electric field the electroosmotic flow velocity will increase linearly for lower electric fields as shown in Figure 4.14b. As applied voltage on a capillary is increased, the temperature inside the capillary also increases and this is called Joule heating. Resistance, dielectric constant, pH and viscosity are also temperature dependent. Therefore, by increasing the electric field all these parameters may also change if there is Joule heating.



**Figure 4.13: Concentration effect on EOF for a) EOF versus concentration, and b) EOF versus inverse square root of concentration. The error bars are shown for each experiment (n = 5)**

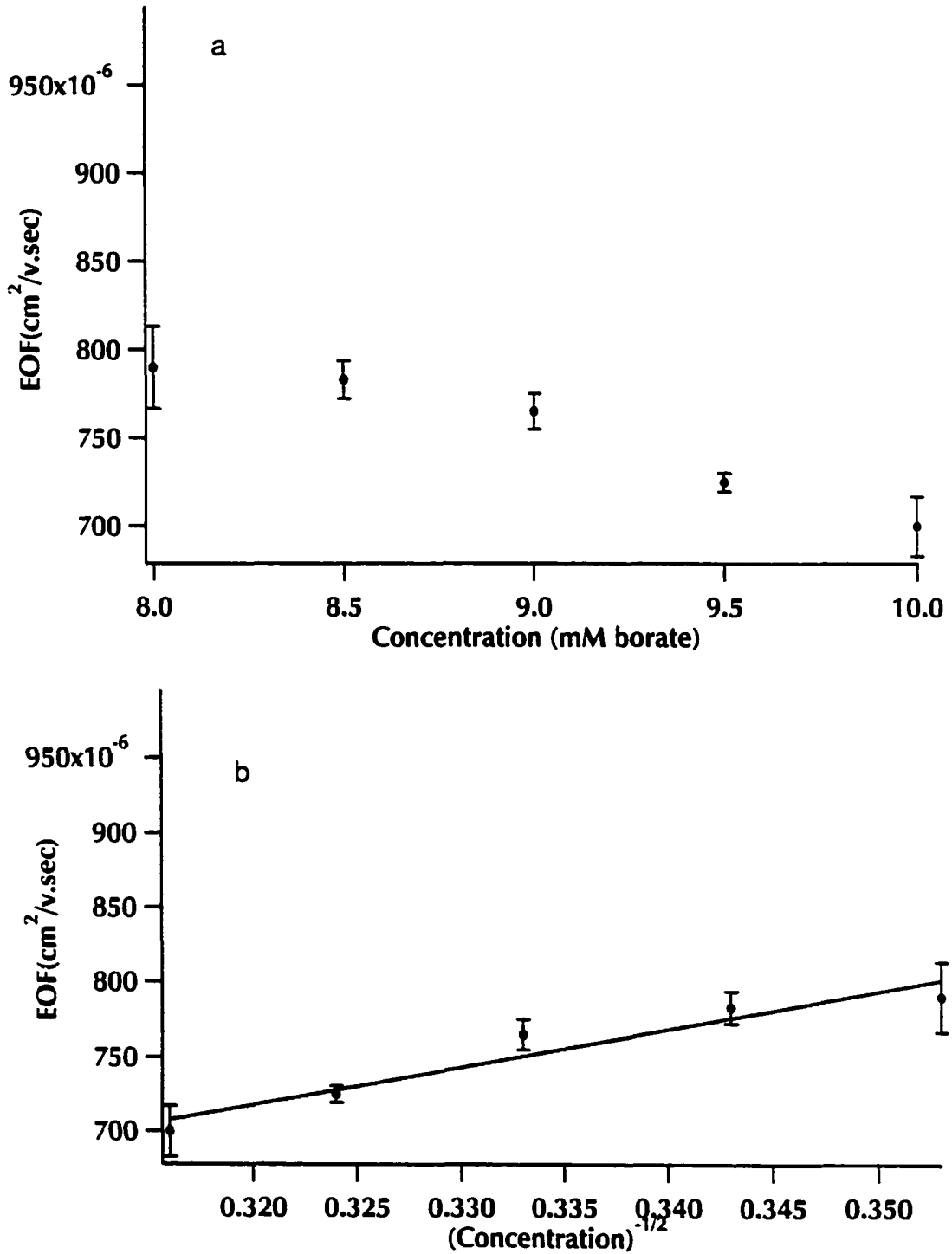
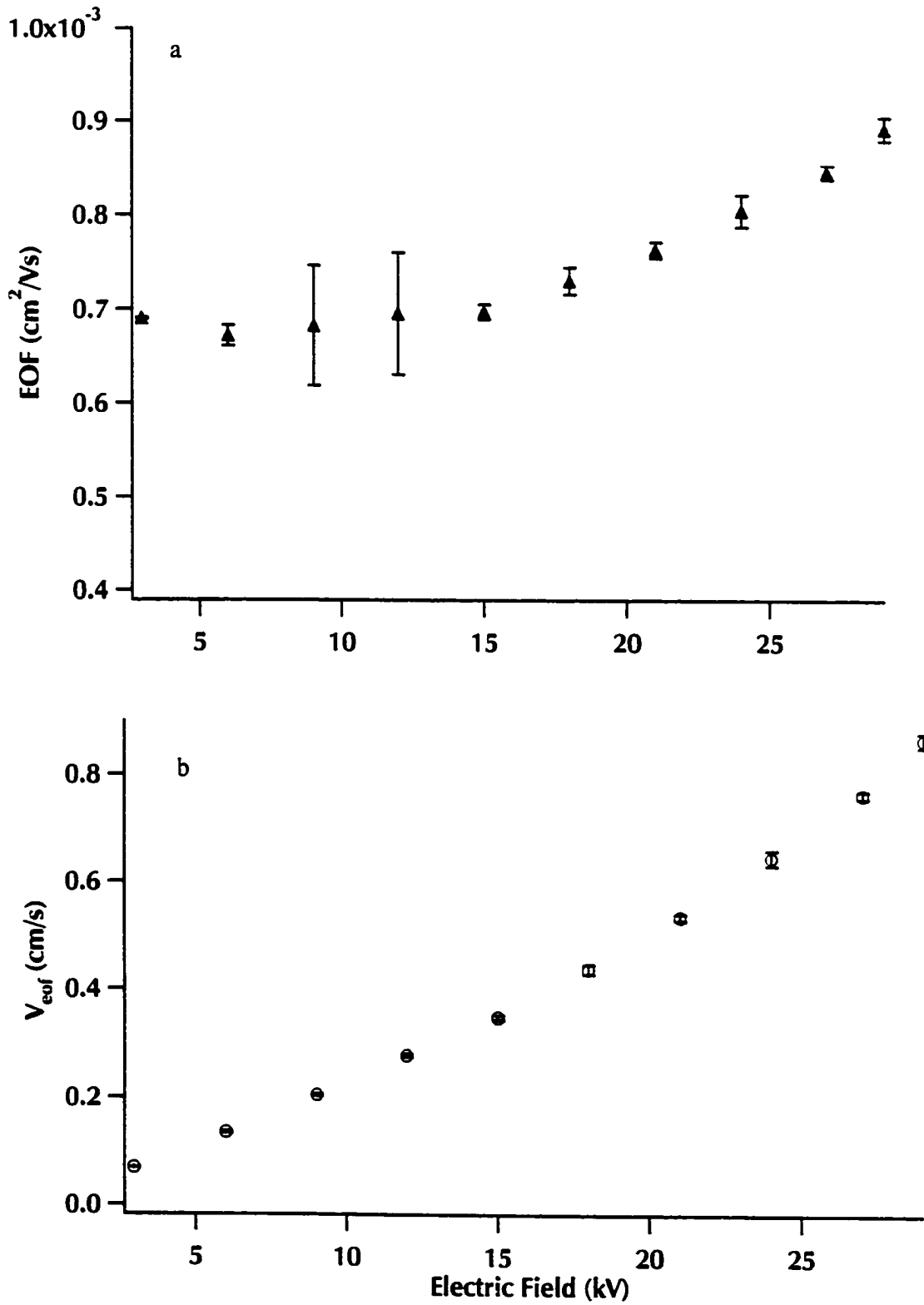


Figure 4.14: Electric field effect on a) EOF mobility b) EOF velocity. The error bars are shown for each measurement (n = 5)



This is the reason for nonlinearity in Figure 4.14b when the electric field is high. This point of change in linearity corresponds to the point that deviation from Ohm's law,

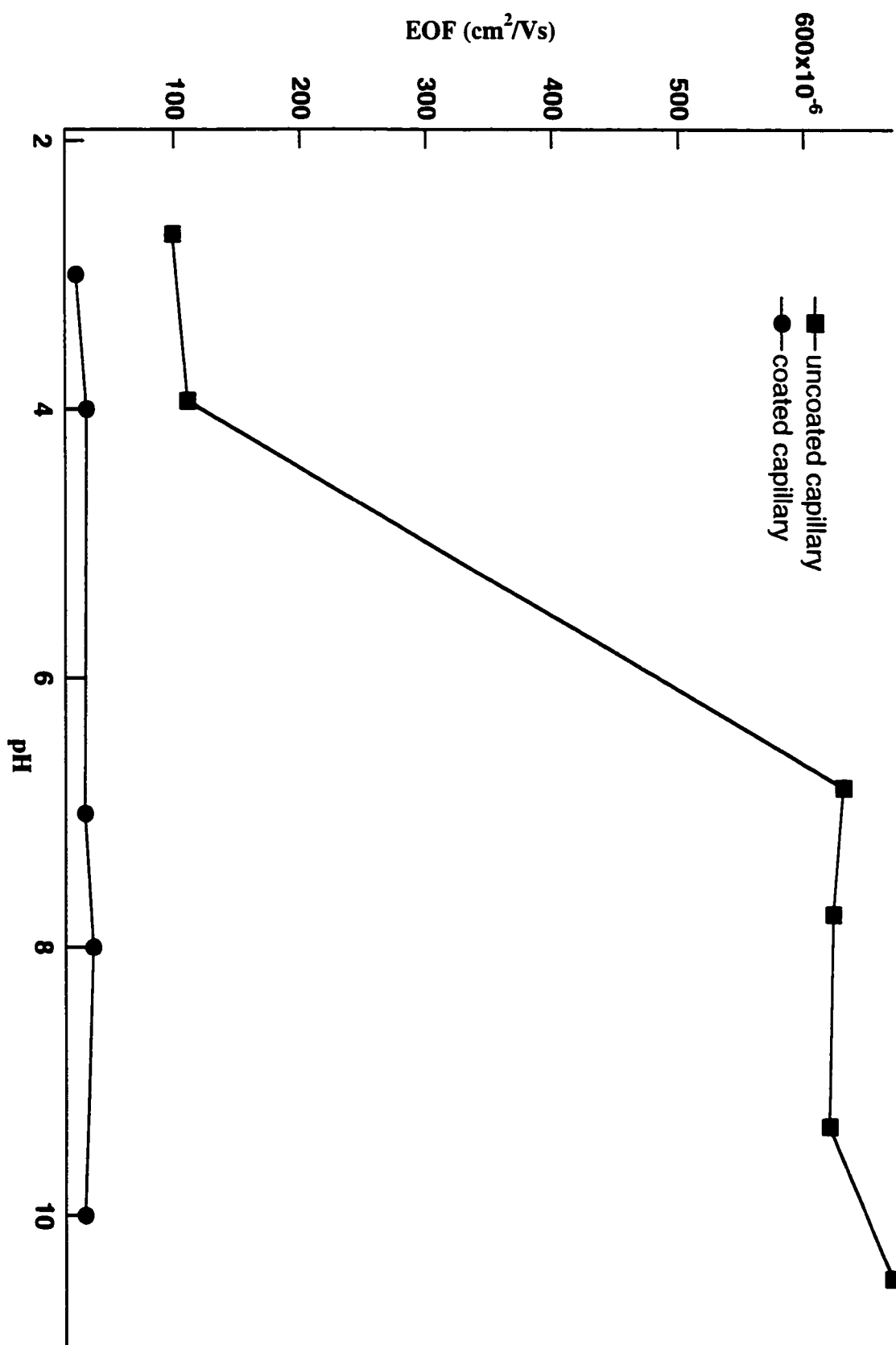
$V = IR$ , is observed. According to equation  $\mu_{\text{eof}} = \epsilon \zeta / 4 \pi \eta$ , there is no direct relation between  $E$  and EOF mobility, but by increasing the electric field the viscosity of the run buffer solution will decrease and this will cause EOF mobility to increase for higher electric fields as it is shown in Figure 4.14a.

#### 4.3.2.3 pH effect on EOF

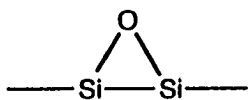
To study how changing of run buffer pH affects EOF, we measured  $\mu_{\text{eof}}$  from pH 2.0 to 11. Attofluor, the neutral marker, gains a charge at acidic pHs and, therefore, all the experiments were done using the current monitoring method. Change in the ionic strength of the run buffer during the course of the pH study was a major concern while preparing the run buffer solutions with different pHs. To eliminate this problem all the buffers were swamped with KCl solution to get a constant ionic strength for each pH.<sup>25</sup>

Figure 4.15 shows the effect of pH on EOF. By increasing the pH, the EOF increases like a titration curve. The silanol groups on the capillary wall act as a monoprotic acid and, therefore, the sigmoidal increase of charge on the surface corresponds to deprotonation of silanol groups. By increasing the pH the negative charge on the capillary surface increases and this causes the EOF to increase proportionally. If the silanol groups are masked, the pH effect on deprotonation of these silanol groups on the surface is negligible as it is shown in lower trace of Figure 4.15 for a coated capillary. Figure 4.16 shows different active silanol groups commonly found on fused-silica capillary walls. These silanol groups are not homogenous, i.e., there is a microheterogeneity among these silanol groups and therefore the pKa of silanol varies from 5 to 7.<sup>26</sup> This is a reason that reproducibility of the pH effect in the intermediate range was not very impressive. At

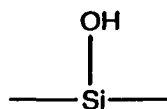
Figure 4.15: The effect of pH on EOF for an uncoated capillary (upper trace) and a coated capillary (lower trace)



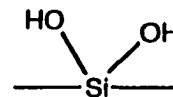
**Figure 4.16: Chemical formulas showing a) siloxane, b) free silanol group, c) geminal silanol group, d) vicinal or bound silanol group, and e) bound water that are present as different types of active silanol groups on fused-silica capillary wall**



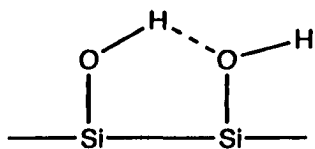
**a**



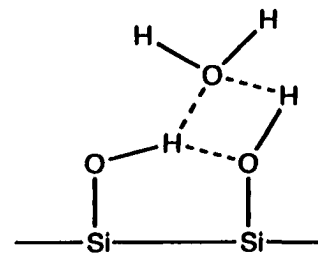
**b**



**c**

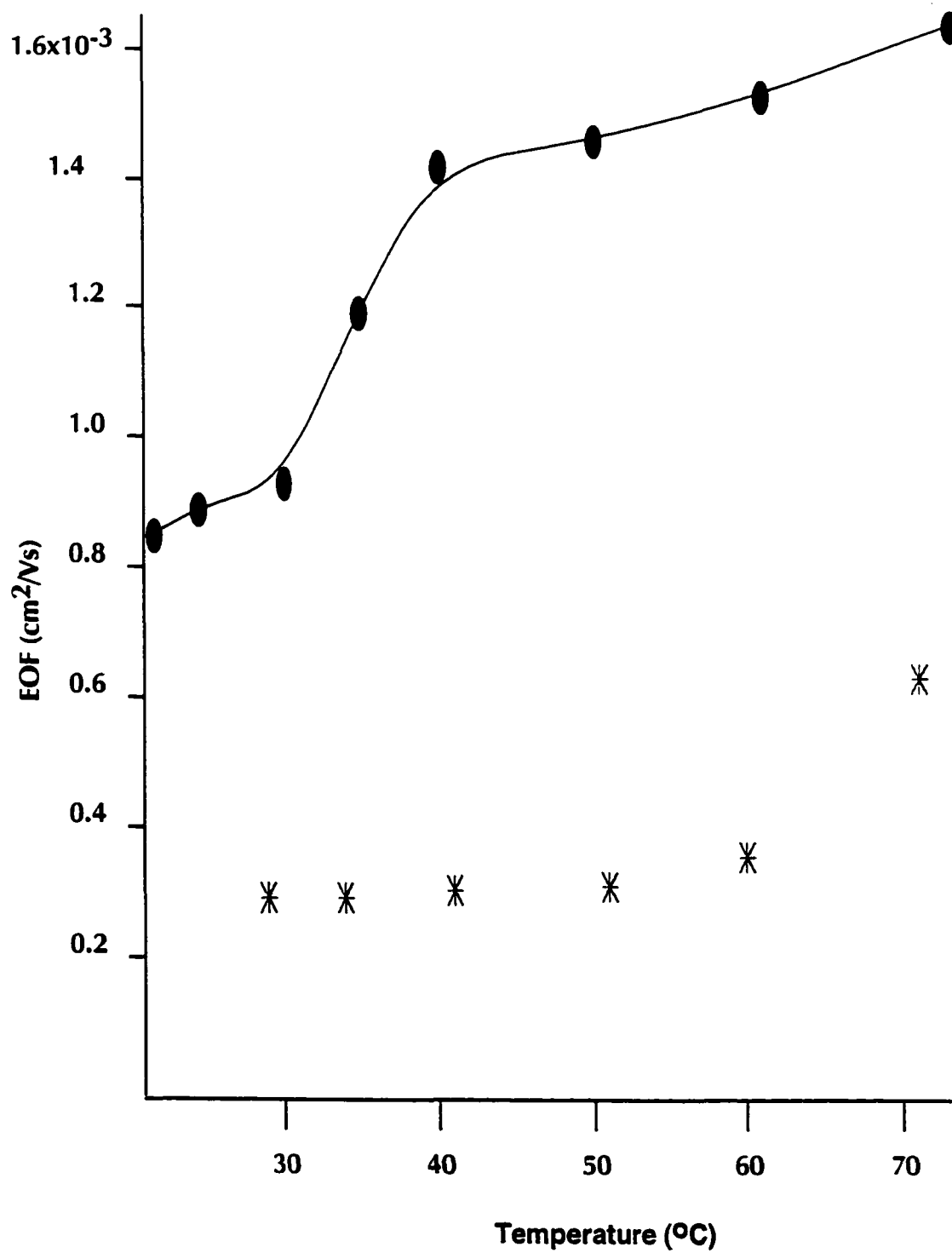


**d**



**e**

**Figure 4.17: Temperature effect on EOF for an uncoated capillary (upper part) and a coated capillary (lower part)**



pH > 10, there was another increase in EOF. At this point the capillary wall was dissolving at alkaline pH.

#### 4.3.2.4 The effect of temperature on EOF

Increasing the temperature lowers the viscosity of the run buffer and this will increase the EOF according to equation 4.10 ( $\mu_{\text{eof}} = \epsilon \zeta / 4 \pi \eta$ ). Temperature can affect the buffer pH as well and this will change the ionization of silanol groups. Therefore, stable temperature control becomes critical in capillary electrophoresis.<sup>27</sup>

Figure 4.17 depicts temperature effect on EOF. If pH and ionic strength of the run buffer are kept constant, the increase in temperature causes an increase in EOF. Between 30 to 40 °C, the slope of uncoated capillary rises. This may be due to a change in pKa of silanol groups with temperature. The smooth increase in EOF after 40° C is due to a smooth decrease in run buffer viscosity. Figure 4.18 shows how the viscosity of the solution decreases by increasing the temperature. Data are taken from CRC handbook.<sup>28</sup>

There are two parameters that change simultaneously with increasing temperature, viscosity of the run buffer solution and the ionization constants of silanol groups at the fused-silica capillary wall. As Figure 4.17 shows, in the case of uncoated capillary the change in EOF with the change in temperature is more pronounced, because both viscosity and ionization constant of silanol groups affect the EOF for an uncoated capillary. Between the temperatures of 30 and 45 °C, the viscosity changes 0.2 units; while for the range of 45 to 60 °C the viscosity changes by 0.1 units. That may explain the sharper rise in EOF of an uncoated capillary. Viscosity change with temperature could not be the main reason because a similar effect is not observed for a coated capillary. Change in pKa of silanol groups with temperature could be a more important factor for an uncoated capillary because the rise in EOF is higher than that of a coated capillary.

Figure 4.18 compares the decrease in viscosity with an increase in EOF for an uncoated capillary. Except between the range of 30 to 45 °C, the decrease in viscosity and increase in EOF could be correlated.

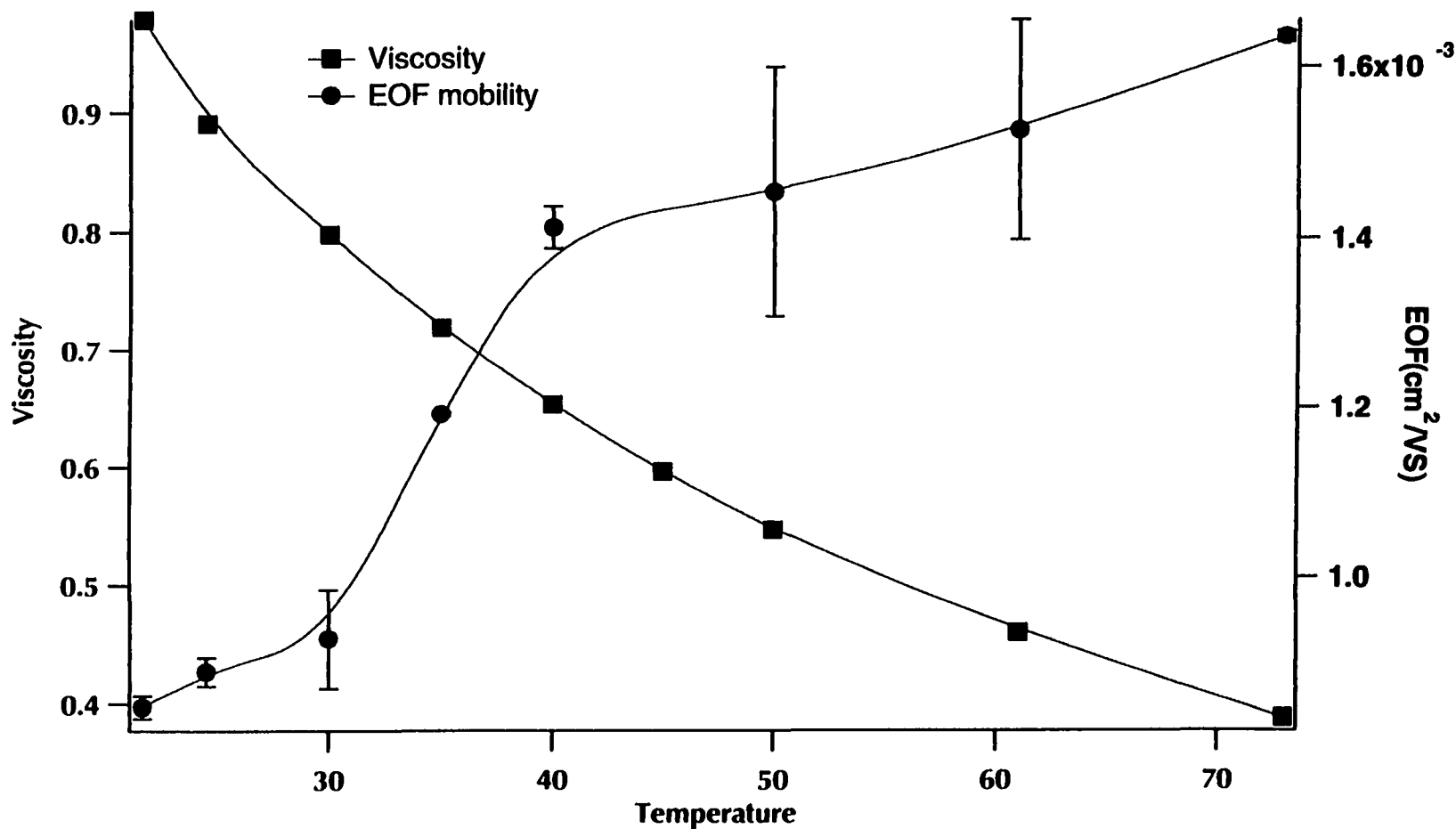
For a coated capillary, there is no silanol groups. This will reduce the possible variables to just the viscosity. Because the EOF is about one order of magnitude lower for a coated capillary as compared to an uncoated capillary, the small change in EOF for a coated capillary is not very visible especially when the Y axis is set for an uncoated capillary with EOF about 10 times higher than that of an uncoated capillary. The high error bars at higher temperature indicated the generation of air bubbles at elevated temperatures.

#### **4.4 Conclusions**

The current monitoring method for EOF measurement is as precise as the neutral marker method if the concentration difference between run buffer and replacing buffer is between 10% to 20%. The student t-test shows that there is no statistically significant difference between the means of the neutral marker and current monitoring methods. No special type of detector is needed for this method and, therefore, it is very simple method. In situations where there is not a neutral marker that is truly neutral in a specific pH, the current monitoring method could be used. This method could be used to study the fundamental properties of the capillary surface and the effect of these properties on electroosmotic mobility. For coated capillaries that EOF is reduced, the current monitoring method could be used to measure the EOF. Using this method, the experimenter need not worry about the possibility of the adsorption of the neutral marker on the capillary wall and/or gaining partial charge at a different pH.



**Figure 4.18: Decrease in viscosity by increasing temperature (Data extracted from CRC handbook) and corresponding increase in EOF by increasing temperature for an uncoated capillary**



#### 4.5: References

1. Shaw, D. J., Introduction to Colloid and Surface Chemistry, 3<sup>rd</sup> edition, Butterworths. Toronto, 1980.
2. Strain, H. H., J. Am. Chem. Soc., 61, 1292, 1939.
3. Strain, H. H. and Sullivan, J. C., Anal. Chem., 23, 816, 1951.
4. Mould, D. L. and Synge, R. L. M., Biochem. J., 58, 571, 1954.
5. Kowalczyk, J., J. Chromatogr., 71, 459, 1972.
6. Jorgenson, J. W. and Lukacs, K. D., J. Chromatogr., 208, 3, 1981.
7. Robson, M. M., Cikalo, M. G., Myers, P., Euerby, M. R. and Bartle, K. D., J. Micro. Sep., 9, 357-372, 1997.
8. Shaw, D. J., Electrophoresis, Academic Press, London, 1969.
9. Liu, H. and Cantwell, F. F., Anal. Chem., 63, 993-1000, 1991.
10. Cantwell, F. F. and Puon, S., Anal. Chem., 51, 623, 1979.
11. Taylor, T. A. and Yeung, E. S., Anal. Chem., 65, 2928, 1993.
12. Robson, M. M., Cikalo, M. G., Myers, P., Euerby, M. R. and Bartle, K. D., J. Micro. Sep., 9, 357-372, 1997.
13. Stevens, T. S. and Cortes, H. J., Anal. Chem., 55, 1365, 1983.
14. Chien, R. and Helmer, J. C., Anal. Chem., 63, 1354-1361, 1991.
15. Tsuda, T., Nakagawa, G.; Sato, M. and Yagi, K., J. Appl. Biochem., 5, 330, 1983.
16. Lauer, H. H. and McManigill, D., Anal. Chem., 58, 166, 1986.
17. Walbroehl, Y. and Jorgenson, J. W., Anal. Chem., 58, 479, 1986.
18. Altria, K. D. and Simpson, C. F., Anal. Proc., (London), 23, 453, 1986.
19. Williams, B. A. and Vigh, G., Anal. Chem., 68, 1174-1180, 1996.
20. Lee, T. T., Dadoo, R. and Zare, R. N., Anal. Chem., 66, 2694-2700, 1994.
21. Huang, X., Gordon, M. J. and Zare, R. N., Anal. Chem., 60, 1837-1838, 1988.

22. Harris, D. C., Quantitative Chemical Analysis, 3<sup>rd</sup> Edition, W. H. Freeman and Company, New York, 1991.
23. Hjerten, S.; Jerstedt, S., and Tiselius, A., Anal. Biochem., 11, 219-233, 1965.
24. Salomon, K., Burgi, D. S. and Helmer J. C., J. of Chromatogr., 559, 69-88. 1991.
25. Elving, P. J., Markcwitz, J. M., and Rocsenthal, I., Preparation of Buffer Systems of Constant Ionic Strength, 28, 7, 1956.
26. Dorsey, J. G. and Cooper, W. T., Anal. Chem., 66, 857A-867A, 1994.
27. McLaughlin, G.M., Nolan, J. A., Lindahl, J. L., Palmieri, R. H., Anderson, K.W., Moris, S. C., Morrison, J. A., and Bronzert, T. J., J. liq. Chromatogr., 15 (6 and 7), 961-1021, 1992.
28. Weast, R. C., Lide, D. R., Astle, M. J., and Beyer, W. H., CRC handbook of Chemistry and Physics, CRC Press, Inc. Boca Raton, Florida, USA, 1989-1990.
29. Harris, D. C., and Kratochvil, B., An Introduction to Chemical Analysis, Saunders College Publishing, Philadelphia, 1981.



# *Volume 2*

# Chapter 5

## Surface modification based on Si-O and Si-C sub-layers and a series of N-substituted acrylamide top-layers for capillary electrophoresis<sup>1</sup>

---

<sup>1</sup> A version of the results presented in this chapter has been published in different journals shown below and some other parts of the results is under preparation for future publications:

1. Surface modification based on Si-O and Si-C sublayers and a series of N-substituted acrylamide top-layers for capillary electrophoresis; C. Gelfi, M. Curcio, P. G. Righetti, R. Sebastiano, A. Citterio, **Hossein Ahmadzadeh** and N. J. Dovichi, *Electrophoresis*, 19, 1677-1682, 1998.
2. SDS-Capillary Electrophoresis of Proteins in a Sieving Matrix Utilizing Two-Spectral Channel Laser-Induced Fluorescence Detection; Douglas B. C, R M. Polakowski, J. C. Y. Wong, **Hossein Ahmadzadeh**, C. Stathakis and N. J. Dovichi, *Electrophoresis*, 19, 2175-2178, 1998.
3. Labeling effects on the isoelectric point of green fluorescent protein; Dawn P. Richards, Costas Stathakis, Robert Polakowski, **Hossein Ahmadzadeh**, Norman J. Dovichi; *J. Chromatogr. A.*, 853, 21-25, 1999.

## 5.1 Introduction

The development of inert and stable coatings in capillary electrophoresis is driven by the need to obtain high efficiency protein separation and high resolution DNA sequencing, both of which require effective sieving matrix immobilization and minimal electroosmotic flow (EOF).

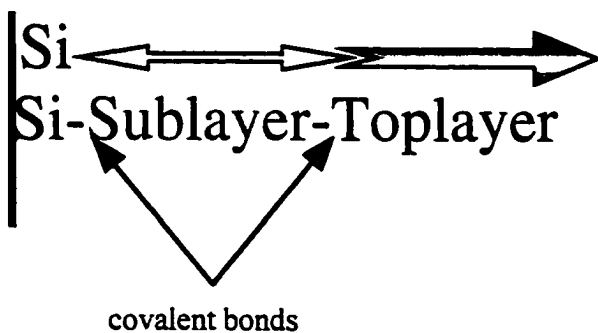
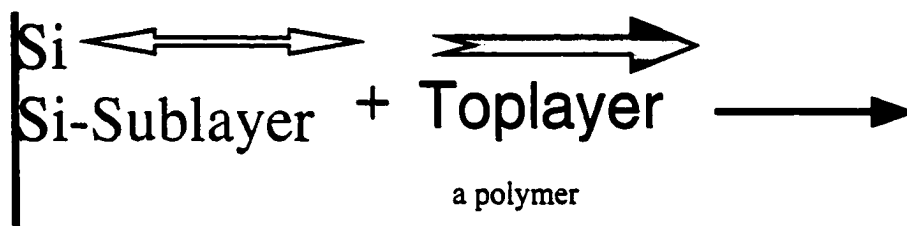
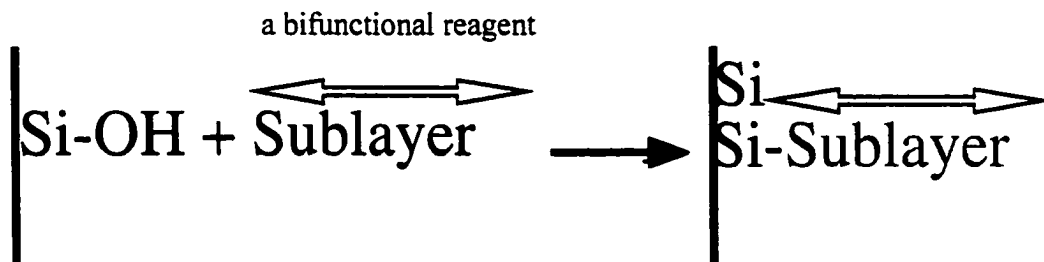
Chemical separation of many biomolecules and pharmaceuticals are limited by their electrostatic interaction with the inner surface of the capillary wall. Furthermore, the theory of capillary electrophoresis predicts that biological macromolecules such as proteins should have efficiencies on the order of  $10^6$  theoretical plates because of the low diffusion coefficient of these molecules. However, in practice we are far from this ideal case mostly because of the adsorption of proteins to the capillary wall. This problem hindered method development, and, therefore, the full potential of CE in protein separation has yet to be realized.<sup>1-3</sup>

The study of surface modification to prevent protein-surface interactions is extremely popular. However, capillaries with modified surfaces are difficult to fabricate since they exhibit hydrolytic instability over a wide pH range, wide temperature range and lack batch-to-batch reproducibility during separation. Polymeric coatings generally demonstrate greater stability than those of their non-polymeric counterparts do, and, therefore, most studies of capillary-wall coating involve polymer chemistry.

Capillaries can be coated in two steps: first, a sub-layer is covalently linked to the surface and, second, a monomer is polymerized as a top-layer, covalently linked to the sub-layer. Figure 5.1 depicts schematic steps and strategy in coating a capillary.

Hjerten was the first to apply silane chemistry in capillary electrophoresis.<sup>4</sup> He used a Si-O bond as a sub-layer that undergoes alkaline hydrolysis at  $\text{pH} > 8$  and polymerized acrylamide as a top-layer that also undergoes alkaline hydrolysis to leave a layer of polyacrylate on the capillary wall. The chemical formulas for Hjerten's coating method are

Figure 5.1: Schematic diagram showing the strategy for permanent coating





shown in Figure 5.2. For a complete structural formula of all reagents including TEMED and APS see Figures 3.7 and 3.8 in chapter 3 of this thesis.

Novotny used the Grignard method to change the Si-O bond to a Si-C bond, the latter of which is much more resistant to alkaline hydrolysis.<sup>5</sup> This method works better than the silane-coupling chemistry, but still uses polyacrylamide as the top-layer, and because of alkaline hydrolysis of polyacrylamide, electroosmotic flow (EOF) is observed at  $\text{pH} > 8$ . Figure 5.3 shows chemical formulas and reaction steps in making a Si-C bond using Grignard method and polymerizing a polyacrylamide as a top-layer (Novotny's coating method).

Righetti introduced and optimized the performance of some novel polymers of acrylamide substitutes. The monomers are acrylamide (AA), dimethylacrylamide (DMA), N-acryloylaminoethoxyethanol (AAEE) and acryloylaminoopropanol (AAP). These polymers were chosen as top-layers because they have both alkaline hydrolysis resistance and a range of hydrophilicity-hydrophobicity.<sup>6-13</sup> These top-layers show much less protein adsorption on the capillary wall; however, despite the use of hydrophilic polymers, Righetti's method involves a Si-O bond sub-layer and therefore is vulnerable to alkaline hydrolysis. The chemical formula of the monomers introduced by Righetti are shown in Figure 5.4 and the sub-layer used by him is depicted in Figure 5.2.

We report a new method of coating which combines both the hydrolytic stability of the Si-C bond (Novotny's method) and the hydrophilicity-hydrophobicity selectivity of Righetti's method. This method of coating could be called modified Novotny-Righetti's coating method.

A good coating should completely cover the surface, and not interact with the analyte.<sup>13</sup> We evaluated the coverage efficiency by measuring the EOF: the lower the EOF, the higher the surface coverage.

Figure 5.2: Chemical formulas for Hjersten coating method

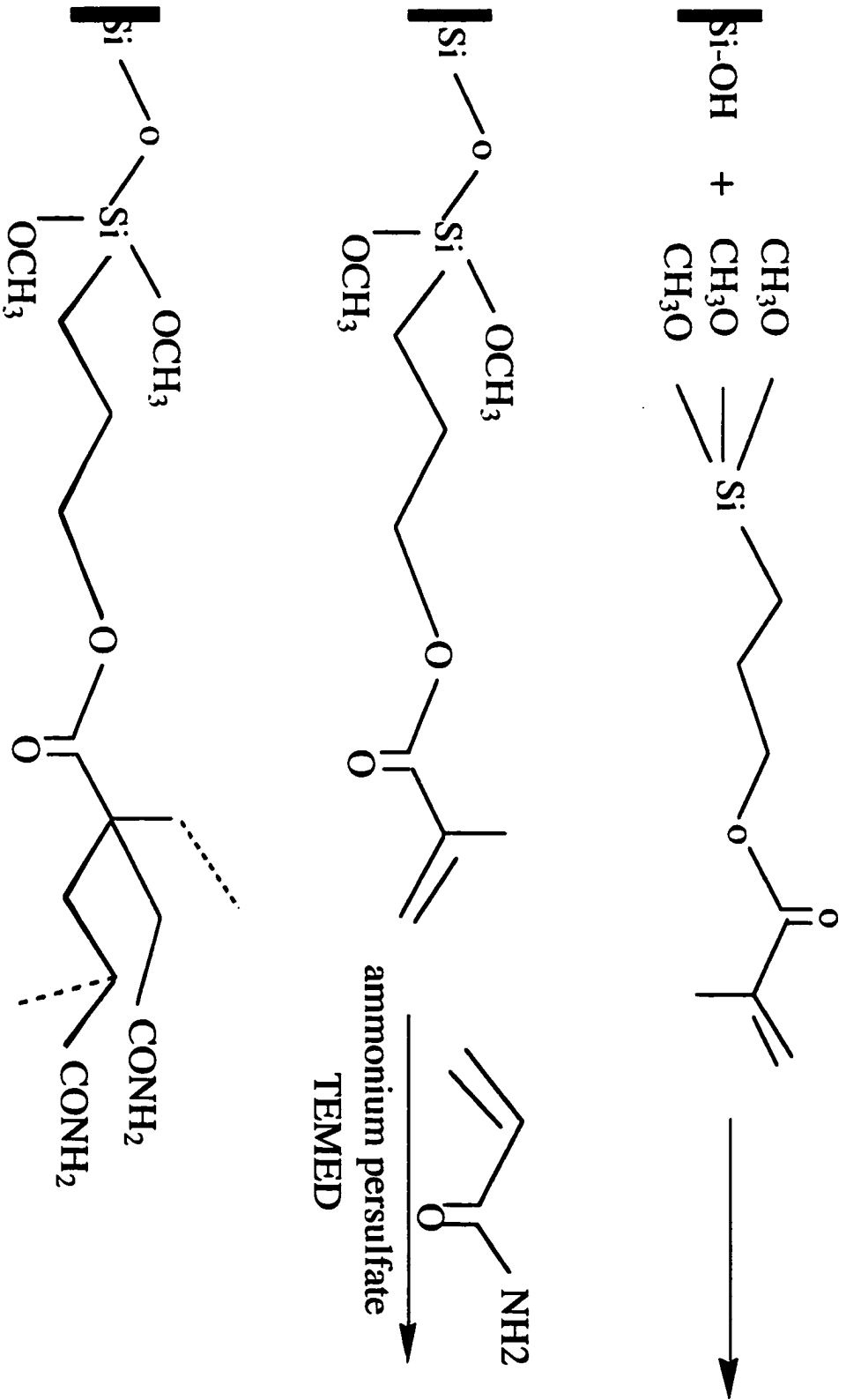


**Figure 5.3: Chemical formulas and reaction steps in making a Si-C bond using Grignard method and polymerization of acrylamide as a top-layer (Novotny's method)**

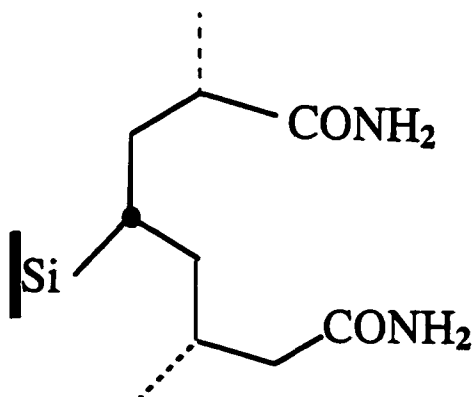
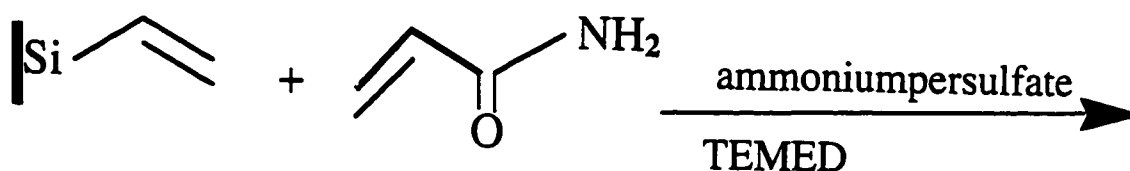
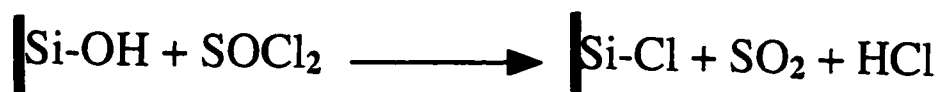
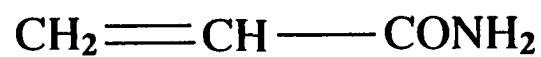
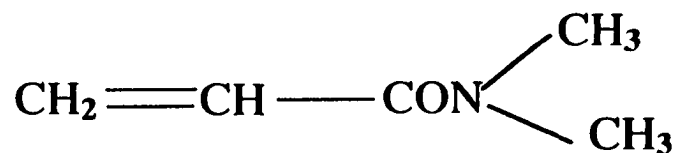


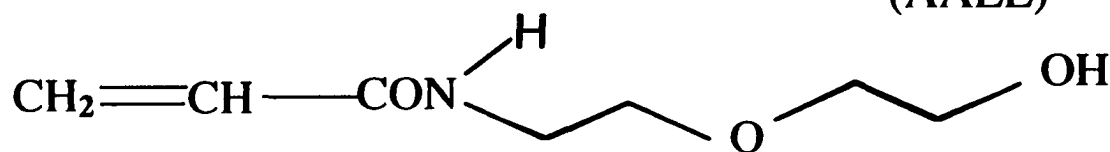
**Figure 5.4: Chemical formulas of the monomers introduced by Righetti**



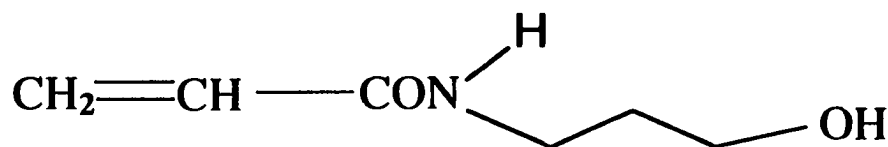
acrylamide (AA)



dimethyl acrylamide  
(DMA)



N-acryloylaminoethoxyethanol  
(AAEE)



acryloylaminopropanol  
(AAP)

In this chapter we also studied a series of acrylamide (AA), dimethylacrylamide (DMA), N-acryloylaminoethoxyethanol (AAEE), and N-acryloylaminopropanol (AAP) coated capillaries based on either one of two approaches. These involved either the coupling of a bifunctional reagent (3-methacryloxypropyltrimethoxysilane) onto the silanol groups (Si-O bond) or silanol chlorination followed by the Grignard-coupling of vinylmagnesiumbromide (Si-C bond). After free-radical polymerization of the monomers onto different sub-layers, EOF versus temperature (20-75 °C) studies revealed superior stability of Si-C as compared to Si-O based sub-layers. The Grignard-based sub-layer was employed further to compare the performance of all 4 monomers. EOF versus pH (pH 3-11) profiles were more stable for polyAAP and polyDMA as compared to polyAAEE and polyAA. PolyAA, which is widely used in DNA sequencing and protein separation, showed evidence of irreversible degradation at pH > 9. In addition, after Si-O-polyAA, EOF for Si-C-polyAA coated capillaries were higher than those of Si-C-polyAAEE, Si-C-polyDMA, and Si-C-polyAAP coated capillaries.

In terms of efficiency and migration time reproducibility, Si-C-polyAAP coated capillaries were superior as demonstrated for fluorescently labeled ovalbumin (200,000 ±18,000 theoretical plates and 0.4% RSD in migration time). Si-C-polyAAP coated capillaries showed the least adsorption of labeled ovalbumin, while the Si-C-polyDMA showed the most adsorption. Si-C-polyAAP coated capillary was successfully used for protein separation.

## **5.2 Experimental**

### **5.2.1 Instrument**

Experiments were carried out using either a single-capillary or a five-capillary

instrument; both instruments were in-house constructed CE-LIF with a detector based on a Sheath-flow cuvette as previously described.<sup>14-17</sup> Unless otherwise stated, fused-silica capillaries were 40 cm x 50  $\mu\text{m}$  (ID), 141  $\mu\text{m}$  OD (Polymicro Technologies, Phoenix, AZ) for the five-capillary instrument, and 25 cm or 30 cm x 50  $\mu\text{m}$  (ID) for the single-capillary instrument. Only one laser and one spectral channel of the five-capillary instrument were active during the experiments. The in-house constructed instruments used a 0-30 kV DC power supply (CZE 1000, Spellman, Plainview, NY). For the sheath-flow cuvette detector, excitation was provided by the 488-nm line of an argon-ion laser operated at 12 mW (Model 2211-55 SL, Uniphase, San Jose, CA or Model Innova 90-4, Coherent, Mountainview, CA), which was focused approximately 30  $\mu\text{m}$  from the tip of the capillary with a 6.3x objective (Melles Griot, Nepean, ON, Canada). Fluorescence was collected by a 60x, 0.7 NA microscope objective (Mo-0060LWD, Universe Kokagu, Oyster Bay, NY) filtered with a spatial filter, and either a 615 DF 45 or a 630 DF 30 band pass filter (Omega Optical, Brattleboro, VT) was used to remove stray light and scattered light, respectively. Fluorescence was imaged onto a photomultiplier tube (R1477, Hamamatsu, Middlesex, NJ) biased at 1,000 V. The photocurrent was passed through a current-to-voltage converter and a low pass filter (RC = 47 ms) and then digitized with a 16-bit data acquisition board (NB-MIO 16 XH-18, National Instruments, Austin, TX) connected to a Macintosh computer.

The applied voltage was 400 V/cm for the five-capillary instrument and 400-800 V/cm for the single-capillary instrument. The running buffer was 10 mM borate for all coated capillaries using the five-capillary instrument and either 10 mM borate or 10 mM borate containing 5 mM sodium dodecylsulphate (SDS) for the single- capillary instrument. When doing pH studies, the run buffer was prepared in a way to keep the ionic strength constant. The procedure to prepare constant ionic strength run buffers at different pHs was described in chapter 4 of this thesis.

### 5.2.2 Reagents

Borax (sodium tetraborate), SDS and sodium citrate were purchased from BDH (Toronto, ON, Canada). For most of the experiments the running buffer and sheath flow buffer were 10 mM borate (2.5 mM borax) and 5 mM SDS or 10 mM borate and no SDS. All buffers were made with Milli-Q de-ionized water and were filtered using a 0.2- $\mu$ m filter. Ovalbumin (dissolved in 10 mM borate pH 9.4), acetic acid, and 3-methacryloxypropyltrimethoxysilane were purchased from Sigma (St. Louis, MO). Derivatizing reagents, 5-furoyl quinoline-3-carboxaldehyde (FQ) and potassium cyanide (KCN), were purchased from Molecular Probes (Eugene, OR). KCN was dissolved in 10 mM borate at a concentration of 25 mM, and this solution was diluted with run buffer to 5 mM before being used. A stock solution of 10 mM FQ was prepared in methanol: 10  $\mu$ L aliquots were then placed into 500  $\mu$ L micro centrifuge tubes and the solvent removed under vacuum using a Speed Vac (Savant Instruments Inc., Farmingdale, NY). The dried FQ aliquots, which were 100 nmol each, were stored at  $-20$  °C. These precautions were necessary since it was observed that FQ degraded slowly in solution even if the solution was stored at  $-20$  °C.

Type 4-A molecular sieves and sodium phosphate were purchased from Fisher Scientific Company (Fair Lawn, NJ, USA). Molecular sieves type 4-A was used as a moisture trap reagent for the nitrogen gas.

Anhydrous THF and vinyl magnesium bromide (with a septum to draw the solution out of the bottle without exposing the solution to air) were purchased from Aldrich (Milwaukee, WI). TEMED and ammonium persulfate were from Bio-Rad (Hercules, CA) and acrylamide (AA) from GibcoBRL (Gaithersburg, MD). Dimethylacrylamide (DMA), N-acryloylaminoethoxyethanol (AAEE), and N-acryloylaminopropanol (AAP) were prepared at Professor Righetti's laboratory. Phosphoric acid was purchased from Caledon Laboratories (Georgetown, ON, Canada).

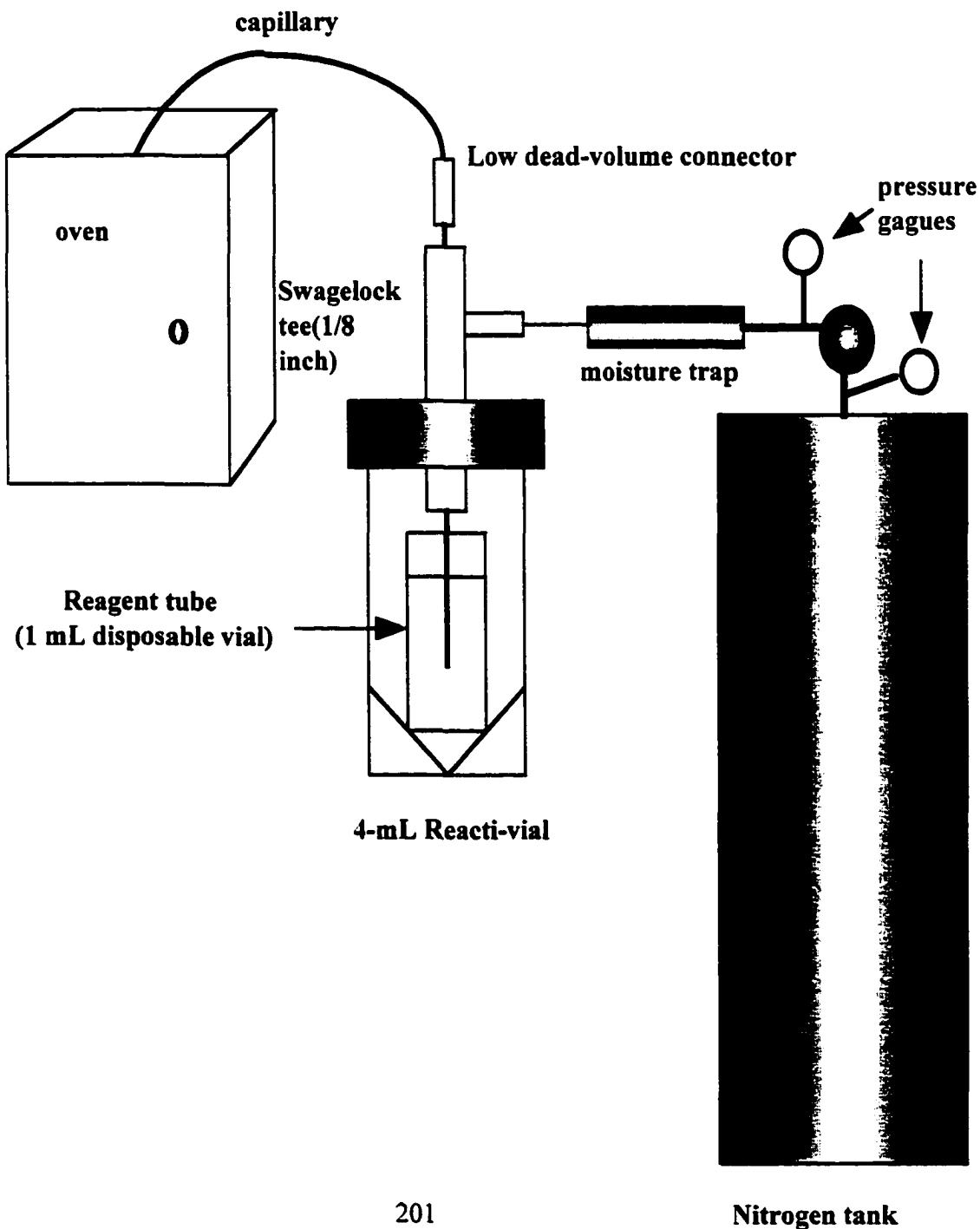
### 5.2.3 Capillary coating protocol

Figure 5.5 shows the simple apparatus that was constructed to deliver reagents onto the capillary. Reagents were prepared in 1-mL disposable vials. Each reagent vial was placed inside a 4 mL Reacti-vial from Pierce. The reacti-vial lid was drilled to accommodate a 1/8 inch stainless steel Swegelok tee. This Swegelok tee was held in place with the aid of copious amounts of Teflon tape. One side of the tee was connected with Teflon tubing to a nitrogen cylinder. A guard column filled with molecular sieves type 4-A as a moisture trap was connected to the nitrogen tank to remove water impurity from nitrogen gas before being used to purge the capillaries. The top side of the Swegelok tee was connected to a 1/16 inch adaptor. This adaptor was connected to a low dead-volume fitting.

The coating of capillaries was done either based on silanization or Grignard reaction (see Figures 5.2 and 5.3). In the former method the capillary (4-5 m long, 50  $\mu\text{m}$  ID) was flushed with 0.1M NaOH for 30 min and then with water for another 30 min. Finally, a 4% solution of 3-methacryloxypropyltrimethoxysilane in a 1:1 mixture of glacial acetic acid and water was prepared, and the capillary was flushed with this solution for 20 min. The reaction was allowed to go to completion for 1 hour. Next, the capillary was flushed with water for 10 min. To 1 mL of a 3%T solution of acrylamide monomer, 4  $\mu\text{L}$  of freshly prepared 10% ammonium persulfate and 1  $\mu\text{L}$  of TEMED were added. This undegassed solution was immediately flushed through the capillary. After 3 hours the polymerization was complete and the gel was replaced with water. The capillary was stored in this water, and before doing a CE run the water inside the capillary was replaced manually with running buffer using a syringe with a proper fitting. Flushing the solutions through the capillary was done using nitrogen gas at 20 psi equipped with a moisture trap (molecular sieves Activated type 4A; Anachemia Montreal, QC, Canada). Figure 5.2 shows the silanization chemistry.



**Figure 5.5: Apparatus for filling capillaries (not to scale). Nitrogen gas pressure was used to force different reagents through the capillary. The reagents were held in a disposable vial held by Reactival. The fittings were used to connect the capillary to the reagents**



The second coating method was the Grignard-based method. Figure 5.3 shows the Grignard reaction with AA polymerization as a top-layer.

The outlet of the low dead-volume fitting was connected to a 3 cm long piece of 1/16 inch outer diameter Teflon tubing. The capillary was threaded through the Teflon tube, the connector and the tee. The capillary tip was located near the middle of Reacti-vial inside the disposable vial. For some solvents like THF and some reagents like vinylmagnesium bromide, this disposable vial has to be glass. When the capillary was inside the vial in the Reacti-vial, the top nut was tightened and the capillary was in place. Unless noted, reagents were flushed through the capillary under nitrogen gas pressure at 20 psi.

The coating procedure has four steps that will be described in the following sections.

#### **5.2.3.1 Capillary pre-treatment**

Fused-silica capillaries, 50  $\mu\text{m}$  ID, 4-5 m long, were conditioned by flushing with 1M NaOH for 3 h, water for 1 hr and methanol for another hour using 20 psi nitrogen pressure. Using a clean and dry tube, the capillary was dried inside a 140  $^{\circ}\text{C}$  oven overnight by flushing with 5 psi nitrogen.

#### **5.2.3.2 Chlorination of silanol groups**

The following day while the capillary was inside the oven and nitrogen was flowing through it, the oven temperature was reduced to 65  $^{\circ}\text{C}$  and then thionylchloride was flushed under 20 psi nitrogen pressure for 30 min. The outflow was checked to identify any plugged capillaries, and was tested for acidity using a pH paper. After 30 min one end of the capillary was sealed with a GC septum while the outlet end remained connected to the vacuum line for an additional 15 min to remove the excess thionylchloride. This step

was done while the capillary was inside the oven. Before doing the chlorinating step, the color of thionylchloride was checked, and whenever the solution was faint in color it was changed to a fresh solution. Then the outlet end of the capillary was sealed using a GC septum, and it was heated in the oven for 8 hr or overnight. In some cases this step was repeated to obtain a more rugged coating. Excess thionyl chloride was decomposed by the addition of water in a fumehood.

### **5.2.3.3 Grignard reaction**

A fresh 0.25 M solution of vinylmagnesiumbromide in dry THF was prepared under nitrogen atmosphere using dried and newly distilled THF to dilute the stock solution of vinylmagnesiumbromide. To prepare this solution, 0.75 mL of dry THF and 0.25 mL of 1M vinylmagnesiumbromide in THF were added to a tube filled with nitrogen gas. A freshly cut end of the capillary was submerged into the solution and the outlet end of the capillary was uncapped, a few centimeters were cut from the end and the capillary was placed in a tube containing methanol. Nitrogen pressure (20 psi) was applied to the other end of the capillary to rinse it with Grignard solution. If the capillary was plugged and no flow was observed, the capillary was placed back inside the oven briefly. If still plugged, it was checked for blockage using a microscope and cut to appropriate lengths. Rinsed for 30 min., the capillaries were capped at both ends using a GC septum, and heated for 6-8 hr or overnight at 70 °C. Then the capillary was uncapped, 5-10 cm of both ends were cut, and then the capillary was rinsed with anhydrous THF for 30 min followed by water for another 30 min. The Grignard step could be repeated to get more rugged capillaries.

Initially, about 10% of the capillaries would be plugged at the Grignard reaction step. We observed that the failure rate dropped to zero in winter, when the relative humidity in the laboratory environment dropped and as experienced was gained in handling the

reagents. Novice experimenters in humid environments may expect difficulty with this sub-layer coating step.

#### **5.2.3.4 Polymerization step**

The capillary was cut into four, 1 m long sections, and coated with different top-layers. A 3%T solution of each of the four monomers (AA, DMA, AAEE, and AAP) was prepared by diluting each stock solution in doubly distilled deionized water. 1  $\mu$ L TEMED and 4  $\mu$ L of 10% ammonium persulfate were added to 1 mL of each of the monomers, and then each was immediately flushed onto the capillary at 60 psi for 5 min. After 3 hours of polymerization the gel was flushed out of each capillary and was replaced with water. These coated capillaries were stored in water, and the running buffer was flushed through them prior to use.

If the gel is left inside the capillary longer than 3 h in this step, a gel filled capillary that is suitable for CGE is obtained. Some times this polymerization step, if the reaction time is long enough, will plug the capillaries.

#### **5.2.3.5 FQ labeling**

The labeling protocol used was a modification of the procedure first introduced by Novotny.<sup>18</sup> 7.5  $\mu$ L of  $10^{-7}$  M ovalbumin solution was added to 100 nmol of dry FQ, and then 2.5  $\mu$ L of 5 mM KCN in water was added. After 30 min the reaction was stopped by adding 740  $\mu$ L of run buffer. This FQ-labeled ovalbumin, with final concentration of  $10^{-9}$  M, was used to evaluate the coated capillaries. In earlier studies this group showed that a 30 min reaction time was the optimized time required to obtain the highest signal intensity for the labeling reaction.<sup>19</sup>

### **5.2.3.6 Electroosmotic flow (EOF) mobility measurement**

To evaluate each coated capillary, the EOF was measured by the current monitoring method.<sup>20</sup> In this method the capillary was filled with 10 mM borate and the current channel was monitored while the high voltage was applied. After having a stable current the run buffer was changed to 8 mM borate. The current started decreasing and after a certain time it reached a constant value. This time was measured and used to calculate EOF. For a thorough discussion and method validation of the current monitoring method, you may refer to chapter 4 of this thesis.

### **5.2.3.7 Safety precautions**

Potassium cyanide is highly poisonous. It reacts rapidly with acids to form lethal HCN gas. Stock solutions should be made in a basic buffer and the experimenter should be aware of any change to acidic pH during the experiment. Neutralization of the waste containing KCN should be made by addition of 1% NaOH solution followed by slow addition of bleach. Excess thionyl chloride should be decomposed by the addition of water to the solution in a fume hood.

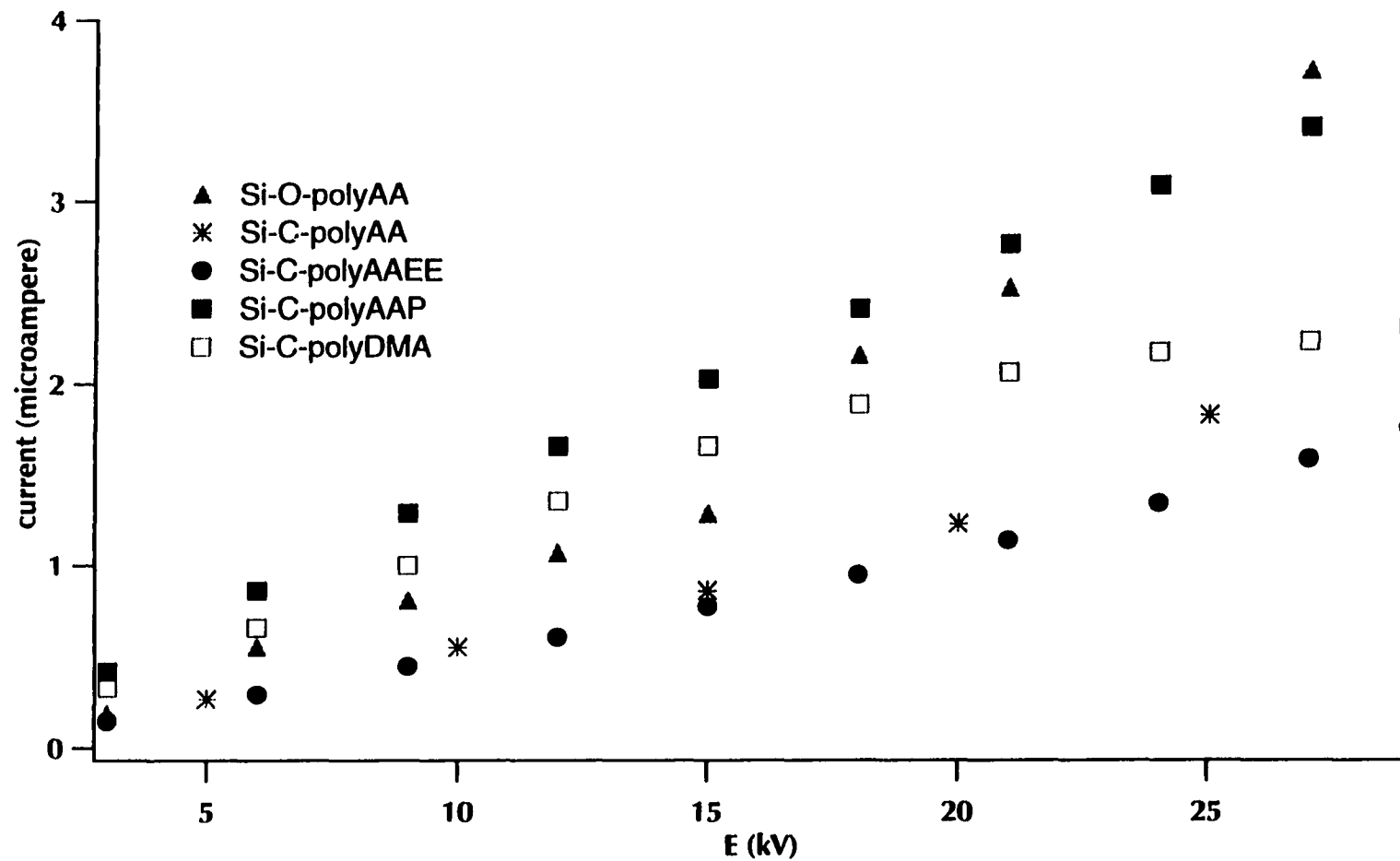
## **5.3 Results and discussion**

### **5.3.1 EOF comparison**

We proved that this current monitoring method to measure EOF is as accurate as the neutral marker method, especially for coated capillaries.<sup>21</sup>

Before each EOF comparison experiment, an Ohm's plot determination was performed on each coated capillary. Figure 5.6 shows the Ohm's plot for a Si-C sub-layer with polyAA, polyDMA, polyAAEE and polyAAP top-layers. For each coated capillary the

**Figure 5.6: Ohm's plot for si-O and Si-C coated capillaries with polyAA, polyAAEE, poly AAP and polyDMA top-layers. The run buffer is 10 mM borate with pH 9.4 for all the experiments. The ionic strength and temperature is kept constant for all the runs.**



current was monitored while the voltage was changed from 3 kV to 6, 9, 12, 15, 18, 21, 24, 27 and 29 kV for a 30 cm long capillary. The maximum voltage in the linear portion of current versus voltage curve was chosen for the applied voltage for each coated capillary. It is not known why each different top-layer is producing different current when the same voltage is applied under the same experimental conditions.

To compare alkaline-hydrolysis stability of the Si-C and Si-O sub-layers, two capillaries were chosen. The first one was based on a silanization reaction having a Si-O sub-layer and the second one was based on the Grignard reaction having a Si-C sub-layer. Both had a polyacrylamide (AA) top-layer. Using 10 mM borate pH 9.4 at room temperature, the EOF of both capillaries was measured. For the silanized-coated capillary, the EOF was  $5.6 \times 10^{-4} \text{ cm}^2/\text{V s}$  ( $n=10$ , RSD = 54%) and the EOF of the Grignard-coated capillary was  $1 \times 10^{-5} \text{ cm}^2/\text{V s}$  ( $n=20$ , RSD = 51%). For the silanized-coated capillary we could not get more than 10 runs because of a gradual increase in EOF which caused longer and longer time for the current to approach to a constant level.

Note that the typical EOF values for uncoated capillaries are around  $8.4 \times 10^{-4} \text{ cm}^2/\text{V s}$ . We have also measured EOF at intermediate steps, just after attachment of vinyl group ( $-\text{CH}_2-\text{CH}=\text{CH}_2$ ) to the capillary wall and before the covalent attachment of the polymer chains. It turns out that when a proper Si-C bond is established by a carefully controlled Grignard reaction, the EOF is reduced by about one order of magnitude.

It is also evident from Figure 5.7 that the final EOF after polymer coating is much lower, typically by more than one order of magnitude, if the sub-layer attachment is done via a direct Si-C bond rather than a Si-O bond. This means that, probably, a well-done reaction is able to cover many more silanol sites as compare to the similar reaction via conventional silane bifunctional reagent. Also note that the coating with N-substituted acrylamide produces a further decrease of EOF as compared to similar coatings with

standard acrylamide. A good coating produces capillaries with a 2-3 orders of magnitude decrease in EOF as compared to uncoated capillaries.

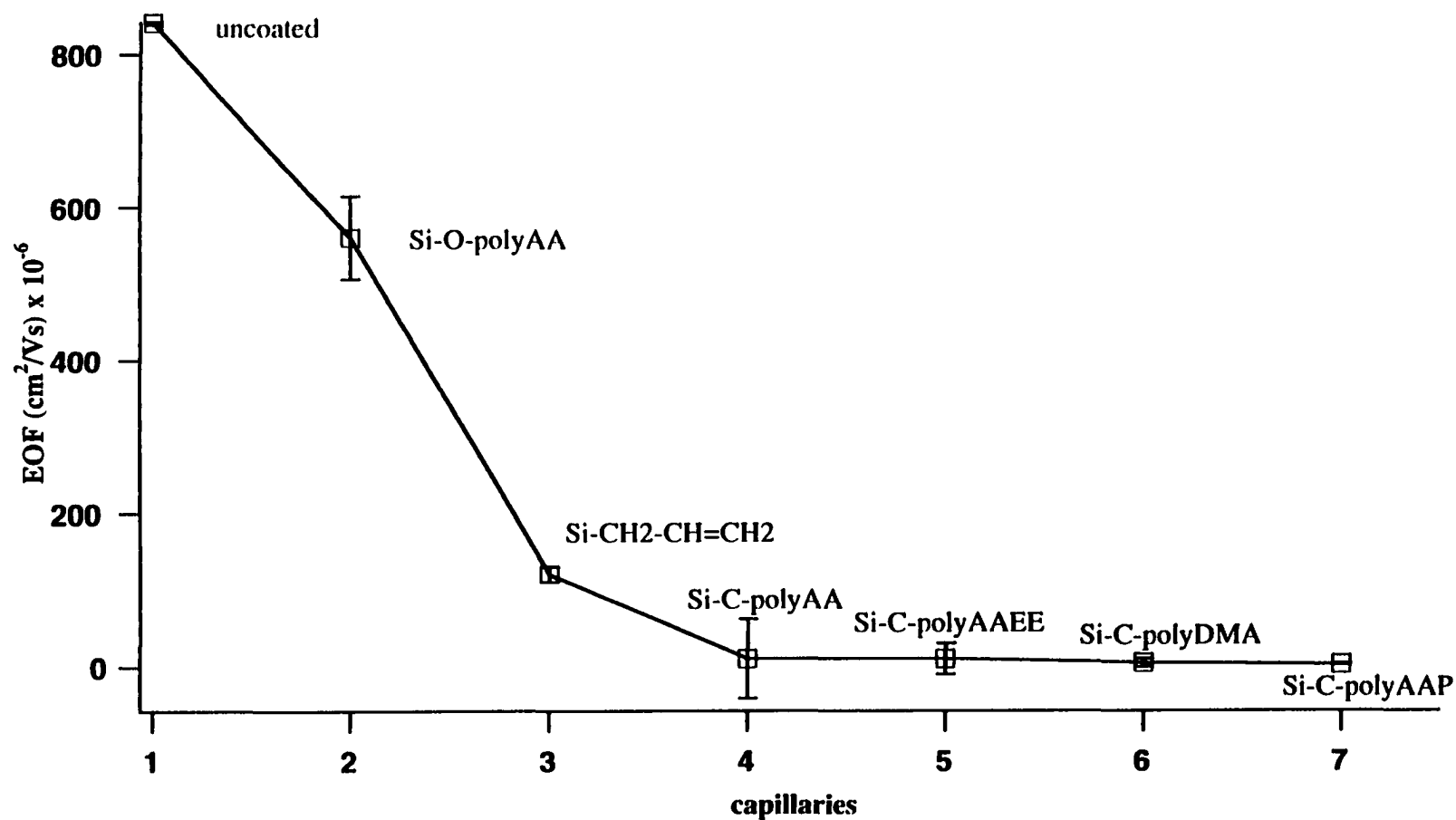
Figure 5.7 compares the EOF measurement and precision for uncoated capillaries, different Si-C coated capillaries and a Si-O-polyAA coated one. This figure shows that the EOF of Si-O-polyAA at pH 9.4 and room temperature is very high, and the precision is very poor (RSD = 54% as compared to uncoated capillaries RSD = 2%). Changing the sub-layer from Si-O to Si-C reduced the EOF and improved the precision. The Si-C-polyAA precision was also very poor (RSD = 51%), even though the EOF was lower than that of Si-O-polyAA. For the Si-C-poly AAEE, we saw an improvement in precision (RSD = 20%) but the same EOF as Si-C-polyAA. It is worth mentioning that for pH < 9 the EOF for a Si-C-polyAAEE was lower than that of the Si-C-polyAA. For the Si-C-polyDMA, the EOF was reduced to very low values and precision was also very good (RSD = 5%). Finally, for the Si-C-polyAAP even lower EOF and excellent precision (RSD = 0.4%) in EOF measurement was observed.

### 5.3.2 Temperature stability

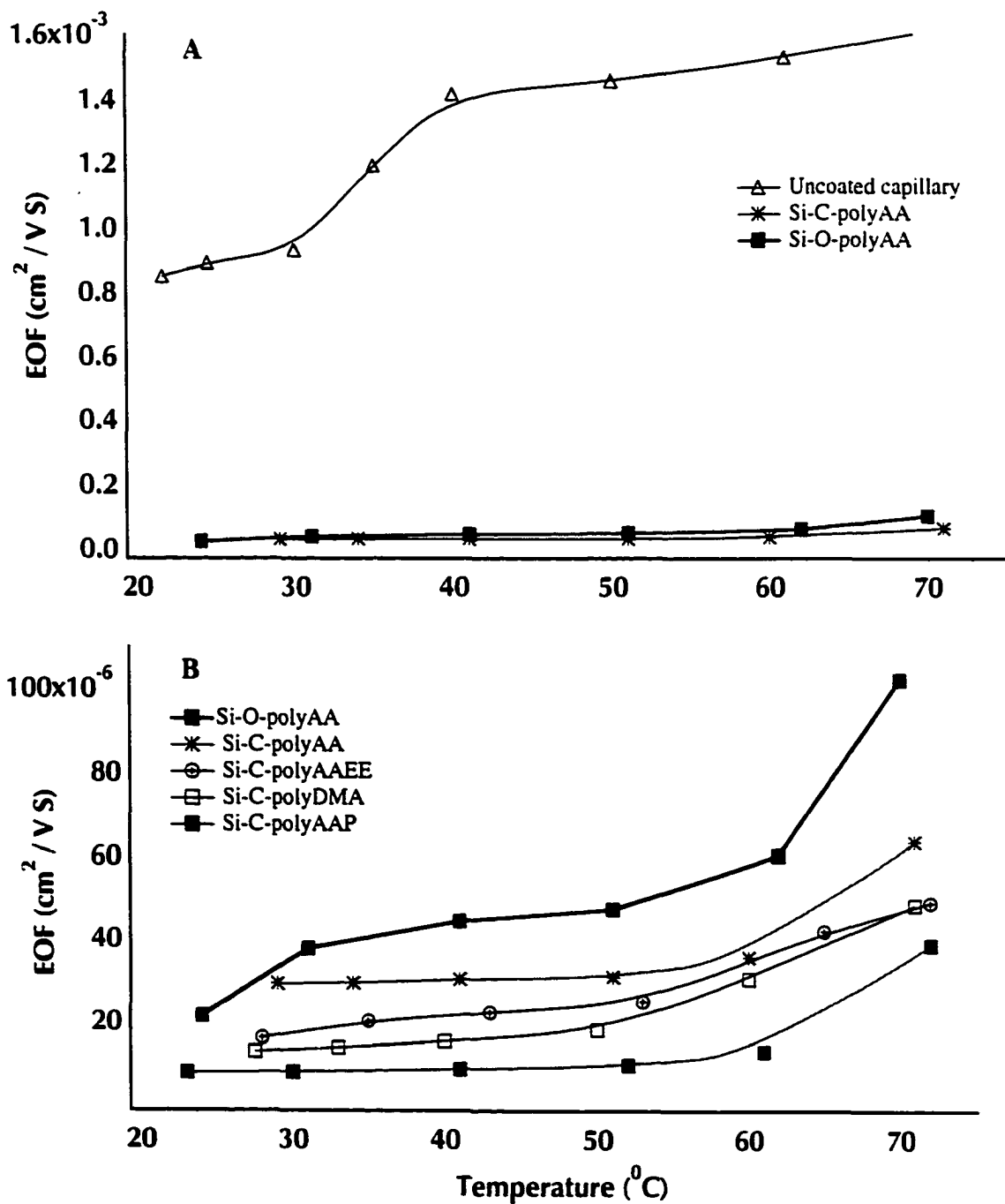
Figure 5.8 compares the temperature stability and top-layer of the coated capillaries from room temperature to 75 °C, at pH 9.4. Figure 5.8a compares uncoated, silanized-coated and Grignard-coated capillaries with acrylamide top-layers. Both Si-O and Si-C sub-layers with similar top-layers (AA) show reduced EOF as compared to uncoated capillaries, and Si-C coated capillaries had much less EOF than those of Si-O coated ones in all the temperatures studied. In part 5.3.1 we showed that the Si-C sub-layer was more stable than the Si-O sub-layer and this experiment confirmed that result. At high temperatures the rate of alkaline hydrolysis of the Si-O sub-layer was higher than that of the Si-C sub-layer, as can be seen by a gradual increase of EOF versus temperature. There are some other



**Figure 5.7: EOF values and relative standard deviations for 1) an uncoated capillary , 2) Si-O-polyAA, 3) Si-CH<sub>2</sub>-CH=CH<sub>2</sub> 4) Si-C-polyAA, 5) Si-C-polyAAEE, 6) Si-C-polyDMA and 7) Si-C-polyAAP coated capillaries. All the EOF measurements are done under constant ionic strength, pH (10 mM borate with pH 9.4), and room temperature.**



**Figure 5.8: Temperature effect on EOF of A) uncoated capillary compared with a Si-C-polyAA coated one, B) Si-C-polyAA, Si-C-polyAAEE, Si-C-polyDMA and Si-C-polyAAP coated capillaries. Ionic strength and pH are kept constant and the fitted line is just a guide to the eye.**



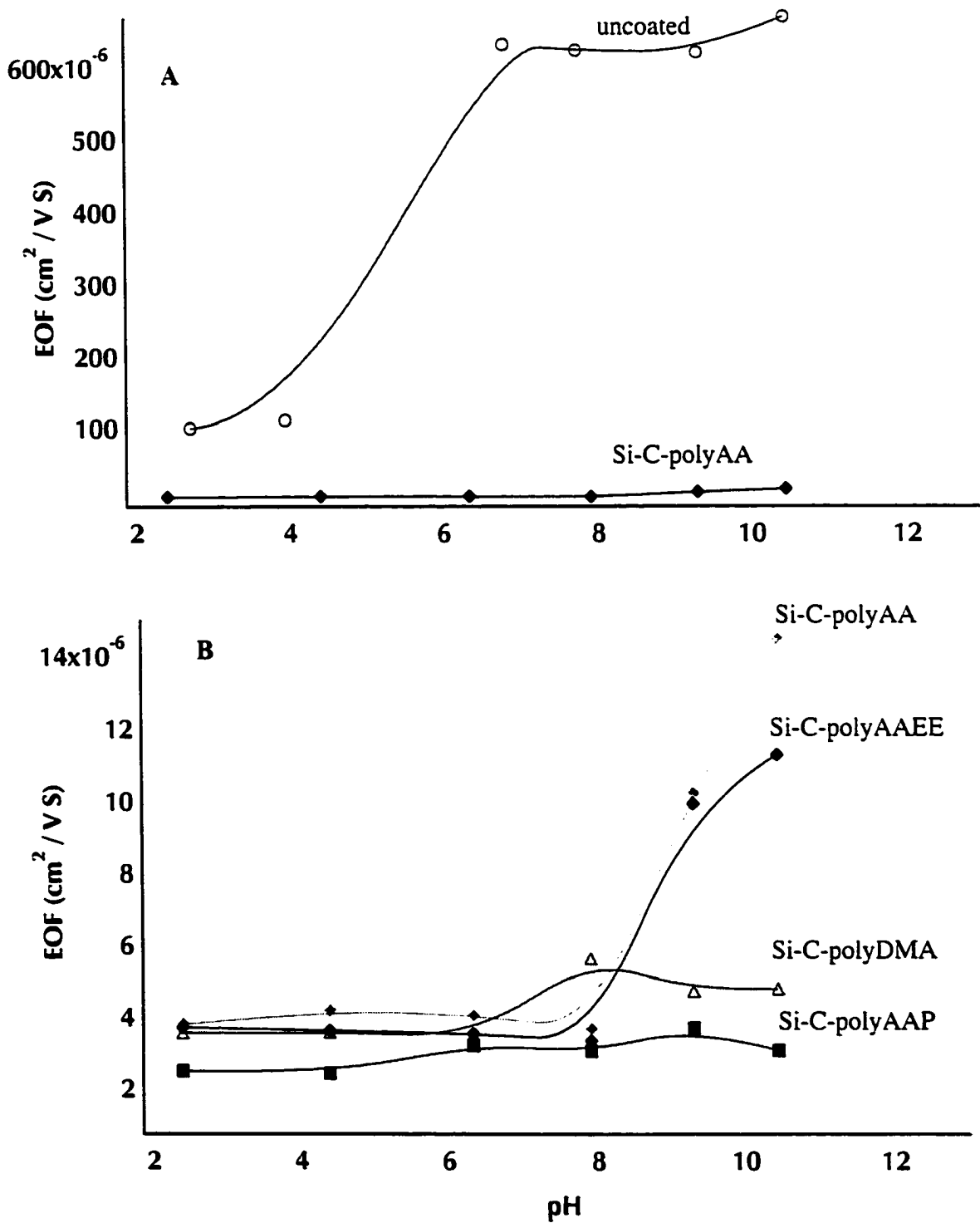
parameters that are temperature dependent and might have played a role in changing the EOF. A discussion about these parameters is given in chapter 4 of this thesis.

Figure 5.8b compare polyAA, polyDMA, polyAAEE, and polyAAP coated capillaries with a Si-C sub-layer. The Si-C-polyAA had lower EOF than the Si-O-polyAA and uncoated capillaries, and higher EOF than other coated capillaries with a Si-C sub-layer. The Si-C-polyDMA had slightly higher EOF than the Si-C-polyAAP but lower than that of the Si-C-polyAAEE. This experiment was done using an AAEE monomer that was stored for a long time. Righetti found that the AAEE monomer undergoes autopolymerization and this may be the reason for the Si-C-polyAAEE coated capillary to show higher EOF as compared to Si-C-polyDMA and Si-C-polyAAP coated ones.<sup>8</sup>

### 5.3.3 pH stability

Figure 5.9 compares the EOF stability of four different top-layers, all having a Si-C sub-layer, over a wide range of pH (2-11) and at constant room temperature. The change of EOF with pH for uncoated capillaries is also shown for comparison. All of these coated capillaries show about one order of magnitude reduction in EOF compare to uncoated capillaries over the pH range of 5-11. Figure 5.9b compares Si-C capillaries having different top-layers. Confirming what we concluded from temperature stability (Figure 5.8), we see that the Si-C-polyAAP and the Si-C-polyDMA coated capillaries show the lowest EOF and, the Si-C-polyAA one has a higher EOF, at most of the pH ranges studied. The Si-C-polyAAEE shows lower EOF than that of the Si-C-polyAA. This is in agreement with what Righetti reported, that a Si-C-polyAAEE is 500 times more resistant to alkaline hydrolysis as compared to polyAA.<sup>26</sup> Above pH 9 we observe a slight increase in EOF for

**Figure 5.9: pH effect on EOF A) uncoated capillary compared with Si-C-polyAA, and B) Si-C-polyAAP, Si-C-polyDMA, Si-C-polyAAEE and Sic-polyAA comparison. The fitted lines are just a guide to the eye.**



the Si-C-polyAA and Si-C-polyAAEE. When the pH increases to 11, the Si-C-polyAAEE, despite a slight increase in EOF, still shows about one order of magnitude lower EOF than that of an uncoated capillary. The Si-C-polyAA shows an EOF almost as high as uncoated capillaries, suggesting that alkaline hydrolysis of the polyAA top-layer has left a layer of polyacrylate, and despite covalent attachment of the polymer to the Si-C sub-layer, the EOF has been regenerated so strongly that this capillary could only be used if the power supply polarity is switched back to positive polarity.

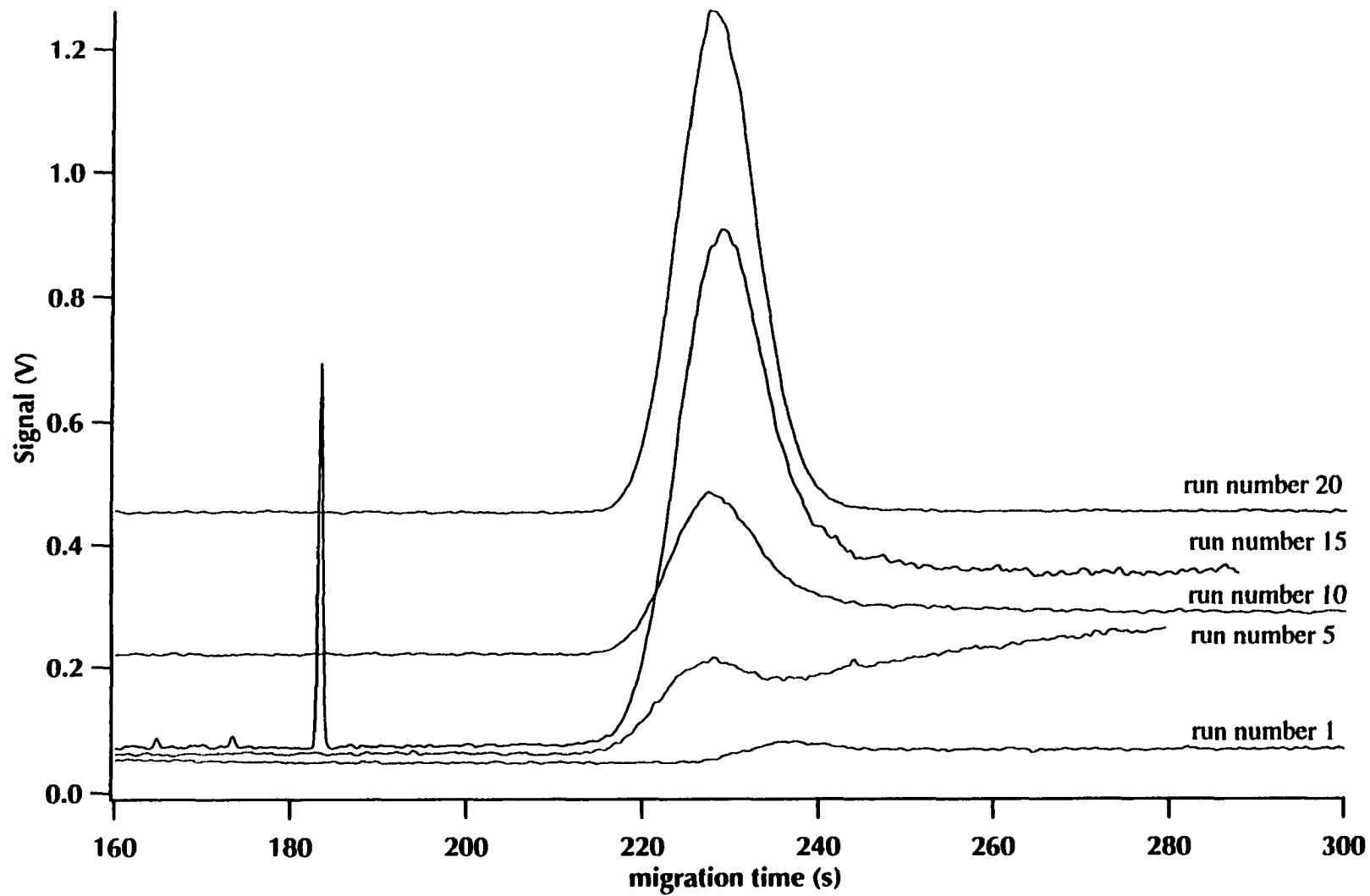
#### **5.3.4 Peak shape comparison and adsorption study**

For each coated capillary 22 identical injections were done; Figure 5.10-5.13 shows run numbers 1, 5, 10, 15, 20 and 22. The differences in migration times among these coated capillaries occur because of different applied voltages for each case chosen according to Ohm's plot (Fig. 5.6).

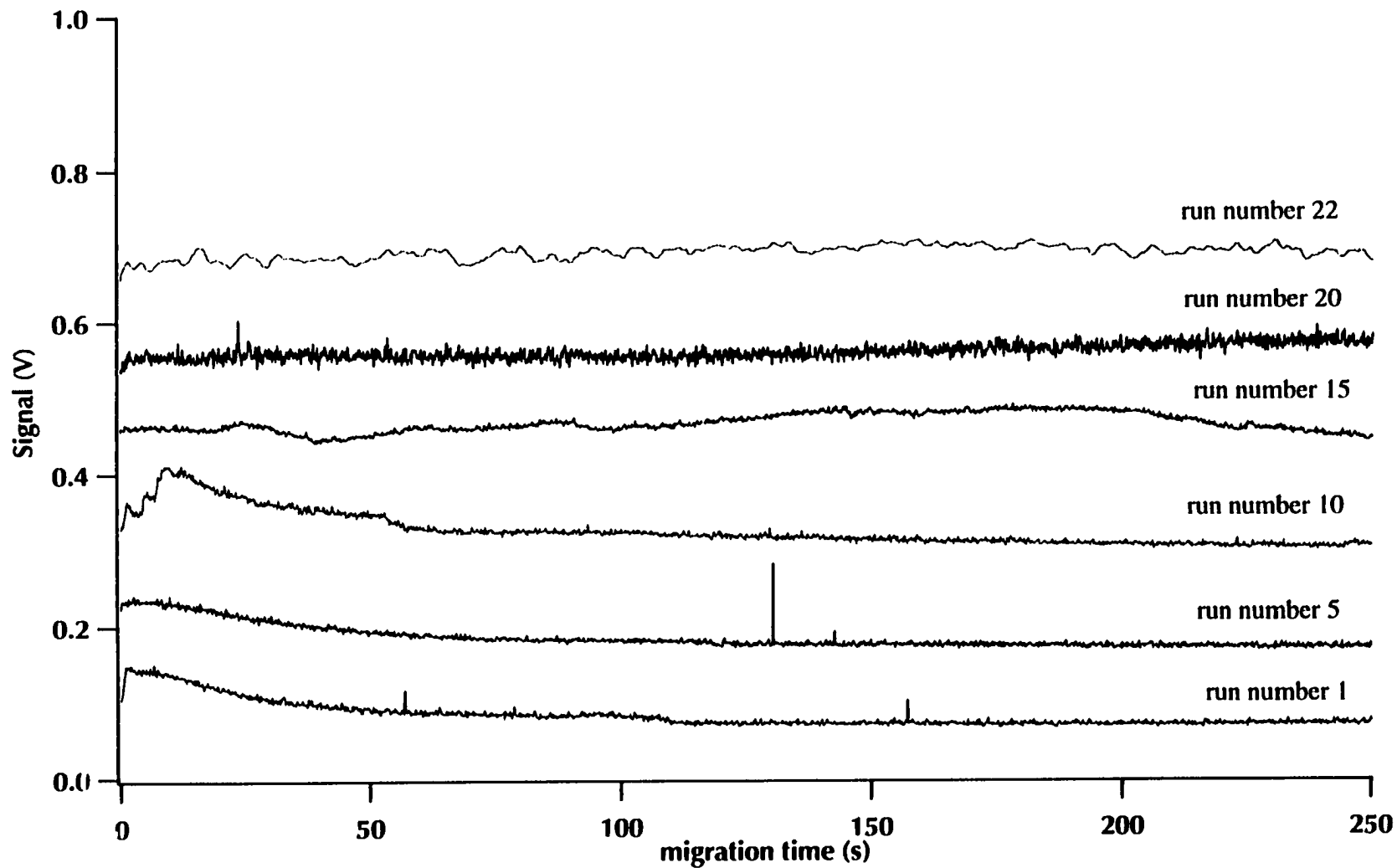
Ovalbumin, chosen to evaluate adsorption onto the coated capillaries, is a useful model protein because it consists of 20 lysine groups that could react with the fluorogenic dye FQ.<sup>19</sup> Figure 5.10 shows electropherograms from 22 successive injections of FQ-labeled ovalbumin onto a Si-C-polyAA coated capillary. The peaks show severe tailing, some of them with a change in background after protein migration, and we also observe fluctuation in the signal intensity. It suggests there was a severe adsorption of ovalbumin onto the capillary wall.

Figure 5.11 also shows a selected electropherograms from 22 successive injections onto a Si-C-polyDMA coated capillary. In this case the adsorption is even worse: adsorption is so strong that no analyte migrates out of the capillary. When the experiment was allowed to run for a long time, there was a gradual drop of the background to the normal value because of a gradual desorption of ovalbumin (data not shown). Even this

**Figure 5.10: Peak shape comparison of 22 successive injections onto a Si-C-polyAA coated capillary**



**Figure 5.11: Peak shape comparison for a Si-C-polyDMA coated capillary selected from 22 successive injection of FQ-labeled protein**



increase/decrease of the background was not reproducible. Therefore, adsorption of ovalbumin onto a Si-C-polyDMA coated capillary was much higher than that of a Si-C-polyAA coated capillary.

Figure 5.12 shows the migration of the same analyte in a Si-C-polyAAEE coated capillary. This coated capillary was much better than Si-C-polyAA and Si-C-polyDMA coated ones. Some tailing and fluctuation in the signal intensity was still seen, suggesting that there was adsorption onto the capillary wall, though not as severe as for the coated capillaries in Fig. 5.10 and Fig. 5.11.

Figure 5.13 depicts adsorption of FQ-labeled ovalbumin onto a Si-C-polyAAP coated capillary. There was no tailing, no change in the background, and no fluctuation in the signal intensity. Therefore, the adsorption was minimal as compared to the other three coated capillaries.

To test the idea that adsorption was one of the major contributors to band broadening, in addition to the contribution from multiple labeling and injection plug, we designed another experiment. After injection of FQ-labeled ovalbumin, the CE run was carried out at 18 kV (600 V / cm). For the second run the same reaction and injection times were chosen, but the CE voltage was reduced to 15 kV. The next experiments were repeated under the same injection conditions but the applied voltage was reduced to 12, 9, 6, and 3 kV. Therefore, the analyte have longer times to adsorb onto the capillary wall in successive runs.

Figure 5.14 shows the result of these experiments for a Si-C-polyAA coated capillary. All of the migration times are normalized to visualize the change in peak width by changing the applied voltage. The lower the CE voltage run, the longer the migration time of FQ-labeled ovalbumin; and therefore, the longer time the protein was in contact with the surface of the capillary, hence leaving more time for the adsorption. The peak widths increased as a result of decreasing applied voltage. By lowering the applied voltage the



Figure 5.12: Peak shape comparison of a Si-C-polyAAEE coated capillary

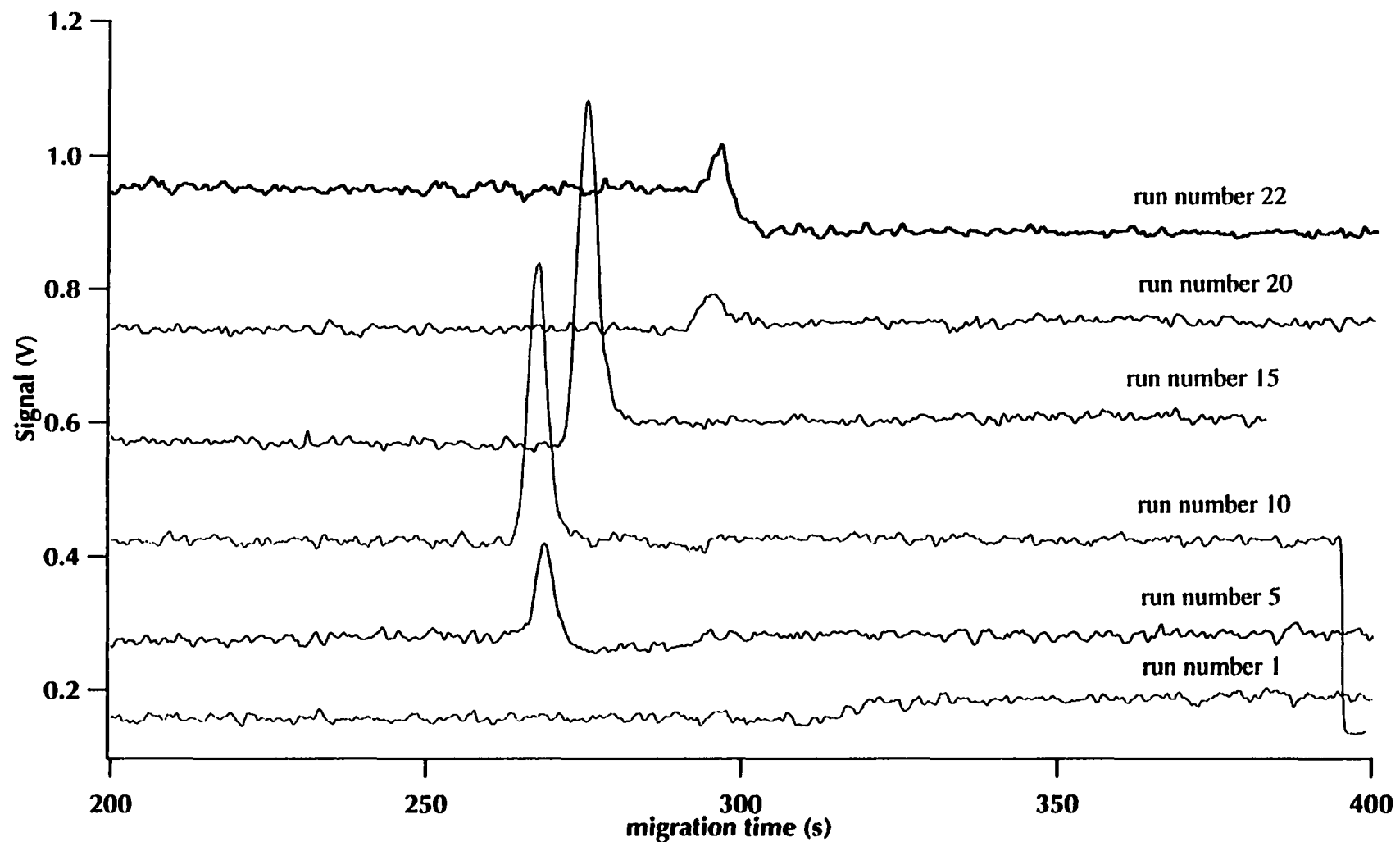


**Figure 5.13: Peak shape comparison for a Si-C-polyAAP coated capillary**

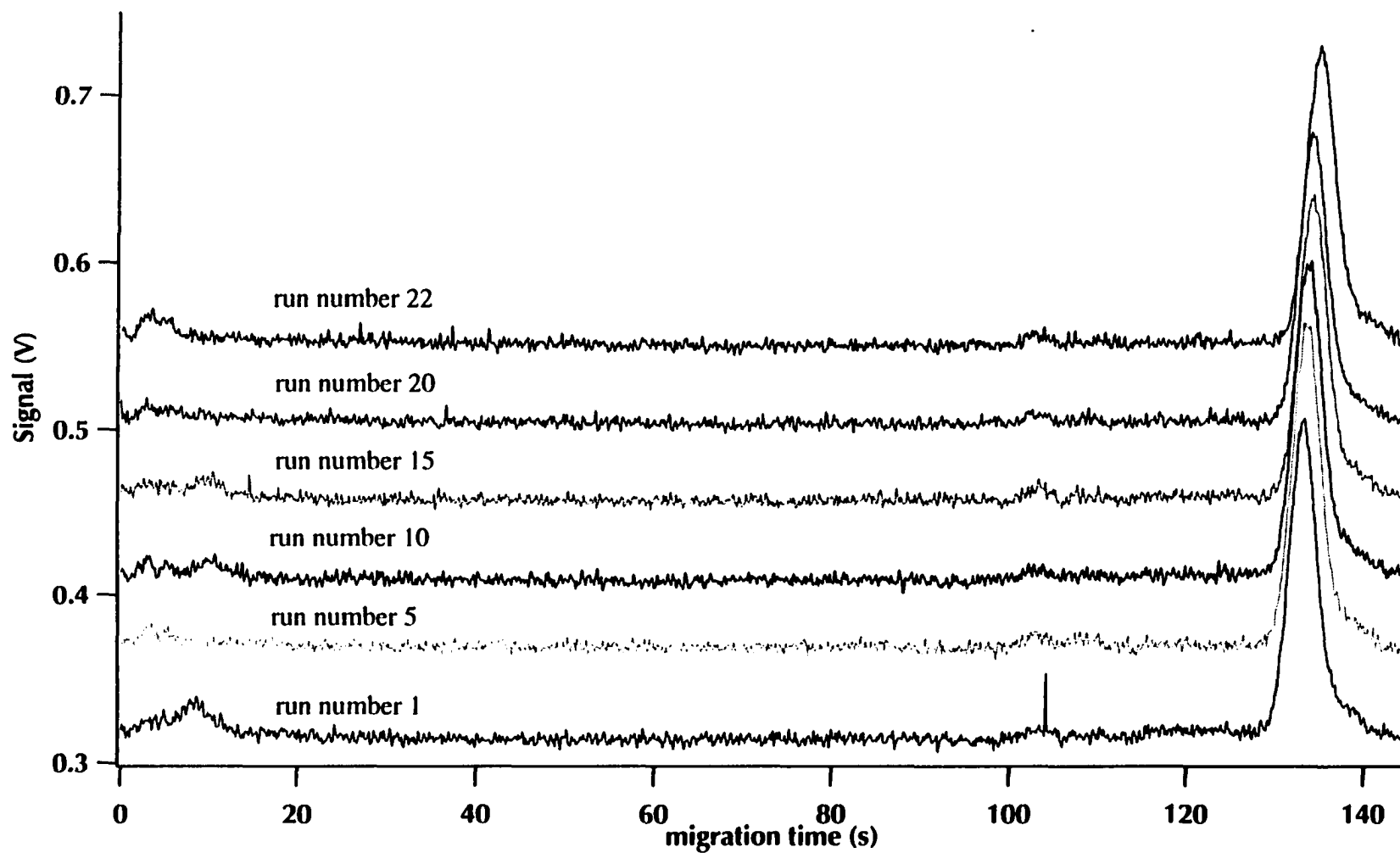
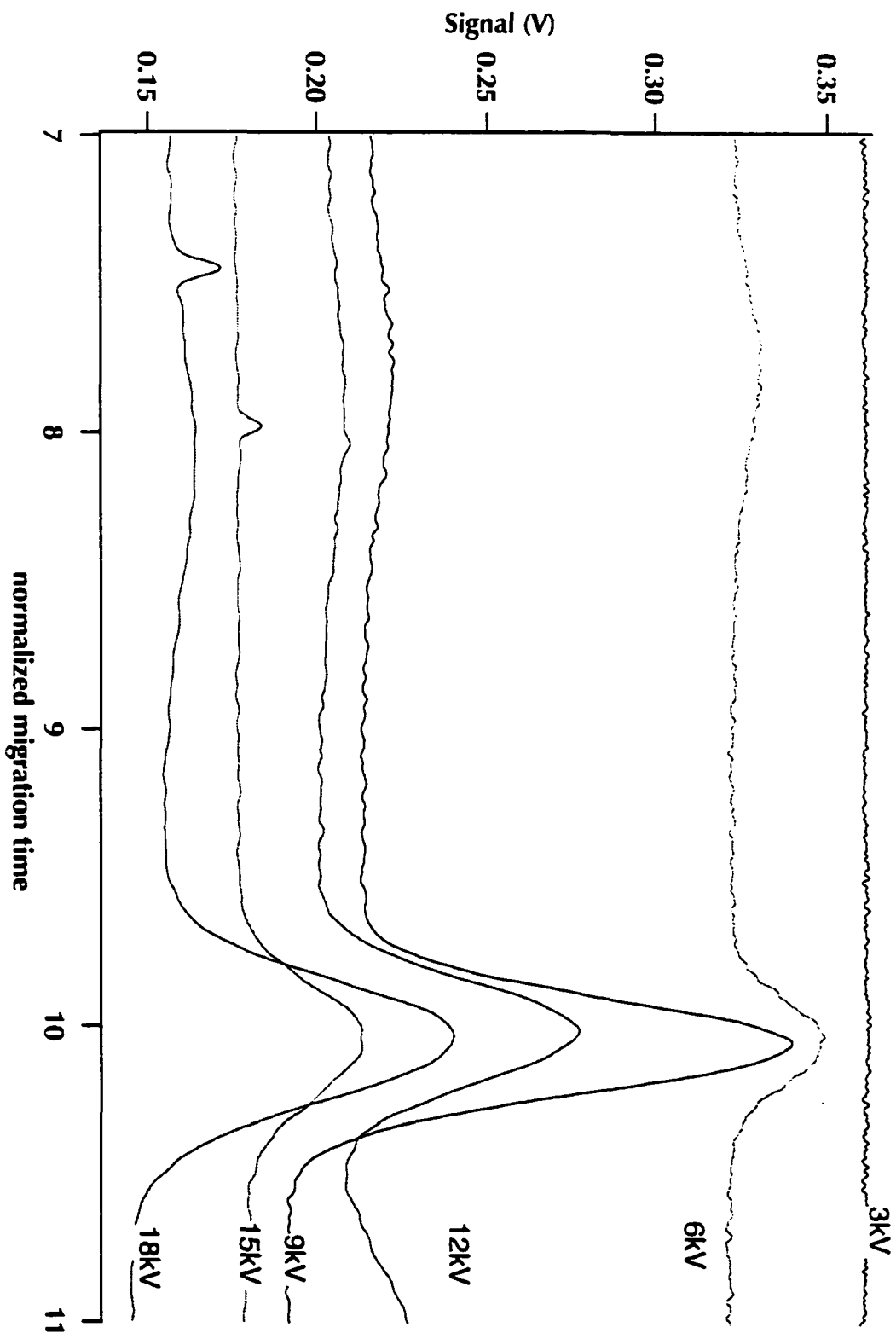


Figure 5.14: Protein adsorption onto a Si-C-polyAA coated capillary



migration times are increased, and therefore, the peak widths increase because of more time for longitudinal diffusion.

The same trend was observed for Si-C-polyAAEE and Si-C-polyAAP (see Figures 5.15 and 5.16). For the Si-C-polyDMA we concluded that the adsorption was so strong and the peaks were so broad that nothing was observed to migrate out of the capillaries, there was only a gradual change in the background. The run buffer was changed to a fresh one and the electrophoresis was continued for a long time after each injection until the background dropped to the original value, indicating that the desorption of the analyte is complete and the capillary is ready for the next injection.

Figure 5.17 shows the peak with the lowest applied voltage (3 kV). The same labeling reaction time and the same injection time for each experiment were chosen and, therefore, we assumed that the contribution from multiple labeling and the injection plug to band broadening was the same for each experiment.<sup>23, 24</sup> The only effect was the contribution of adsorption to band broadening. As we can see in Figure 5.17, the peak at 3 kV for a Si-C-polyAA was so broad that it was not distinguishable from the background, and, therefore, with the exception of the Si-C-polyDMA, this coated capillary showed the maximum adsorption. The peak for the Si-C-polyAAEE was less broad, and, therefore, there was less adsorption as compared to a Si-C-polyAA. Finally, the peak for the Si-C-polyAAP showed the least broadening and hence the least adsorption.

Therefore, we concluded that among these coated capillaries in terms of alkaline hydrolysis, the Si-O-polyAA was the worst coated capillary because of a combination of the worst sub-layer and the worst top-layer. With respect to adsorption the Si-C-polyDMA, which had a very low EOF and very high stability over a wide pH range and temperature range, was worse than all of the other Si-C coated capillaries and also Si-O-polyAA. Si-C-polyAAEE and Si-C-polyAAP both worked very well, although the latter performed slightly better.

Figure 5.15: Adsorption of proteins onto a Si-C-poly-AAFE coated capillary

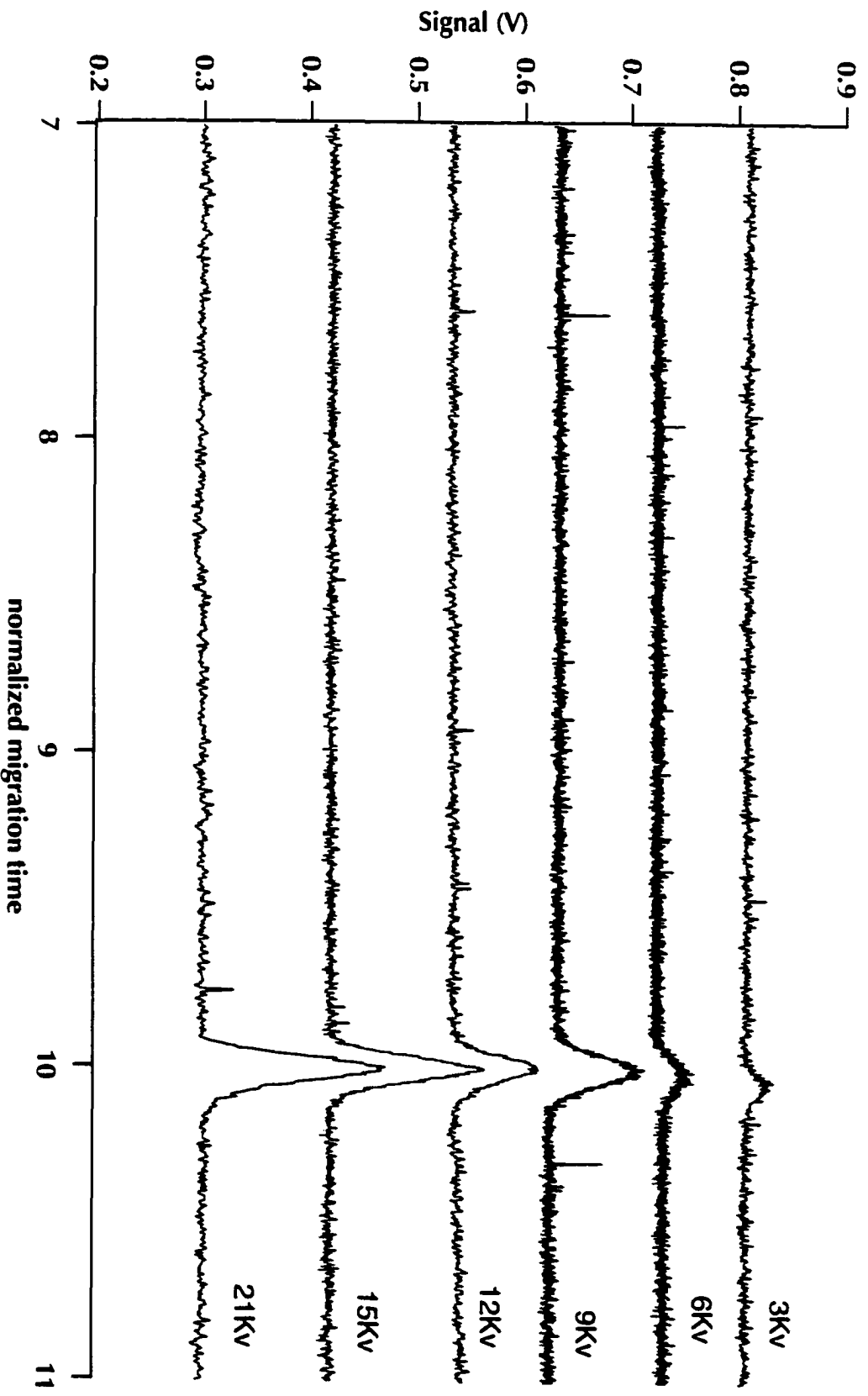
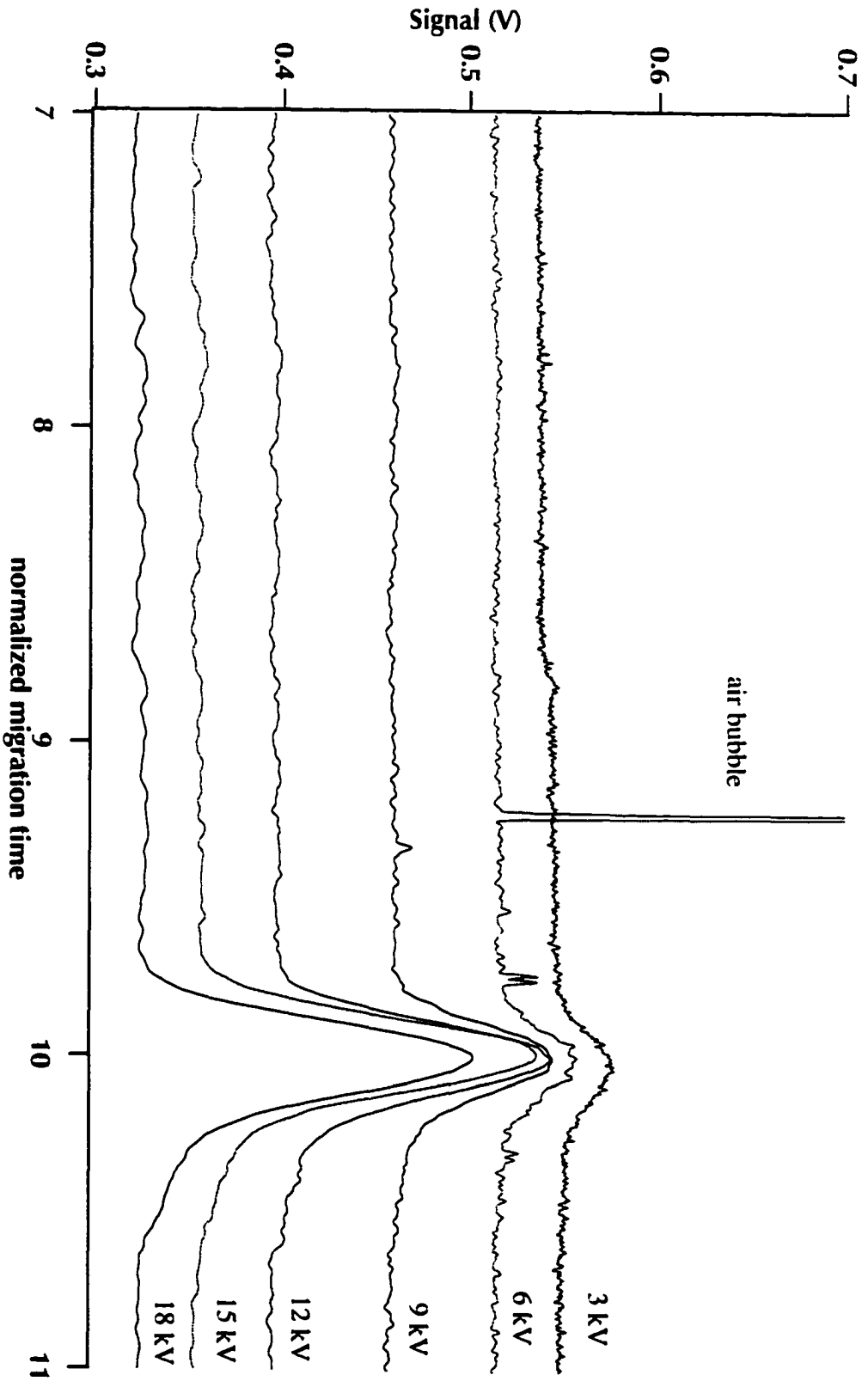
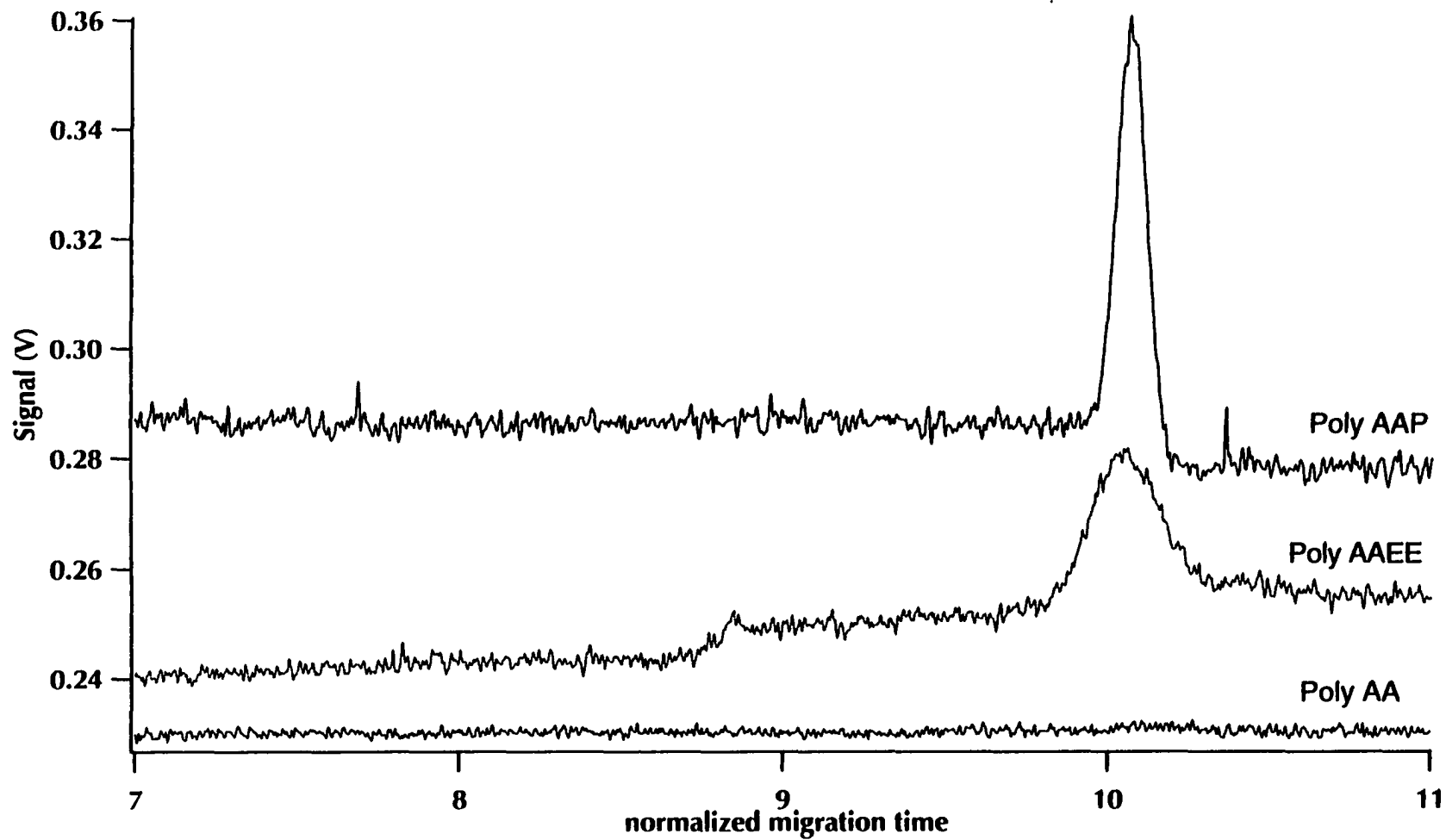


Figure 5.16: Protein adsorption onto a Si-C-polyAAP coated capillary



**Figure 5.17: Peak width comparison among Si-C-polyAA, Si-C-polyAAEE and Si-C-polyAAP coated capillaries**



### 5.3.5 Five-capillary instrument

A major concern in evaluating different monomers in coated capillaries was the aging effect. All the capillaries were coated at the same time, but they were studied one at a time using a single capillary instrument. This might have caused aging of the later studied capillaries as compare to those that studied earlier. To rule out the aging effect, a 5-capillary instrument was used. In this case, the sample was injected onto the all 5 capillaries and the high voltage was applied to run the same sample in 5 capillaries at the same time. Each capillary was 42 cm long. The injection voltage was 100 V/cm for 5 s and the applied voltage was 400 V/cm for all the capillaries. Each capillary has a different Ohm's plot and this applied voltage was chosen in a way that none of the capillaries experienced Joule heating.

A batch of capillaries was coated, and ten successive injections of fluorescein and 22 successive injections of FQ-labeled ovalbumin were done.

Figure 5.18 shows the 10<sup>th</sup> electropherogram of this experiment. 1 nM fluorescein was injected simultaneously onto each coated capillary.

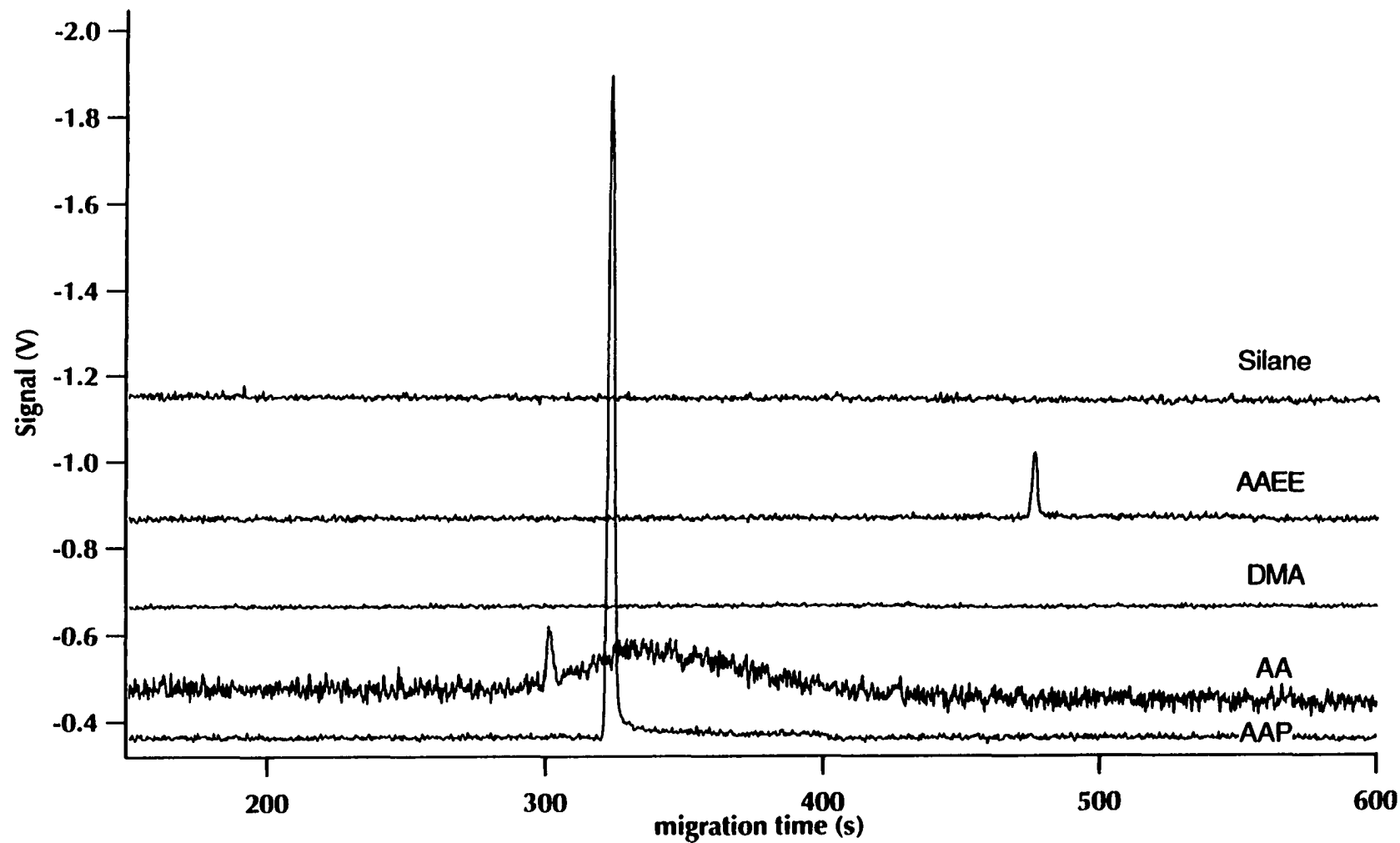
This experiment confirmed what we observed on the single-capillary instrument when running one capillary at a time. The Si-O-polyAA was the first to gain a high EOF; by applying negative polarity we could not detect analyte migrating out of it because high EOF in the opposite direction prevented the analyte from reaching the detector.

To align the system we had to run fluorescein continuously through the five capillaries to optimize S/N ratio. Five fluorescence spots were observed during the alignment, but because of the high pH of the run buffer and the high rate of alkaline hydrolysis of both the Si-O sub-layer and the polyAA top-layer, the Si-O-polyAA coated capillary gained an EOF so rapidly that after alignment nothing could migrate out of it.

When working with the single-capillary instrument, it was easy to show that the coating was not effective anymore. After the power supply polarity was inverted to



**Figure 5.18: The 10th run of simultaneous evaluation of coated capillaries using 5-capillary instrument (1 nM fluorescein injection for 5 s at 100 V/cm, voltage run 400 V/cm and capillary length 42 cm)**



positive, the fluorescein which was negatively charged, would migrate out of the Si-O-polyAA coated capillaries. When the experiment was done at positive polarity, the first migration times were longer but they decreased to the normal migration times for uncoated capillaries. The reason that migration times were longer for the first runs was the gradual regeneration of the EOF, and, therefore, shorter and shorter migration times. Using positive polarity, the EOF is co-directional with the electrophoretic mobility and, therefore, gradual regeneration of EOF causes the migration time become shorter.

The Si-C-polyAA was the second capillary that gained EOF presumably because of alkaline hydrolysis of the polyAA top-layer, and leaving a layer of immobilized polyacrylate on the capillary wall with a stable Si-C sub-layer. After aligning the instrument, and running 10 CE experiments with fluorescein, we observed FQ-labeled ovalbumin migrating out of this capillary for another 10 runs with a gradual increase in migration times. This was not surprising, because when negative polarity was used, the EOF was in the opposite direction away from the detection end, and a gradual increase of the EOF caused a similar increase in migration times.

As we observed for the single-capillary instrument, when the same sample was injected simultaneously with the same injection times and injection voltages onto all the capillaries, every coated capillary showed migration of the FQ-labeled ovalbumin except the Si-C-polyDMA because of the severe adsorption of the protein onto the capillary wall. In the case of fluorescein injection, in which the molecule was smaller but still hydrophobic, we observed either a total adsorption of fluorescein (see Figure 5.18) or a very broad peak for the Si-C-polyDMA coated capillary (see Figure 5.19).

Figure 5.20 shows simultaneous injection of 1 nM FQ-labeled ovalbumine onto five coated capillaries. The same injection conditions and the same applied voltage were used for both fluorescein and FQ-labeled ovalbumine injections.

**Figure 5.19: Simultaneous evaluation of coated capillaries using 5-capillary instrument**

(conditions the same as Fig. 5.18, run number 20)

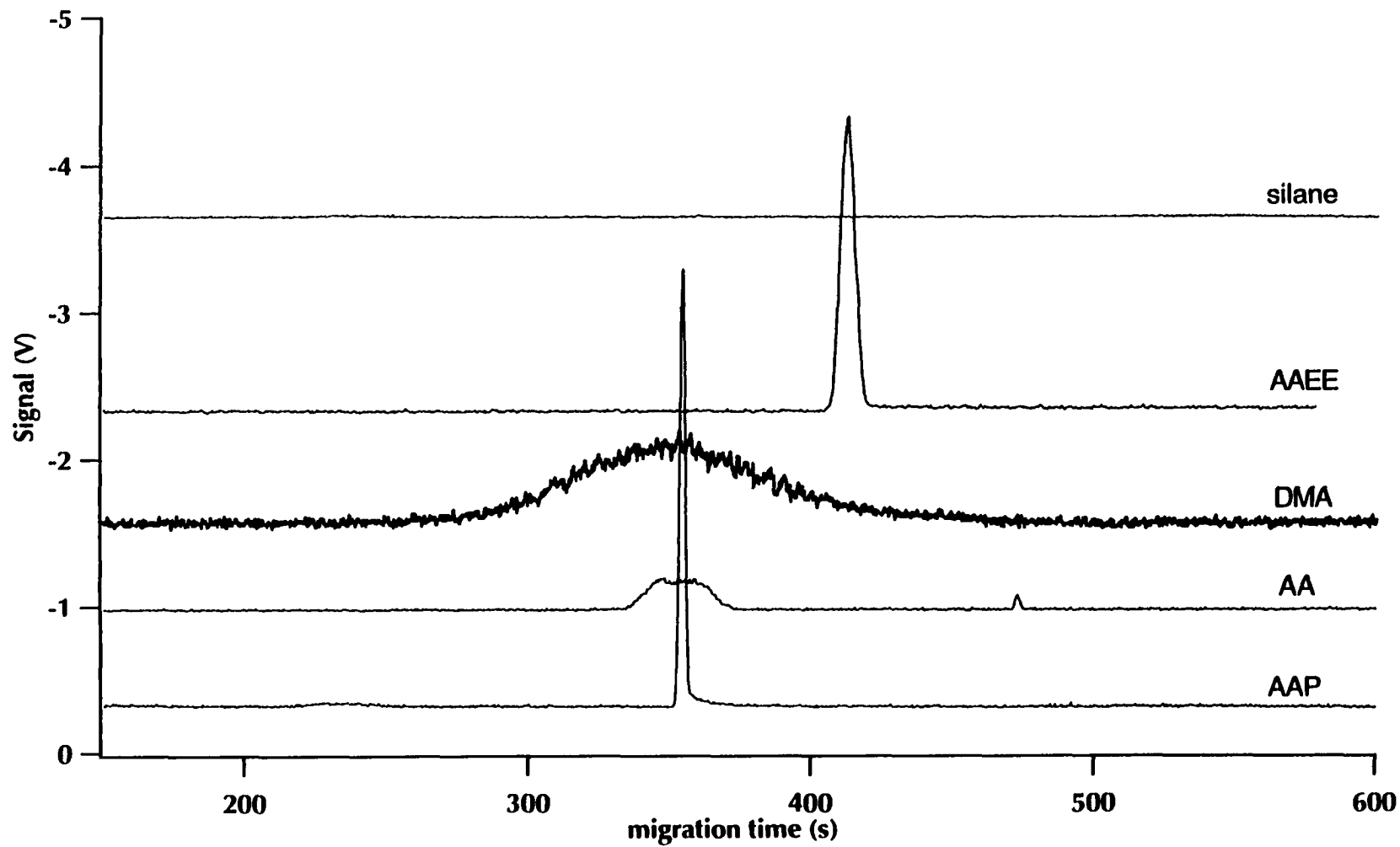
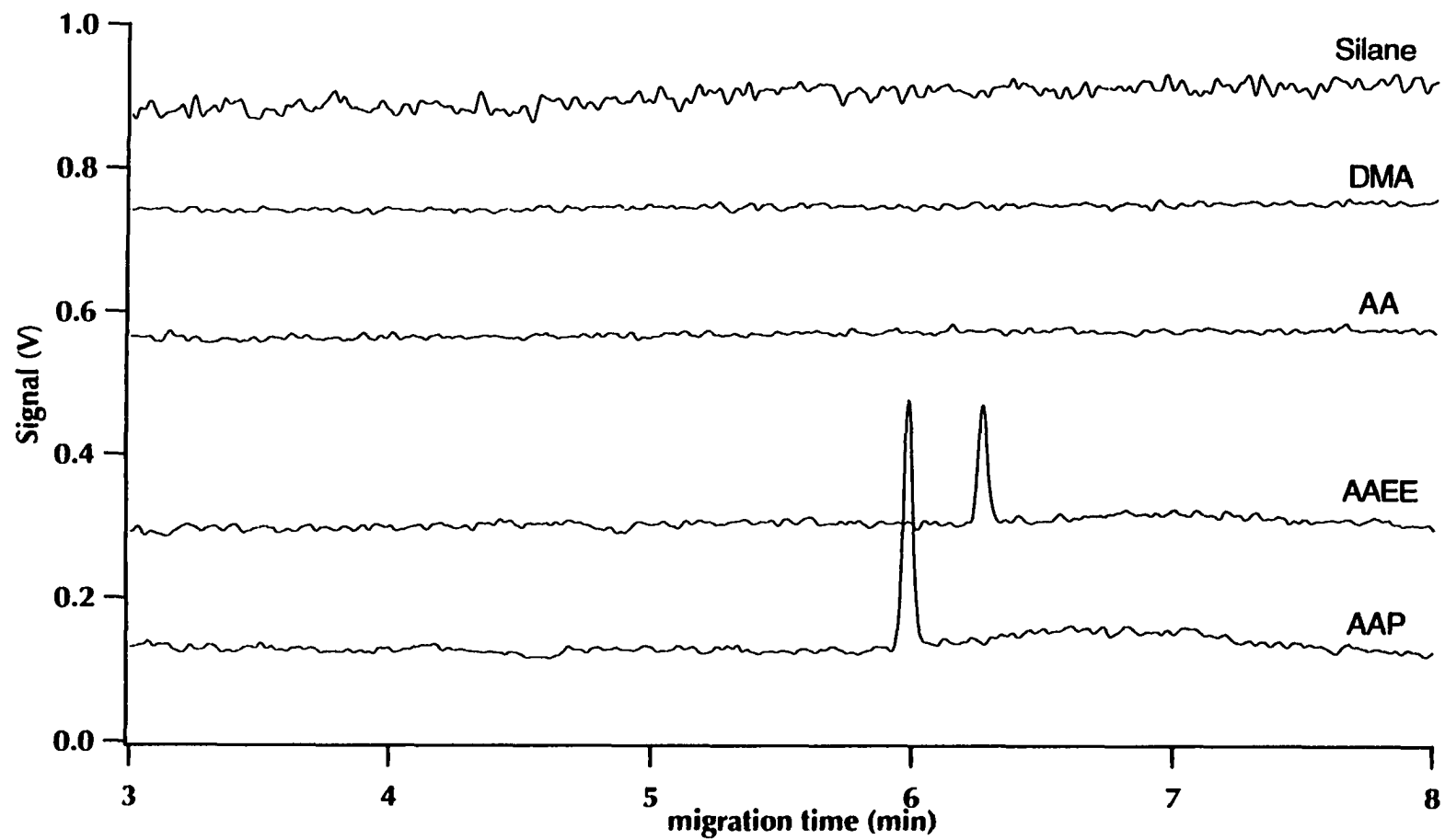


**Figure 5.20: Simultaneous evaluation of five coated capillaries using 5-capillary instrument (FQ-labelled ovalbumin injection for 5 s at 100 V/cm, voltage run 400 V/cm, capillary length 42 cm, run number 1)**



The two best coated capillaries were Si-C-polyAAEE and Si-C-polyAAP. It was very difficult to draw a conclusion from Figure 5.18-5.20 concerning which one performed better. It was observed that the Si-O-polyAA coated capillary gains EOF after 10 runs and the Si-C-polyAA after 20 runs. Si-C-polyDMA showed total adsorption of FQ-labeled ovalbumin and total adsorption or broad desorption peak, after many injections were adsorbed, for fluorescein injection. To have a clear comparison of these two coated capillaries, we coated another batch of capillaries and repeated the five-capillary instrument experiment with the three capillaries of Si-C-polyAAP and two capillaries of Si-C-polyAAEE. There are reports in the literature that shows AAEE monomer could be used in more than 300 runs at pH 8.5 without changing the EOF.<sup>29-30</sup>

Figure 5.21 shows the run number 1 for the comparison of Si-C-polyAAP and Si-C-polyAAEE coated capillaries using 5-capillary instrument. Figure 5.22 shows the run number 20 of the same experiment. FQ-labeled ovalbumine was injected and CE was performed under the same conditions as previous experiment. The Si-C-polyAAP coated capillaries showed narrower and sharper peaks as compared to Si-C-polyAAEE coated ones.

Figure 5.23 compares the peak area of 22 successive, simultaneous injections of FQ-labeled ovalbumin onto these capillaries. Under similar conditions scattered peak areas for polyAAEE coated capillaries were observed, but less scattered than for Si-C-polyAAP coated capillaries. The average peak area for Si-C-polyAAEE was less than that of the Si-C-polyAAP coated one. This means that there is a slight adsorption onto a Si-C-polyAAEE as compared to a Si-C-polyAAP coated capillary.

Figure 5.24 compares the number of theoretical plates ( $N$ ) for Si-C-polyAAEE and Si-C-polyAAP coated capillaries. Figure 5.24a shows the average  $N$  versus run number for Si-C-polyAAEE coated capillaries and Figure 5.24b for Si-C-polyAAP coated ones. The average number of theoretical plates for Si-C-polyAAP coated capillaries is 200,000 with

Figure S.21: Comparison of Si-C-polyAAP and Si-C-polyAEE coated capillaries using 5-capillary instrument (run number 1)

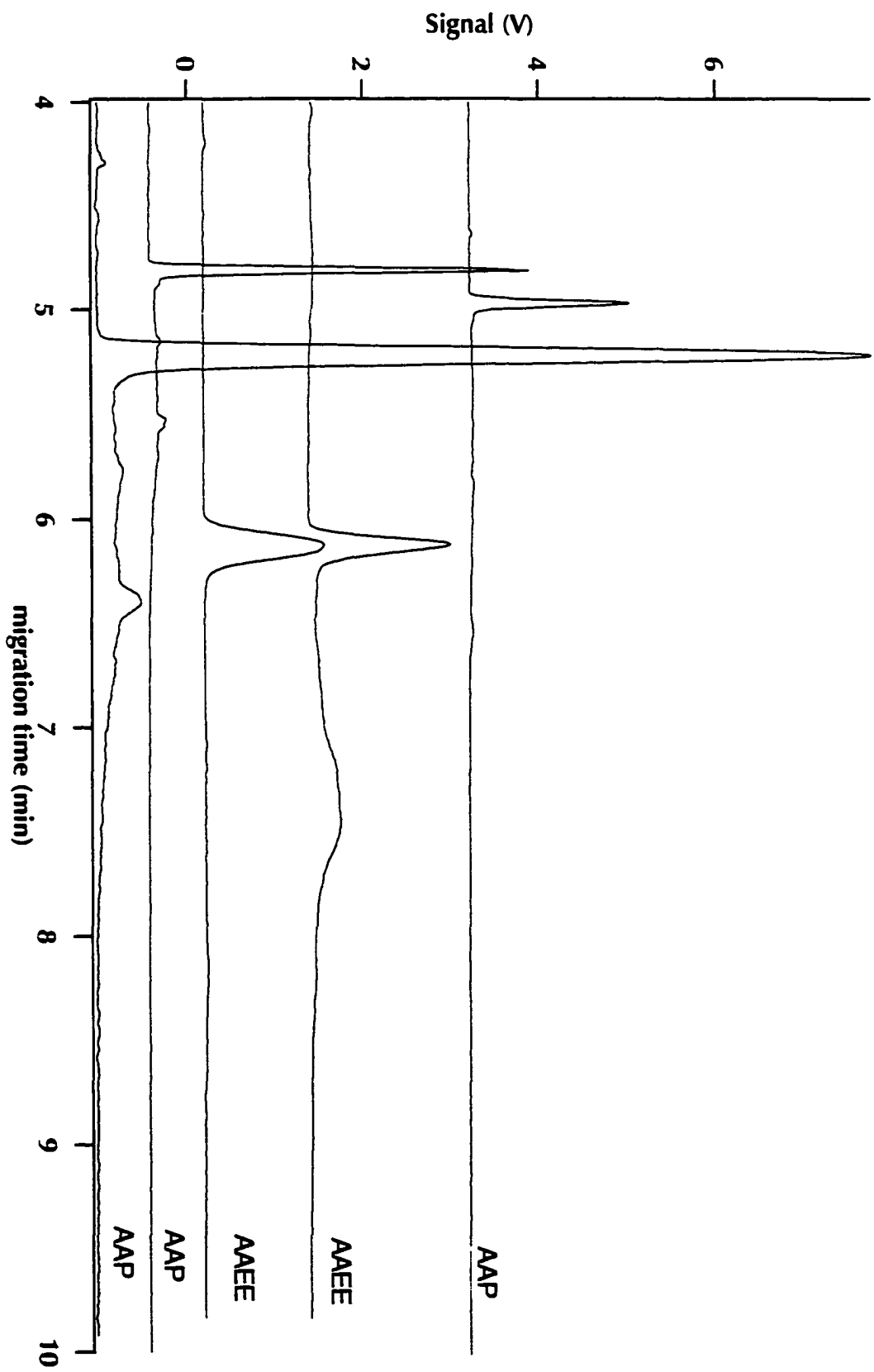


Figure 5.22: Comparison of Si-C-polyAAP and Si-C-polyAAEE coated capillaries using 5-capillary instrument (run number 20)

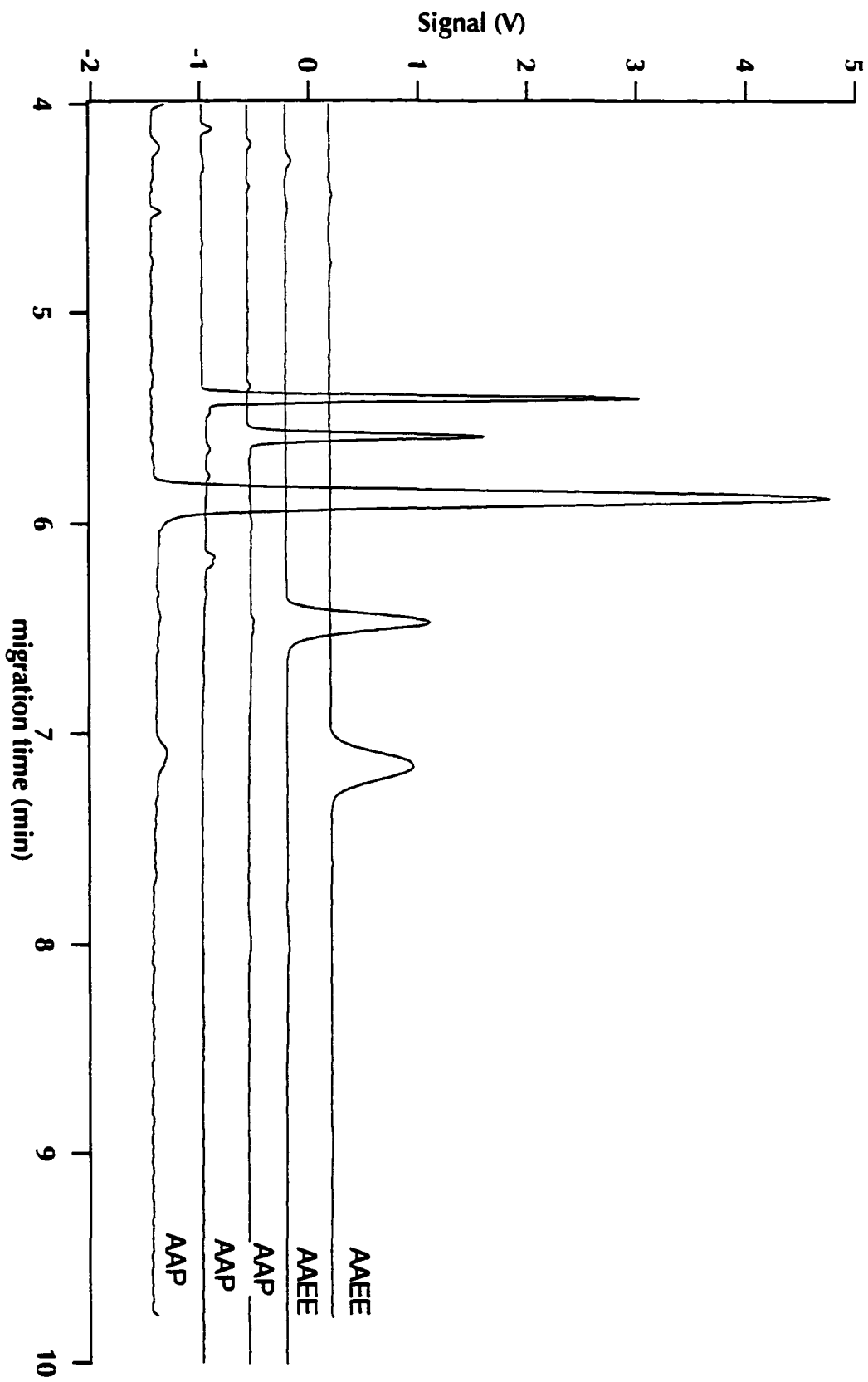
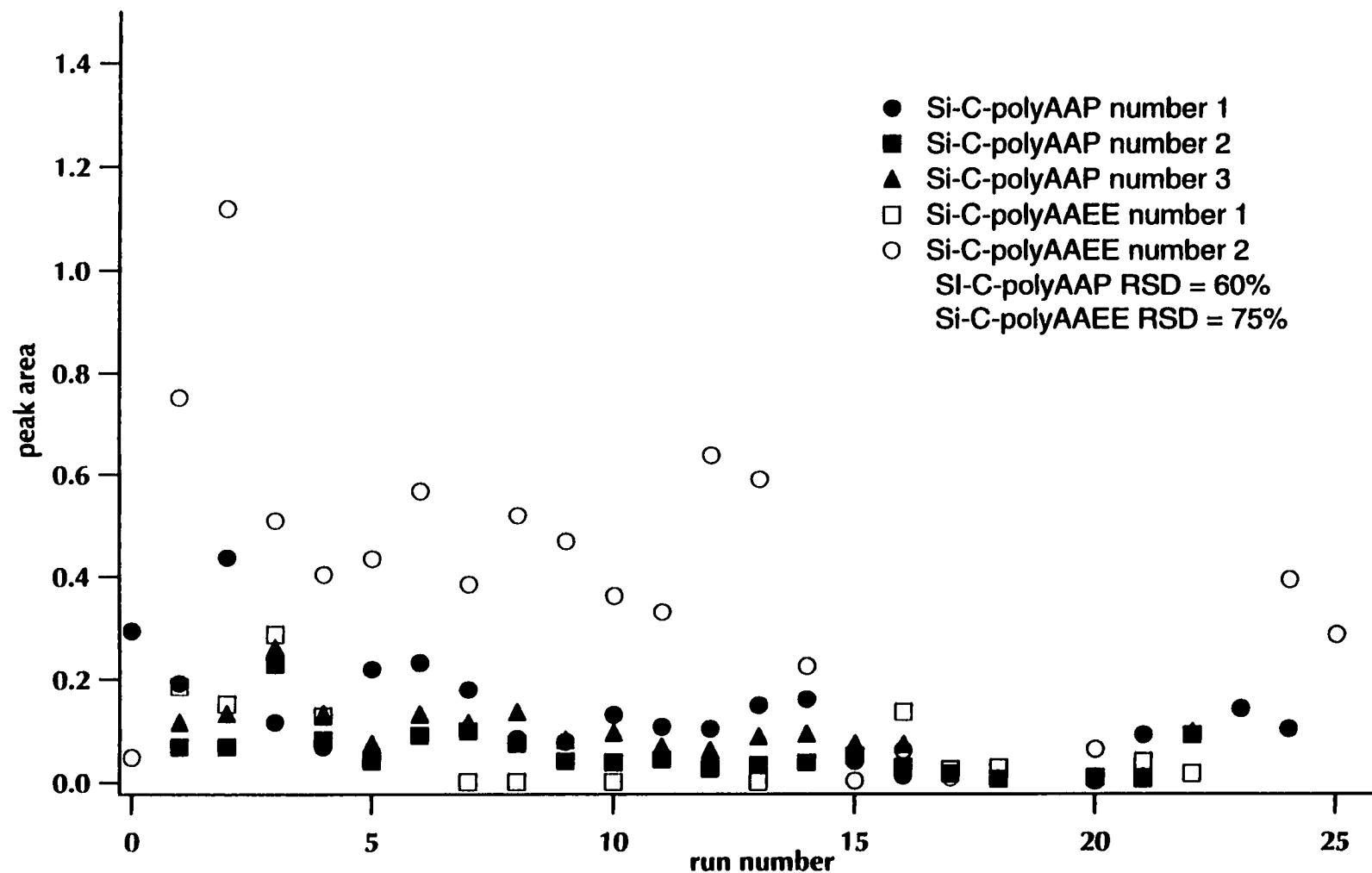
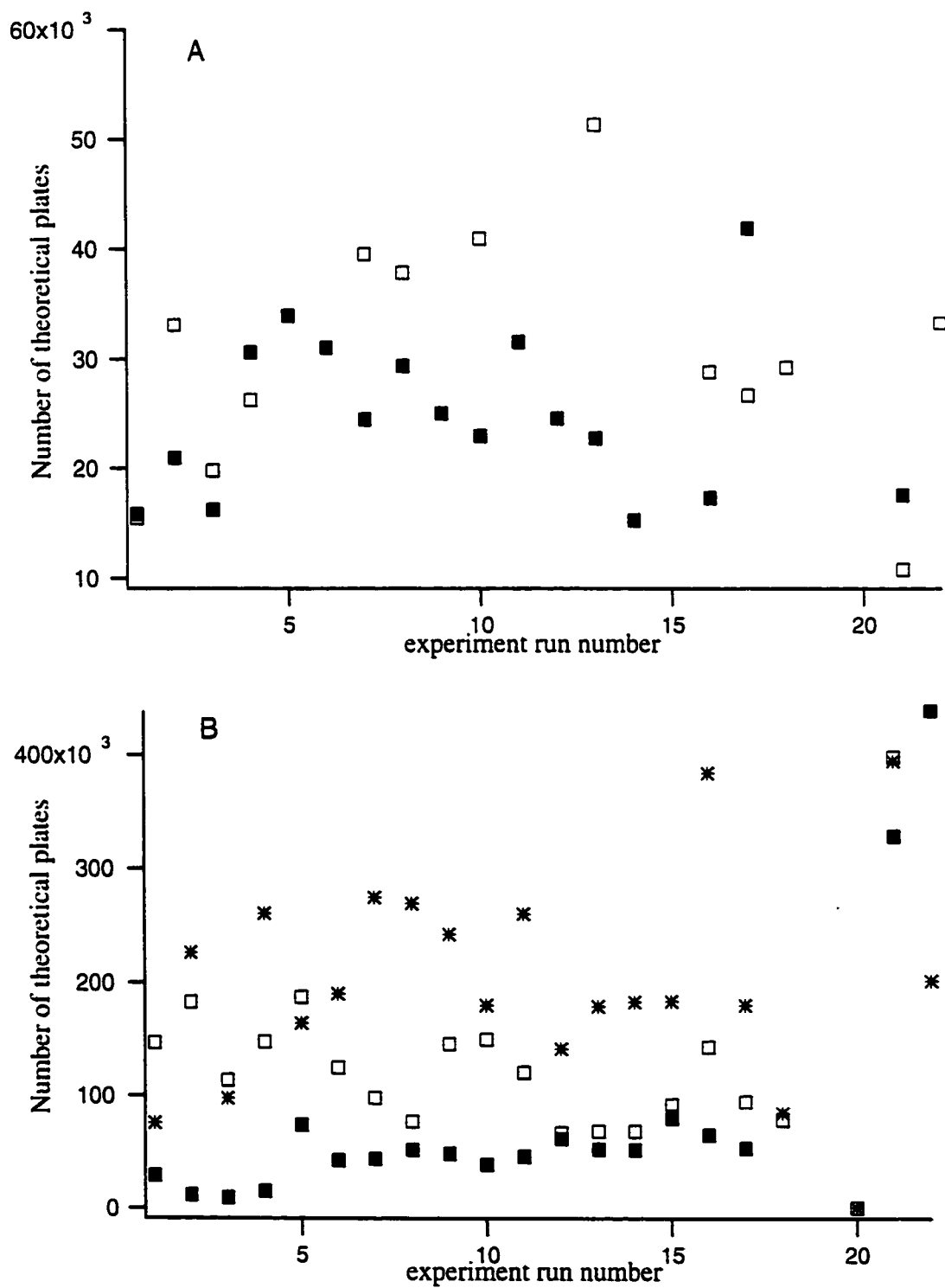


Figure 5.23: Peak area comparison for 22 injection onto Si-C-polyAAP and Si-C-polyAAEE coated capillaries using 5-capillary instrument





**Figure 5.24: Theoretical plate comparison for a) Si-CpolyAAEE and b) Si-CpolyAAP coated capillaries using 5-capillary instrument**



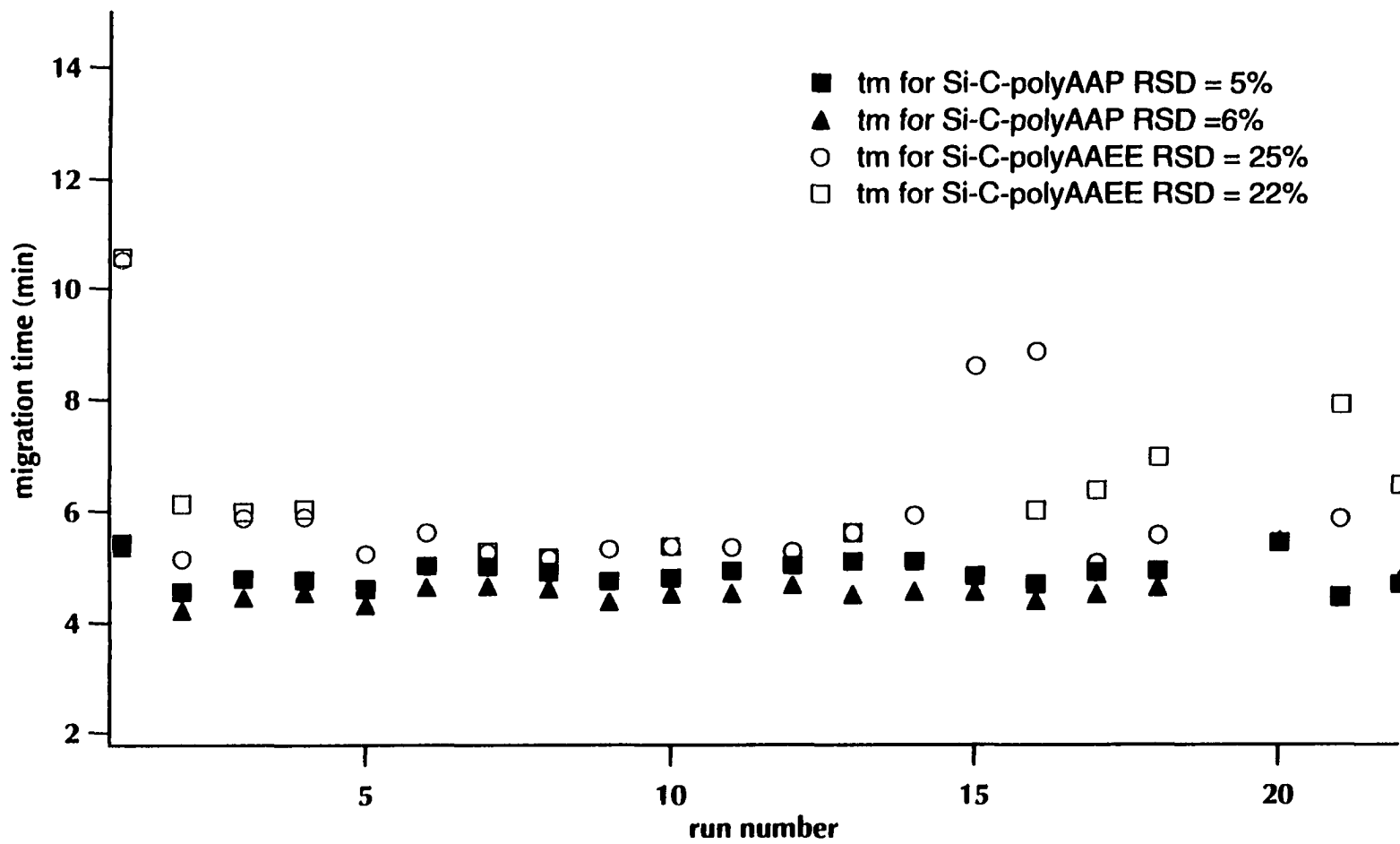
RSD of 45%, while average number of theoretical plates for Si-C-polyAAEE coated capillaries is 36,000 with the RSD of 147%.

Our laboratory already reported that injection and multiple labeling are primary causes of band broadening.<sup>24-25</sup> In these experiments the same injection voltages, injection times and run voltages were applied. The only parameter with no experimental control was adsorption of protein onto the capillary walls. As with the single-capillary instrument, we came to the same conclusion. As compared to other coated capillaries, both the Si-C-polyAAEE and Si-C-polyAAP worked well, although the Si-C-polyAAP coated one performed slightly better. It is worth mentioning that the viscosity of the AAEE monomer from batch-to-batch coatings kept changing, and also the EOF batch-to batch reproducibility of the Si-C-polyAAEE was not as good as the Si-C-polyAAP coated ones. Righetti has explained this phenomenon in terms of the 1-6 H-transfer mechanism and auto-polymerization of the AAEE monomer.<sup>26</sup> From batch-to-batch reproducibility point of view, Si-C-polyAAP coated capillaries were much better than Si-C-polyAAEE coated ones, with a change in EOF of 5% and 22%, respectively.

### **5.3.6 Migration time reproducibility**

Figure 5.25 presents migration time reproducibility of two Si-C-polyAAEE coated capillaries and two Si-C-polyAAP coated capillaries from the five-capillary experiment data. For the Si-C-polyAAP, RSD is 5% and 6% while the RSD for the Si-C-polyAAEE is 25% and 23%. Basically the reproducibility of the EOF and migration time for each coated capillary was the same because migration time was measured experimentally and EOF was calculated based on the migration time. This figure shows the results of 22 successive, simultaneous injections of FQ-labeled ovalbumin onto the 5 capillaries without washing the

**Figure 5.25: Migration time reproducibility comparison of Si-C-polyAAP and Si-C-polyAAEE coated capillaries using 5-capillary instrument. FQ-labeled ovalbumin is injected for 5 sec at 100 V/cm, voltage run 400 V/cm, capillary length 42 cm and 22 identical injections.**



capillaries in-between runs. The same injection conditions and the same run voltage as the other 5-capillary experiments were chosen for this experiment.

Table 5.1 shows migration time reproducibility of Si-C-polyAA, Si-C-polyAAEE, and Si-C-polyAAP coated capillaries for 22 successive injections using the single-capillary instrument with the capillaries being washed with run buffer in-between runs.

Washing in-between runs caused desorption of FQ-labeled ovalbumin, and, therefore, dramatically improved migration time reproducibilities. The Si-C-polyAAEE migration time reproducibility improved from 25% to 3.6% by washing the capillary in-between runs and the Si-C-polyAAP migration time improved from 5% to 1.9%. This Si-C-polyAAP coated capillary was chosen to study long-term stability.

### **5.3.7 Long-term stability**

To study long-term stability of Si-C-polyAAP coated capillaries, one capillary was chosen to do all the experiments including pH studies, temperature studies, EOF measurement, and migration time reproducibility. Changing the conditions from low to high temperature and back to low temperature did not significantly affect EOF nor migration time reproducibility of fluorescein or FQ-labeled ovalbumin.

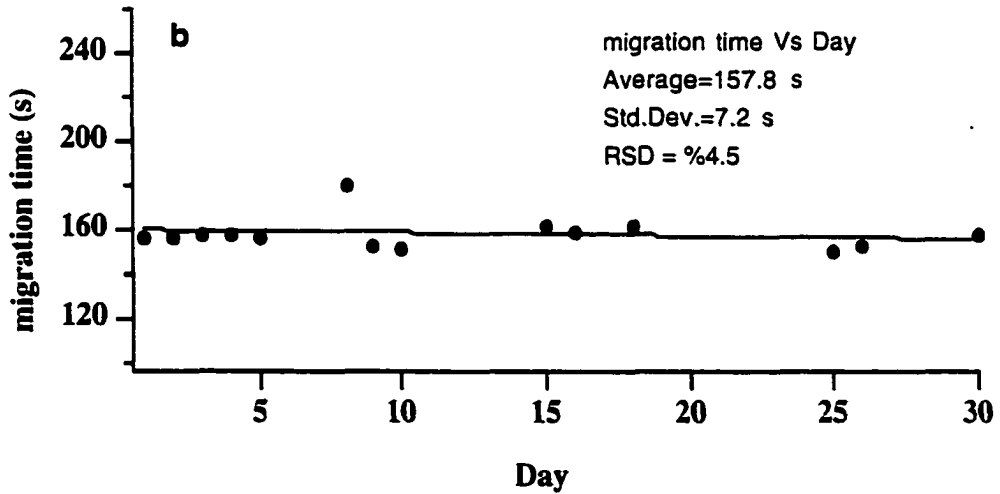
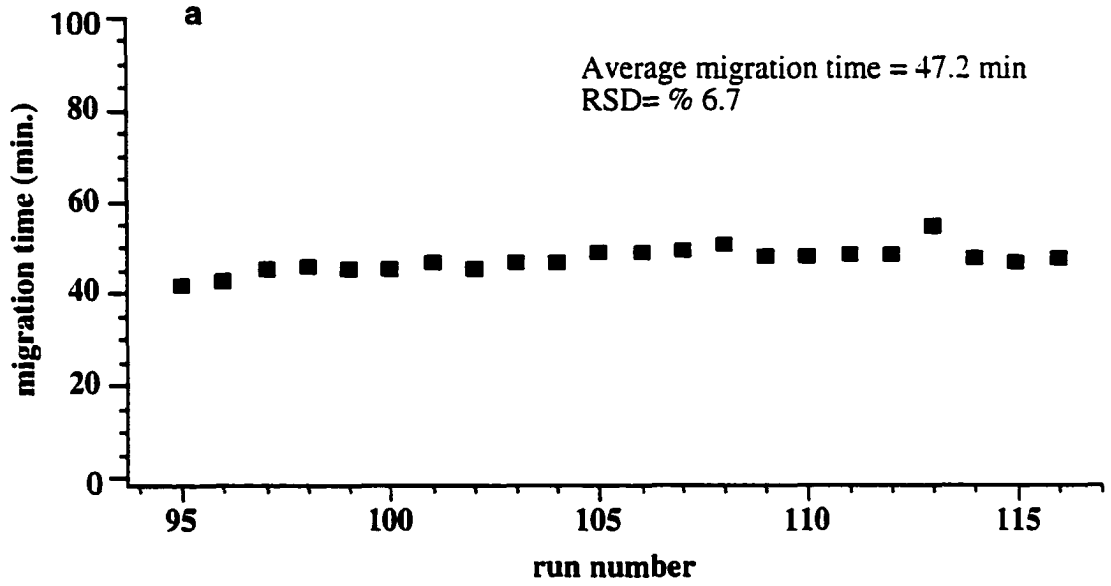
Figure 5.26a shows that Si-C-polyAAP was quite stable under such harsh and variable conditions for more than 100 runs, with a 7% RSD in EOF and / or migration time.

We observed that the Si-C-polyAA, after Si-O-polyAA, was most susceptible to alkaline hydrolysis. To increase the life-time of this capillary, after each injection we replaced the 10 mM borate- 5mM SDS run buffer (pH 9.4) with distilled water and stored the capillary in water overnight before doing another experiment next day. As a result of

**Table 5.1: Migration time reproducibility of coated capillaries using single-capillary instrument with the capillaries being washed with run buffer in between runs. Sample FQ-labeled ovalbumin injected for 5 s at 1 kV. Capillary length 35 cm, voltage run 400 V/cm, and 22 identical injections**

Capillary	Migration time RSD
Si-O-polyAA	Unstable
Si-C-polyAA	10.0%
Si-C-polyDMA	Variable
Si-C-polyAAEE	3.6%
Si-C-polyAAP	1.9%

Figure 5.26: Long term stability of a) Si-C-polyAAP, and b) Si-C-polyAA coated capillaries



this simple method, the life time of this capillary was extended to more than a month as shown in Figure 5.26b.

In another experiment Si-C-polyAA and Si-C-polyAAP coated capillaries were chosen for the comparison of long-term stability. Both capillaries were subjected to electrophoresis at 25 °C in a pH 9.0 buffer (90 mM Tris-acetate). EOF was measured every 20th run and each run lasted 30 min. The results of this experiment are shown in Figure 5.27. As this Figure shows, the Si-C-polyAAP coated capillary has roughly the same EOF after 300 runs, but EOF for the Si-C-polyAA coated one starts increasing after 20 runs. In other publications AAEE coated capillaries have shown 300 reproducible CE runs at pH 8.5.<sup>29-30</sup>

### **5.3.8 Si-C-polyDMA coated capillary**

We observed that this capillary showed so strong an adsorption of FQ-labeled ovalbumin that no analyte migrated out, whereas its pH stability was as good as Si-C-polyAAP coated capillaries. This capillary was very stable under a wide range of temperatures.

Preliminary experiments showed that Si-C-polyDMA could be used for DNA analysis at high temperatures using replaceable gels (data not shown). The results of using Si-C-polyDMA for DNA sequencing at high temperatures and replaceable gels is under preparation for publication in collaboration with other members of this group.

### **5.3.9 Separation of alkaline protein markers**

Figure 5.28a adopted with permission from the collaborative work with Professor Righetti's group in Italy shows four separate runs of the standard set of four alkaline protein markers (lysozyme, chymotrypsin, ribonuclease A and trypsinogen, respectively)

**Figure 5.27: EOF regeneration of a Si-C-polyAA (top) and a Si-C-polyAAP (bottom) coated capillary. Both capillaries were subjected to electrophoresis at room temperature in a pH 9.4 borate buffer.**

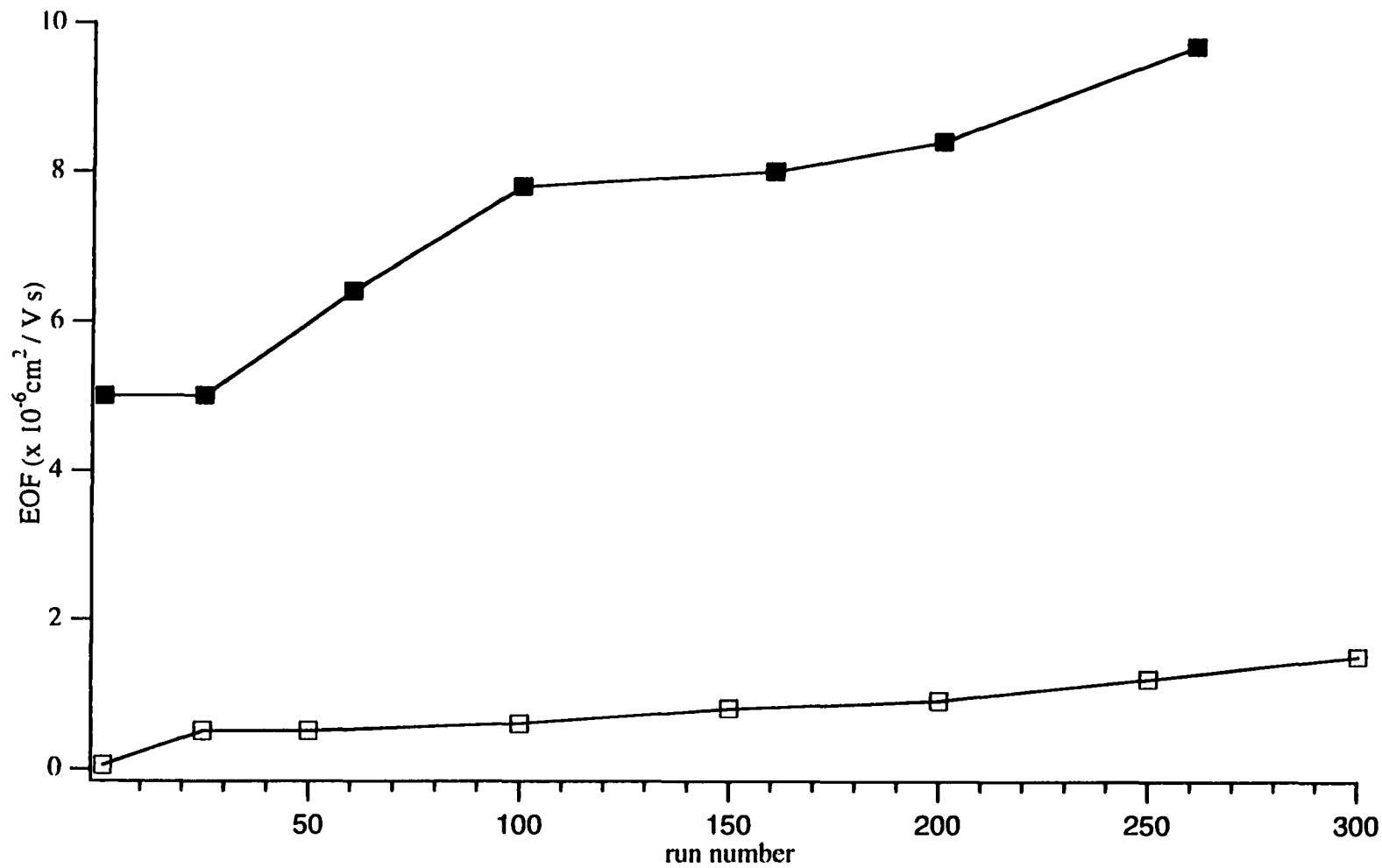
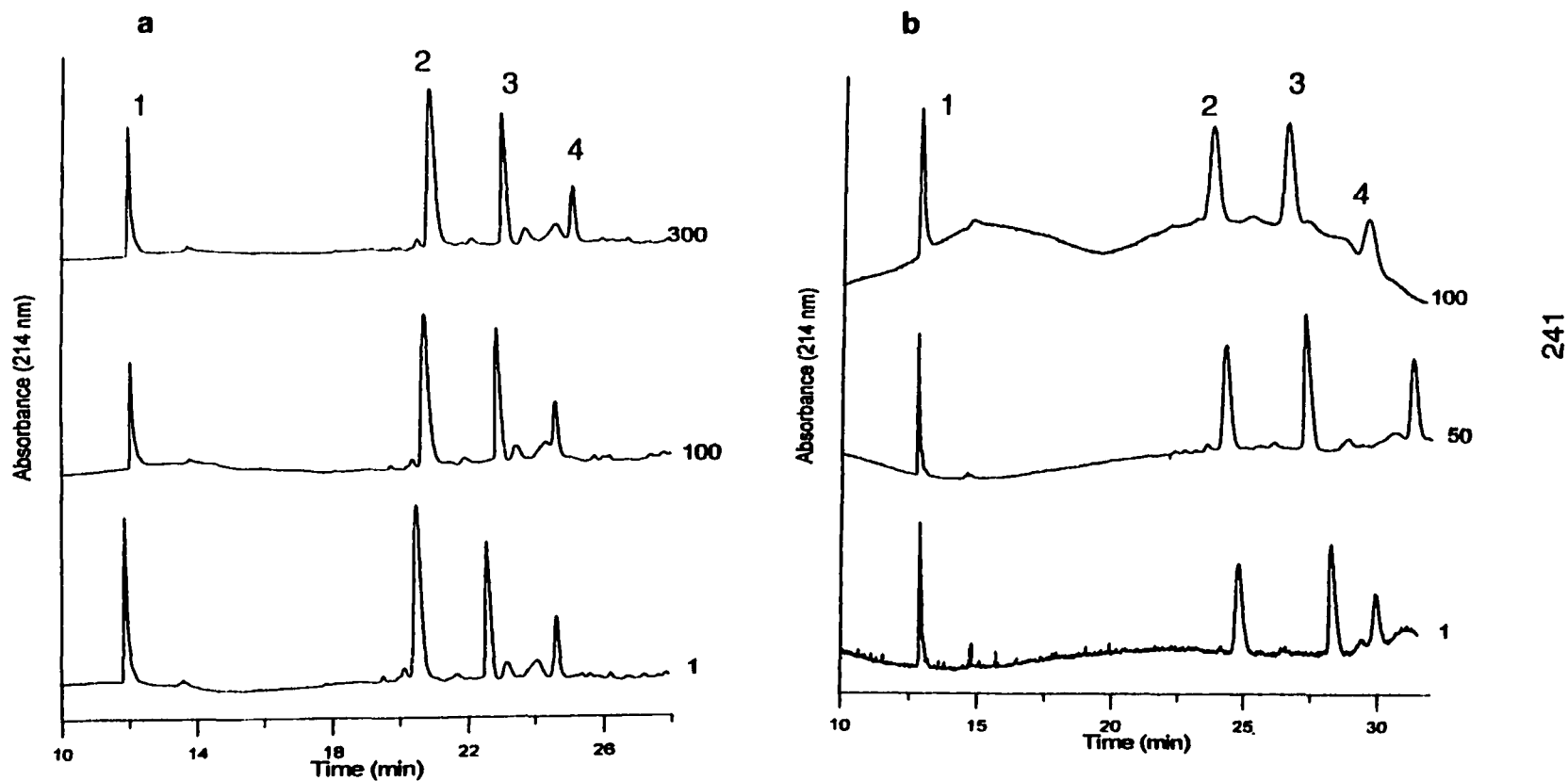




**Figure 5.28: Separation of alkaline protein markers using a) Si-CpolyAAP and b) Si-CpolyAA coated capillaries.**

**A standard set of four alkaline protein markers (peaks are: 1 lysozyme, 2 chymotrypsin, 3 ribonuclease A, and 4 trypsinogen). The numbers show the CE run number for each coated capillary.**



overlaid in a single tracing. A Si-C-polyAAP coated capillary that was coated in Edmonton and shipped to Italy was used for this separation.

It is seen that the peaks are sharp and symmetric for a Si-C-polyAAP coated capillary (Figure 5.28a), with a return of the baseline to the original value before and after the peak. These are taken as indicators of the absence of interaction of the protein with the capillary wall.<sup>27-28</sup>

The separation was performed at pH 7.0 at which all proteins bear a net positive charge. When the same separation is performed in a mixture of the four protein markers on a Si-C-polyAA coated capillary, the same pattern is observed (Figure 5.28b). A series of minor peaks is visible which probably representing minor contaminants, possibly also alkaline proteins. This experiment was done with a Bio-Rad (Hercules, CA, USA) Biofocus 3000, equipped with a UV detector. At pH 9.4 the Si-C-polyAA coated capillary degraded rapidly, but by lowering the pH its life time increased to 100 runs (Figure 5.28b).

#### **5.4 Conclusions**

Our new method improved the performance of coated capillaries in terms of pH stability from pH 2-11, temperature stability from 20 °C to 75 °C, migration time reproducibility with FQ-labeled ovalbumin, and EOF reproducibility. We also showed that Si-C- sub-layers for coating were much more stable than Si-O sub-layers and also polyAA top-layers were susceptible to alkaline hydrolysis for both Si-C sub-layers and Si-O sub-layers. Both Si-C-polyAAEE and Si-C-polyAAP showed less adsorption as compared to Si-C-polyDMA and Si-C-polyAA. It was difficult to decide which one was better if both AAEE and AAP monomers were fresh, but lack of batch-to batch reproducibility for the Si-C-polyAAEE was observed due to auto-polymerization of AAEE monomers. The

Si-C-polyAAP showed less adsorption and better batch-to-batch reproducibility than that of the Si-C-polyAAEE. Preliminary results showed that Si-C-polyDMA, which was very stable in terms of EOF over a wide range of pH and temperature, could be successfully applied for DNA analysis. In this work we reported a new modified method of coating capillaries which was a combination of selected hydrophilicity of polymers as top-layers and high resistance toward alkaline hydrolysis of Si-C as sub-layers.

## 5.5 References

1. Wirth, M. J., Pieter Fair Bank, R.W., Fatumbi, H. O., *Science*, 275, 44-47, 1997.
2. Jorgenson, J. W., and Lukacs, K. DeArman., *Anal.Chem.*, 53, 1298-1302, 1981.
3. Schoneich, C., Andreas, F.R., Huhmer, S. R., Stobaugh, J. F., Seetharama D.S., Jois, C., Larive, K., Teruna J. S., Squier, T. C., Bigelow, D. J., and Williams. T. D., *Anal.Chem.*, 67, 155R-181R, 1995.
4. Hjertten, S., *J. Chrom.*, 347, 191, 1985.
5. Kelly A. Cobb, Vladislav Dolnik, and Milos Novotny, *Anal.Chem.* 1990, 62. 2478-2483
6. Chiari, M., Micheletti, C., Nesi, M., Fazio, M., and Righetti, P. G., *Electrophoresis*, 15, 177-186, 1994.
7. Chiari, M., Nesi, M., and Righetti, P. G., *Electrophoresis*, 15, 616-622, 1994.
8. Gelfi, C., Perego, M., Libbra, F., and Righetti, P. G., *Electrophoresis*, 17, 1342-1347, 1996.
9. Simo-Alfonso, E., Gelfi, C., Sebastiano, R., Citterio, A., and Righetti, P. G., *Electrophoresis*, 17, Artikel 224, 2247, 2248, 1996.
10. Blanco, S., Clifton, M. J., Joly, J. L., and Righetti, P. G., *Electrophoresis*, 17, 1126-1133, 1996.
11. Gelfi, C., Perego, M., and Righetti, P. G., *Electrophoresis*, 17, 1407-1475, 1996.
12. Chiari, M., Nesi, M., Ottolina, G., and Righetti, P. G., *J.Chrom. A*, 680, 571-577, 1994.
13. Righetti, P. G., *Capillary Electrophoresis in Analytical Biotechnology*, CRC Press Inc., 1996.
14. Wu, S., and Dovichi, N. J., *J.Chrom.*, 480, 141-155, 1989.
15. Zhang, J., Ph.D. thesis, University of Alberta, 1994.

16. Wu, S., Dovichi, N.J., *Science*, 480, 141-155, 1989.
17. Cheng, Y.F., Dovichi, N.J., *Science*, 242, 562-564, 1988.
18. Beale, S.C., Hsieh, Y-Z, Wiesler, D. and Novotny, M., *J.Chrom. A.*, 499, 579-587, 1990.
19. Pinto, D. M., Arriaga, E. A., Craig, D., Angelova, J., Sharma, N., Ahmadzadeh, H., Boulet, C. A., and Dovichi, N. J., *Anal.Chem.*, 69, 3015-3021, 1997.
20. Huang, X., Gordon, M. J., and Zare, R. N., *Anal.Chem.*, 60, 1837-1838, 1988.
21. Ahmadzadeh, H., et al, in preparation
22. Miertus, S., Righetti P. G., and Chiari, M., *Electrophoresis*, 15, 1104-1111, 1994.
23. Terabe, S., Otsuka, K., and Ando, T., *Anal.Chem.*, 61, 251-260, 1989.
24. Cheng, Y. F., Wu, S., Chen, D. Y., and Dovichi, N. J., *Anal.Chem.*, 62, 496-503, 1990.
25. Craig, D., et al, submitted.
26. Simo-Alfonso, E., Gelfi, C., Sebastiano, R., Citterio, A., and Righetti, P. G., *Electrophoresis*, 17, Artikel 2246, 1996.
27. Zhukov, M.Y., Ermakov, S.V. and Righetti, P.G., *J. Chromatogr A*, 766, 171-185, 1997.
28. Ermakov, S.V, Zhukov, M.Y., Capelli, L. and Righetti, P.G., *J. Chromatogr. A.* , 699, 297-313, 1995.
29. Chiari, M., DellOrto, N., and Gelani, A., *Anal. Chem.*, 68, 2731-2736, 1996.
30. Chiari, M., Nesi, M., Sandoval, J. E., and Pesek, J. J., *J. Chromatogr. A.*, 717, 1-13, 1995.

# PART III

## Development of labeling chemistry and its characterization for ultra-sensitive assay of natural toxins and environmental samples using capillary electrophoresis and flow injection analysis with laser-induced fluorescence detection<sup>1</sup>

---

<sup>1</sup> Some parts of the amine labeling of this chapter have already been published as "Picomolar Assay of Native Proteins by Capillary Electrophoresis Pre-column Labeling, Sub-micellar Separation, and Laser-Induced Fluorescence Detection" by Devanad M. Pinto, Edgar A. Arriaga, Doug Craig, Jordanka Angelova, Neepun Sharma, Hossein Ahmadzadeh, and Norman J. Dovichi; Anal. Chem. 69, 3015-3021, 1997. The amine labeling chemistry will not be discussed here.

# **Chapter 6**

## **Carboxylic acid labeling and method development for microcystin analysis**

## 6.1 Introduction

### 6.1.1 Microcystins and shellfish toxins

Microcystins are a group of potent natural toxins with LD<sub>50</sub> as low as 50 µg / kg of body weight.<sup>1</sup> Microcystins are potential liver toxins and neurotoxins (anatoxin-a).<sup>2-4</sup> These toxins are commonly produced by certain planktonic cyanobacteria or blue-green algae (cyanobacterial blooms). Microcystins may be found in lakes, ponds and municipal water supplies. The presence of these toxins in natural waters impose problems for the maintenance of safe water supplies.<sup>1</sup> These toxins have been correlated to several incidents of animal illnesses and a few incidents of human illnesses. Many drinking water supplies throughout the world have experienced periodic blooms of cyanobacteria that contribute significantly to a wide range of water-related problems. Toxic cyanobacterial blooms have been documented in the USA, New Zealand, the former USSR, Bangladesh, India, Israel, several European countries, South Africa, Japan, China, Portugal, Finland, England, and Australia and western Canada.<sup>6</sup> Natural toxins in seafood and water have been responsible for several poisonings throughout the world. A seafood toxin, domoic acid, was the cause for the amnesic shellfish poisoning that resulted in 3 deaths and left over 20 neurological victims after they consumed some blue mussels harvested from Prince Edward Island in 1987.<sup>5-6</sup>

Some of these toxins can inhibit enzymes at concentration levels that are below the detection limit of the current analytical techniques. Understanding of the possible health risks and environmental quality assessments required with regard to these natural toxins has been limited by the lack of a sensitive and reliable analytical method to determine specific forms of toxins at trace levels.

Microcystins contain three D-amino acids (glutamic acid, alanine, and methylaspartic acid), two unusual amino acids (N-methyl-dehydroalanine (Mdha) and

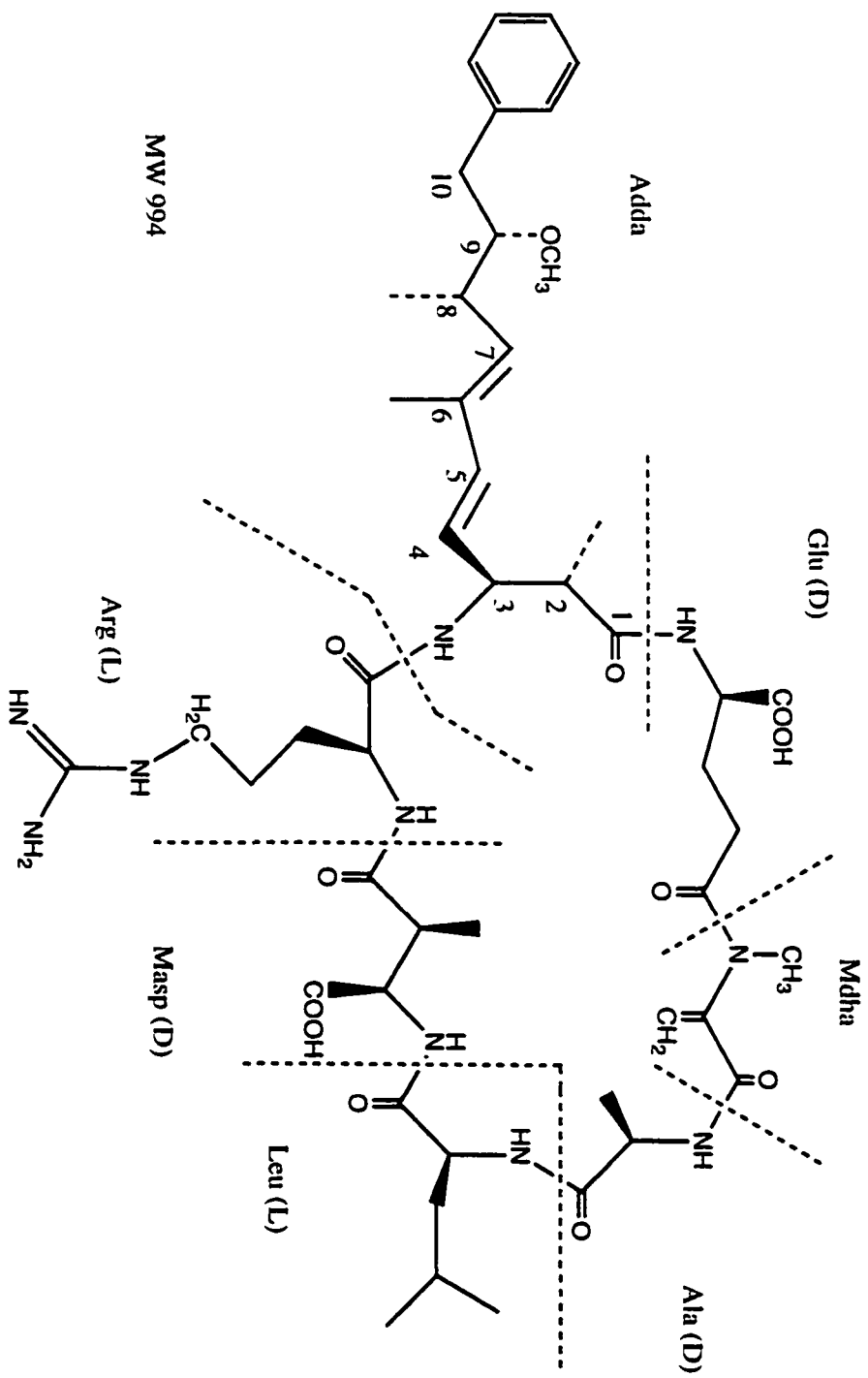


3-amino-9-methoxy-2, 6, 8-trimethyl-10-phenyldeca-4,6-dienoic acid (Adda) and two variable L-amino acids (leucine and arginine). Figure 6.1 shows the chemical structure of microcystin-LR. The general structure is cyclo(-D-Ala-L-X-D-erythro- $\beta$ -methyl-Asp-L-Z-Adda-D-Glu-N-methyldehydro-Ala), where X and Z represent the two variable L-amino acids and Adda is (2S, 3S, 8S, 9S)-3-amino-9-methoxy-2, 6, 8-trimethyl-10-phenyldeca-4, 6-dienoic acid.<sup>6</sup>

There are over 50 different microcystin variants, which all have similar methylation and demethylation patterns on the two unusual amino acids. The toxicity among these different microcystins varies and, therefore, it is essential to quantitate different forms of microcystin in order to evaluate health risks and environmental impacts. However, the most sensitive method available, enzyme-linked immunosorbent assay (ELISA) (detection limit 0.2 nM or 10 pg per assay) is unable to differentiate among the different forms of toxins.<sup>7</sup> The other sensitive assay for natural toxins is protein phosphatase bioassay.<sup>8</sup> These assays are not very specific for individual chemical forms of a group of toxins, although immunoassays are usually specific because antibodies generally possess high specificity targeting unique structural elements called epitopes.<sup>9</sup> Immunological recognition is based on the spatial complementary groups in the epitope of the antigen with those of antibody.<sup>9</sup> However, because antibodies target epitopes, not the whole antigen, antibodies can fail to discriminate structurally similar species by cross-reacting.

It is possible to solve this cross-reactivity problem by using CE separation prior to immunological recognition. The cross-reactivity, therefore, changes to an advantage and simultaneous measurement of a group of individual toxins is possible. A mixture of toxins, after being separated by CE, are sequentially eluted from the separation capillary, recognized by the antibody, and then monitored by the laser-induced fluorescence detector.<sup>9</sup>

**Figure 6.1: Chemical structure of microcystin-LR. There are two variable L-amino acids, leucine and arginine, three D-amino acids, and two unusual amino acids, N-methyl-dehydroalanine (Mdha), and 3-amino-9-methoxy-10-phenyldeca-4,6-dienoic acid(Adda)**



Antibodies against microcystin-LR have been prepared by Chu in collaboration with Carmichael. They obtained anti-microcystin antibody from rabbit serum after immunizing rabbits with bovine serum albumin-microcystin-LR conjugate. We are collaborating with Dr. Xc. Le from the Department of Public Health at the University of Alberta. Dr. Carmichael is providing the antibody for Dr. Xc. Le.

It is proposed that a standard microcystin-LR will be labeled at its carboxylic acid group of glutamic acid with 5-bromomethylfluorescein (5-BrMF), using a similar procedure as for penicillin-G labeling. This labeling does not affect the antibody-antigen recognition. It is known that recognition of microcystins by antibody is through the binding of the unusual amino acid Adda group that is present in all microcystin variants, and this group will not be affected by the fluorescent labeling (because of the presence of two -COOH groups in microcystin structure and the possibility of multiple labeling we had to label arginine side chain of microcystin).

### **6.1.2 Objectives**

The objective for this project is to fluorescently label microcystin-LR. The chemical structure of microcystin-LR (Fig. 6.1) shows two carboxylic acid and one arginine group.

In this chapter carboxylic acid labeling will be presented. The next chapter presents the result of arginine labeling and microgram-scale organic synthesis of an arginine specific fluorescent labeling reagent.

In the first part, penicillin-G was chosen as a model compound to optimize the chemistry of carboxylic acid labeling. The reason to choose penicillin-G is that an antibody against penicillin-G is commercially available and both penicillin-G and microcystins have carboxylic acid functional groups.

### 6.1.3 Carboxylic acid labeling

The quantitation of carboxylic acid containing analyte in a biological matrix is important in cell structure and function. The labeling reagents for carboxylic acid derivatization are adopted from HPLC separation and quantitation of fatty acids.<sup>10-16</sup> Fatty acids have been labeled with a detection limit of 7.5 nanomolar.<sup>17-18</sup>

In the analysis of carboxylic acids, choosing an appropriate labeling reagent with no side reactions with other functional groups in the molecule is very important. The chosen reagent must react at a low molar concentration and its absorption spectrum should match that of the common laboratory lasers such as an argon-ion laser with 488-nm emission line.

The most common way of carboxylic acid labeling is esterification of carboxylic acid functional group. There are many esterification reagents commercially available for carboxylic acid derivatization.<sup>19</sup> One class of these reagents is diazoalkanes. The most common fluorescent diazomethyl derivative is 9-anthryldiazomethane (ADAM), a reagent that is used to label several types of biological compounds. Unfortunately, ADAM is unstable and decomposes during storage.<sup>19</sup> The second class of carboxylic acid labeling reagents is trifluoromethanesulfonates. They react with the anion of carboxylic acids in acetonitrile to give adducts that are detectable by adsorption at 394 nm with 4 femtomoles limit of detection.<sup>19</sup> This labeling reagent has the disadvantage of requiring a UV laser that is expensive as compared to visible-light lasers.

The third class of carboxylic acid esterification reagents is fluorescent alkylhalides. Molecular Probes Inc. has marketed many of these alkylhalides. Among these compounds 5-bromomethyl fluorescein (5-BrMF) and BODIPY methyl bromide have the strongest absorptivity and fluorescence emission of the currently available carboxylic acid labeling reagents. Figure 6.2 shows the excitation and emission spectrum of 5-BrMF. The excitation wavelength of 492 nm matches well with the 488-nm line of an argon-ion laser.

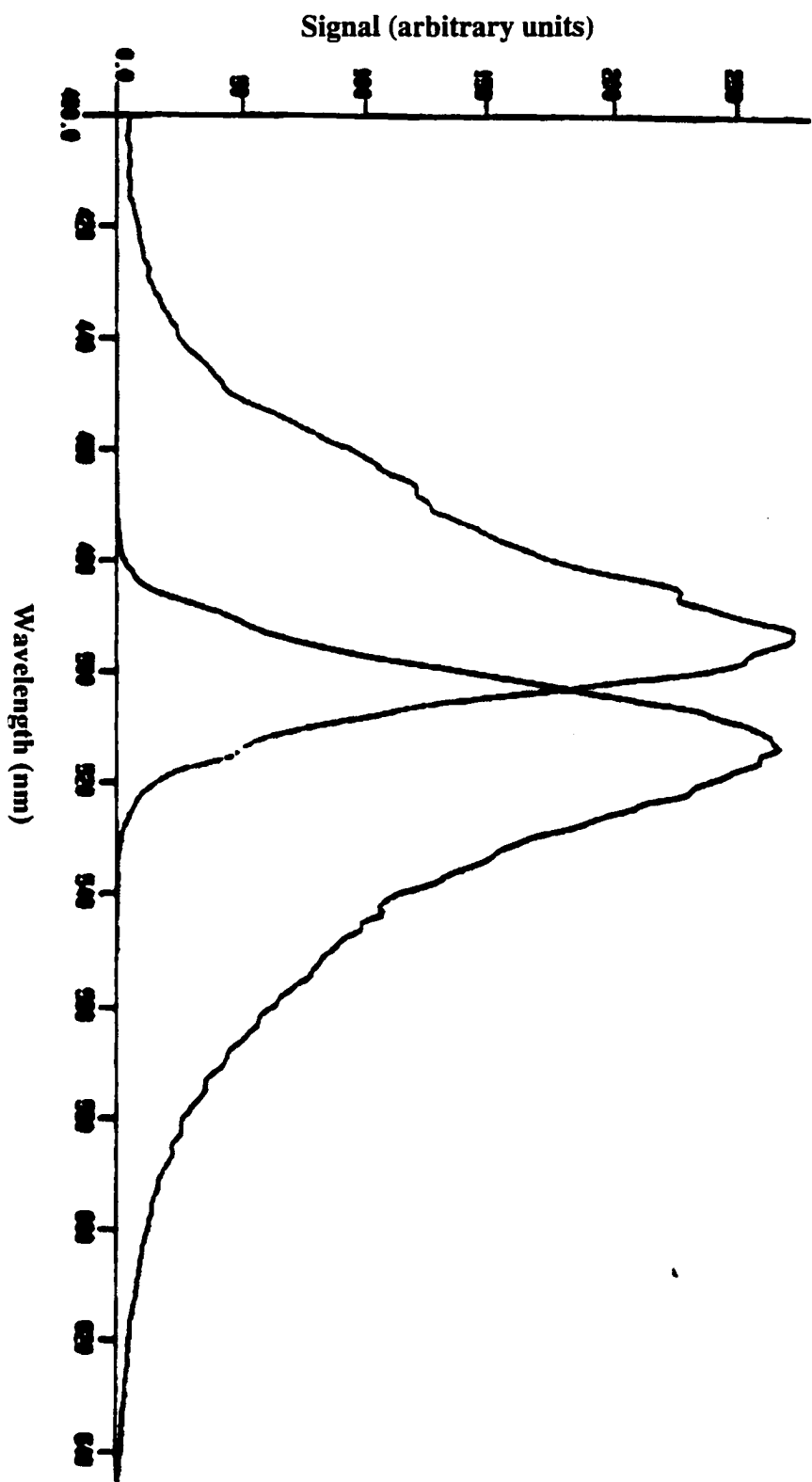


Figure 6.2: Excitation/emission spectra of 5-Br-MF as a fluorescent labeling reagent for carboxylic acid derivatization 19

5-BrMF has an excitation coefficient of 81,000 L/mol-cm. Its emission wavelength is 515 nm. I chose 5-BrMF to study the labeling chemistry of carboxylic acids and penicillin-G, in particular, because many other research groups used 5-BrMF for carboxylic acid labeling, but not for labeling of penicillin-G.<sup>20</sup>

#### **6.1.4 The use of penicillins as model analytes**

Microcystins are expensive and highly toxic. Optimization studies had to be performed on an inexpensive and safer compound. Penicillin-G was chosen as a model analyte to optimize the labeling reaction. The carboxylic acid group in penicillin-G is linked to

$\beta$ -lactam ring. The carboxylic acid groups of microcystins are also linked to a heptapeptide ring and this makes the penicillin-G a good candidate to simulate the microcystins. Penicillin-G is fluorescently labeled by reacting it with a carboxylic acid-reactive probe, 5-BrMF. This fluorescent dye reacts with salts of carboxylic acids during heating in an organic solvent such as methanol or acetonitrile. This dye has the strongest fluorescence of the currently available carboxylic acid-reactive probes. The high absorbance and intense green fluorescence at 515 nm of this probe make it the preferred choice for high sensitivity analysis.

Although penicillin itself does not elicit immune responses, it can be immunogenic when conjugated to a protein. Antibodies against penicillin are commercially available and can also be prepared by immunizing rabbits with penicillin-BSA conjugate. I used commercially available anti-penicillin antibodies in this study.

Because this project is a collaborative work, I concentrated on the labeling chemistry of microcystin and Professor Le's research group used the labeled antigen to do laser-induced fluorescence polarization (LIFP) immunoassay.

### 6.1.5 Organic synthesis

The reaction mechanism of 5-BrMF with penicillin-G is an  $\text{SN}^2$  nucleophilic substitution. In this reaction the oxygen atom of the carboxylate group in penicillin-G attacks, as a nucleophile, the methylene carbon of 5-BrMF and displaces its bromide ion. The reaction is shown in Figure 6.3. There are some practical difficulties in controlling this reaction. One problem is that 5-BrMF may attack itself because of the presence of two nucleophilic sites on the molecule. The carboxylic acid and phenolic protons may dissociate at higher pH and act as a nucleophile to displace the bromine of the second 5-BrMF. The second problem is the fast proton exchange between 5-BrMF carboxylic acid and the carboxylate site on the potassium salt of penicillin-G. This proton exchange will cause the carboxylate ion to change to carboxylic acid and reduces the nucleophilicity of the penicillin-G, while increasing self-reaction of 5-BrMF. Steric hindrance of the methyl groups next to the carboxylate ion on the  $\beta$ -lactam ring of penicillin-G is another problem for this reaction. The last point is the necessity of nonaqueous conditions. Esterification of carboxylic acids in aqueous solution is usually not possible, and esters tend to be unstable in water under basic conditions. This last problem imposes practical considerations on careful control of moisture content of the solvents that we choose.

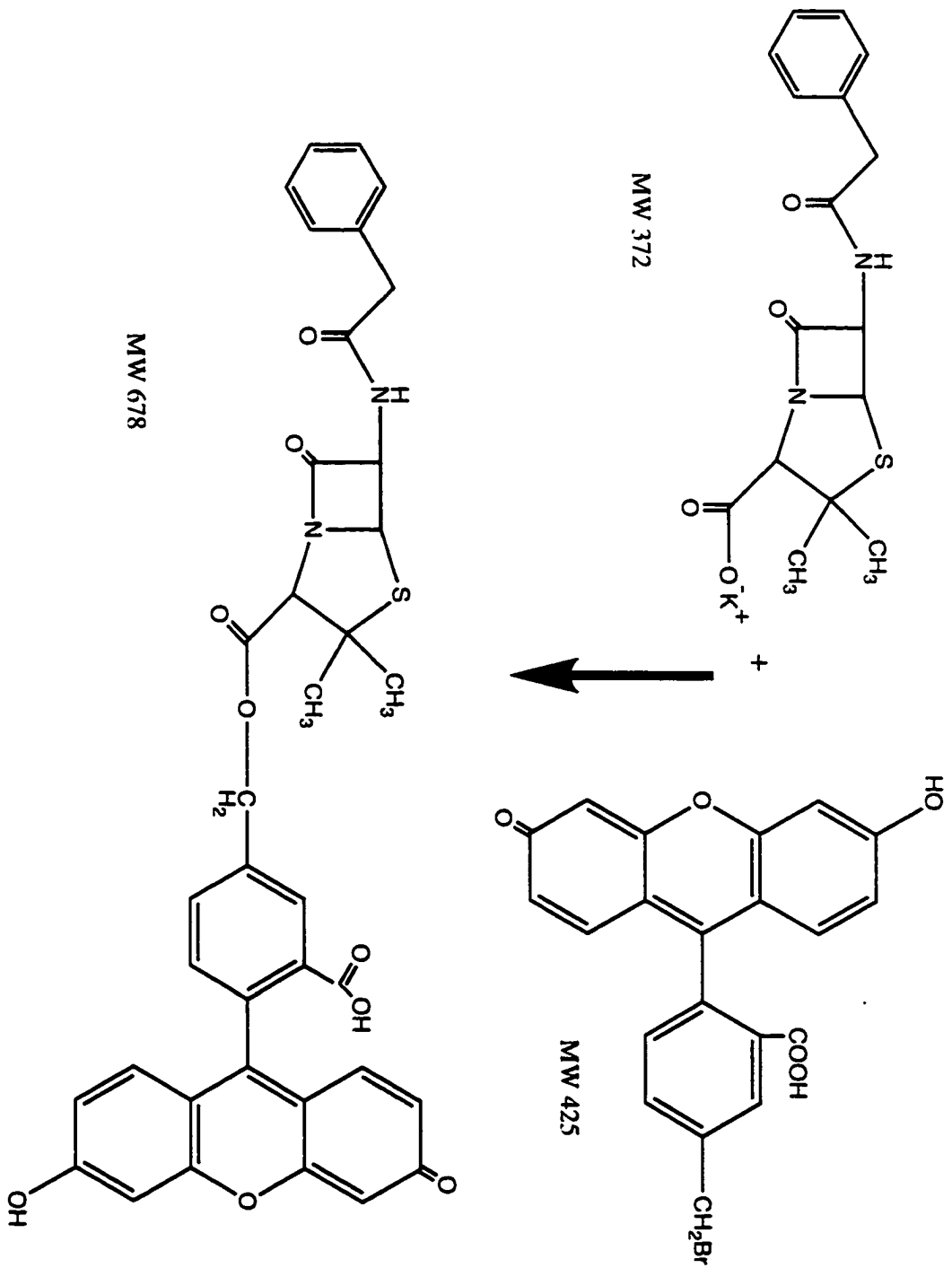
## 6.2 Experimental

The experiments may be divided into three parts. The first part consists of organic synthesis of fluorescently labeled penicillin-G, the second part is purification and isolation of the labeled penicillin-G, and the third part is analytical quantitation of the product.

### 6.2.1 Reagents

5-BrMF was purchased from Molecular Probes, Eugene, OR, USA. 18-crown-6 was purchased from Fluka Chemika, Switzerland. DMF was purchased from Aldrich,

Figure 6.3: The chemical equation showing the labeling of penicillin-G with a fluorescent tag 5-Br-MF





Millwaukee, WI, USA. Penicillin-G potassium salt and anti-Penicillin antibodies. Type I (Mouse) were purchased from Calbiochem-Novabiochem, LaJolla, CA, USA. Antibody was constructed using a penicillinG-BSA conjugate and was reactive toward the  $\beta$ -lactam ring of penicillin. Antibody was supplied in 15 mM potassium phosphate, 150 mM NaCl and 0.1%  $\text{NaN}_3$  at pH 7.2. Upon receiving, the anti-penicillin antibody was stored in a freezer at  $-20^\circ\text{C}$ . The product data sheet from the manufacturer says that if the antibody is stored below  $-20^\circ\text{C}$  or on dry ice, it will precipitate. The manufacturer also recommends that freeze/thaw cycles be avoided. The Bio-Gel P-4 Gel for gel permeation chromatography was purchased from Bio Rad Laboratories, Richmond, CA, USA.

### 6.2.2 Instruments

The CE-LIF instrument is a home-built instrument that has been described in Chapters 2 and 3 of this thesis.

A SpeedVac, to dry out the solvents, was purchased from Savant of Farmingdale, NY, USA. The electrospray ionization mass spectrometer (ESI-MS) was a PE/Sciex API 100 (Thornhill, ON, Canada) single quadrupole equipped with an ion spray source. A  $50\ \mu\text{m}$  ID x  $184\ \mu\text{m}$  OD fused-silica capillary was connected to the hold-down tee of the ion sprayer on one side and to a syringe pump on the other side. The coaxial sheath flow liquid of 100% methanol was pumped by a Harvard Apparatus low pressure syringe infusion pump (South Natick, MA, USA). Before analysis, while the analytes were infused at a flow rate of  $2.0\ \mu\text{L}/\text{min}$ , the ion sprayer was adjusted for maximum sensitivity. Operation parameters such as ion spray voltage (IS), orifice voltage (OR), ring voltage (RNG) and curtain gas flow were optimized for maximum total ion chromatogram (TIC) signals over a range of 50-1000 using flow injection method. Lower OR was chosen to generate less in-source collision-induced dissociation (CID) to monitor the protonated molecular ions. A

working pressure of  $1.7 \times 10^{-5}$  Torr was maintained in the analyzer chamber (CEM), and the voltage of 2.3 kV was kept constant during routine operation of the instrument. The IS was set to 4.6 kV, OR was 45 V, RNG was 320 V, curtain gas flow was 8 (0.95 L/min). Nebulizing assistance was provided by passing purified nitrogen through the nebulizer tube at a rate of 0.41 L/min or 0.67 L/min, unless otherwise stated. Full scan analysis of sample ions was accomplished by scanning the quadropole in 1.0 amu from 50.0 to 900.0 in 0.56 s. Mass spectra were acquired by a LCTune software, and then processed by Multiview 1.2 and MacQuant software from Sciex.

An HPLC system consisting of a Dionex (Sunnyvale, CA, USA) Gradient pump DX300, Waters 712 WISP Auto-sampler, and Waters 484 Tunable Absorbance Detector was used for purification of the synthesized product.

### **6.2.3 Reaction conditions optimization**

#### **6.2.3.1 Procedure 1**

A 78.7  $\mu\text{g/mL}$  solution of penicillin-G in distilled water was prepared and 300  $\mu\text{L}$  of the solution was transferred to a 2 mL glass vial. 250  $\mu\text{L}$  of 125  $\mu\text{g/mL}$  solution of 5-BrMF in acetonitrile (AcN) was added to the glass vial. Then 200  $\mu\text{L}$  of 700  $\mu\text{g/mL}$  18-crown-6 and 200 mg of  $\text{K}_2\text{CO}_3$  was also added to the reaction vial. The reaction components were mixed and heated at 87  $^\circ\text{C}$  for 90 min.

#### **6.2.3.2 Procedure 2**

2  $\mu\text{L}$  of 5 mM penicillin-G in distilled water was transferred to a 1 mL glass vial. 2  $\mu\text{L}$  of 5 mM KOH in water was added to neutralize the solution. After drying the water

using SpeedVac, 1  $\mu\text{L}$  of 1.79 M KOH in MeOH was added. Then 2.8 mg of potassium carbonate was added to 700  $\mu\text{L}$  of 100 mM 18-crown-6 in acetonitrile and transferred to the penicillin-G vial. Acetone (85  $\mu\text{L}$ ) was added to the above solution. After the solution was vortexed, 2  $\mu\text{L}$  of 5 mM 6-BrMF in acetone was added and the solution vial was incubated at 70  $^{\circ}\text{C}$  for 30 min.

The reaction mixture was diluted 100 times using 10 mM borate at pH 9.4 and then injected onto a 50  $\mu\text{m}$  ID and 35 cm long capillary. The injection was done electrokinetically at 1 kV for 5 s. The separation voltage was 400 V/cm and the argon-ion laser power was adjusted to 12.1 mW.

### 6.2.3.3 Procedure 3

Penicillin-G (2.4 mg) was dissolved in MeOH (100  $\mu\text{L}$ ) and 10  $\mu\text{L}$  of this solution was transferred to a reaction vial. 2.5 mL of 125  $\mu\text{g} / \text{mL}$  5-BrMF solution in AcN was added to the penicillin-G reaction vial. Then 250 mg of potassium carbonate was added followed by 2.43 mL of AcN. Finally, 60  $\mu\text{L}$  of 0.1 M solution of 18-crown-6 in acetonitrile (AcN) was added and the solution/suspension reaction mixture was refluxed at 80  $^{\circ}\text{C}$  for 90 min. At the end of the 90 min period the reaction contents were vacuum-filtered twice using standard filter paper to remove solid potassium carbonate. The filtrate was diluted 10,000 times with distilled water and injected onto a capillary L = 35 cm, OD 151  $\mu\text{m}$ , ID 50  $\mu\text{m}$ . A voltage of 14 kV was applied and excitation accomplished with an argon-ion laser. The PMT was biased at 1000V for detection. The sample was further

studied with HPLC using a C<sub>18</sub> reversed phase column with a tunable absorbance detector: the mobile phase was 60:40 water:methanol.

#### **6.2.3.4 Procedure 4**

4 mg of dye and 37 mg of Penicillin-G were dissolved in 10 mL of reaction grade acetone. To this mixture tetramethylammonium hydroxide was added to adjust the pH of the solution to 10-12. The reaction mixture was refluxed in the dark for 5 hs.

#### **6.2.3.5 Procedure 5**

4 mg of dye and 37 mg of Penicillin-G were dissolved in 15 mL of reaction grade acetone and 18-crown-6 was added to the solution until everything dissolved. The reaction was refluxed for 5 hs in the dark. The reaction was monitored by TLC using unreacted 5-BrMF as a standard every 30 min. Further analysis using an ESI-MS was also carried out.

#### **6.2.3.6 Procedure 6**

3.7 mg of Penicillin-G and 0.4 mg of 5-BrMF were dissolved in 1 mL of DMF such that the molar ratio of analyte to 5-BrMF was 10 to 1 respectively (1 / 1 and 100 / 1 mole ratios were also studied). 0.5 mL of 0.27 mg / mL 18-crown-6 in DMF was added to the solution so that the total reaction volume was 1.5 mL. The reaction was stirred and heated to 80 °C for 2 hs. The product was isolated from solution using a C<sub>18</sub> Sep-Pak cartridge. The reaction mixture was loaded onto the column and then washed with water repeatedly. Washing removed any unreacted 5-BrMF, 18-crown-6, and DMF, but left the hydrophobic derivative on the column. The derivative was eluted by washing the column with copious amount of 100% methanol. The methanol was evaporated with a rotary speed-vac. The pure product was redissolved in running buffer (to prepare a 10<sup>-8</sup> M

solution) and injected onto a capillary similar to the one described for other procedures. To confirm the formation of the product, an electrospray mass spectrometer was used and the correct molecular weight was detected and the structure was in agreement with <sup>1</sup>H-NMR spectroscopy.

It was next decided to purify the product by an HPLC to avoid sample decomposition while doing preparative TLC. The sample and several standards were injected onto the HPLC with a C<sub>18</sub> reversed phase column and a tunable absorbance detector in order to optimize the mobile phase composition for best separation. Mobile phase compositions ranging from 100% water to 100% methanol were used. After many trial and error experiments, it was found that a mobile phase of 60% water to 40% methanol gives the best resolution within an acceptable run time.

#### **6.2.3.7 Procedure 7**

This procedure was similar to procedure 6 except that 18-crown-6 was not used for the reaction.

#### **6.2.3.8 Preparative TLC and purification method**

The reaction was monitored with TLC. After optimizing the developing solvent, the reaction was repeated at a larger scale. The reaction mixture was loaded on TLC plates (Kieselgel 60 F<sub>254</sub> from Merck) and the band corresponding to the product was cut out. The product was extracted from the silica gels of TLC plate by soaking the silica gel in MeOH. After extraction was complete, the MeOH was evaporated and the product was dissolved in water and injected onto a C<sub>18</sub> Sep-Pak column. The labeled penicillin-G stuck to the C<sub>18</sub> and impurities were washed away using copious amount of water. When the washing procedure was complete, the product was washed out of the Sep-Pak column using MeOH.

Finally MeOH was evaporated and the pure product was ready for IR and NMR studies and also for standard solution preparation.

The second approach in purifying the product was using preparative HPLC.

#### **6.2.3.9 Quantitation and Calibration curve**

Purified labeled penicillin-G was dissolved in methanol at a concentration of 1.0 mM. This stock solution was used to prepare several standard solutions of the labeled penicillin-G by diluting with 10 mM borate buffer, pH 9.4, for injection onto the CE column as described above. An injection voltage of 1000 V was applied for 5.0 s that approximately transfers one nL of the analyte onto the capillary.

### **6.3 Results and Discussion**

Figure 6.4 shows the electropherogram of the product of procedure 1. There are many peaks present in the electropherogram mainly because of the aqueous solvent used for the reaction. Water, in basic pH due to the presence of potassium carbonate, can act as a nucleophile. This nucleophilicity of water will compete with the carboxylate ion of the penicillin-G and as a result, a mixture of products is observed. This electropherogram shows that an aqueous condition is not an ideal condition for the carboxylic acid labeling.

The electropherogram represented by Figure 6.5 was obtained by diluting (10,000 times) the products of Procedure 2 to give a final concentration of approximately  $10^{-9}$  M, followed by immediate injection onto the capillary. Another solution containing unreacted 5-BrMF, which served as a blank, was also injected onto the capillary under the same conditions as the product. The electropherogram in Figure 6.5 shows that several products have been formed in the course of the reaction and unreacted 5-BrMF is still present even though it was the limiting reagent. This indicated that the reaction had many

**Figure 6.4: Penicillin-G labeling reaction with 5-BrMF in aqueous  $K_2CO_3$  solution (procedure 1).  $10^{-9}$  M solution of the reaction mixture has been injected for 5s at 1000V. CE voltage run is 400 V/cm and the capillary length is 35 cm. The blank reaction was performed exactly similar to the main reaction, but penicillin-G was not present.**

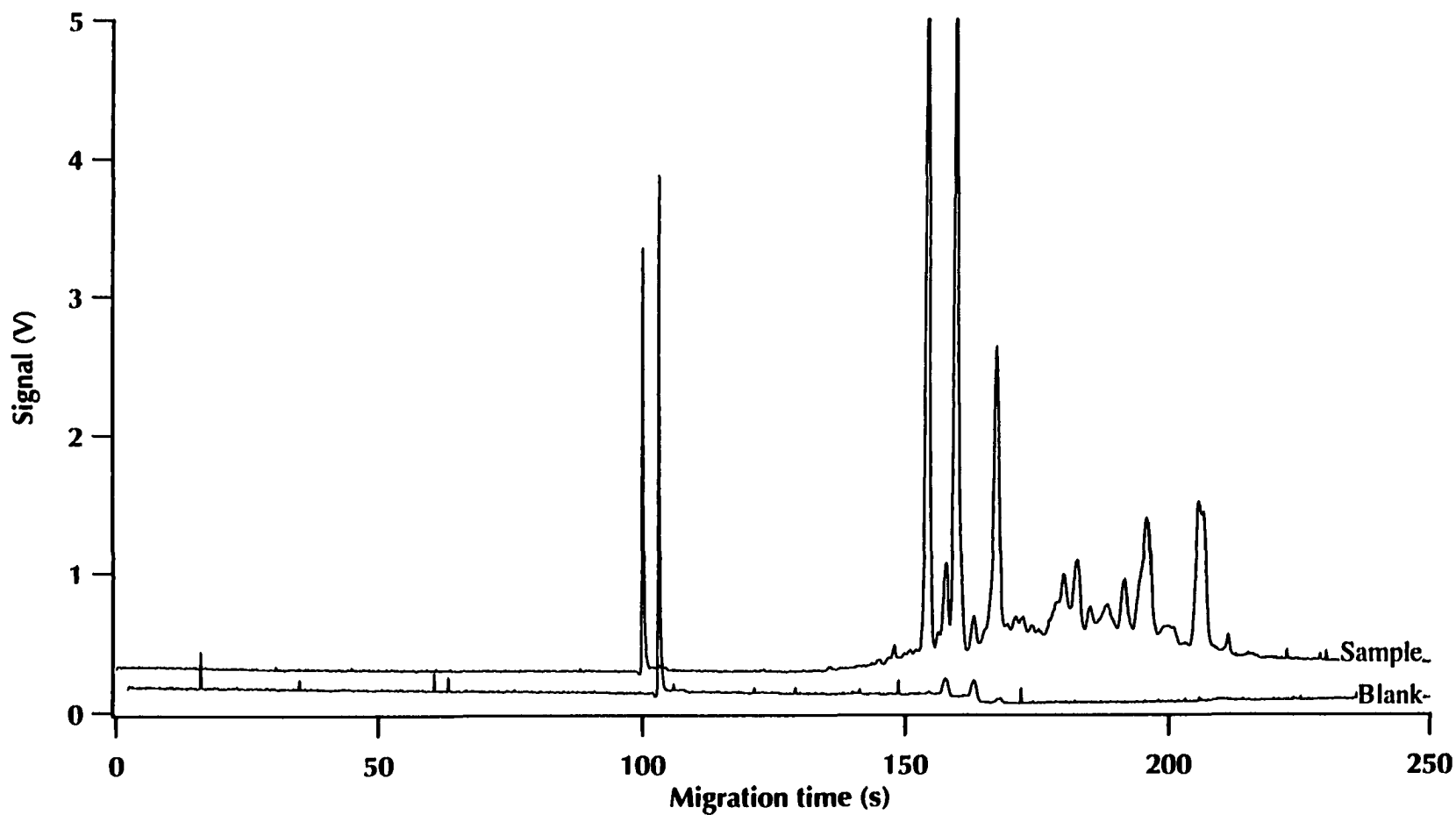
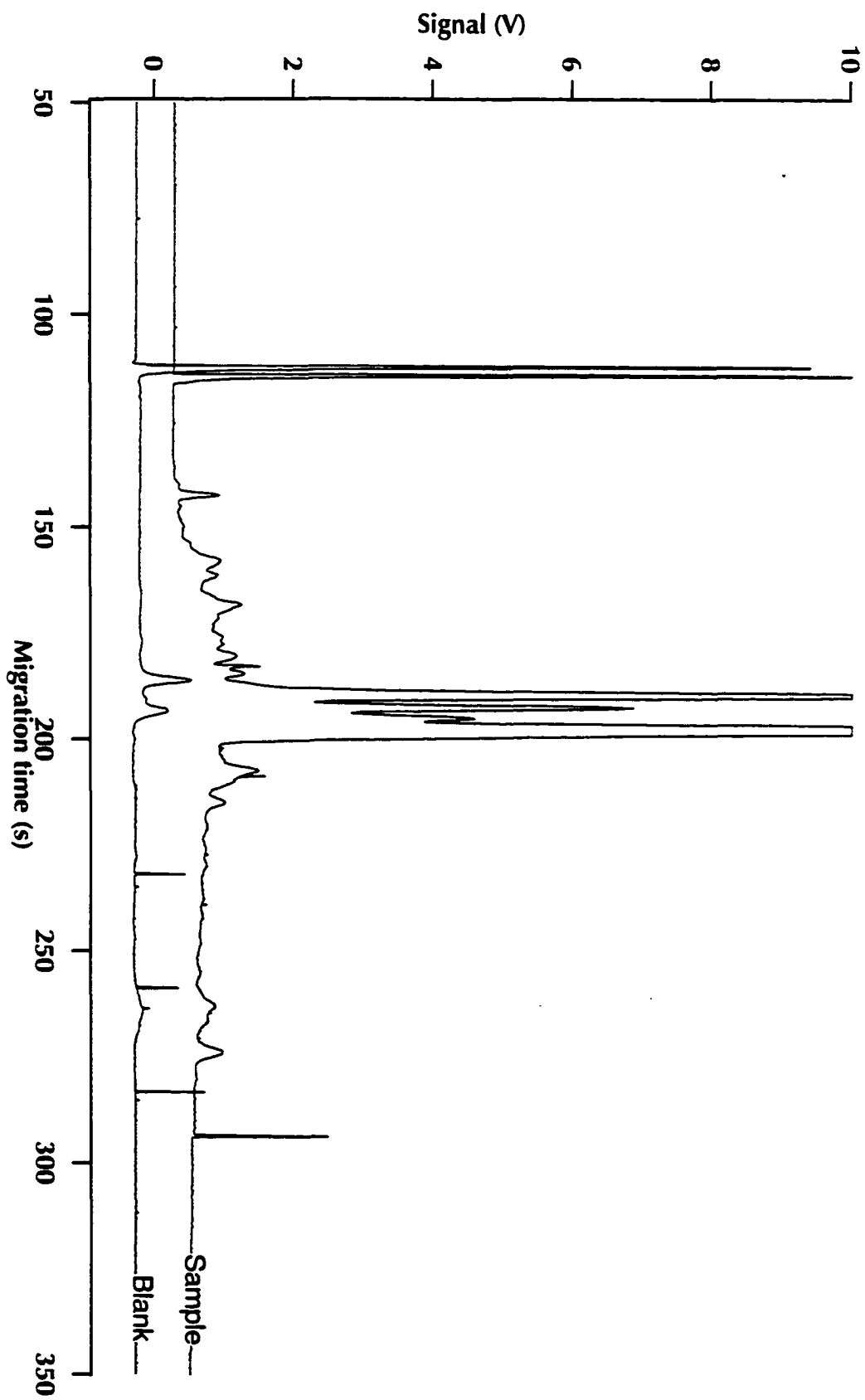


Figure 6.5: Labeling reaction in MeOH solution (procedure 2). CF conditions are similar to Fig. 6.4.





side products and it did not go to completion, possibly due to the presence of a strong base, KOH, that effectively displaced the bromide ion of the 5-BrMF, leaving 5-HMF (5-hydroxymethylfluorescein). Hydroxide ion is not as good a leaving group as bromide ion, and therefore, some side products were formed that consumed the starting material before obtaining the labeled penicillin-G.

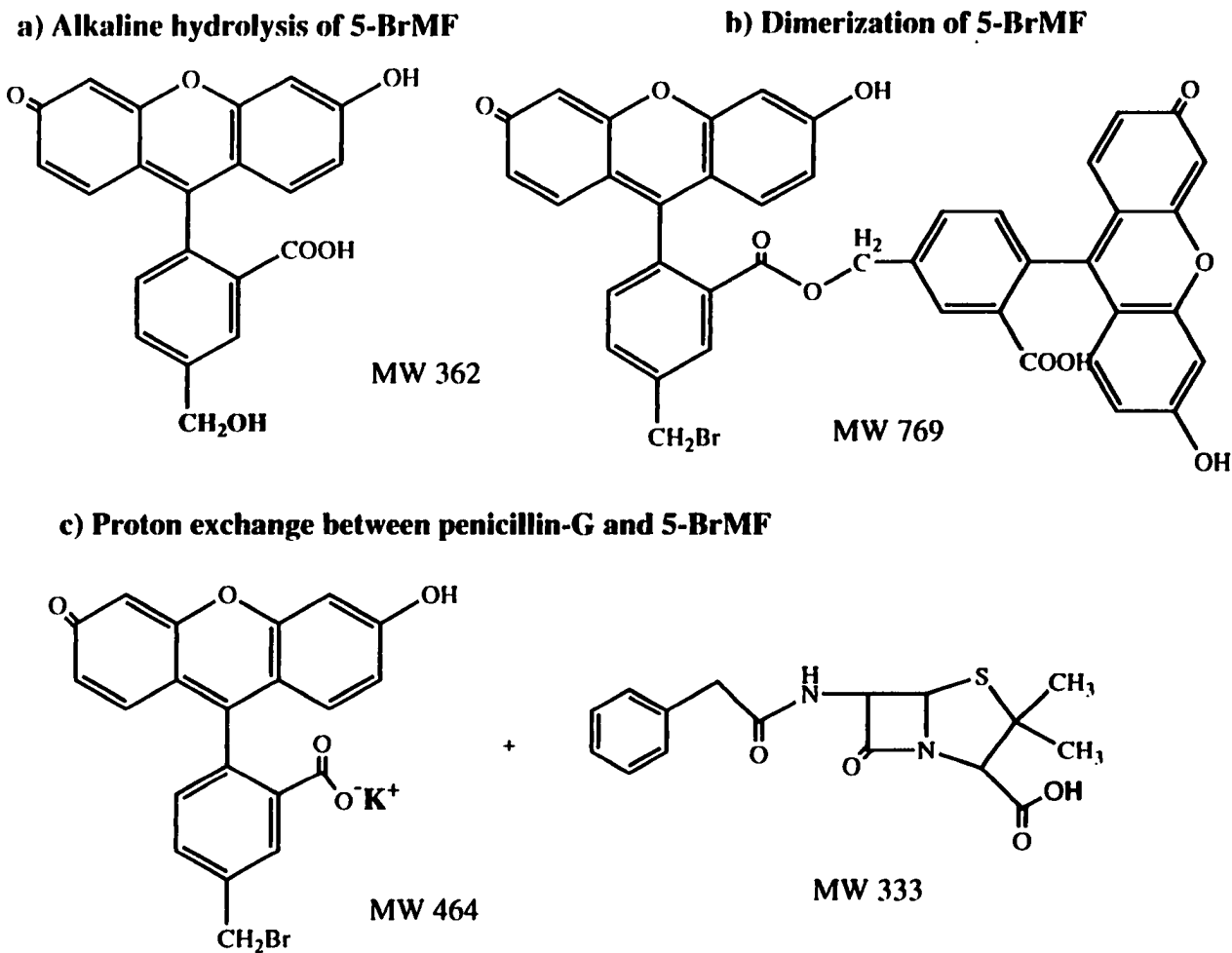
Figure 6.6 represents some possible side reaction products that may form under these conditions. 5-BrMF shows multiple pH-dependent ionic equilibria in aqueous solution. Both the carboxylic acid and phenol functional groups are ionized in aqueous solution at high pH.

Figure 6.7 shows the positive ion mode ESI-MS spectrum of the product of procedure 3. Solvent for this reaction was a mixture of MeOH and AcN in the absence of KOH. This procedure is done under nonaqueous conditions. The side products are reduced using nonaqueous conditions, but still the molecular ion intensity is lower than the side products and starting material. The peak at 335 amu is a protonated penicillin-G cation that indicates the reaction had not gone to completion. This spectrum shows the necessity of the presence of a base for the reaction. There are also some side products present. One reason could be the presence of MeOH as a solvent. The methoxide ion can react as a nucleophile and displaces the bromide ion, leaving 5-methoxymethyl fluorescein.

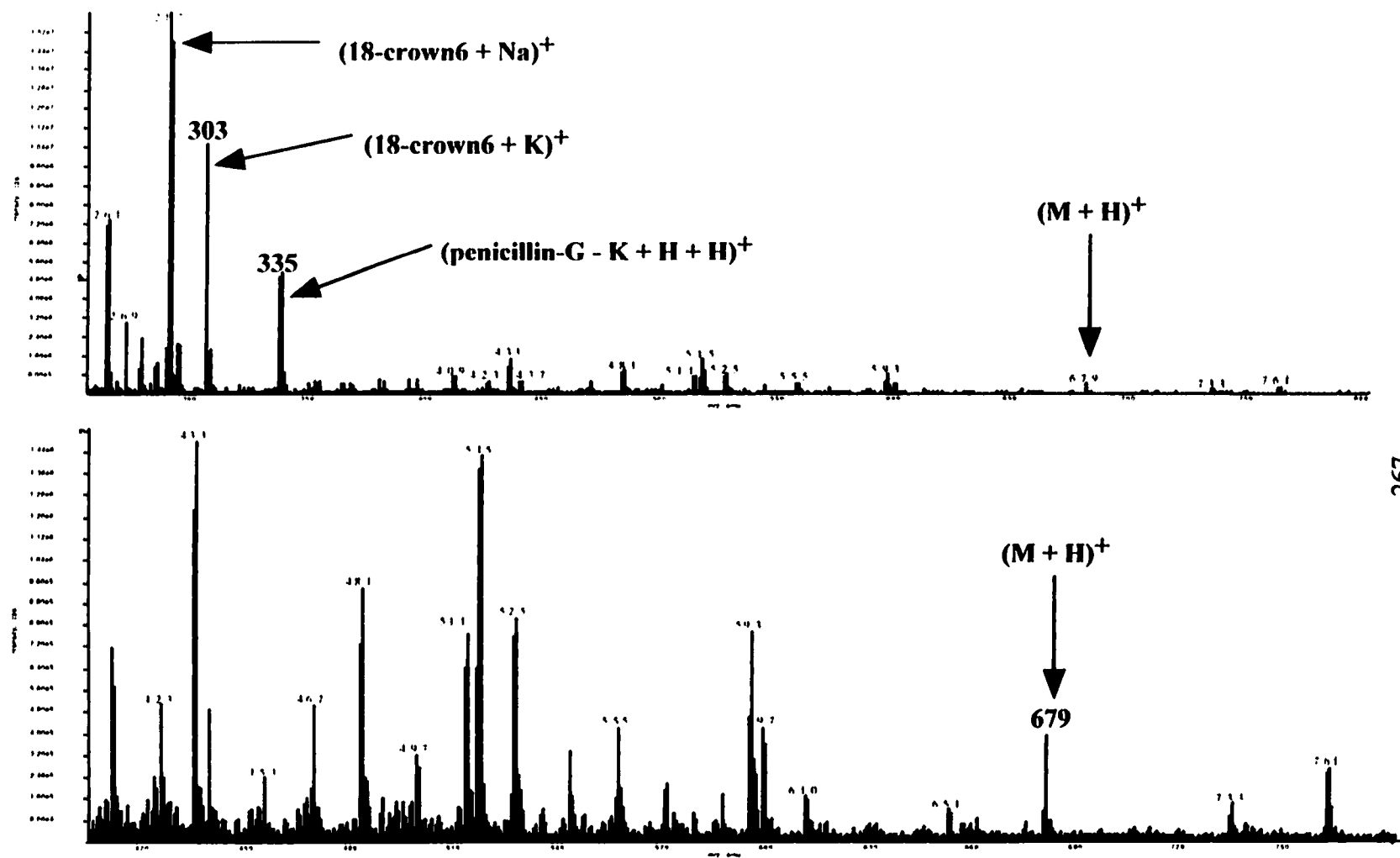
Procedures 4 and 5 were done in acetone as a solvent, with and without an organic base tetraethylammonium hydroxide. Figure 6.8 shows the equilibria and pKa for mono-anion, di-anion, neutral and cationic forms of fluorescein<sup>19</sup>. The mono-anion of 5-BrMF may dimerize itself by replacing the bromide ion. This dimerized peak is observed in the ESI-MS spectrum of the reaction (Fig. 6.9).

Figure 6.9 shows the ESI-MS spectrum of the reaction mixture of procedure 4. The (molecular ion + H + Na)<sup>+</sup> is weakly observed at 701 amu. However further analysis

Figure 6.6: Possible side reactions for penicillin-G labeling with 5-BrMF in aqueous KOH solution<sup>19</sup>



**Figure 6.7: ESI/MS for the product of procedure 3. The labeling reaction is done in MeOH/AcN solvents in the absence of KOH. Top spectrum shows the whole mass range and the bottom spectrum is the expansion of 400 to 800 amu.**



267

Figure 6.8: Dianion, monoanion, neutral, cationic and lactone form of fluorescein<sup>19</sup>

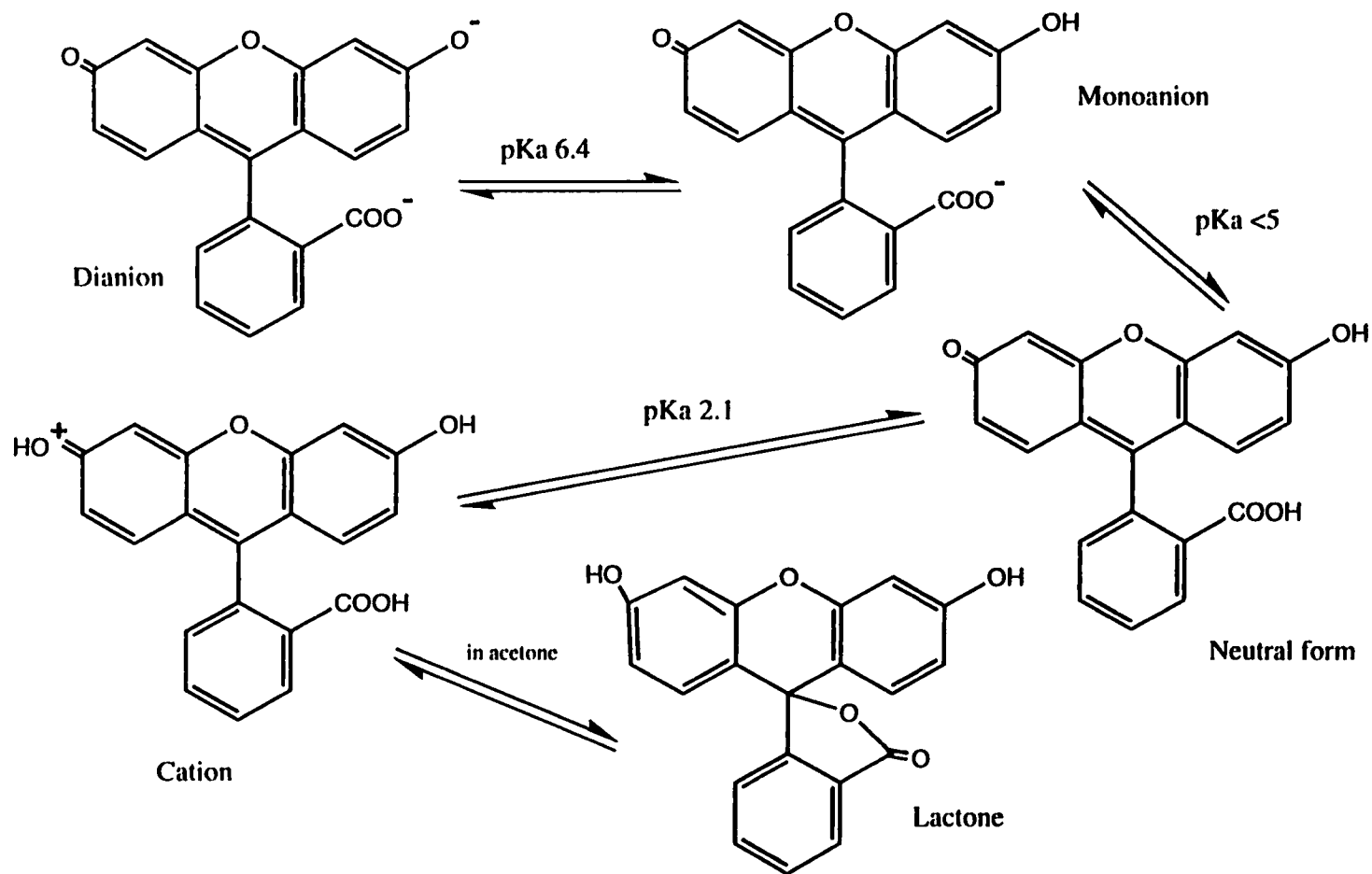
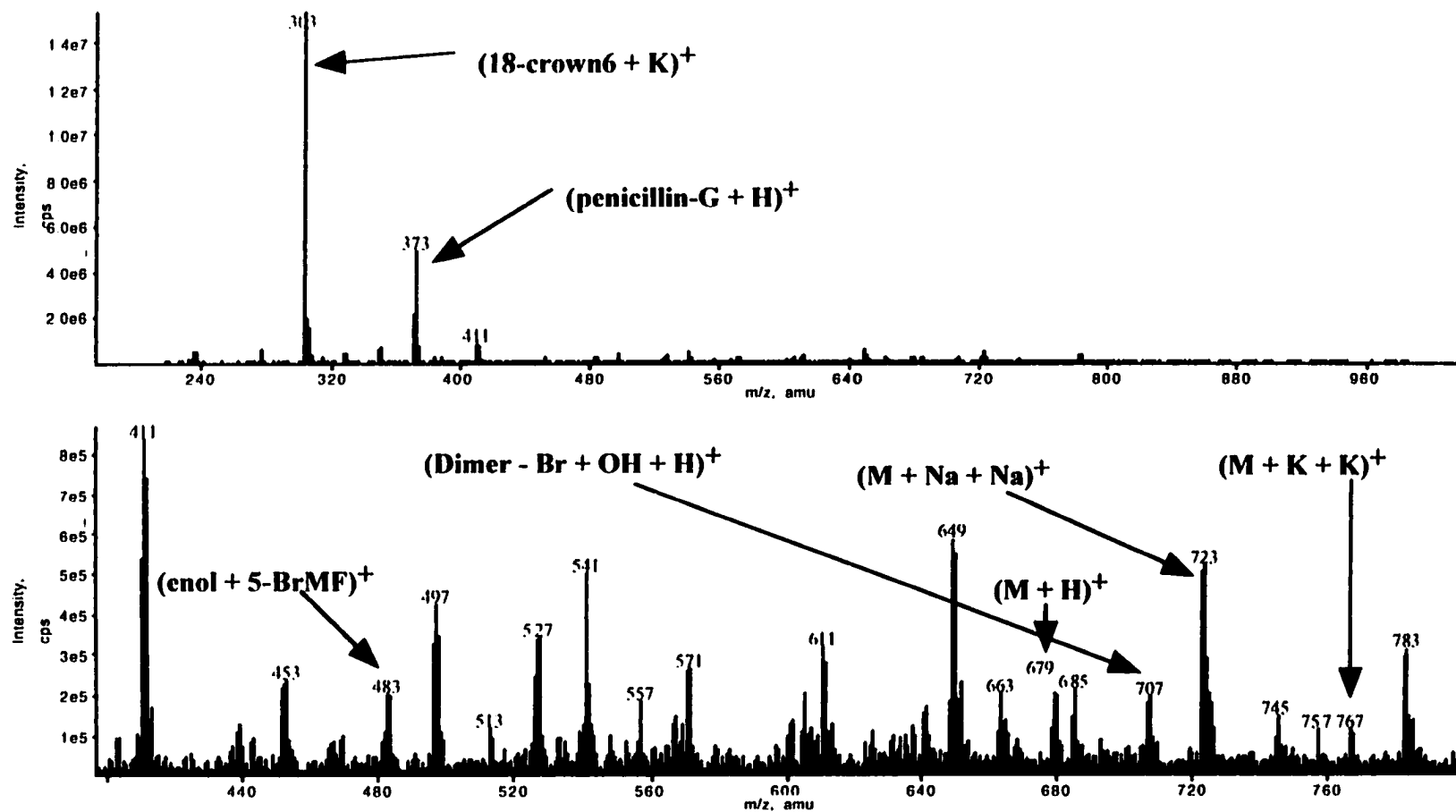


**Figure 6.9: ESI/MS spectrum of the labeling reaction in acetone solvent in the presence of an organic base. Top spectrum shows the whole range and the bottom spectrum is the expansion of 400 to 800 amu.**



269

reveals that many other species are present in the spectrum and have swamped the signal of the desired product, indicating that the yield and purity of this reaction was not satisfactory. The peak at 679 amu is  $(\text{M} + \text{H})^+$ . The 679 amu suggests the presence of the labeled penicillin-G. The peak at 701 amu is  $(\text{M} + \text{H} + \text{Na})^+$  and the stronger peak at 723 amu is  $(\text{M} + \text{H} + \text{Na} + \text{Na})^+$  suggesting that both the carboxylic proton and phenolic protons have been substituted by sodium ions. There is also another peak at 767 amu that is probably  $(\text{M} + \text{K} + \text{K})^+$ , in this case both carboxylic acid and phenolic protons have been replaced by potassium ions. The peaks at 287 amu and 303 amu are  $(18\text{-crown-6} + \text{Na})^+$  and  $(18\text{-crown-6} + \text{K})^+$  ions that were identified by separate running of ESI-MS of the 18-crown-6. Figure 6.9 also shows that there are many side products present for this reaction. for example the peak at 783 amu could be the potassium salt of the dimerized 5-methoxymethyl fluorescein. This means that most of the 5-BrMF was destroyed under these conditions. The peaks at 745 amu and 767 amu should be dimerized 5-hydroxymethyl fluorescein potassium salt  $(5\text{-HMF} + \text{H} + \text{K})^+$  and  $(5\text{-HMF} + \text{Na} + \text{K})^+$  ions respectively. Under these conditions acetone is in its enolate form and reacts as a nucleophile to displace the bromide ion from 5-BrMF. The peak at 483 amu should be the result of this reaction that destroys the 5-BrMF. There was no further attempt to assign other peaks. This ESI-MS spectrum clearly indicated that the acetone, which is the common solvent for carboxylic acid labeling, leads to many side products and is not a good solvent.

After consultation with other organic chemists at the university of Alberta (Prof. Hindsgaul and Prof. Stryker) it was deduced that the major problem arises from the reaction of tetraethylammonium hydroxide with acetone to form enolates, which will further react with 5-BrMF to give a host of undesired products that are observed by ESI-MS. It was, therefore, decided to abandon the base altogether and use 18-crown-6 as a catalyst. When the reaction time was completed TLC would be used to separate the product from side products for further study.

Procedure 4 was repeated in the absence of tetramethyl ammonium hydroxide (Procedure 5) and the reaction was monitored using TLC. 5-BrMF and labeled penicillin-G fluoresced and were visible on the TLC plate. Penicillin-G and 18-crown-6 were made visible by exposing the TLC plate to iodine vapor or dipping the TLC plate in 5% sulfuric acid solution in ethanol. Table 6.1 shows the  $R_f$  values for optimizing the TLC experiment to separate the products of Procedure 5. Mobile phase compositions that were tried to optimize reaction mixture separations are also listed in Table 6.1. A mobile phase of 1:9 methanol-to-chloroform was used to separate the product from unreacted 5-BrMF on a silica column. Five-mL fractions were collected and analyzed with mass spectrometry to determine whether the product formed. None of the fractions collected showed that product was present. This was probably because the product had not formed at all, or it decomposed in the silica column. These results indicated that a new reaction scheme and better separation techniques must be devised that will eliminate the presence of acetone and allow us to isolate the product without decomposition. When the TLC showed the disappearance of 5-BrMF, the reaction was stopped and the reaction mixture was passed through a column packed with silica gel 60A mesh size 320 - 400. Twenty fractions were collected, the UV/Vis spectrum of each fraction was obtained and compared with the spectrum of individual starting materials to identify which compound was eluting from the column.

Table 6.2 shows the UV/Vis maximum absorption wavelength ( $\lambda_{\max}$ ) of starting materials and the fractions collected from the column. UV spectrum of the reaction and each fragment collected show that reaction had occurred, but it does not say whether it was 5-BrMF reacting with itself or with penicillin-G.

Figure 6.10 shows the ESI-MS spectrum of the reaction mixture of Procedure 5 before separation. The sodium adduct of the product is observed at 701 amu.

**Table 6.1:  $R_f$  values for separation of the reaction components of procedure 5 (labeling reaction in acetone in the absence of tetramethylammonium hydroxide)**

Mobile Phase	Product	5-BrMF	Penicillin-G	18-crown6
MeOH/H <sub>2</sub> O 9/1	0.67	0.8	1.0	1.0
MeOH/H <sub>2</sub> O 1/1	0.78	0.89	1.0	
MeOH/H <sub>2</sub> O 3/7	0.57	0.82	---	
MeOH/CH <sub>2</sub> Cl 1/3	0.72	0.57	---	
MeOH/CH <sub>2</sub> Cl 1/9	0.65	0.41	0.46	
MeOH/CH <sub>2</sub> Cl 5/9	---	---	---	
CH <sub>2</sub> Cl/AcN 9/1	0.0	0.0	0.0	
100% AcN	---	---	---	
100% MeOH	0.67	0.72	0.90	
100% H <sub>2</sub> O	0.64	0.86	1.0	1.0

Dashed lines indicate that the spot was not observed on the plate after the run was completed.



**Table 6.2:  $\lambda_{\max}$  for starting material and different collected fractions of reaction mixture of procedure 4**

	$\lambda_{\max}$ (nm)	Reference solvent	Absorbance
<b>18-crown-6</b>	----	DMF	----
<b>Penicillin-G</b>	330	DMF	
	324	MeOH/H <sub>2</sub> O 8/2	
<b>5-BrMF</b>	528, 492, 464	DMF	
<b>(no heating)</b>			
<b>Blank 5-BrMF</b>	310	AcN, 18-crown-6	0.27, 0.26, 0.24
<b>reaction mixture</b>	524	5-BrMF in DMF	1.24
	492		0.72
	460		0.48
<b>reaction mixture</b>	524	DMF	2.05
	520		2.05
	492		1.36
<b>Fraction 1-5</b>	----	DMF	----
<b>Fraction 6-10</b>	330	DMF	----
<b>Fraction 11-15</b>	310, 528, 492, 464	DMF	----
<b>Fraction 16-20</b>	524, 520, 492, 454, 310	DMF	----

Figure 6.10: MS spectra of the labeling reaction product in acetone (procedure 5)

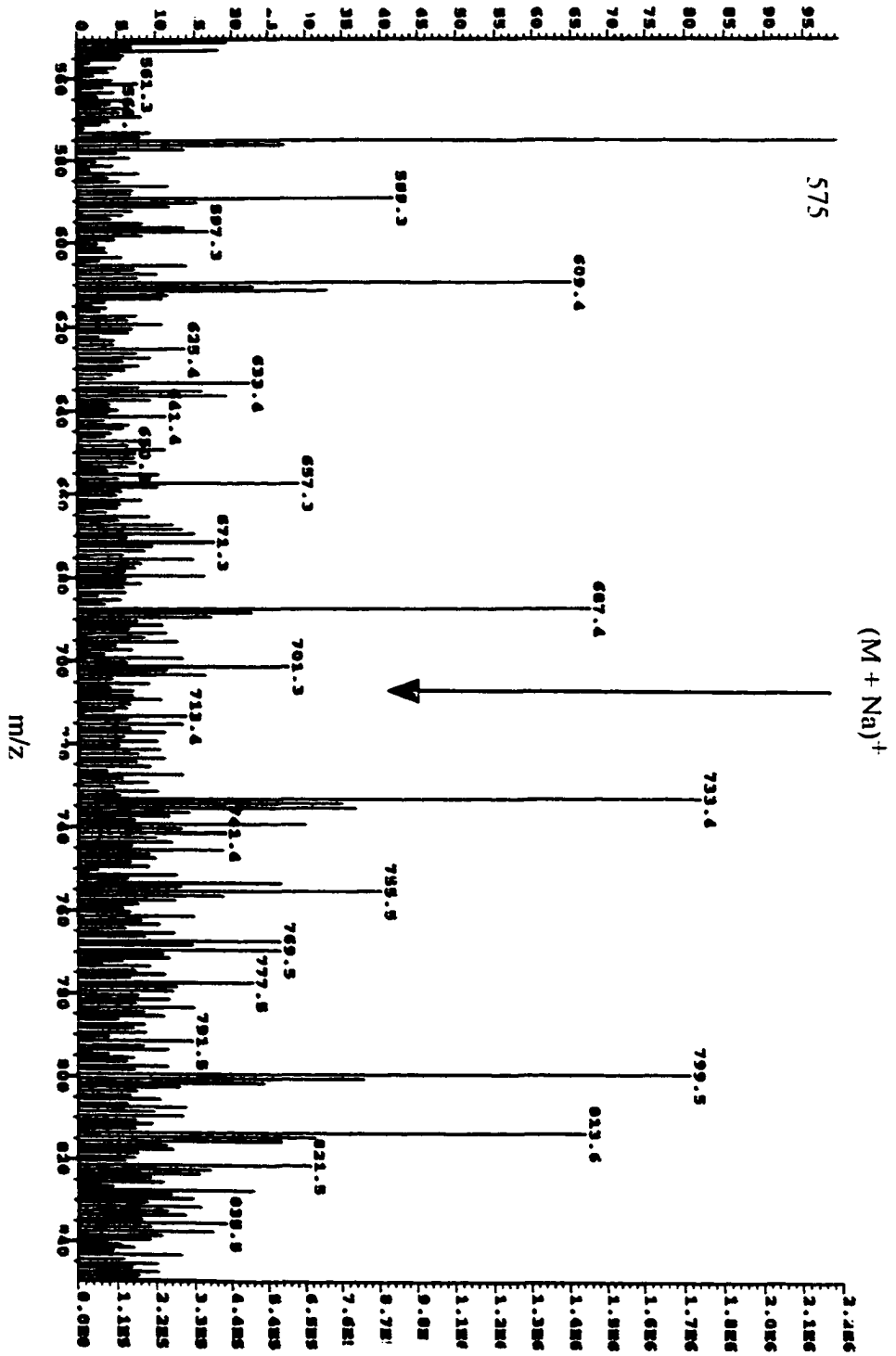
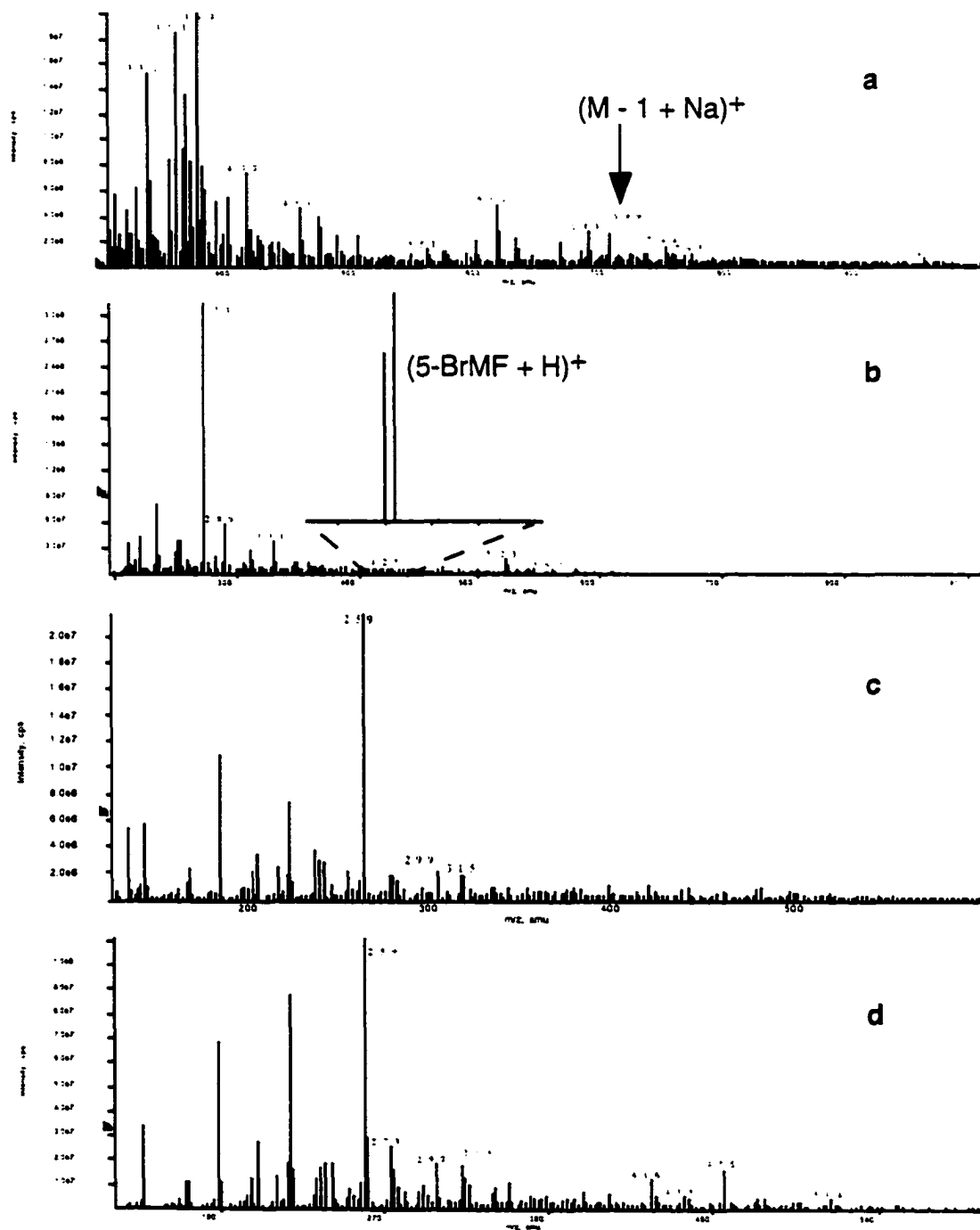


**Figure 6.11: ESI/MS spectra of reaction in acetone in the absence of tetraethyl ammonium hydroxide organic base after passing the reaction mixture from a silica gel column. From top to bottom a) fraction 20, b) fraction 15, c) fraction 10, d) fraction 5 collected from the column**



275

but there are also many other higher molecular weight peaks present indicating the possibility of other side reactions.

Figure 6.11 shows the ESI-MS spectra for fractions 5, 10, 15 and 20 of the reaction of Procedure 5. This procedure lacks the organic base tetramethyl ammonium hydroxide. The reaction mixture was passed through a silica gel column and each collected fraction was injected into a ESI mass spectrometer. The weak peak at 701 amu could be (molecular ion + Na)<sup>+</sup> that indicates the presence of the product, but there are also many more peaks that suggest side products are also present.

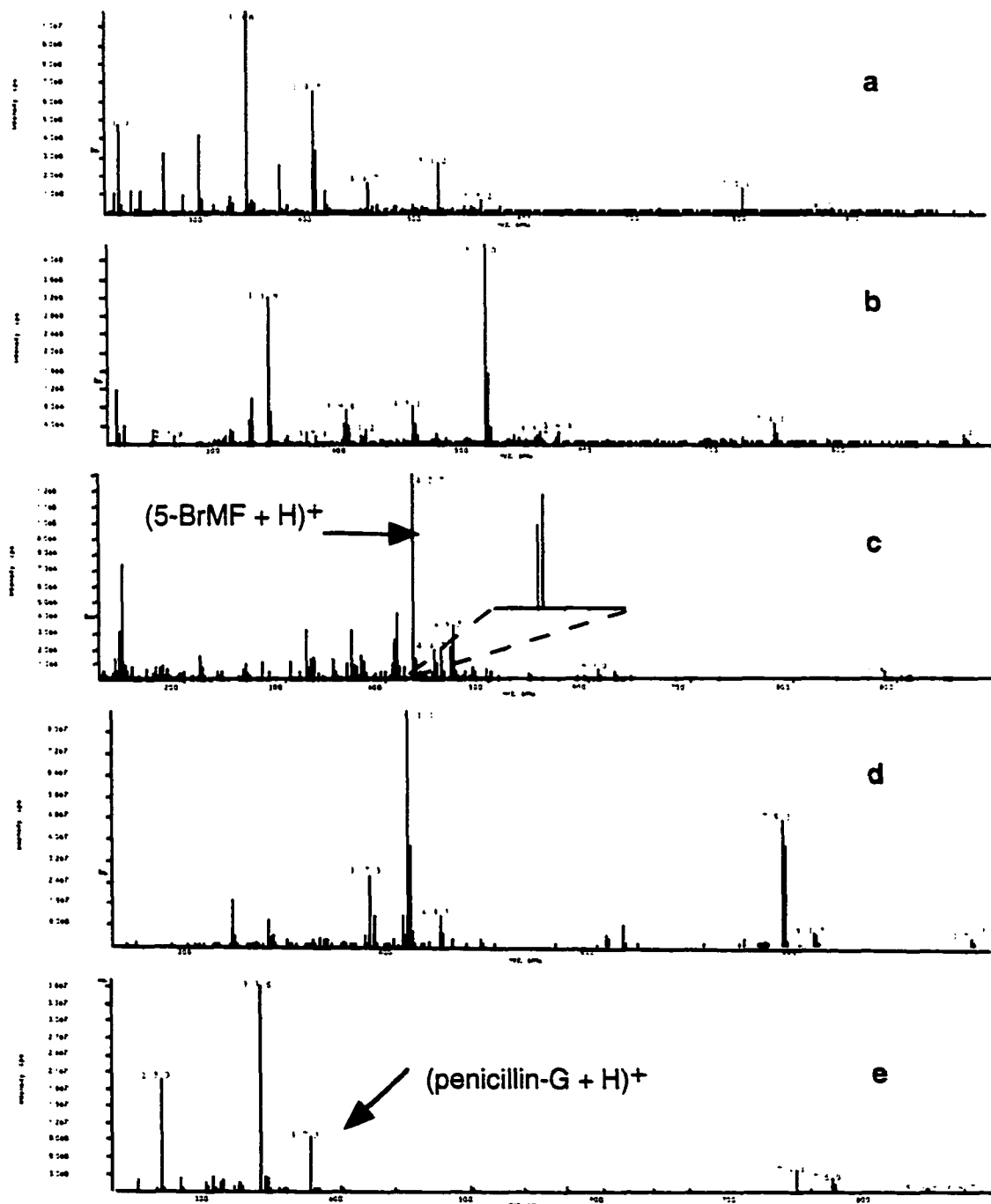
Figure 6.12 shows the ESI-MS spectra of a) blank 5-BrMF, b) blank penicillin-G, c) 5-BrMF without heating, d) penicillin-G without heating and e) a mixture of 5-BrMF and penicillin-G without heating. This figure also shows that a mixture of 5-BrMF and penicillin-G without heating (Fig. 6.11e) lack the 5-BrMF peak.

Figure 6.13 is the negative ion ESI-MS spectra for the fractions 5, 10, 15 and 20 collected from the column when procedure 5 was done. Procedure 5 uses acetone as a solvent, but lacks the presence of tetraethylammonium hydroxide. The product, with a very low intensity, is observed but many side products from self-reaction of 5-BrMF are also present.

Figure 6.14 shows the negative ion mode ESI-MS spectra for a) blank reaction of 5-BrMF, b) 5-BrMF without heating, c) blank reaction of penicillin-G and d) a mixture of penicillin-G and 5-BrMF without heating. Figures 6.10-6.14 show that acetone is not a good solvent for this labeling reaction despite being used by many researchers (Mukhrejee, et al).<sup>17, 18, 20</sup>

In procedure 6 the reaction was repeated in DMF solvent. Before purification, the reaction mixture was injected onto a capillary for 5 s at 1000V. The capillary length was 35 cm and the applied voltage was 400 v / cm. Figure 6.15 shows the electropherogram of the

**Figure 6.12: ESI/MS spectra of reaction in acetone in the absence of an organic base. From top to bottom a) blank 5-BrMF, b) blank penicillin-G, c) 5-BrMF without heating, d) penicillin-G without heating, e) mixture of 5-BrMF and penicillin-G without heating**



**Figure 6.13: Negative ion mode ESI/MS of labeling reaction in acetone in the absence of an organic base. The reaction mixture is passed through a column and a) fraction 20, b) fraction 15, c) fraction 10, and e) fraction 5 are collected from the silica gel column**

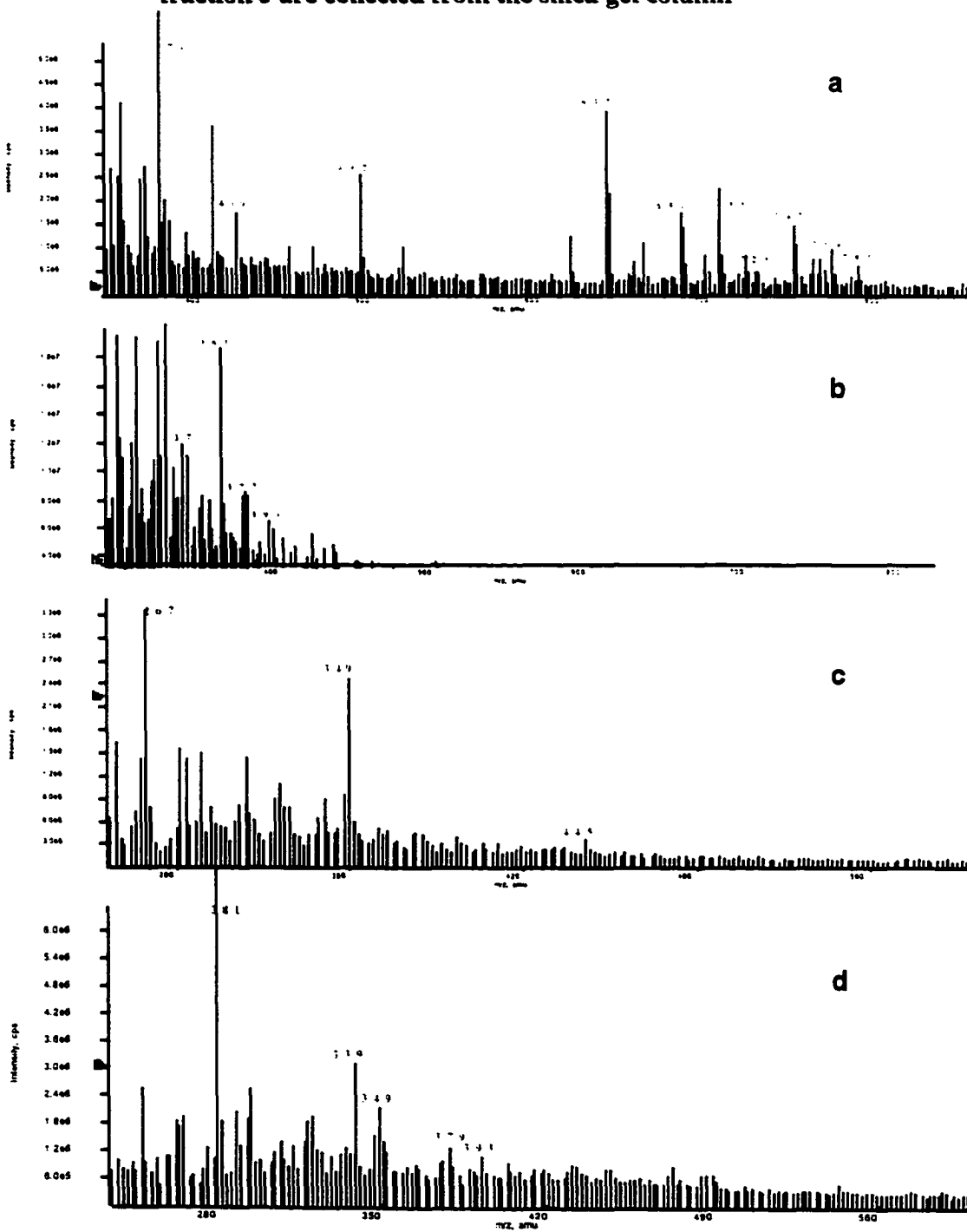
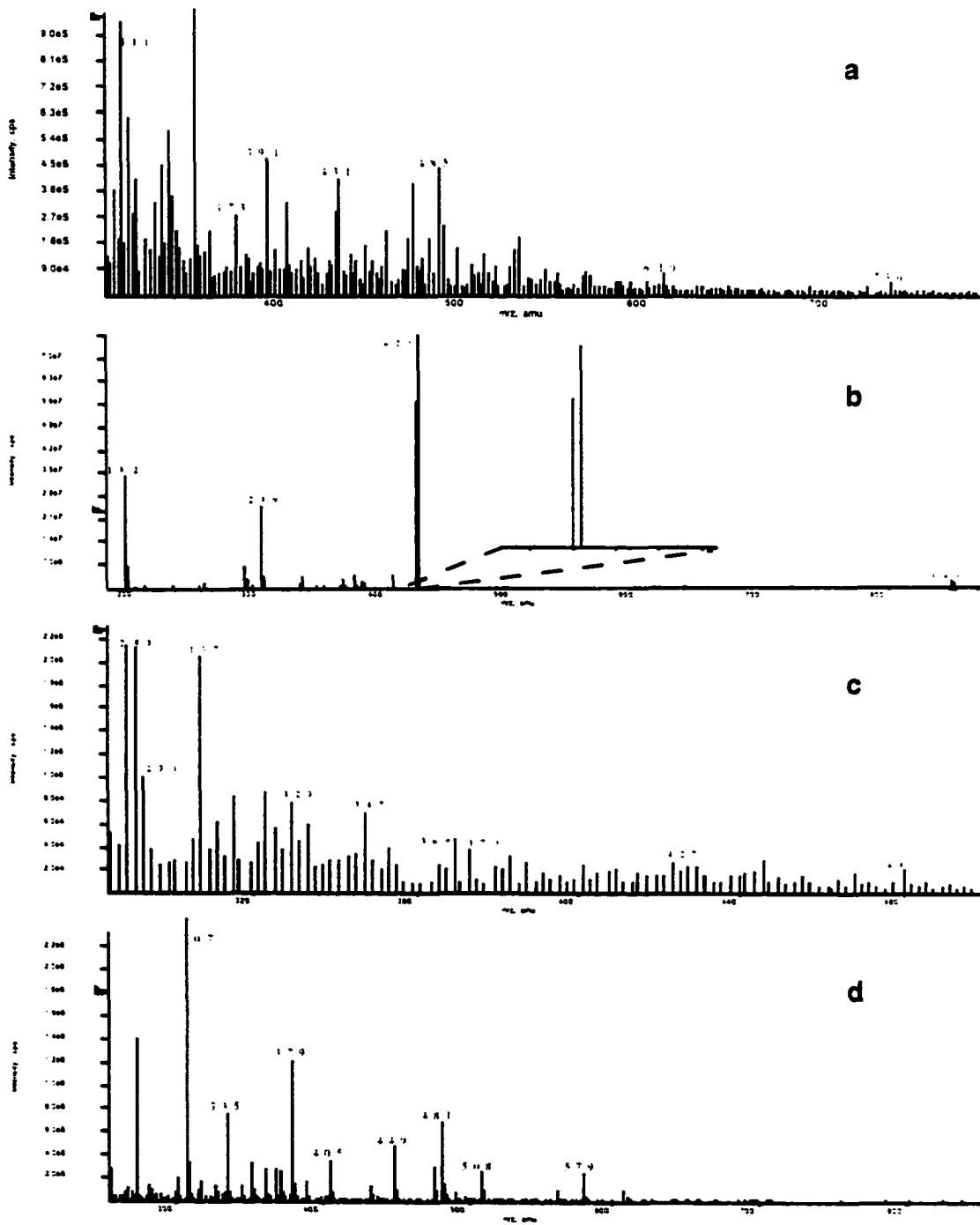


**Figure 6.14: Negative ion mode ESI/MS of reaction in acetone in the absence of an organic base. a) blank reaction of 5-BrMF, b) 5-BrMF without heating, c) blank reaction of penicillin-G and d) mixture of 5-BrMF and penicillin-G without heating**



reaction mixture. For DMF solvent, there are not as many products present as compared to when acetone is used as the solvent.

Figure 6.16 shows the chromatograms obtained by injecting the sample and blank of the reaction of procedure 6 under optimized conditions. Standards such as 18-crown-6, penicillin-G, and 5-BrMF were also injected onto the column separately and were used to assign some of the peaks on the chromatogram from the sample. Figure 6.16 shows a peak at 17.5 minutes which was not present in the blank, and thus was concluded to be labeled penicillin. However this did not resolve our initial problem of trying to isolate labeled product from the host of other side products that were seen in the electropherogram of Figure 6.15.

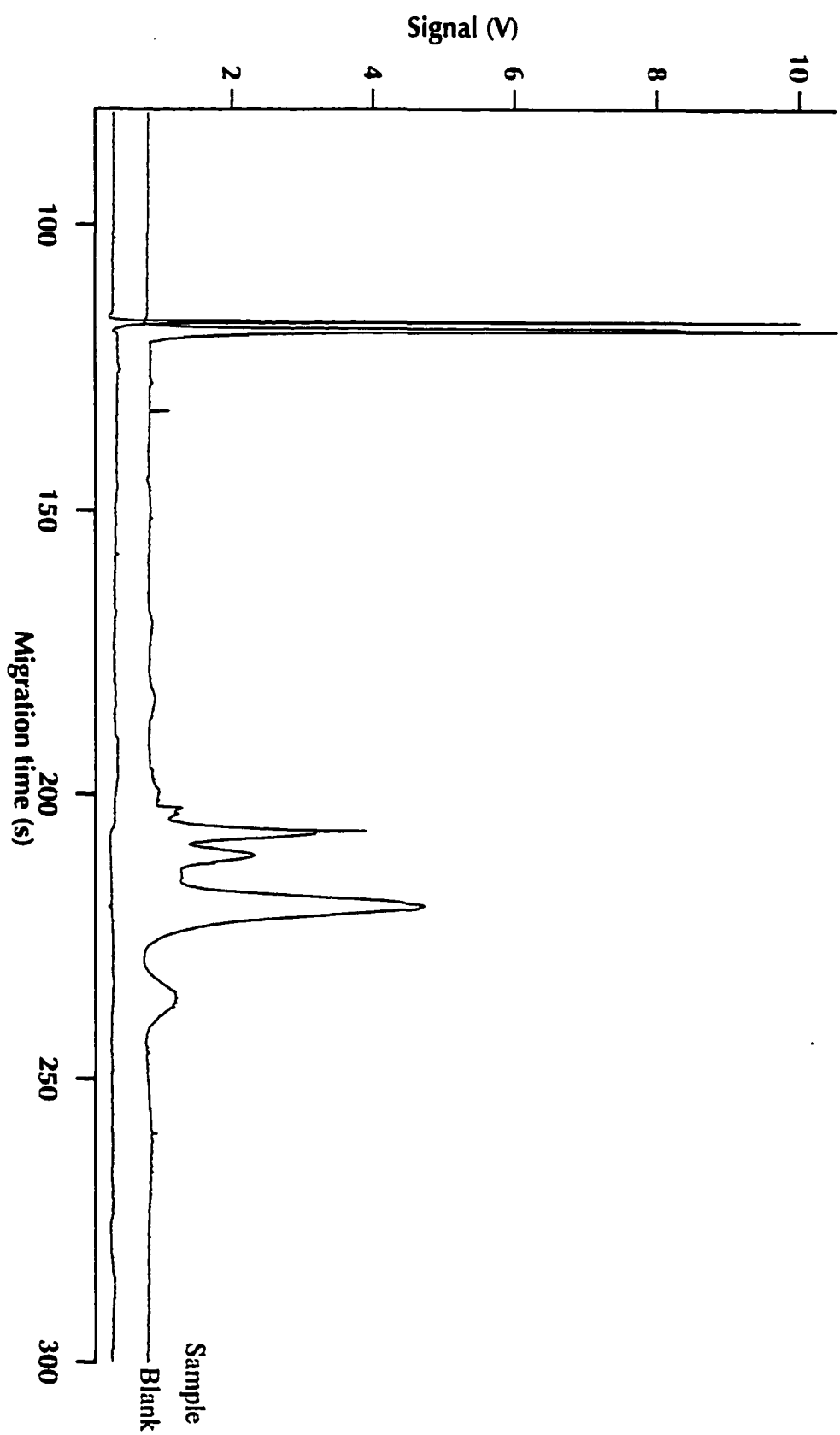
Figure 6.15 shows the electropherogram of the reaction mixture of the Procedure 6. HPLC gives one peak for the product whereas CE gives 4 peaks. These results clearly illustrate the superiority of CE over HPLC in separating and detecting these compounds. A single peak in HPLC may be further separated by CE to show that multiple compounds are present and that they have coeluted to give one peak, in HPLC as demonstrated by this example.

Figure 6.17 shows the positive ion mode ESI-MS spectrum of the HPLC purified product of Procedure 6 before HPLC separation. The positive ion spectrum further shows that sodium and potassium adducts are also present at  $m/z$  values of 701.0 amu and 717.0 amu which correspond to the (molecular ion + Na)<sup>+</sup> and (molecular ion + K)<sup>+</sup> respectively. Isotope patterns of the (molecular ion + 1)<sup>+</sup>, (molecular ion + Na)<sup>+</sup>, and (molecular ion + K)<sup>+</sup> were also calculated for comparison.

Figure 6.18 shows the expansion of the peak at 679 amu and 717 amu along with the theoretical molecular weight calculations considering isotopic contribution to the molecular weight. Very close matching of theoretical molecular weights, considering isotope contributions and natural abundances of each isotope, indicated the presence of



Figure 6.15: Electropherograms of labeling reaction products in DMF solvent (procedure 6). CE conditions are similar to Fig. 6.4.



**Figure 6.16: HPLC separation of the labeling reaction component. a) 490 nm channel, b) 310 nm channel of a diode array detector for HPLC. Peak A is penicillin-G, B is 5-BrMF and its dimer, C is 18-crown6 and D is the labeled penicillin-G (final product)**

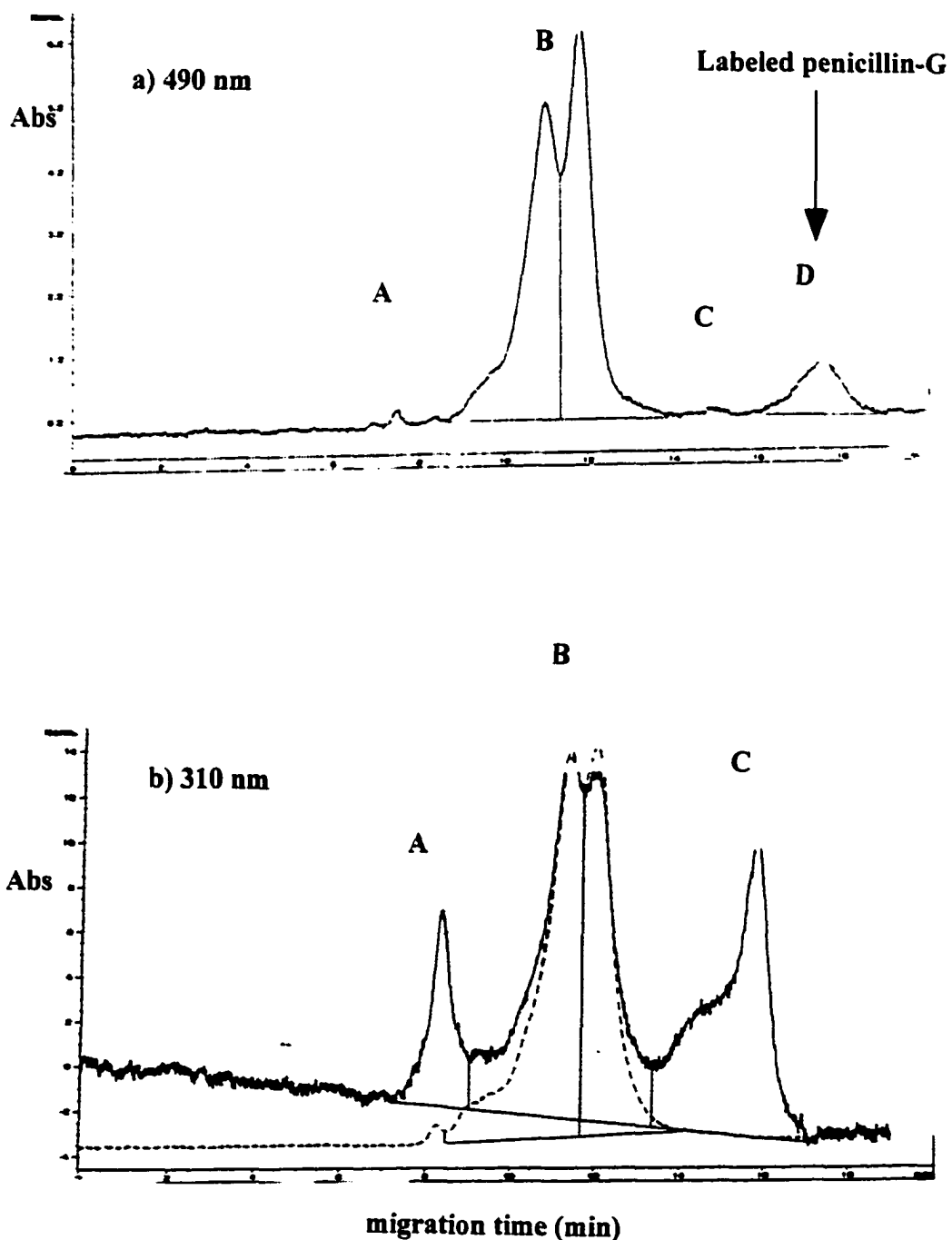
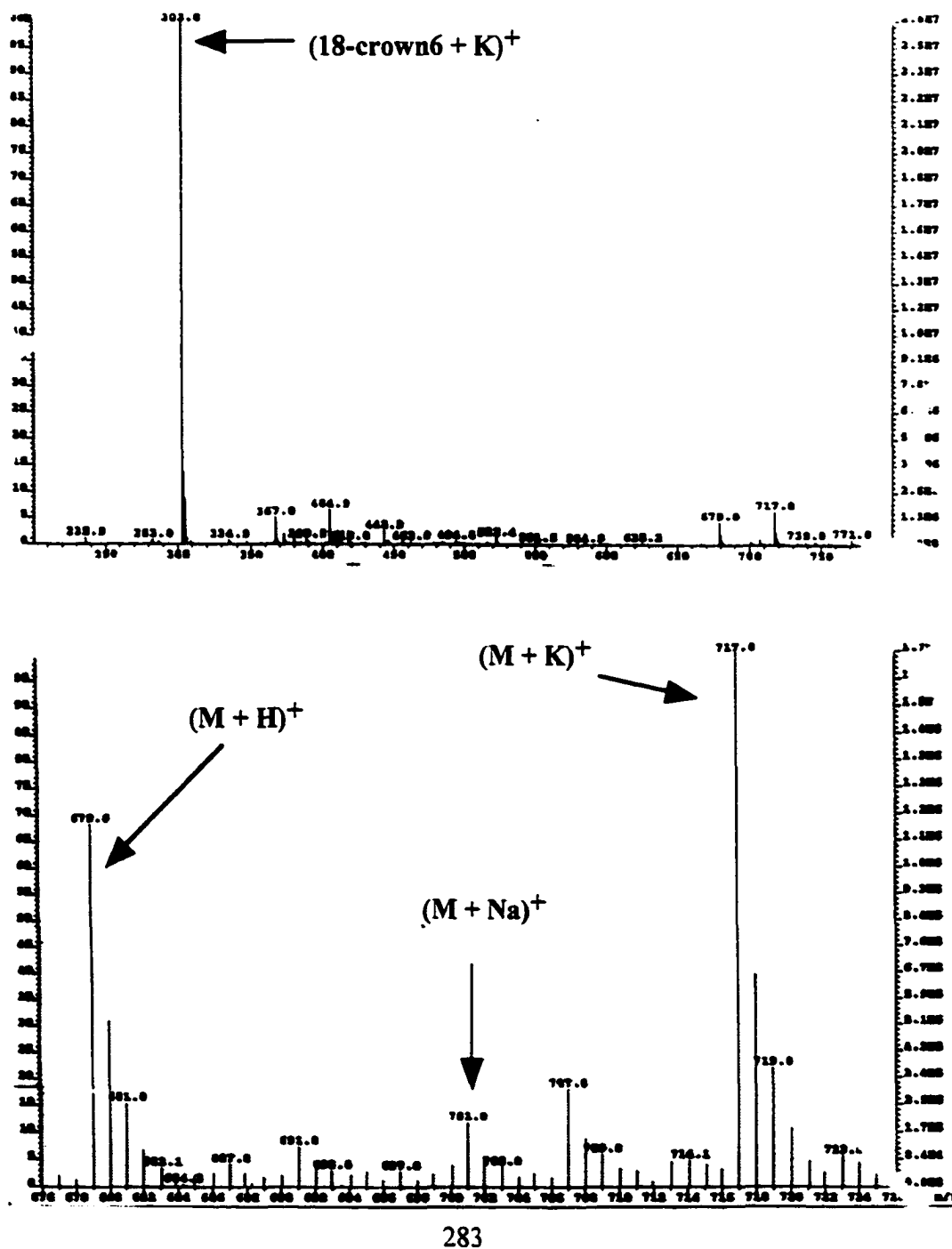
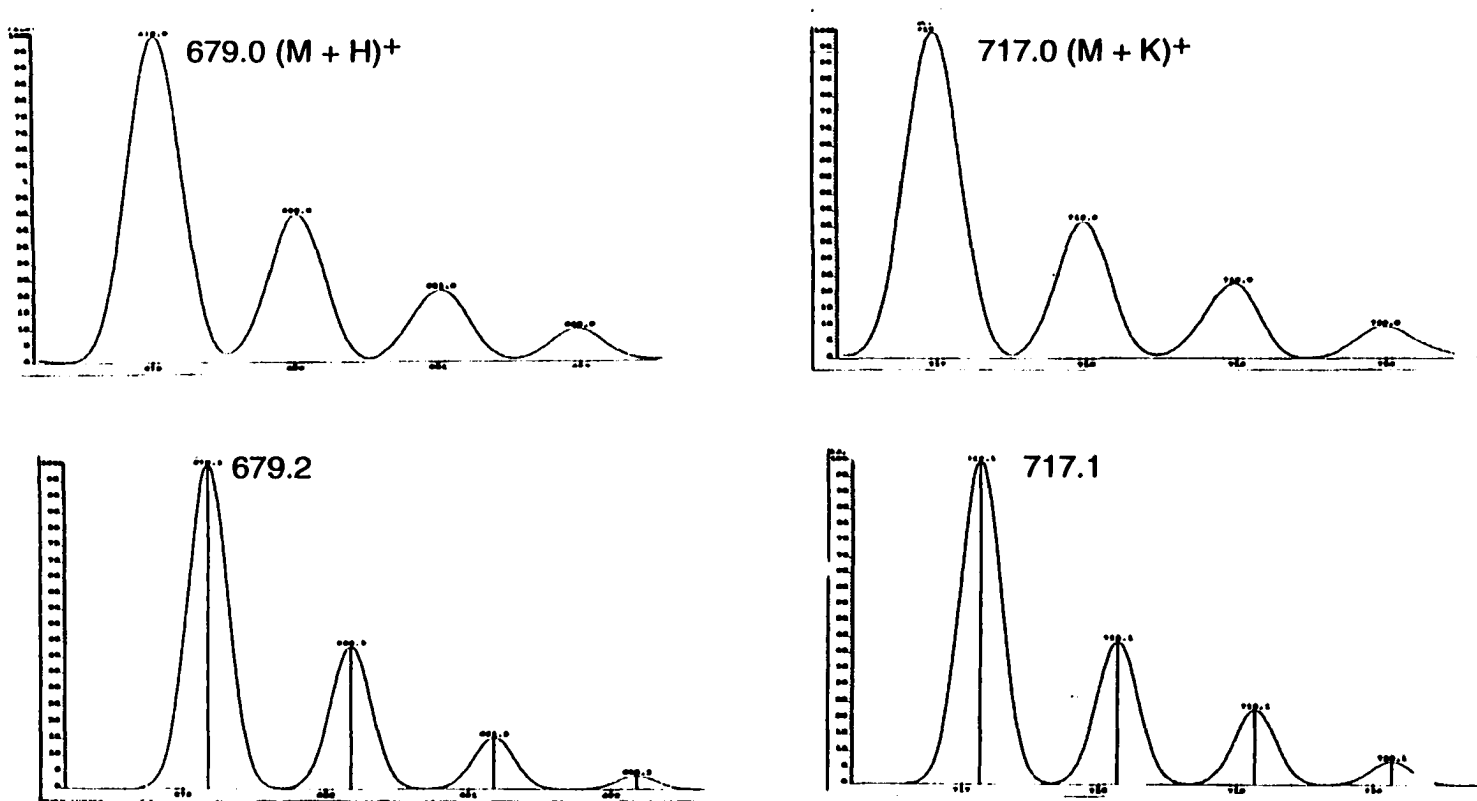


Figure 6.17: Positive ion ESI/MS spectra of the labeling reaction in DMF

(procedure 6) before HPLC separation (preparation TLC purification). Top spectrum shows the whole range and the bottom spectrum is the expansion of  $M^+$  and its related adducts



**Figure 6.18: Hydrogen and potassium adducts of the labeling reaction in DMF. The top spectra are the expansion of the experimental positive ESI/MS spectra and the bottom ones are theoretical molecular weight calculations and corresponding isotope patterns of the molecular weights with relative abundances for the isotopes.**



labeled penicillin-G. Procedure 6 was suggested after realizing that DMF, unlike acetone, is a non-reactive aprotic solvent that can enhance  $\text{SN}^2$  reactions and furthermore all the reactants needed for the synthesis were readily soluble in DMF.

Figure 6.19 shows the positive ion mode ESI-MS spectrum of the product of procedure 6 after HPLC purification. The strong peak of  $(18 \text{ crown-6} + \text{K})^+$  at 303 is eliminated by separation and the major peak at 733 is  $(\text{M} + \text{K})^+$ .

Procedure 7 was repeated under the same conditions as Procedure 6 except the presence of 18-crown-6. Figure 6.20 and Figure 6.21 show both positive ion mode and negative ion mode ESI-MS spectra of the reaction product of Procedure 7 after purification by a Sep-Pak  $\text{C}_{18}$  cartridge. A very clean spectrum is shown with the molecular ion present by itself in the negative ion mode at 677.2 amu (Figure 6.21) and in positive ion mode (Figure 6.20) at 701 amu (sodium adduct) and 723 amu (potassium adduct). The peaks at 701 and 723 amu,  $(\text{molecular ion} + \text{H})^+$  and  $(\text{molecular ion} + \text{Na})^+$ , confirm the presence of the labeled penicillin-G, but the peak at 425 amu shows the presence of non-reacted dye. This experiment demonstrates the need for the presence of 18-crown-6, to act as a catalyst to complex the potassium ion of the penicillin-G, producing a bare carboxylate ion as a nucleophile to replace the bromide ion of the 5-BrMF.

The reaction represented by Procedure 7 did not yield better results than that of Procedure 6, as once again side reactions were detected. The peak at 425 amu shows the presence of non-reacted 5-BrMF (Figure 6.20).

After HPLC purification and structure elucidation of the product, this material was injected into an ESI-MS instrument to verify that its purity matched the MS standards. Both the positive ion mode and negative ion mode ESI-MS spectra of the HPLC-purified product with one sharp peak for the labeled penicillin-G indicated its purity. UV/Vis spectrum of the purified labeled penicillin-G showed an absorption maximum at 500 nm that has a red shift from 488 nm of 5-BrMF, indicating that the reaction has occurred.

**Figure 6.19: Positive ion ESI/MS spectrum of the HPLC-purified product of labeling reaction in DMF (Procedure 6). The sodium adduct of the 18-crown-6 is separated and the potassium adduct of the labeled penicillin-G is the major ion.**

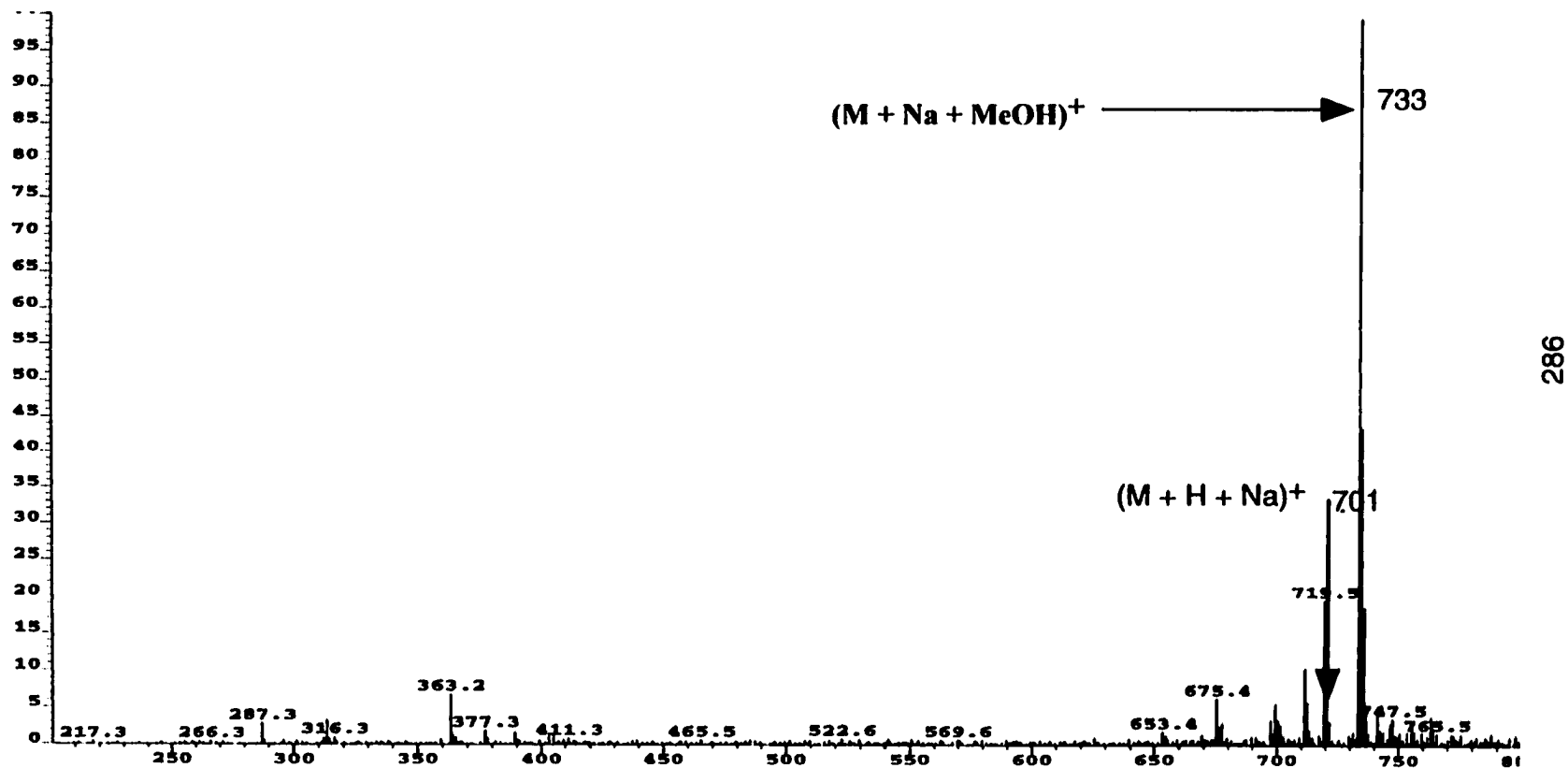


Figure 6.20: Positive ion mode ESI/MS of the labeling reaction in DMF with no 18-crown6 present (procedure 7)

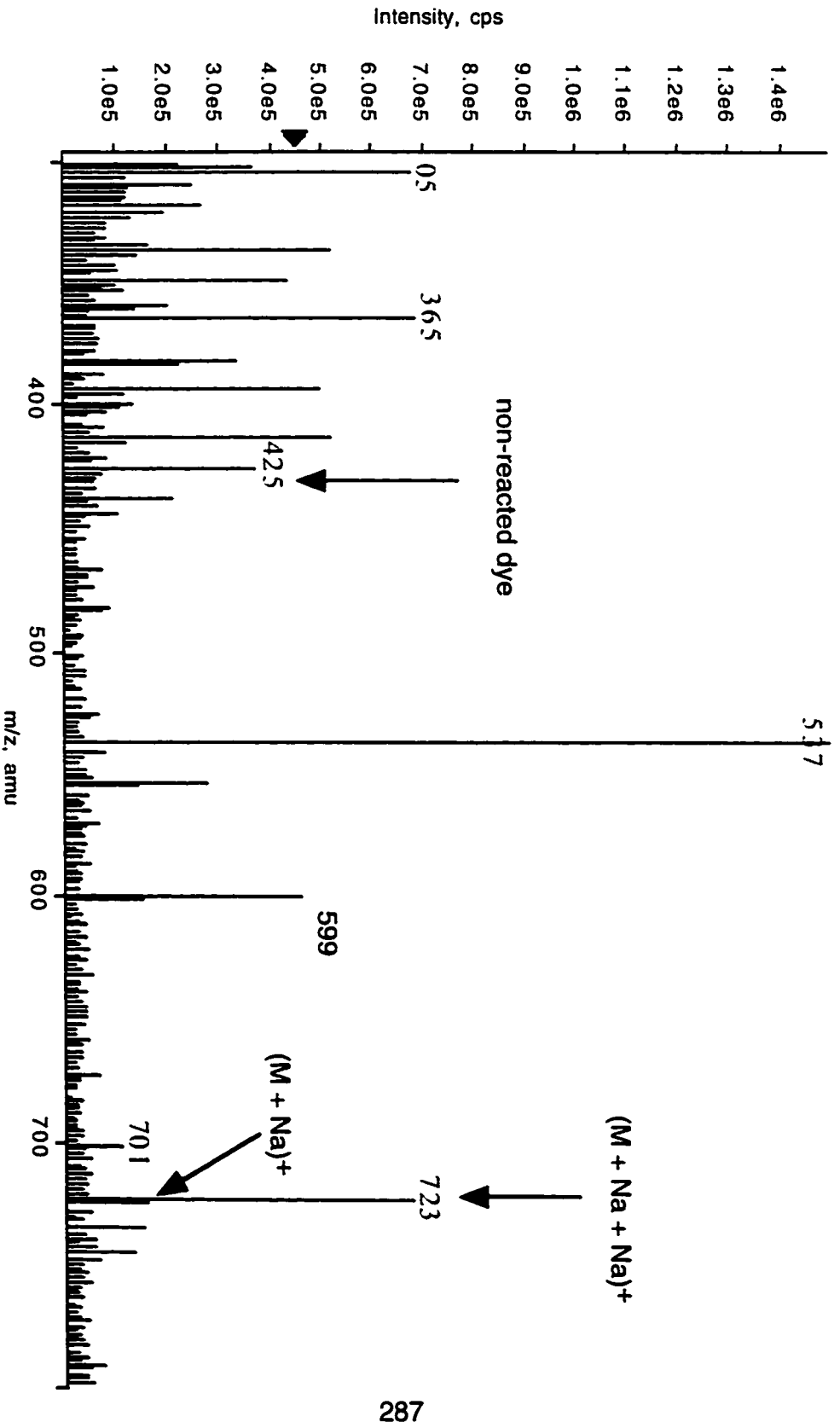


Figure 6.21: Negative ion mode ESI/MS of the labeling reaction in DMF with no 18-crown-6 present (Procedure 7)

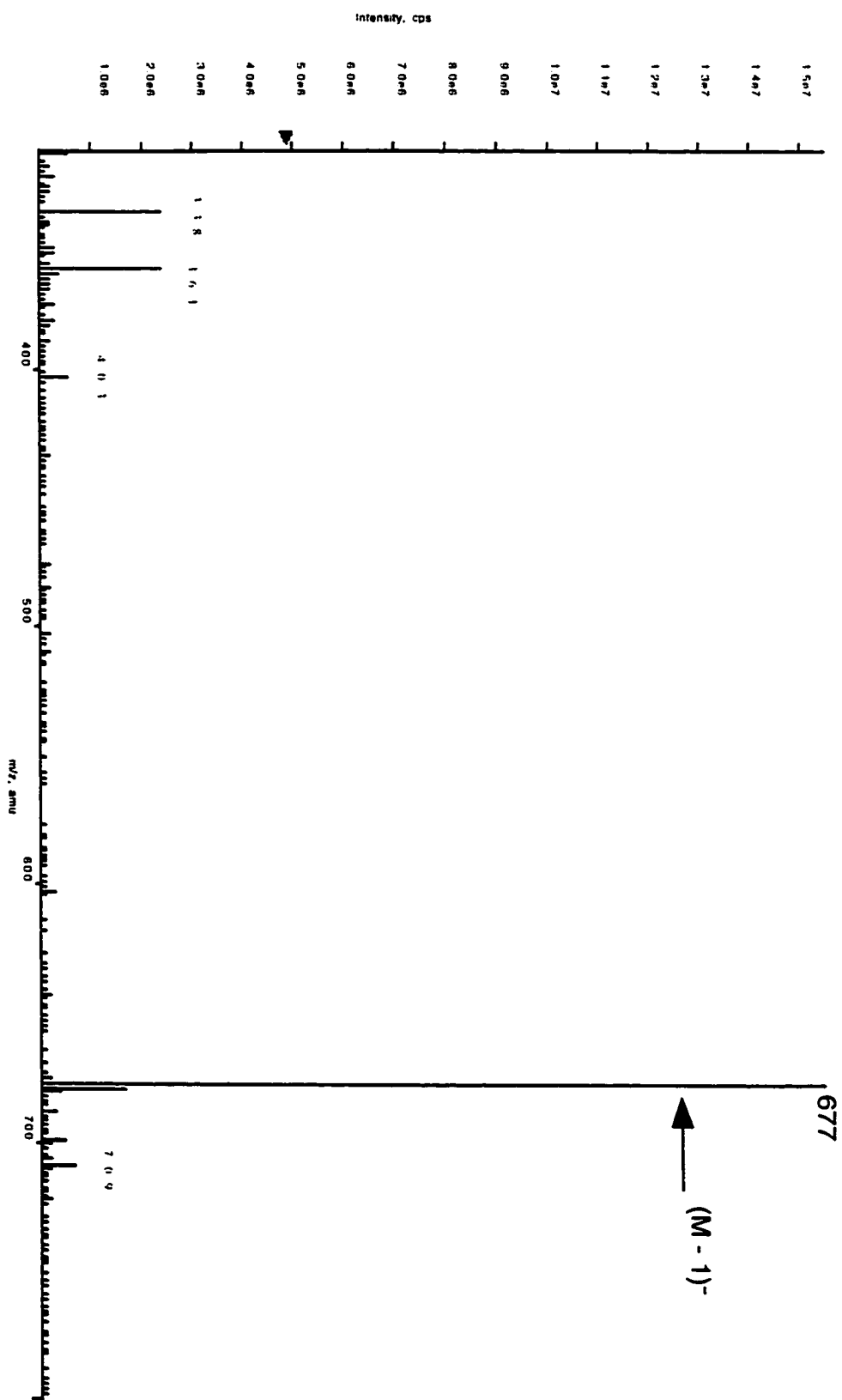




Figure 6.22: 600 MHz NMR  $^1\text{H}$  NMR spectrum of labeled penicillin-G

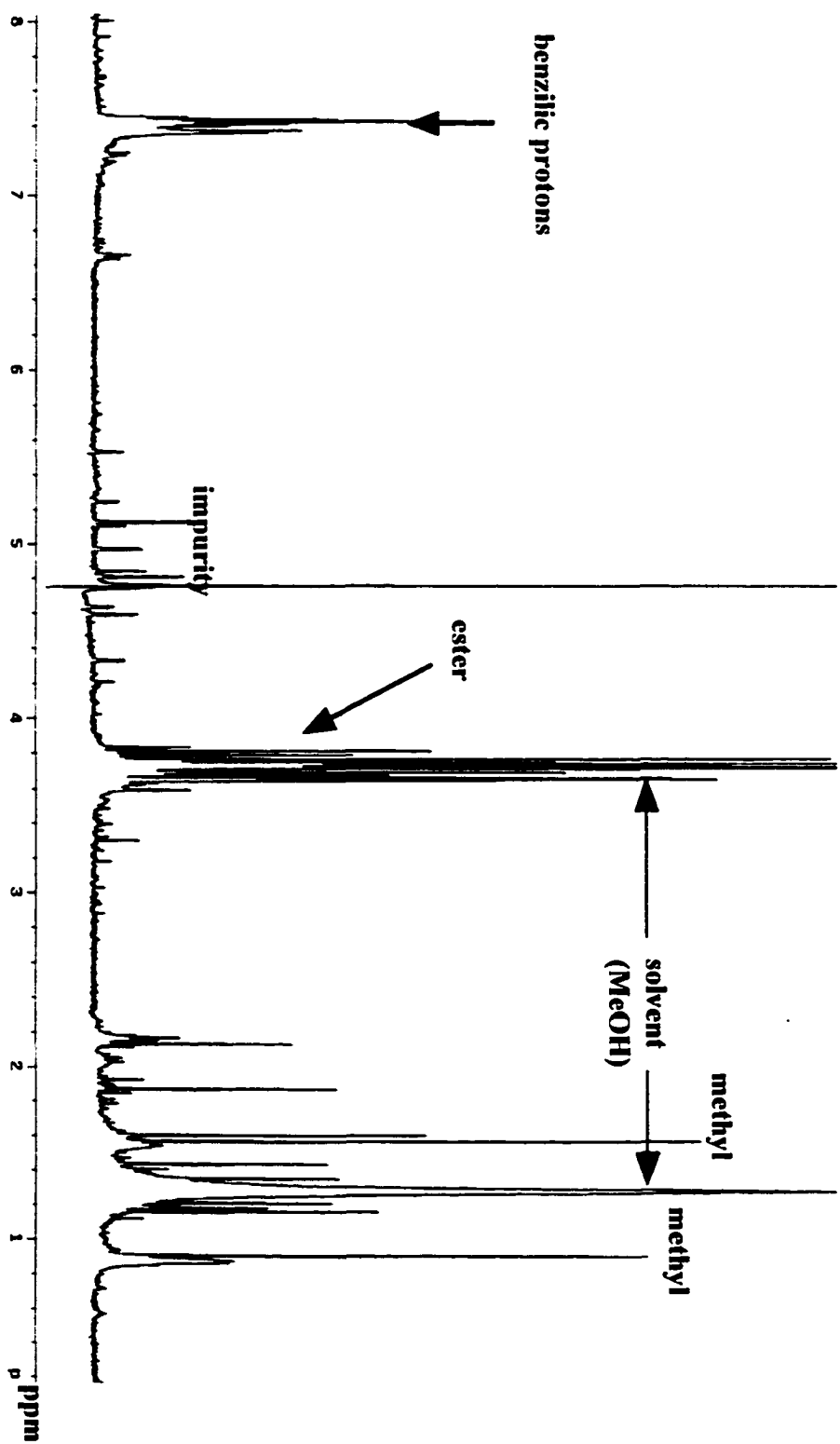
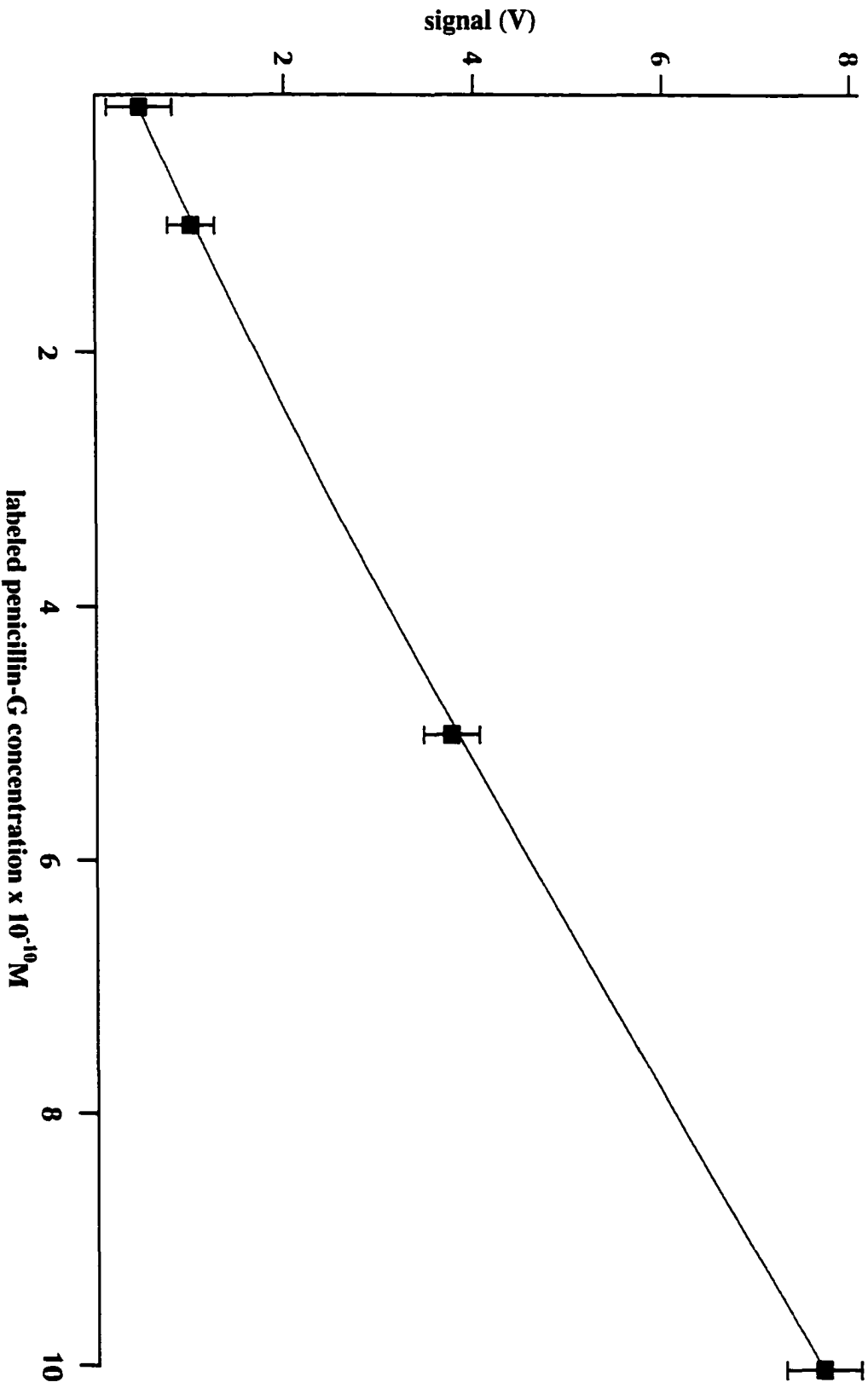


Figure 6.23: Calibration curve of labeled penicillin-G for 5 s injection at 1000 V and CE voltage run 400 V/cm (n = 3)



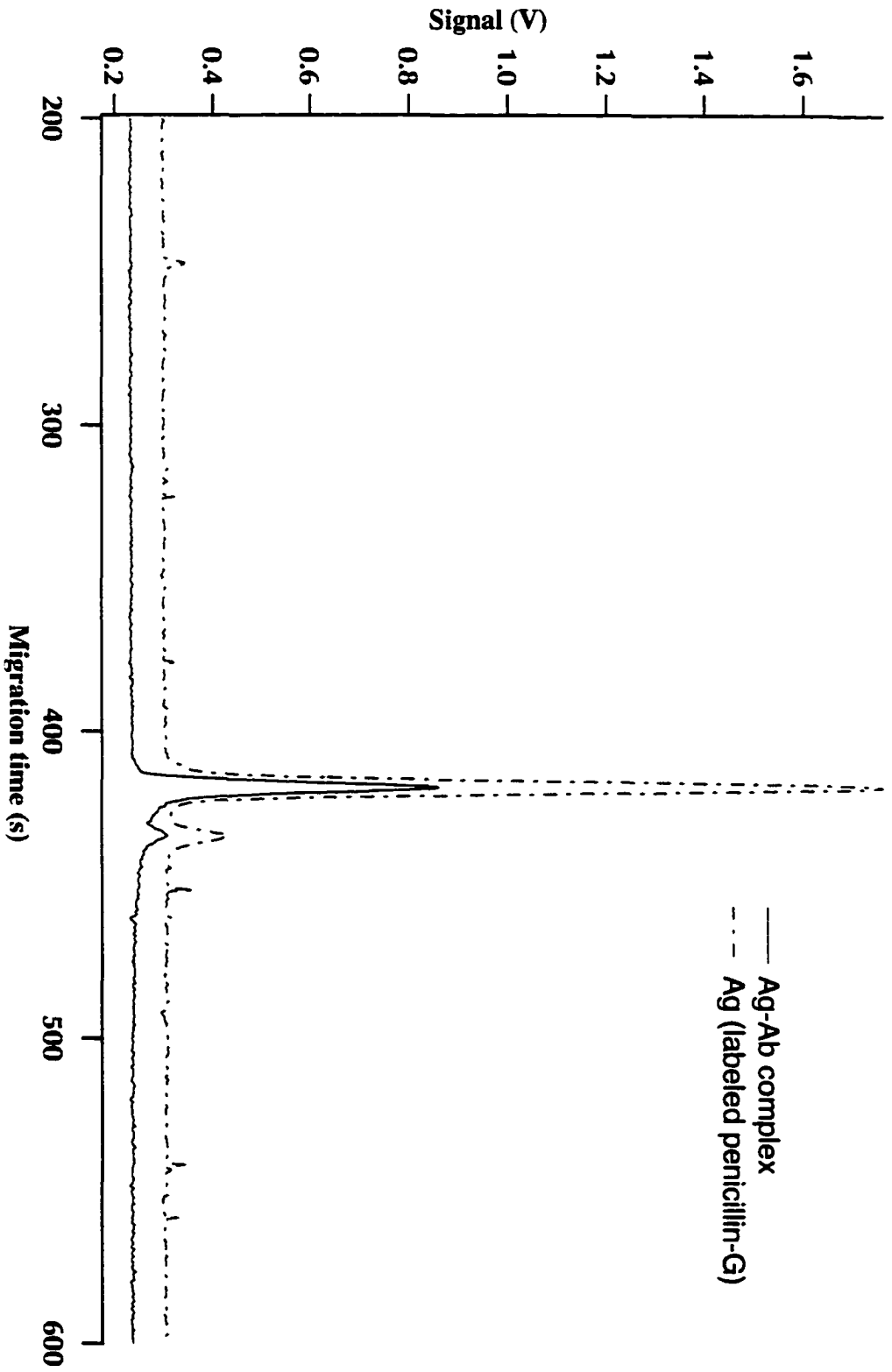
NMR was used for to elucidate the structure. Figure 6.22 is a 600 MHz <sup>1</sup>H-NMR spectrum of the labeled penicillin-G showing peaks that correspond to the expected functional groups. At 7.5 ppm aromatic benzyl protons are found, and at 3.8 ppm peaks which correspond to the ester functionality, O=C-O-CH<sub>2</sub>-, are found. Ester bond formation is in agreement with the structure of the product because this bond should only be seen if a penicillin-dye derivative is present. The NMR solvent was deuterated MeOH with some water impurities that could be seen in NMR spectrum. The Methyl and hydroxyl groups of the MeOH are also observed in NMR spectrum.

After the structure was confirmed the next step was to construct a calibration plot of the product, and to determine its detection limit by using CE-LIF. Figure 6.23 is the calibration plot of product ranging from 10<sup>-9</sup> M to a detection limit of 5.0x10<sup>-12</sup> M. All samples were injected by applying 1000V for 5 s on the capillary, which corresponds to approximately 1 nL of sample per injection. At the detection limit of 5.0x10<sup>-12</sup> M, each injection corresponds to approximately 5.0 x 10<sup>-21</sup> moles of product or about 3000 molecules. This is the lowest detection limit reported for penicillin-G quantitation.

These results lead to the next step in my research to design an ultra sensitive immunoassay for microcystins using the labeled penicillin-G. However, it was found that the antibody does not bind to its antigen and antibody-antigen interaction of penicillin-G does not occur. This suggests that attachment of 5-BrMF, a large molecule, to penicillin-G, disturbs the epitope of the antigen. If this is true, then, an immunoassay involving labeled penicillin-G and its antibody would be impossible and alternative strategies must be developed.

Figure 6.24 shows an electropherogram of labeled penicillin-G before and after it is introduced to the antibody. It would be expected that once the labeled penicillin attaches to its antibody, a significant change in its mobility would occur depending on the

Figure 6.24: Immunoassay reaction of labeled penicillin-G (Ag) with anti penicillin-G (Ab)



weight and charge that antibody carries. However there was no change in migration time even though all other parameters were kept constant, indicating the antibody does not recognize the labeled penicillin-G.

#### **6.4: Conclusion**

Penicillin-G has been labeled with the fluorescent marker 5-BrMF using DMF as the reaction solvent and a trace amount of 18-crown-6 as a catalyst. The product was separated and purified from solution by a C18 reversed phase Sep-Pak column. Preparative TLC and preparative HPLC were used to purify the product. The structure and molecular weight of the derivative was in agreement with mass spectrometry and 600 MHz <sup>1</sup>H-NMR spectroscopy. The separation technique was very effective in isolating pure product from impurities as were seen by the MS and NMR results. 3000 molecules of labeled penicillin-G were detected. It was also shown that the solvents of choice according to the literature for carboxylic acid labeling, i.e MeOH or acetone, are not good solvents and DMF was proven to be the best polar and aprotic solvent. Unfortunately, the labeled product does not complex with anti-penicillin antibody.

## 6.5: References

1. Nishiwaki-Matsushima, R., Ohta T., Nishiwaki, S., Suganuma, M., Kohyama, K., Ishikawa, T., Carmichael, W. W. and Fujiki, H., *J Cancer Res Clin Oncol.* 118, 420-424, 1992.
2. Carmichael, W. W., *Scientific American*, 78-86, January 1994.
3. Falconer, I. R. (Ed.), *Algal Toxins in Seafood and Drinking Water*, Academic Press: London, 1993.
4. Lambert, T. W., Holmes, C. F. B., and Hurdy, S.E., *Environmental Reviews*, 2, 167-186, 1994.
5. Quillam M. A. and Wright, J. L. C., *Anal Chem.*, 61, 1053A-1060A, 1989.
6. Lambert, T. W., Holmes, C. F. B., and Hrudey, S. E., *Environ. Rev.*, 2, 167-168, 1994.
7. Chu, F. S., Huang, X. and Wei, R. D., *J. Assoc. Anal. Chem.*, 73, 451-456, 1990.
8. Lambert, T. W., Boland, M. P., Holmes, C. F. B., and Hrudey, S. E., *Environmental Science & Technology*, 28, 753-755, 1994.
9. Weir, D. M., Herzenberg, L. A., and Blackwell, C., *Handbook of Environmental Immunology*, 4<sup>th</sup> Ed., Vol. 1, Blackwell Scientific Publications: Boston, 1986.
10. Yamamura, Y., Kawakami, J., Santa, T., Kotaki, H., Uchino, K., Sawada, Y., and Iga, T., *J. Chrom., Biomedical Applications*, 567, 151-160, 1990.
11. Van Der Horst, F. A. L., Reijn, J. M., Post, M. H., and Bult, A., *J. Chrom.*, 507, 351-366, 1990.
12. Wolf, J. H., and Korf, J., *J. Chrom.*, 502, 423-430, 1990.
13. Jungling, E., and Kammermeier, H., *Anal. Biochem.*, 171, 150-157, 1988.
14. Elbert, W., Breitenbach, S., Neftel, A., and Hahn, J., *J. Chrom.*, 328, 111-120, 1985.

15. Hayashi, K., Kawase, K., Yoshimura, K., Ara, K., and Tsuji, K., *Anal. Biochem.* 136, 314-320, 1984.
16. Farinotti, R., Siard, Ph., Bourson, J., Kirkiacharian, S., Valeur, B., and Mahuzier, G., *J. Chrom.*, 269, 81-90, 1983.
17. Mukhrejee, P. S., and Kanes, H. T., *Analyst*, 121, 1573, 1996.
18. Mukhrejee, P. S., Desilva, K. H., and Kanes, H. T., *Pharm. Res.*, 12(6), 930-936, 1995.
19. Haugland, Richard P. "Handbook of Fluorescent probes and Research Chemicals". 6<sup>th</sup> Ed., *Molecular Probes*, p. 76, 1996.
20. Mukhrejee, P. S.; and Kames, T., *Anal. Chem.*, 68, 327-332, 1996.

# Chapter 7

## **Arginine labeling chemistry and microgram-scale organic synthesis of an arginine-specific fluorescent reagent and microcystin immunoassay<sup>1</sup>**

---

<sup>1</sup> Some parts of this chapter are being prepared for publication as “microgram-scale organic synthesis of an arginine-specific reagent and microcystin chemical analysis” by **Hossein Ahmadzadeh**, X. C. Le and Norman J. Dovichi.



## 7.1 Introduction

Since 1878 when George Francis of Adelaide, Australia, published the first description of the lethal effects produced by cyanobacteria, research has been done to study cyanobacteria. Paul R. Gorham at the University of Alberta in Edmonton was one of the first scientists to study the properties of toxic cyanobacteria and he has continued since the 1950s.<sup>1</sup>

These microbes are responsible for dramatic die-off of wild and domestic animals. After consuming water contaminated by toxic cyanobacteria, thousands of migrating ducks and geese have perished in the mid-western USA. These toxins and their derivatives are being considered as potential medicines for Alzheimer's disease and other disorders and serve as invaluable tools for exploring questions in cell biology.<sup>1</sup>

Cyanobacterial poison damages the liver and kills animals by causing the blood to pool in the liver. This can lead to fatal circulatory shock within a few hours or to death over several days by liver failure. The symptoms of cyanobacteria poisoning are loss of consciousness, dizziness, falling and remaining quiet, as if asleep, unless touched. When convulsions come, the head and neck are drawn back by rigid spasms that subside shortly before death.

The liver toxins form a family of at least 53 related cyclic peptides. The seven amino acid peptides are called microcystins and five amino acid peptides are called nodularins.

In chapter 6, I described the development of carboxylic acid labeling chemistry for a model compound. Unfortunately, the antibody did not recognize the labeled antigen because of the proximity of the epitope to the labeling site. The carboxylic acid groups of the microcystins are also directly attached to the peptide ring. It is not known whether the peptide ring is part of the epitope. However there must be a spacer arm bridging the biological molecule and the fluorescent tag in order to be recognized by the antibody.<sup>2</sup> To

eliminate the possibility of not being recognized by the antibody, it was decided to label the arginine side-chain of the microcystin. This arginine group is five atoms away from the peptide ring and adding a fluorescent tag to it should not disturb the epitope. The other advantage of labeling the arginine group is that it eliminates the possibility of multiple labeling. There are two carboxylic acid functional groups in microcystin and this leads to three possible products in labeled microcystins. A great amount of effort will be needed to separate these labeled microcystins and check them one-by-one to see which one binds to the antibody. To bypass all these problems, I decided to work on arginine-labeling chemistry.

### **7.1.1 Model compounds for microcystin labeling**

Due to their expense, the reaction could not be optimized directly on microcystins. After optimizing all reaction parameters on the model compounds, it would be then feasible to label microcystin.

The first model compound chosen was N<sub>α</sub>-acetyl-L-arginine. This compound was chosen because of its similarity to the arginine side chain of microcystin. The N-terminus of this amino acid is blocked in order to eliminate the possibility of free amine labeling and to mimic microcystin structure in which the N-terminus of arginine is changed to a peptide bond.

The second model compound chosen was cyclo (Arg-Gly-Asp-D-Phe-Val). This model compound is very similar to microcystin. Both are cyclic peptides with arginine side chains. The chemistry that is optimized for a single amino acid may not be true for a cyclic peptide like microcystin unless it is checked on a similar cyclic peptide.

### **7.1.2 Microgram-scale organic synthesis and labeling**

For the first model compound, N-acetyl-L-arginine, the optimized weight of the arginine reagent was 10 mg. The second model compound, cyclo (Arg-Gly-Asp-D-Phe-Val), was purchased in 1-mg vials and the whole 1 mg was used. Finally, the microcystin itself was purchased from Cal-Biochem in 500- $\mu$ g scales and all the subsequent labeling chemistry was practiced at this scale. By this point, enough experience was gained to handle microgram-scale organic synthesis.

One limitation of microgram-scale organic synthesis is that we had to rely on the mass spectrometry data to optimize the reactions. An insufficient amount of product was a major problem for doing NMR studies to cross validate the results. Most of the peaks were considered as the possible products of the reactions and there were no further identification studies.

### **7.1.3 Introduction to arginine-labeling chemistry**

Fluorescent labeling is gradually replacing radioactive labeling in immunoassays. Usually the fluorescent label has a spacer arm to separate the biomolecule from the signal generator or label. Traditional spacer arms consisted of aliphatic and/or aromatic hydrocarbons containing two reactive functional groups on the termini. The length of the spacer arm is usually 6-15 carbons to prevent steric interference between the signal generator and the biomolecule.<sup>2</sup>

One amino acid for which a selective fluorescent reagent has not been proposed is arginine. The guanidinium group of the arginine does not react with substances that modify lysine groups, at least not under the mild conditions (neutral pH, aqueous solution, and low temperature) that are preferred for studying functional proteins.

I decided to choose arginine as a labeling site to bypass the need for a spacer arm and also to prevent the possibility of multiple labeling of the carboxylic acid side chain of microcystin.

Arginine itself plays a general role as an anionic binding site in enzymes.<sup>3</sup> Arginine-specific reagents may inactivate the enzyme; loss of enzyme activity is correlated with arginine-lead substrate recognition. It is a common procedure to modify the arginine of an enzyme and reevaluate its activity to see if arginine was involved in binding to the substrate.<sup>4-19</sup>

#### **7.1.4 The chemical properties of the guanidinium group of arginine**

Among the various reactions for modifying functional groups in proteins, the most recent that have been discovered are those for the chemical modification of arginine residues. One reason for this delay is the unique chemistry of the guanidinium group. Its two  $-NH_2$  functional groups do not have the same chemical reactivity as the  $\epsilon-NH_2$  group of the lysine amino acid. The guanidinium ion can be represented by three equivalent resonance forms. This feature is responsible for the pKa being 12.5 for arginine. Another feature of the guanidinium group is the coplanarity of the three nitrogens and the central atom due to the partial double bond character of each of the C-N bonds. This bonding conformation enables the guanidinium side chain of arginine to enter into extended patterns of hydrogen bonding that are unique and perhaps explains the evolutionary selection of arginine as a constituent of proteins.<sup>20-21</sup>

#### **7.1.5 Microgram-scale organic synthesis of an arginine-specific fluorescent labeling reagent**

1, 2 diketones have been used to modify the arginine in different proteins and

enzymes and to study structure-function relationships of proteins.<sup>22-30</sup> Cyclohexane dione, 2, 3 butane dione, and phenylglyoxal have been the most frequent arginine-labeling reagents for the past 50 years.

In order to synthesize a fluorescent labeling reagent specifically for arginine, I decided to couple a diketone functional group to a fluorescent molecule. This coupled reagent has the ability to selectively bind to an arginine group via its diketone functional group and fluoresces via its fluorescent molecule. To link a diketone to a fluorescent molecule is not easy because the nucleophilic group introduced onto a diketone to displace the Br atom of 5-bromomethylfluorescein (5-BrMF) will destroy the diketone functional group faster than doing the displacement reaction. To bypass this problem, I decided to link a mono ketone functionality to a fluorescent molecule and have a second oxidizable group in close proximity to the ketone and oxidize this group to get the second ketone functional group.

## **7.2 Experimental**

### **7.2.1 Reagents**

$N_{\alpha}$ -acetyl-L-arginine, cyclo (Arg-Gly-Asp-D-Phe-Val), and gentisic acid (2, 5-dihydroxybenzoic acid) were purchased from Sigma (St. Louis Mo, USA). Tetramethylrhodamine succinimidyl ester (TMR), 5-bromomethyl fluorescein (5-BrMF), KCN and 3-(2-furoyl) quinoline-2-carboxaldehyde (FQ) were acquired from Molecular Probes (Eugene, OR, USA). Fused-silica capillary (50  $\mu$ m ID, 140  $\mu$ m OD) was obtained from PolyMicro Technologies (Phoenix, AZ, USA). Sodium hydroxide, 2, 3-butanedione, hydroxylamine hydrochloride, and furfurylamine were purchased from Lancaster at

Caledon Laboratories (Georgetown, ON, Canada). Disodium tetraborate and iodine were obtained from BDH Chemicals (Toronto, ON, Canada). HPLC grade MeOH was purchased from Burdick & Jackson, B & J brand (Muskegon, MI, USA). DMF, 3, 5-dimethoxy-4-hydroxy-cinnamic acid, aminoacetophenone, hydrazine, N-methylmorpholine, ninhydrin, EtOH, butanol, acetic acid, ammonium molybdate, ceric sulfate, and benzylbromide were purchased from Aldrich Chemical Company Inc. (Milwaukee, WI, USA). AG 50W and AG MP-50 cation exchanger resins were purchased from Bio-Rad Laboratories (Richmond, CA, USA). Sulfuric acid was purchased from Fischer Scientific (Nepean, ON, Canada). The Bio-Gel P-4 Gel for gel permeation chromatography was purchased from Bio Rad Laboratories, Richmond, CA, USA.

### **7.2.2 Instruments**

ESI-MS was described in the experimental part of the Chapter 6. The positive ion mode was chosen for ESI and usually the sample was dissolved in a mixture of HOAc and MeOH at a 1/9 ratio unless otherwise stated. After optimization the following experimental parameters were chosen: IS 5100, OR 10.0, RNG 330, Q<sub>0</sub> -10, IQ1 -12, ST -16, ROI -11, DF -200, CEM 2300, Neb 4, and Cur 8.

MALDI was performed with a commercial KRATOS-MALDI instrument. Sep-Pak C<sub>18</sub> cartridges were purchased from Waters Millipore Corporation (Milford, Mass, USA). Silica gel plates for TLC were acquired from Eastman Kodak Company (Rochester, NY, USA).

### **7.2.3 Visualizing spots on TLC<sup>30</sup>**

A stock solution of N-acetylarginine (10 mM) in doubly distilled deionized water was prepared to do the TLC experiments.

### **7.2.3.1 Ninhydrine solution**

N-acetyl-arginine was spotted on a TLC plate and dipped into a 0.2% ninhydrine solution in 80% ethanol. Then the plate was heated on a heating block until solvent on the plate was dried. The spot turned white/colorless while the rest of the TLC plate turned brown.

### **7.2.3.2 Iodine vapor**

N-acetyl-arginine was spotted on a TLC plate and was developed with a solvent containing 60% butanol, 15% HOAc and 15% water. The TLC plate was exposed to iodine vapor for 1 hour and a brown spot for N-acetylarginine was observed.

### **7.2.3.3 Sulfuric acid solution**

One droplet of N-acetylarginine was spotted on a TLC plate. After being dried, the TLC plate was dipped into a solution of 5% H<sub>2</sub>SO<sub>4</sub> in 95% EtOH and heated. No spot was observed.

### **7.2.3.4 Molibdo-Cerric solution**

A solution containing 10.64 g ammonium molibdate, 0.5 g cerric sulfate, 80 mL water and 10 mL of concentrated H<sub>2</sub>SO<sub>4</sub> was prepared. The arginine solution was spotted on the TLC plate. After the spot was dried, the plate was dipped into the above mentioned solution and heated gently. While the background on the TLC plate turned blue, the arginine spot was dark blue.

#### 7.2.4 Developing solvent for TLC<sup>31</sup>

Different combinations of two and three component mixture of solvents were used to measure the  $R_f$  values for TLC of N-acetylarginine. BuOH/AcOH/H<sub>2</sub>O with different ratios were tested. A 60:15:15 ratio gave an  $R_f$  value of 0.22, while 60:15:25 ratio gave an  $R_f$  value of 0.25. If both water and acetic acid were increased to a 60:25:25 ratio, the  $R_f$  value also increased to 0.39. This solvent mixture was chosen to develop the TLC plates and monitor the reaction.

#### 7.2.5 Free amine generation from N<sub>α</sub>-acetyl-L-arginine model compound

Arginine with a pKa of 12.5 is the strongest base among the amino acids. To label arginine the most challenging problem is deprotonating it to get a free amine. There are many amine-labeling reagents and labeling free amines is a routine procedure. I have optimized the reaction time and temperature for an amine labeling procedure that will not be discussed here.<sup>32</sup>

Figure 7.1 shows the four different approaches taken to deprotonate the N-acetyl-arginine or convert arginine to ornithine. Sodium hydroxide and sodium hydride bases were chosen to deprotonate the acidic proton on the arginine. Hydrazine and hydroxylamine were chosen to convert arginine to ornithine.

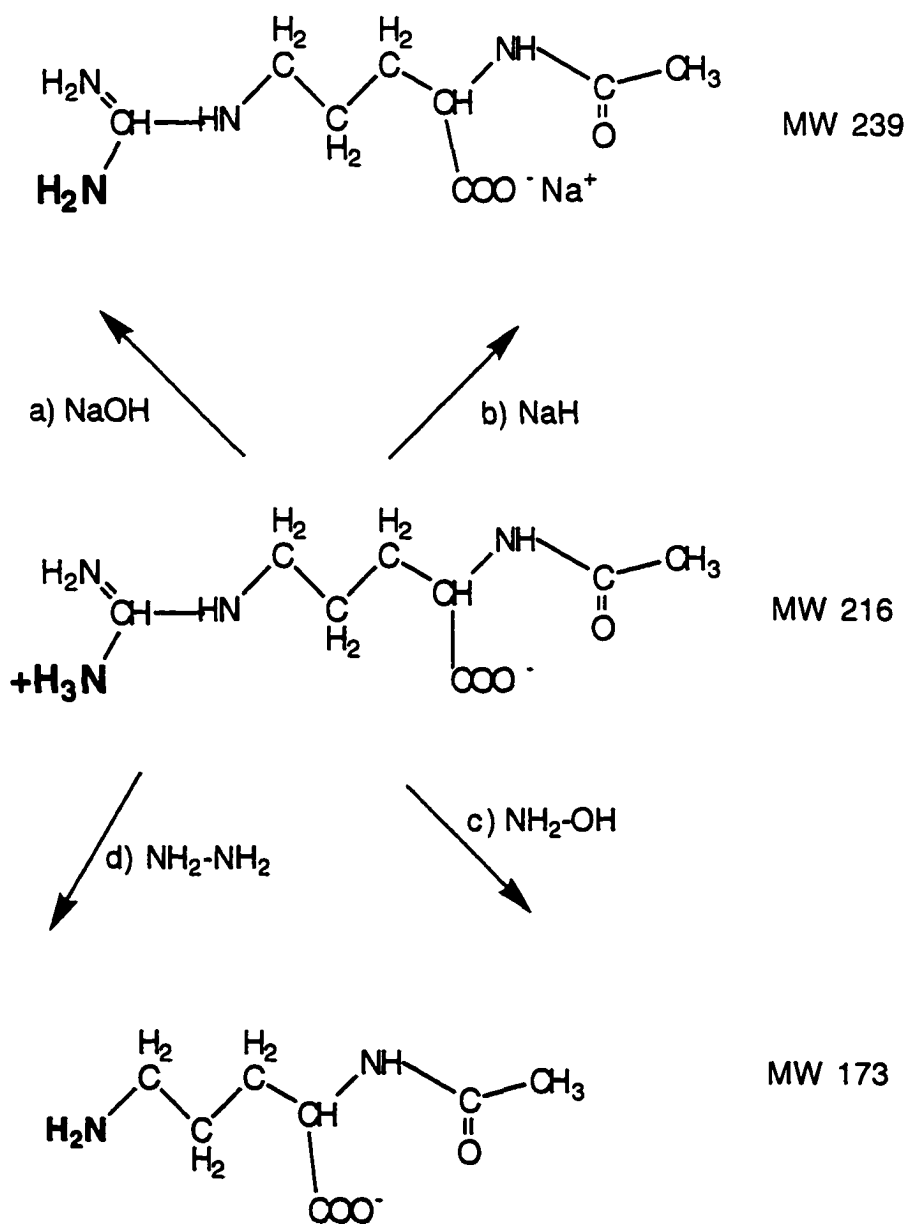
#### 7.2.6 Direct labeling of arginine with amine-labeling reagent FQ

N-acetyl-arginine (0.00216 g) was dissolved in doubly-distilled water (10 mL) to make a solution of N-acetyl-arginine ( $10^{-3}$  M). It was then diluted to  $10^{-4}$  M with NaOH (10 mM) solution to adjust the pH to 13.0.



**Figure 7.1: Four different feasible strategies to deprotonate**

**$N_\alpha$ -acetyl-arginine. a) direct deprotonation using aqueous NaOH, b) NaH reaction under nonaqueous conditions, c) arginine to ornithine conversion using hydroxyl amine, and d) hydrazinolysis reaction**



To a vial containing 100 nmol of dry FQ, 7.5  $\mu\text{L}$  of the N-acetyl-arginine solution (pH 13) was added. Then 2.5  $\mu\text{L}$  of 5 mM KCN was added and the reaction was allowed to go to completion for 30 minutes. Next, the reaction mixture was diluted to 500  $\mu\text{L}$  with 10 mM borate. Arginine concentration after dilution was  $7.5 \times 10^{-4} / 500$  or  $1.5 \times 10^{-6}$  M.

The same reaction was repeated for the blank. All the reagents and conditions were similar except for the presence of N-acetyl-L-arginine. Both sample and the blank were injected onto a 50  $\mu\text{m}$  ID x 141  $\mu\text{m}$  OD uncoated capillary for 5 s at 1000 V. The separation voltage of 400 V/cm was applied and the electropherogram was recorded.

### **7.2.7 Direct labeling of N-acetyl-L-arginine with tetramethylrhodamine N-hydroxysuccinimidyl ester at pH 12**

For this labeling reaction, a pure DMF solution was required. The solvent has to be smelled to be sure that there is no amine present in DMF. If there is a trace amount of amine, it will inhibit the reaction. DMF was heated to remove volatile amine and have a clean solvent in which to dissolve the tetramethylrhodamine N-hydroxysuccinimidyl ester (TMR).

100  $\mu\text{L}$  of aqueous 1 M NaOH was added to 900  $\mu\text{L}$  of distilled DMF in an Epindorf vial. This basic DMF solution was used to prepare a 9 mM N-acetylarginine solution. A small amount of N-acetylarginine was removed for the TLC experiment. 2 - 2.5 mg of TMR was dissolved in 250  $\mu\text{L}$  of distilled DMF. This intensely red solution was added to N-acetylarginine solution and the reaction mixture in the Epindorf vial wrapped in aluminum foil was stirred with a small stir bar, at room temperature. Using a clamp, the reaction vial was held in a beaker filled with water. Stirring the water in the beaker caused the reaction mixture in the vial to be agitated. Each hour the reaction progress was checked

on a TLC plate. The solvent system was  $\text{CHCl}_3:\text{MeOH}:\text{H}_2\text{O}$  with a 65:35:1 ratio. After 3–4 h, the reaction was complete.

The TLC experiment showed that at least three components were present in the reaction mixture. The ESI-MS spectrum confirmed that two of these components were TMR and hydrolyzed TMR.

### **7.2.8 Hydrazine reaction**

Three samples of N-acetylarginine (10.8 mg, 43.2 mg, and 216 mg) were chosen and 1 mL of 35% hydrazine was added to each sample in a test tube. All the test tubes were heated at 75 °C for 1 h.

### **7.2.9 Hydrazinolysis reaction time optimization**

The reactions were repeated for 2, 3, 4, 5, 10 and 24 h. Monitoring the reaction with TLC was not possible because hydrazine itself is an amine that darkens the TLC plate after developing. For each test tube when the reaction time elapsed, the mixture was evaporated using a rotary evaporator. N-methyl morpholine (5 mL) was added twice and evaporated each time to remove hydrazine. TLC was performed by spotting arginine by itself, the reaction mixture by itself, and a cospot of arginine and the reaction mixture. The TLC solvent was BuOH, AcOH and water with 65:25:25 ratio and the developing TLC solution was ceric-molibdate buffer.

### **7.2.10 Ornithine TMR labeling reaction**

The hydrazine reaction using 10.8 mg of N-acetyl-L-arginine dissolved in 30% hydrazine solution in water was repeated using the procedure of section 7.2.8. After adding

N-methyl morpholine (5 mL) twice and using the rotary evaporator to remove the hydrazine, the labeling reaction was performed on the ornithine product of the reaction.

The hydrazine reaction converted N-acetyl-L-arginine to the primary amine ornithine, which was confirmed by ESI-MS. The side product was also an amine that had to be separated before doing the TMR labeling reaction.

TMR (2 - 2.5 mg) was dissolved in distilled DMF (250  $\mu$ L). This intensely red solution was added to the reaction mixture (ornithine) solution and it was stirred with a small stir bar at room temperature for 4 hours in an aluminum foil wrapped vial. The solvent system was  $\text{CHCl}_3/\text{MeOH}/\text{H}_2\text{O}$  (65:35:1).

#### **7.2.11 Hydroxylamine reaction**

A 35% solution of hydroxylamine hydrochloride in water was neutralized with a 100 mM solution of NaOH. To 3 mL of this solution 10.8 mg of N-acetyl-L-arginine (50  $\mu$ moles) was added. The mixture was heated at 70  $^{\circ}\text{C}$  for 10 hours. The TLC was checked each hour and when the spot corresponding to N-acetyl-L-arginine disappeared the reaction was stopped. Hydroxylamine was evaporated and the TMR labeling reaction was repeated using the procedure described for the ornithine-labeling reaction (section 7.2.10).

#### **7.2.12 Sodium hydride reaction**

N-acetyl-L-arginine (10.8 mg or 50  $\mu$ mol) was added to dry DMF (3 mL). The mixture was heated for 5 min to get a suspension of very fine particles of arginine in DMF. NaH (12 mg) suspended in 60% oil was added to N-acetyl-L-arginine in DMF and the mixture was stirred and heated at 40  $^{\circ}\text{C}$  for 3 h. Excess NaH was filtered using a Whatman qualitative filter paper 5.5 cm.

### **7.2.13 TMR labeling reaction on the NaH reaction mixture before separation**

Excess NaH was filtered from and 0.185 M NaHCO<sub>3</sub> (100 μL) was added to the reaction mixture to adjust the pH to 8.5. Then TMR (5 mg) was dissolved in dry DMF (300 μL) and 100 μL of this solution was added to the reaction mixture. The solution was allowed to incubated at room temperature for 5 h.

### **7.2.14 Ion-exchange separation of the Hydrazinolysis and NaH reaction products**

A 10-cm long column containing AG 50W and AG MP-50 cation exchanger resins (Bio Rad), which are a strong cation exchanger resin (-SO<sub>3</sub>H type), was filled using the slurry method. The column was washed with 5 mL of MeOH three times. The reaction mixture was dissolved in 1 mL of water and applied on top of the column. The column was washed with 30 mL of MeOH to elute the products. After MeOH was evaporated, TLC showed that no product eluted from the column. The column, then, was washed with 2 M NaCl solution and TLC showed the product eluted. The water of the eluted product was evaporated and NaCl was the major precipitate. 1 mL of heated MeOH was added to the precipitate to dissolve the ornithine and NaCl solid was filtered. MeOH was removed using a rotary evaporator and the labeling reaction was done on the separated product as described in Sections 7.2.13 and 7.1.2.17.

### **7.2.15 Preparative TLC for NaH and Hydrazinolysis reaction product**

TLC was repeated on a larger scale for both the NaH and hydrazine reactions after the completion of labeling reaction. The reaction mixture was deposited as a continuous band on a preparative TLC plate (25 x 25 cm). The colored bands on the TLC plate were

removed by scraping with a razor blade. The adsorbed components of each product on the silica gel was dissolved in copious amounts of MeOH. The colored MeOH solution, which contained the extracted product, was decanted and the extraction procedure was repeated. MeOH dissolved both the silica gel powders on the TLC plate and the desired product. When MeOH was evaporated, the product had to be recovered from silica gel by extraction with MeOH again. Most of the product was separated by dissolving the extract in water and filtering out the silica gel precipitate. To obtain a pure product, this solution was applied onto a Sep-Pak C<sub>18</sub> cartridge and all the undesired side products were washed away using water and the pure product was recovered as described below.

#### **7.2.16 C<sub>18</sub> Sep-Pak separation of the NaH and Hydrazinolysis reaction products**

A C<sub>18</sub> Sep-Pak cartridge was equilibrated by washing several times with 30 mL of water. Then the reaction mixture for the NaH or hydrazinolysis reaction was injected separately onto the Sep-Pak cartridge. The cartridge was washed with water and the effluent was collected for identification by mass spectrometry. Then the Sep-Pak cartridge was washed with HPLC grade MeOH and the colored fractions were collected into separate vials. The solvent of each collected fraction was evaporated and product identified by mass spectrometry.

#### **7.2.17 TMR labeling of the NaH reaction after ion exchange separation of the product**

TMR (5 mg) was dissolved in dried-distilled DMF (300  $\mu$ L) and 1/5 of this solution was taken for each labeling reaction experiment. The separation procedure was described in Section 7.2.14. To each of fraction 1 (MeOH washed portion of the column), fraction 2

(NaCl washed portion of the column) and the reaction mixture before separation, the following reagents were added: water (100  $\mu\text{L}$ ), 0.185 M  $\text{NaHCO}_3$  (100  $\mu\text{L}$ ), and TMR (100  $\mu\text{L}$ ) solution. Then each vial was incubated at room temperature for 5 hours.

A  $\text{C}_{18}$  Sep-Pak cartridge was equilibrated with water and washed several times with 30 mL of water. Then the reaction mixture for each of the three vials mentioned above was applied separately onto the Sep-Pak cartridge. The cartridge was washed with water and the effluent was collected to be checked for identification by mass spectrometry. Then the Sep-Pak cartridge was washed with HPLC grade MeOH and the colored fractions were collected into separate vials. The MeOH in each vial was evaporated and then the identity of the product was determined by mass spectrometry.

For the NaH reaction, 21 mg of the labeled arginine was obtained from 10 mg of arginine. The theoretical value of the product for 10 mg arginine is  $(631 \times 10)/216 = 29$  mg of labeled arginine. The labeling efficiency, therefore, is  $21/29 = 0.73$  or 73%.

#### **7.2.18 Two-layer sample deposition for MALDI**

The MALDI sample probe consists of a 1 x 10 cm stainless steel plate with 20 platinum-coated sample locations in a row. The sample preparation and two-layer sample deposition method for MALDI was adapted from reference 35. DHB (2, 5 dihydroxybenzoic acid) matrix solution was prepared at a concentration of 10 mg/mL in 30% acetonitrile/water. The matrix solution was mixed on a vortex for 1 min and then centrifuged and the supernatant was taken off to remove nondissolved matrix crystals. A 0.5  $\mu\text{L}$  aliquot of matrix solution was applied to the probe and allowed to dry and then another 0.5  $\mu\text{L}$  of analyte solution was placed on the sample probe and allowed to dry. The same procedure was repeated to place the sample on each of the 20 spots on the sample

probe and then all 20 samples were inserted onto the MALDI instrument and using a computer controlled program each sample was targeted one by one and the MALDI spectrum was recorded.

From Sections 7.2.7 and 7.2.11, it was concluded that the direct labeling reaction at high pH and hydroxylamine reactions were not suitable for further studies. To compare the hydrazine and NaH reactions, the two reactions were repeated under optimized conditions and then the separation was performed to obtain pure product. TMR labeling reaction was done on each of the pure products. The result for each step of the reaction was monitored with MALDI.

#### **7.2.19 Hydrazine reaction on cyclic peptide**

To cyclic peptide (1 mg) 35% hydrazine (1 mL) was added. The clear solution of cyclic peptide in hydrazine was transferred to a capped test tube and heated at 75 °C for 5 h. This reaction time was optimized for the hydrazinolysis reaction on N-acetyl-L-arginine. After 5 h, excess hydrazine solution was removed by adding N-methyl morpholine and rotary evaporating the solution. Then the TMR labeling reaction was done as described next.

#### **7.2.20 TMR labeling on the product of Hydrazinolysis reaction of cyclic peptide**

The hydrazine reaction mixture of cyclic peptide was dried under reduced pressure and then redissolved in dry DMF (300  $\mu$ L). TMR (5 mg) was also dissolved in dry DMF (500  $\mu$ L) in a separate vial. This TMR solution (100  $\mu$ L) was added to the peptide solution



(100  $\mu\text{L}$ ) and this 200  $\mu\text{L}$  of mixture was stirred at room temperature for 5 h. TLC was checked every 1 h.

#### **7.2.21 NaH reaction on cyclic peptide**

The weight of each cyclic peptide purchased from Sigma was 1 mg. Therefore it was not feasible to use a 10-mg scale reaction. The reaction, then, was scaled down to 1 mg.

To cyclic peptide (1 mg), NaH (0.3 mg) and dried DMF (1 mL) were added. The reaction vial was isolated from humidity by using a  $\text{CaCl}_2$  guard column at the top of a reflux system. While it was under dry argon, the reaction vial was placed in an oil bath and stirred at 60  $^\circ\text{C}$  for 5 h. For the NaH reaction with N-acetyl-L-arginine, the optimum reaction time was 5 hs. The excess NaH was filtered and decomposed by adding water. The supernatant was used for TMR labeling.

#### **7.2.22 TMR labeling on the product of NaH reaction of cyclic peptide**

The NaH reaction mixture was filtered to remove excess NaH. Then it was washed with dry DMF (1200  $\mu\text{L}$ ) and 1/2 of this solution was added to 150  $\mu\text{L}$  of TMR (5 mg in 500  $\mu\text{L}$  of dry DMF) solution. Then this 750  $\mu\text{L}$  solution of cyclic peptide and TMR in DMF was stirred at room temperature for 5 hs. TLC was checked each hour. The reaction mixture was applied onto a Sep-Pak cartridge and then it was washed with water (30 mL) and the effluent was collected. Then the cartridge was washed with MeOH and ten 5-mL fractions were collected. The MALDI-MS of each of the collected fractions was recorded.

### 7.2.23 Furfurylamine reaction with 5-BrMF

Dried molecular sieves (type 4A) were put in a round-bottom flask equipped with a refluxing unit. 5-BrMF (5 mg or 20  $\mu\text{mol}$ ) was dissolved in dry DMF (1 mL). To the flask containing molecular sieves and the 5-BrMF solution in DMF, furfurylamine (88  $\mu\text{L}$  or 100  $\mu\text{mol}$ ) was added. To prevent carbon dioxide adsorption by furfurylamine from the air, a calcium chloride trap was placed on top of the refluxing system. The reaction vial was stirred at room temperature for 2 hs.  $\text{CHCl}_3/\text{MeOH}/\text{H}_2\text{O}$  (65:35:0.5) was not a good solvent for developing TLC runs.  $\text{MeOH}/\text{CHCl}_3$  (10:90) was used for TLC and  $R_f$  values for 5-BrMF and furfurylamine were 0.46 and 1.0 respectively. An  $R_f$  value of 0.2 for the product was measured after 2 hs of reflux.

Because furfurylamine is an aliphatic amine, it is a good nucleophile and the reaction goes to completion after 2 hs at room temperature. Preparative TLC was used to separate the product from the starting material. The pure product was extracted from the silica gel of TLC plates by washing with copious amounts of MeOH. MeOH dissolved both product and silica gel and when MeOH was evaporated silica gel coprecipitated with the product. The product was reextracted from silica gel by washing with water. The water was evaporated and the product was redissolved in water and applied to a Sep-Pak cartridge. Only a small fraction of the product attached to Sep-Pak.

The product was recovered from the Sep-Pak, the solvent was evaporated, and the product redissolved in water. TLC was performed on the product and it showed two spots with  $R_f$  values of 0.0 and 0.45 when using a  $\text{MeOH}/\text{CH}_2\text{Cl}_2$  (10:90) as the solvent. To purify the product, it was applied on a column that was packed with fine particles of silica gel. The first fraction with  $R_f$  values of 0.45 on TLC was collected using the same mobile phase as TLC. Then the eluent was changed to  $\text{MeOH}/\text{CH}_2\text{Cl}_2/\text{H}_2\text{O}$  (30:70:3) to mobilize and recover the second fraction with  $R_f$  values of 0.0 in TLC.

Each fraction collected from Sep-Pak and from the normal phase column was checked for the product using MALDI-MS. The MALDI matrix, DHB, was dissolved in AcN:H<sub>2</sub>O 200 μL:300 μL. 0.5 μL of DHB and 0.5 μL of each fraction collected from the Sep-Pak and normal phase columns were placed on a MALDI tip and checked for the desired product.

#### **7.2.24 Ozonolysis of 5-BrMF and furfurylamine reaction**

Fluorescein-furfurylamine adduct was dissolved in a solution of 9 mL of dichloromethane and 1 mL of dry methanol in a three-neck round-bottom flask. The flask was equipped with a thermometer and a reflux unit and an adapter to fit in the ozone input tube. The flask was put in dry ice and acetone to cool to -78 °C. To the ozone generator 90 V was applied and the ozone produced was purged into the solution for 5 minutes at -78 °C. When the solution turned blue the voltage of the ozone generator was set to zero and oxygen was purged into the solution for another 5 minutes. Then 200 μL of (CH<sub>3</sub>)<sub>2</sub>S was added to the solution and left to warm up to room temperature for 1 hour. The solvent was evaporated and the product was checked using MALDI-MS.

Two blank solutions were also run for the Ozonolysis of 5-BrMF by itself and furfurylamine alone. After 5 minutes blue color appeared in the solution. MALDI-MS experiments were performed on both the blanks and the sample.

#### **7.2.25 Reaction of 4-aminoacetophenone with 5-BrMF**

Type 4A molecular sieves were put in a round-bottom flask equipped with a refluxing unit. 5-BrMF (5 mg or 20 μmol) was dissolved in dry DMF (1 mL).

Aminoacetophenone (13.5 mg or 100 μmol) was added to the fluorescein solution in DMF.

A  $\text{CaCl}_2$  guard column was placed on top of the refluxing unit. The reaction vial was stirred over night at  $75\text{ }^\circ\text{C}$ .

$\text{MeOH}/\text{CHCl}_3$  (10:90) was used for TLC and  $R_f$  values for 5-BrMF and 4-aminoacetophenone were 0.46 and 1.0 respectively. An  $R_f$  value of 0.3 for the product was measured after overnight reflux at  $75\text{ }^\circ\text{C}$ . A rotary evaporator was used to evaporate DMF. The product was extracted in water and excess 4-aminoacetophenone precipitate was discarded. MALDI-MS for this intermediate was checked and  $\text{SeO}_2$  oxidation was performed on the product.

#### **7.2.26 $\text{SeO}_2$ oxidation of 5-BrMF and aminoacetophenone reaction**

Dioxane (9 mL) and water (1 mL) were added to fluorescein acetaminophenone adduct. Then  $\text{SeO}_2$  (8 mg) was added to the solution and it was refluxed for 2 hs. Excess  $\text{SeO}_2$  was filtered out and the solvent was evaporated. MALDI-MS was checked for the presence of the product.

#### **7.2.27 Reaction of 2, 3-butanedione with benzylbromide**

60% NaH in oil (1 mg) was washed with THF to remove the oil. Then 2, 3-butanedione (0.8 g) was also dissolved in THF (1 mL) and half of the washed NaH was added to it. Benzylbromide was passed through an  $\text{Al}_2\text{O}_3$  column to get 1 mL of clear solution. This benzylbromide was added to the 2, 3-butanedione solution and NaH while the reaction vial was cooled to  $-78\text{ }^\circ\text{C}$  with dry ice. When the reaction vial was allowed to warm to room temperature, the color of the solution turned brown and the reaction was completed. The solution was decanted to remove the excess NaH. Then NaH was decomposed by adding water. The THF solvent was removed by evaporation and MALDI-MS of the product was recorded.

### **7.2.28 Reaction of 2, 3-butanedione with 5-BrMF**

This reaction was repeated under similar conditions as benzylbromide reaction with 2,3 butanedione in section 7.2.27 except that 5-BrMF was used instead of benzylbromide.

### **7.2.29 Arginine labeling using 5 (pentane 2,3 dione) methylfluorescein**

Arginine modification by 5(2, 3 pentane dione) methylfluorescein was performed in borate buffer (50 mM, pH 8.0) at 25 °C. A 20 mM solution of 5(2, 3 pentanedione) methyl fluorescein in borate buffer (50 mM) was made by diluting the original solution 500 times into borate buffer (50 mM, pH 8.0).<sup>40-42</sup> The pH decreased to 7.5 upon mixing. Small volumes of a NaOH (5 M) solution were added in order to compensate for the pH drop. Equal volumes of this solution and a 10 μM solution of N<sub>α</sub>-acetyl-arginine (in 50 mM borate buffer) were mixed. The reaction was allowed to stand overnight and then checked by the MALDI-MS spectrum for the product.

A similar reaction of arginine labeling was repeated in the absence of water to investigate the effect of complex formation of the product with borate and identify the product peak in MALDI-MS spectrum.

### **7.2.30 Microcystin labeling with TMR using NaH deprotonation**

The NaH deprotonation and labeling reaction conditions were similar to the conditions for cyclic peptide labeling reaction with TMR in Sections 7.2.21 and 7.2.22 except that microcystin was used instead of cyclic peptide.

NaH (0.15 mg) and dried DMF (500 μL) were added to microcystin (500 μg). The reaction vial was isolated from humidity in the air by using a CaCl<sub>2</sub> guard column at the top of a reflux system. While it was under dry argon, the reaction vial was placed in an oil bath

and stirred at 60 °C for 5 hs. For the NaH reaction with N-acetyl-L-arginine the reaction time was optimum at 5 hs. The excess NaH was filtered out and decomposed by adding water. The supernatant liquid was used for TMR labeling.

The supernatant liquid was dried using a rotary evaporator and redissolved in dry DMF (600  $\mu$ L) and 1/2 of this solution was added to 150  $\mu$ L of TMR (5 mg in 500  $\mu$ L of dry DMF solution). Then this 750  $\mu$ L solution of microcystin and TMR in DMF was stirred at room temperature for 5 hs. TLC was checked each hour. The reaction mixture was injected onto a Sep-Pak cartridge and then it was washed with 30 mL of water and the effluent was collected. Then the cartridge was washed with MeOH and each fraction was collected. The MALDI-MS of each of the collected fractions was recorded.

### **7.2.31 Separation of the labeled microcystin-LR**

Components of the microcystin labeling reaction were applied to a Waters C<sub>18</sub> Sep-Pak cartridge. The same procedure that was described for the separation of cyclic peptide labeling reaction product (7.2.16) was repeated for the separation in this experiment.

Another attempt to separate the mixture by gel permeation chromatography was done. A glass column was filled with polyacrylamide gel and the reaction mixture was applied on top of the column and it was eluted with water. The column was equipped with a fraction collector and all the fractions were collected until the effluent was colorless.

### **7.2.32 Microcystin labeling using 5-BrMF**

The procedure for microcystin labeling with 5-BrMF is exactly similar to TMR labeling of microcystin (section 7.2.30) except using 5-BrMF solution in DMF instead of TMR solution.

### **7.2.33 Microcystin immunoassay**

A  $10^{-5}$  M solution of labeled microcystin in 10 mM borate solution, pH 9.2, was prepared from the stock solution of  $10^{-3}$  M in DMF. The solution was diluted to  $10^{-9}$  M with the run buffer and then injected onto a 35 cm long capillary by applying 1000 V for 5 s. CE was performed by applying 400 V/cm run voltage.

A solution of  $10^{-5}$  M antimicrocystin was prepared in 10 mM phosphate buffer, pH 7.0.

To 10  $\mu$ L of the  $10^{-5}$  M solution of labeled microcystin 2, 4, 6, 8 and 10  $\mu$ L of 1 mg/mL antibody solution were added and in each case a CE experiment was performed after dilution to check the antigen-antibody complex formation.

## **7.3 Results and discussion**

### **7.3.1 Direct labeling of arginine with amine labeling reagent FQ**

Direct labeling of N-acetyl-L-arginine with the amine-labeling reagent FQ was not successful. The procedure was described in Section 7.2.6. Figure 7.2 shows the electropherograms of both a blank solution and the product of the FQ reagent with N-acetyl-L-arginine. The blank and labeled-arginine electropherograms are both quite similar indicating that no labeling reaction has occurred. The pKa for arginine is 12.5. However the experiment was performed at pH 13, in which a significant fraction of arginine was deprotonated, but the 0.1 M free hydroxide ion destroyed the FQ and no labeling reaction took place.

In section 7.2.12 for the reaction of NaH with N-acetyl-L-arginine (10.8 mg), the product weight was 14.15 mg and consisted of deprotonated N-acetyl-L-arginine. 60%

Figure 7.2: Arginine deprotonation and labeling reaction electropherogram. 5 s injecton at 1000 V. CE voltage 400 V/cm

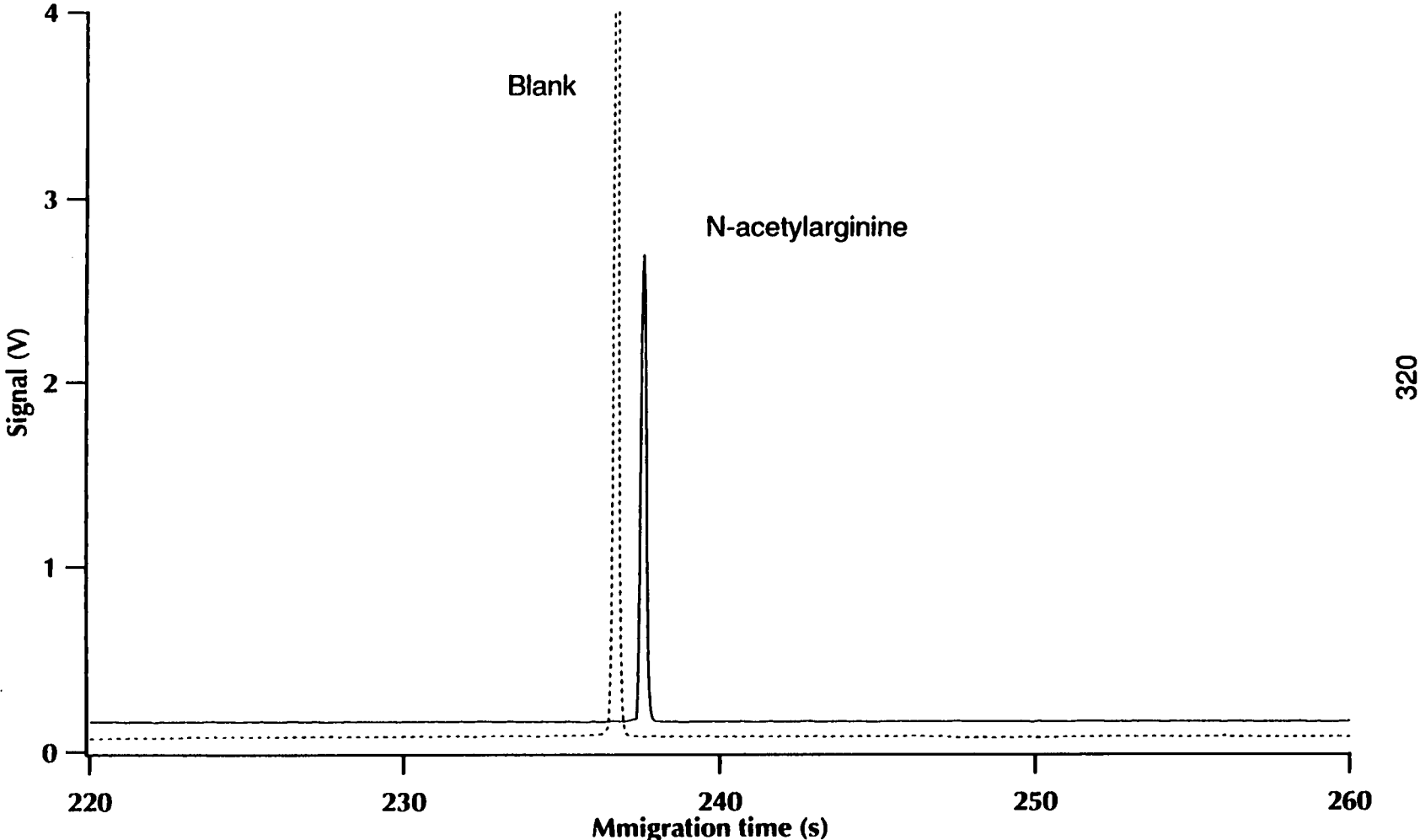




**Figure 7.3: Direct arginine labeling reaction at high pH with TMR**

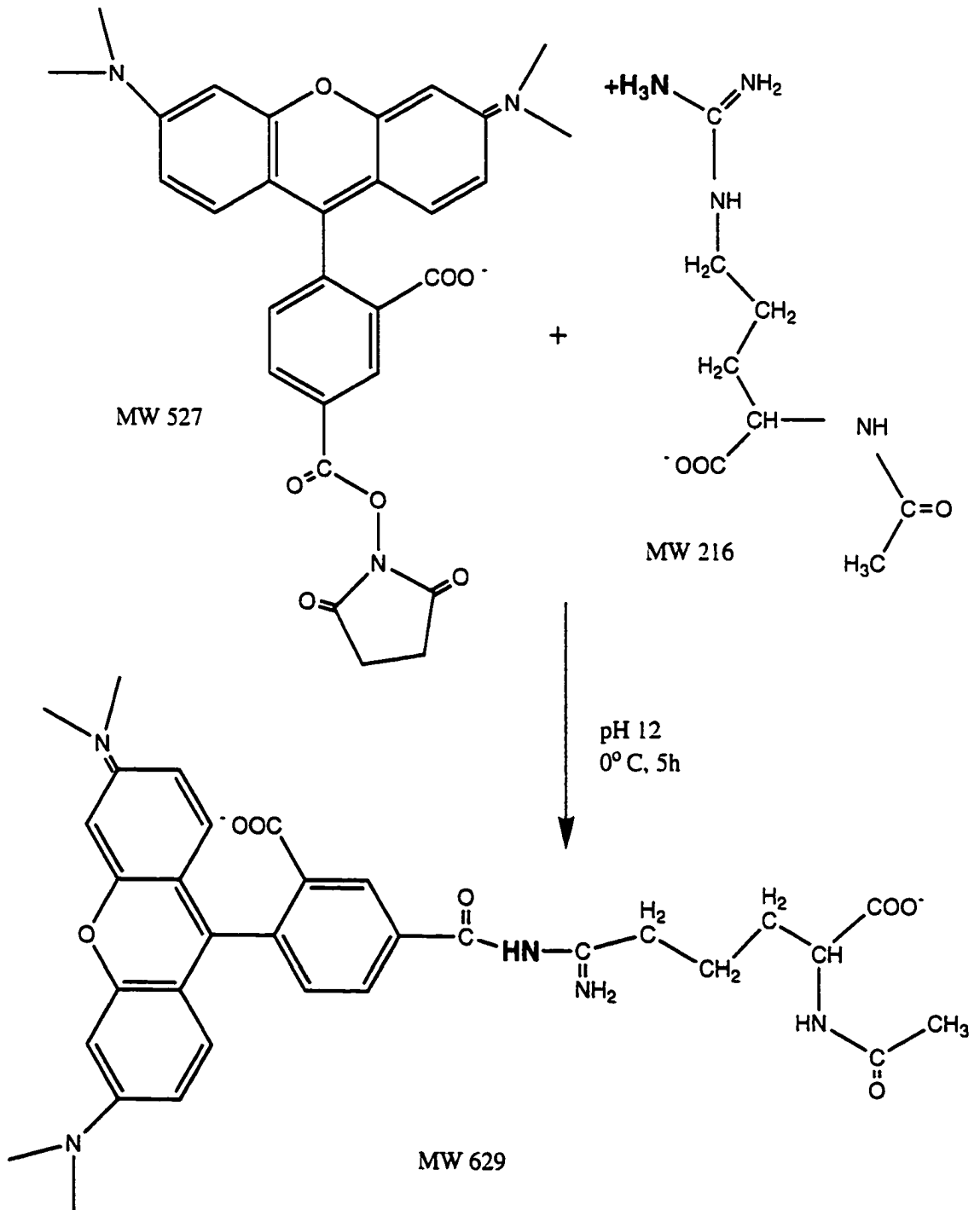
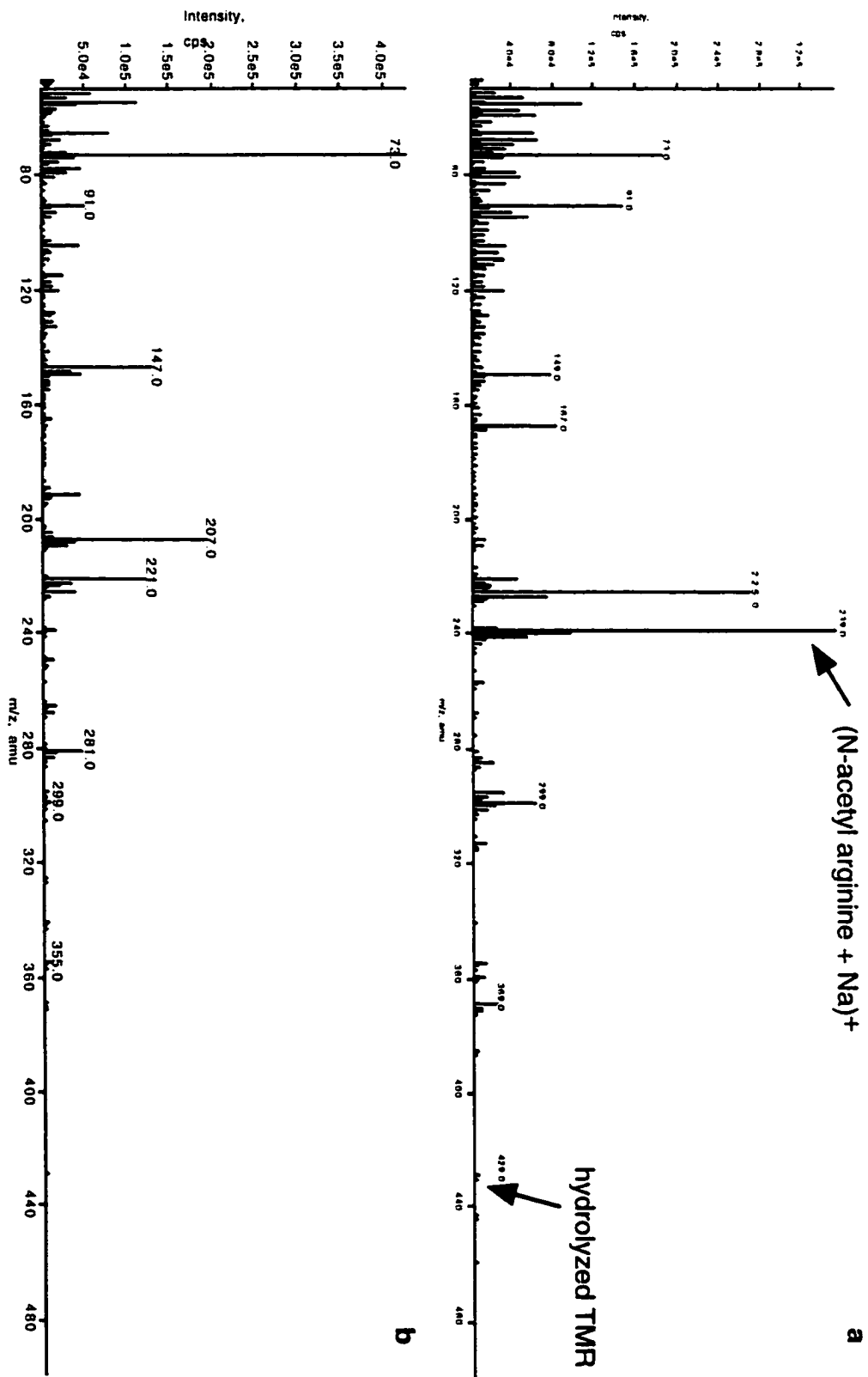


Figure 7.4: ESI-MS spectra of a) reaction mixture of TMR with arginine at high pH and b) blank MeOH/HOAc 9/1



NaH in oil (12 mg) will add 4.8 mg of oil to the total weight of the product. Therefore, the weight of pure product is  $14.1 - 4.8 = 9.3$  mg. If the reaction efficiency is 100%, we would expect to have ~ 12 mg of the product. The actual yield of the NaH reaction, therefore, is  $(9.3/12) \times 100 \sim 80$  % yield.

### **7.3.2 Direct labeling of arginine with TMR at pH 12**

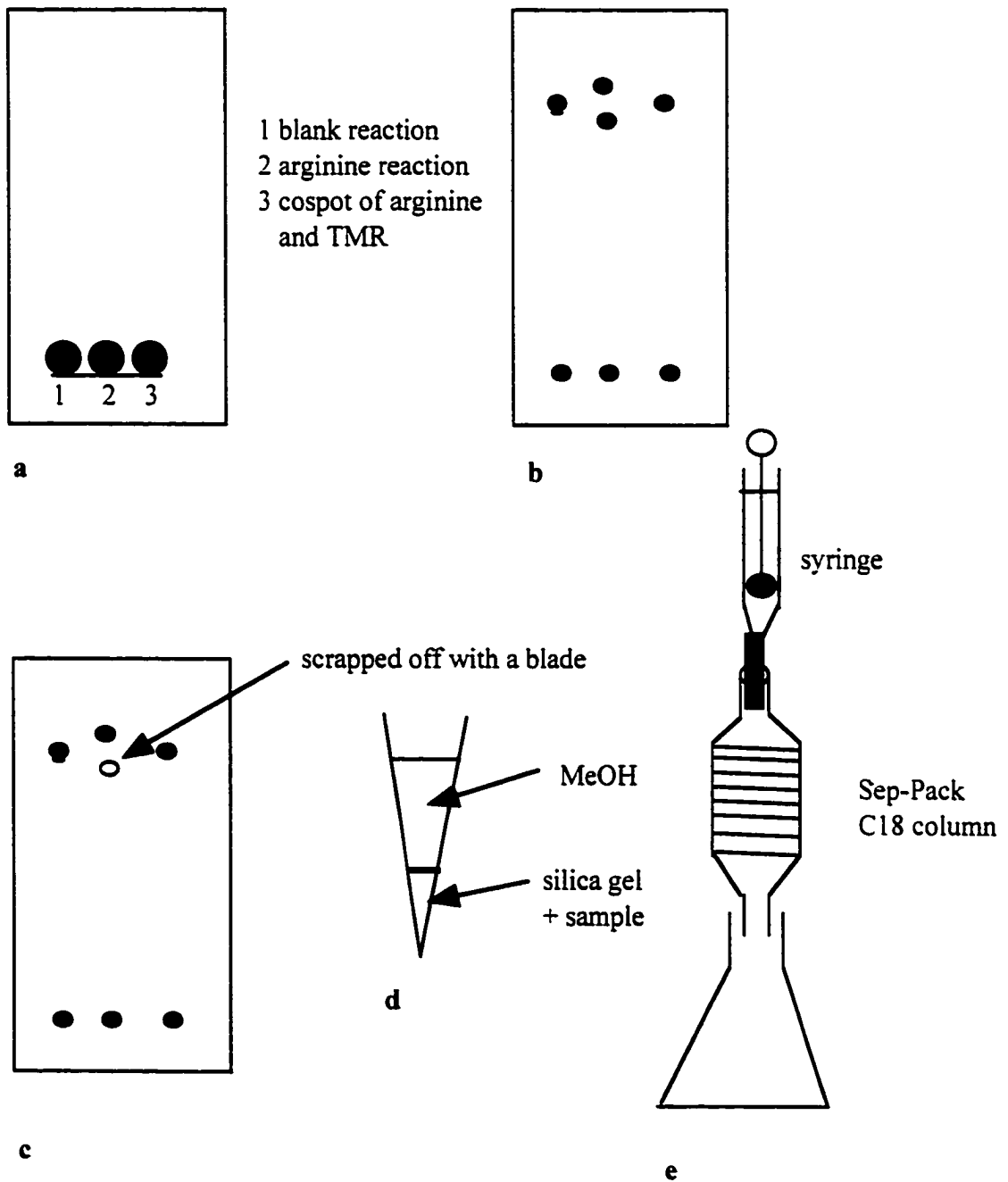
Figure 7.3 shows the reaction of N-acetyl-L-arginine with TMR at pH 12 as described in section 7.2.7. The reaction was done in 0 °C for 5 hours. Figure 7.4 shows the blank and the reaction mixture ESI-MS spectra. The sodium adduct of N-acetyl-L-arginine at 239 amu indicates that the TMR has not reacted with the arginine. The peak at 429 amu shows that TMR has been hydrolyzed by the hydroxide ion in the solution. This experiment clearly indicated that the labeling reaction at high pH did not work because TMR hydrolyzed very quickly and it could not react with the free amine of N-acetyl-L-arginine. The hydroxide ion rapidly displaced the succinimidyl ester leaving group and hydroxide ion itself is not a good leaving group. TMR-OH is a stable molecule and did not react with protonated N-acetyl-L-arginine.

### **7.3.3 Hydrazine reaction with arginine and reaction time optimization**

It is well known that hydrazine can remove the guanidinium group of arginine and form a free amine called ornithine.<sup>32</sup> It has been observed that arginine-to-ornithine conversion may give rise to peptide-bond cleavage if the reaction is not controlled properly.<sup>33</sup>

Figure 7.5 shows the schematic representation of TLC for the arginine-to-ornithine conversion reaction (section 7.2.8) and the practical method to cut out the desired product from the silica gel, extraction of the product out of the silica gel and further separation and

**Figure 7.5: Schematic representation of arginine-to-ornithine conversion reaction and purification processes of a) before running the TLC, b) after running the TLC, c) removal of the desired spot for further purification, d) extraction of the product from silica gel, and e) Sep-Pak separation and purification of the product**



purification with Sep-Pak.  $R_f$  values for arginine by itself was 0.43 and for the product, ornithine, was 0.28.

#### 7.3.4 Hydrazine reaction time optimization

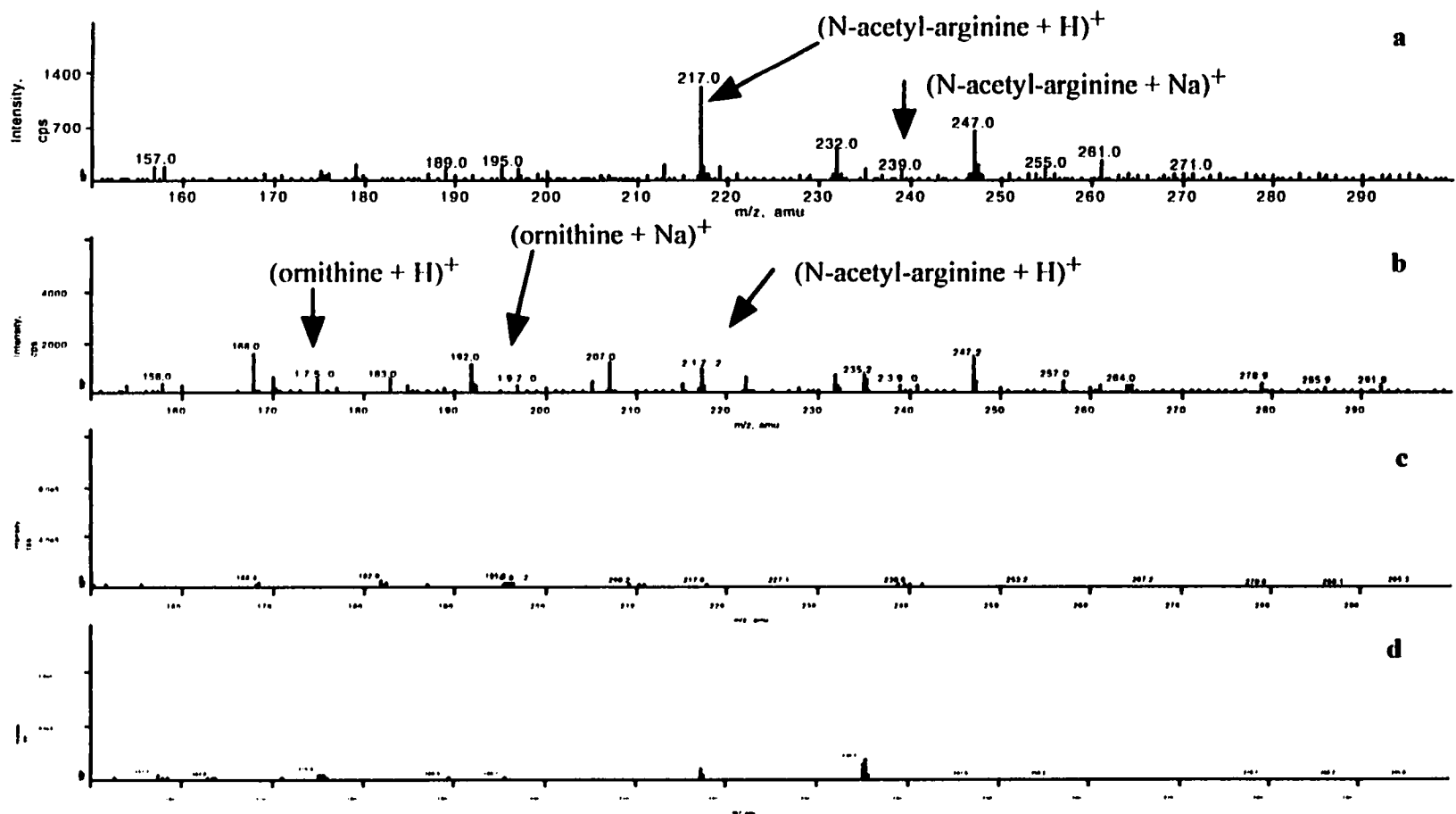
Figure 7.6 shows the ESI-MS spectra for the hydrazine reaction after 1 h and 5 h (Section 7.2.9). After 1 h reaction time the peak at 175 amu (ornithine + H)<sup>+</sup> is observed, but the presence of an intense peak at 217 amu (arginine + H)<sup>+</sup> indicates that the reaction is not completed. The spectrum for 5 h reaction time shows both arginine and ornithine in addition to some unknown side products. This experiment shows that increasing the reaction time does not necessarily improve the reaction. The ESI-MS spectrum of the reaction mixture for more than 64 h of reaction time did not show any improvement (data not shown).

N-acetylarginine is a small amino acid and hydrazine does not react with the molecule, but hydrazine will break any peptide bonds present in peptides and proteins if the reaction is not controlled properly.<sup>33</sup>

#### 7.3.5 Ornithine TMR labeling reaction

Figure 7.7 shows the TMR labeling of ornithine produced from Hydrazinolysis of N-acetyl-L-arginine and Figure 7.8 shows the ESI-MS spectra of the Hydrazinolysis reaction before and after addition of TMR labeling reagent (Section 7.2.10). The peak at 197 amu, sodium adduct of ornithine, shows that the hydrazinolysis reaction was successful and the appearance of the peak at 609 amu, TMR-labeled ornithine sodium adduct, shows that the labeling reaction has also occurred. Not all of the ornithine peak disappeared in the MALDI-MS spectrum indicating that the labeling reaction had not gone to completion. By comparing the two spectra, the disappearance of ornithine and the

**Figure 7.6: ESI-MS spectra of the arginine-to-ornithine conversion reaction of a) blank reaction of arginine in the absence of hydrazine for 1 h heating, b) 1h, c) 5 h, and d) 64 h heating of arginine in the presence of hydrazine**



326

Figure 7.7: TMR labeling reaction formula of ornithine by hydrazinolysis of N-acetyl-L-arginine

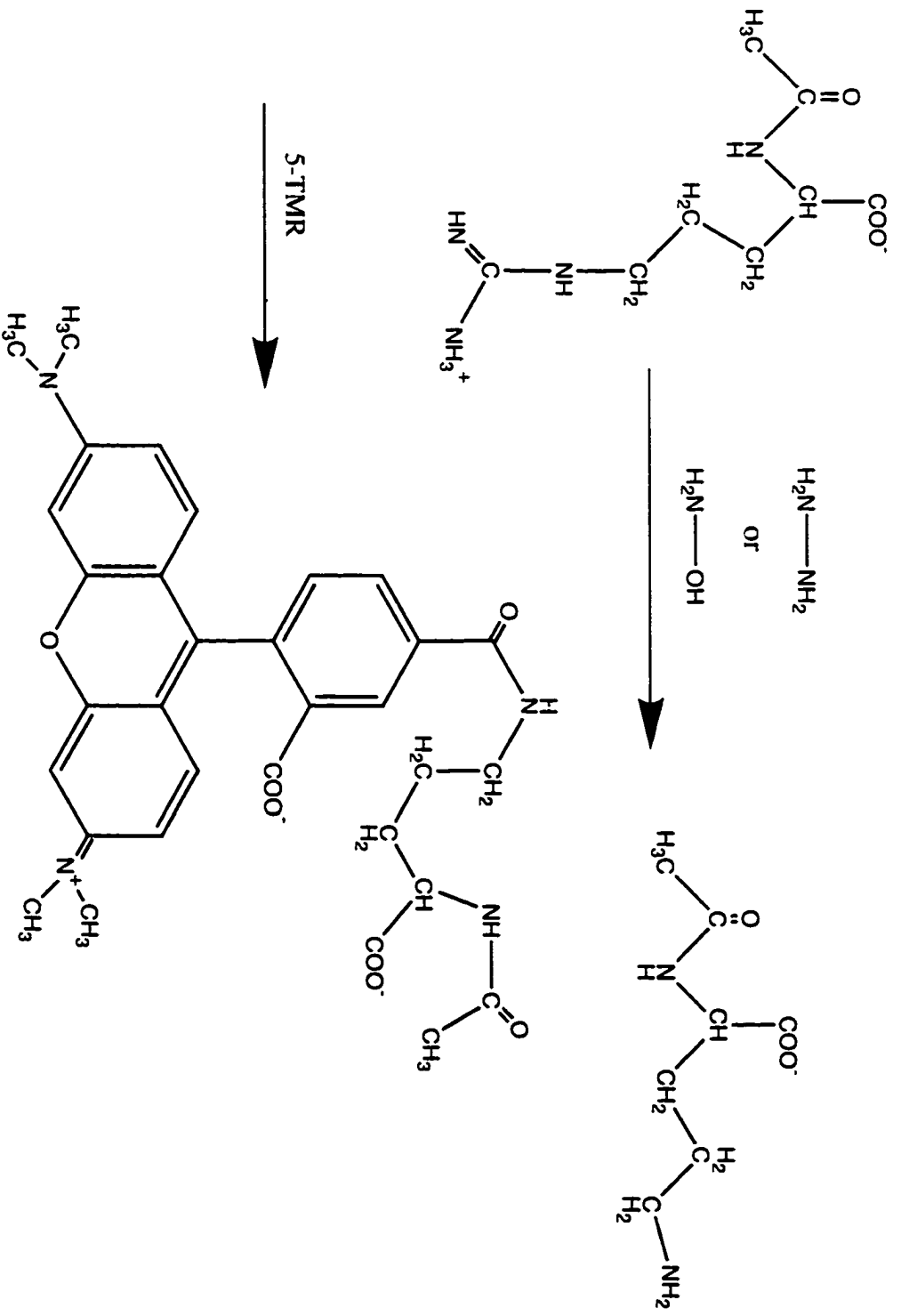
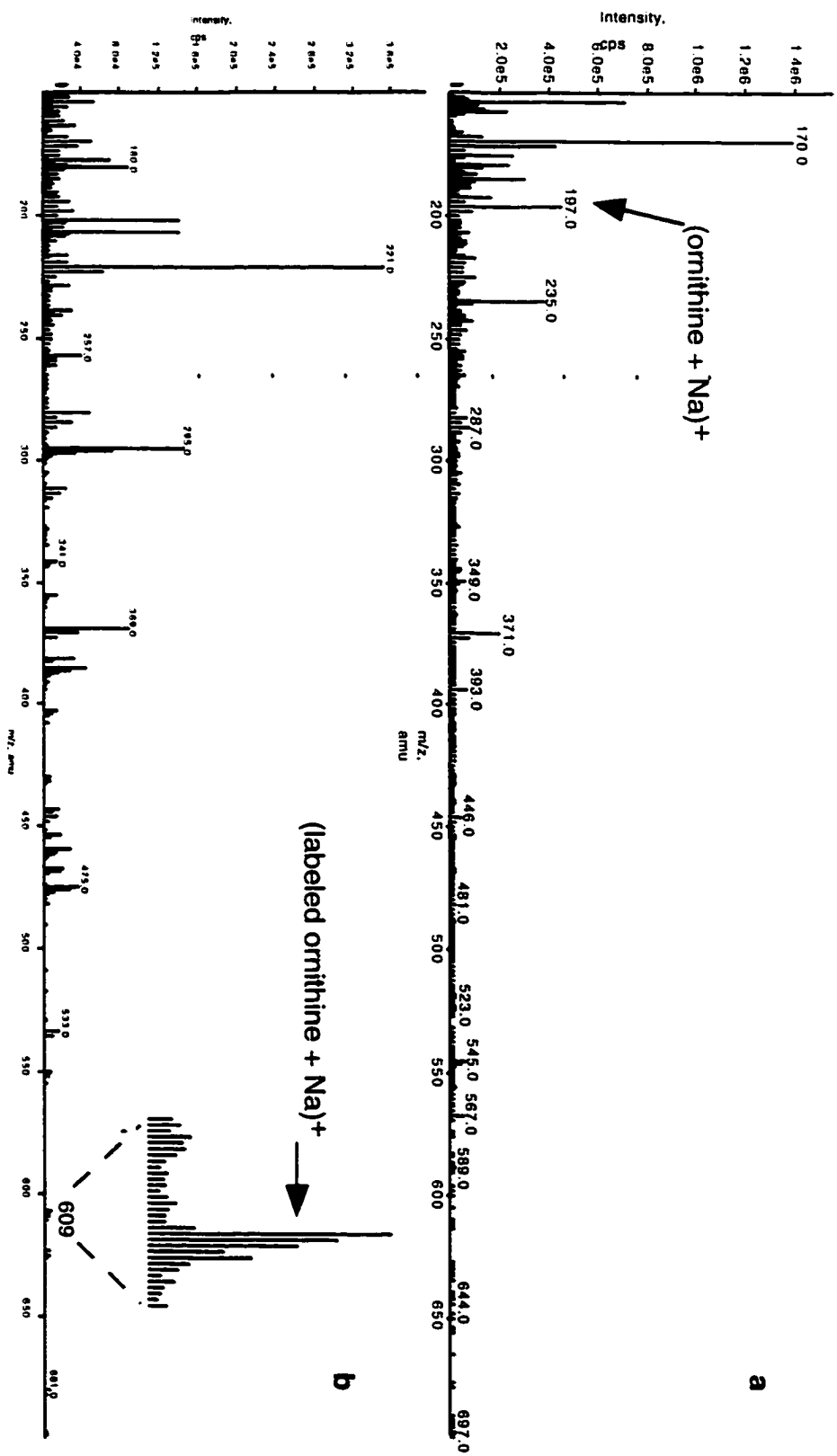


Figure 7.8: ESI-MS spectra of the hydrazinolysis reaction of N-acetyl-L-arginine, a) before labeling reaction with TMR, and b) after labeling reaction with TMR





appearance of labeled ornithine, suggests that both labeling of the free amine and arginine peptide bond breaking occurred. The product of peptide bond cleavage has a low molecular weight and it could not be easily identified in the ESI-MS spectrum.

### **7.3.6 Hydroxylamine reaction with arginine**

Figure 7.9 shows the ESI-MS spectrum of the hydroxylamine reaction before and after the labeling reaction with TMR (section 7.2.11). Hydroxylamine is a weaker nucleophile compared to hydrazine and we expected less arginine peptide bond cleavage and hence more product to be observed; but no significant improvement could be seen. Even the peak at 217 amu indicates that most of the starting material is present and the reaction has not gone to completion.

### **7.3.7 Sodium hydride reaction with arginine and TMR labeling of the product before separation**

Figure 7.10 shows the chemical equations for sodium hydride deprotonation of N-acetyl-L-arginine and immediate labeling of the deprotonated form of the arginine with TMR under nonaqueous conditions (sections 7.2.12 and 7.2.13). Figure 7.11 shows the ESI-MS spectra of the NaH deprotonation of N-acetyl-L-arginine before and after labeling reaction with TMR reagent. The peak at 239 amu is probably the sodium adduct of the deprotonated arginine and the peak at 261 amu could be the disodium salt of deprotonated arginine. Upon addition of the labeling reagents, both of these peaks disappeared. The peak at 631 amu is the TMR-labeled arginine. The strong peak at 431 amu is the hydrolyzed TMR, suggesting the need for better control of the labeling reaction and separation of the desired product before labeling reaction.

Comparing all the results, we conclude that direct deprotonation of arginine at high pH in aqueous solution and the hydroxylamine conversion of arginine to ornithine are not

**Figure 7.9: ESI-MS spectra of hydroxylamine reaction with N-acetyl-L-arginine a) before and b) after TMR labeling reaction**

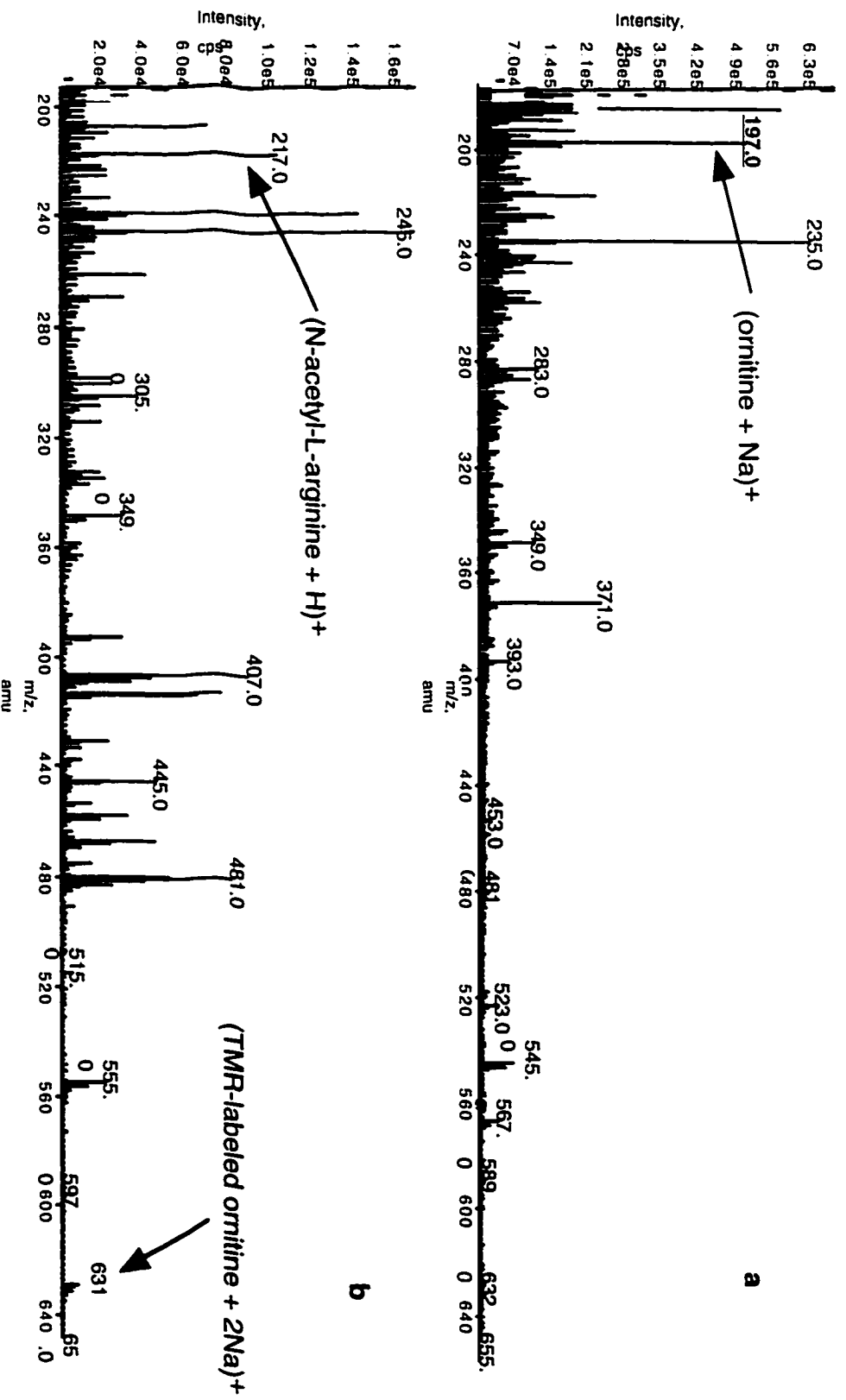


Figure 7.10: Chemical equations of NaH deprotonation of N-acetyl-L-arginine and TMR labeling of the product

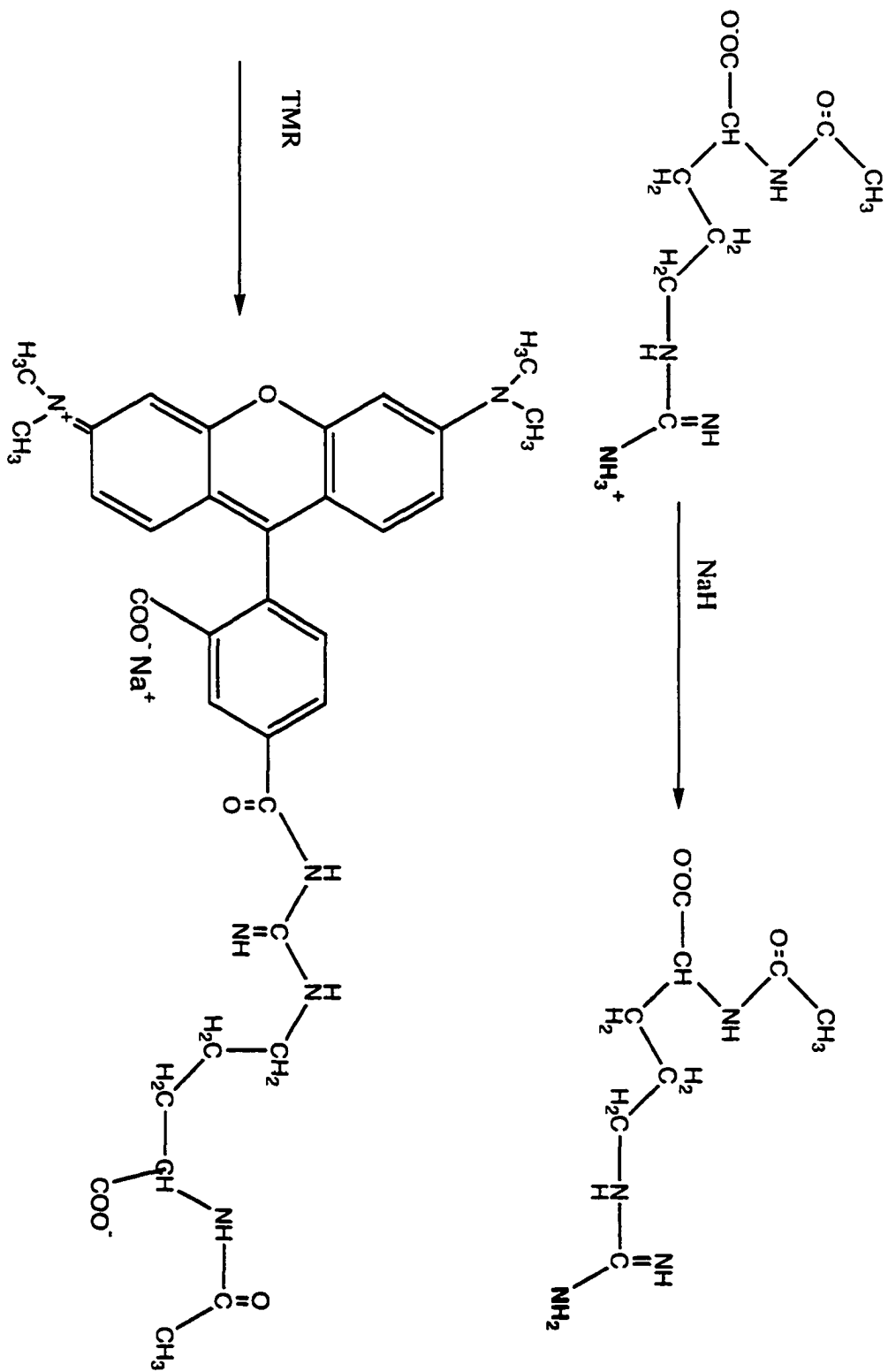
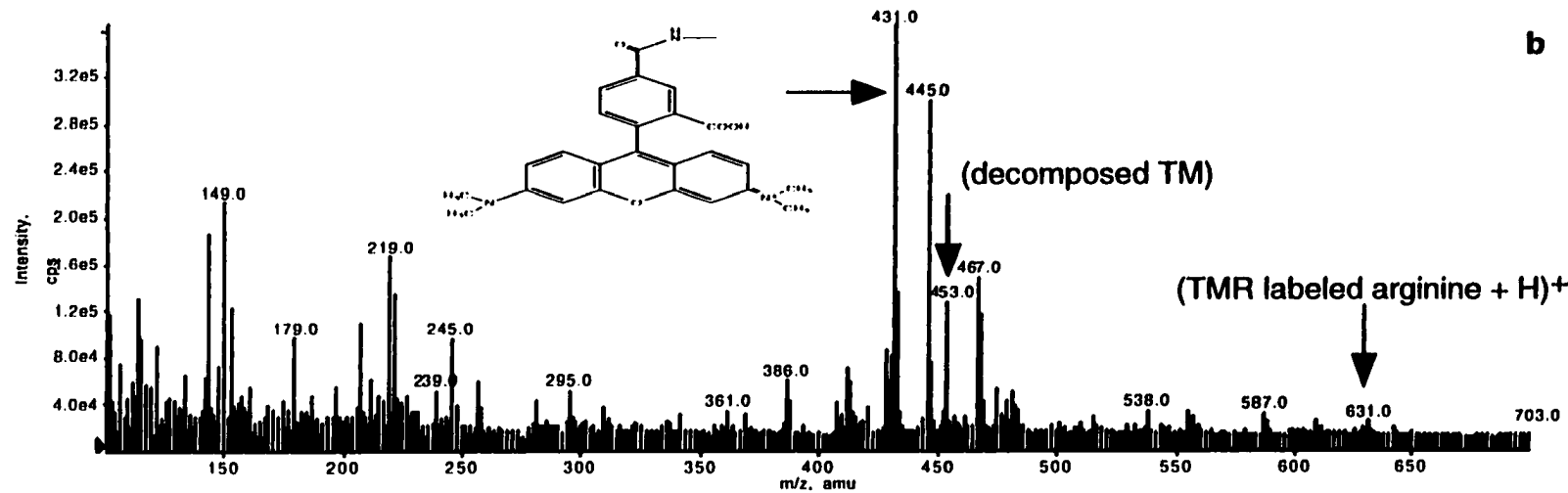
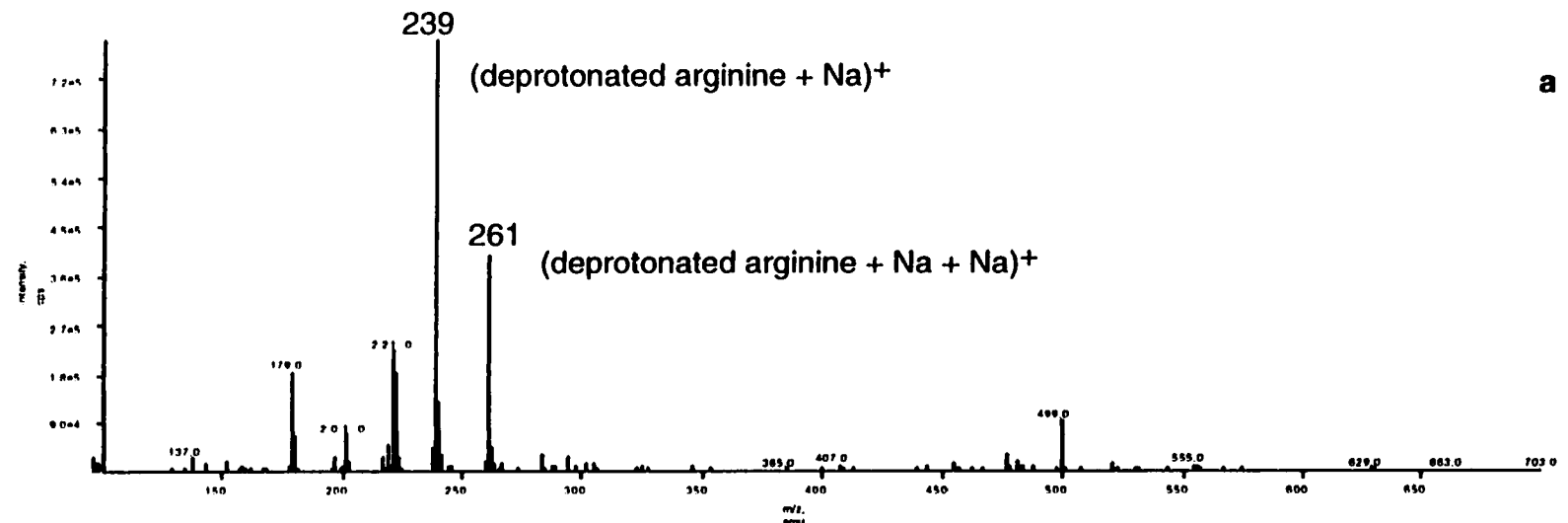


Figure 7.11: ESI-MS spectra of NaH reaction with N-acetyl-L-arginine a) before and b) after labeling reaction with TMR



332

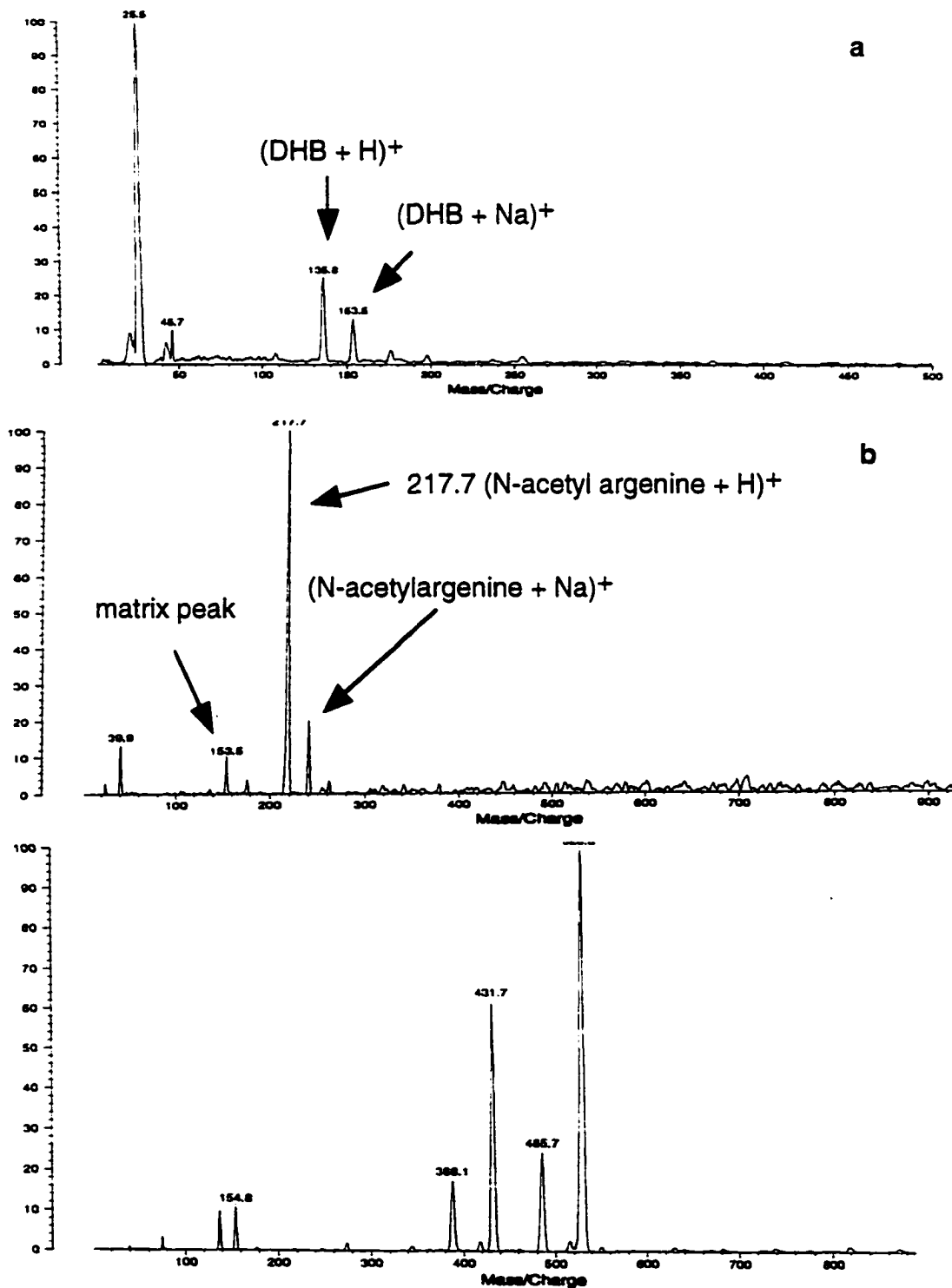
successful. The hydrazinolysis and NaH reactions had to be compared to see which reaction was more practical for arginine labeling. Here, these two reactions were repeated and the products were identified with MALDI-MS.

Figure 7.12 shows MALDI-MS spectra of a) DHB (matrix) and starting materials of b) N-acetyl-arginine and c) TMR. The peaks at 154 amu and 176 amu in Figure 7.12a are hydrogen and sodium adducts of the matrix DHB. The peak at 138 amu of the same figure is DHB with the loss of hydroxide ion. These three peaks (136 amu, 154 amu and 176 amu) are the characteristic peaks for the matrix and can be seen in almost all of the MALDI-MS spectra using DHB. The peak at 217 amu in Figure 7.12b is the protonated form of N-acetyl-L-arginine. The presence of this peak, when monitoring a labeling reaction, indicates that the reaction was not completed. In Figure 7.12c, the peak at 528 amu is the protonated form of TMR and the peak at 432 amu is hydrolyzed TMR that can be seen in most of the labeling reactions indicating that a fraction of the labeling reagent was lost because of the hydrolysis.

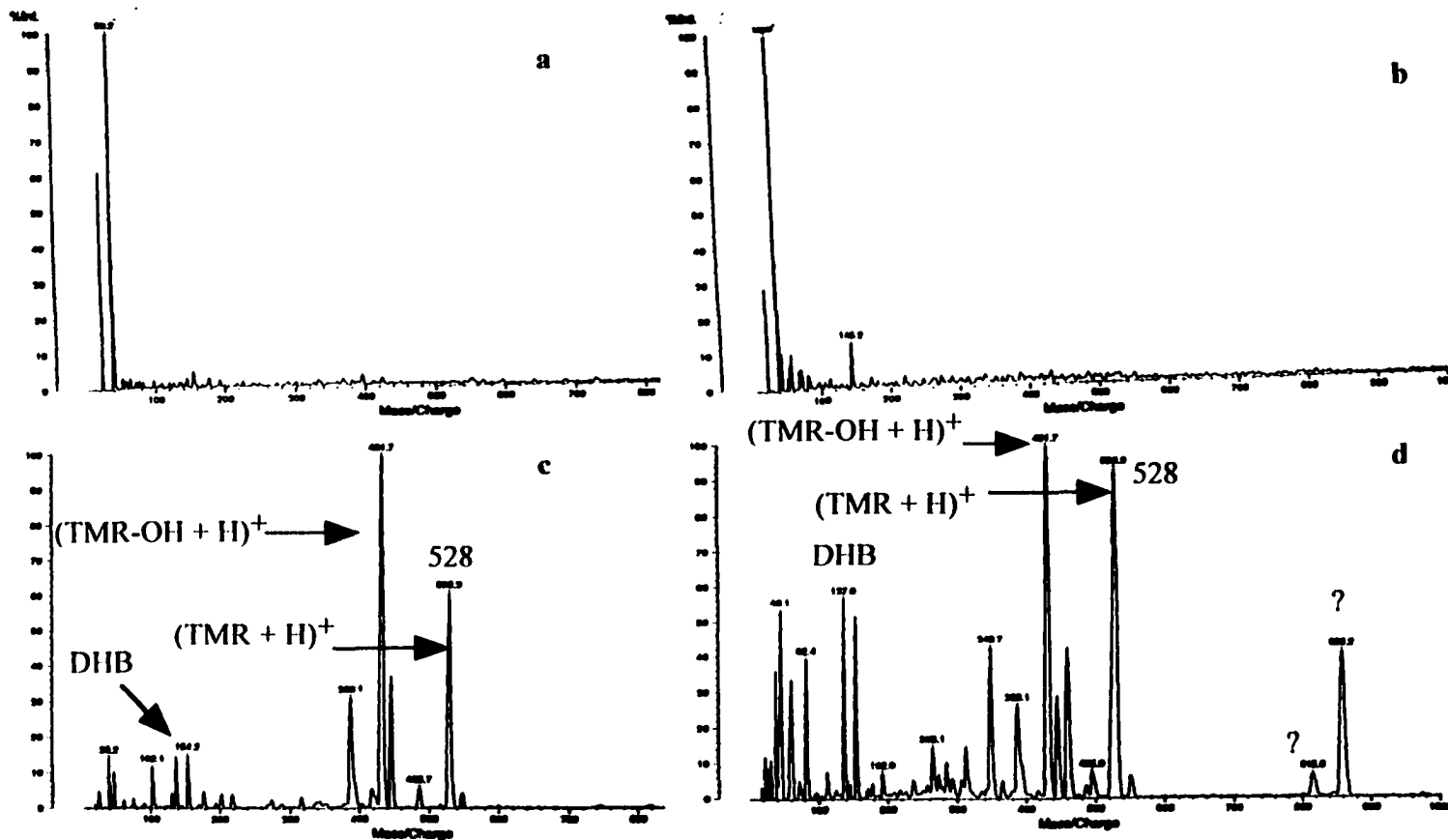
### **7.3.8 Hydrazine and NaH reactions with arginine and TMR labeling of the product after separation with ion-exchange resin**

Figure 7.13 shows the MALDI-MS spectra of the hydrazine reaction mixture after the reaction components were passed through the AG 50W and MP-50 cation-exchange resin (section 7.2.14). Figure 7.13a shows the MALDI-MS spectrum of the product eluting out of the column when washed with MeOH. The presence of no peak indicates either strong adsorption of the product to the cation-exchanger resin or the inability of MALDI to detect low molecular weight ions (173 amu for ornithine). Figure 7.13b shows the MALDI-MS spectrum of the product eluted from the column when it is washed with 2 M NaCl solution. Similar to the MeOH washed fraction, no ornithine peak was observed. The possibility that arginine was not converted to ornithine has been already ruled out by

**Figure 7.12: MALDI-MS spectra of a) dihydroxy benzoic acid (DHB) used as a matrix, b) N-acetylarginine used as a sample and c) 5-TMR used as a labeling reagent**



**Figure 7.13: MALDI analysis of hydrazine reaction mixture passed through AG50W and AGMP-50 cation-exchange resin and washed with a) MeOH, b) 2M NaCl, c) TMR labeling reaction on a and d) TMR labeling reaction on b**



ESI-MS results of the same experiment without separation (Figures 7.6 and 7.8). Figure 7.13c and Figure 7.13d show the MALDI-MS spectra of the labeling reaction on each of the MeOH-washed and NaCl-washed fractions of the hydrazine reaction after passing through the ion-exchange column. In both cases the hydrolyzed TMR peaks were observed but not the expected product. This experiment indicated that the ion-exchange technique was not suitable for this separation probably because of strong adsorption of primary amines (ornithine) on the  $R-SO_3^-H^+$  resin.

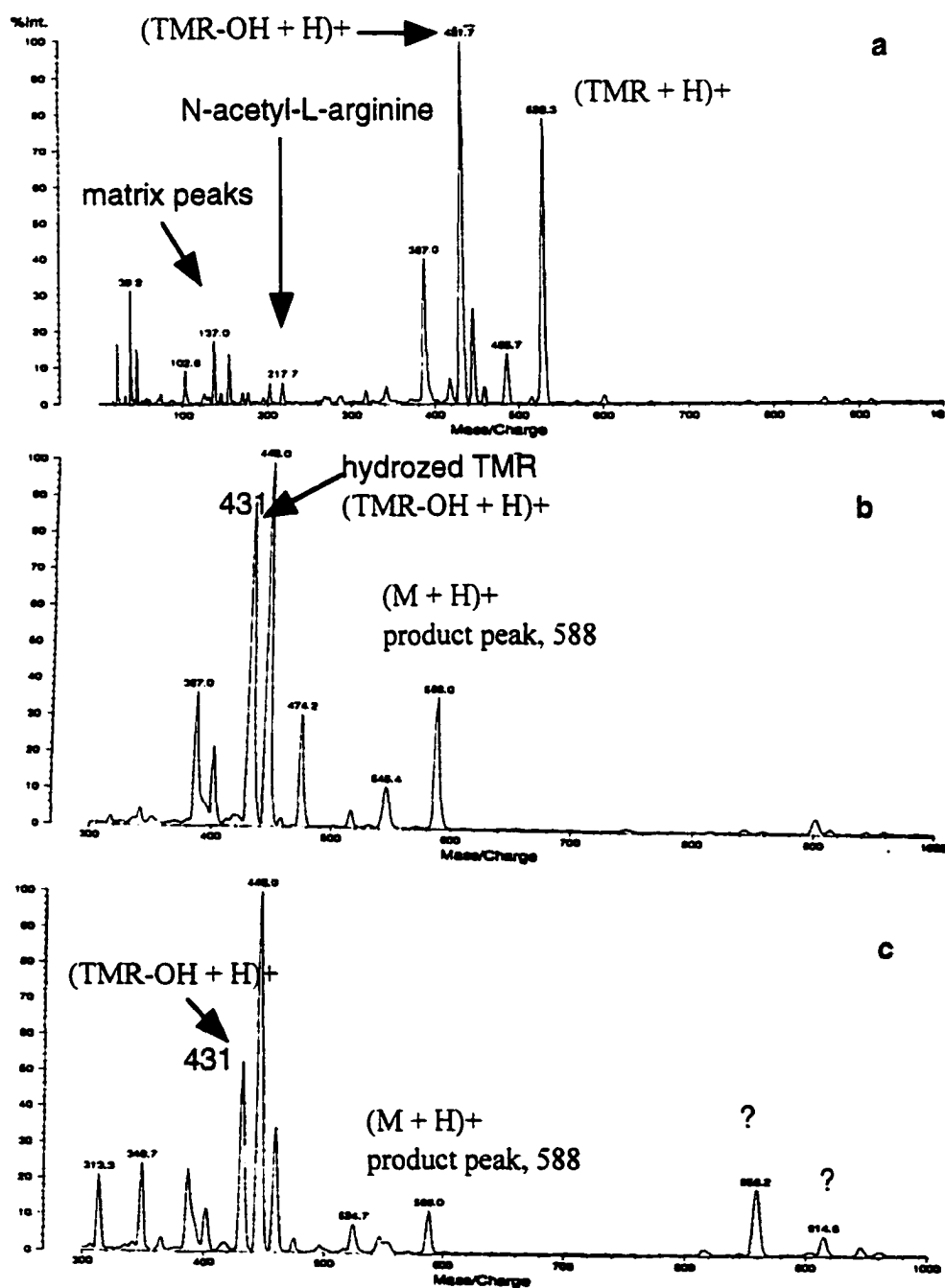
### **7.3.9 Hydrazine and NaH reactions with arginine and TMR labeling of the product after separation with Sep-Pak**

Figure 7.14 show the MALDI-MS spectrum of the hydrazine reaction mixture when labeled with TMR and separated with  $C_{18}$  Sep-Pak cartridge (7.2.16 and 7.2.17). Figure 7.14a shows the MALDI-MS spectrum of the first fraction washed with 5 mL of water. The peak at 528 amu shows the presence of excess TMR and the peak at 432 amu is due to hydrolyzed TMR. Figure 7.14b shows the MALDI-MS spectrum of the fourth fraction washed with 5 mL of water. The peak at 588 amu is the labeled ornithine and the one at 431 amu is the hydrolyzed TMR indicating the partial separation of the labeled ornithine. Figure 7.14c shows the MALDI-MS spectrum of the MeOH-washed fraction of the hydrazine reaction. The peaks at 588 amu and 431 amu indicate the coelution of the labeled ornithine and hydrolyzed TMR.

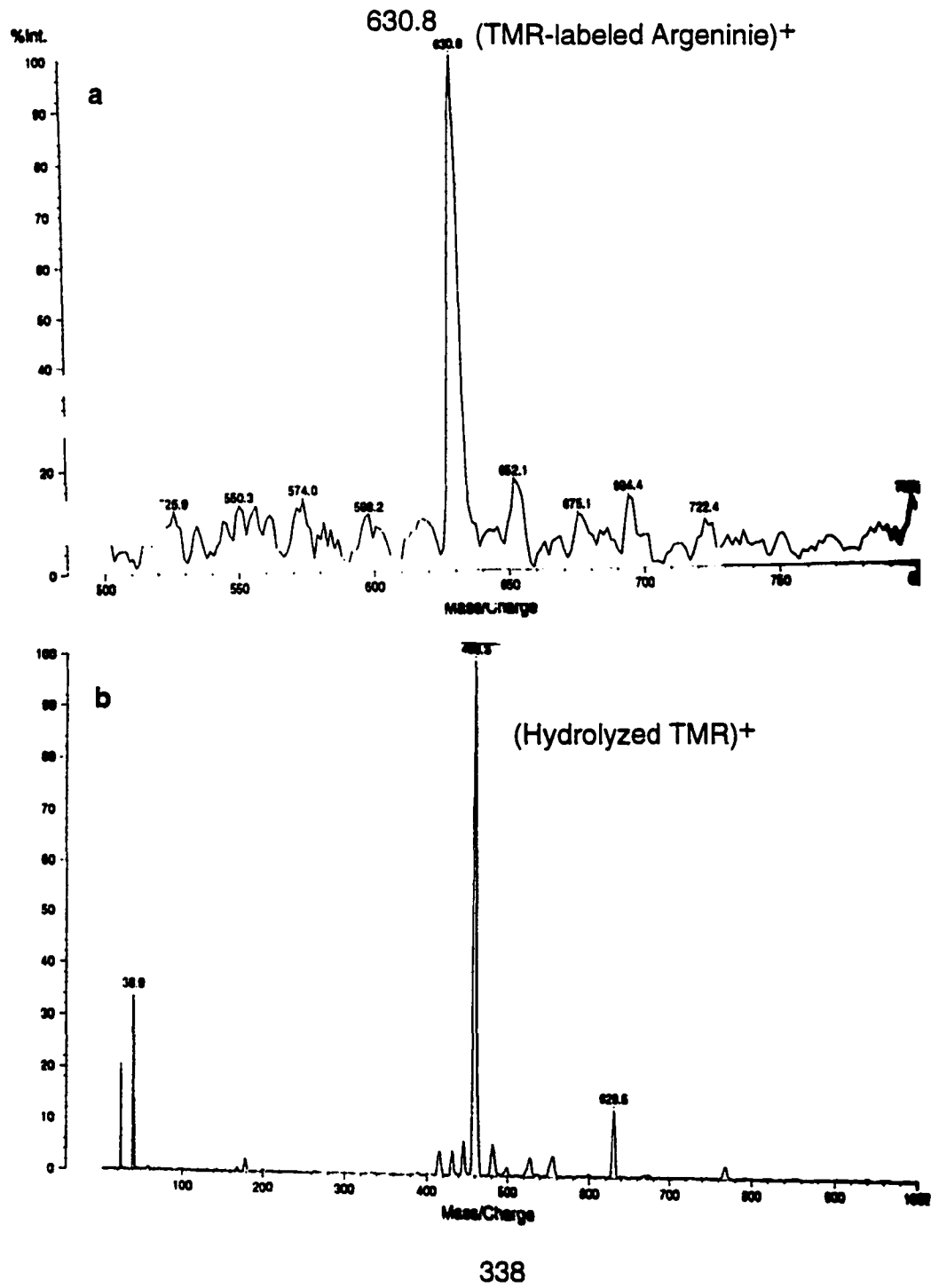
Figure 7.15 shows the MALDI-MS spectra of the NaH reaction mixture labeled with TMR and separated with  $C_{18}$  Sep-Pak column. Figure 7.15a shows the spectrum of the first fraction washed with 5 mL of water and Figure 7.15b shows the spectrum of the first MeOH-washed fraction. The peak at 631 amu is TMR-labeled arginine and the peak at 458 amu is the excess hydrolyzed TMR.



**Figure 7.14: MALDI analysis of hydrazine reaction mixture labeled with TMR and separated by C<sub>18</sub> Sep-Pak cartridge. a) first fraction washed with 5 mL of water, b) fourth fraction washed with 5 mL of water and c) first fraction washed with 5 mL of MeOH**



**Figure 7.15: MALDI analysis of sodium hydride reaction mixture labeled with TMR and separated by C18 Sep-Pak cartridge, a) first fraction washed with 5ml of water and b) first fraction washed with 5 mL of MeOH**



### 7.3.10 Hydrazine and NaH reactions with cyclic peptide

Figure 7.16 shows the chemical equations for the hydrazinolysis of cyclic peptide and the TMR labeling reaction of the expected product (sections 7.2.19 and 7.2.20).

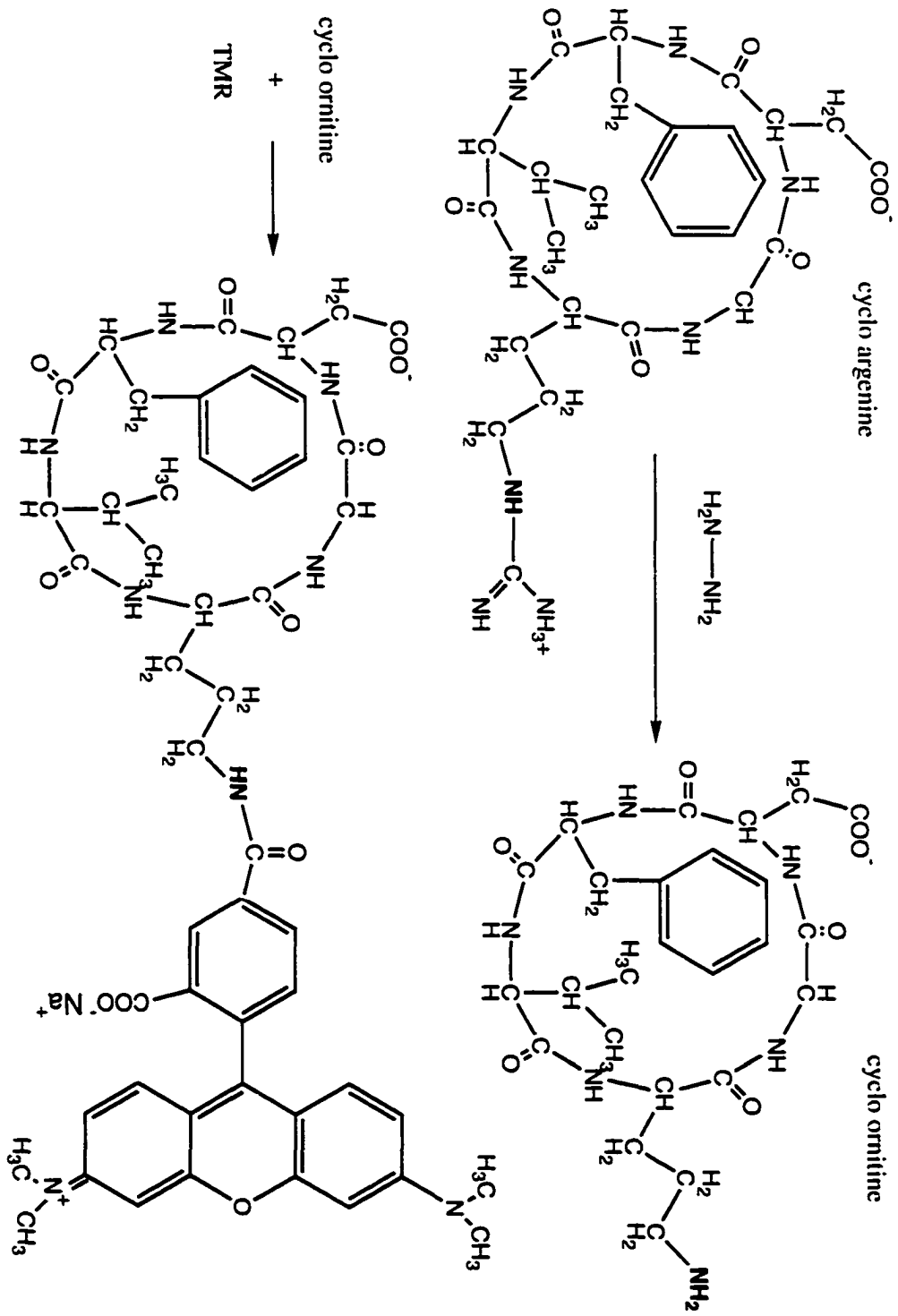
Figure 7.17 shows the chemical equations for the NaH reaction on the cyclic peptide model compound followed by TMR labeling of the arginine-deprotonated cyclic peptide (section 7.2.21 and 7.2.22).

Figure 7.18 shows the TLC for the TMR labeling reaction products of NaH and hydrazinolysis reactions of the arginine-containing cyclic peptide. TMR itself was also spotted to compare with the labeling products. TMR on TLC shows two spots, while NaH reaction shows three spots two of which having exactly the same  $R_f$  values as TMR. One extra spot on the NaH reaction column indicated that the NaH-deprotonated cyclic peptide was labeled. TLC for hydrazine reaction shows seven bands, two of which match with the  $R_f$  values of TMR. The five extra bands in the TLC of the hydrazine reaction indicates that the hydrazine cleaved all five peptide bonds producing 5 amino acids that were subsequently labeled with TMR at their N-terminal amine groups.

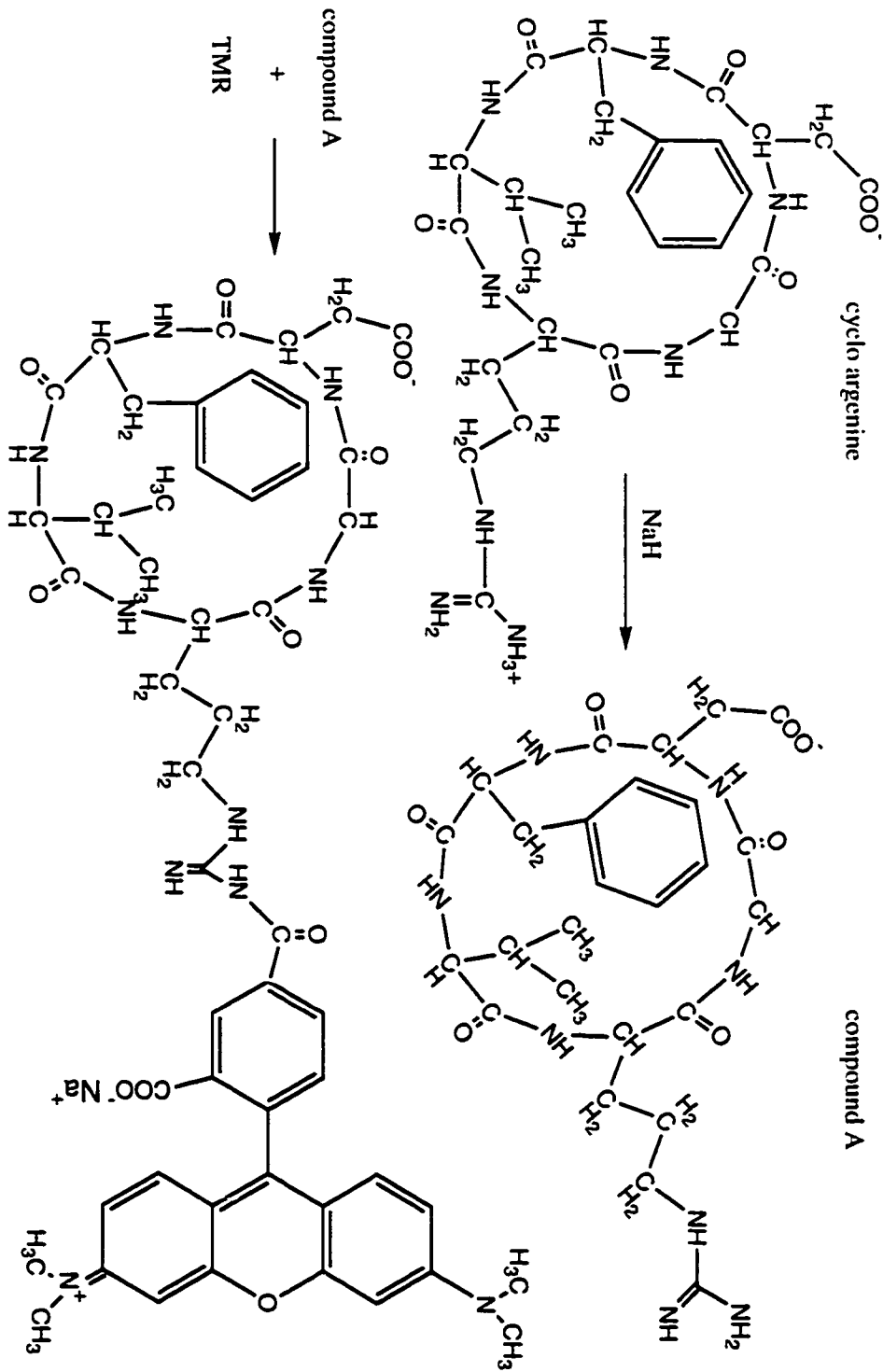
Figure 7.19 shows the positive-ion mode MALDI-MS spectra of the starting material for NaH and hydrazine reactions. Despite the presence of all the components in Figure 7.19c, the manufacturer claims the cyclic peptide to be pure. The cyclic peptide MALDI-MS spectrum shows 7 peaks indicating that the peptide itself is a mixture of two or three peptides. MS spectrum of TMR heated in DMF for 5 hours shows that TMR underwent hydrolysis, photolysis and/or pyrolysis during the course of the reaction and not all the peaks in an MS spectrum could be assigned to a labeled product.

Figure 7.20 shows the positive-ion mode MALDI-MS spectra of the hydrazine reaction of the cyclic peptide before and after labeling reaction but without separation and for different fractions collected from C<sub>18</sub> Sep-Pak cartridge. This figure shows that in the

**Figure 7.16: Chemical reaction of cyclo (Arg-Gly-Asp-Phe-Val) by hydrazine and TMR labeling of the product**



**Figure 7.17: NaH reaction with arginine containing cyclic peptide and TMR labeling of the resulting product**



**Figure 7.18: TLC of a) TMR, b) hydrazinolysis reaction product of cyclic peptide (Arg-Gly-Asp-Phe-Val) and c) NaH reaction product of cyclic peptide**

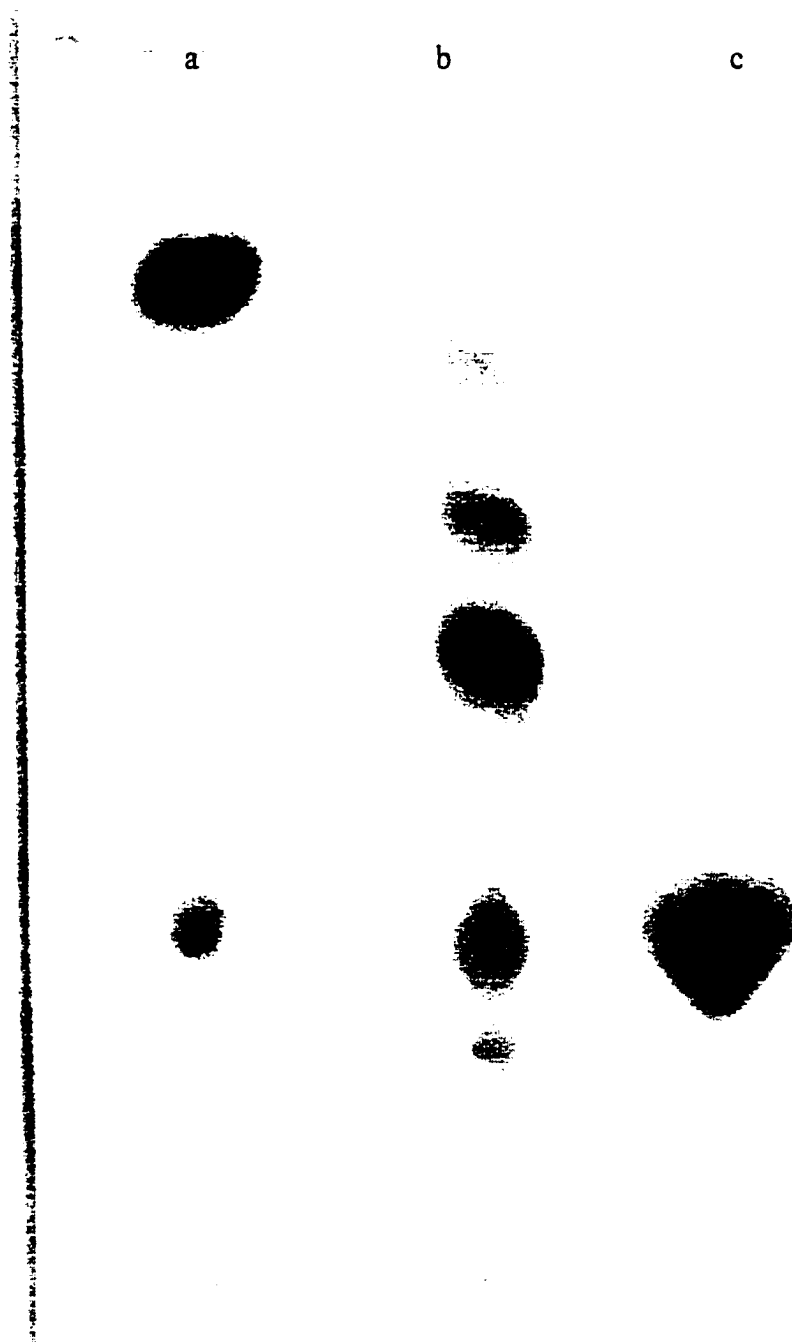
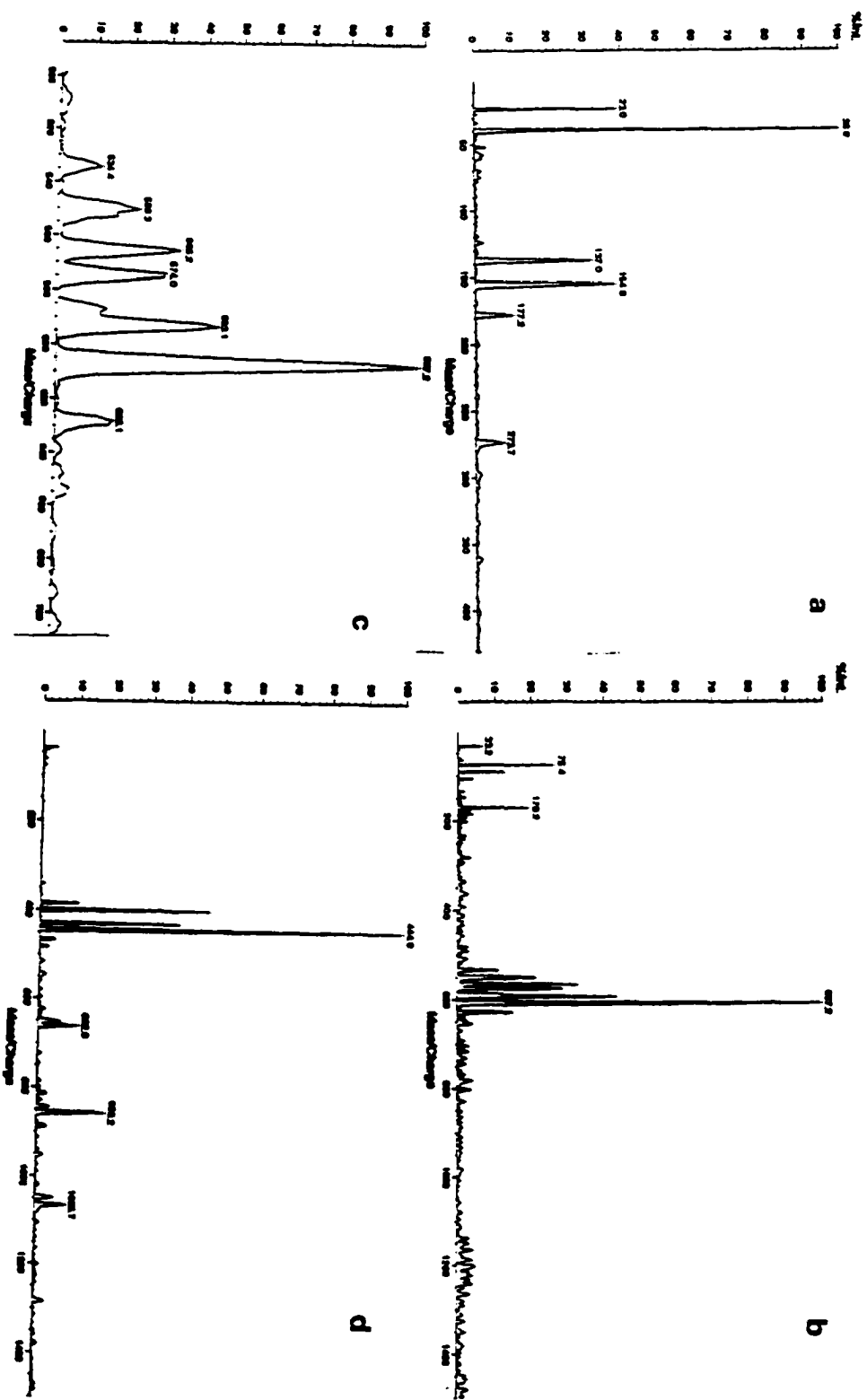
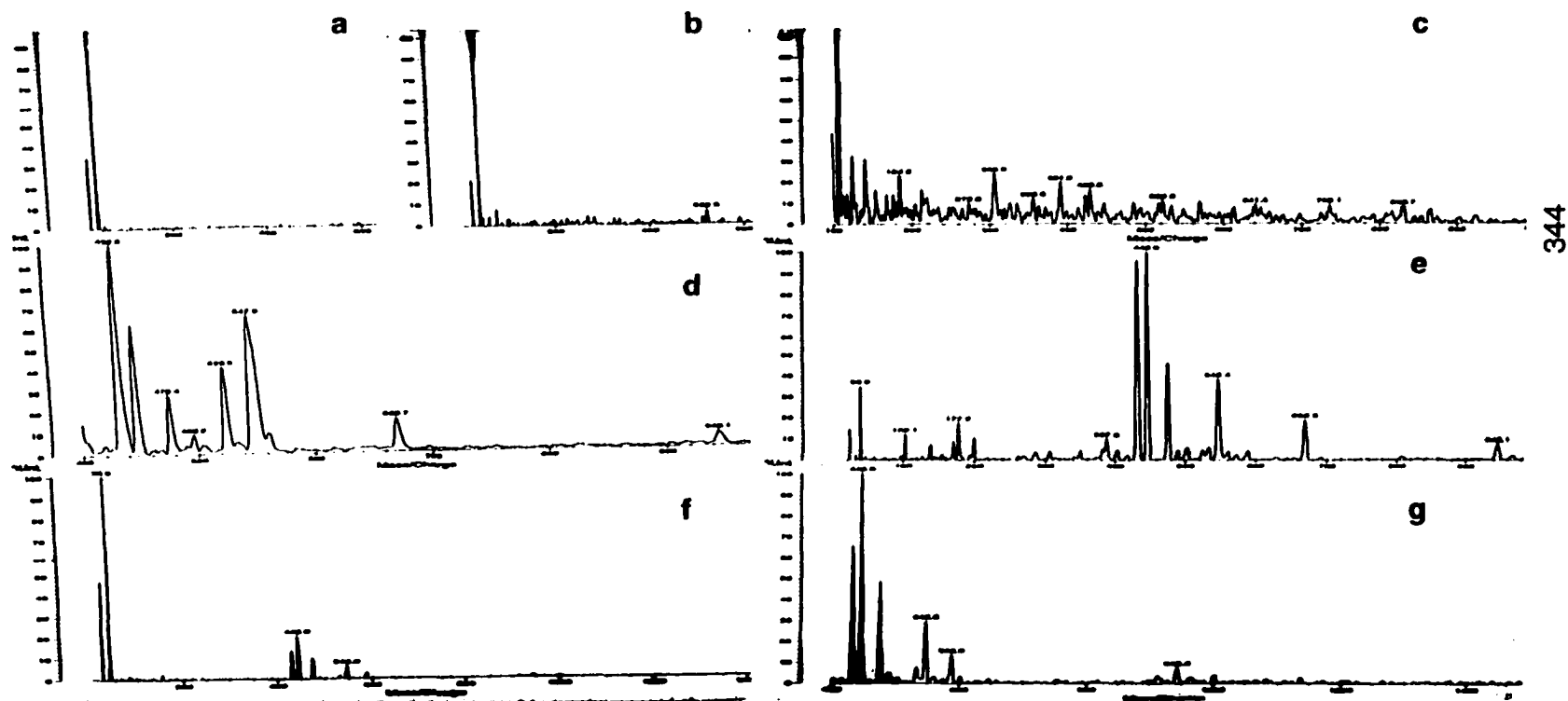


Figure 7.19: MALDI-MS spectra of a) DHB matrix, b) cyclic peptide, c) expansion of b, and d) TMR in DMF



**Figure 7.20: MALDI-MS spectra of the hydrazine reaction products of cyclic peptide a) before labeling reaction and before separation, b) after labeling reaction but before separation, c) after labeling reaction and the first water washed out of the Sep-Pak cartridge, d) after labeling reaction and first MeOH washed out of Sep-Pak cartridge, e) after labeling reaction and 5th MeOH wash, f) 10th MeOH wash and g) 15th MeOH wash out of the Sep-Pak cartridge**





absence of separation, the product peak is swamped by many other side products. It also shows many other unidentified side products resulting from peptide bond cleavage.

Figure 7.21 shows the MALDI-MS spectra for NaH reaction with cyclic peptide before and after labeling. The MALDI-MS spectra for different fractions washed out of Sep-Pak with MeOH indicate most of the decomposed TMR coelutes with labeled cyclic peptide and Sep-Pak separation by itself is not efficient enough to separate all of the present components and the Sep-Pak separation has to be combined with TLC separation.

There was another attempt to identify all the peaks in different fractions collected from preparative TLC. Preparative TLC (Figure 7.18) was repeated and each band was cut out and extracted in MeOH.

Figure 7.22 shows MALDI-MS spectra for the blank TMR dissolved in DMF and separated by preparative TLC. Trace a is the DHB matrix, trace b is the first band recovered from TLC and trace c is the second band recovered from TLC. Despite having two different  $R_f$  values in TLC, the two separated bands have the same molecular weight. This suggests that the purchased TMR, claimed to be pure by the manufacturer, is a mixture of 5-TMR and 6-TMR. The two isomers have the same molecular weight but they may have different  $R_f$  values on TLC. Trace b shows a small peak at 528 amu for TMR, but trace c shows just the hydrolyzed TMR at 431 amu.

Figure 7.23 shows the MALDI-MS spectra for band 1 to band 7 of the preparative TLC performed on hydrazinolysis reaction of cyclic peptide followed by TMR labeling of the resulting product. None of the separated bands correspond to TMR-labeled cyclic peptide. This indicates that most of the peptide bonds of the cyclic peptide are cleaved by hydrazine and these bands are probably labeled amino acids.

**Figure 7.21: MALDI-MS spectra for NaH reaction with cyclic peptide followed by TMR labeling of the product, a) cyclic peptide reaction with NaH before labeling, b) after labeling but before separation, c) Sep-Pak separation of first MeOH washed fraction, d) second MeOH washed, e) third MeOH washed and f) expansion of e**

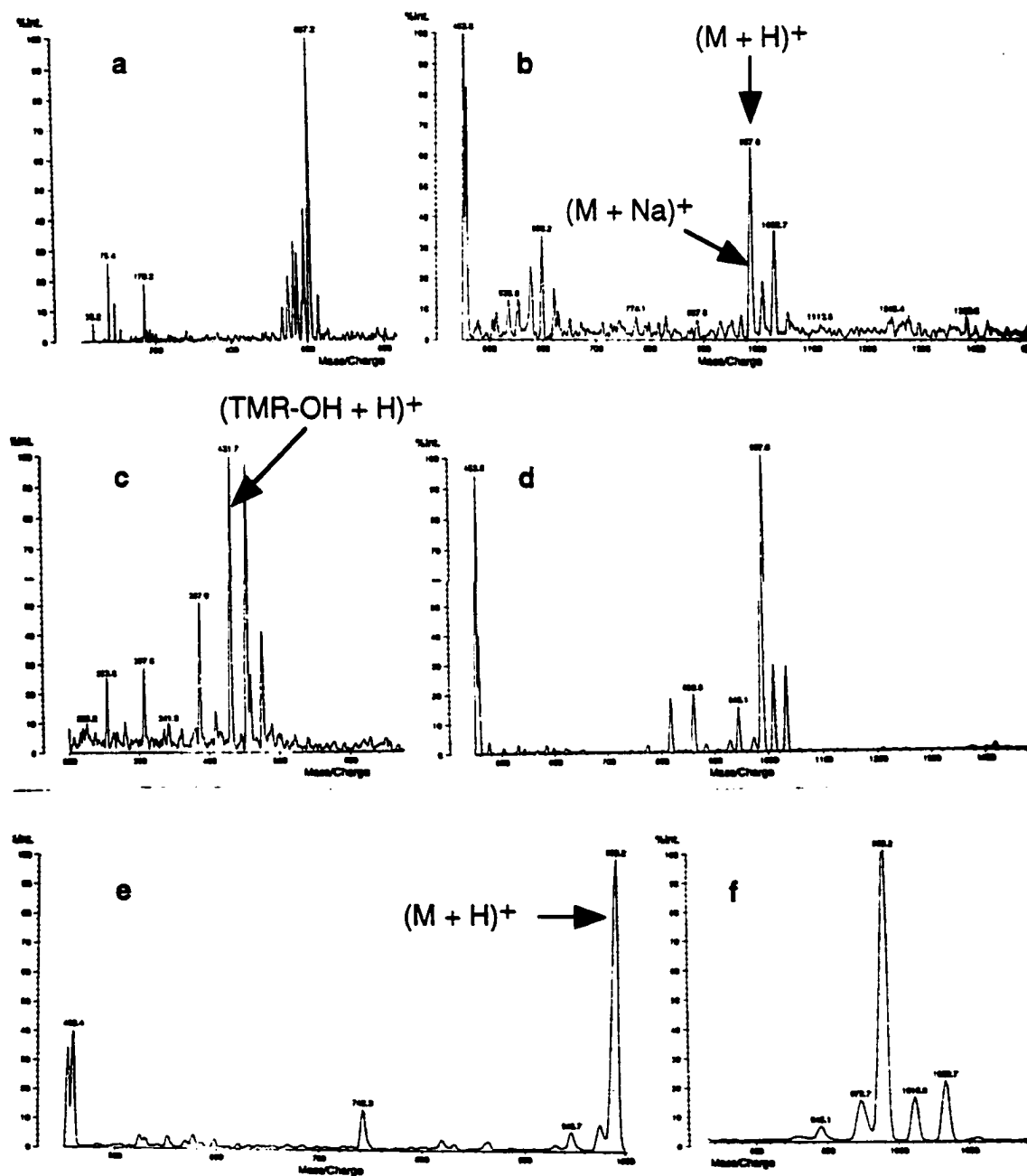
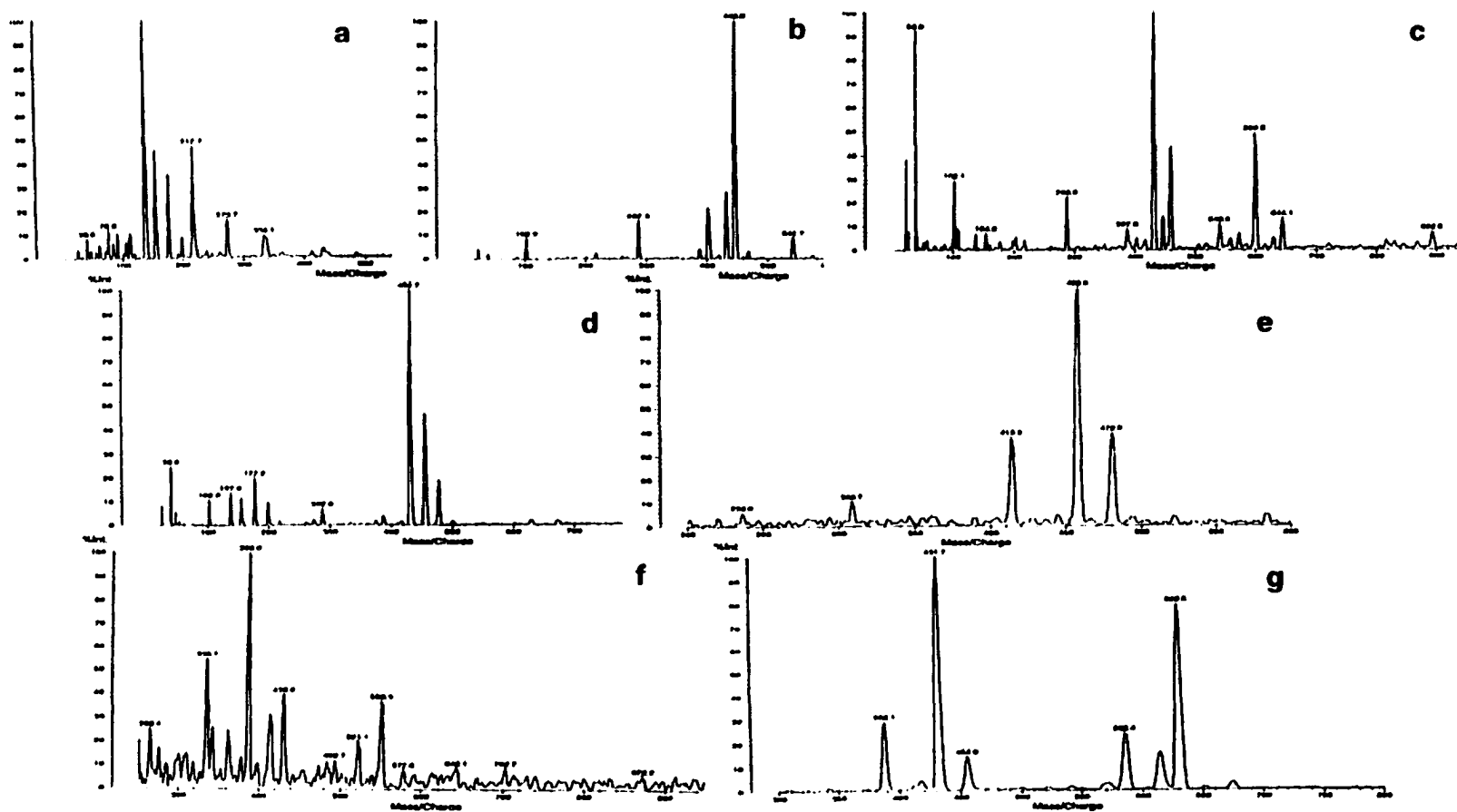




**Figure 7.23: MALDI-MS spectra of the hydrazinolysis reaction of cyclic peptide followed by TMR labeling of the products.**

**The labeled product is separated by preparative TLC and spectra a - g show fractions 1 to 7, respectively**



### **7.3.11 Furfurylamine and 4-aminoacetophenone reactions with 5-BrMF followed by the oxidation of the resulting products**

Figure 7.24 shows the reaction of 5-BrMF and furfurylamine followed by the ozonolysis of the product (Sections 7.2.33 and 7.2.34). Because furfurylamine is an aliphatic amine and a good nucleophile, it reacts quickly and efficiently with 5-BrMF.

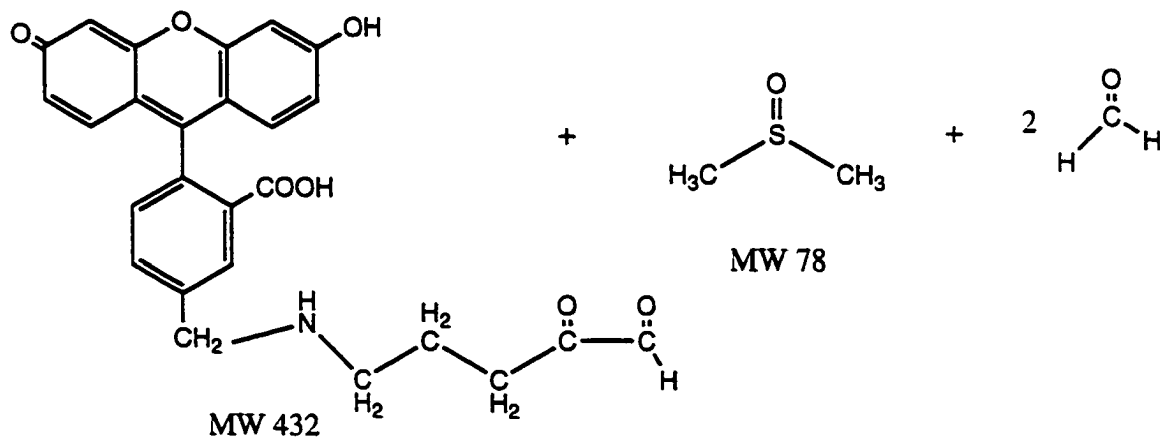
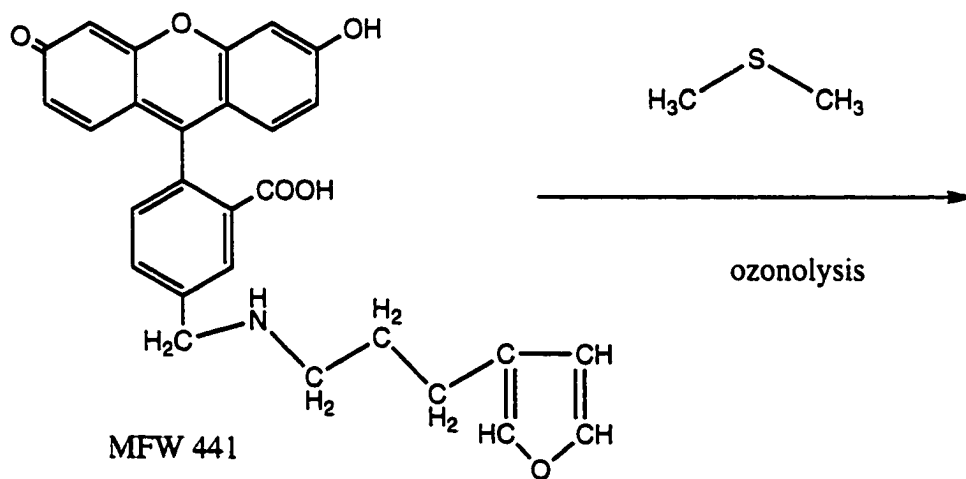
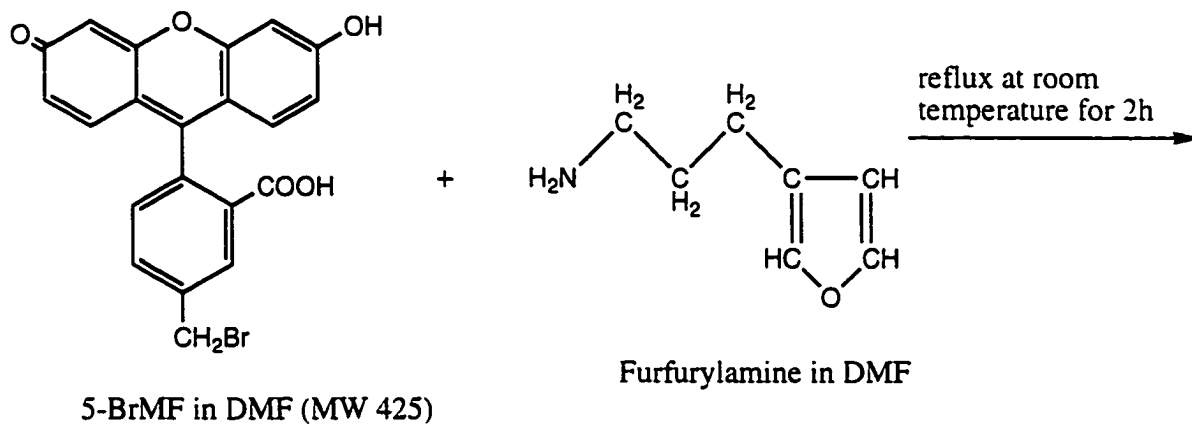
Figure 7.25 shows the chemical equations for the reaction of 5-BrMF and 4-aminoacetophenone followed by the oxidation of the reaction product with  $\text{SeO}_2$  (Sections 7.2.25 and 7.2.26). Because 4-aminoacetophenone is an aromatic amine and, therefore, a poor nucleophile; it reacts slowly and has a low yield.

Figure 7.26 shows the MALDI-MS spectra of the furfurylamine reaction with 5-BrMF and the ozonolysis of the reaction product. The first step of the reaction went to completion, i.e. furfurylamine displaces the bromide ion of 5-BrMF efficiently. The second step did not happen. Ozonolysis of the blank shows the destruction of aromatic rings in 5-BrMF if the reaction time is long. The peak at 705 amu in trace b is an unidentified oxidized product.

Figure 7.27 shows the MALDI-MS spectra of the 4-aminoacetophenone reaction with 5-BrMF and  $\text{SeO}_2$  oxidation of the resulting product. Because 4-aminoacetophenone is an aromatic amine and, therefore, a weak nucleophile, the reaction is slow. The first step of the reaction went to completion, but the oxidation yield was low. Oxidation of the blank 5-BrMF with  $\text{SeO}_2$  shows that the aromatic conjugated rings of fluorescein were destroyed because of oxidation (data not shown).

Condensation of an aliphatic or aromatic amine with 5-BrMF was possible, but the second step of oxidation, ozonolysis, was not as easy and needed much more optimization of conditions. The  $\text{SeO}_2$  oxidation yield is low. To bypass this oxidation step, I decided to couple a molecule that already contains a diketone functionality with benzyl bromide as a

**Figure 7.24: Chemical equations for the synthesis of an arginine-specific reagent using furfurylamine followed by ozonolysis of the product**



**Figure 7.25: Chemical equations for the synthesis of an arginine-specific reagent using aminoacetophenone followed by oxidation of the product**

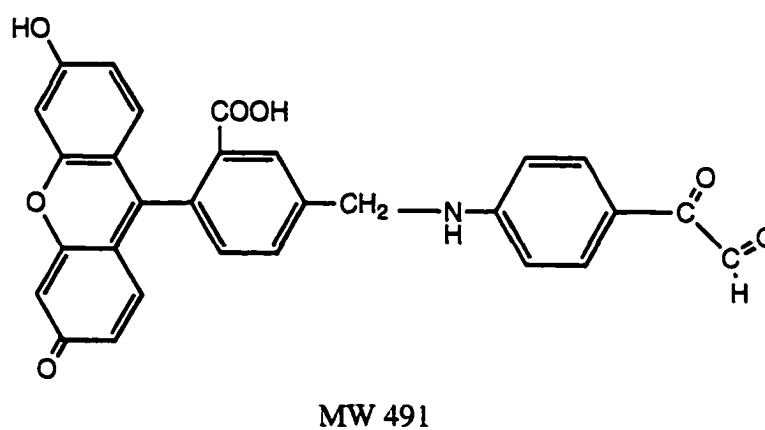
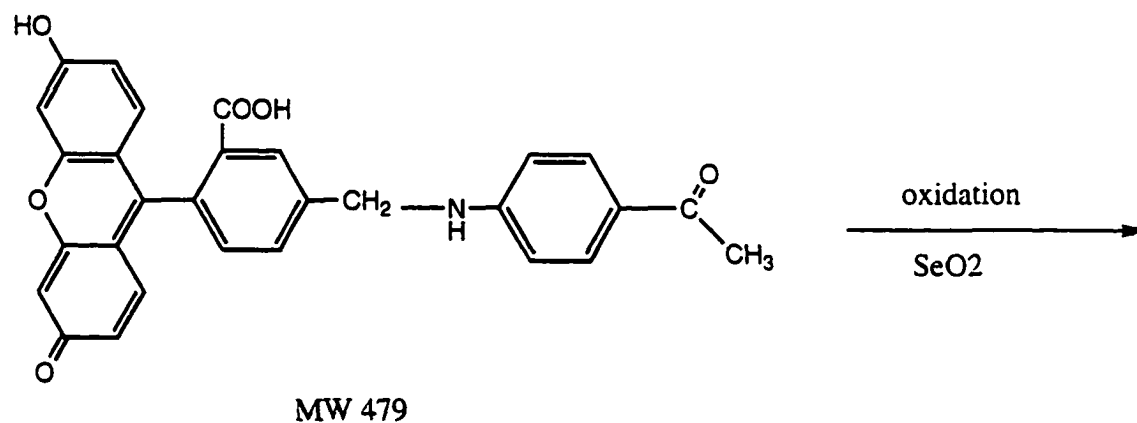
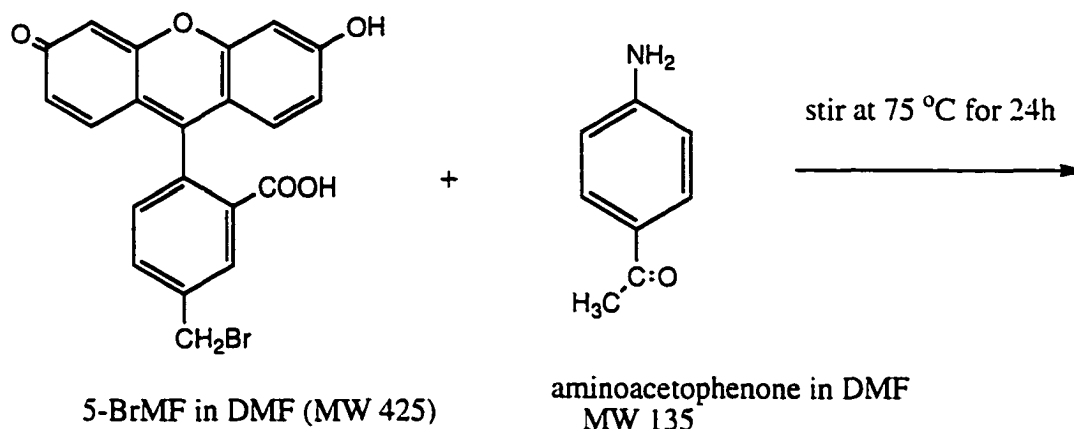


**Figure 7.26: MALDI-MS spectra of a) furfurylamine condensation reaction with 5-BrMF and b) ozonolysis of the furfurylamine condensation product**

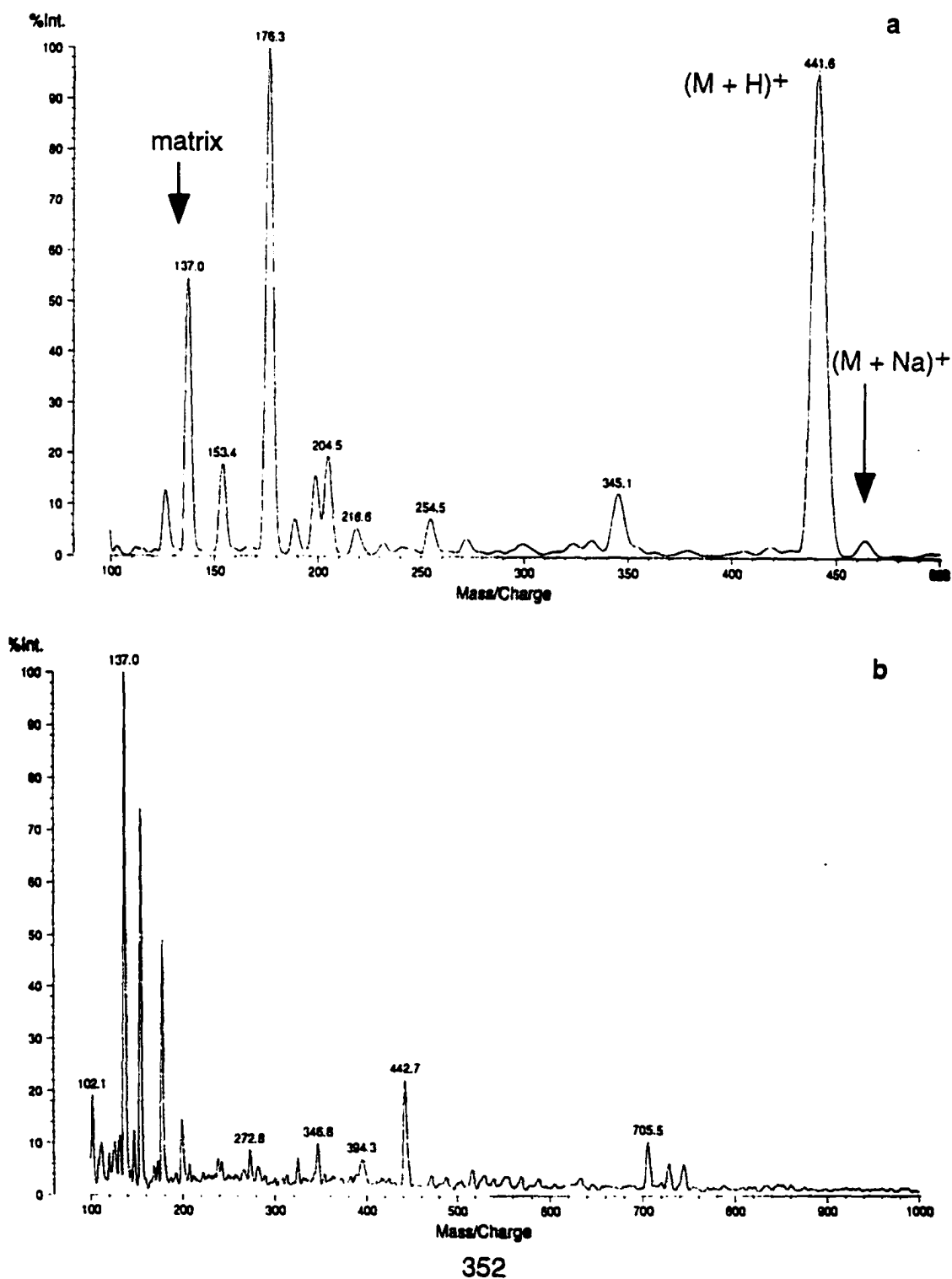
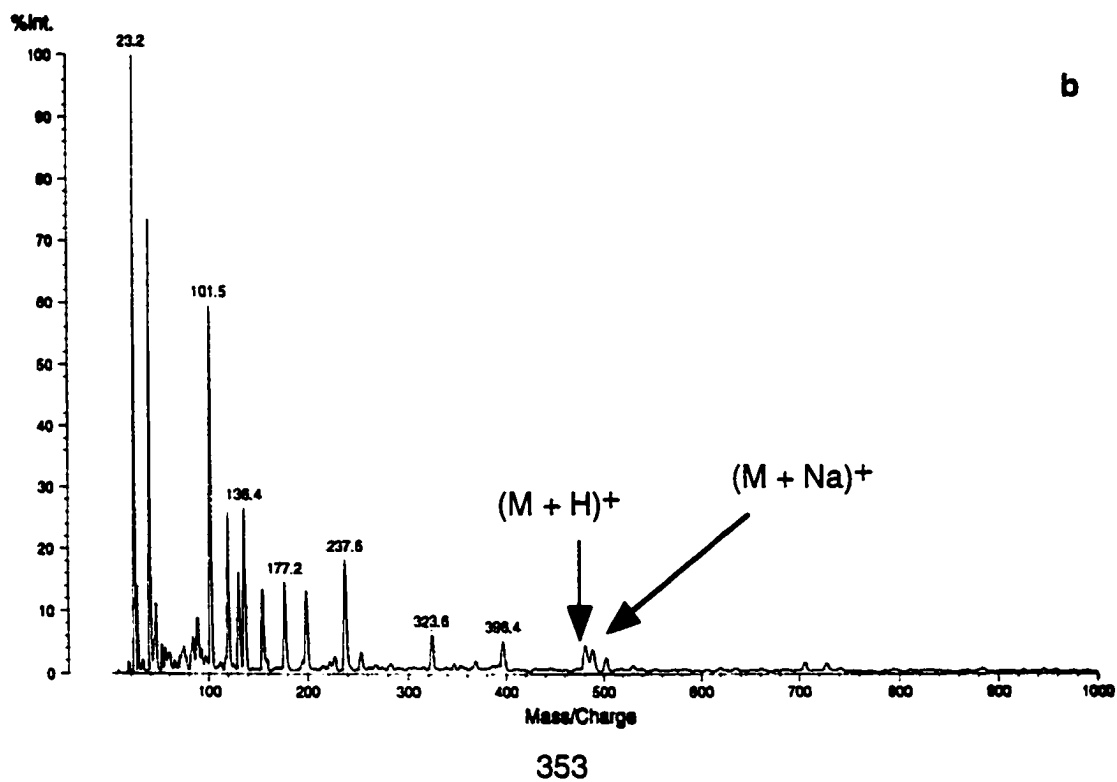
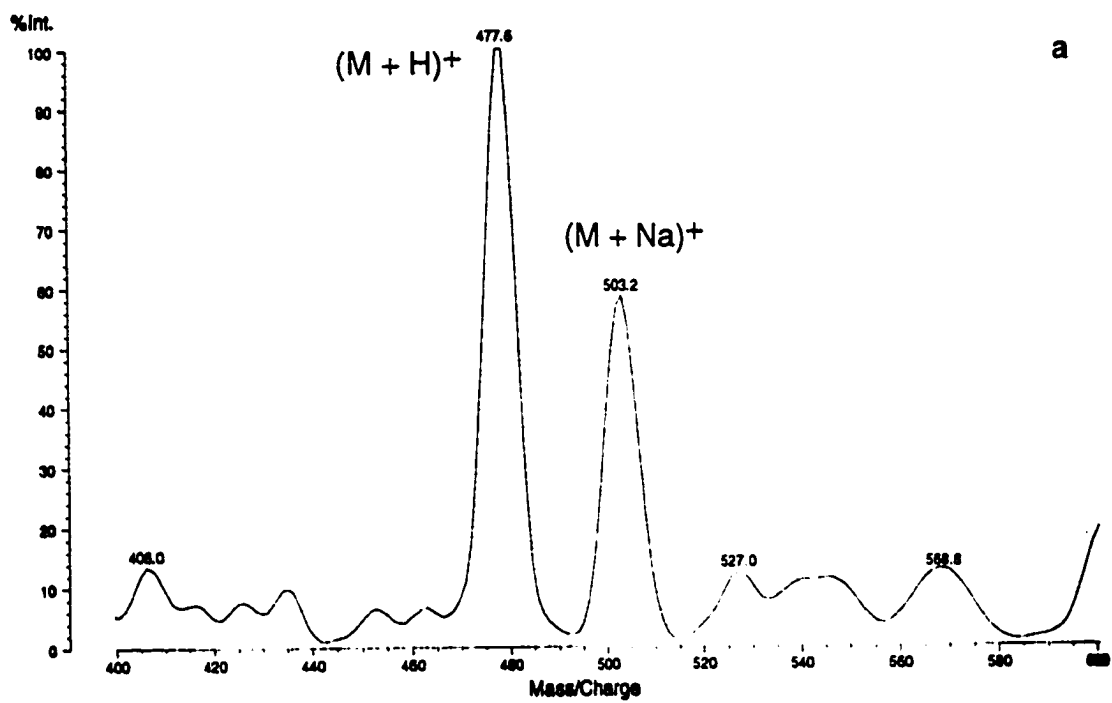




**Figure 7.27: MALDI-MS spectra of a) 4-aminoacetophenone condensation reaction with 5-BrMF and b) SeO<sub>2</sub> oxidation of the resulting product from condensation**



model compound for 5-BrMF. A similar reaction for the synthesis of 5-thiomethylpentane-2,3-dione has been reported in the literature.<sup>35</sup>

### 7.3.12 Butanedione reaction with benzylbromide

Figure 7.28 shows chemical equations for the 2, 3 butanedione reaction with benzylbromide and possible condensation of 2,3 butane dione (Section 7.2.27).

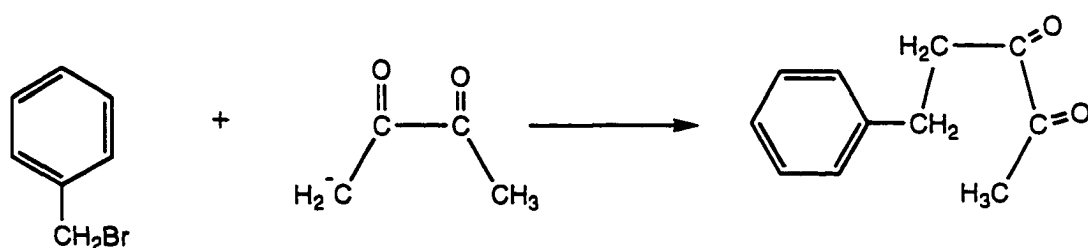
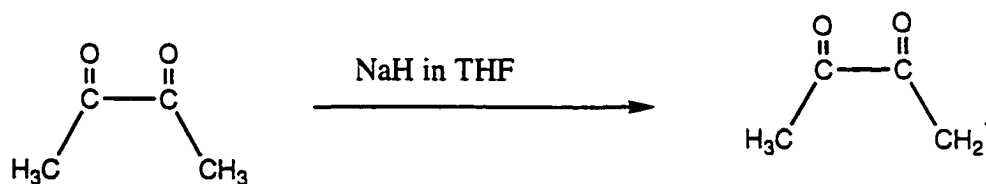
Figure 7.29 shows the MALDI-MS spectra for 2,3 butanedione dimerization in basic conditions and also the product formed from the 2,3 butane dione reaction with benzylbromide. The same reaction under similar conditions was repeated with 5-BrMF and a diketone derivative of fluorescein was prepared.

### 7.3.13 Butanedione reaction with 5-BrMF

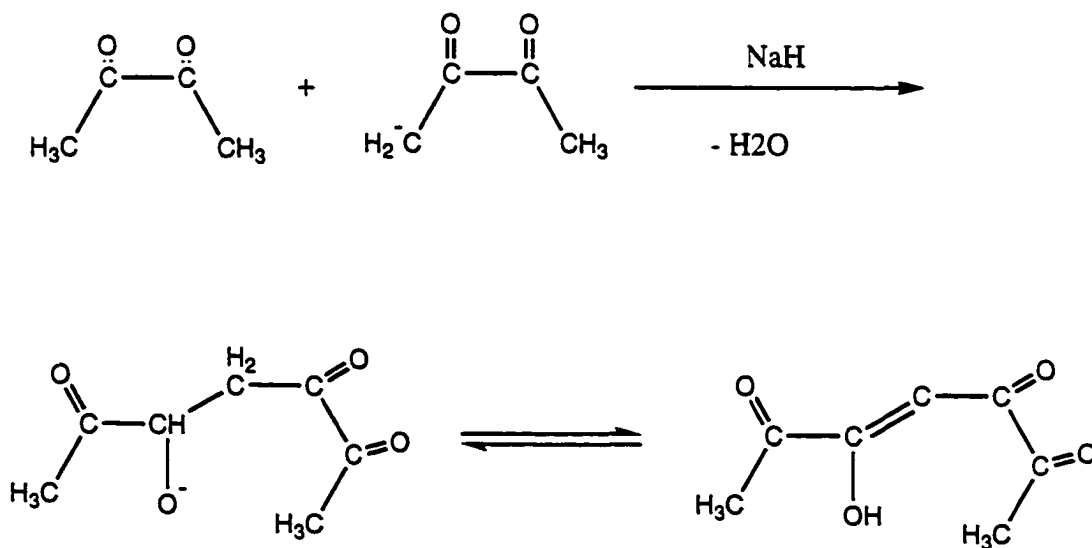
Figure 7.30 shows the chemical equations for the 2,3-butanedione trimerization and its reaction with 5-BrMF to synthesize an arginine-specific labeling reagent (section 7.2.28). It has been showed that 2,3-butane dione in acidic media (DHB matrix for MALDI) changes to a tricyclic trimer compound.<sup>14, 36-37</sup> This trimer was observed in the MALDI-MS spectrum of butane dione.

Figure 7.31 shows the MALDI-MS spectra for the product of the 2,3 butanedione reaction with 5-BrMF. The peak at 431 amu is 5 (pentane 2,3 dione) fluorescein. The peak at 453 amu is the sodium adduct of the arginine-specific reagent. Higher molecular weight peaks are not identified. They could either be side products or dimer/trimer adducts of butane dione and 5-BrMF and/or sodium/potassium adduct of these side products.

**Figure 7.28: Chemical equations showing 2, 3 butanedione coupling to benzyl bromide and dimerization of diketone**



benzyl bromide in THF



**Figure 7.29: MALDI-MS spectra of a) 2, 3, butanedione, b) benzylbromide and c) 2, 3, butanedione condensation reaction with benzyl bromide**

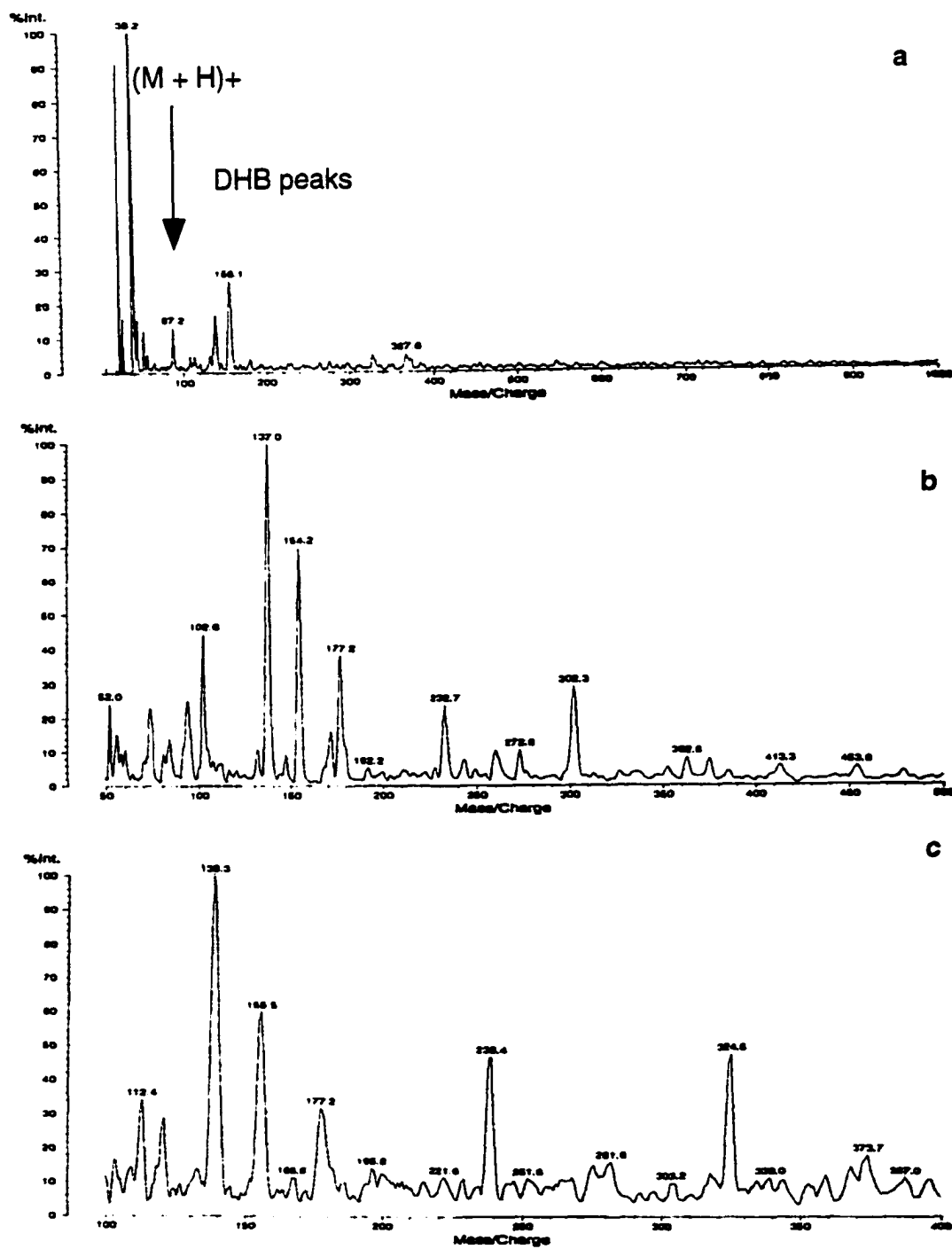


**Figure 7.30: Chemical equations showing 2, 3 butanedione trimerization and its reaction with 5-BrMF to synthesize an arginine-specific labeling reagent**

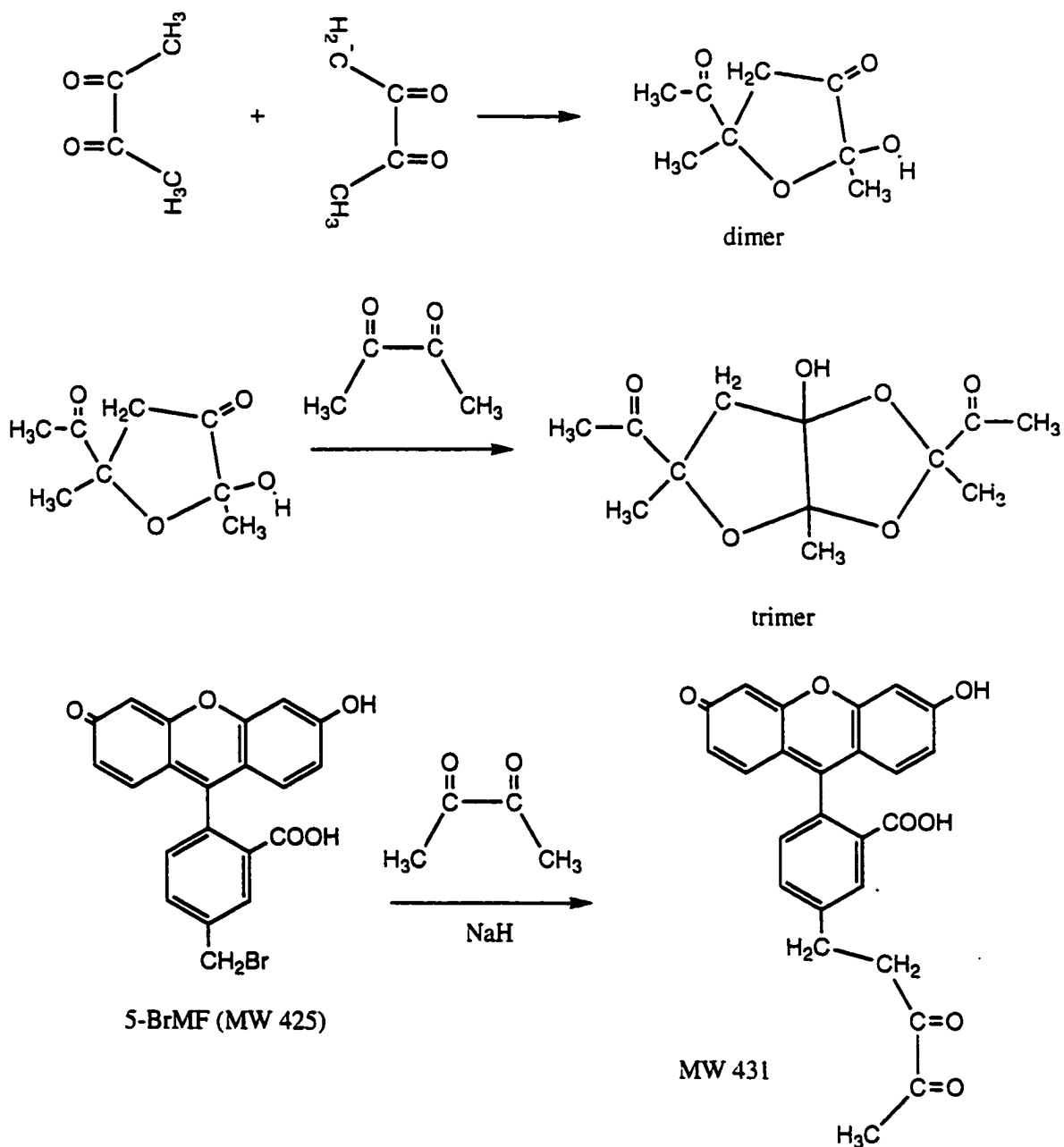
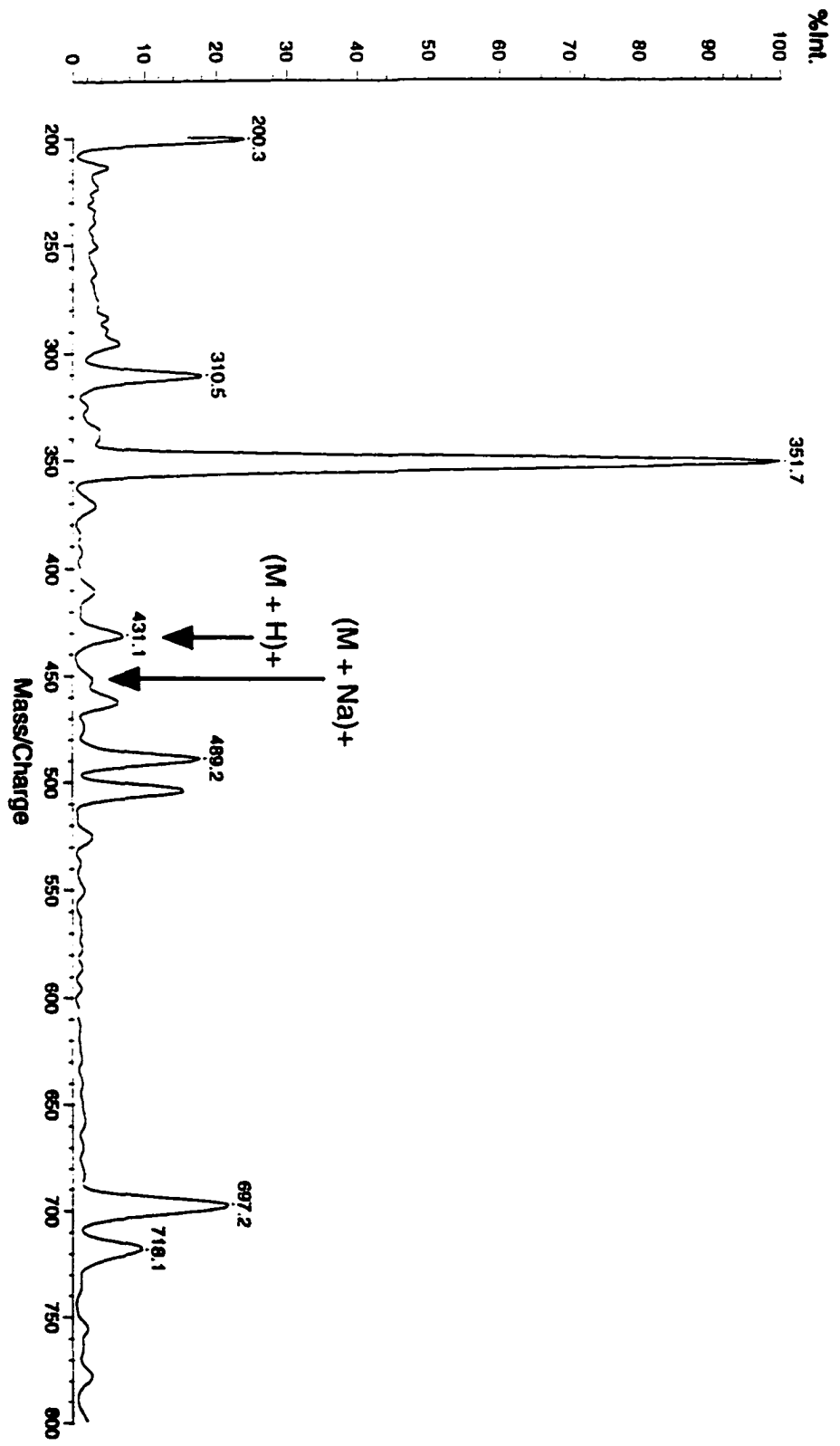


Figure 7.31: MALDI-MS spectra of 2, 3, butane dione reaction with 5-BrVMF for the synthesis of an arginine-specific fluorescent reagent



The positive charge of the arginine is effectively distributed over the entire guanidinium group. In the protonated form, the guanidinium group is nonreactive, and only very small fractions of the nonionized form are present at physiological pH values.

The exact mechanism of arginine reaction with a diketone is not known, but it is said that the formation of heterocyclic condensation products of 1, 2 and 1, 3-dicarbonyl compounds, such as glyoxal, phenyl glyoxal, 2, 3-butane dione and 1,2-cyclohexane dione reacts with the arginine group. The reaction is favored because the distance between the two carbonyl groups of the reagents also matches that between the two unsubstituted nitrogen atoms of the guanidinium group.<sup>38-39</sup>

#### **7.3.14 Arginine labeling reaction with synthesized 5(pentane 2, 3 dione) methylfluorescein**

Figure 7.32 shows the chemical equations of arginine labeling with the synthesized fluorescent diketone reagent (section 7.2.29). The product could form a borate complex or a water molecule will be lost in acidic conditions of MALDI sample preparation.<sup>13</sup>

Arginine could react with a monomer biacetyl, a dimer biacetyl, a trimer biacetyl or a combination of them and this will cause a mixture of different products that is difficult to isolate and identify. From an analytical point of view, arginine is the limiting reagent and the reaction is quantitative for arginine.<sup>13, 16-19, 43-44</sup>

Figure 7.33 shows the MALDI-MS spectra of arginine and its reaction product with 5 (2, 3 pentane dione) methylfluorescein in the presence and absence of borate buffer. When the borate is absent (Figure 7.33b) all the starting material peaks are observed along with the product peak indicating that the reaction is not complete. The peak at 217 amu is unreacted arginine, the peak at 431 amu is unreacted 5 (2, 3 pentane dione) methylfluorescein and the peak at 413 amu is the hydrolyzed 5 (2, 3 pentane dione) methylfluorescein in acidic media of matrix. The peaks at 691 amu and 725 amu are sodium

**Figure 7.32: Chemical equations of arginine labeling with the diketone derivative**

**of fluorescein**

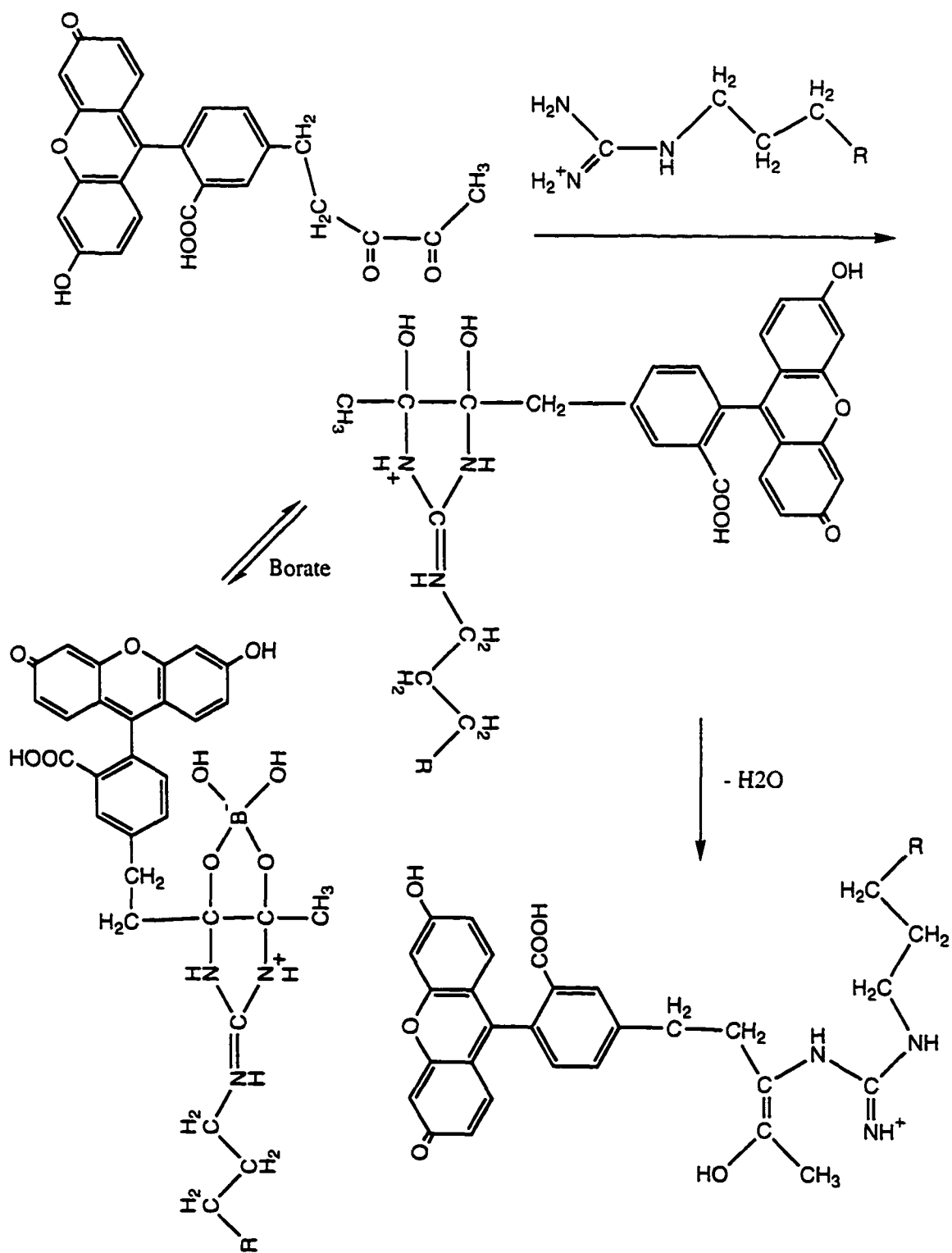
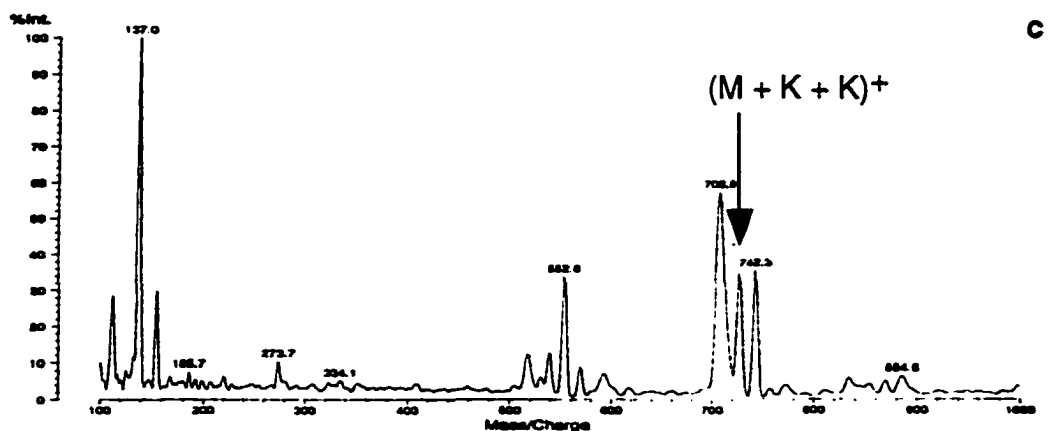
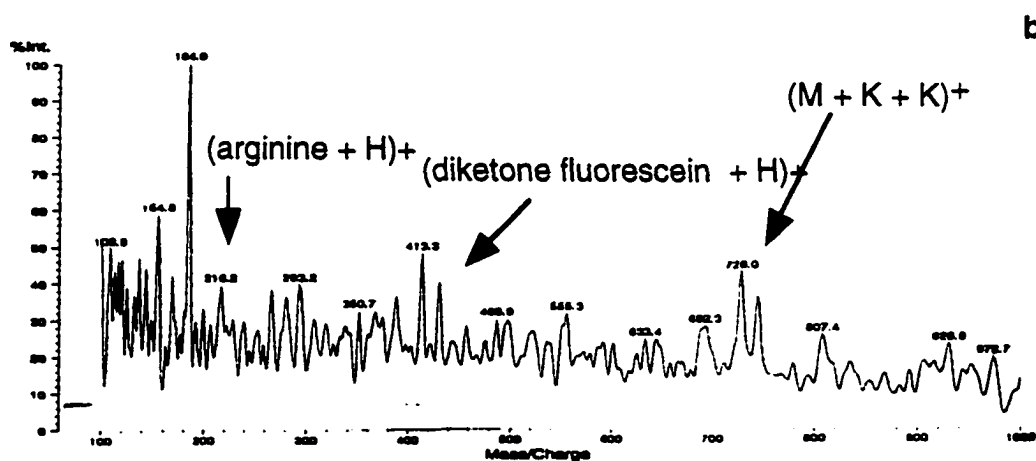
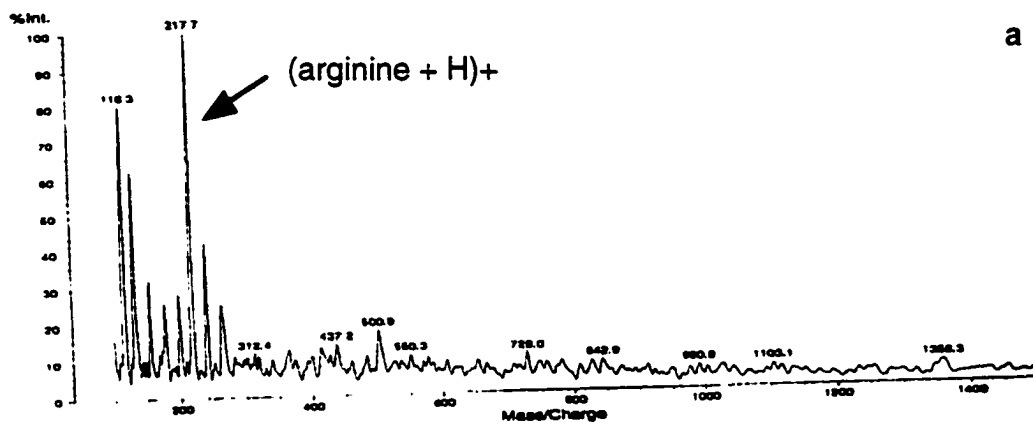




Figure 7.33: MALDI-MS spectra of a) N-acetyl-L-arginine, b) arginine-labeling reaction with 5(2, 3 butanedione) methylfluorescein in the absence of borate and c) arginine-labeling reaction with 5(2, 3 butanedione) methylfluorescein in the presence of borate



and potassium adducts of the product, respectively. When the reaction is repeated in borate buffer (Figure 7.33c) both the arginine and 5(2, 3 pentane dione) methyl fluorescein peaks disappeared indicating the completion of the reaction. In this case, however, the product peaks at 691 amu and 725 amu have shifted to higher molecular weight peaks suggesting that the product and borate formed a complex.

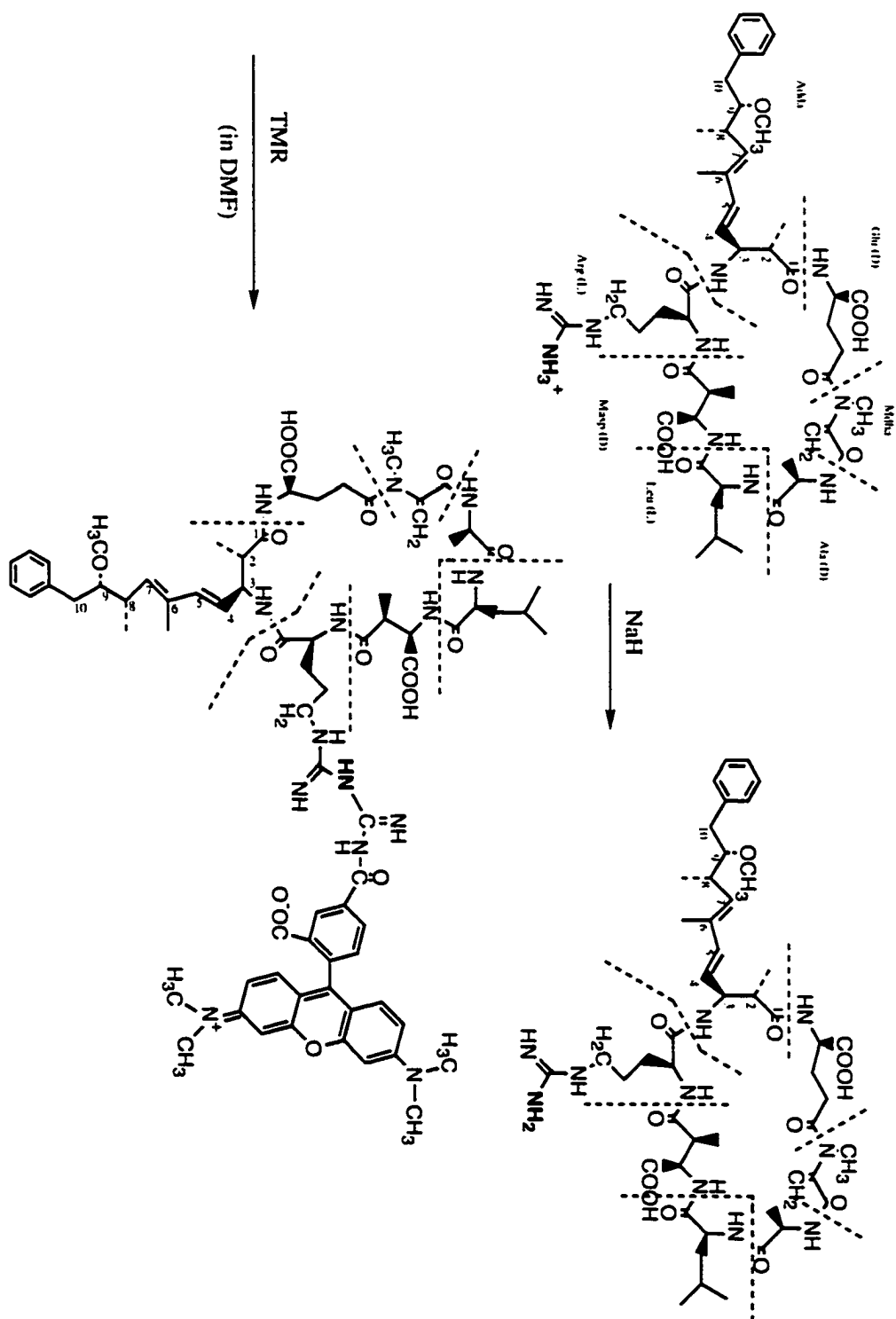
### 7.3.15 Microcystin labeling with TMR using NaH deprotonation

Figure 7.34 shows the microcystin-labeling reactions with TMR using NaH for deprotonation (section 7.2.30).

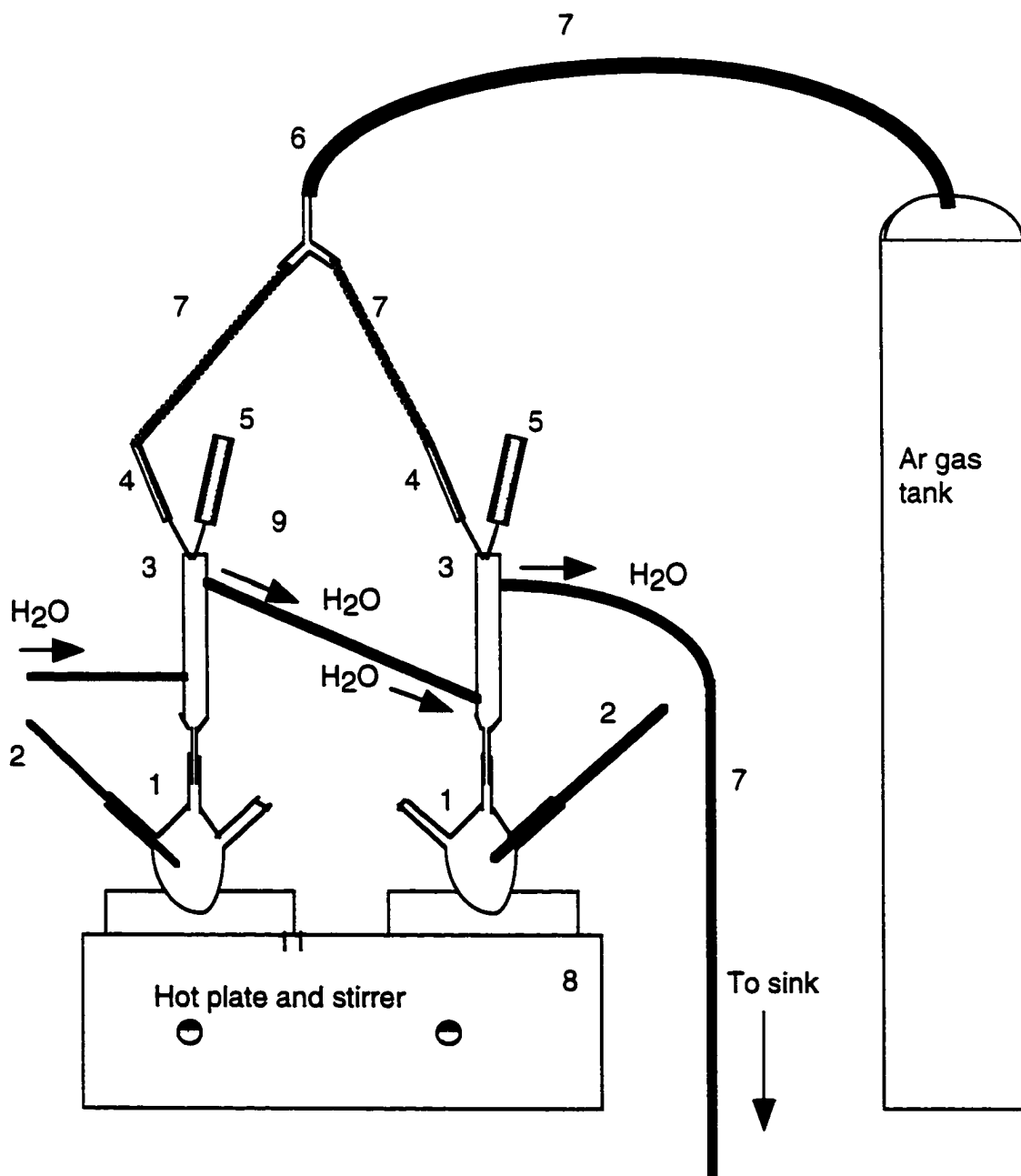
Figure 7.35 shows the schematic diagram of the apparatus used to perform labeling reactions of microcystin-LR with TMR under nonaqueous conditions. There are two 5-mL 3-necked flasks, one for the labeling reaction and the second one for TMR so that microcystin-LR will not be exposed to all the thermal and photochemical conditions of the labeling reaction. The latter solution was used as a blank for comparison with the labeled microcystin. The reaction is performed under argon inert atmosphere. Two calcium chloride guard columns attached to each of the reflux apparatus ensures that the moisture content of the air does not hydrolyze NaH to NaOH. If this happens, the hydroxide ion will displace the succinimidyl ester group of the TMR and change the desired succinimidyl ester leaving group to a poor -OH leaving group and the reaction will stop before microcystin is labeled.

Figure 7.36 shows the MALDI-MS spectra of microcystin, TMR and the product of the labeling reaction of microcystin and TMR. The negative ion mode peak for the product of the labeling reaction is at 711 amu that may be the molecular ion with two negative charges resulting from the loss of two carboxylic acid protons. The matrix for the negative ion MALDI experiment was 3-aminoquinoline. The positive ion mode MALDI-

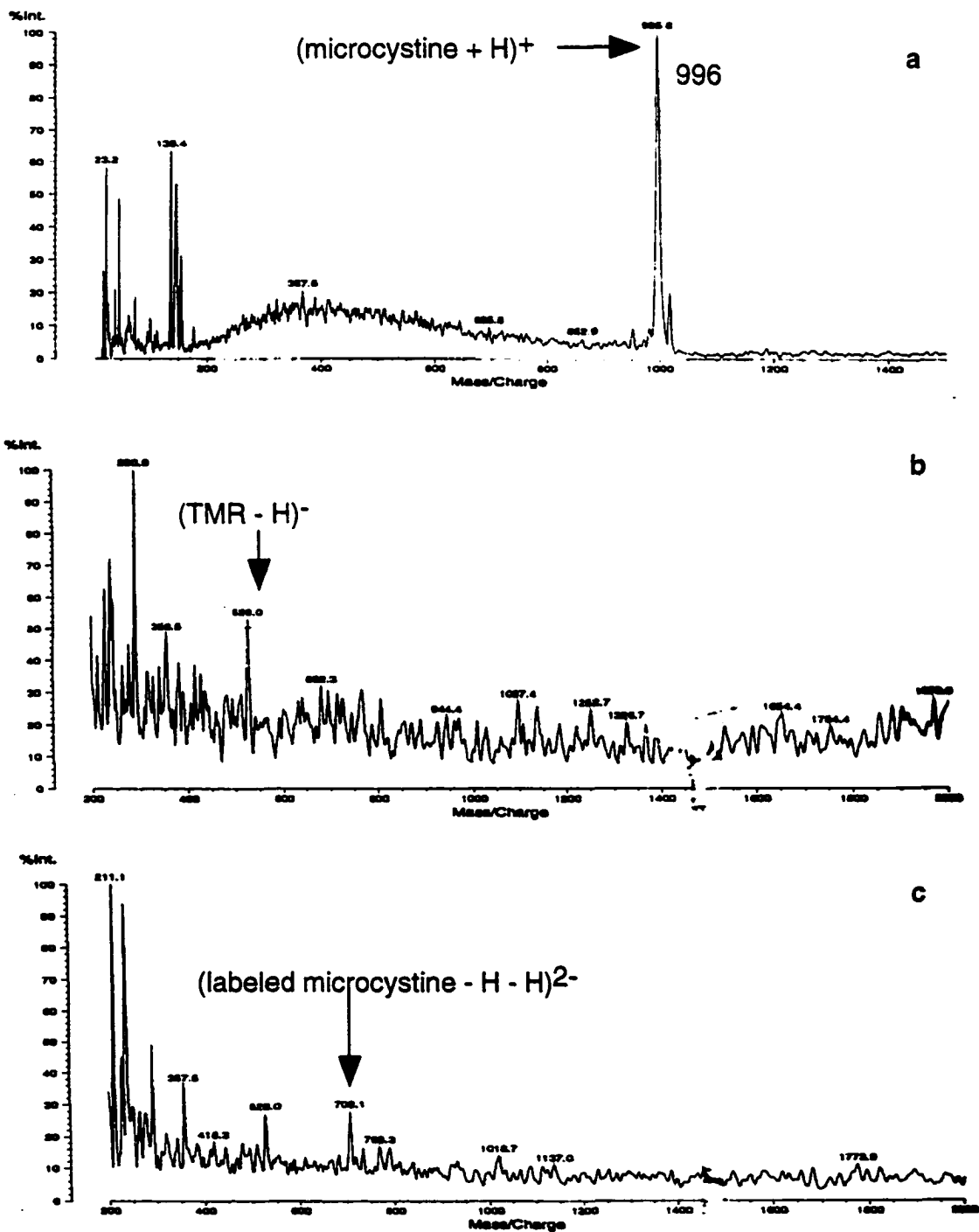
Figure 7.34: Chemical equations of microcystin-LR labeling reaction with TMR using NaH to deprotonate arginine group



**Figure 7.35: Schematic diagram of the apparatus for performing labeling reaction of microcystin. 1) 5-ml three-necked flask, 2) thermometer, 3) reflux apparatus, 4) syringe with needle, 5) calcium chloride guard column, 6) three-way connector, 7) tubing, 8) hotplate and stirrer**



**Figure 7.36: MALDI-MS spectra of microcystine-LR labeled with TMR, a) positive-ion mode spectrum of microcystine, b) negative-ion mode of TMR, and c) negative-ion mode MALDI-MS spectrum of the labeled microcystin with TMR**



MS spectrum of the labeled product is so crowded with the adduct peaks that it is very difficult to assign each one before separation.

### 7.3.16 Separation of the labeled microcystin

Figure 7.37 shows MALDI-MS spectra of different fractions collected from the column of gel permeation chromatography (section 7.2.31). In the first fraction (Figure 7.37a) the sodium adduct of the product is observed at 1446 amu. The expansion of the spectrum (Figure 7.37b) shows hydrogen (1425 amu), sodium (1446 amu), and potassium (1462 amu) adducts of the product. There are many other peaks at higher molecular weights that could not be assigned. The negative polarity MALDI-MS spectrum (Figure 7.37c) shows a hydrolyzed product with 3 negative charges at 471 amu. None of the other adducts and side products is observed in negative polarity mode. Figure 7.37d shows the negative polarity MALDI-MS spectrum of the 50<sup>th</sup> fraction indicating that separation is not very effective. In all the fractions collected, product peaks are observed. The MALDI-MS spectrum of the reaction mixture also shows the same peaks indicating that gel permeation chromatography is not effective when the difference in molecular weight of the component is small.

Figure 7.38 shows the Sep-Pak separation of the microcystin-labeling reaction with TMR. When the reaction mixture is injected onto the Sep-Pak cartridge and washed with water all the excess and hydrolyzed TMR will be separated (data not shown). After changing to MeOH the adsorbed labeled microcystin starts desorbing gradually. Figure 7.38a shows MALDI-MS spectrum of the first fraction; no molecular peak is observed. The 5<sup>th</sup> fraction (Figure 7.38b) starts to show the disodium adduct of the product (1469 amu) and the 10<sup>th</sup> fraction (Figure 7.38c) shows the sodium adduct peak at 1447 amu. While washing with MeOH the solvolysis (methanolysis) reaction occurs and MeOH

**Figure 7.37: MALDI-MS spectra of gel chromatography separation of labeled microcystin with TMR for a) first fraction (positive polarity), b) expansion of a, c) second fraction (negative polarity), and d) 50th fraction (negative polarity)**

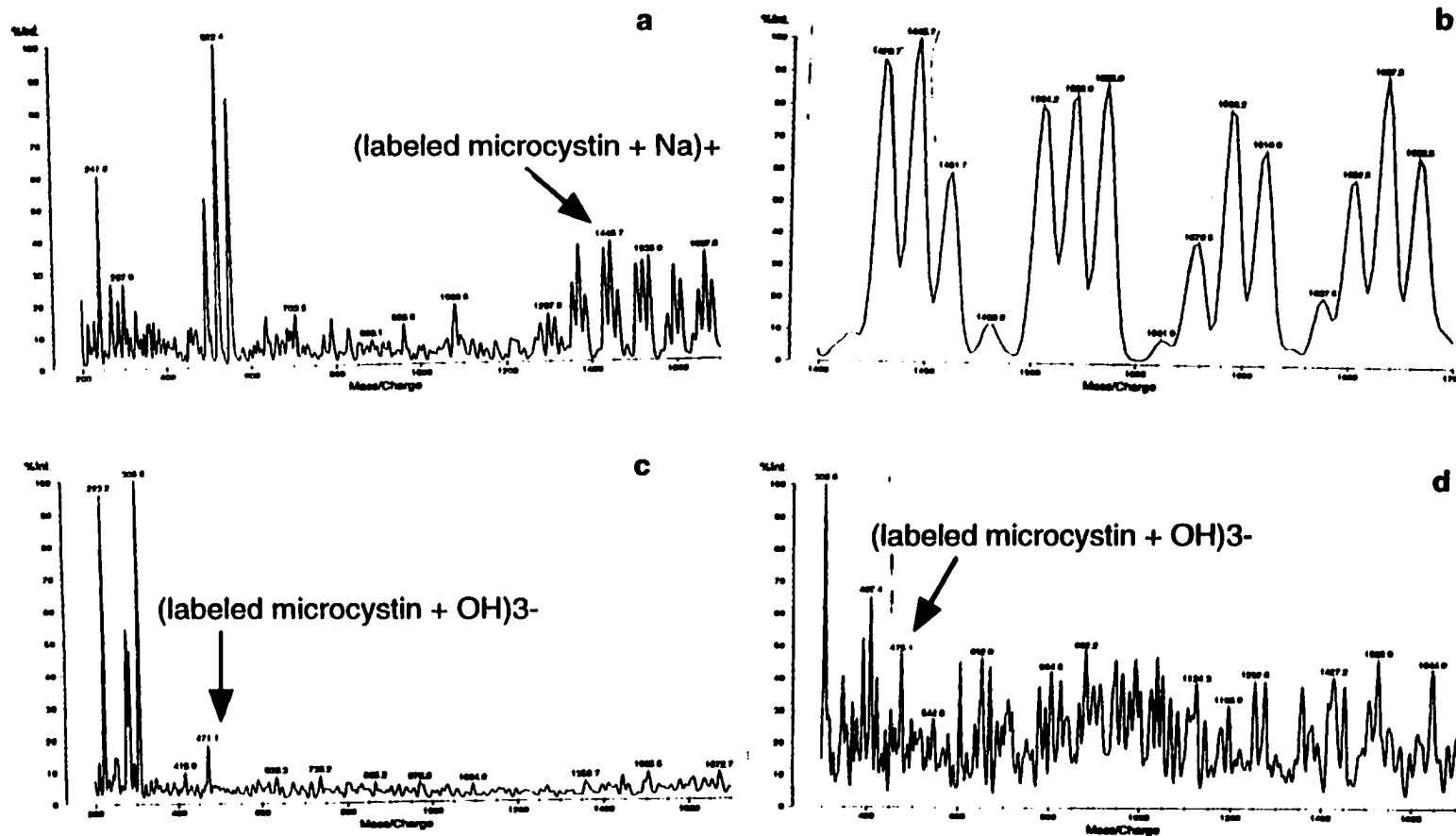
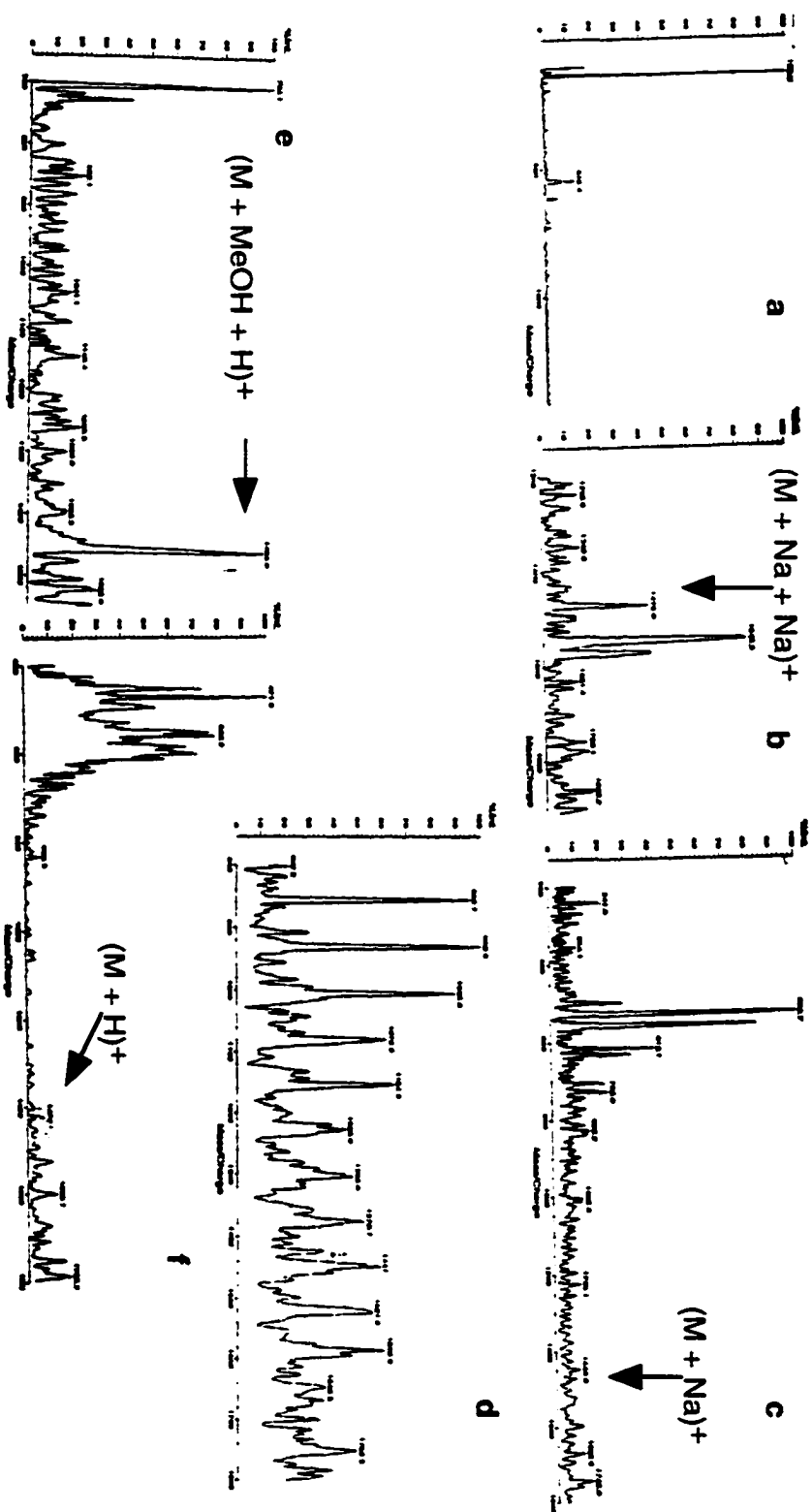


Figure 7.38: MALDI-MS spectra of Sep-Pak separation of labeled microcystin with TMR for collected fractions of a) first, b) 5th, c) 10th, d) 15th, e) 20th MeOH washed fraction, and f) unfractionated





adduct of the product is observed in the 15<sup>th</sup> fraction (Figure 7.38d) at 1457 amu. For the 20<sup>th</sup> fraction the molecular ion peak of the product is still observed at 1425 amu (Figure 7.38e) indicating the gradual desorption of the labeled microcystin from the hydrophobic C<sub>18</sub> column. The MALDI-MS spectrum of the reaction mixture is shown in Figure 7.38f. The hydrogen and sodium adduct of the product are observed at 1425 amu and 1447 amu. This experiment shows that Sep-Pak approach is more effective in separating the excess TMR than gel filtration chromatography. An effective separation strategy is preparative TLC followed by Sep-Pak cleanup of the product.

TMR was chosen for labeling of microcystin for several reasons. First, a fluorescently labeled microcystin is readily excited by the 546 nm spectral line from the mercury-arc lamp used in most fluorescence microscopes. Second, TMR is intrinsically more photo-stable than fluorescein and TMR conjugates often appear to be brighter than the corresponding fluorescein conjugates. Third, TMR is efficiently excited by 543 nm spectral line of the green He-Ne laser that is used for analytical instrumentation.<sup>45</sup> Finally, TMR emission at 579 nm is more effective in eliminating Raman bands from water. Nevertheless, since our collaborator's laboratory (Dr X. C. Le) was not equipped with He-Ne green laser for their CE-LIF polarization system, I had to develop a labeling procedure for microcystin that could be excited by the 488-nm spectral line of the argon ion blue laser.

### **7.3.17 Microcystin labeling with 5-BrMF**

The procedure for microcystin labeling with 5-BrMF was described in section 7.2.32 and the apparatus was the same as shown in Figure 7.35. Figure 7.39 shows the chemical equations for microcystin labeling using 5-BrMF as the labeling reagent and Figure 7.40 shows the negative-ion mode ESI-MS spectrum of the labeled microcystin.

**Figure 7.39: Microcystin-LR labeling reaction with 5-BrMF using NaH to deprotonate arginine group**

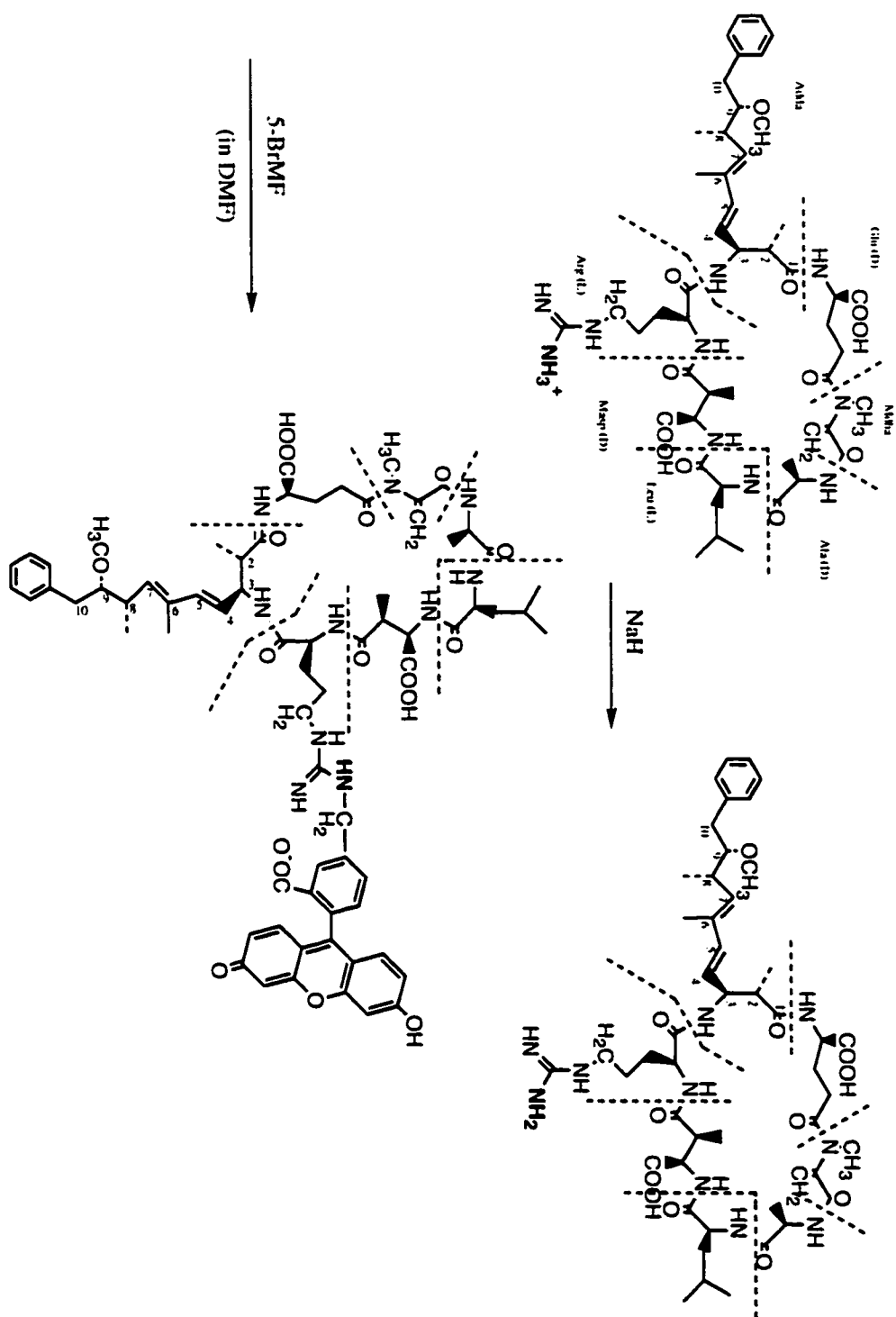
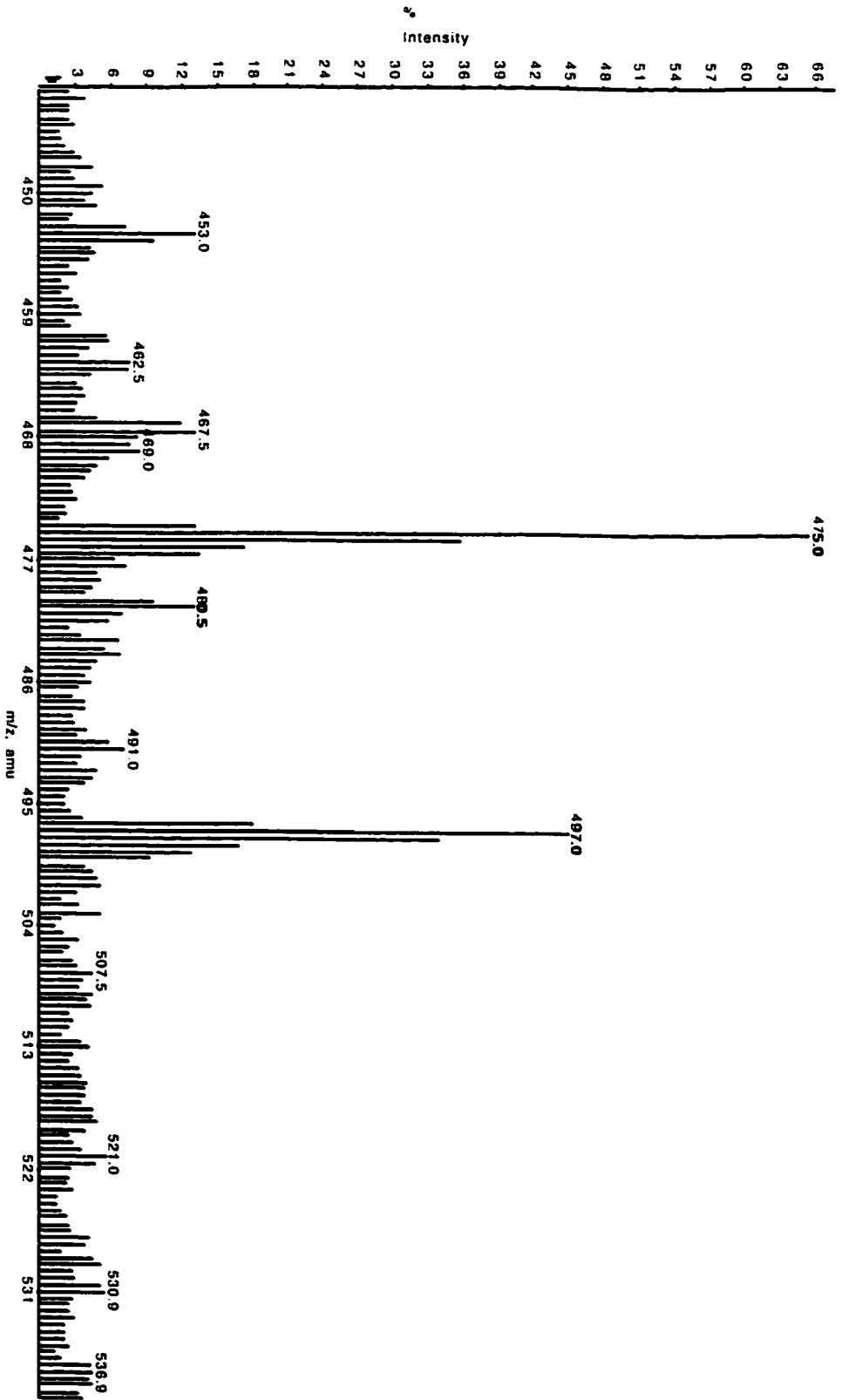


Figure 7.40: Negative-ion mode ESIMS spectrum of microcystine-LR labeled with TMR



The peak at 475 amu is probably  $(M + OH)^3$ . I assume that 5-BrMF reacts much more readily with the nitrogen nucleophile of arginine than with the oxygen nucleophile of carboxylic acids.

### 7.3.18 Microcystin immunoassay using 5-BrMF as labeling reagent

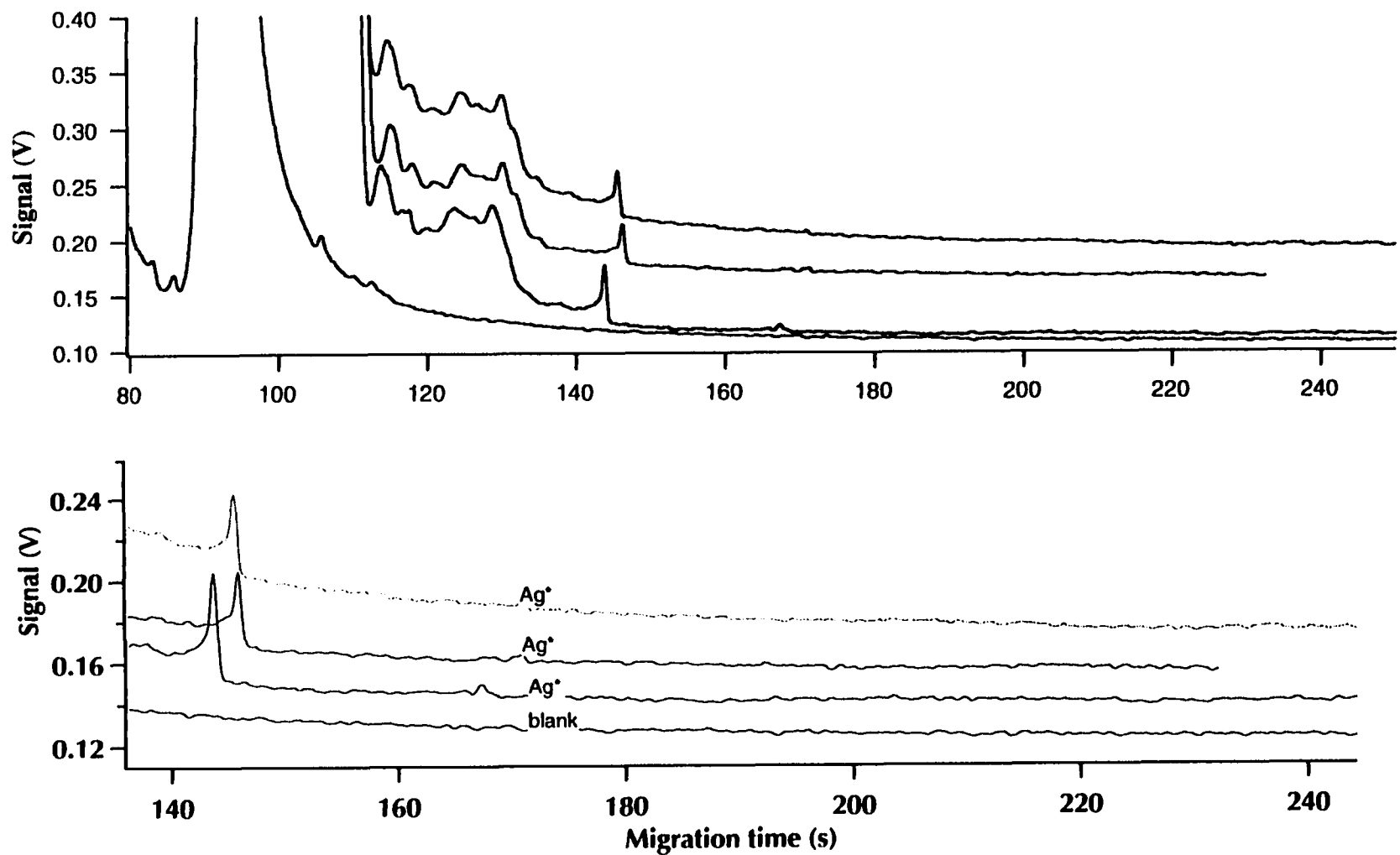
Figure 7.41 shows the reproducibility of the CE experiment and detection of  $10^{-10}$  M labeled microcystin and Figure 7.42 shows the titration of labeled microcystin with anti-microcystin antibody (section 7.2.33). By adding 2, 4, 6, 8 and 10  $\mu$ L of antibody solution, the resulting decrease in microcystin signal intensity is shown.

Figure 7.43 shows the working curve for the addition of anti-microcystin antibody to the microcystin solution. Peak area was calculated for each increment using Igor Pro software and plotted against  $\mu$ L of antibody added to the microcystin solution. The microcystin peak area drops as antibody solution is added.

The labeled microcystin peak area decreased nonlinearly with the addition of antimicrocystin antibody, but the complex peak was not observed in CE. The experiment was performed using a poly-AAP coated capillary and still the complex peak was not observed. A Laser Induced Fluorescence Polarization (LIFP) CE experiment was also performed (data not shown) to detect the complex peak but without success. Washing the capillary with 10 mM NaOH solution after the CE experiment showed a gradual increase in signal intensity. After a while the signal dropped to the background level. This experiment showed that the complex adsorbs strongly to the capillary wall even if the capillary surface was coated with poly-AAP.

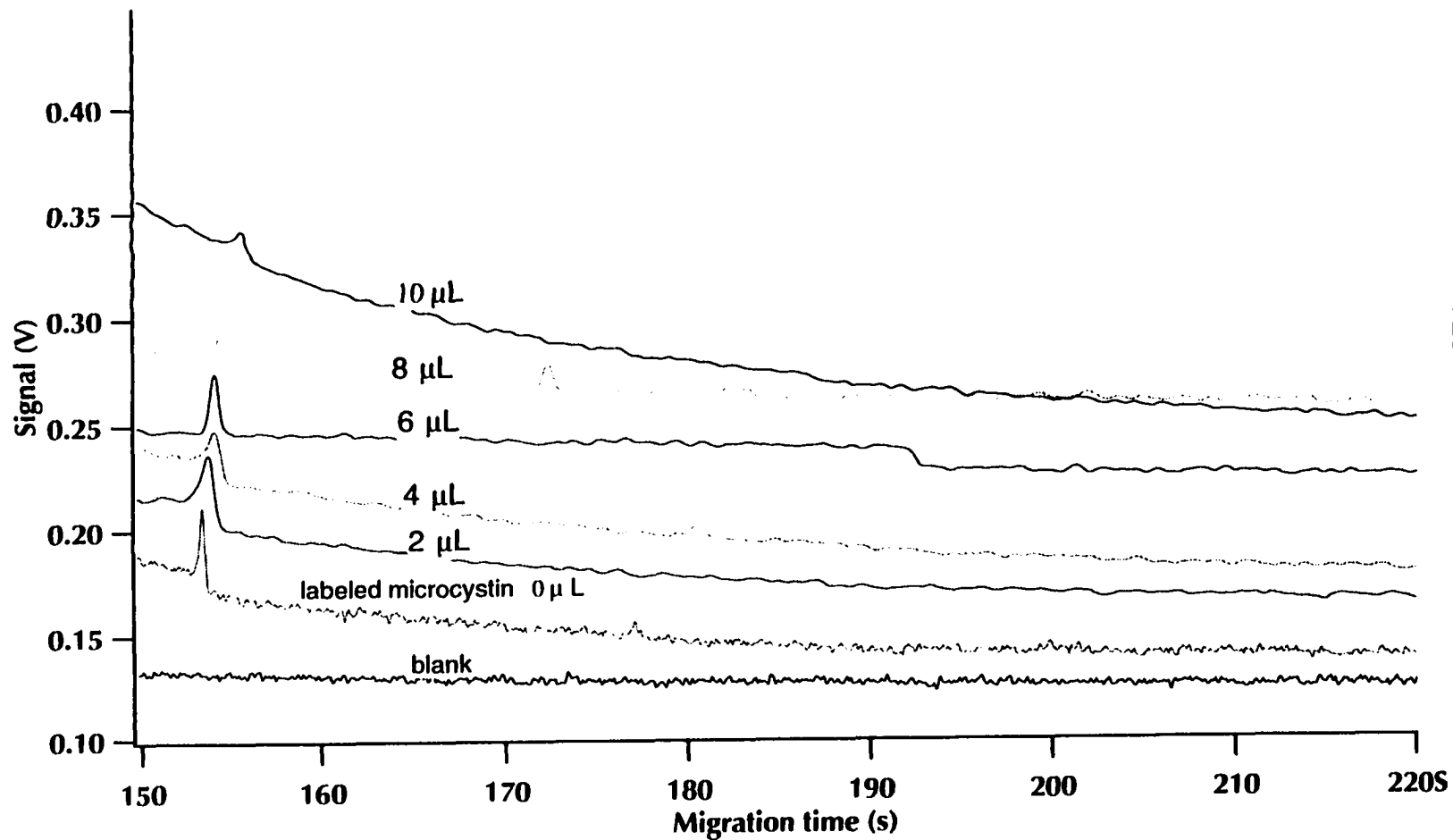
It was decided next to repeat the immunoassay experiment with the Fab portion of the antimicrocystin antibody in order to have a lower MW protein and reduce adsorption. The investigation on this project is continuing by two other graduate students.

**Figure 7.41: Reproducibility of CE experiment for labeled microcystin. Top electropherogram is the total range and the bottom electropherogram is the expansion of the top electropherogram.**



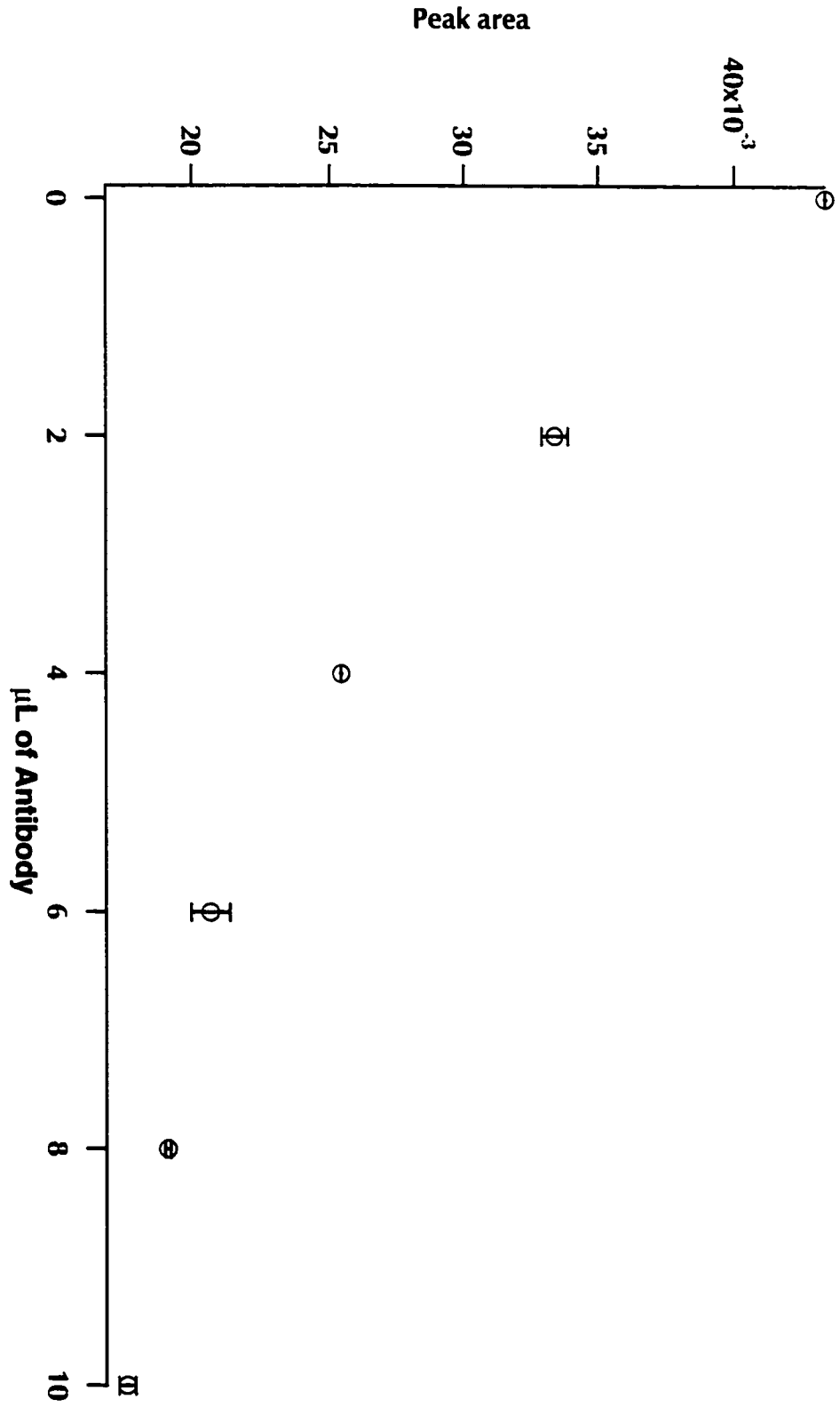
373

Figure 7.42: Titration of labeled microcystin by adding 0, 2, 4, 6, 8, and 10  $\mu\text{L}$  of anti-microcystin antibody



374

Figure 7.43: Calibration curve for the addition of anti-microcystin antibody to labeled microcystine



#### 7.4: Conclusions

Several procedures were tested to optimize the labeling reaction conditions for microcystin-LR. N-acetyl-L-arginine, cyclo (Arg-Gly-Asp-D-Phe-Val) cyclic peptide, and microcystin itself were chosen respectively. The reactants were decreased from 10.8 mg of N-acetyl-L-arginine to 1 mg of cyclic peptide and finally to 500 µg of microcystin. In off-column labeling for LIF detection, the bottle-neck is the labeling reaction itself that has to be done at higher concentrations of reagents. 500 µg is the lowest amounts of reagents consumed for off-column labeling reactions for LIF detection.

Two different labeling reagents were used, TMR and 5-BrMF. The reaction conditions were optimized for TMR and then successfully applied for 5-BrMF. It was demonstrated that direct labeling of arginine at high pH was not feasible because of reagent decomposition. Other bases like hydrazine and hydroxylamine hydrochloride were also tested. Hydrazine worked well for small molecules, but it cleaved the peptide bonds for larger molecules.

Sodium hydride was chosen as a strong base that worked well in nonaqueous conditions to remove the proton of arginine and produce a free amine functional group ready for labeling. This base worked well for both small and big molecules. Using this base, all the model compounds, N-acetyl-L-arginine, cyclo (Arg-Gly-Asp-D-Phe-Val) cyclic peptide, including microcystin itself, were labeled with TMR labeling reagent. For microcystin-LR, another labeling reagent (5-BrMF) also worked well.

The labeled microcystin bonded to antimicrocystin antibody in an immunoassay reaction. The peak corresponding to labeled microcystin decreased by the addition of antimicrocystin antibody and there was a linear relationship between labeled microcystin peak and volume of antimicrocystin antibody added. A working curve for this titration was obtained.



We expected to see an increasing antigen-antibody complex (Ag\*.Ab) peak correlating to the labeled microcystin decreasing peak. Unfortunately, this peak was not observed in several attempts of optimizing CE experimental conditions. It was thought that the adsorption of the Ag\*.Ab to the capillary wall could be the main reason for the complex not being detected. When the Ag\*.Ab was injected onto the capillary and CE showed no corresponding signal, the CE run buffer was changed to 10 mM NaOH. In this case an increase in the background was observed that after a while dropped to the base line. This was in agreement with the feasibility of adsorption.

Several synthetic routes were tried to produce an arginine-specific reagent. A diketone functional group was suggested in the literature as the best arginine-specific reagent. Our goal was to have a fluorescent labeling reagent for arginine and that was the reason why we tried to couple a fluorescent molecule with a diketone functional group. The first attempt was to couple a molecule with one ketone functionality to the fluorescent molecule and oxidize the second ketone group. This approach worked very well when we used an aliphatic amine to be linked to the fluorescence molecule, however ozonolysis as an oxidation technique to make a diketone did not work well. The other approach was using an aliphatic amine (4-aminoacetophenone) to be linked to the fluorescein and SeO<sub>2</sub> oxidation of the methyl group in aminoacetophenone to an aldehyde. This synthesis worked, but the reaction yield was low. The last synthetic scheme was direct coupling of a diketone (2, 3-butanedione) with 5-BrMF under nonaqueous conditions. This synthesis worked and the product was confirmed using MALDI-MS. This arginine specific reagent is not listed in the Handbook of Fluorescent Probes and Research Chemicals.<sup>46</sup> Still however it is difficult to purify a molecule with a diketone functional group. It was proven that this reagent does react to the arginine, but purification and isolation is left for future work. Another graduate student is working on this project.

## 7.5: References

1. Carmichael, W. W.; *Scientific American*, 78-86, January 1994.
2. Crisp, G. T., and Gore, J., *Tetrahedron*, 53, 4, 1505-1522, 1997.
3. Riordan, J. F., *Molecular & Cellular Biochemistry*, 26, 2, 71-91, 1979.
4. Lange, L. G., Riordan, J. F., and Vallee, L. B., *Biochemistry*, 13, 21, 4361-4370, 1974.
5. Borders, C. L., and Riordan J. F., *Biochemistry*, 14, 21, 4699-4704, 1975.
6. Lobb, R. R., Strokes, M. A., Hill, O. H. A., and Riordan, J. F., *Eur. J. Biochem.*, 70, 517-522, 1976.
7. Daemen, F. J. M., and Riordan, J. F., *Biochemistry*, 13, 14, 2865-2871, 1974.
8. Lange, L. G., Riordan, J. F., Vallee, B. L., and Branden C. I., *Biochemistry*, 14, 15, 3497-3502, 1975.
9. Riordan, J. F., and Scandurra, R., *Biochemical and Biophysical Research Communication*, 66, 1, 417-424, 1975.
10. Lawlis, V. B., and McFadden, B. A., *Biochemical and Biophysical Research Communication*, 80, 3, 580-585, 1978.
11. Powers, S. G., and Riordan, J. F., *Proc. Nat. Acad. Sci., USA*, 72, 7, 2616-2620, 1975.
12. Riordan, J. F., McElvany, K. D., and Borders, C. L. Jr., *Science*, 195, 884-886, Mar 4, 1977.
13. Riordan, J. F., *Biochemistry*, 12, 20, 3915-3923, 1973.
14. Yankeelov J. A. Jr., *Biochemistry*, 9, 12, 2433-2439, 1970.
15. Jornvall, H., Lange, L. G., Riordan, J. F., and Vallee, B. L., *Biochemical and Biophysical Research Communication*, 77, 1, 73-78, 1977.
16. Borders, C. L. Jr., Riordan, J. F., and Auld, D. S., *Biochemical and Biophysical Research Communication*, 66, 2, 490-495, 1975.

17. Scholoss, J. V., Norton, I. L., Stringer, C. D., and Hartman, F. C., *Biochemistry*, 17, 26, 5628-5631, 1978.
18. Chollet, R., *Biochemical and Biophysical Research Communication*, 83, 4, 1267-1274, Aug. 29, 1978.
19. Chollet, R., *Biochemica et Biophysica Acta*, 658, 177-190, 1981.
20. Riordan, J. F., *Molecular & Cellular Biochemistry*, 26, 2, 71-91, July 31, 1979.
21. Miklos, B., *Principles of Peptide Synthesis*, 2<sup>nd</sup> Ed. Springer-Verlag, 147-152, 1984.
22. Takahashi, K., *The Journal of Biological Chemistry*, 243, 23, 6171-6179, Dec.10, 1968.
23. Guttman, P., and Boissonnas, R. A., *Helvetica Chemica Acta*, XLI, 199, 1852-1882, 1958.
24. Tso, J. Y., and Zalkin, H., *The Journal of Biological Chemistry*, 266, 19, 9901-1981, Oct. 1981.
25. Kettlun, A. M., Urib, L., Silva, S., Rivera J., Antonieta Valenzuela M., and Traverso-Cori A., *Arch. Biol. Med. Exp.*, 14, 171-175, 1981.
26. Kawakami, M., and Goodman, DeWitt S., *Biochemistry*, 20, 5881-5887, 1981.
27. Lusty, C. J., and Ratner, S., *Proc. Natl. Acad. Sci., USA*, 84, 3176-3180, 1987.
28. Narayanan, C. S., and Krakow, J. S., *Nucleic Acids Research* 11, 9, 1983.
29. Ali, F. E., Bennet, D. B., Calvo, R. R., Elliot, J. D., Hwang, S., Ku T. W., Lago, M. A., Nichols, A. J., Romoff, T. T., Shah, D. H., Vasco, J. A., Wong, A. S., Yellin, T. O., Yuan, C., and Samanen, J. M., *J. Med. Chem.*, 37, 769-780, 1994.
30. Egon, S., *Thin-layer chromatography a laboratory handbook*, 2<sup>nd</sup> edition, Springer-Verlay, NY 1969.
31. Pinto D. M., Arriaga E. A., Craig D., Angelova J., Sharma N., Ahmadzadeh H., and Dovichi N. J., *Anal. Chem.*, 69, 3015-3021, 1997.
32. Laursen, R. A., Horn, M. J., and Bonner, A. G., *Febs Letters.*, 21, 1, 67-70, 1972.

33. Honegger, A., Hughes, G. J., and Wilson, K. J., *Biochem. J.*, 199, 53-59, 1981.
34. Whittall, R. M., Palcic, M. M., Hindsgaul, O., and Li, L., *Anal. Chem.*, 67, 19, 3509, 3514, 1995.
35. Kalbag, S. M., and Roeske, W., *Journal of the American Chemical Society*, 97, 441, 1975.
36. Baldenius, K., Dallman, P., and Hudec, J., *Tetrahedron Letters.*, 34, 9, 1517-1520, 1993.
37. Yankeelov, Jr. J. A., and Crawford, T. H., *Journal of the American Chemical Society*, 90, 6, 1664-1666, 1968.
38. Smith, E. L., *Methods in Enzymol.*, 47, 156-161, 1977.
39. Yamasaki, R. B., *Anal. Biochem.*, 109, 32-40, 1980.
40. Wijnands, R. A., Muller, F., and Visser, A. J. W. G., *J. Biochem.*, 163, 535-544, 1987.
41. Shen, S. and Strobel, H. W., *Archives of Biochemistry and Biophysics*, 304, 1, 257-265, July 1993.
42. Shah, M. A., Tayyab, S., and Ali R., *International Journal of Biological Macromolecules*, 18, 77-81, 1996.
43. Yankeelov, Jr. J. A., *Biochemistry*, 9, 12, 1970.
44. Petz, D., Loffler H. G., and Schneider, F., *Zeitschrift fur Naturforschung Section C Biosciences* 34, 9-10, 742-746, Sept-Oct. 1979.
45. Haugland, R. P., *Handbook of Fluorescent Probes and Research Chemicals, Molecular Probes, 6<sup>th</sup> Ed.*, 1996.

# Chapter 8

## **Capillary-based and microchip flow injection analysis of TNT using displacement immunoassay with laser-induced fluorescence detection<sup>1</sup>**

---

<sup>1</sup> This chapter is a collaborative work with The Center for Bio/Molecular Science and Engineering, Naval Research Laboratory, Washington, D.C. 20375, USA and Professor Jed Harrison's group at the Chemistry Department, University of Alberta.

## 8.1. Introduction

### 8.1.1 Immunoassay techniques for environmental/clinical sample analysis

Immunoassay techniques can be classified as competitive or noncompetitive. In a noncompetitive assay an excess of labeled antibody is added to the sample solution. When the complexation reaction is completed the antigen concentration of the sample solution can be determined.<sup>1</sup> The labeled antibody forms a complex specifically with the antigen of interest. The resulting equilibria is



where  $\text{Ab}^*$  is fluorescently labeled antibody and  $\text{Ag}$  is antigen. A CE-LIF analysis of a noncompetitive assay should result in two peaks, one corresponding to the excess free  $\text{Ab}^*$  and the other for the  $\text{Ab}^*.\text{Ag}$  complex. If the complex is stable enough, it should be possible to quantify  $\text{Ag}$  based on the amount of  $\text{Ab}^*.\text{Ag}$  complex formed or the decrease in free  $\text{Ab}^*$ .

In a competitive immunoassay, there is a competition between the fluorescently labeled antigen,  $\text{Ag}^*$ , and non-labeled antigen,  $\text{Ag}$ , to bind to  $\text{Ab}$ . In this case the antibody,  $\text{Ab}$ , is not fluorescently labeled and nonlabeled antigens compete for the same antibody. To perform a competitive immunoassay, a limiting amount of  $\text{Ab}$  is mixed with the sample containing  $\text{Ag}$  and a fixed concentration of  $\text{Ag}^*$ . The competition is between the following two equilibria:





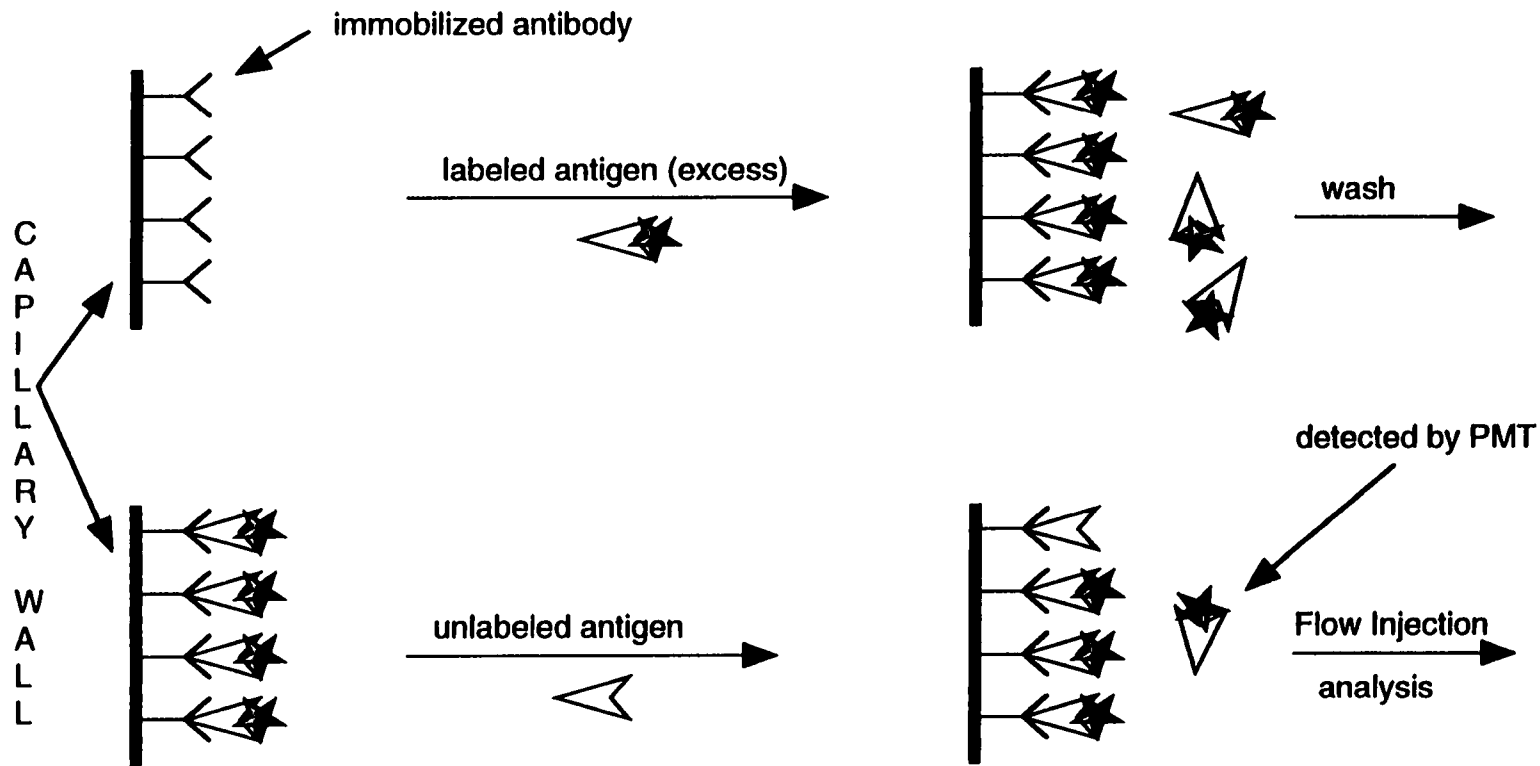
After the complexation reaction is complete,  $\text{Ag}^* \cdot \text{Ab}$  complex and  $\text{Ag}^*$  are separated and quantified. As the equilibrium governs, a large  $\text{Ag}$  concentration will result in lower  $\text{Ag}^* \cdot \text{Ab}$  and higher  $\text{Ag}^*$  concentrations. Therefore, the amount of analyte can be directly determined by measuring the concentration of either  $\text{Ag}^* \cdot \text{Ab}$ , free  $\text{Ag}^*$ , or their ratio.<sup>2</sup>

One other class of immunoassay techniques is fluorescence polarization. In this technique the intensity of the polarized light emitted by the fluorescence compound is measured. Fluorescence polarization depends on the fluorescence lifetime (the time interval between excitation and emission) and the rotational relaxation time of the molecule, i.e. the time required for an oriented molecule to return to a random orientation in solution. Smaller molecules, such as fluorescently labeled antigen ( $\text{Ag}^*$ ), rotate rapidly in solution and have shorter relaxation times and, therefore, do not show significant fluorescence polarization. For an  $\text{Ag}^* \cdot \text{Ab}$  or  $\text{Ag} \cdot \text{Ab}^*$  complex, fluorescent polarization is significant because the large complex molecule rotates slowly in solution and the relaxation time is much longer.<sup>3</sup>

Another class of immunoassay techniques is displacement immunoassay. This method has the advantage of detecting nonlabeled  $\text{Ag}$ . In both competitive and noncompetitive immunoassay, there is a need for a labeling step of the  $\text{Ag}$  or  $\text{Ab}$  that is very time consuming and difficult. Figure 8.1 shows the schematic diagram of displacement immunoassay. In this technique, one  $\text{Ag}$  from a class of compounds is chosen to be labeled. The  $\text{Ab}$  is immobilized on a surface and the surface is exposed to a copious amount of labeled antigen ( $\text{Ag}^*$ ). When the binding reaction is complete and the  $\text{Ag}^* \cdot \text{Ab}$  complex is formed, excess  $\text{Ag}^*$  is washed out. Now unlabeled  $\text{Ag}$  is injected on the surface and it will displace the equivalent amount of  $\text{Ag}^*$  which is detected.

Figure 8.1: Schematic diagram of displacement immunoassay. Labeled antigen (  ) is detected and

unlabeled antigen (  ) is measured indirectly





### **8.1.2 Microfabrication devices for performing capillary electrophoresis and flow injection analysis of explosives**

Photolithography and chemical etching technology provide a route to sample injection and separation schemes based on micromachining CE. Low dead volume and very short separation distances can be achieved. Miniaturization technology can increase measurement speed and allow parallel measurement. Compared to conventional systems, microfabricated devices could reduce solvent and sample consumption and decrease analysis times because of their decreased dimensions.

Insulating substances, glass and fused silica, are used to allow high voltages to be applied to the chips to deliver samples and reagents through the channels on the chip. The technology developed for the semiconductor industry can be transferred directly to chip fabrication using insulating substances.

The sequence of photolithographic steps have been discussed in detail elsewhere.<sup>+7</sup> Briefly the sequence of photolithographic fabrication are:

- a) A glass is coated with Cr and Au and then this masked glass is coated with photoresist.
- b) The chip is exposed to light through a master mask and the channel design is transferred to the substrate using this mask.
- c) After exposing to UV light, the photoresist is developed.
- d) The exposed areas are etched with aqua regia and a commercial Cr etch.
- e) Now the exposed glass is etched using a dilute HF / NH<sub>4</sub>F bath.
- f) After the photoresist and metal mask are stripped, a glass cover plate is bonded to the substrate over the etched channels to form the closed network of channels.

### **8.1.3 Capillary electrophoresis for performing immunoassay analysis of explosives**

The advantages of immunoassay techniques are selectivity, sensitivity, and cost

effectiveness for screening clinical and environmental samples.<sup>3</sup> The selectivity of immunoassay allows the measurement of a target compound at trace levels in the presence of potential interferences at much higher concentrations. The main drawback of common immunoassay techniques is that they are slow and manually intensive procedures.

Capillary electrophoresis has proven to be one of the most powerful separation techniques. Combining capillary electrophoresis with immunoassay techniques could be useful in performing rapid, automated immunoassays.<sup>9</sup> In this chapter we have combined an immunoassay technique for TNT analysis with the high surface-to-volume ratio of the capillaries. The objective of this work was to develop a technique that combines the advantages of immunoassay, CE separation and LIF detection.

#### **8.1.4 The analysis of explosive compounds**

There is a need for fast, reliable, and cost-effective sensors to detect explosives for environmental monitoring and the transportation industry. An ideal explosive sensor has to be sensitive, selective, and simple to use on-site. Because of the necessity to demilitarize and clean up the areas previously used for munitions storage and processing, the Naval Research Laboratory (NRL), USA, has investigated TNT immunosensing schemes using packed-column and membrane displacement immunoassay formats. Our research group collaborated with NRL to design a field portable and cost effective sensor for explosive monitoring.

Immunoassay techniques are selective, sensitive and inexpensive methods for screening clinical and environmental samples.<sup>8-13</sup> Enzyme-linked immunosorbent assay (ELISA) is limited because of the need for trained personnel and long assay times.<sup>14</sup> These limitations have sparked the development of antibody-based immunosensors, so called biosensors, using different immunoassay techniques.

One class of immunosensor is based on displacement immunoassay (Figure 8.1) at the surface of antibody-coated beads or membranes.<sup>15-17</sup> This chapter describes a capillary-based and microchip-based displacement continuous flow immunosensors with LIF detection for 2, 4, 6-trinitrotoluene (TNT) and other explosives. These sensors are at least two to three orders of magnitude more sensitive as compared to the previously used packed columns and membrane flow-immunosensors or to an ELISA technique using the same antibody reagent.<sup>15-17</sup>

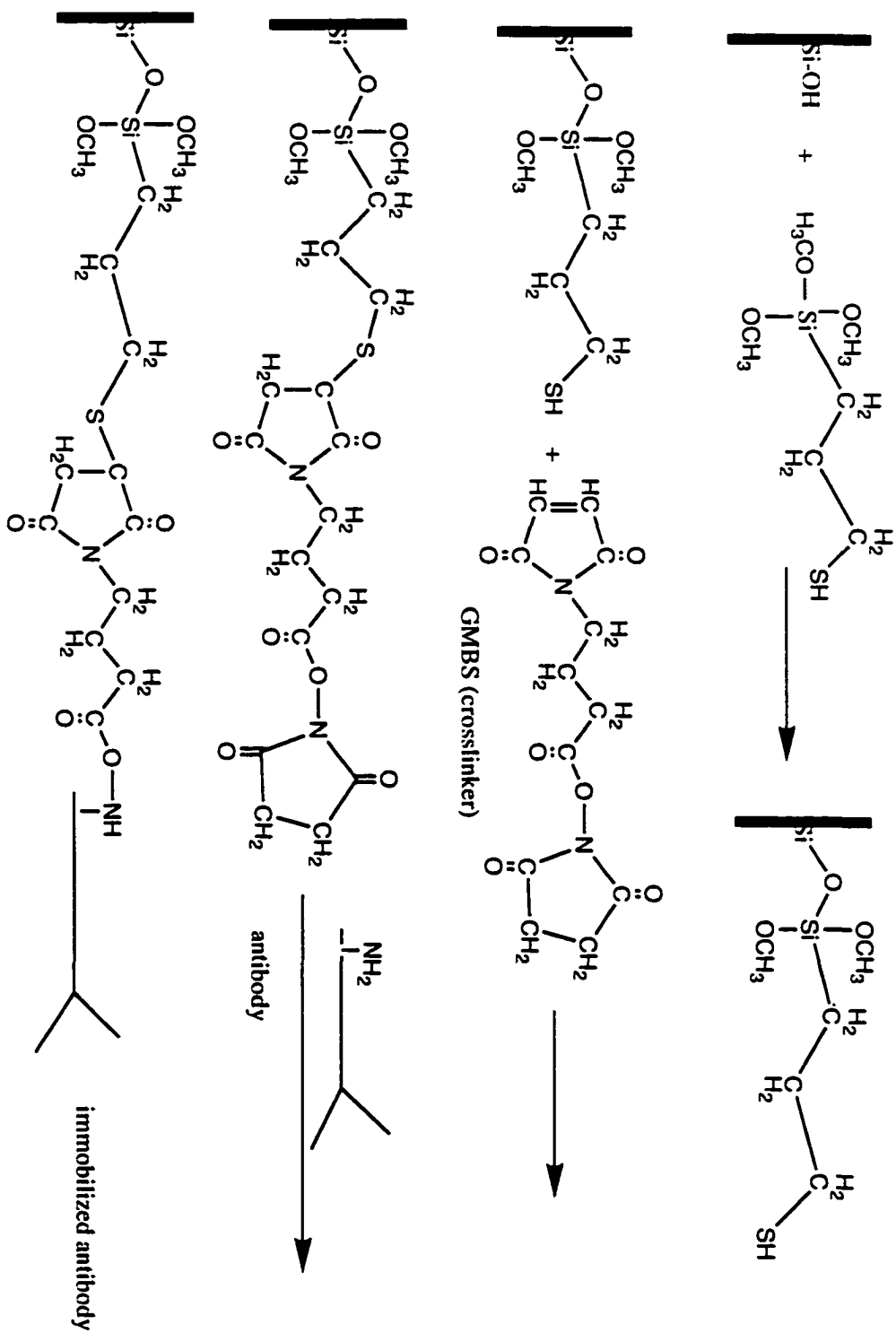
Capillaries have the advantage of high surface-to-volume ratios, laminar flow, and reduced band broadening as compared to packed columns.<sup>18</sup> Although capillaries have proven to be very successful in separation science, there are no reports on them being used in displacement flow immunosensors. LOD as low as 7 femtomoles of TNT for 100  $\mu\text{L}$  of 15 pg / mL of TNT has been reported.<sup>19</sup>

### **8.1.5 Antibody immobilization on silica surfaces<sup>20</sup>**

The strategy to immobilize antibodies on the capillary wall is similar to the strategy to coat capillaries that was discussed in Chapter 5 of this thesis. Antibody immobilization involves four steps. In the first step, the capillary surface is cleaned and washed with NaOH, water and then MeOH. Then, in the second step, the capillary wall is coated with a silane reagent with a thiol functional group. Third, this thiol functional group is bound to a hetero-bifunctional crosslinker with different reactive groups on each end. In the fourth step, the protein or antibody is immobilized via its terminal amino groups forming an amide bond with the free end of the crosslinker.

Figure 8.2 shows the chemical equations for the covalent attachment of proteins and antibodies to the silica surfaces.

**Figure 8.2: Chemical equations of the antibody immobilization on the capillary wall**



## 8.2 Experimental

### 8.2.1 Reagents and materials

Fused-silica capillaries (50  $\mu\text{m}$  ID, 140  $\mu\text{m}$  OD) were purchased from PolyMicro Technologies (Phoenix, AZ, USA). 35-cm long capillaries were used for flow injection analysis with LIF detection. 3-mercaptopropyltrimethoxysilane (MTS) and N-succinimidyl-4-maleimidobutyrate (GMBS) were purchased from Fluka Chemie AG (Switzerland). Ethanol (200 proof, Warner-Graham); toluene (Mallinckrodt); Tween 20, phenylalanine, and glycine were from Sigma (St. Louis Mo, USA); sodium monophosphate was from Aldrich chemical company Inc., (Milwaukee, WI, USA). 2, 4, 6-trinitrotoluene (TNT), 1, 3, 5-trinitrobenzene (TNB), 4-amino-2, 6-dinitrotoluene (ADNT), nitrobenzene (NB), 2, 4-dinitrotoluene (DNT), 2-nitrotoluene (NT), hexahydro 1, 3, 5 trinitrotriazine (RDX), and octahydro 1, 3, 5, 7 tetranitro 1, 3, 5, 7-tetrazocine (HMX), anti-TNT antibody, 1, 3 dinitroglycerol, and dinitroethylenglycol were kindly provided by the Naval Research Laboratory, Washington DC, USA. All reagents were used as received without further purification and aqueous solutions were prepared in distilled-deionized water unless otherwise stated.

### 8.2.2 Equipment

The in-house instrument for post-column detection was a CE-LIF system with a sheath-flow cuvette. It was equipped to a 0-30 kV power supply (CZE1000, Spellman, Plainview, NY, USA). For flow injection analysis the power supply was off. For the sheath-flow cuvette detector, excitation was provided by the 635-nm line of a diode laser at 3 mW (Melles Griot, Nepean, ON, Canada), which was focused approximately 30  $\mu\text{m}$

from the tip of the capillary with a 6.3 x objective. Fluorescence was collected by a 60 x, 0.7 NA microscope objective (MO-0060LWD, Universe Kokagu, Oyster Bay, NY, USA), filtered with a spatial filter to remove stray light and a  $682 \pm 11$  bandpass filter (Omega Optical, Brattleboro, VT, USA) to remove scattered light, and imaged onto a photomultiplier tube (R1477, Hamamatsu, Middlesex, NJ, USA) biased at 1.0 kV. Figure 8.3 shows the schematic diagram of a flow injection analysis system with LIF detection. It is similar to CE-LIF system that was described in Chapter 2 of this thesis. Hydrodynamic injection was performed by placing the capillary in an Eppendorf vial containing the sample and lifting up the sample vial to a specific height for a period of time. A Hamilton syringe (Hamilton Company, Reno, Nevada, USA) was filled with the buffer solution and attached to the capillary. Pressure injection was performed by a syringe pump (Harvard Apparatus Inc., Saint-Laurent, Quebec, Canada) to drive the buffer solution on to the capillary.

CE experiments were performed using either the in-house system with a sheath flow cuvette for post-column detection or a Beckman P/ACE 2100 CE instrument for on-column detection. P/ACE system software was used for data acquisition of the Beckman instrument.

The set-up for microchip-based technology used the same excitation laser and emission filters as described for sheath-flow cuvette capillary electrophoresis. The chip had 10 channels with 200  $\mu\text{m}$  depth and 400  $\mu\text{m}$  width and 5 cm length, but a single channel was used for the experiment until the coated antibody on the inner surface of the microchip was removed during the course of the experiment.

The optical set up for flow injection analysis on the microchip is shown in Figure 8.4a and the top view of the layout of the channels integrated on a planar glass substrate is shown in Figure 8.4b. Diode laser light was focused with a lens onto the separation channel of a microchip that was held in place with a Plexiglas holder. Fluorescence

**Figure 8.3: Schematic diagram of the displacement immunoassay flow injection analysis with a sheath-flow cuvette and LIF detection**

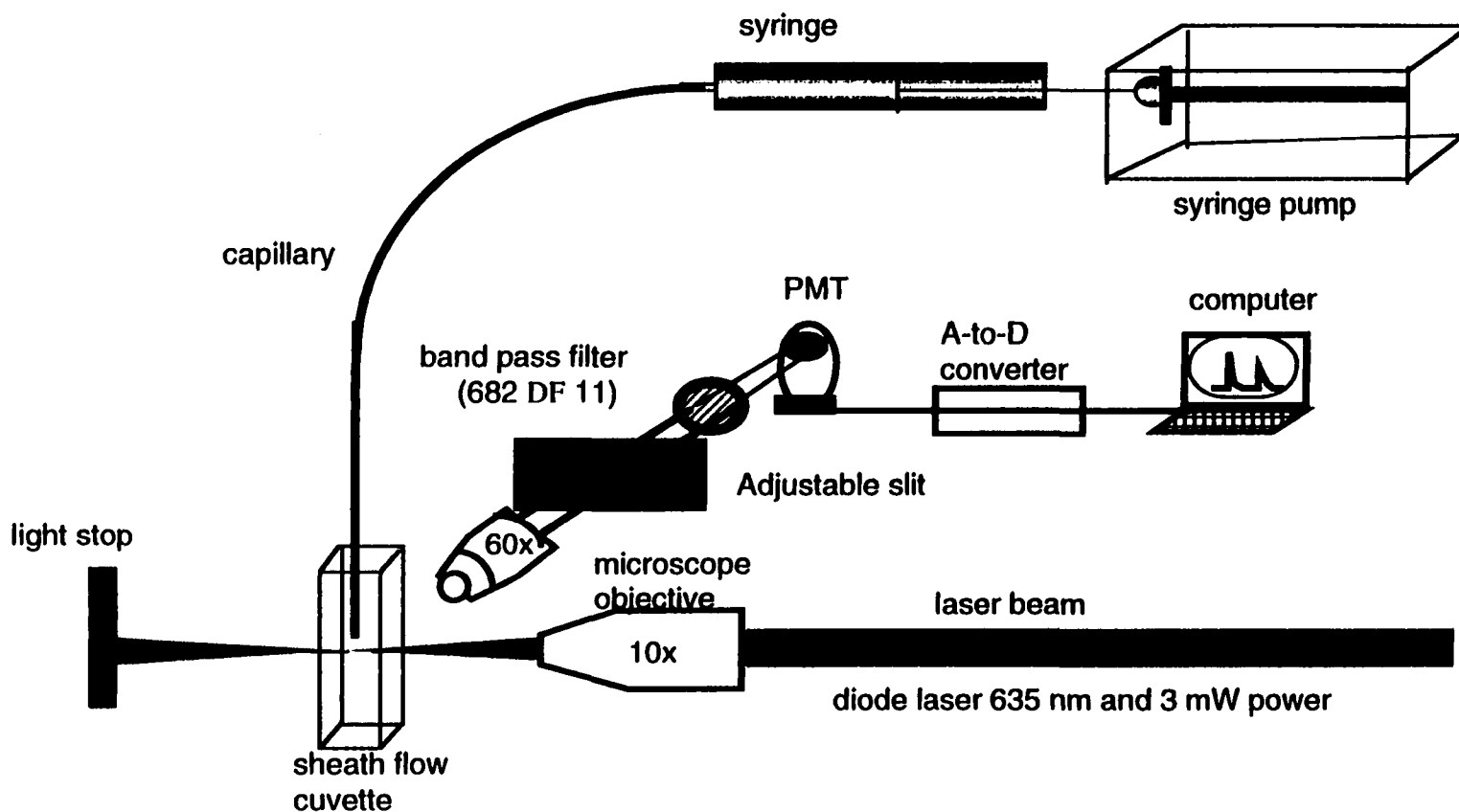
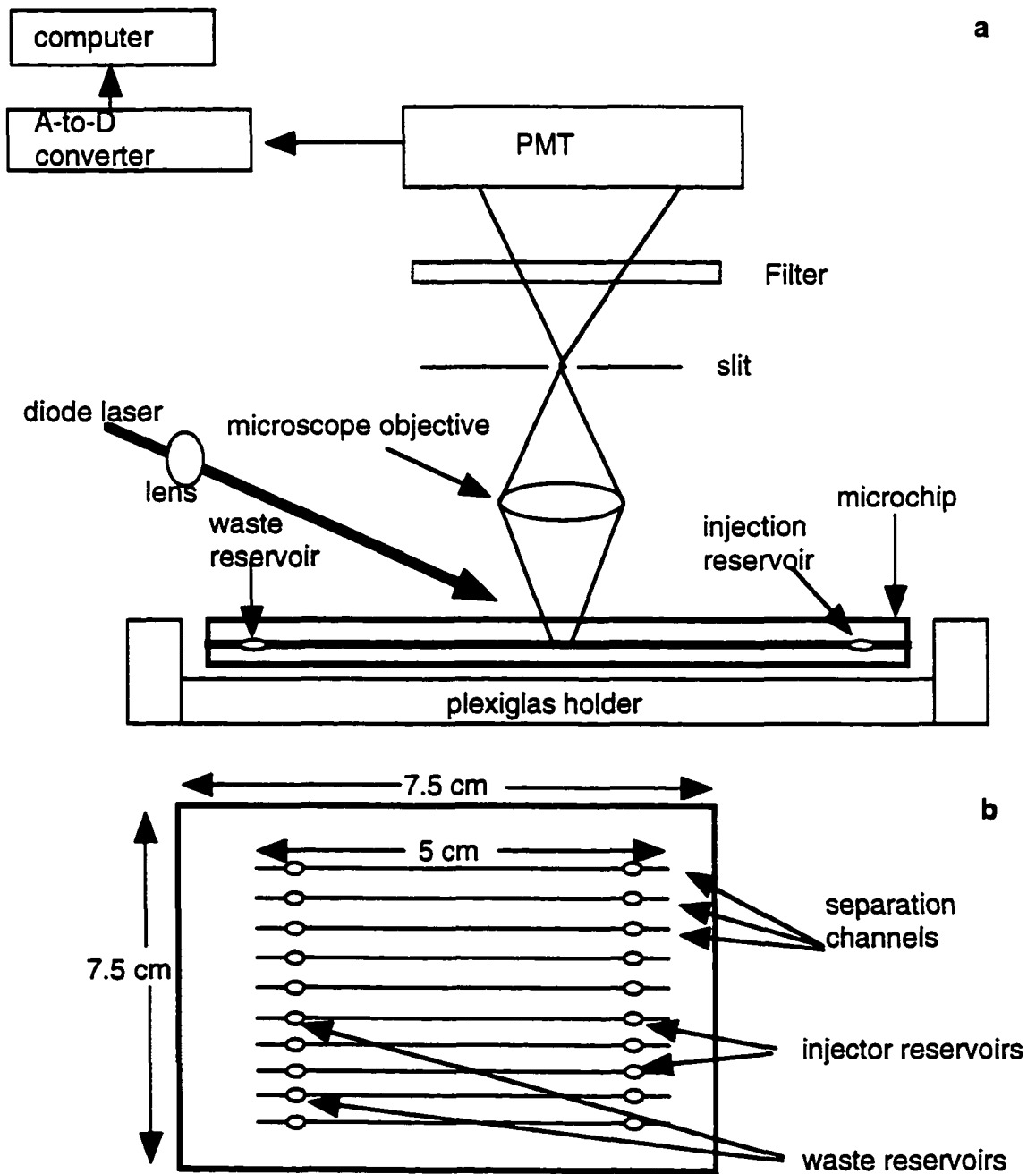


**Figure 8.4: a) Schematic of the optical detection system for flow injection analysis of TNT with LIF detection using a microfabricated chip, and b) The top view of the channels integrated on a planar glass substrate used as a microchip.**





emission was collected with a microscope objective, focused onto slit, filtered, and then detected with a photomultiplier tube.

The optical setup was constructed on an optical breadboard (3 ft x 3 ft, Melles Griot). A diode laser operated at 3 mW was used as the fluorescence excitation source. The laser was focused onto the channels of the microchip at  $\sim 45^\circ$  to the surface using a lens with a focal distance of 30 cm, as shown in Figure 8.4a. The surfaces of the microchip device were roughened during the bonding process, so the beam diameter focused in the channels tended to vary between 100 and 200  $\mu\text{m}$ , depending on the position. The paths of the reflected beams were arranged so that they did not strike the other channels elsewhere, in order to avoid photobleaching.

The fluorescence emission was detected with the optical assembly perpendicular to the plane of the microchip device. Emitted fluorescence light was collected with a microscope objective (10:1, NA 0.3, working distance 6 mm, Rolyn Optical) mounted on a microscope body (Melles Griot). A photomultiplier tube (Hamamatsu Model R1477) powered by a high-voltage supply (Hamamatsu HC123-01) was mounted in a sealed housing at the exit of the microscope. A 100- $\mu\text{m}$  air slit (Melles Griot) was placed at the field stop plane of the microscope in a specially made adaptor, to restrict the channel length viewed by the detector to  $\sim 10 \mu\text{m}$ . An interference filter was mounted over the entrance to the PMT housing to eliminate scattered laser light. The entire assembly was covered with a large box to reduce, but not eliminate, the ambient light. Both the device mounting stage and the microscope assembly were mounted on Newport Research x-y translation stages.

The PMT output was connected to a 1-M $\Omega$  resistor. The potential was recorded with a Linear Instruments strip chart recorder (Model 500). It was also filtered through two sets of active, six-pole Butterworth filters (Krohn-Hite Model 3342, Avon, MS) both set at

50 Hz, before inputting the signal to the A-D converter. The response time of the detector was 40 ms with this configuration. The sampling rate of the A-D converter varied between 10 and 20 Hz. Once acquired digitally, the peak parameters (center of gravity, peak area, variance) were obtained by statistical moment analysis.

### **8.2.3 Flow buffer**

The flow buffer was a mixture of 10 mM sodium monophosphate, 2.5% ethanol, and 0.01% Tween. All compounds to be analyzed using the capillary immunosensor were prepared in this flow buffer.

### **8.2.4 Antibody immobilization on a capillary<sup>15</sup>**

The same set-up for coating capillaries, described in Figure 5.5 of this thesis, was used to deliver the reagents onto the capillary to immobilize the antibody. A 5-m long capillary (50  $\mu\text{m}$  ID, 140  $\mu\text{m}$  OD) was cut and, using proper connections and fittings, was connected to the nitrogen tank. A molecular sieve (type A4) trap was in place before delivering gas onto the solutions used in the capillary. This trap ensured the dryness of nitrogen gas.

A 4% solution of mercaptopropyltrimethoxysilane (MTS) in toluene was drawn onto the capillary by applying 20 psi pressure. Both ends of the capillary were sealed using a GC septum and then the capillary with MTS solution in it was incubated for one hour at room temperature. After the capillary was flushed with toluene three times, a 2 mM GMBS solution (crosslinker) was introduced onto the capillary and incubated at room temperature for another hour. Then the capillary was rinsed with deionized water and a 1 mg/mL solution of anti-TNT antibody 11B3 was introduced onto the capillary for one hour. The

capillary was then rinsed with water three times. A 30  $\mu\text{M}$  solution of Cy5-trinitrobenzene (Cy5-TNB) was introduced onto the capillary and incubated in a refrigerator at 4 °C for a minimum of 12 hours.

### **8.2.5 Antibody immobilization on a microchip**

The microchip was donated by Dr. Jed Harrison, Chemistry Department, University of Alberta. On the microchip there was a sample reservoir and a waste reservoir. The sample reservoir was filled with reagent. A glass funnel was attached to a hose that was connected to the vacuum line. A very gentle vacuum was applied to a glass funnel that was placed on top of the waste reservoirs of the microchip. In this way the reagent was delivered onto the channels of the microchip and the same procedure as described for capillary-based was used to coat the antibody on the microchip internal walls.

### **8.2.6 Displacement immunoassay**

The detection end of the capillary was inserted onto a sheath-flow cuvette. From the injection end of the capillary, the flow buffer was pumped onto the capillary using a syringe pump. The excitation wavelength of the Cy5-TNB was provided by a red laser at  $632 \pm 4$  nm and the fluorescence emission was monitored at  $662 \pm 4$  nm.

At first, we observed a constantly changing slope of the background fluorescence intensity as a function of time. This was an indication of the washing of the excess and nonspecifically adsorbed Cy5-TNB from the capillary wall. After 10-15 min the background fluorescence stabilized. At this point, about 1-nL aliquots of flow buffer containing explosives were hydrodynamically injected onto the capillary. The injection end of the capillary was attached to the syringe pump with a proper fitting. The resulting

peaks due to the displacement of the fluorescently labeled antigen were recorded and the area under the peaks was quantified using Igor Pro software. Injections at each concentration and for each of the explosives were made three times and the average value was used in all the graphs.

In microchip flow injection analysis, 1  $\mu\text{L}$  of the explosives were injected manually onto the channel using a Hamilton syringe. The total volume of each channel is 5 cm x 200  $\mu\text{m}$  x 400  $\mu\text{m}$  or 4  $\mu\text{L}$ .

### **8.3 Results and discussion**

#### **8.3.1 Injection time and flow rate optimization for flow injection analysis of Cy5-TNB with a sheath-flow cuvette and LIF detection**

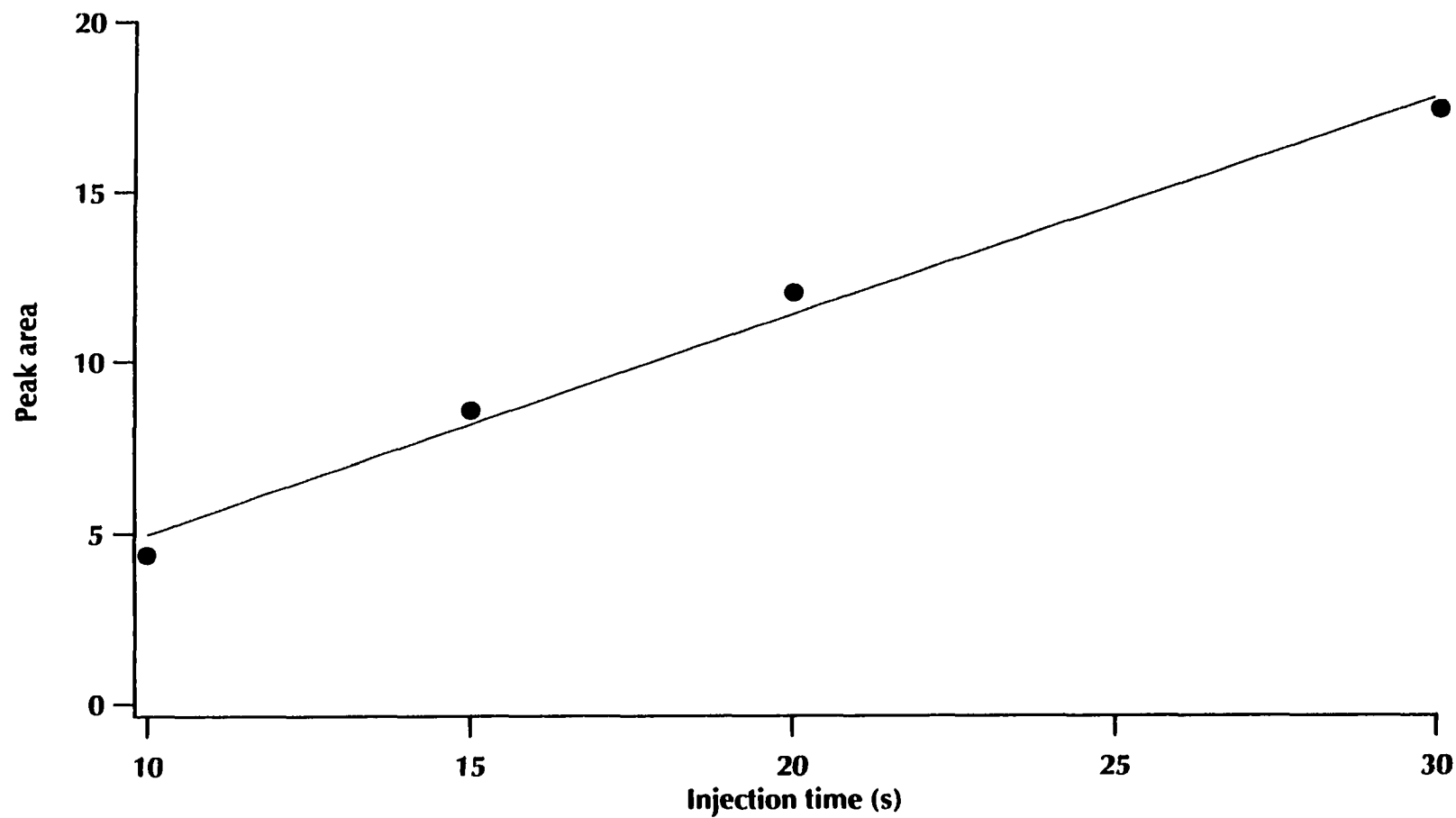
Figure 8.5 shows the linear relationship between Cy5-TNB peak areas and hydrodynamic injection times in an antibody-immobilized coated capillary. Each Cy5-TNB injection was repeated three times and the average value of the peak areas is plotted against the injection time. The instrument used for this experiment was a flow injection analysis system with a sheath-flow cuvette post-column LIF detection with 680 nL/min flow rate in a 35-cm long capillary.

Figure 8.6 shows the effect of the flow rate in  $\mu\text{L} / \text{min}$  on the retention time of Cy5-TNB. By increasing the flow rate an inverse drop in retention time was observed.

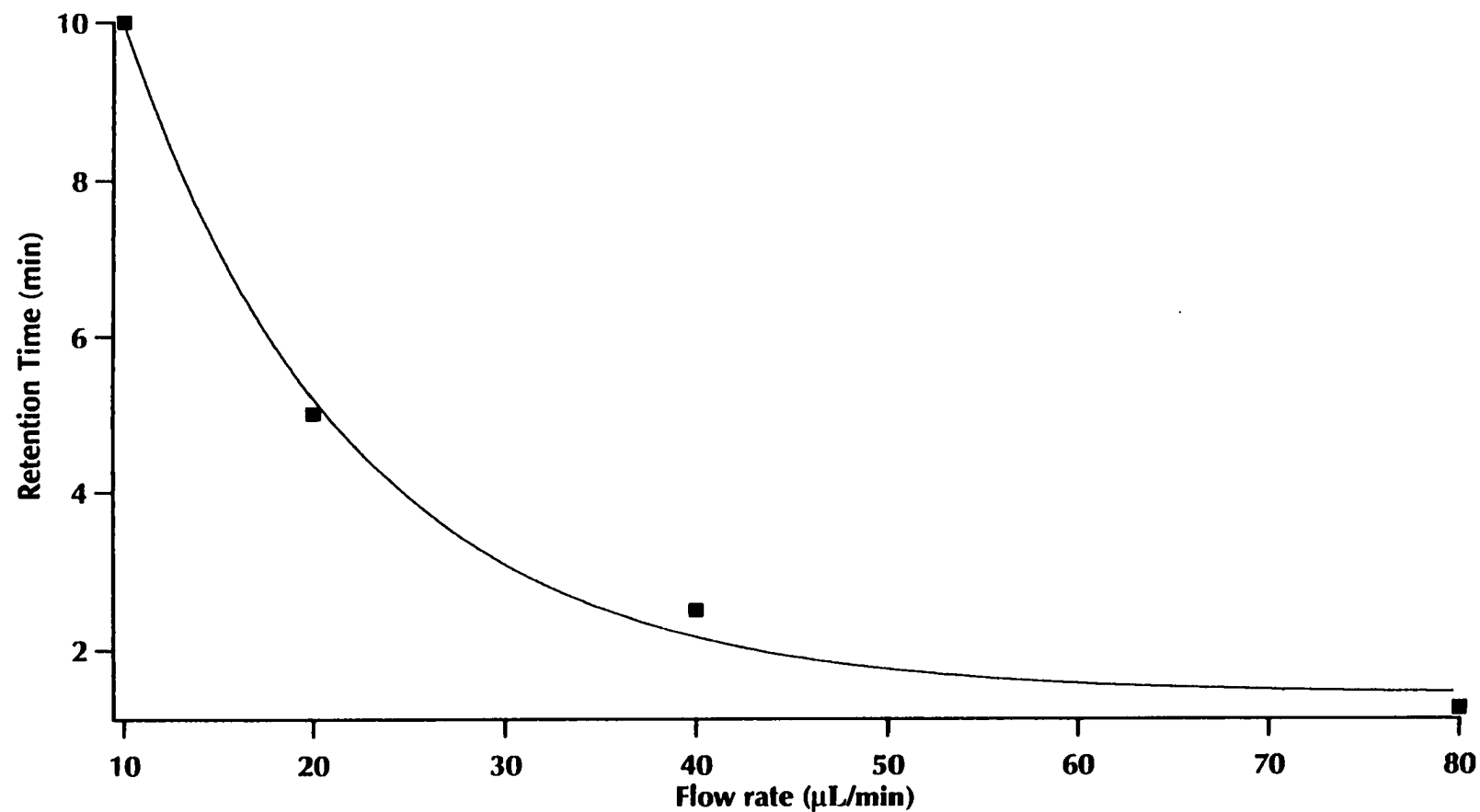
#### **8.3.2 Comparison of calibration curves for Cy5-TNB using flow injection analysis with a sheath-flow cuvette, a commercial Beckman instrument, and a microchip system**

A series of Cy5-TNB solutions in run buffer from  $10^{-8}$  M to  $10^{-12}$  M was prepared

**Figure 8.5: The effect of injection time on peak area for displacement immunoassay flow injection analysis of TNT with a sheath-flow cuvette and LIF detection. Capillary length is 35 cm, 10 s injection for 20 cm height difference and 680 nL/min flow rate. The TNT concentration is 100 ng/mL.**



**Figure 8.6: The effect of the flow rate on retention time in displacement flow injection analysis of TNT using a sheath-flow cuvette with LIF detection. Capillary length is 35 cm, and 10 s injection is done hydrodynamically with 20 cm height difference. The curve is a guide to the eye.**



and hydrodynamically injected onto a 35-cm long antibody-immobilized coated capillary. The flow rate was 680 nL/min, height difference for hydrodynamic injection was 25 cm and the injection time was 10 s.

Figure 8.7 shows the calibration curve for Cy5-TNB using post-column LIF detection with a sheath-flow cuvette. The linear dynamic range is from 0.1 to at least 30 nM Cy5-TNB. Six back-to-back injections of 1 nM Cy5-TNB were performed on the same capillary for 10 s each. The average peak area was 5.3 with a standard deviation of 0.6 that corresponds to 5.3/0.6 or 9% RSD for hydrodynamic injection.

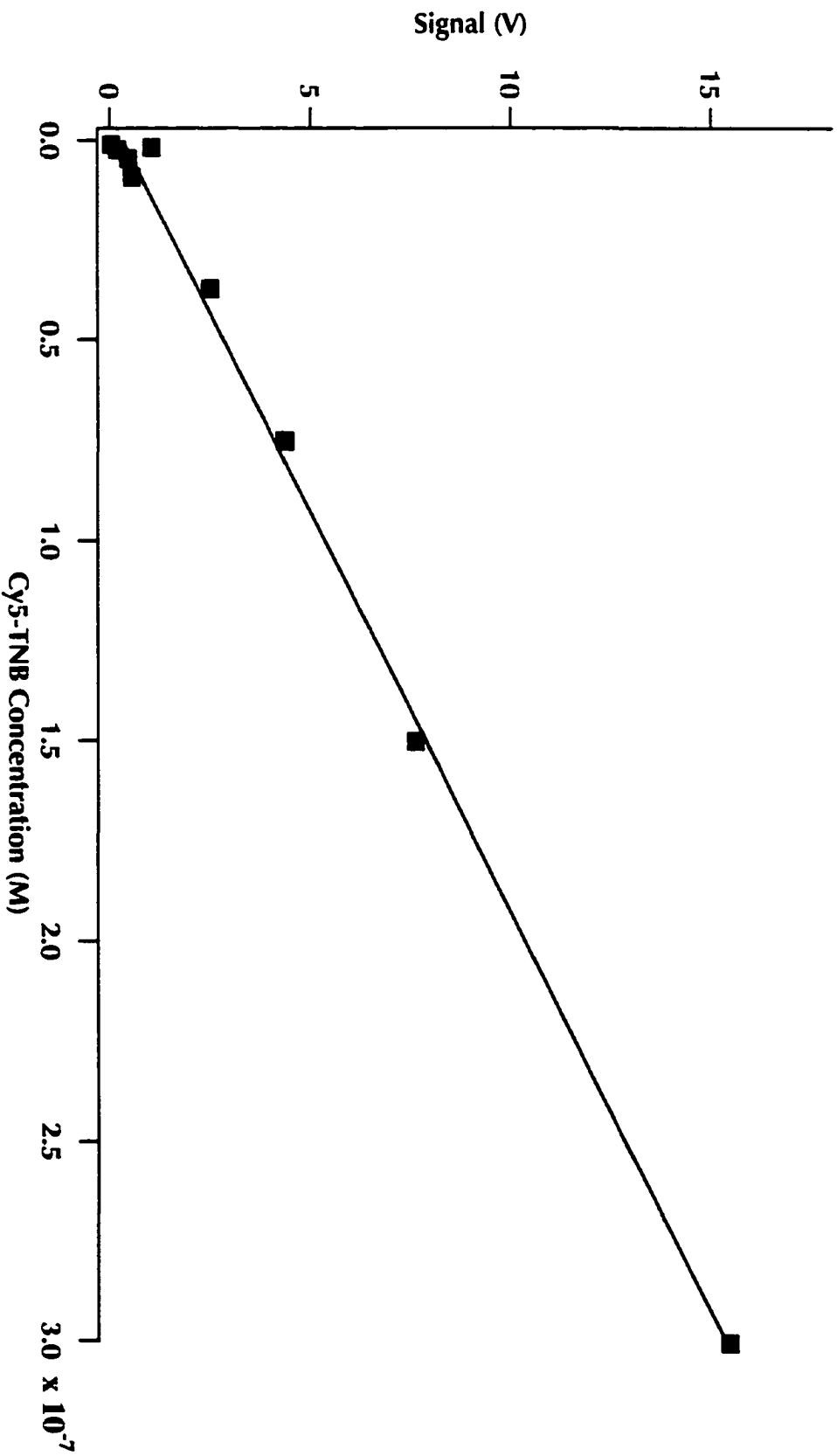
Figure 8.8 is a similar calibration curve as Figure 8.7 using the commercial Beckman instrument with on-column LIF detection. The total capillary length was 27 cm and 20 cm to the detection end. The injection was done under 0.5 psi for 20 s that is equivalent to 40 nL. The pressure to perform FIA was 20 psi. The linear dynamic range is 1 to at least 300 nM Cy-5 TNB.

Figure 8.9b shows the same calibration curve for Cy5-TNB using the microchip system. In this case the 1- $\mu$ L injection was done on a microchip channel followed by FIA with LIF detection. The injection volume is about 3 orders of magnitude higher than that of the two previous calibration curves. Figure 8.9a shows the peaks detected from the microchip using FIA with on-channel LIF detection and Figure 8.9b is the calibration curve resulting from peak areas obtained from Figure 8.9a versus concentration of Cy5-TNB for 1- $\mu$ L injection.

### **8.3.3 Displacement immunoassay of TNT using flow injection analysis with a sheath-flow cuvette, microchip, and a Beckman instrument**

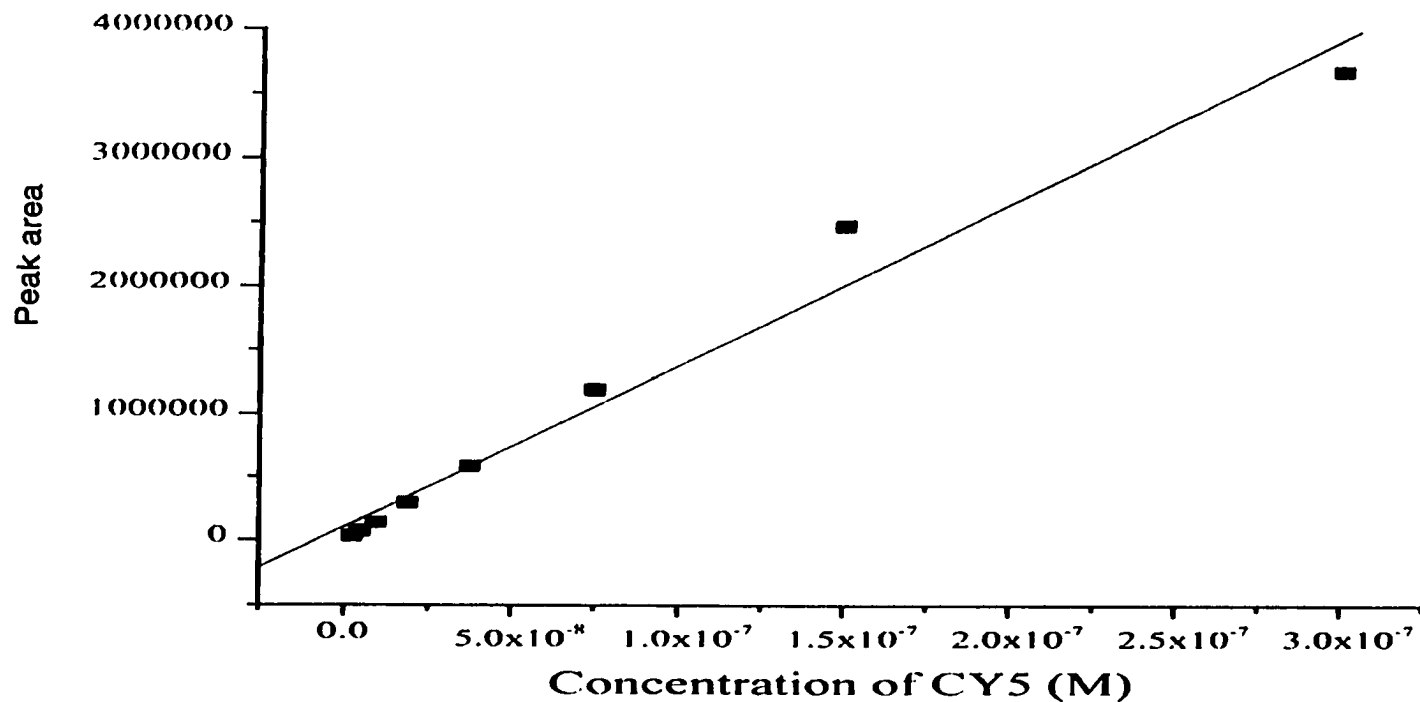
TNT is not fluorescently labeled, but it displaces the Cy5-TNB that is fluorescently labeled. By detecting the displaced Cy5-TNB, the concentration of TNT could be

**Figure 8.7: Calibration curve for Cy5-TNB using flow injection analysis with a sheath-flow cuvette and LIF detection. Capillary length is 35 cm, and 10 s hydrodynamic injection is done with 20 cm of height difference.**



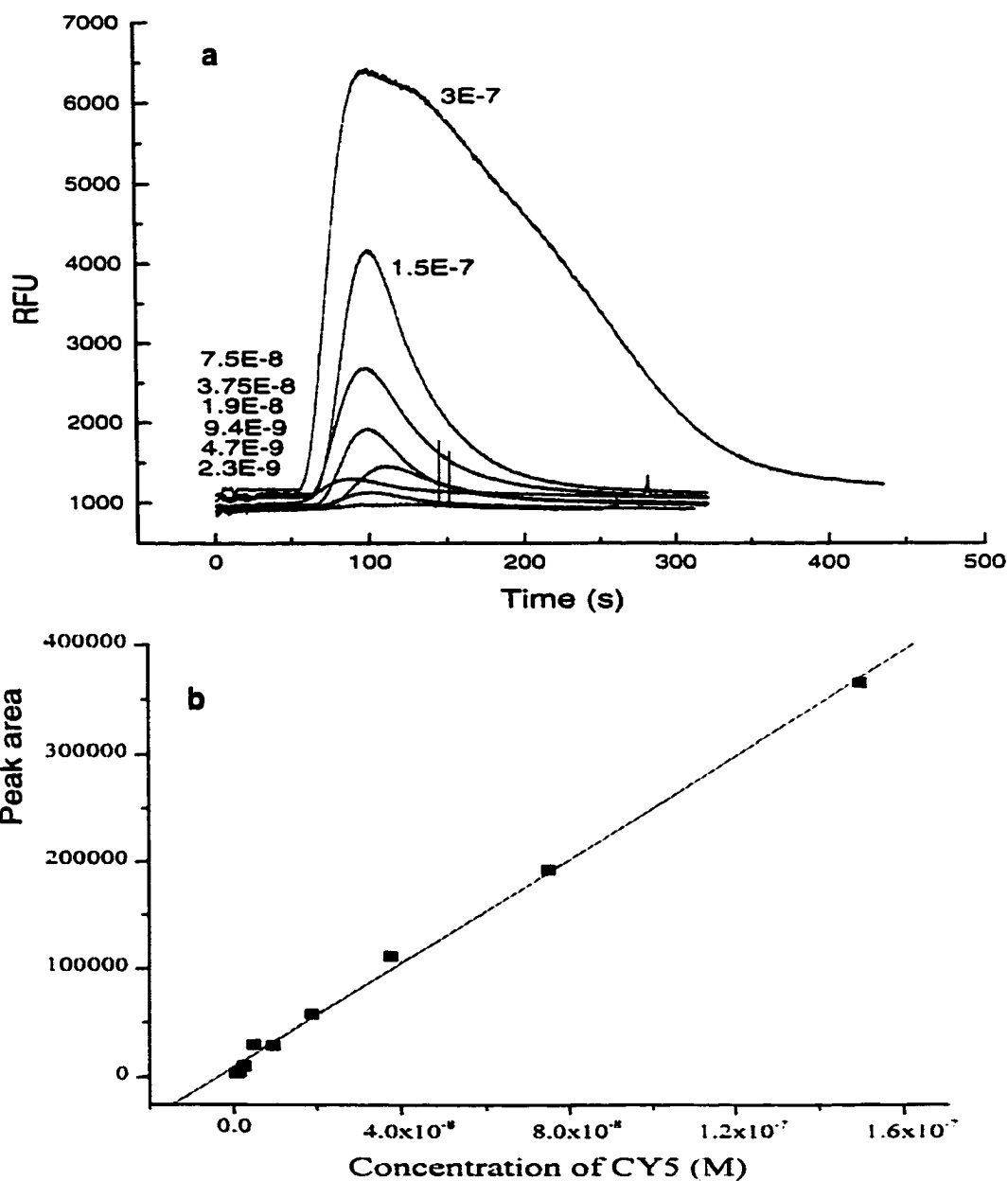


**Figure 8.8: Calibration curve for Cy5-TNB using flow injection analysis with on-column LIF detection. The Beckman instrument has been used for this experiment with 20 s injection at 0.5 psi and 20 psi for separation. The capillary length was 27 cm end-to-end and 20 cm from injection end to the detection window. RFU is relative fluorescence unit.**



401

**Figure 8.9:** a) Peak shape for flow injection analysis of Cy5-TNB on a microchip with on-column LIF detection, and b) Calibration curve for Cy5-TNB using the peak areas of part a. The injection volume is 1  $\mu\text{L}$  and the flow is maintained using gravity with 20 cm height difference.



determined. In this experiment, I compared the TNT analysis using 3 different instruments. The capillary format with a post-column LIF detection and a sheath-flow cuvette was compared to the microchip format with on-column LIF detection. Post-column and on-column LIF detections were also compared using the Beckman instrument for on-column detection and an in-house sheath-flow cuvette for post-column detection.

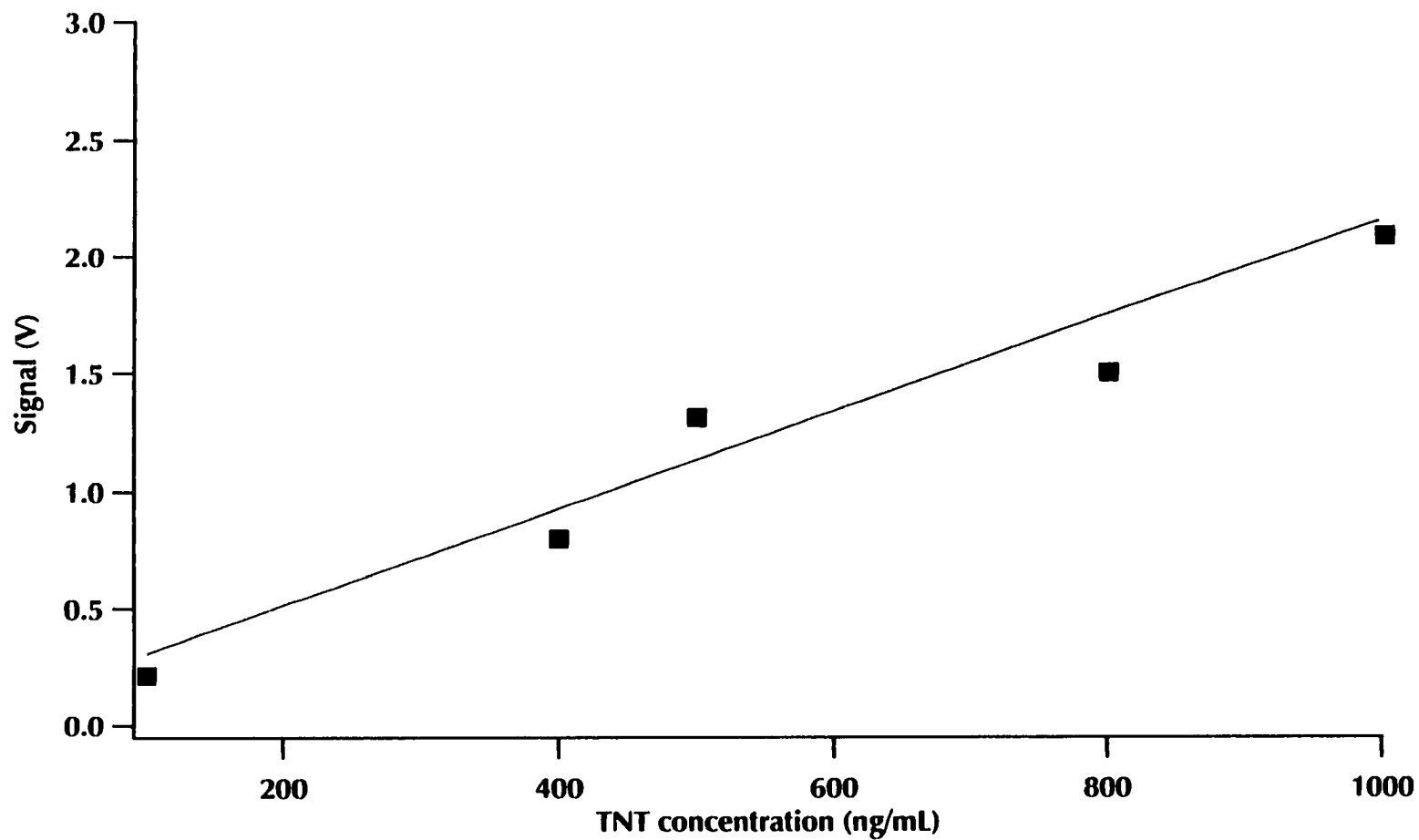
Figure 8.10 shows the flow injection analysis of Cy5-TNB displacement by TNT injection using post-column LIF detection with a sheath-flow cuvette. The linear dynamic range is from 100 to 1000 ng/mL of TNT for a 1 nL injection. Figure 8.11a shows the flow injection analysis of unlabeled TNT for a 1- $\mu$ L injection on the microchip. The linearity between the peak area and concentration of the TNT was poor for microchip-based flow injection analysis. Figure 8.11b shows the calibration curve for TNT detection and a 1- $\mu$ L injection. Figure 8.12a shows the flow injection analysis with on-column LIF detection using the Beckman CE instrument. Figure 8.12b is the calibration curve for CE-LIF detection of 1 to 10  $\mu$ g/mL of TNT.

#### **8.3.4 Cross-reactivity studies of explosive compounds**

In order to study the cross-reactivity of the Ab for TNT and other explosive compounds, 5000 ng/mL of TNT followed by 5000 ng / mL each of the following reagents: RDX; HMX; 2 nitrotoluene; 2 amino 4, 6 dinitrotoluene; 1, 3 dinitroglycerol; and 2, 4 dinitrotoluene, were injected onto the capillary for 10 s and 25 cm height difference. Figure 8.13 shows the chemical formulas for each of the explosives studied for cross-reactivity. Figure 8.14 shows the cross-reactivity of the family of explosives as compared to TNT as the control reagent. This Figure is the FIA with post-column LIF detection using a sheath-flow cuvette. If the peak area for TNT is assigned 100%, relative to TNT the

**Figure 8.10: TNT analysis using Cy5-TNB displacement immunoassay and a sheath-flow cuvette with LIF detection.**

**Capillary length is 35 cm, and 10 s hydrodynamic injection of TNT is done with 20 cm height difference.**



404

**Figure 8.11: a) Peak shape for TNT analysis using microchip with flow injection analysis and on-channel LIF detection, and b) Calibration curve for TNT using the peak areas from Fig. 11a. The injection volume onto the microchip is 1  $\mu$ L.**

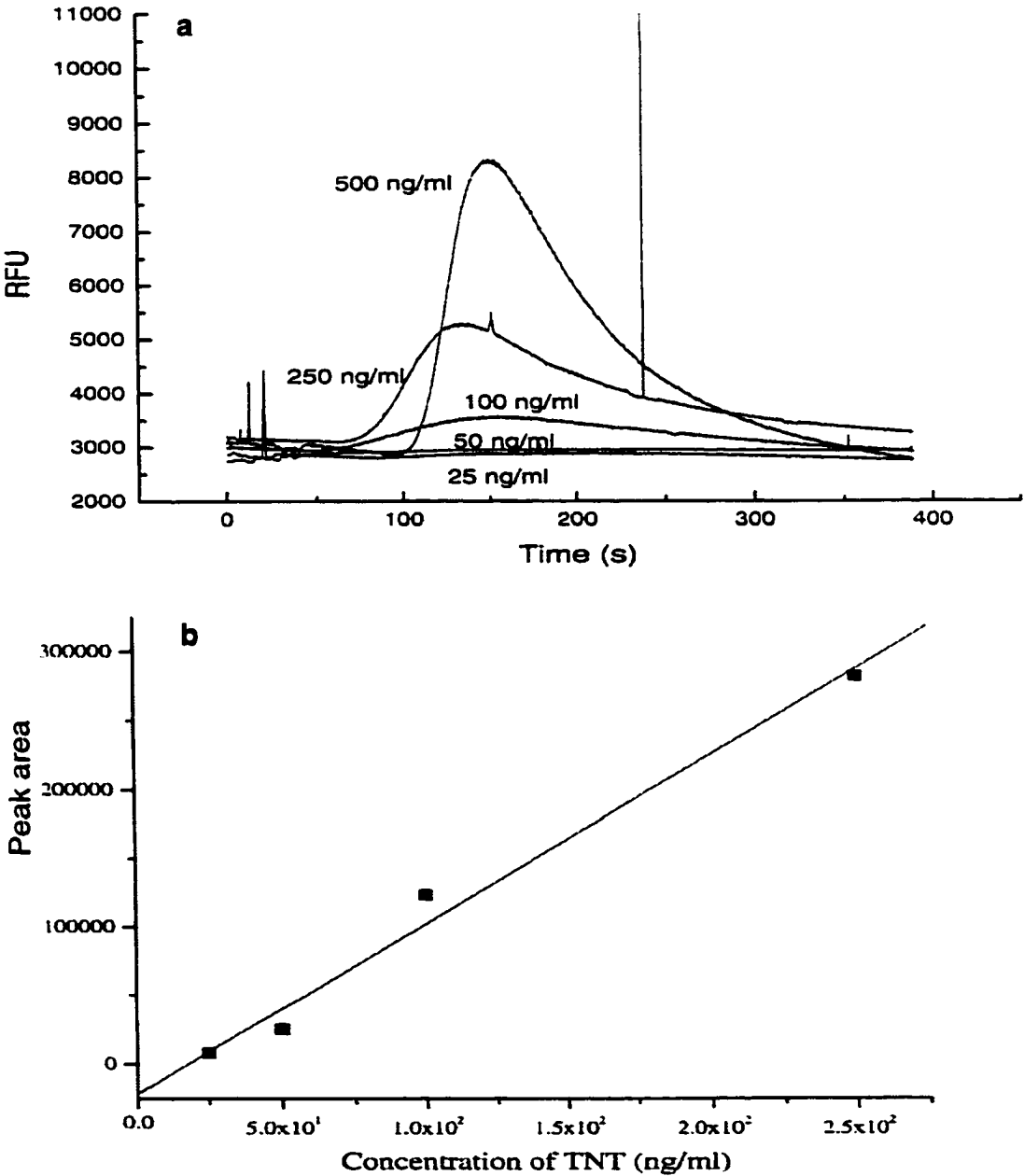


**Figure 8.12: a) Peak shape for TNT flow injection analysis with on-column LIF detection, and b) Calibration curve for TNT with 20 s injection at 0.5 psi. Flow pressure was 20 psi. Commercial Beckman instrument has been used for this experiment Capillary length was 27 cm end-to-end and 20 cm injection to detection length.**

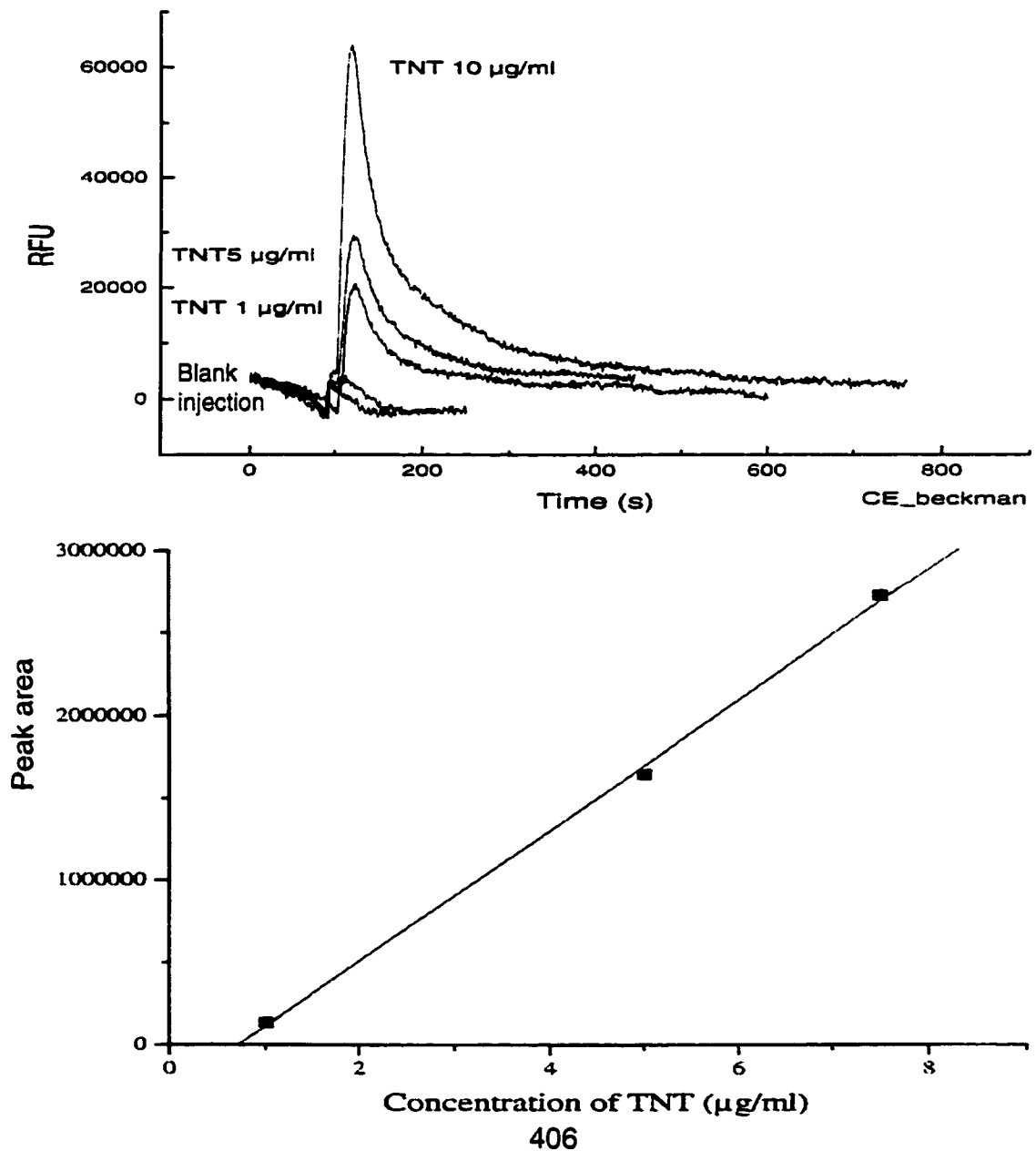
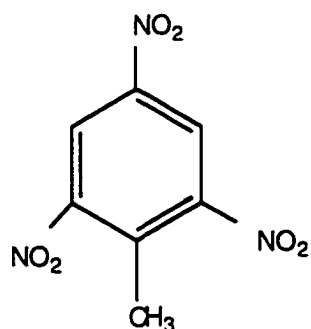
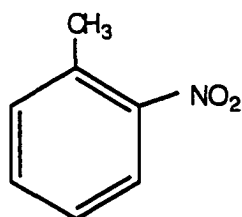


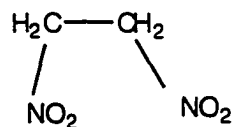
**Figure 8.13: Chemical formulas for different explosives used for cross-reactivity studies**



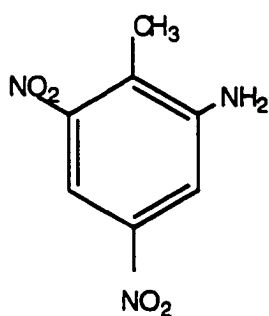
TNT (trinitrotoluene)



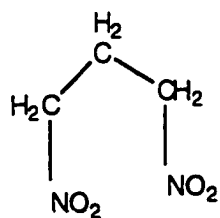
2-nitrotoluene



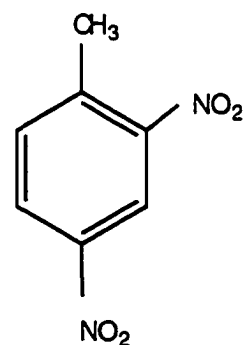
dinitroethylene glycol



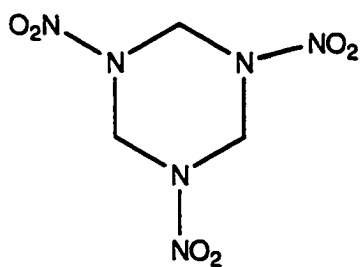
2-amino 4,6 dinitrotoluene



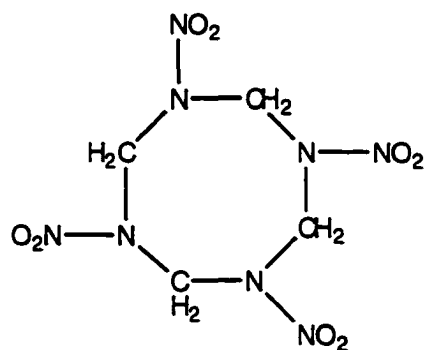
1,3 dinitrolycerol



2,4 dinitrotoluene

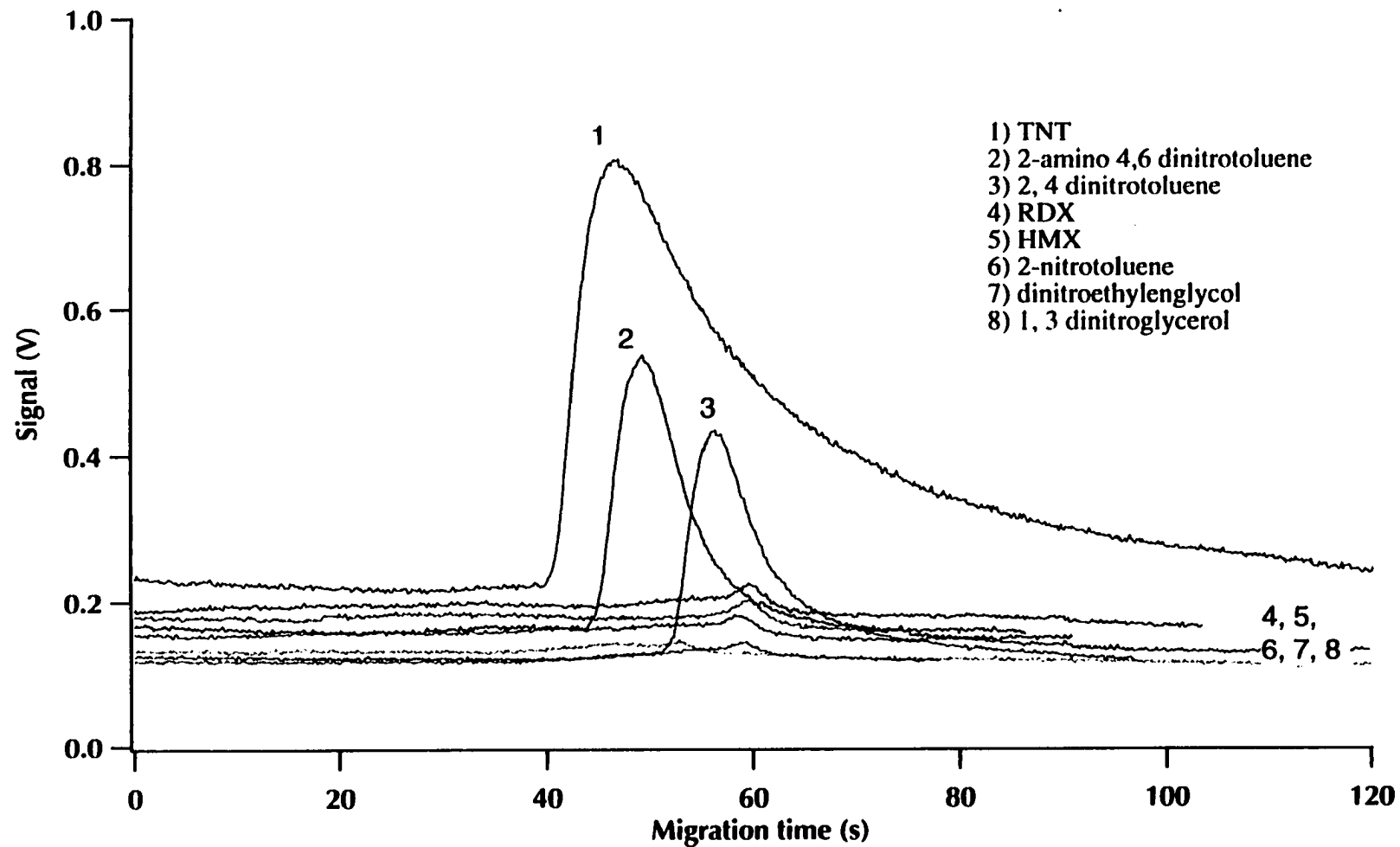


RDX (hexahydro 1,3,5 trinitrotriazine)



HMX (octahydro 1,3,5,7-tetranitrotetrazocine)

**Figure 8.14: Cross-reactivity of explosive compounds as compared to TNT using Flow Injection Analysis with a sheath-flow cuvette and LIF detection**



408



cross-reactivity of the explosives are as follows: RDX (1%); HMX (0.4%); 2-nitrotoluene (0.2%); 2-amino, 4, 6 dinitrotoluene (24%); 1, 3 dinitroglycerol (1.5%); and 2, 4 dinitrotoluene (22%). The cross-reactivity of the capillary immunosensor is due to the antibody employed.<sup>21</sup> Polyclonal antibodies are quite heterogeneous, and therefore, bind to many compounds from the same family of explosives. Monoclonal antibodies, on the other hand, are homogenous and their cross-reactivity is much less than those of polyclonal antibodies. The Ab that was provided by NRL was polyclonal and we expected to observe some degrees of cross-reactivity.

High cross-reactivity of TNB and DNT, which are breakdown products of TNT, make the capillary immunosensor more effective as a detector for this family of explosive compounds.

Displacement efficiency ( $D_e$ ) is defined as:<sup>22</sup>

$$D_e = \text{moles of Ag* detected} / \text{moles of Ag injected} \quad (8.4)$$

where Ag\* and Ag represent the Cy5-TNB and TNT, respectively. The displacement efficiencies of the packed-column flow immunosensors was reported to be 0.001 l.<sup>21-22</sup> A capillary-format immunosensor improves the sensitivity due to the enhanced interaction of the antigen with the immobilized antibodies, because of the high surface-to-volume ratio.

Table 8.1 shows the surface-to-volume ratio versus internal diameter of the capillary. As this table shows, reducing the capillary internal diameter causes the surface-to-volume ratio to rise accordingly. 1000 ng/mL TNT (4.4  $\mu$ M TNT) was hydrodynamically injected onto the capillary for 10 s at 25 cm height difference and the corresponding Cy5-TNB peak area that was displaced was calculated to be 2.1. This peak area is equivalent to 0.37 nM concentration of Cy5-TNB injected hydrodynamically under the same conditions as TNT. For 1 nL injection volume the amount of TNT injected is

**Table 8.1: Theoretical calculations of surface-to-volume ratio versus capillary ID**

<b>Capillary ID (<math>\mu\text{m}</math>)</b>	<b>% surface-to-volume ratio</b>
550	0.73
250	1.60
100	4.00
75	5.33
50	8
25	16

$4.4 \times 10^{-15}$  moles and the amount detected is  $3.7 \times 10^{-17}$  moles. The displacement efficiency is, therefore,  $3.7 \times 10^{-17} / 4.4 \times 10^{-15}$  or 0.08 which is about 80 times higher than reported for the packed-column immunosensor.<sup>22, 23</sup>

Figure 8.15 shows the cross-reactivity of the same family of explosives as Figure 8.14, but using microchip flow injection analysis with on-channel LIF detection and a 1- $\mu$ L injection of the explosives with a concentrations similar to that used for flow injection analysis with a sheath-flow cuvette. When using the Beckman instrument and applying high voltage to drive the analyte to the detection end by electroosmotic flow, the results were not consistent and the peaks were very broad and irreproducible.

### **8.3.5 Comparison of electroosmotic and hydrodynamic analysis**

Electroosmotic analysis was not reproducible and applying high voltage caused bleeding of Cy5-TNB probably because the high electric field might have changed the folding of the antibody and the epitope topology. Figure 8.16 compares the peak shape for electrokinetic and hydrodynamic injections. When doing electrokinetic injection the peaks were very broad and the reproducibility was very poor. For hydrodynamic injection the band broadening was reduced but still the reproducibility was very poor. The commercial CE Beckman instrument with on-column LIF detection was equipped with a vacuum injector.

### **8.3.6 LOD comparison among a sheath-flow cuvette, a microchip, and a commercial Beckman instrument**

Table 8.2 compares the concentration LOD and mass LOD for displacement FIA in a capillary format and microchip format. In the microchip mode at least 1- $\mu$ L of the sample has to be injected, but in the capillary format the injected volume is in the nL range which is

**Figure 8.15: Cross-reactivity of explosive compounds compared to TNT using flow injection analysis with LIF**

**detection on a microchip channel with 1  $\mu$ L injection of the explosives each at 500 ng/mL concentration.**

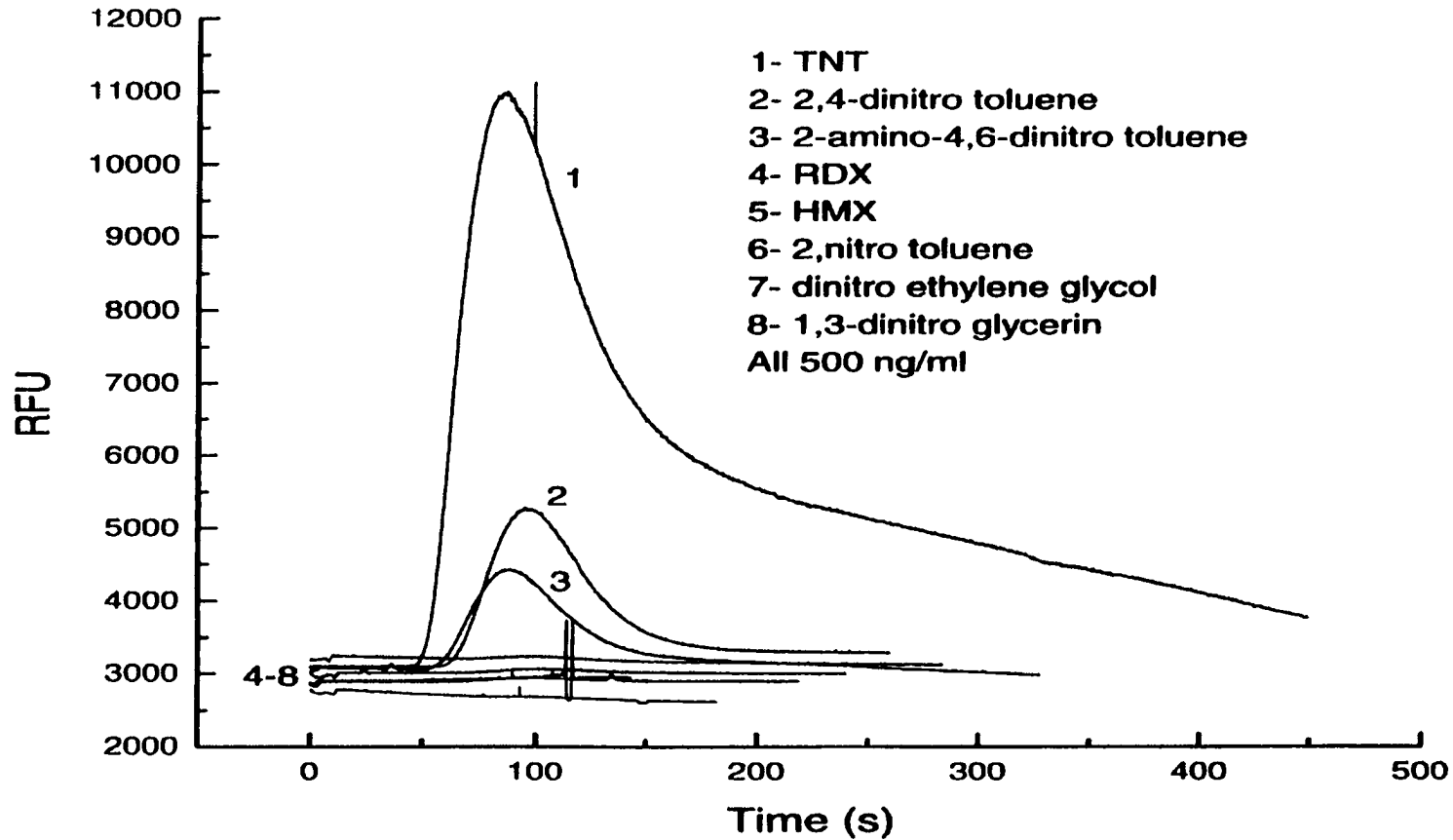


**Figure 8.16: Displacement immunoassay of TNT using a sheath-flow cuvette and LIF detection with a) Hydrodynamic injection and b) Electrokinetic injection of TNT. Capillary length is 20 cm and 400 V/cm voltage was applied to transfer the TNT to the detection end using electroosmotic flow.**

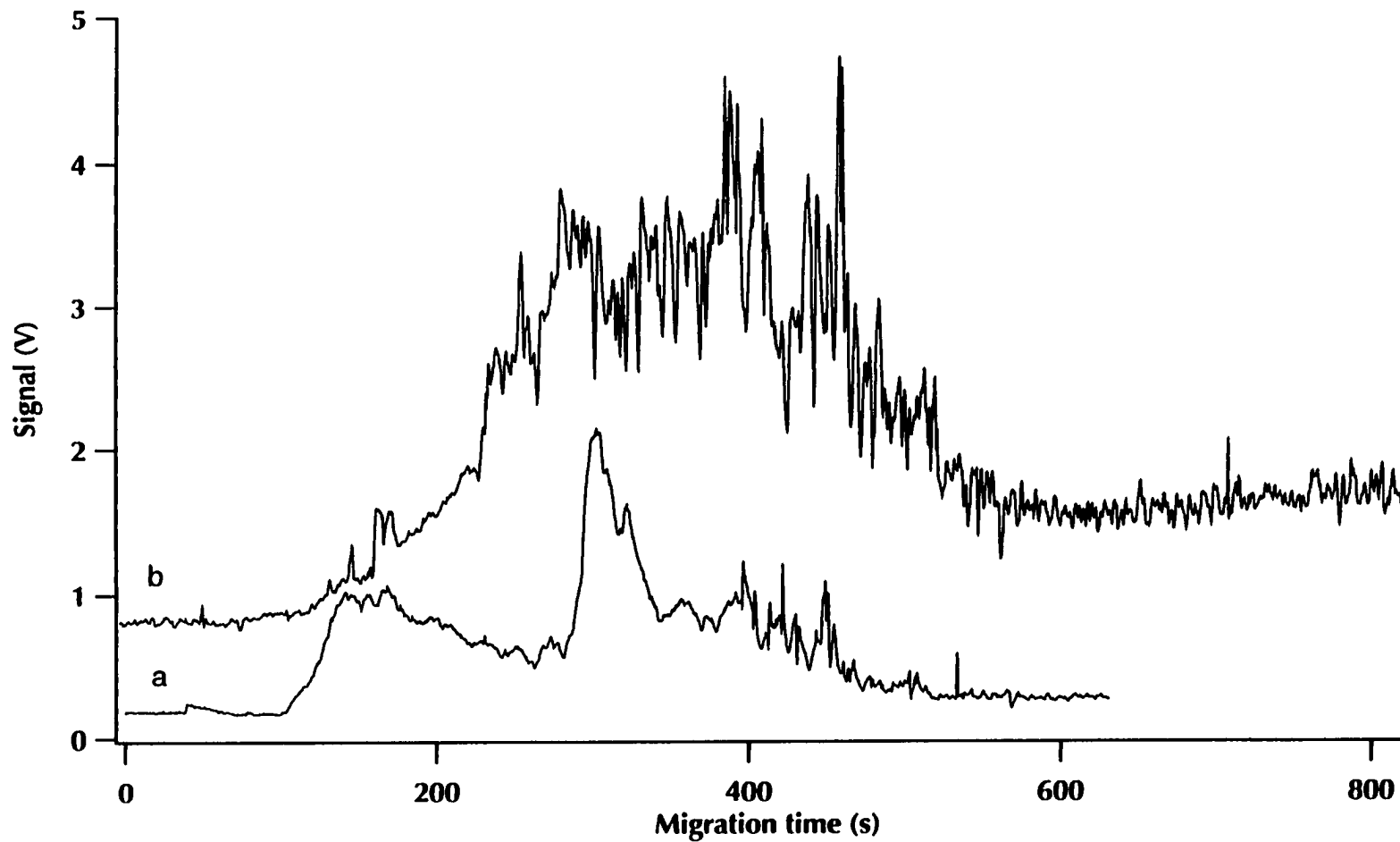


**Table 8.2: LOD comparison among FIA and LIF detection with a) on-column detection using a commercial Beckman instrument, b) on-column detection on a microchip, and c) post-column detection with a sheath flow cuvette**

	<b>Commercial Beckman Instrument</b>	<b>Microchip</b>	<b>In-house CE with a sheath- flow cuvette</b>
<b>Volume injected</b>	40 nL	1 $\mu$ L	1 nL
<b>Mass LOD</b>	176 femtomoles	110 femtomoles	440 attomoles
<b>Conc. LOD</b>	100 ng/mL	25 ng/mL	100 ng/mL

3 orders of magnitude less than that for a microchip. The concentration LOD for the capillary format was 100 ng/mL, while for microchip format was 25 ng/mL of TNT. Calculating the amount of TNT injected shows that the mass LOD for a capillary is 40 attomole and for a microchip is 4 femtomoles, and for a commercial Beckman instrument is 176 femtomoles.

#### **8.4 Conclusions**

In this chapter, I have shown that when using small ID capillaries as compared to packed-bed columns surface-to-volume ratio increases, laminar flow decreases and band broadening is reduced. Sensitivity of a displacement continuous flow immunosensor improves as compared to packed-bed column immunosensors. It is also shown that using capillaries, smaller volumes of sample, solvent, and other reagents are consumed. Concentration LOD for the microchip based format was better than that of the capillary when injecting 1000 times more sample, while mass LOD was about 4000 times better for capillary-based immunoassay than for the microchip-based immunoassay. Cross-reactivity studies using the microchip-based and capillary-based immunoassay resulted the same conclusion that the assay is a general technique for the determination of this class of explosives.

## 8.5: References

1. Cass, A. E. G., *Biosensors A Practical Approach*, IRL Press at Oxford University Press, 1990.
2. Schlitz, N. M., Kennedy, R. T., *Anal. Chem.*, 65, 3161, 1993.
3. Ye, L., Le, C. X., Xing, J. Z., Ma, M., Yatscoff, R., *J. of Chromatogr., B.* 414, 59-67, 1998.
4. Landers, *Handbook of Capillary Electrophoresis*, Chapter 29, CRC press Inc., 1997.
5. Fan, Z. H., Harrison, D. J., *Anal. Chem.*, 66, 1, 177-184, 1994.
6. Seiler, K., Harrison, D. J., *Anal. Chem.*, 65, 10, 1481-1488, 1993.
7. Harrison, D. J., Fluri, K., Seiler, K., Fan, Z., Effenhauser, C. S., Manz, A., *Science*, 261, 895-897, 13 Aug. 1993.
8. Van Emon, J. M., Mumma, R. O., *Immunological Methods for Environmental Analysis*, ACS Symposium 442, Washington, 1989.
9. Schultz, N. M., Kennedy, R. T., *Anal. Chem.*, 65, 3161-3165, 1993.
10. Meulenberg, E. P., Mudler, W. H., Stoks, P. G., *Environ. Sci. Tech.*, 29, 553-561, 1995.
11. Hunter, W. M., Corrie, J. E. T., *Immunoassays for Clinical Chemistry*, 2<sup>nd</sup> ed., Churchill Livingstone: Edinburg, 1983.
12. Rabbany, S. Y., Donner, B. L., Ligler, F. S., *Crit. Rev. Biomed. Eng.*, 225, 307-346, 1994.
13. Ahren, H., *The Scientist*, 10, 18-20, 1995.
14. Kemeny, D. M., *A Practical Guide to ELISA*, Pergamon Press: Oxford, 1991.
15. Warden, B. A., Allam, K., Sentissi, A., Cecchini, D. J., Giese, R. W., *Anal. Biochem.*, 162, 363-369, 1987.



16. Whelan, J. P., Kusterbeck, A. W., Wemhoff, G. A., Bredhorst, R., Ligler, F. S..  
Anal. Chem., 65, 3561-3565, 1993.
17. Judd, L. L., Kusterbeck, A. W., Charles, P. T., Ligler, F. S., Field screening  
Methods for Hazardous Wastes and Toxic Chemicals, Air and Waste Management  
Assoc., Pittsburg, PA, 2, 732-736, 1993.
18. Poole, C. F., Poole, S. K., Chromatography Today; Elsevier Science: New York.  
NY, 1991.
19. Narang, U., Gauger, P. R., and Ligler, F. S., Anal. Chem., 69, 1961-1964, 1997.
20. Bhatia, S. K., Shriver-Lake, L. C., Prior, K. J., George, J. H., Calvert, J. M.,  
Bredehorst, R., Ligler, F. S., Anal. Biochem., 178, 408-413, 1989.
21. Whelan, J. P., Kusterbeck, A. W., Wemhoff, G. A., Bredhorst, R., Ligler, F. S..  
Anal. Chem., 65, 3561-3565, 1993.
22. Rabbany, S. Y., Kusterbeck, A. W., Bredehorst, R., Ligler, F. S., Sens. & Actuat.B.  
29, 72-78, 1993.
23. Narang, U.; Gauger, P. R.; and Ligler, F. S.; Anal. Chem., 69, 1961-1964, 1997.

# **Chapter 9**

## **Conclusions and future work**

## **9.1 Introduction**

The objective of this research was combining the high sensitivity of LIF detection and high selectivity of immunoassay to quantitate natural toxins and explosives in the environment. The immunoassay technique was chosen because it was already used for this class of chemicals, but the classical immunoassay technique lacked the sensitivity that was compensated by LIF detection. The first step was to assemble a CE-LIF instrument and optimize its performance. Then I had to prevent the analyte from adsorption and finally fluorescently label the analyte, called antigen in immunoassay, in order for it to be detectable.

This thesis has three parts. In part one assembling the instrument, parameter optimization and evaluating the injection techniques are presented. Because of very low concentration of analyte and because of bias in electrokinetic injection, different injection methods were studied. Finally, sample depletion in electrokinetic injection was studied to evaluate the effect of multiple injections on the original concentration of the analyte. Part one includes three chapters: Chapters 1, 2, and 3.

## **9.2 CE-LIF instrument and performance optimization**

In Chapter 2 a compact CE-LIF instrument and performance optimization of this miniaturized CE is shown. Different injection techniques in CE are discussed and experimental results show the high sensitivity of the CE-LIF method. This CE-LIF instrument is the first generation of instruments in the development of mobile instruments. The injector box had to be modified for reproducible vacuum injection. If the bias in electrokinetic injection is not important, this method is very precise. The limit of detection of the instrument is 150 fluorescein molecules.

The first generation of the instrument had to be operated in the dark because of light leakage into the PMT. To avoid this difficulty, a light shield was designed. It was proved that this simple design prevents stray light from reaching the detector. The light shield allows the CE-LIF instrument to be operated in day light and takes us one step ahead in having a mobile CE-LIF instrument.

The next generation of the miniaturized CE-LIF should improve the performance of the system. The laser and the power supply could be replaced with more compact units to reduce the size of the instrument. The alignment of the instrument is a time consuming task for a novice experimenter that should be improved.

In Chapter 3 electrokinetic injection sample depletion are presented. There are several techniques to introduce the sample onto the capillary. The most common one is electrokinetic injection that is biased and components with higher mobility are differentially injected onto the capillary. The analyte concentration changes with subsequent injections. These problems are addressed in this chapter.

DNA samples that were re-suspended in low ionic strength formamide were efficiently introduced onto a separation capillary. This efficient sample introduction technique suggests that dilute DNA sequencing samples can be used for analysis. As a result, it should be possible to modify the DNA sequencing reaction to use lower concentration of template, enzyme, nucleotides, and primer. A significant cost savings could be achieved by decreased consumption of these reagents. This is particularly important in large-scale sequencing efforts, such as the human genome initiative and large-scale genomic disease screening efforts.

When DNA fragments are being injected onto the capillary, they are also being driven through the separation medium. In this case peak width should increase with an increase in the injection time. Instead there is, presumably, an isotachophoretic focusing effect at the capillary tip. More work is required to characterize this phenomenon.

### 9.3 Electroosmotic flow measurement and manipulation

The microcystin antibody is a large protein that adsorbs to the capillary wall and, hence, obscures the separation. This problem is addressed in part two of the thesis. To minimize the adsorption, a capillary was coated with a hydrophilic polymer. To evaluate the efficiency of the surface coverage, a reliable method for EOF measurement was developed and used as a criterion to evaluate the effectiveness of surface coverage. Part two includes Chapters 4 and 5.

The driving force to run the analyte from the injection end to the detection end could be EOF. In this part a method to measure the EOF is presented. Reducing the EOF could reduce the analyte loss due to adsorption to the capillary wall.

In Chapter 4, two methods for EOF measurement, the current monitoring method and neutral marker method, have been compared. The current monitoring method for EOF measurement is as precise as the neutral marker method if the concentration difference between run buffer and replacing buffer is between 10% to 20%. If the concentration gradient is less than 10% or more than 20%, the F-test shows that the difference between the standard deviation of the two methods is significant. The student t-test shows that there is no statistically significant difference between the means of the neutral marker and the current monitoring methods if the concentration gradient is between 10% to 20%. No special type of detector is needed and, therefore, it is a very simple method. In situations where there is not a marker that is truly neutral at a specific pH, the current monitoring method could be used. This method could be used to study the fundamental properties of the capillary surface and the effect of these properties on electroosmotic mobility. For coated capillaries when EOF is reduced, this current monitoring method could be used to measure the EOF. Using this method, the experimenter need not worry about the possibility of the adsorption of the neutral marker on the capillary wall and/or gaining partial charge at a different pH.

Coating the capillary inner surface with a polymer to eliminate EOF is presented in Chapter 5. A series of polymers from the most hydrophobic to the most hydrophilic are compared to find which polymer shows the lowest EOF and minimum adsorption of proteins and antibody to the capillary wall.

Our new method improved the performance of coated capillaries in terms of pH stability from pH 2-11, temperature stability from 20 °C to 75 °C, migration time reproducibility with FQ-labeled ovalbumin, and EOF reproducibility. We also showed that Si-C- sub-layers for coating were much more stable than Si-O sub-layers and also polyAA top-layers were susceptible to alkaline hydrolysis for both Si-C sub-layers and Si-O sub-layers. Both Si-C-polyAAEE and Si-C-polyAAP showed less adsorption as compared to Si-C-polyDMA and Si-C-polyAA. It was difficult to decide which one was better if both AAEE and AAP monomers were fresh, but lack of batch-to batch reproducibility for the Si-C-polyAAEE was observed due to auto-polymerization of AAEE monomers. The Si-C-polyAAP showed less adsorption and better batch-to-batch reproducibility than that of the Si-C-polyAAEE. Preliminary results showed that Si-C-polyDMA, which was very stable in terms of EOF over a wide range of pH and temperature, could be successfully applied for DNA analysis. In this work we reported a new modified method of coating capillaries which was a combination of selected hydrophilicity of polymers as top-layers and high resistance toward alkaline hydrolysis of Si-C as sub-layers.

In this part some other polymers could be used to evaluate the adsorption of proteins onto the capillary wall. Much more work is needed to separate different classes of proteins. Most probably each protein may have its best performance for a special type of coating that has to be studied.

## 9.4 Labeling chemistry and environmental sample analysis

Having gained experience in introducing the sample effectively onto the capillary and preventing the sample loss by adsorption, the third part of the thesis involved fluorescently labeling the analyte in order to be able to detect it. This part includes Chapters 6, 7, and 8.

The labeling chemistry for CE-LIF immunoassay of carboxylic acid labeling is presented in Chapter 6. Despite being optimized by the author, amine labeling chemistry with FQ fluorogenic dye is not discussed because it is widely used in CE and the analytes of interest lack an amine group. Microcystin lacks an amine group, but it has two carboxylic acid groups and one arginine group.

Penicillin-G has been labeled with the fluorescent marker 5-BrMF using DMF as the reaction solvent and a trace amount of 18-crown-6 as a catalyst. The product was separated and purified from solution by a C18 reversed phase Sep-Pak cartridge. Preparative TLC and preparative HPLC were used to purify the product. The structure and molecular weight of the derivative were confirmed by mass spectrometry and 600 MHz <sup>1</sup>H-NMR spectroscopy. The separation technique was very effective in isolating pure product from impurities as was seen by the MS and NMR results. 3000 molecules of labeled penicillin-G were detected. It was also shown that the solvents of choice according to the literature for carboxylic acid labeling, i.e. MeOH or acetone, are not good solvents and DMF was shown to be better.

The carboxylic acid labeling procedure can be applied for fatty acids and peptide analysis. A graduate student, Heather Cain, is working on labeling different fatty acids and peptides using the optimized Procedure 7 mentioned in Chapter 6 of this thesis.

Microgram-scale organic synthesis of an arginine-specific reagent is shown in Chapter 7. Microcystin contains an arginine group. In this chapter an optimized procedure to label the arginine group is presented. Because the sample quantity is very limited, the

synthetic approach was developed in a way to reduce the weight of the starting material to a microgram in order to minimize the reagent consumption.

Some other strategies to synthesize this arginine-specific reagent have to be studied. Another graduate student, Hans Osthoff, is continuing this part of the project.

Several procedures were tested to optimize the labeling reaction conditions for microcystin-LR. N-acetyl-L-arginine, cyclo (Arg-Gly-Asp-D-Phe-Val) cyclic peptide, and microcystin itself were chosen respectively. The reactants were decreased from 10.8 mg of N-acetyl-L-arginine to 1 mg of cyclic peptide and finally to 500  $\mu$ g of microcystin. In off-column labeling for LIF detection, the bottle-neck is the reaction itself that has to be done at higher concentrations of reagents.

Two different labeling reagents were used, TMR and 5-BrMF. It was demonstrated that direct labeling of arginine functionality at high pH was not feasible because of reagent decomposition at high pH. Other bases like hydrazine and hydroxylamine hydrochloride were also tested. Hydrazine worked well for small molecules, but it cleaved the peptide bonds for larger molecules.

Sodium hydride was chosen as a strong base that worked well under nonaqueous conditions to remove the proton of arginine and produce a free amine functional group ready for labeling site. This base worked well for both small and large molecules. Using this base all the model compounds, N-acetyl-L-arginine, cyclo (Arg-Gly-Asp-D-Phe-Val) cyclic peptide, including microcystin itself were labeled with the TMR reagent. For microcystin-LR, another labeling reagent (5-BrMF) also worked well.

The labeled microcystin bound to anti-microcystin antibody in an immunoassay reaction. The peak corresponding to labeled microcystin decreased with the addition of antimicrocystin antibody and there was a linear relationship between labeled microcystin peak and volume of anti-microcystin antibody added. A linear calibration curve for this titration was obtained.



We expected to observe an increase in the antigen-antibody complex (Ag\*.Ab) peak correlating to a decrease in the labeled microcystin peak. Unfortunately, this peak was not observed in several attempts of optimizing CE experimental conditions. It was thought that the adsorption of the Ag\*.Ab to the capillary wall could be the main reason for the complex not being detected. When the Ag\*.Ab was injected onto the capillary and CE showed no corresponding signal, the CE run buffer was changed to 10 mM NaOH. In this case an increase in the background was observed that after a while dropped to the base line. This observation was in agreement with the possibility of adsorption.

Several synthetic routes were tried to synthesize an arginine-specific reagent. A diketone functional group was suggested in the literature as the best arginine-specific reagent. Our goal was to have a fluorescent labeling reagent for arginine. That was the reason why we tried to couple a fluorescent molecule with a diketone functional group. The first attempt was to couple a molecule with one ketone functionality to the fluorescent molecule and oxidize the second ketone group. This approach worked very well when we used an aliphatic amine to be linked to the fluorescence molecule, however ozonolysis as an oxidation technique to make a diketone did not work as well. The other approach was using an aliphatic amine (4-aminoacetophenone) to be linked to the fluorescein molecule and SeO<sub>2</sub> oxidation of the methyl group in aminoacetophenone to an aldehyde. This synthesis worked, but the reaction yield was low. The last synthetic scheme was direct coupling of a diketone (2, 3-butanedione) with 5-BrMF under nonaqueous conditions. This synthesis worked and the product was confirmed using MALDI-MS. Still the main difficulty was purification of a molecule with a diketone functional group. It was proven that this reagent does bind to the arginine, but purification and isolation is left for future work.

In Chapter 8 different immunoassay techniques are discussed and displacement immunoassay of explosive compounds is presented in order to have another approach for environmental samples. In this chapter, I have shown that when using small ID capillaries

as compared to packed-bed columns surface-to-volume ratio increases, laminar flow decreases and band broadening is reduced. Sensitivity of a displacement continuous flow immunosensor improves as compared to packed-bed column immunosensors. It is also shown that using capillaries, smaller volumes of sample, solvent, and other reagents are consumed. Concentration LOD for the microchip based was 4 times poorer than that of the capillary while the mass LOD was about 3 orders of magnitude better for capillary-based immunoassay than for microchip-based immunoassay. Cross-reactivity studies using microchip-based and capillary-based immunoassay came to the same conclusion that the assay is a general technique for explosive determination. Polyclonal antibodies were used for TNT immunoassay, but if a sensor exclusively for TNT is the goal, a monoclonal Ab should be used instead.